New Activation Modes in Anion-Binding Catalysis: Enantioselective Synthesis of Amino Esters

New Activation Modes in Anion-Binding Catalysis:

Enantioselective Synthesis of Amino Esters

A thesis presented by

Andrew James Bendelsmith

to

The Department of Chemistry and Chemical Biology

in partial fulfillment of the requirements

for the degree of

Doctor of Philosophy

in the subject of

Chemistry

Harvard University

Cambridge, Massachusetts

June 2019

Dissertation Advisor: Eric N. Jacobsen *Andrew James Bendelsmith*

New Activation Modes in Anion-Binding Catalysis:

Enantioselective Synthesis of Amino Esters

Abstract

Dual hydrogen-bond donors (HBDs) function as soft Brønsted- or Lewis-acid catalysts. Two principal modes of catalysis have been identified for HBDs: via direct activation of π-electrophiles, or via anion-abstraction binding. In the latter context, the dual N-H's can associate with leaving groups to generate reactive chiral ion-pairs, which can be intercepted by nucleophiles to form a variety of products. Chiral HBDs have been designed and identified as highly enantioselective catalysts in a broad range of transformations. However, due to the relatively weak nature of hydrogen bonds in typical HBD catalysts, the scope of substrates that can be engaged is limited. The vast majority of successful HBD-catalyzed anion-abstraction reactions involve halide, and specifically chloride, leaving groups. Additionally HBDs generally only heterolyze labile C-Cl bonds to produce heteroatom-stabilized cations, such as *N*-acyl iminium ions, oxocarbeniums, and 3-membered onium intermediates. These requirements have resulted in important limitations to the substrates that can be activated toward enantioselective substitution reactions. The dissertation presented herein presents three strategies to overcome these limitations to HBD catalysis.

In Chapters 2 and 3, highly enantio- and diastereoselective syntheses of α-allyl and α-aryl amino esters are presented. Kinetic and computational studies provide evidence for an HBD-

catalyzed S_N2 reaction between the α-chloroglycinate electrophile and allylsilane nucleophile. This represents a new mode of anion-binding catalysis in which catalyst can effect an S_N2 substitution to a substrate for which ionization is energetically inaccessible, potentially expanding the range of substrates amenable to activation. Computational and regression modeling indicate that catalyst achieves enantioinduction by preferentially stabilizing the pathway to the major enantiomer of product through a precisely controlled network of attractive non-covalent interactions.

The ability to achieve strong rate enhancements by chiral HBDs in Lewis acid promoted reactions would greatly expand the scope of enantioselctive anion-abstraction chemistry. In Chapter 4, an HBD and $BF_3 \cdot OEt$ co-catalyzed allylation of α-aryl-α-methoxy glycinates for the synthesis α,α-disubstituted amino esters is described. The HBD catalyst does not sufficiently accelerate an enantioselective pathway over the racemic background reaction catalyzed by just $BF_3 \cdot OEt_2$, and thus the product could not be obtained in high enantioselectivity. A Sakurai model reaction and Gutmann-Beckett NMR study were developed to screen for synergistic HBD and Lewis acid combinations in which the complex is more active than the Lewis acid alone. This study determined BCl_3 and squaramides as a viable combination with promising preliminary results.

The ability to use chiral HBD catalysts in mineral acid-promoted transformations would open new avenues in asymmetric catalysis. In Chapter 5, an HBD and HCl co-catalyzed semi-pinacol rearrangement to synthesize α-quaternary cyclobutanones is described. The HBD promotes the model reaction in moderate enantioselectivities and is proposed to stabilize the chloride anion, perturbing the HCl dissociation equilibrium, K_a. Enantioselectivity then arises from this HCl-HBD adduct, which serves as a more acidic, chiral H+ source.

Table of Contents

Acknowledgements

I am extremely grateful to Professor Eric N. Jacobsen for his continued mentorship, support, and advice during graduate school. Eric's devotion to teaching both in the laboratory and in the classroom have provided me with all of the tools I hoped to gain in graduate school and more. I have benefited greatly from his ambitious vision for his research program, his mechanistic acumen, and his ability to give constructive criticism. I have experienced a lot of personal growth and challenges in his laboratory. Eric has taught me how to push through failure and hardship and to challenge myself to meet and overcome obstacles, and I am both a better person and chemist as a result. Eric has created a group dynamic in which everyone teaches and learns from each other; it is a special environment, highly conducive to learning and generating quality science. I was extremely fortunate to have the opportunity to be a part of such an amazing group of people and chemists.

My thesis committee members have been extremely supportive and have challenged me to pursue interesting questions and push the boundaries of my research and knowledge. Both Profs. Emily Balskus and Dan Nocera have taken the time to meet with me outside of committee meetings to give me guidance, for which I am deeply grateful. Watching Emily's new lab mature into a highly successful powerhouse has been a privilege and honor. I was never able to anticipate Dan's questions, and often flubbed them and continued to think about them over the next weeks to months. Dan has been a scientific role model for me since even before I attended graduate school, and it has been an honor having him serve on my committee; furthermore, his amazing body of work has influenced and inspired my scientific directions after graduate school.

My Professors at Macalester, namely Becky Hoye, Tom Varberg, and Keith Kuwata encouraged me to pursue graduate school and have been invaluable mentors, advisors and friends. I had the opportunity to interact with them in the classroom and in the lab, and they have instilled in me a love for both chemistry and teaching.

Nicole Minotti is the unsung hero of the Jacobsen lab. She keeps the lab running so smoothly and with so little error or complaints, that most members have no idea how much she does for us. On top of the amazing work Nicole does, she has also become a personal friend. Nicole is always willing to chat and serve as a sounding board and support system, whether it is at noon or at 2 AM. Nicole, I am not sure what the lab would do without you.

I have been fortunate to have had amazing mentors during my formative years in graduate school. Dr. Pam Tadross was my first mentor and she taught me experimental rigor and organization, the latter of which I never acquired. I came with almost no synthetic knowledge, and through her hands-on mentorship and exacting standards, I was able to quickly learn the ropes. Next, I had the opportunity to join team Bar^F, under the fantastic leadership of Dr. Andreas Rötheli. Andy led through example, and taught me the rigor and beauty of pursing mechanistic chemistry. I have never seen anyone as passionate about his work as Andy; his devotion to his work and vision is truly inspirational. Last, although I never worked directly under Dr. Steven Banik, he served as a mentor to me and all of the younger graduate students in the lab at the time. Steven is a brilliant chemist, with boundless ideas and visions. He knows how to take risks and devote the time and energy to see projects come to fruition. Although gruff at first, Steven is incredibly caring and will go out of his way to help anyone in need. I greatly admire him and consider him a personal role model.

In addition to mentors, I have had a wonderful set of younger graduate student and undergraduate mentees. Dan Strassfeld was my first mentee. Dan is one of the most passionate, intelligent, hard-working and thinking student I have seen. He is uniquely talented and I am absolutely convinced he will go on to do great things. Although I was technically Dan's mentor, we learned together and he probably taught me more than I taught him. Next I had the opportunity to work with Mitchell Pleasure, and working with him was, obviously a pleasure. Mitchell is incredibly bright, kind, and has a broad range of interests and will go on to become an amazing doctor. Eve Xu is the most delightful mentee one could imagine. She has limitless enthusiasm for chemistry, is incredibly hard working, and is astonishingly intelligent. Her passion for chemistry is infectious and seeing her brightened my day each day. She has all the skills to have an amazing graduate career. Last, my most recent mentee is Katherine Forbes. I have already seen Katherine grow so much in her first 4 months in the lab. She already has her own project up and running, has a million more ideas, and the sky is the limit. Don't let people underestimate you or squash your enthusiasm, you are a force to be reckoned with.

I had the good fortune to overlap with a number of other talented postdocs and graduate students in the lab. Dr. Rose Kennedy was my lab bay-mate and I greatly enjoyed chatting at our hoods and getting guidance from her. I look forward to following her career at Rochester. Dr. Alison Wendlandt helped me during personally challenging times in graduate school and was always a great person to go to for personal or scientific advice (or just exchange 30 Rock jokes with). Her students are lucky to have such a supportive and down to earth mentor, who also happens to be a brilliant chemist. Dr. Russ Algera has been extremely generous with his time and helpful in mechanistic discussions and interpretations. He is always willing to help me and anyone else in lab. Russ is an absolute genius and will do great work in whatever he pursues next. Last,

during the middle of my graduate career, I briefly overlapped with Dr. Daisuke Suzuki, who tragically passed away. I wish I would have taken the time to get to know him better, as I deeply felt his absence only when it was too late.

There are a number of my peers and younger students who I need to thank. I am proud to call Dr. Andrew Mayfield my classmate and my friend. Andrew is a talented chemist, an amazing lab citizen, and makes wherever he works a better place. I am glad we were able to form a close friendship early on in graduate school and experiences the good and bad together. I look forward to watching your career continue to grow. Prithvi Vangal has been a great friend and a positive influence on the lab and in my life. Prithvi and I think about problems very similarly, but he has a unique talent to see the good in things where I see the bad. I have a lot to learn from him, and can't wait to see how this mechanistic genius finishes out his graduate career. I have been incredibly fortunate to have had the opportunity to work next to Qiuhan Li over the past 3 years, I could not imagine a better bay-mate. Qiuhan is so incredibly nice and giving; I deeply appreciate appreciate his willingness to let me borrow his chemicals, manifold, and synthetic intermediates. Qiuhan is such a talented synthetic chemist and has made so much scientific progress in the first half of his Ph.D. First he conquered mannosylation and then site selective glycosylation, and I can't wait to see what challenging problem he solves next.

Drs. Sam Levi and Katrina Mennie formed the other two thirds of the "front office mafia" and made graduate school much more enjoyable. Every lunch and afternoon Google spent with them was truly splendid. They were always willing to listen to my complaints and allow me to distract them from their work. They are both extraordinary chemists, in completely different ways. Katrina is extremely focused and can solve any problem through hard work and determination.

Sam enjoys thinking about philosophy and arriving at a solution though a combination of creativity and experiment. Merck is so lucky to have both of you.

I entered Harvard with an fantastic cohort of students, who served as a fun support mechanism for me. Amymarie Bartholomew, Ben Levin, and Jordan Wilkerson have all not only been my closest friends but my roommates during graduate school. They have made the last 6 years much more enjoyable and I have been fortunate to see them all grow as scientists. Drs. Nancy Li and Claudia Kleinlein have not only been wonderful friends throughout graduate school, but I have also had the pleasure to collaborate with and learn a ton of inorganic chemistry from both of them.

The person I am most indebted to and thankful for on both a scientific and personal level is Chris Kim. Chris entered graduate school with me and he immediately found immense success. It is only because of Chris's success and willingness to let me finish his work that I can write this dissertation; this is as much his work as it is mine. On a personal level, Chris has been my closest friend and greatest support system. He has gone above and beyond what one could expect for a friend, and his support was often the only thing that kept me going. Chris, it has been an honor to watch you and learn from you over the past 6 years. Your ability to restart in the Szostak lab, reinvent yourself in a new field, and find a great deal of success there has been inspirational. You are deeply intelligent, you know how to plan things well, you know yourself and your values, and you put thought into everything you do. You are truly a continuing source of inspiration, and I cannot wait to see where your journey takes you, as I know you have the tools to succeed in all future endeavors.

Last I am deeply thankful to my family (Anne, Dick, Charlie, Quinn, and Emily) for all the support they have provided me in graduate school and in life. Graduate school was my first time

away from home. I did not truly appreciate all the support you give or how much I would miss all of you, until I left home. My dad, is an organic chemist, and the reason I pursued this in the first place. I hope that I can become as good of a chemist as you and use chemistry to make as much of an impact on the world as you have. My mom, is the hardest working person I know. She is relentlessly devoted to her work and she loves it. Her work ethic and passion has been inspirational to me, and I look to her as an example and for guidance during both graduate school and in life.

List of Abbreviations

α	One carbon away
$[\alpha]^{T}_{D}$	Specific rotation at temperature T at the sodium D line
Å	Ångstrom
Ac	Acetyl
Ac2O	Acetic anhydride
Alloc	Allyloxycarbonyl
Anth	Anthracenyl
aq.	Aqueous
β	Two carbons away
B3LYP	Becke-3-Lee-Yang-Parr
BArF	Tetrakis[3,5-bis(trifluoromethyl)phenyl]borate
BCF	Tris(pentafluorophenyl)borane
BINAP	2,2'–Bis(diphenylphosphino)–1,1'–binaphthyl
BINOL	[1,1′-Binaphthalene]-2,2′-diol
*t*BME	Tert-butyl methyl ether
Bn	Benzyl
Boc	Tert–Butyloxycarbonyl
Boc_2O	Di-tert-Butyldicarbonate
BOX	Bisoxazoline
Bu	Butyl
*n*Bu	Normal-butyl
*s*Bu	Sec–butyl
*t*Bu	Tert–butyl
Bz	Benzoyl
C_2	Containing a 2-fold rotational axis and identity as the sole symmetry elements
cal	Calorie

cat	Catalyst
CBz	Carbobenzyloxy
Cinnamyl	3-phenyl-2-propenyl
cis	Same side
conc.	Concentration
δ	Chemical shift in ppm
Δ	Change
°C	Degree Celsius
D or *d*	Deuterium
DCE	1,2-Dichloroethane
DCM	Dichloromethane
DFT	Density functional theory
DIPEA	Diisopropylethylamine; Hünig's base
DKR	Dynamic kinetic resolution
DMAP	4–Dimethylaminopyridine
DMF	N,N-Dimethylformamide
DMSO	Dimethylsulfoxide
d.r.	Diastereomeric ratio
η	Hapticity
E	Electronic energy
E	Entgegen (German for opposite)
ee	Enantiomeric Excess
ent	Enantiomeric
E_2O	Diethyl ether
Et	Ethyl
Et3N	Triethylamine
EtOAc	Ethyl acetate
equiv.	Equivalents

Fmoc	9-Fluorenylmethyloxycarbonyl
g	Gram
G	Gibbs energy
h	Hour
HBD	Hydrogen-bond donor
HBTU	N,N,N′,N′-Tetramethyl-O-(1H-benzotriazol-1-yl)uronium hexafluorophosphate
HMDS	Hexamethyldisilazide
HOMO	Highest occupied molecular orbital
HPLC	High performance/pressure liquid chromatography
HRMS	High resolution mass spectrometry
Hz	Hertz
IDPi	Imidodiphosphorimidate
IPA	Isopropanol
IRC	Intrinsic reaction coordinate
ITC	Isothermal calorimetry
J	Coupling constant in Hz
k	Kilo
k	Rate constant
K	Unspecified equilibrium
K_a	Acid dissociation equilibrium constant
K_{dim}	Dimerization constant
KIE	Kinetic isotope effect
t-Leu	Tert-leucine
LFER	Linear free energy relationship
LUMO	Lowest unoccupied molecular orbital
µ	Micro
m	Meta
M	Molar or Mega

m	Milli
Me	Methyl
MeOH	Methanol
mol	Mole
MS	Mass spectrometry or molecular sieves
N	Number of
Nap	Naphthyl
NBS	N–Bromosuccinimide
ND	Not determined
NHC	N-Heterocyclic carbene
NMR	Nuclear Magnetic Resonance
Nuc	Nucleophile
o	Ortho
obs	Observed
p	Para
p	Negative of the base ten logarithm
PCM	Polarization continuum model
Ph	Phenyl
Phen	Phenanthryl
PHOX	Phosphinooxazoline
Ppm	Parts per million
Pr	Propyl
iPr	Iso–propyl
Prenyl	3-methylbut-2-en-1-yl
PTC	Phase transfer catalysis
Pyr	Pyrenyl
R	Unspecified substituent
rac	Racemic

Rf	Retention factor
rt	Room temperature
σ_m	Hammett meta parameter
s	Second
Salen	2,2′-Ethylenebis(nitrilomethylidene)diphenol, N,N′-ethylenebis(salicylimine)
SAPT	Symmetry adapted perturbation theory
sat.	Saturated
SIR	Selective inversion recovery
S_N1	Unimolecular nucleophilic substitution
S_N2	Bimolecular nucleophilic substitution
t	Time
T	Temperature
TADDOL	α,α,α',α'-tetraaryl-2,2-disubstituted 1,3-dioxolane-4,5-dimethanol.
TBS	Tert–butyldimethylsilyl
TEPO	Triethylphosphine oxide
TFA	Trifluoro acetic acid
TFAA	Trifluoro acetic acid anhydride
TfOH	Triflic acid
THF	Tetrahydrofuran
TIPS	Triisopropylsilyl
TLC	Thin layer chromatography
TMS	Trimethylsilyl
TMSCl	Trimethylsilyl chloride
Tol	Tolyl
trans	Opposite side
TS	Transition state
TsOH	Tosic acid
Z	Zusammen (German for together)

Chapter 1

Enantioselective Syntheses of Amino Acids with a Focus on α-Allyl and α-Aryl Amino Acids

1.1 Overview on asymmetric amino acid synthesis

One can envision a number of viable disconnections in the synthesis of amino acids, as shown in Figure 1.1. The α-carbon of mono-substituted amino acids, by definition, contains an amine, a carbonyl, an H atom, and a side chain with a C-C bond (with the exception of glycine, which lacks a side chain). All four bond disconnections at the α-carbon are highly precedented and are highlighted in Figure 1.1. This section will discuss select enantioselective methods, using both chiral auxiliaries and chiral catalysts, capable of forging each of the four bonds to the α-carbon.

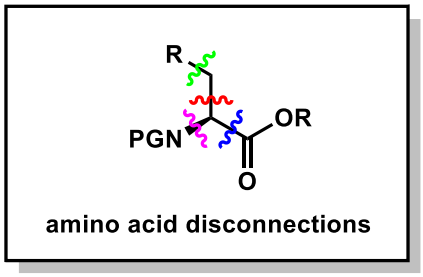

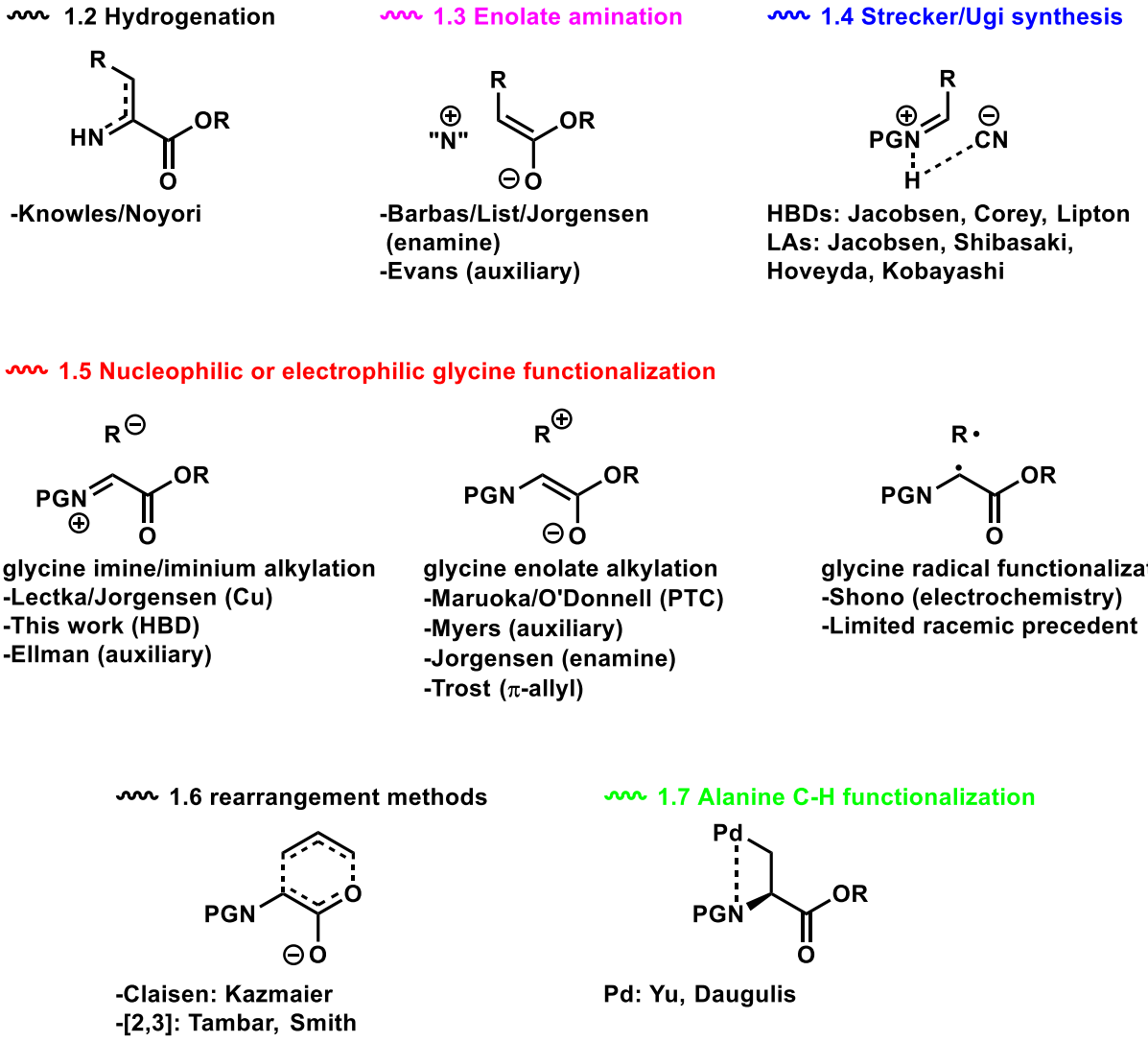

Figure 1.1 Overview of synthetic methods for enantioenriched amino acid synthesis

1.2 Enantioselective methods for introduction of the α-hydrogen in amino acid synthesis

Given the ease of reduction of α,β-unsaturated esters, enamines and imines, as well as the ease of enolate formation and subsequent protonation, both protic and hydrogenative methods

have been widely utilized in the enantioselective synthesis of amino acids (Figure 1.2). Asymmetric hydrogenation chemistry has emerged as a powerful tool to set the stereochemistry at the α-carbon of amino acids, and the 2001 Nobel Prize in chemistry was partially awarded to Knowles and Noyori, in recognition of their success in asymmetric hydrogenations applied to the syntheses of amino acids. Rhodium complexes with either mono or bidentate phosphine ligands have emerged as a broad class of compounds that catalyze highly enantioselective reductions of amino acid derived enamines (Figure 1.2 A).[1] To a lesser extent, the hydrogenation of α-imino carboxylates (Figure 1.2 B) has been explored with transition metal phosphine complexes; due to rapid tautomerization to the enamine, this has often been explored in the context of reductive aminations.[2] In the event that the R group on the nitrogen is a chiral auxiliary, most often Ellman's *tert*-butyl sulfinamine, hydride sources can be employed in a diastereoselective manner.[3] There is extensive precedent on hydrogenations of either enamines or imines to amino acids and numerous reviews have been written on this subject; however we will only mention them briefly because they are neither complexity generating nor generally amenable to the synthesis of α-allyl or α-aryl amino acids.[1,4]

[1] For highlights in hydrogenation of amino acids see: a) D. Vineyard, B.; S. Knowles, W.; J. Sabacky, M.; L. Bachman, G.; J. Weinkauff, D. Asymmetric Hydrogenation. Rhodium Chiral Bisphosphine Catalyst. *J. Am. Chem. Soc.* **1977**, *99* (18), 5946–5952. b) S. Knowles, W. Asymmetric Hydrogenation. *Acc. Chem. Res.* **1983**, *16* (3), 106–112. c) Zhu, G.; Zhang, X. Highly Enantioselective Rhodium-Catalyzed Hydrogenation of Dehydroamino Acids with New Chiral Bisphosphinites. *J. Org. Chem.* **1998**, *63* (9), 3133–3136. d) Qiao, S.; C. Fu, G. The First Application of a Planar-Chiral Phosphorus Heterocycle in Asymmetric Catalysis: Enantioselective Hydrogenation of Dehydroamino Acids. *J. Org. Chem.* **1998**, *63* (13), 4168–4169. e) D. Fryzuk, M.; Bosnich, B. Asymmetric Synthesis. Production of Optically Active Amino Acids by Catalytic Hydrogenation. *J. Am. Chem. Soc.* **1977**, *99* (19), 6262–6267.

[2] Tararov, V. I.; Börner, A. Approaching Highly Enantioselective Reductive Amination. *Synlett* **2005**, *2*, 203–211.

[3] Reddy, L. R.; Gupta, A. P.; Liu, Y. Asymmetric Synthesis of α-Amino Acids by Reduction of *N*-*Tert*-Butanesulfinyl Ketimine Esters. *J. Org. Chem.* **2011**, *76* (9), 3409–3415.

[4] For a comprehensive review on amino acid synthesis see: Nájera, C.; M. Sansano, J. Catalytic Asymmetric Synthesis of α-Amino Acids. *Chem. Rev.* **2007**, *107* (11), 4584–4671.

Catalytic addition of the the α-hydrogen atom

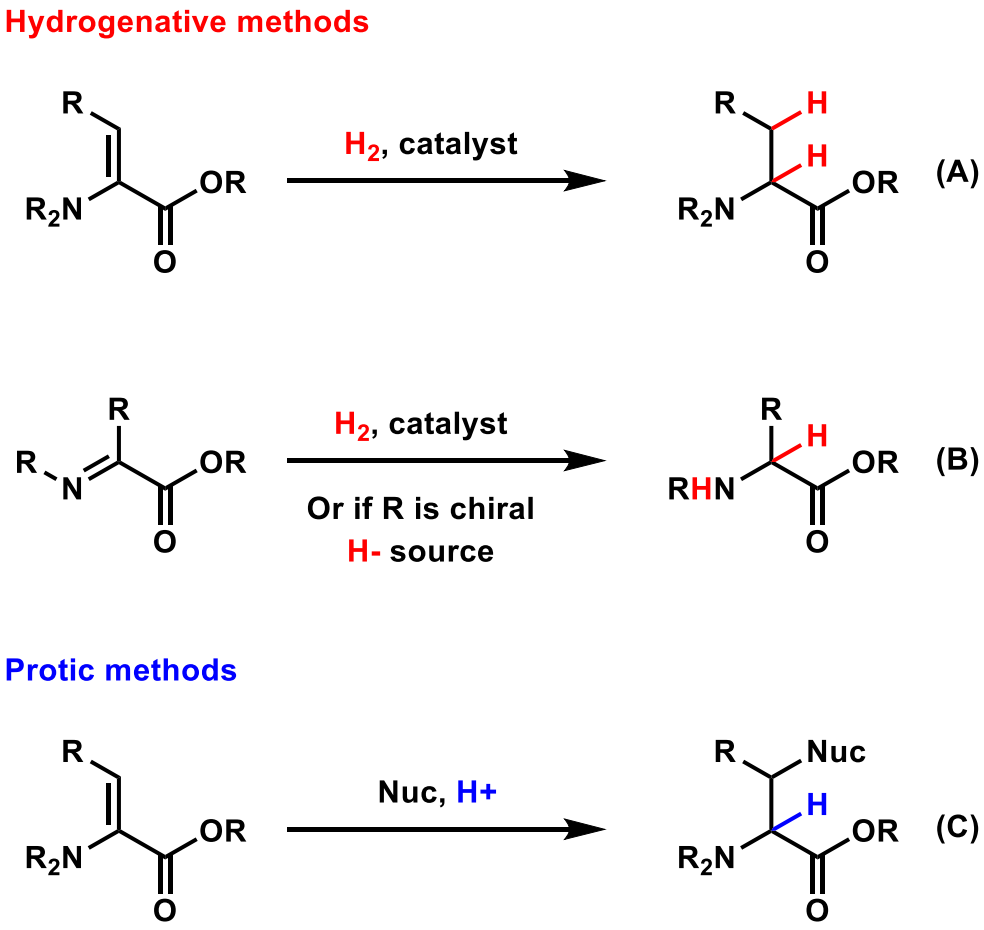

Figure 1.2 The H atom side chain can be added via hydrogenative or protic methods

The protonation of an amino acid enolate with a chiral acid is conceptually a very simple way to set the α-stereocenter, yet this strategy often provides low levels of enantioselectivity.[5] This can fail for a number of reasons including: 1) poor E/Z selectivity in enolate formation, 2) finding an appropriate chiral acid pKa, 3) poor stereochemical information in protonation events, 4) the strong basicity and facile protonation of amino acid derived enamines. As an example of the

[5] Duhamel, L.; Duhamel, P.; Plaquevent, J.-C. Enantioselective Protonations: Fundamental Insights and New Concepts. *Tetrahedron: Asymmetry* **2004**, *15* (23), 3653–3691.

challenge of this strategy, Figure 1.3 shows the poor enantioselectivities in the protonation of phenylglycine enolate with 3 equivalents of tartarate derivatives.[6]

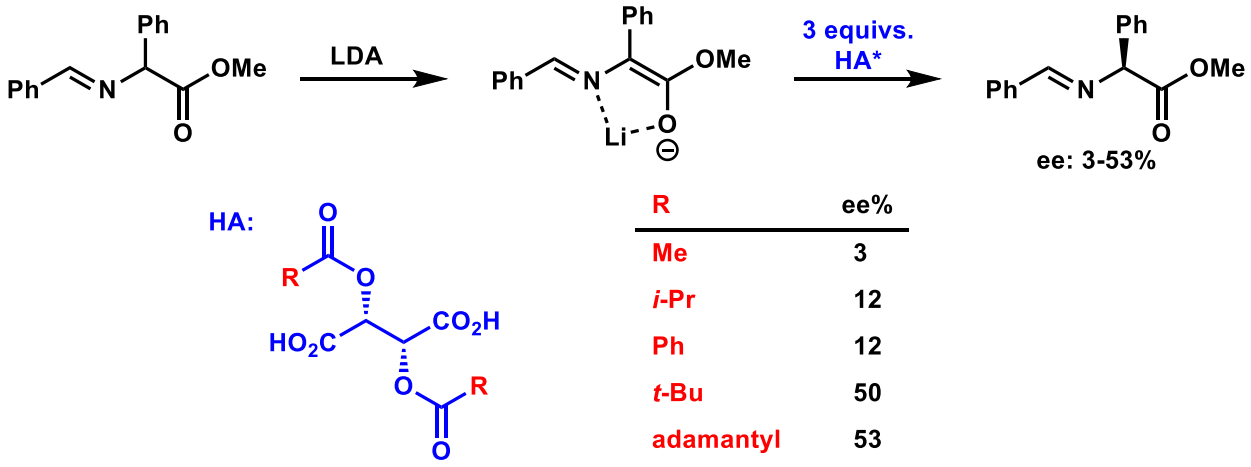

R	ee%
Me	3
i-Pr	12
Ph	12
t-Bu	50
adamantyl	53

Figure 1.3 Challenge with asymmetric protonation of amino ester enolates

While direct protonation of amino ester enolates is challenging, a rhodium or copper catalyzed Michael addition to an α,β-unsaturated amino acid can generate a chiral enolate as an intermediate, which can be trapped with achiral proton sources (Figure 1.2 C).[7] Formation of a chiral enolate allows for better transfer of stereochemical information (Figure 1.4), although enantioselectivies are still much lower than with hydrogenation methods (~90% vs. 99%).

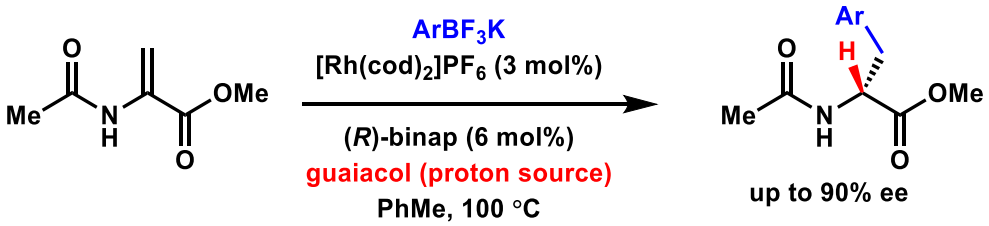

Figure 1.4 Chiral rhodium enolates allow for enantioselective protonations

[6] Duhamel, L.; Plaquevent, J. C. Deracemization by Enantioselective Protonation. A New Method for the Enantiomeric Enrichment of .Alpha.-Amino Acids. *J. Am. Chem. Soc.* **1978**, *100* (23), 7415–7416.

[7] a) Manfred T. Reetz, *; Dominique Moulin, and; Gosberg, A. BINOL-Based Diphosphonites as Ligands in the Asymmetric Rh-Catalyzed Conjugate Addition of Arylboronic Acids. **2001**, *3*, 4083–4085. https://doi.org/10.1021/OL010219Y. b) Navarre, L.; Darses, S.; Genet, J.-P. Tandem 1,4-Addition/Enantioselective Protonation Catalyzed by Rhodium Complexes: Efficient Access Toα-Amino Acids. *Angew. Chemie Int. Ed.* **2004**, *43* (6), 719–723.

1.3 Enantioselective methods for introduction of the α-amine in amino acid synthesis

One appealing disconnection to amino acids is the addition of electrophilic "N+" reagents to enolates, enamines, or other enolate equivalents. The wide availability of carbonyl compounds and the wide spread effort in developing chiral auxiliary and asymmetric catalytic methods for enolate functionalization makes this route particularly intriguing. However, there are only limited examples of electrophilic enolate aminations due to the small number of electrophilic aminating reagents. This creates a second problem; removal of additional functionality on electrophilic aminating reagents to reveal desired amino acid product often requires a number of chemical steps or harsh conditions to break N-N or N-O bonds (e.g. Raney Nickel, H_2) (Figure 1.5).

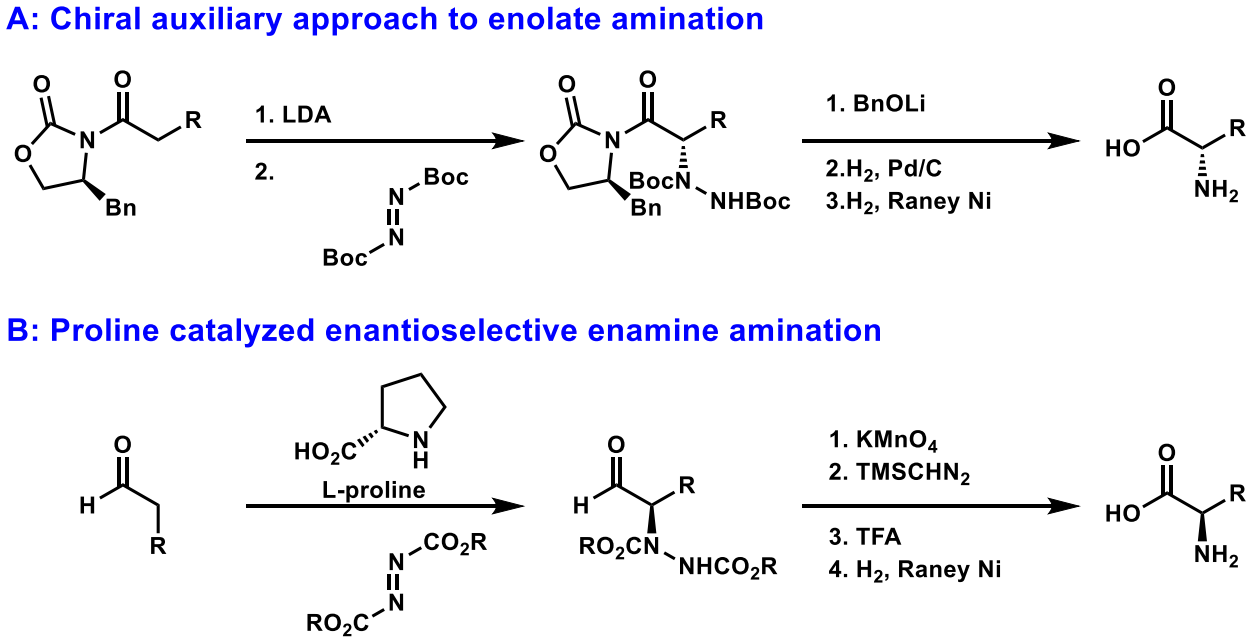

Figure 1.5 Enolate/enamine electrophilic amination to synthesize amino acids

The Evans' auxiliary is used to control enolate geometry and facial addition to the di-*tert*-butylazodicarboxylate (DBAD) amino acid derivatives in extremely high dr (>97:3).[8] However,

[8] A. Evans, D.; C. Britton, T.; L. Dorow, R.; F. Dellaria, J. Stereoselective Amination of Chiral Enolates. A New Approach to the Asymmetric Synthesis of .Alpha.-Hydrazino and .Alpha.-Amino Acid Derivatives. *J. Am. Chem. Soc.* **1986**, *108* (20), 6395–6397.

removal of the auxiliary and reduction of the N-N bond take a number of steps (Figure 1.5 A). The Evans' auxiliary has also been used to affect electrophilic azidations, using 2,4,6-triisopropylbenzenesulfonylazide, which can be easily reduced under Staudinger conditions.[9] List and Jorgensen simultaneously developed proline catalyzed enantioselective aminations α-to an aledehyde, proceeding through an enamine mechanism.[10] Both methods use dialkyl azodicarboxylates, the same substrates, and proline as catalyst; ee's tend to be in the low 90's (Figure 1.5 B). Due to the ease of deprotonation of malonates and 1,3-dicarbonyl compounds, these enolates are commonly employed nucleophiles in this class of reactions.

An alternate method to introduce the nitrogen substituent is to perform asymmetric aziridinations of α,β-unsaturated esters, most commonly cinammates or acrylates, followed by opening the aziridine with a nucleophile. This has been accomplished in an enantioselective context, up to 95% ee, by employing chinchona alkaloid quaternary ammonium salts as phase transfer catalysts (PTC).[11] While not technically addition of a nitrogen substituent, a useful and related transformation is the addition of ethyldiazoacetate to aldimines. Wulff has accomplished this transformation in 96% ee and perfect diastereoselectivities (favoring the *cis* diasteresomer) by

---

[9] Evans, D. A.; Britton, T. C.; Ellman, J. A.; Dorow, R. L. The Asymmetric Synthesis of .Alpha.-Amino Acids. Electrophilic Azidation of Chiral Imide Enolates, a Practical Approach to the Synthesis of (R)- and (S)-.Alpha.-Azido Carboxylic Acids. *J. Am. Chem. Soc.* **1990**, *112* (10), 4011–4030.

[10] a) List, B. Direct Catalytic Asymmetric α-Amination of Aldehydes. *J. Am. Chem. Soc.* **2002**, *124* (20), 5656–5657. b) Bøgevig, A.; Juhl, K.; Kumaragurubaran, N.; Zhuang, W.; Jørgensen, K. A. Direct Organo-Catalytic Asymmetricα-Amination of Aldehydes—A Simple Approach to Optically Active α-Amino Aldehydes, α-Amino Alcohols, And α-Amino Acids. *Angew. Chemie Int. Ed.* **2002**, *41* (10), 1790–1793.

[11] Murugan, E.; Siva, A. Synthesis of Asymmetric *N* -Arylaziridine Derivatives Using a New Chiral Phase-Transfer Catalyst. *Synthesis (Stuttg).* **2005**, *2005* (12), 2022–2028.

employing chiral (*S*)-Vapol derived boron complexes.[12] Wulff has subsequently found deprotection and ring opening conditions.[13]

1.4 Enantioselective methods for introduction of the carboxylate in amino acid synthesis: Strecker reactions for amino acid synthesis

The Strecker reaction is one of the oldest organic reactions, and is the first reported synthesis of amino acids. In 1850, Adolph Strecker discovered that the addition of HCN to acetaldehyde and ammonia could produce an α-amino nitrile; subsequent hydrolysis furnished the amino acid alanine.[14] Furthermore, in 1953, Stanley Miller showed in a landmark experiment, that one could produce amino acids via the Strecker reaction under conditions that mimic those of the early earth.[15]

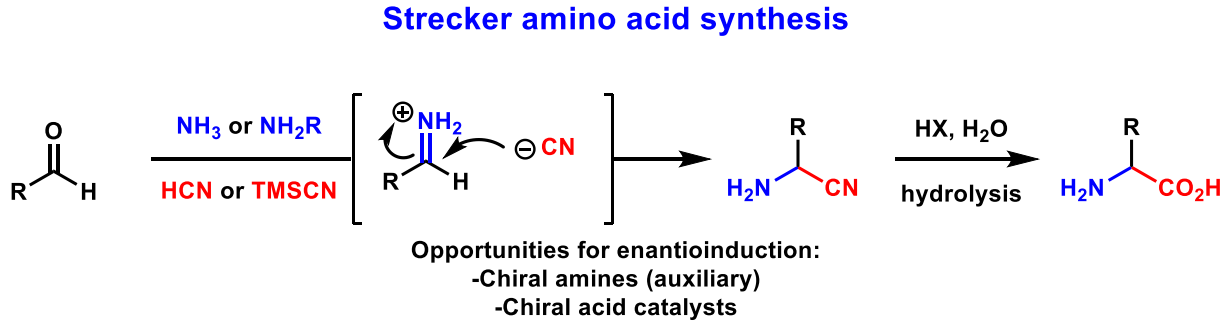

Figure 1.6 Overview of Strecker amino acid synthesis

In general, the Strecker reaction is a 3-component reaction in which HCN or TMSCN is added to an imine that may be preformed or formed *in situ* from an aldehyde and amine (Figure

[12] C. Antilla, J.; D. Wulff, W. Catalytic Asymmetric Aziridination with a Chiral VAPOL−Boron Lewis Acid. *J. Am. Chem. Soc.* **1999**, *121* (21), 5099–5100.

[13] Aniruddha P. Patwardhan; Zhenjie Lu; V. Reddy Pulgam, and; Wulff*, W. D. Novel Ozone-Mediated Cleavage of the Benzhydryl Protecting Group from Aziridinyl Esters. **2005**, *7*, 2201–2204.

[14] Strecker, A. Ueber Die Künstliche Bildung Der Milchsäure Und Einen Neuen, Dem Glycocoll Homologen Körper; *Ann. der Chemie und Pharm.* **1850**, *75* (1), 27–45.

[15] Miller, S. L. A Production of Amino Acids under Possible Primitive Earth Conditions. *Science* **1953**, *117* (3046), 528–529.

1.6). Due to the wide accessibility of benzaldehyde derivatives, Strecker reactions have been particularly useful in the synthesis of α-aryl amino acids, which will be discussed in depth in Chapter 2. The Strecker reaction has been the attention of several chiral auxiliary studies. Since the mid 1990's, numerous asymmetric Strecker reactions have been developed in transition metal, lewis acid, and organocatalytic contexts; several reviews have been written on asymmetric Strecker syntheses.[16]

If either the amine or aldehyde starting material bear a stereocenter, then the addition of cyanide to the aldimine is a diastereoselective reaction. In principle, the aldehyde could serve as a convenient source of chirality due to the number of chiral pool carboxylic acids and alcohols, which can be reduced and oxidized to the aldehyde, respectively. A number of highly diastereoselective Strecker syntheses of chiral aldehydes have been realized.[16] However, as the chiral information from the aldehyde is non-cleavable and incorporated into the amino acid side-chain in the product, these syntheses are not general.

A much more attractive source of chiral information is the use of chiral amines that can be cleaved in the product. The first asymmetric Strecker reaction was achieved by Harada in 1963, employing (*S*)-α-phenylethylamine as a chiral auxiliary (Figure 1.7 A). Harada reported the combined procedure for the Streker reaction followed by deprotection, which provided the amino acid 17% yield with 90% ee; however, it was later discovered, the intrinsic d.r. was just 3.3 : 1 and the purification methods involved multiple accidental recrystallizations up to 90% ee.[17] This

[16] For a review on Strecker reactions see: Wang, J.; Liu, X.; Feng, X. Asymmetric Strecker Reactions. *Chem. Rev.* **2011**, *111* (11), 6947–6983.

[17] M. Stout, D.; A. Black, L.; L. Matier, W. Asymmetric Strecker Synthesis: Isolation of Pure Enantiomers and Mechanistic Implications. *J. Org. Chem.* **2002**, *48* (26), 5369–5373.

transformation was subsequently improved to more synthetically useful yields and selectivities (>20 : 1 d.r.) by using a cyanide-modified hemin-copolymer as the cyanide source.[18]

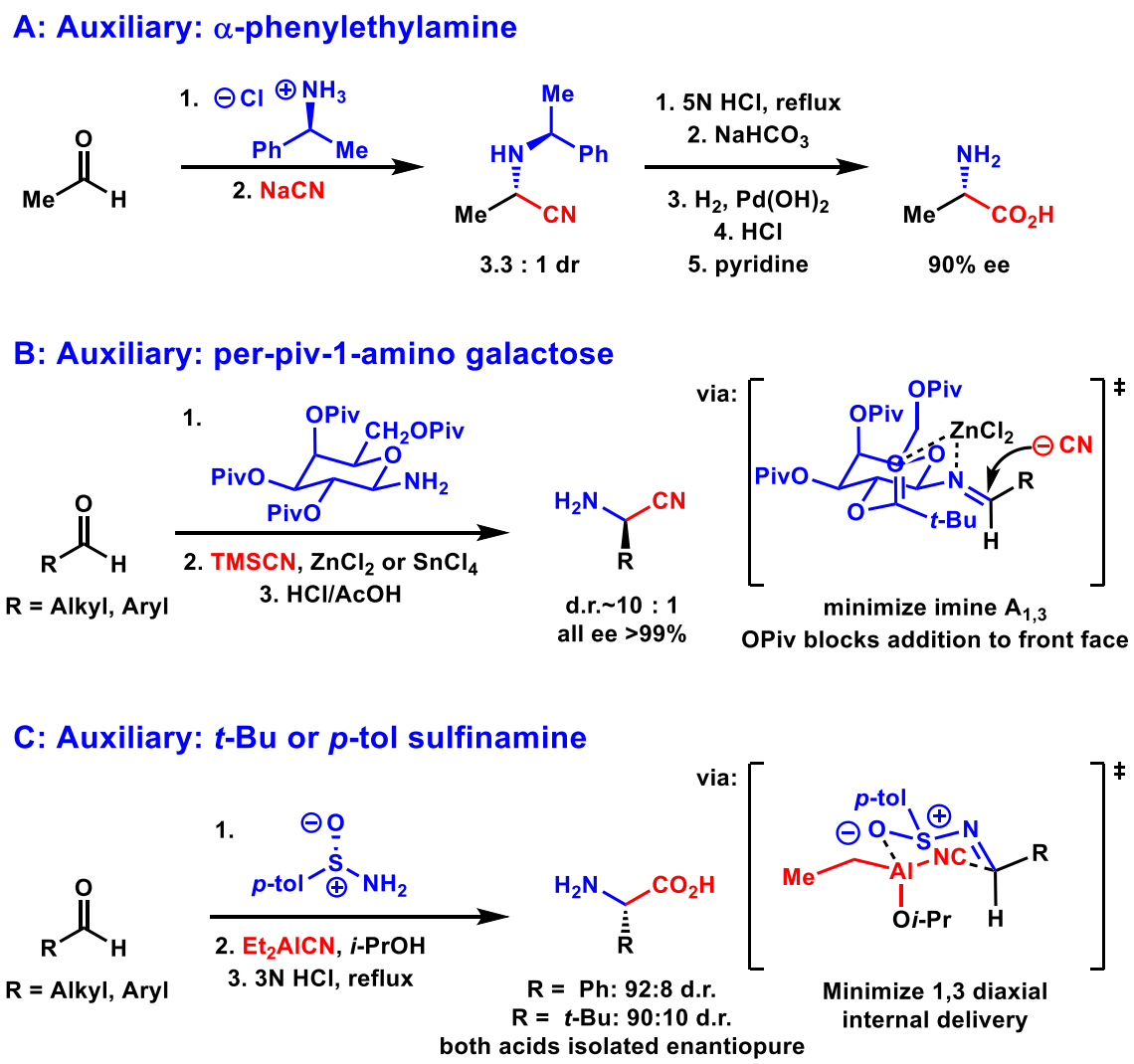

Figure 1.7 Chiral amine auxiliaries in the Strecker reaction

2-aminoglycosides make for particularly appealing chiral auxiliaries due to their abundance and low cost, as well as the relative ease of deprotecting an aminoglycosidic linkange. 1-amino-per-pivaloyl galactose has been found to impart high levels of selectivity (~10 : 1 d.r.)

[18] Saito, K.; Harada, K. Asymmetric Syntheses of Amino Acids by Addition of Cyanide to the Schiff Bases in the Presence of Cyanide-Modified Hemin-Copolymer. *Tetrahedron Lett.* **1989**, *30* (34), 4535–4538.

and an ability to upgrade to enantiopure products.[19] A clear downside being that as the enantiomer of galactose does not exist, this method can only make one enantiomer of amino acids (Figure 1.7 B). The stereochemical model for this reaction proposes that the imine and the 2-OPiv oxygen chelate $ZnCl_2$ in a 7 membered ring. The imine forms exclusively in the (*E*)-conformation, which has been confirmed via NOE, and minimizes $A_{1,3}$ interactions. The 2-OPiv then blocks addition of cyanide from the front face, to give the amino acid in high d.r.

The most practical diastereoselective Strecker reactions are additions of cyanide to sulfinamines; both Ellman's *t*-butylsulfinamine and Davis' *p*-tolylsulfinamine have been used extensively.[20] These reactions have a number of benefits including the low cost of the auxiliary, high diastereoselectivities, ease of separating diastereomers via chromatography or recrystallization, and removal of the auxiliary under the same conditions as cyanide hydrolysis. In 1994, Davis reported the first diastereoselective Strecker reaction to a sulfinamine (Figure 1.7 C).[20c,21] While d.r. is modest (~9 : 1 up to 99 : 1), compounds can easily be obtained enantiopure and numerous improvements have been made on the original conditions over the last 25 years. Davis found that common cyanide sources, KCN and CuCN gave little to no reactivity, while Et_2AlCN afforded the products in 62-78% yield and up to 83:17 d.r.[20c] The addition of isopropanol generated ethylene gas and provided greatly improved d.r. up to 98:2. These results taken together suggest the transition state model depicted in Figure 1.7 C, in which the reaction proceeds via a closed 6-

[19] Kunz, H.; Sager, W. Diastereoselective Strecker Synthesis of α-Aminonitriles on Carbohydrate Templates. *Angew. Chemie Int. Ed. English* **1987**, *26* (6), 557–559

[20] For lead references on Streckers employing sulfinamines see: a) Jonathan A. Ellman, *; Timothy D. Owens, and; Tang, T. P. N-Tert-Butanesulfinyl Imines: Versatile Intermediates for the Asymmetric Synthesis of Amines. **2002**. b) Robak, M. T.; Herbage, M. A.; Ellman, J. A. Synthesis and Applications of *Tert* -Butanesulfinamide. *Chem. Rev.* **2010**, *110* (6), 3600–3740. c) Davis, F. A.; Reddy, R. E.; Portonovo, P. S. Asymmetric Strecker Synthesis Using Enantiopure Sulfinimines: A Convenient Synthesis of α-Amino Acids. *Tetrahedron Lett.* **1994**, *35* (50), 9351–9354.

[21] Davis, F. A.; Portonovo, P. S.; Reddy, R. E.; Chiu, Y. Asymmetric Strecker Synthesis Using Enantiopure Sulfinimines and Diethylaluminum Cyanide: The Alcohol Effect. *J. Org. Chem.* **1996**, *61* (2), 440–441.

membered ring transition state with internal delivery of the aluminumcyanide. These methods can also be used to make α,α-disubstituted amino acids from ketamine starting materials, which will be discussed briefly in Chapter 3.

In 1996, Lipton reported the first catalytic enantioselective Strecker reaction, catalyzed by a dipeptide bearing a guanidine, which is the source of catalytic activity.[22] Since then, Strecker reactions have been extensively explored in the context of asymmetric catalysis, with catalysts falling broadly into three classes, guanidines, Lewis acids, and hydrogen-bond donors (for these purposes considered a distinct class from guanidines due to more complicated functionality and mechanisms of enantioinduction) (Figure 1.8). Numerous reviews have been written on asymmetric catalytic Strecker reactions.[16,23]

[22] Mani S. Iyer; Kenneth M. Gigstad; Nivedita D. Namdev, and; Lipton*, M. Asymmetric Catalysis of the Strecker Amino Acid Synthesis by a Cyclic Dipeptide. **1996**, *118* (20), 4910-4911.

[23] For reviews on asymmetric Strecker reactions see: a) Yet, L. Recent Developments in Catalytic Asymmetric Strecker-Type Reactions. *Angew. Chemie Int. Ed.* **2001**, *40* (5), 875–877. b) Gröger*, H. Catalytic Enantioselective Strecker Reactions and Analogous Syntheses. *Chem. Rev.* **2003**, *103* (8), 2795–2828.

Guanidines:

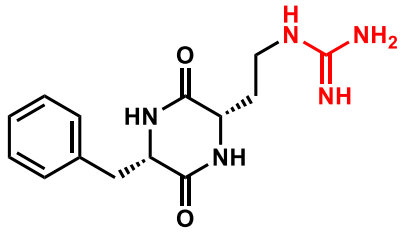

Lipton

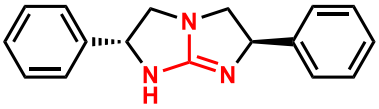

Corey

Lewis Acidic Metal Complexes

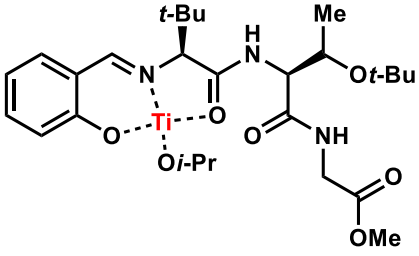

Hoveyda

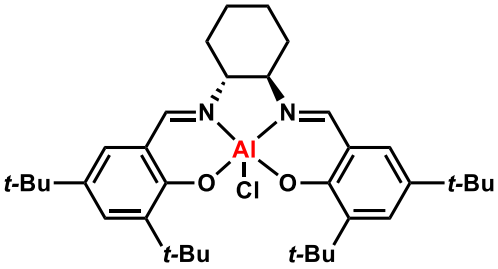

Jacobsen and Sigman

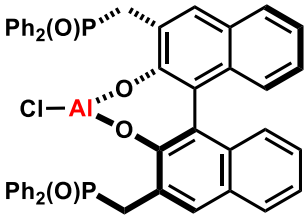

Shibasaki

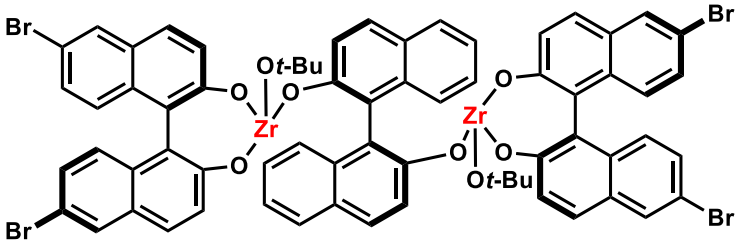

each Zr has an additional N-Me imidazole ligand not depicted

Kobayashi

Hydrogen-Bond Donors

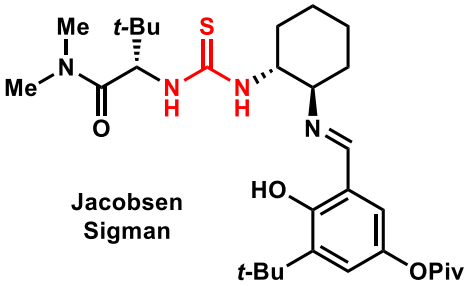

Jacobsen
Sigman

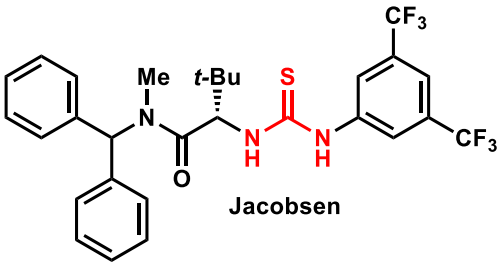

Jacobsen

Figure 1.8 Summary of classes of catalysts for asymmetric Strecker reactions

In addition to the guanidine catalyst reported by Lipton, Corey and Grogan have reported the C_2 symmetric guanidine derivative shown in Figure 1.8.[24] In both the Lipton and Corey work, benzaldehyde derived aldimines are good substrates giving much higher ee's than aliphatic substrates (Lipton: 90- >99% ee for aromatic vs. 10-20 for alkyl; Corey 80-88% ee for aromatic vs. 63-84% for alkyl). This difference in aliphatic and aromatic substrates is proposed to be the result of better recognition of aryl substrates engaging in π-π interactions. Guanidine catalysts are proposed to operate via simultaneous activation of cyanide by protonating the guanidine of catalyst, while also binding and activating the imine substrate via an H-bond to catalyst, in what is called a pre-transition state assembly.

There are a multitude of Strecker reactions catalyzed by Lewis acidic metals, a few of which will be discussed in some detail here. Jacobsen and Sigman developed the first asymmetric Lewis acid catalyzed Strecker reaction, employing the chiral (salen)AlCl complex shown in Figure 1.8.[25] Similar to the guanidine based catalysts, this method provides α-aryl glycines from arylimines in generally >90% ee, while affecting mildly enantioselective aliphatic imine hydrocyanations at 30-50% ee. Hoveyda and Snapper have investigated somewhat similar Ti(IV) Schiff base catalysts, which are able to catalyze both aryl and aliphatic imines with high enantioselectivity.[26] They have investigated the mechanism and determined that the Titanium

[24] Corey, E. J.; Grogan, M. J. Enantioselective Synthesis of α-Amino Nitriles from N-Benzhydryl Imines and HCN with a Chiral Bicyclic Guanidine as Catalyst. *Org. Lett.* **1999**, *1* (1), 157–160.

[25] Sigman, M. S..; Jacobsen, E. N. Enantioselective Addition of Hydrogen Cyanide to Imines Catalyzed by a Chiral (Salen)Al(III) Complex. *J. Am. Chem. Soc.* **1998**, *120* (21) 5315–5316.

[26] Krueger, C. A.; Kuntz, K. W.; Dzierba, C. D.; Wirschun, W. G.; Gleason, J. D.; Snapper, M. L.; Hoveyda, A. H. Ti-Catalyzed Enantioselective Addition of Cyanide to Imines. A Practical Synthesis of Optically Pure α-Amino Acids. *J. Am. Chem. Soc.* **1999**, *121* (17), 4284–4285.

coordinates the imine, which stacks with the phenolate, while the threonine derived amide precisely directs addition of HCN.[27]

Kobayashi reported the dimeric, BINOL derived zirconium catalyst, which is able to catalyze the addition of Bu_3SnCN to aldimines derived from 2-aminophenol.[28] Again, aromatic substrates give better enantioselectivities than aliphatic substrates. Kobayashi was able to make modifications to the catalyst counterion, which allowed for a 3-component coupling, wherein the imine can be formed *in situ*.[29] Additionally, this modified procedure has both alphatic and aromatic substrates with >86% ee. Shibasaki developed a bifunctional BINOL derived AlCl complex, which similar to all previously discussed methods, synthesizes aromatic products in >86% ee, with aliphatic substrates in the 70-80% ee range.[30] This complex is proposed to proceed through dual activation by coordination of the amine to the aluminum complex while the phosphine oxide engages in Brønsted or Lewis activation of HCN or TMSCN to direct addition to the imine.

The last class of chiral catalysts that promote strecker reactions shown in Figure 1.8 is the thiourea dual hydrogen-bond donor catalysts. Sigman and Jacobsen, are able to affect hydrocyanation of *N*-allyl imines in 70-92% yield and with 70-91% ee, in what is the first generation of thiourea catalyzed Strecker reactions.[31] Mechanistic studies revealed that the

---

[27] Josephsohn, N. J.; Kuntz, K. W.; Snapper, M. L.; Hoveyda, A. H. Mechanism of Enantioselective Ti-Catalyzed Strecker Reaction: Peptide-Based Metal Complexes as Bifunctional Catalysts. *J. Am. Chem. Soc.* **2001**, *123* (47), 11594–11599.

[28] Ishitani, H.; Komiyama, S.; Kobayashi, S. Catalytic, Enantioselective Synthesis Ofα-Aminonitriles with a Novel Zirconium Catalyst. *Angew. Chemie Int. Ed.* **1998**, *37* (22), 3186–3188.

[29] Ishitani, H.; Komiyama, S.; Hasegawa, Y.; Kobayashi, S. Catalytic Asymmetric Strecker Synthesis. Preparation of Enantiomerically Pure α-Amino Acid Derivatives from Aldimines and Tributyltin Cyanide or Achiral Aldehydes, Amines, and Hydrogen Cyanide Using a Chiral Zirconium Catalyst. *J. Am. Chem. Soc.* **2000**, *122* (5), 762–766.

[30] Takamura, M.; Hamashima, Y.; Usuda, H.; Kanai, M.; Shibasaki, M. A Catalytic Asymmetric Strecker-Type Reaction: Interesting Reactivity Difference between TMSCN and HCN. *Angew. Chemie Int. Ed.* **2000**, *39* (9), 1650–1652.

[31] For seminal reports on HBD catalyzed asymmetric Strecker reactions see: a) Sigman, M. S.; Jacobsen, E. N. Schiff Base Catalysts for the Asymmetric Strecker Reaction Identified and Optimized from Parallel Synthetic Libraries. *J.*

thiourea is able to bind to the imine in a 2H mechanism with the R group perpendicular to the plan of the thiourea. The imine undergoes E/Z isomerism under the reaction conditions, and the catalyst is proposed to activate the *Z* isomer, the exact influence the catalyst has on the cyanide addition is unknown.[32]

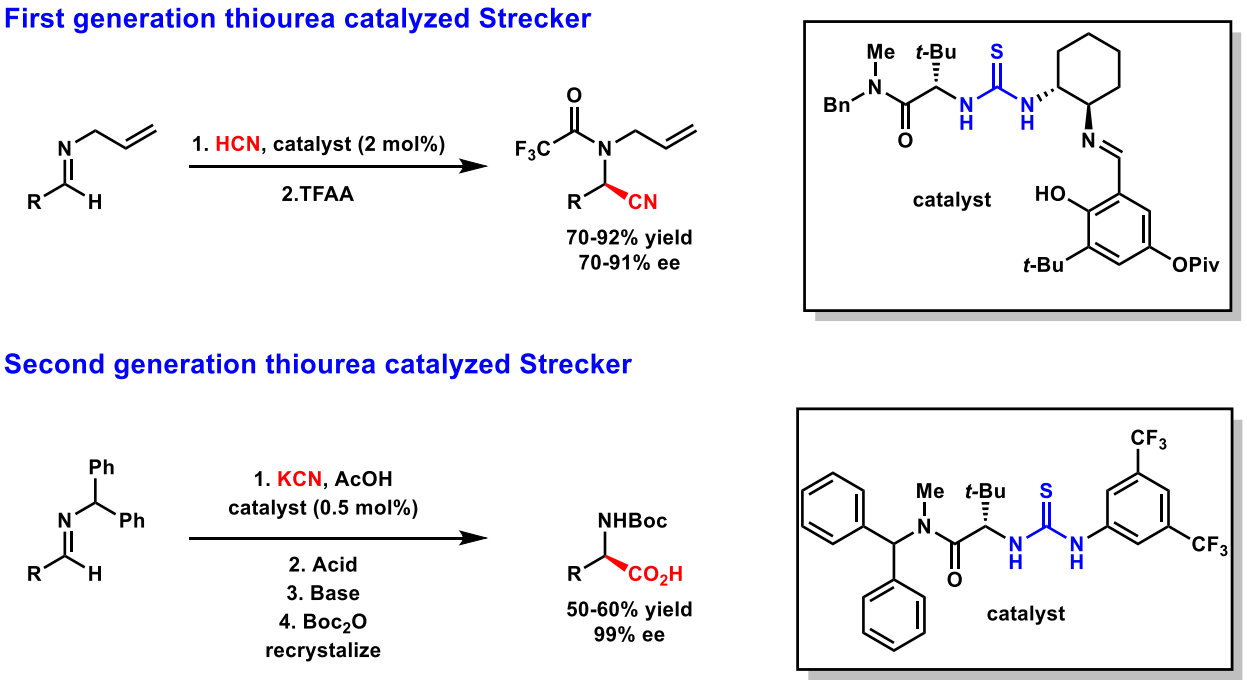

Figure 1.9 Thiourea catalyzed hydrocyanation of imines

The second generation thiourea catalyzed Strecker reaction is aimed at synthetic accessibility. The reaction uses relatively simple HBD catalyst, solid KCN, in biphasic water/toluene, and can be run on multi-gram scale; while ee's range from 73-98%, products can be recrystallized up to 99% ee for a broad range of aliphatic and aryl imine substrates.[33]

Am. Chem. Soc. **1998**, *120* (19), 4901–4902. b) Sigman, M. S.; Vachal, P.; Jacobsen, E. N. A General Catalyst for the Asymmetric Strecker Reaction. *Angew. Chemie Int. Ed.* **2000**, *39* (7), 1279–1281.

[32] Vachal, P.; Jacobsen, E. N. Structure-Based Analysis and Optimization of a Highly Enantioselective Catalyst for the Strecker Reaction. *J. Am. Chem. Soc.* **2002**, *124* (34), 10012–10014.

[33] Zuend, S. J.; Coughlin, M. P.; Lalonde, M. P.; Jacobsen, E. N. Scaleable Catalytic Asymmetric Strecker Syntheses of Unnatural α-Amino Acids. *Nature* **2009**, *461* (7266), 968–970.

Interestingly, this reaction is proposed to proceed via a mechanism divergent from the first generation HBD catalyzed strecker reaction. Rather than thiourea binding of the imine, experiment and computational evidence point to a mechanism involving a catalyst-promoted proton transfer from HCN to imine to generate diastereomeric ion pairs.[34] The iminium is stabilized by H-bonding to the catalyst amide and via cation-π interactions with the benzhydryl group, while CN anion is bound to the thiourea pocket; these ion pairs collapse to form product, with diastereomeric differential imine stabilization being the largest driving force in enantiodiscrimination.

1.5 Enantioselective methods for introduction of the amino acid side chain

All of the diversity in naturally occurring and synthetic amino acids occurs on the side chain. Thus, any general methods asymmetric catalytic methods to introduce the side chain would be highly valuable in having a unified strategy to generate a wide range of amino acids. Importantly, this is the only amino acid disconnection in which 2 stereocenters (α and β) can be set in one step, although high enantio- and diastereoselectivity is rarely achieved in these transformations. Additionally, glycine and glyoxylates/glyoxylate imine, the likely starting materials are both widely available. One can envision disconnecting the side chain in either of the possible polar contexts or in a radical context (Figure 1.10).

[34] Zuend, S. J.; Jacobsen, E. N. Mechanism of Amido-Thiourea Catalyzed Enantioselective Imine Hydrocyanation: Transition State Stabilization via Multiple Non-Covalent Interactions. *J. Am. Chem. Soc.* **2009**, *131* (42), 15358–15374

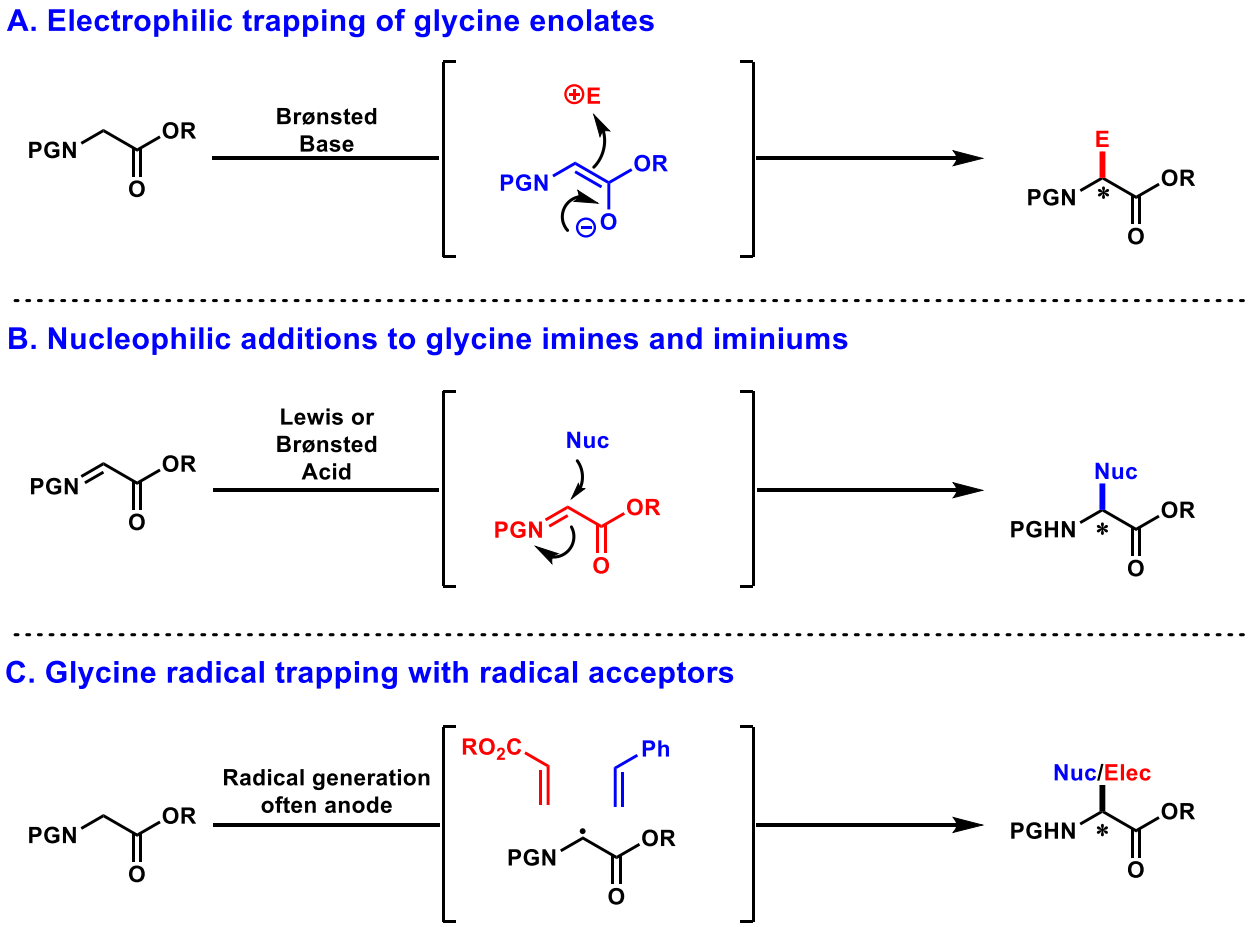

Figure 1.10 General strategies for the addition of amino acid side chains

1.5.1 Radical methods for introduction of the amino acid side chain

The radical disconnection for amino acids (Figure 1.10 C) is largely unexplored, especially in the context of asymmetric catalysis, although there is a review on the topic.[35] Despite the ubiquity of glycyl radicals in biological transformations, glycyl radicals are rarely used in organic synthesis, due to challenge of controlling the desired transformation over competing pathways.

Common ways to generate glycyl radicals involve a hydrogen atom abstraction from glycine performed by diarylketones under photolytic conditions.[36] Shono oxidation is bulk

[35] Easton, C. J. Free-Radical Reactions in the Synthesis of α-Amino Acids and Derivatives. *Chem. Rev.* **1997**, *97* (1), 53–82.
[36] Elad, D.; Sperling, J. Photoalkylation of Proteins. *J. Am. Chem. Soc.* **1971**, *93* (15), 3839–3840.

electrolysis of an amino acid in methanol, to generate the α-radical or iminium, which is rapidly trapped by solvent to afford α-methoxy amino acids.[37] One can use NBS to perform free radical bromination of glycine, which can subsequently be trapped by malonate anion or allylstannanes to generate α-allyl amino acids (Figure 1.11).[38,39] These allylations are proposed to proceed through radical transformations, although with no mechanistic evidence. The ease of affecting substitution chemistry at this carbon as discussed extensively in Chapter 2 raises the possibility that these proceed via polar mechanisms. To the best of our knowledge, there are no enantioselective radical syntheses of amino acids.

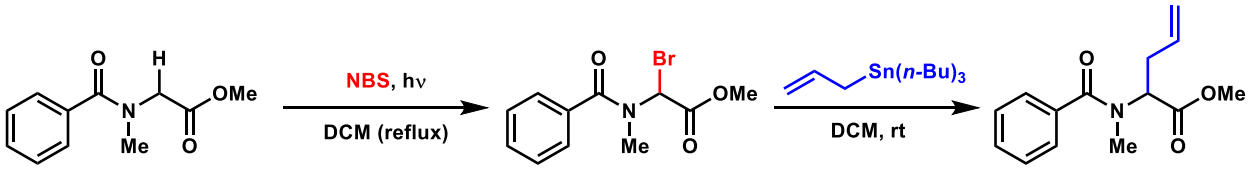

Figure 1.11 radical bromination and subsequent allylstannane addition to glycinate amide

1.5.2 Enolate alkylation methods for introduction of the amino acid side chain

One of the most general and practical ways to make unnatural amino acids, especially α-allyl amino acids is via enolate alkylation, either in the context of chiral auxiliaries or enantioselective catalysis. Myers' pseudoephedrine glycinamide auxiliary can be used to make α-alkyl/α-allyl and in some cases α,α-disubstituted amino acids by deprotonating with LDA to form the enolate, which can add into alkyl, allyl, or benzyl halides in an S_N2 fashion.[40] These reactions

[37] Shono, T.; Hamaguchi, H.; Matsumura, Y. Electroorganic Chemistry. XX. Anodic Oxidation of Carbamates. *J. Am. Chem. Soc.* **1975**, *97* (15), 4264–4268

[38] Easton, C. J.; Scharfbillig, I. M.; Wui Tan, E. Selective Modification of Glycine Residues in Dipeptides. *Tetrahedron Lett.* **1988**, *29* (13), 1565–1568.

[39] Baldwin, J. E.; Adlington, R. M.; Lowe, C.; O'Neil, I. A.; Sanders, G. L.; Schofield, C. J.; Sweeney, J. B. Reactions of a Glycidyl Radical Equivalent with 2-Functionalised Allyl Stannanes. *J. Chem. Soc. Chem. Commun.* **1988**, No. 15, 1030.

[40] a) Myers, A. G.; L. Gleason, J.; Yoon, T. Practical Method for the Synthesis of D- or L-.Alpha.-Amino Acids by the Alkylation of (+)- or (-)-Pseudoephedrine Glycinamide. *J. Am. Chem. Soc.* **2002**, *117* (32), 8488–8489. b) Myers, A. G.; Gleason, J. L. Asymmetric Synthesis of α-Amino Acids by the Alkylation of Pseudoephedrine Glycinamide: L

have high d.e. of 90-98% and can be recrystallized to enantiopure products. Deprotection is facile under standard saponification conditions. The main limitation to this chemistry is that due to the steric requirements in the S_N2 transition state, secondary electrophiles are challenging.

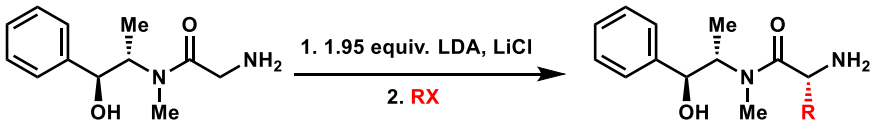

RX	d.e.
EtI	97 (>99)
AllylBr	93 (>99)
i-BuI	97 (>99)
BnBr	91 (>99)

Figure 1.12 Enolate alkylation with pseudoephederine glycinamides

Among catalytic approaches to asymmetric enolate alkylation, the phase-transfer-catalyzed (PTC) allylation of Schiff base, ester enolates was pioneered by O'Donnell.[41] O'Donnell first discovered that enolates could be alkylated via PTC by employing BTEAC as a catalyst for the alkylation of benzophenoneimine protected α-aminonitriles.[42] The choice of benzophenone imine is ubiquitous and judicious in PTC enolate alkylations. It serves two roles: 1) it stabilizes the enolate, facilitating deprotonation of the starting material and 2) if the enolate of the product is inaccessible because the newly added side chain would engage in a high energy $A_{1,3}$ interaction with the phenyl group, and thus product stereochemistry is not eroded. While enantioselectivities initially reported cinchona alkaloid catalysts are only moderately enantioselective (Figure 1.13 A),[43] this chemistry was advanced to the current state-of-the-art by Maruoka through the discovery

-Allylglycine and N-Boc- L -Allylglycine. In *Organic Syntheses*; John Wiley & Sons, Inc.: Hoboken, NJ, USA, 2003; pp 57–57.

[41] For a review on PTC catalyzed enolate alkylations see: O'Donnell, M. J. The Enantioselective Synthesis of α-Amino Acids by Phase-Transfer Catalysis with Achiral Schiff Base Esters. *Acc. Chem. Res.* **2004**, *37* (8), 506–517.

[42] O'Donnell, M. J.; Eckrich, T. M. The Synthesis of Amino Acid Derivatives by Catalytic Phase-Transfer Alkylations. *Tetrahedron Lett.* **1978**, *19* (47), 4625–4628.

[43] O'Donnell, M. J.; D. Bennett, W.; Wu, S. The Stereoselective Synthesis of .Alpha.-Amino Acids by Phase-Transfer Catalysis. *J. Am. Chem. Soc.* **2002**, *111* (6), 2353–2355.

of highly effective, C_2 symmetric, quaternary ammonium salt catalysts (Figure 1.13 B).[44] Maruoka's catalysts and conditions are highly practical, employing less than 1 mol% of catalyst, generally achieving enantioselectivies >95%, and in convenient biphasic conditions.

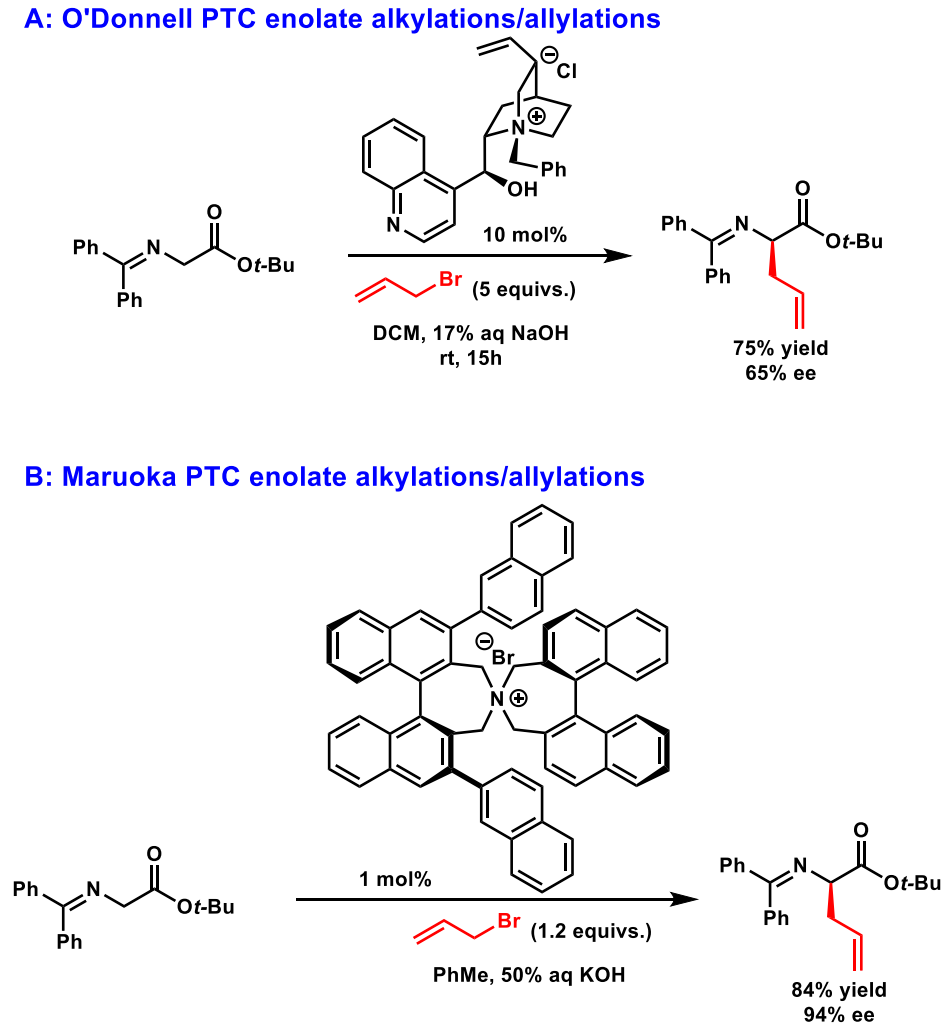

Figure 1.13 enantioselective PTC methods for the synthesis of α-allyl amino acids

Maruoka's chemistry is astonishingly general, affecting enolate alkylation on classes of substrates on would not expect to work. Changing the amine protecting group to *p*-Cl-benzaldehyde imine allows for a second enolization event which makes the highly enantioselective

[44] For a review on enantioselective PTC enolate alkylations see a) Maruoka, K.; Ooi, T. Enantioselective Amino Acid Synthesis by Chiral Phase-Transfer Catalysis. *Chem. Rev.* **2003**, *103* (8), 3013–3028. For initial report see: Ooi, T.; Kameda, M.; Maruoka, K. Molecular Design of a C2-Symmetric Chiral Phase-Transfer Catalyst for Practical Asymmetric Synthesis of α-Amino Acids. *J. Am. Chem. Soc.* **1999**, *121* (27), 6519–6520.

synthesis of α,α-disubstituted amino acids possible (Figure 1.14 A).[45] Maruoka and Jorgensen have both reported chiral PTC S_NAr reactions with nitroarenes.[46] Additionally, Maruoka can engage fluorinated arenes engaging in an η^6 interaction with chromium tricarbonyl in S_NAr chemistry.[47] This chemistry provides remarkably high levels of enantioselectivity for a broad range of α-alkyl-α-aryl glycinates bearing electronically neutral arenes (Figure 1.14 B). While PTC and auxiliary enolate alkylation methods provide access to a numerous unbranched α-alkyl and α-allyl amino esters, the preparation of branched products via PTC is generally not possible due to sterically demanding or contra-steric substitution at a branched electrophilic carbon.

[45] Kitamura, M.; Shirakawa, S.; Maruoka, K. Powerful Chiral Phase-Transfer Catalysts for the Asymmetric Synthesis of α-Alkyl- and α,α-Dialkyl-α-Amino Acids. *Angew. Chemie Int. Ed.* **2005**, *44* (10), 1549–1551.

[46] a) Bella, M.; Kobbelgaard, S.; Jørgensen, K. A. Organocatalytic Regio- and Asymmetric C-Selective SNAr ReactionsStereoselective Synthesis of Optically Active Spiro-Pyrrolidone-3,3‘-Oxoindoles. *J. Am. Chem. Soc.* **2005**, *127* (11), 3670–3671. b) Shirakawa, S.; Koga, K.; Tokuda, T.; Yamamoto, K.; Maruoka, K. Catalytic Asymmetric Synthesis of 3,3′-Diaryloxindoles as Triarylmethanes with a Chiral All-Carbon Quaternary Center: Phase-Transfer-Catalyzed S_N Ar Reaction. *Angew. Chemie Int. Ed.* **2014**, *53* (24), 6220–6223.

[47] Shirakawa, S.; Yamamoto, K.; Maruoka, K. Phase-Transfer-Catalyzed Asymmetric S_N Ar Reaction of α-Amino Acid Derivatives with Arene Chromium Complexes. *Angew. Chemie Int. Ed.* **2015**, *54* (3), 838–840.

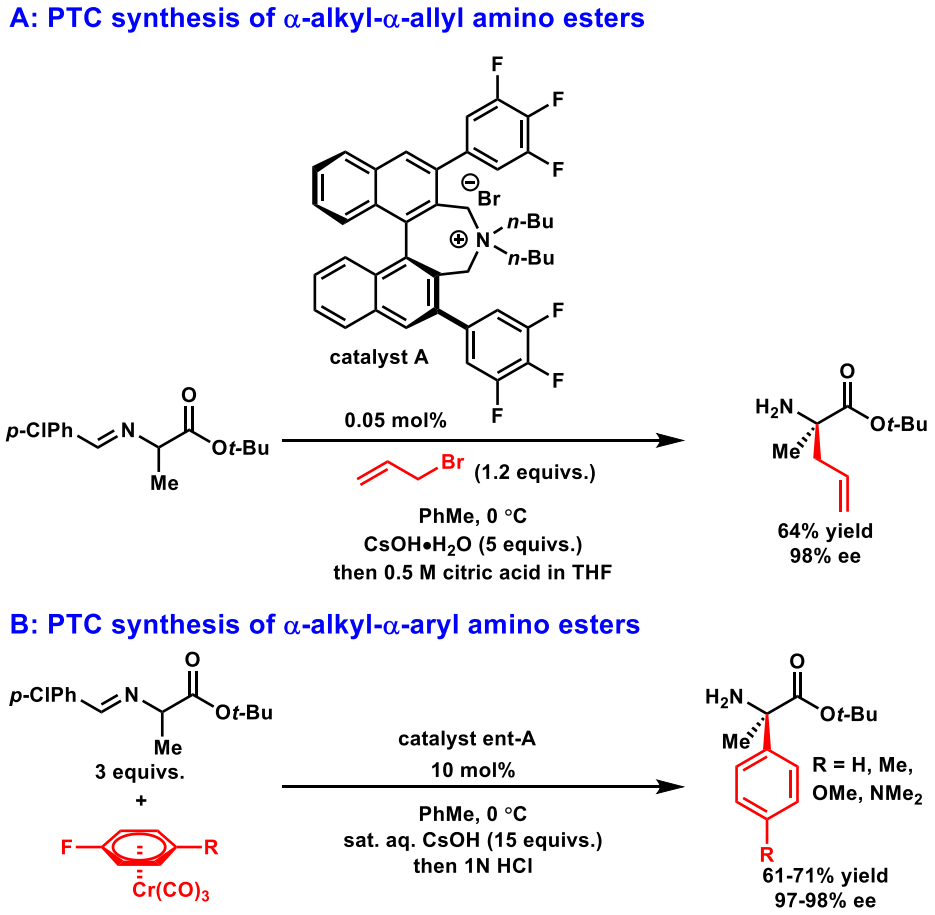

Figure 1.14 enantioselective PTC methods for the synthesis of α,α-disubstituted amino acids

1.5.3 Metal catalyzed allylations of enolates for introduction of the amino acid side chain

While PTC methods cannot produce β-branched products, a number of allylic acetates are known to react at the more hindered site (including iridium, molybdenum, and tungsten). Cinnamyl phosphate, in the presence of a chiral phosphite iridium complex, was found to react with the O'Donnell Schiff base enolate at the more hindered position to afford reverse-cinnamyl amino acids in up to 97% ee (Figure 1.15 A).[48] Interestingly, the identity of the base reverses the major

[48] Kanayama, T.; Yoshida, K.; Miyabe, H.; Takemoto, Y. Enantio- and Diastereoselective Ir-Catalyzed Allylic Substitutions for Asymmetric Synthesis of Amino Acid Derivatives. *Angew. Chemie Int. Ed.* **2003**, *42* (18), 2054–2056.

diastereomer, with KOH giving the *syn* diastereomer in 6:1 d.r. and LiHMDS giving the *anti* isomer in 1:9 d.r.

Trost has had considerable success in synthesizing α,α-disbustitued amino acids via asymmetric allylic alkylations of azalactones derived from amino acids. The first generation is a palladium chiral bidentatephosphine catalyzed addition of 3-acetoxycyclohexene a variety of azalactones.[49] Palladium allyl species generally favor addition at the less substituted carbon, thus switching to molybdenum with the same general chiral framework allowed for reverse-cinnamylation of the same substrates (Figure 1.15 B).[50] Metal catalyzed allylic alkylation works well for cinnamylations in both the syntheses of α-substituted and α,α-disbustituted amino acids; however, crotylations, and in general substrates where branching is aliphatic, remain an unsolved problem in the context of metal catalyzed enolate allylations.

[49] Trost, B. M.; Ariza, X. Catalytic Asymmetric Alkylation of Nucleophiles: Asymmetric Synthesis Ofα-Alkylated Amino Acids. *Angew. Chemie Int. Ed.* **1997**, *36* (23), 2635–2637.

[50] M. Trost, B.; Dogra, K. Synthesis of Novel Quaternary Amino Acids Using Molybdenum-Catalyzed Asymmetric Allylic Alkylation. *J. Am. Chem. Soc.* **2002**, *124* (25), 7256–7257.

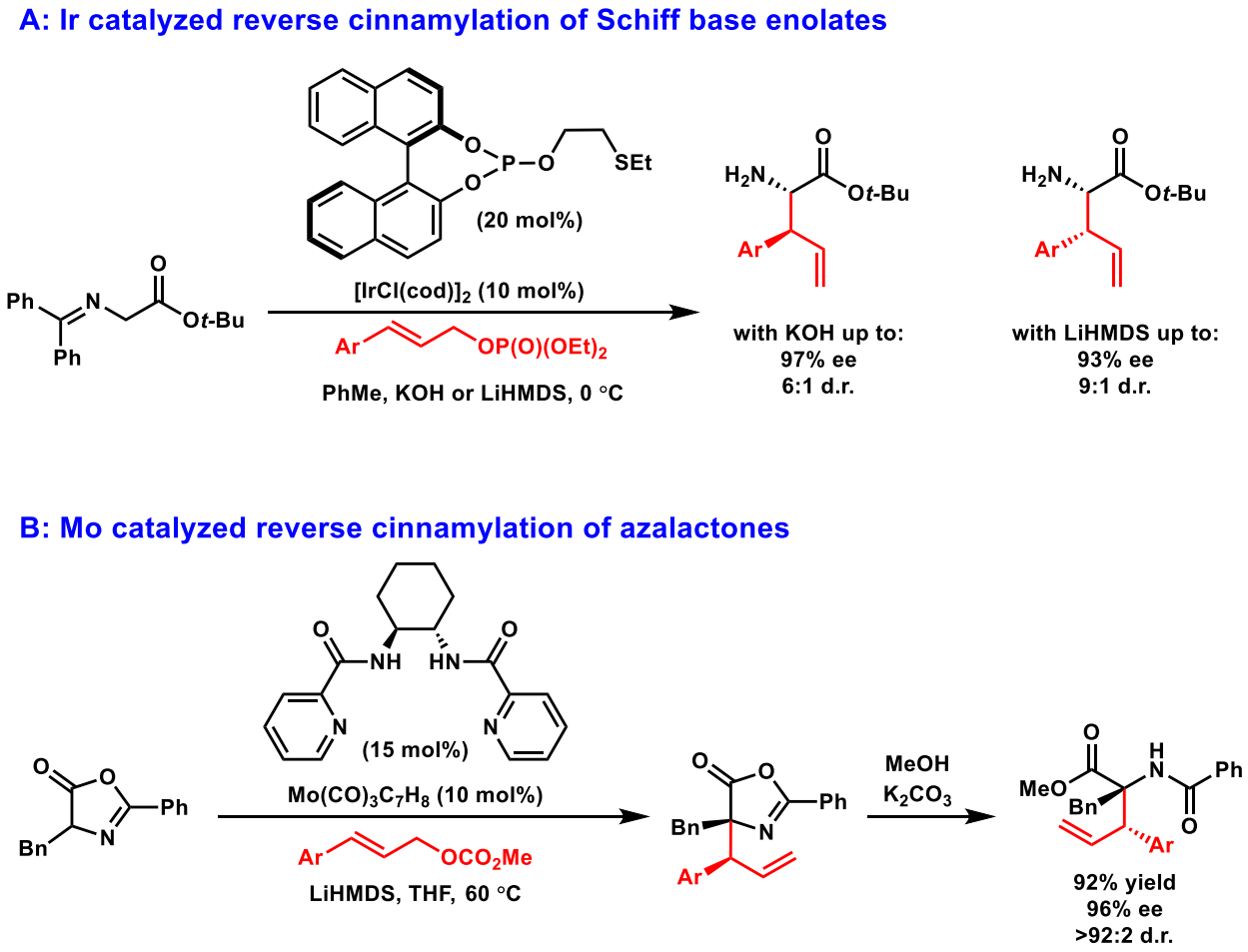

Figure 1.15 Transition metal catalyzed allylations of amino acid enolates

1.5.4 Imine nucleophilic additions for introduction of the amino acid side chain

Umpolung to the enolate alkylation strategy is the addition of nuclophilic side chains to glyoxylate imines or iminiums, as depicted in Figure 1.10 B. The advantage to this disconnection that additions to these imines are relatively slow, but become facile in the presence of Lewis acid organometallic or organocatalysts, which allows for a enantioselective catalysis over background in the addition of a broad range of both weak and strong nucleophiles.[51] Whereas enolate alkylation methods are limited by the range of electrophiles that undergo S_N2 or S_NAr reactions, any

[51] For reviews on catalytic enantioselective additions to imines: a) Vilaivan, T.; Bhanthumnavin, W.; Sritana-Anant, Y. Recent Advances in Catalytic Asymmetric Addition to Imines and Related C=N Systems. *Curr. Org. Chem.* **2005**, *9* (14), 1315–1392. b) Kobayashi, S.; Ishitani, H. Catalytic Enantioselective Addition to Imines. *Chem. Rev.* **1999**, *99* (5), 1069–1094.

organozinc, Grignard reagent, or weak organometallic nucleophile, including those that would lead to β-branched products, could in principle add to these imines greatly increasing the substrate scope. The addition of aryl groups, nucleophilic allylating reagents, as well as ene and Mannich reactions are all precedented in auxiliary and asymmetric catalytic contexts; we will focus on allylation and arylation here (Figure 1.16).[4] The major downside to these methods is the requirement that a relatively unstable and hydrolytically labile imine be preformed as well as often challenging *N*-deprotection of the amino acid or amino ester products.

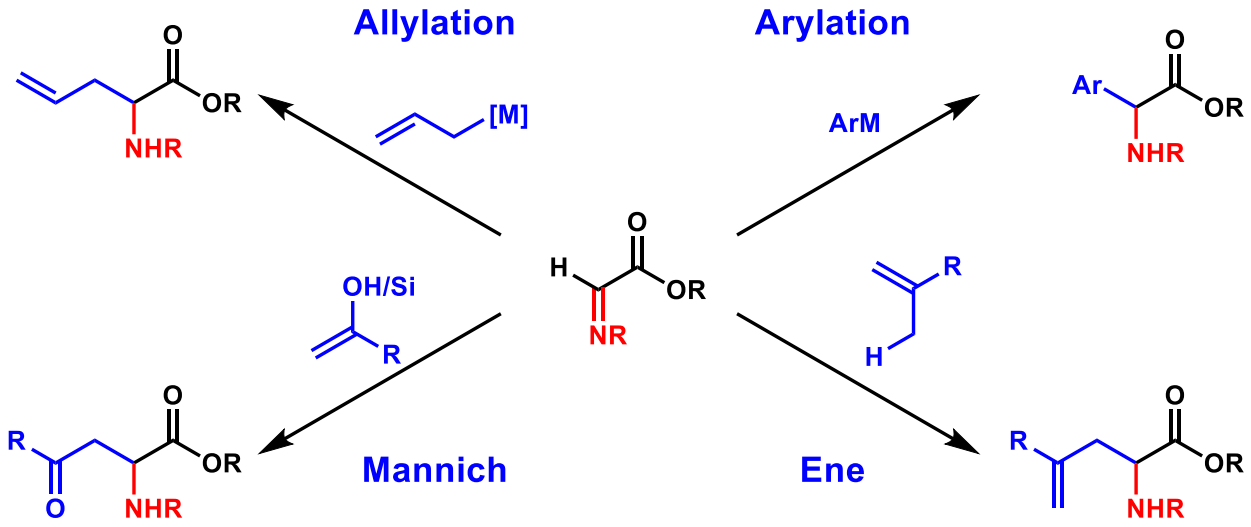

Figure 1.16 Synthesis of amino esters via nucleophilic addition to glyoxylate imines

The condensation product between a chiral amine and glyoxylate, affords a chiral imine, which can be intercepted by a range of nucleophiles in a diastereoselective fashion to generate amino acids. The Ellman and Davis sulfonyl imines generally provide diastereomeric syntheses of amino acids.[20,52] Allyl amino esters have been synthesized via the Ellman auxiliary by the generation of Pd-allylcomplexes from allene, which can transmetallate to indium to affect

[52] Davis, F. A.; McCoull, W. Concise Asymmetric Synthesis of α-Amino Acid Derivatives from N-Sulfinylimino Esters. *J. Org. Chem.* **1999**, *64* (10), 3396–3397.

diastereoselective imine additions.[53] The direct generation of allyl indium reagents from allylbromides also provide high levels of d.r. (Figure 1.17 A).[54] The coupling of arylboronic acids and *N-tert*-butanesulfinyl imino esters has been accomplished with rhodium catalysis to generate α-aryl glycine derivatives in >98:2 d.r. (Figure 1.17 B).[55] The proposed stereochemical model involves the sulfonamide oxygen coordinating rhodium and directing aryl addition. A TMSOTf catalyzed addition of electron rich heteroaromatics has also been reported, giving a d.r.'s in the range of 4:6 to 8:2, with the exception of indole, which adds to furnish a single diastereomer of α-(3-indole) glycine.[56] In limited examples using triorganozincates, additions to phenylglyoxylate imines afford α-alkyl-α-aryl amino acids in high d.r. (Figure 1.17 C).[57]

[53] Grigg, R.; McCaffrey, S.; Sridharan, V.; Fishwick, C. W. G.; Kilner, C.; Korn, S.; Bailey, K.; Blacker, J. Enantioselective Synthesis of Non-Proteinogenic 2-Arylallyl-α-Amino Acids via Pd/In Catalytic Cascades. *Tetrahedron* **2006**, *62* (52), 12159–12171.

[54] Sun, X.-W.; Liu, M.; Xu, M.-H.; Lin, G.-Q. Remarkable Salt Effect on In-Mediated Allylation of N-Tert-Butanesulfinyl Imines in Aqueous Media: Highly Practical Asymmetric Synthesis of Chiral Homoallylic Amines and Isoindolinones. *Org. Lett.* **2008**, *10* (6), 1259–1262.

[55] Beenen, M. A.; Weix, D. J.; Ellman, J. A. Asymmetric Synthesis of Protected Arylglycines by Rhodium-Catalyzed Addition of Arylboronic Acids to N-Tert-Butanesulfinyl Imino Esters. *J. Am. Chem. Soc.* **2006**, *128* (19) 6304–6305.

[56] Andreassen, T.; Hansen, L.-K.; Gautun, O. R. Diastereoselective Synthesis of Heteroaromatic Glycine Derivatives. *Euro. J. Org. Chem.* **2008**, *2008* (29), 4871–4876.

[57] Almansa, R.; Guijarro, D.; Yus, M. Application of the Addition of Triorganozincates to N-(Tert-Butanesulfinyl)Imines to the Enantioselective Synthesis of α-Amino Acids. *Tetrahedron Lett.* **2009**, *50* (28), 4188–4190.

A: Synthesis of α-allyl amino acids using the Ellman auxiliary

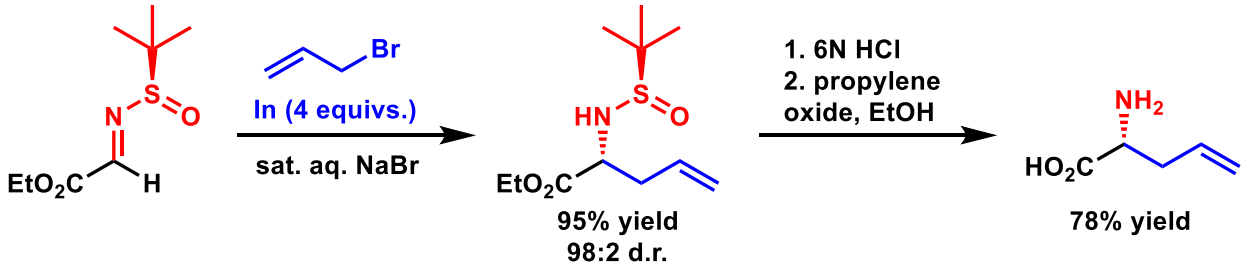

B: Synthesis of α-aryl amino acids using the Ellman auxiliary

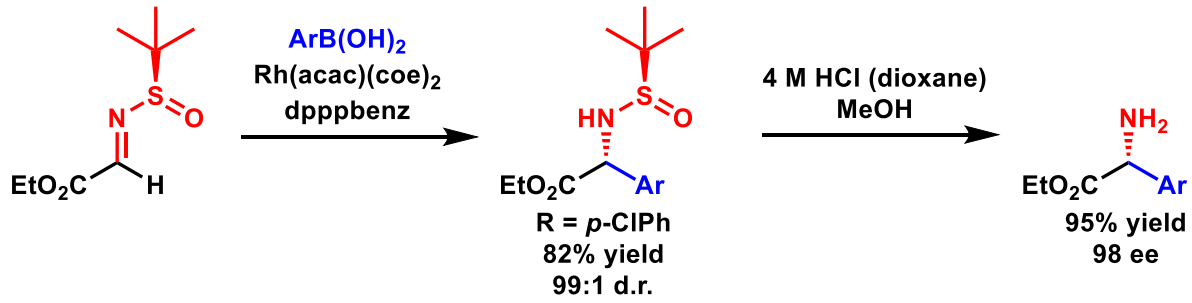

C: Synthesis of α-alkyl-α-aryl amino acids using the Ellman auxiliary

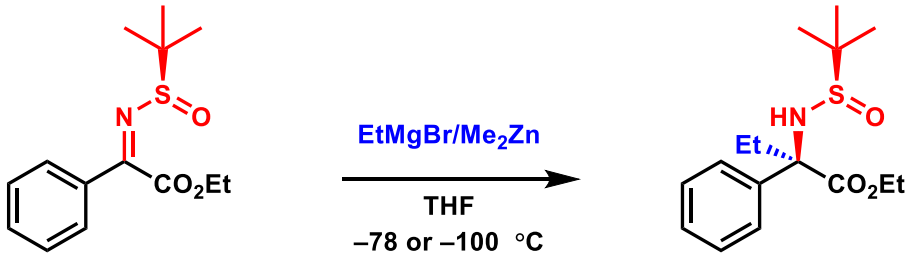

Figure 1.17 enantioselective PTC methods for the synthesis of α,α-disubstituted amino acids

The use of chiral transition metal complexes has emerged as powerful class of catalysts in the addition of nucleophilic allylating and arylating agents to *N*-tosyl α-imino esters. Leckta and Jørgensen independently arrived at (*R*)-*p*-tol-binap copper (I) complexes in the addition of allylsilanes and allylstannanes to *N*-tosyl α-imino esters, which allows stereocontrolled construction of β-branched α-allyl amino acid derivatives in up to 93% ee and 20:1 d.r (Figure

1.18 A).[58] Kobayashi successfully employed 3 equivalents of binap derived bisphosphine oxides to catalyze highly enantioselective and diastereoselective additions of allyltirchlorosilanes to α-hydrozono esters.[59] Recently, Szabó published a related allylation and propargylation of allyl- and propargylboronic acids, catalyzed by binol to the same α-hydrozono esters substrates.[60] The biggest drawback to these reactions is the challenge of removing the amino-protecting group.

The enantioselective additions of arenes to α-imino esters is relatively unexplored, with most reports being in the Friedel-Crafts addition of electron rich aromatics and heteroaromatics. In 1999 Johannsen reported the exact same (*R*)-*p*-tol-binap copper (I) complex used in allylations to affect the addition of indoles and pyrroles to *N*-tosyl α-imino esters with enantioselectivities up to 97%, which can be upgraded to enantiopure products (Figure 1.18 B).[61] Jørgensen found the same copper (I) complex promotes the addition of anilines and furans/thiofurans to *N*-carbamoyl α-imino esters in yields ranging from 33-82% and ee's from 72-96%.[62]

---

[58] a) Ferraris, D.; Dudding, T.; Young, B.; Drury III, W. J.; Lectka, T. Catalytic, Enantioselective Alkylations of N,O-Acetals. *J. Org. Chem.* **1999**, *64* (7), 2168–2169. b) Ferraris, D.; Young, B.; Cox, C.; Dudding, T.; J. Drury, W.; Ryzhkov, L.; E. Taggi, A.; Lectka, T. Catalytic, Enantioselective Alkylation of α-Imino Esters: The Synthesis of Nonnatural α-Amino Acid Derivatives. *J. Am. Chem. Soc.* **2001**, *124* (1), 67–77. c) Fang, X.; Johannsen, M.; Yao, S.; Gathergood, N.; G. Hazell, R.; Anker Jørgensen, K. Catalytic Approach for the Formation of Optically Active Allyl α-Amino Acids by Addition of Allylic Metal Compounds to α-Imino Esters. *J. Org. Chem.* **1999**, *64* (13), 4844–4849.

[59] Ogawa, C.; Sugiura, M.; Kobayashi, S. Stereospecific, Enantioselective Allylation of ?-Hydrazono Esters by Using Allyltrichlorosilanes with BINAP Dioxides as Neutral-Coordinate Organocatalysts. *Angew. Chemie Int. Ed.* **2004**, *43* (47), 6491–6493.

[60] Jonker, S. J. T.; Diner, C.; Schulz, G.; Iwamoto, H.; Eriksson, L.; Szabó, K. J. Catalytic Asymmetric Propargyl- and Allylboration of Hydrazonoesters: A Metal-Free Approach to Sterically Encumbered Chiral α-Amino Acid Derivatives. *Chem. Commun.* **2018**, *54* (91), 12852–12855.

[61] Johannsen, M. An Enantioselective Synthesis of Heteroaromatic N-Tosyl α-Amino Acids. *Chem. Commun.* **1999**, No. 21, 2233–2234.

[62] a) Saaby, S.; Bayón, P.; Aburel, P. S.; Jørgensen, K. A. Optically Active Aromatic and Heteroaromatic α-Amino Acids by a One-Pot Catalytic Enantioselective Addition of Aromatic and Heteroaromatic C−H Bonds to α-Imino Esters. *J. Org. Chem.* **2002**, *67* (12), 4352–4361. b) Saaby, S.; Fang, X.; Gathergood, N.; Jørgensen, K. A. Formation of Optically Active Aromaticα-Amino Acids by Catalytic Enantioselective Addition of Imines to Aromatic Compounds. *Angew. Chemie* **2000**, *39* (22), 4114–4116.

A: Cu (I) catalyzed enantio- and diastereoselective allylations

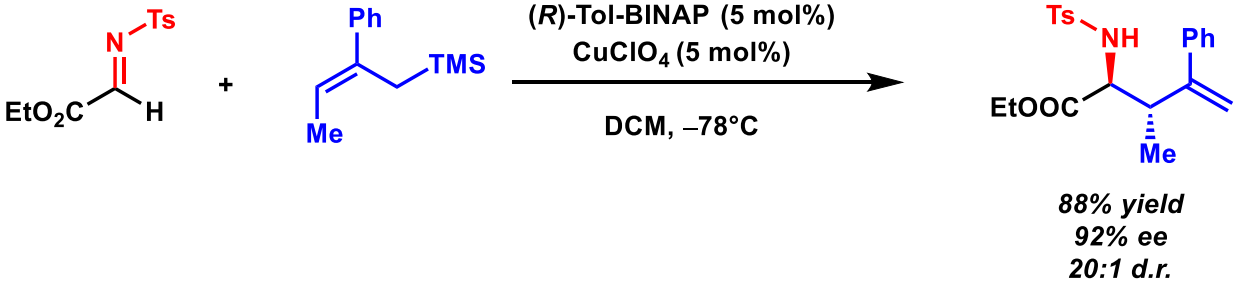

B: Cu (I) catalyzed enantioselective Friedel-Crafts arylations

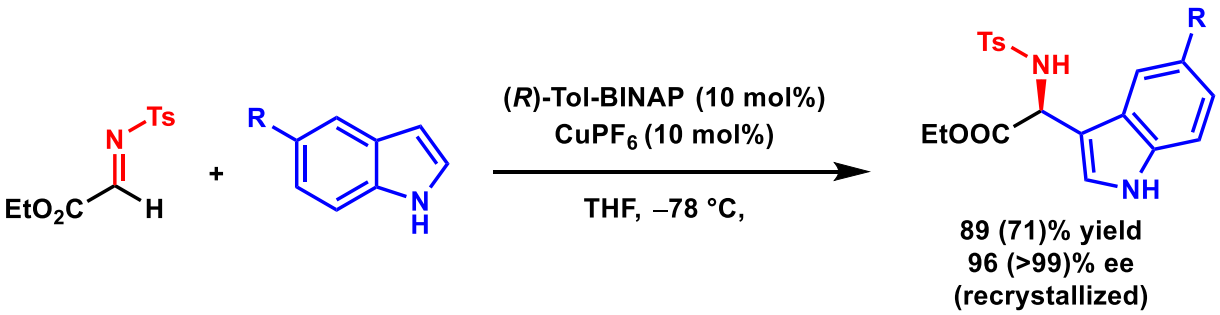

Figure 1.18 Chiral Cu (I) catalyzed nucleophilic additions to glyoxylate imines

1.6 Rearrangement chemistry for installation of the amino acid side chain

One possible route to α-allyl glycine derivatives is to condense allylic alcohols onto *N*-protected glycine and to enolize to affect an ester enolate Claisen rearrangement.[63] Due to the stereospecific nature of [3,3] sigmatropic rearrangements, this ensures high d.r. and only requires a catalyst to impart enantioselectivity. In 1994, Kazmaier reported a diastereoselective chelation controlled enolate Claisen rearrangement to synthesize *syn*-crotylated glycines from (*E*)-crotyl glycine esters in high d.r., proceding through a closed chair transition state.[64] Kazmaier developed

[63] For a review of Claisen rearrangements as applied to amino acid synthesis: Kazmaier, U. Application of the Chelate-Enolate Claisen Rearrangement to The Synthesis of γ,δ-Unsaturated Amino Acids. *Liebigs Ann.* **1997**, *1997* (2), 285–295.

[64] Kazmaier, U. Synthesis of Unsaturated Amino Acids by[3,3]-Sigmatropic Rearrangement of Chelate-Bridged Glycine Ester Enolates. *Angew. Chemie Int. Ed. English* **1994**, *33* (9), 998–999.

an asymmetric variant stoichiometrically promoted by aluminum isopropoxide, with 2.5 equivalents of quinine as a chiral ligand, to afford α-crotylated amino acids in 98% d.r. and 86% ee (Figure 1.19 A).[65] Under the same conditions, prenyl type esters can be rearranged to generate α-amino acids with β-quaternary stereocenters with up to 98% d.r. and 93% ee, although ee's are highly substrate dependent.[66] While enantioselectivies are often modest, the amino acids can be crystallized with α-phenethylamine to enantiopure material.

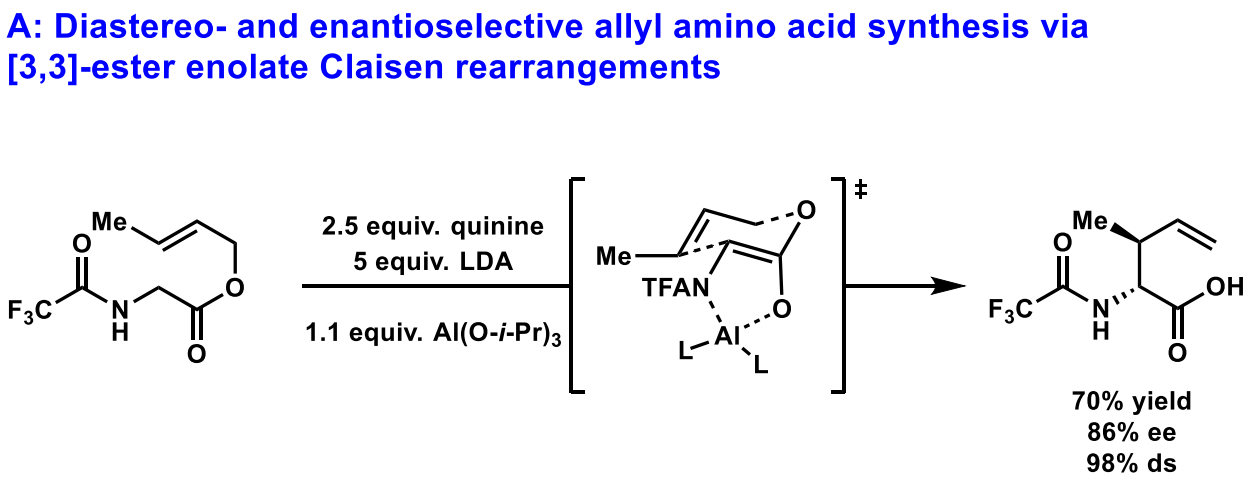

Figure 1.19 Synthesis of allyl amino acids via enantioselective sigmatropic rearrangements

[65] Kazmaier, U.; Krebs, A. Synthesis of Chiral γ,δ-Unsaturated Amino Acids by Asymmetric Ester Enolate Claisen Rearrangement. *Angew. Chemie Int. Ed. English* **1995**, *34* (18), 2012–2014.

[66] Krebs, A.; Kazmaier, U. The Asymmetric Ester Enolate Claisen Rearrangement as a Suitable Method for the Synthesis of Sterically Highly Demanding Amino Acids. *Tetrahedron Lett.* **1996**, *37* (44), 7945–7946.

In addition to Claisen rearrangements, ammonium ylide [2,3]-sigmatropic rearrangements can similarly be used to set β-branched-α-allyl amino esters in a diastereospecific and enantioselective manner. In 2011, Tambar reported a palladium catalyzed allylic amination of *N,N*-dimethyl glycinates, which could form the ylide *in situ* and rearrange to the β-branched-α-allyl amino esters in high yields and 9:1 d.r.[67] When using Oppolzer's camphorsultam as a chiral auxiliary as an amino amide in place of the ester group, the reaction was highly diastereoselective providing access to optically pure products. Inspired by Tambar's precedent, Smith is able to use benzotetramisole as a nucleophilic catalyst to add into the ester of a preformed amino ester quaternary ammonium salt, acting as a transient auxiliary during the rearrangement step, affording cinnamyl amino esters in excellent enantioselectivies of up to >19:1 d.r. and >99% ee (Figure 1.19 B).[68] Smith went on to combine Tambar and his precedent and develop a one-pot tandem relay catalytic system, involving palladium catalyzed allylic amination followed by isothiourea catalyzed [2,3]-rearrangement to furnish the same products shown in Figure 1.19 B without loss in enantioselectivity.[69] While these methods afford very high enantioselectivies, they are limited to cinnamyl type substrates, which can also be made via transition metal catalyzed allylic alkylations, as discuss in section 1.5.3.

1.7 Enantioselective C-H activation in the synthesis of amino acids

Recent advances in the field of C(sp^3)-H activation, catalyzed by transition metals, have made the functionalization of natural amino acids an attractive method for synthesizing unnatural

[67] Soheili, A.; K. Tambar, U. Tandem Catalytic Allylic Amination and [2,3]-Stevens Rearrangement of Tertiary Amines. *J. Am. Chem. Soc.* **2011**, *133* (33), 12956–12959.
[68] H. West, T.; S. B. Daniels, D.; M. Z. Slawin, A.; D. Smith, A. An Isothiourea-Catalyzed Asymmetric [2,3]-Rearrangement of Allylic Ammonium Ylides. *J. Am. Chem. Soc.* **2014**, *136* (12), 4476–4479.

[69] S. M. Spoehrle, S.; H. West, T.; E. Taylor, J.; M. Z. Slawin, A.; D. Smith, A. Tandem Palladium and Isothiourea Relay Catalysis: Enantioselective Synthesis of α-Amino Acid Derivatives via Allylic Amination and [2,3]-Sigmatropic Rearrangement. *J. Am. Chem. Soc.* **2017**, *139* (34), 11895–11902.

amino acids.[70] Amino acid C-H activations can be categorized by the distance the bond that is being activated is from the carbonyl, as well the C hybridization of the C-H bond that is being broken (Figure 1.20).

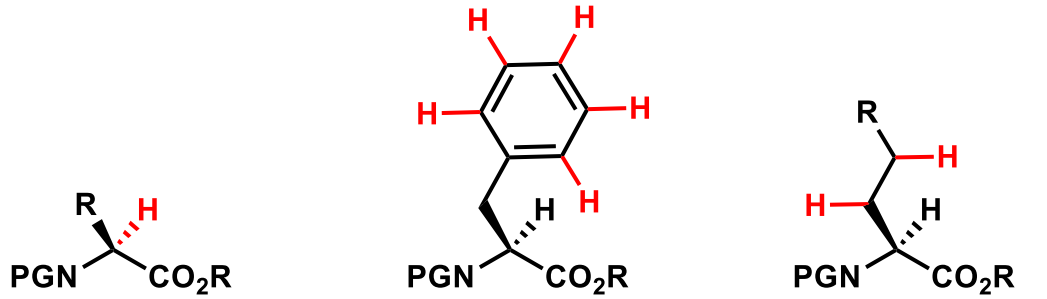

peptide backbone modification α-(Csp^3)-H | **peptide side-chain modification (Csp^2)-H** | **peptide side-chain modification β- or γ-(Csp^2)-H**

Figure 1.20 Classes of C-H functionalization of amino acid residues

Most α-C-H functionalizations have been oxidative methods, which take advantage of the weak α-C-H bond to chemoselectively generate an alpha radical, which can be trapped directly or oxidized to the imine and subsequently trapped. Numerous copper, iron, and cobalt racemic arylations and propargylations, and Mannich reactions of glycine derivatives have been accomplished via this strategy. However, translating this into more challenging functionalizations of α-substituted amino acids for the synthesis of α,α-disubstituted amino acids has been challenging and has required the azalactone enolate alkylation strategy discussed in section 1.5.3.[71]

---

[70] For reviews on C-H activation as applied to amino acid synthesis: a) Noisier, A. F. M.; Brimble, M. A. C–H Functionalization in the Synthesis of Amino Acids and Peptides. *Chem. Rev.* **2014**, *114* (18), 8775–8806. b) He, G.; Wang, B.; Nack, W. A.; Chen, G. Syntheses and Transformations of α-Amino Acids via Palladium-Catalyzed Auxiliary-Directed Sp ^{3} C–H Functionalization. *Acc. Chem. Res.* **2016**, *49* (4), 635–645. c) Brandhofer, T.; García Mancheño, O. Site-Selective C-H Bond Activation/Functionalization of Alpha-Amino Acids and Peptide-Like Derivatives. *Euro. J. Org. Chem.* **2018**, *2018* (44), 6050–6067.

[71] Zhang, G.; Zhang, Y.; Wang, R. Catalytic Asymmetric Activation of a C Sp 3□H Bond Adjacent to a Nitrogen Atom: A Versatile Approach to Optically Active α-Alkyl α-Amino Acids and C1-Alkylated Tetrahydroisoquinoline Derivatives. *Angew. Chemie Int. Ed.* **2011**, *50* (44), 10429–10432.

Enantioselective α-C-H functionalizations have largely remained elusive with the exception of one Michael addition of β-keto esters and one arylation detailed in Figure 1.21.[72,73]

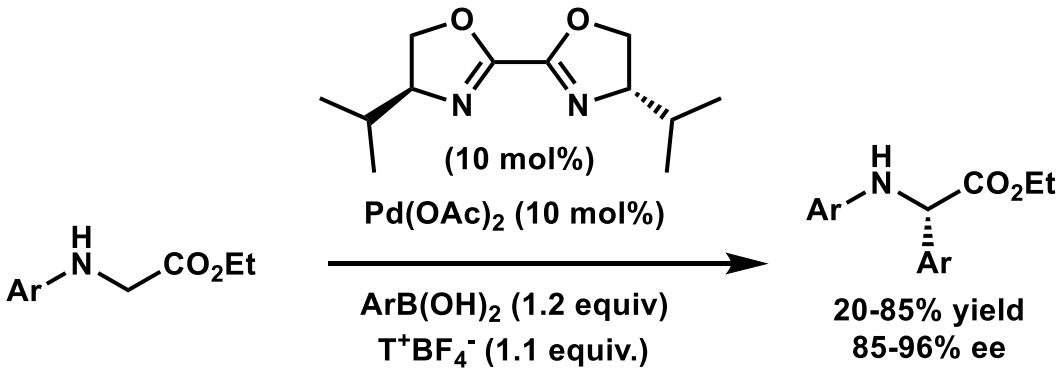

Figure 1.21 Aryl amino acids via chiral C-H oxidative cross-coupling

While controlling enantioselective C-H oxidation at the α-position is challenging, side-chain functionalization is especially appealing, as the stereocenter is already set in the starting material. Palladium catalysis has emerged as the primary tool for performing side-chain functionalization. Palladium catalyzed Csp^2-H functionalizations were developed first, and Yu applied this to the acetoxylation of phenylalanine in 2010.[74] The ability to functionalize alanine would allow for the construction of a wide array of enantiopure amino acids. Thus, as the palladium catalyzed field evolved to allow for Csp^3-H functionalizations, Daugulis applied two different directing group strategies to affect alanine mono- and di-arylation, including in the presence of functionalizable Csp^2-H bonds.[75] Chen demonstrated that this strategy could be applied to perform diastereoselective arylations with longer aliphatic side chains, as well as expand the scope to

[72] Wei, X.-H.; Wang, G.-W.; Yang, S.-D. Enantioselective Synthesis of Arylglycine Derivatives by Direct C–H Oxidative Cross-Coupling. *Chem. Commun.* **2015**, *51* (5), 832–835.

[73] Vickers, C. J.; Mei, T.-S.; Yu, J.-Q. Pd(II)-Catalyzed *o*-C−H Acetoxylation of Phenylalanine and Ephedrine Derivatives with MeCOOO ^{t}-Bu/Ac_2O. *Org. Lett.* **2010**, *12* (11), 2511–2513.

[74] Vickers, C. J.; Mei, T.-S.; Yu, J.-Q. Pd(II)-Catalyzed *o* -C−H Acetoxylation of Phenylalanine and Ephedrine Derivatives with MeCOOO ^{t} Bu/Ac $_2$ O. *Org. Lett.* **2010**, *12* (11), 2511–2513.

[75] Tran, L. D.; Daugulis, O. Nonnatural Amino Acid Synthesis by Using Carbon-Hydrogen Bond Functionalization Methodology. *Angew. Chemie Int. Ed.* **2012**, *51* (21), 5188–5191.

vinylations of alanine, with electronically biased vinyl iodides.[76,77] Yu reported the same palladium catalyst, with pyrimidine ligands, which enable directing group free selective mono- and di-arylation, the diarylated products are produced in high d.r. (Figure 1.22 A).[78] Yu has been able to translate this chemistry into an enantioselective context by employing chiral palladium ligand complexes to desymmetrize 2-aminoisobutyric acid derivatives, which produce α-benzyl-α-methyl amino acids in high enantioselectivities (Figure 1.22 B).[79]

[76] Zhang, S.-Y.; Li, Q.; He, G.; Nack, W. A.; Chen, G. Stereoselective Synthesis of β-Alkylated α-Amino Acids via Palladium-Catalyzed Alkylation of Unactivated Methylene C(Sp ^{3})–H Bonds with Primary Alkyl Halides. *J. Am. Chem. Soc.* **2013**, *135* (32), 12135–12141.

[77] Wang, B.; Lu, C.; Zhang, S.-Y.; He, G.; Nack, W. A.; Chen, G. Palladium-Catalyzed Stereoretentive Olefination of Unactivated C(Sp ^{3})–H Bonds with Vinyl Iodides at Room Temperature: Synthesis of β-Vinyl α-Amino Acids. *Org. Lett.* **2014**, *16* (23), 6260–6263.

[78] He, J.; Li, S.; Deng, Y.; Fu, H.; Laforteza, B. N.; Spangler, J. E.; Homs, A.; Yu, J.-Q. Ligand-Controlled C(Sp^3)-H Arylation and Olefination in Synthesis of Unnatural Chiral α-Amino Acids. *Science* **2014**, *343* (6176), 1216–1220.

[79] Wu, Q.-F.; Shen, P.-X.; He, J.; Wang, X.-B.; Zhang, F.; Shao, Q.; Zhu, R.-Y.; Mapelli, C.; Qiao, J. X.; Poss, M. A.; et al. Formation of α-Chiral Centers by Asymmetric β-C(Sp3)-H Arylation, Alkenylation, and Alkynylation. *Science* **2017**, *355* (6324), 499–503.

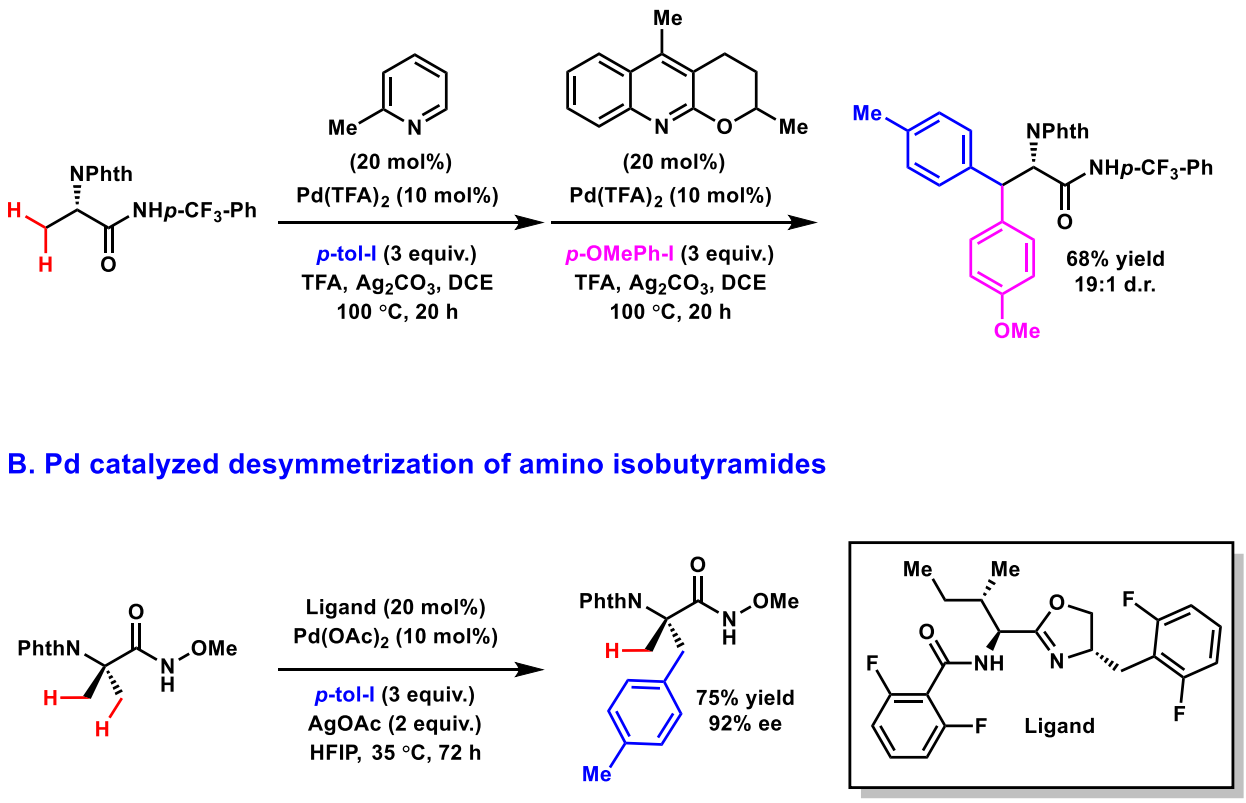

Figure 1.22 Pd catalyzed β-C(sp^3)-H arylations in the synthesis of unnatural amino acids

1.8 Outlook on remaining challenges in amino acid synthesis

The synthesis of enantioenriched amino acids is a mature field in both chiral auxiliary and catalytic enantioselective contexts. While many classes of amino acids can be synthesized with high yields and enantioselectivities via a number of disconnections, there are a few outstanding problems in this field.

The first is the need for methods with easily cleavable nitrogen protecting groups; many syntheses introduce sensitive functionalities that can decompose and have enolizable α-protons, which can racemize under protecting group removal.

The second is general syntheses of β-branched amino acids. Traditionally the only viable disconnection to β-branched amino acids without installing the β-stereocenter in a previous step is certain hydrogenative methods (which require the synthesis of diastereomerically pure enamines)

and imine nucleophilic additions, which have only limited examples and struggle to achieve catalyst controlled high enantio- and diastereoselectivity. The proclivity for palladacycles to form five membered ring C-H activation transition states allows for selective β-C-H functionalization. These methods elegantly simplify the problem of setting two stereocenters enantioselectively and diastereoselectively to the much easier task of achieving β-diastereocontrol relative to the naturally occurring α-stereocenter. While these methods have made great progress in facilitating β-arylation and in some cases halogenation, future methods should focus on diversifying the bonds that can be constructed in this way.

The final remaining challenge is general syntheses of α,α-disubstituted amino acid synthesis. When one of the α-groups is methyl, there are a number of ways to set this stereocenter. However, when neither group is methyl, there are relatively few methods to make these products and the ones that exist rely on complicated protecting or chiral auxiliary groups.

Chapter 2

Enantioselective Synthesis of α-Allyl and α-Aryl Amino Esters via Hydrogen-Bond-Donor Catalysis

2.1 Introduction: applications of α-allyl amino acids

α-Amino acids are essential building blocks in the fields of chemistry and biology. Non-proteinogenic amino acids, especially those that cannot be made via post-translational modification, are, by definition, not produced abundantly in nature, and thus methods for their syntheses are of high value.[4,80] Among the many classes of unnatural amino acids devised by synthetic chemists, α-allyl amino acids have proven particularly valuable in a wide variety of contexts. These building blocks not only map onto biologically active molecules, but also the allyl group provides a versatile handle that can be further functionalized. The alkenyl functional handle in these building blocks can be elaborated for site-selective protein modification,[81,82] preparation of

[80] For reviews on asymmetric catalystic amino acid synthesis see: a) Yamashita, Y.; Kobayashi, S. Catalytic Asymmetric Synthesis of α-Amino Acid Derivatives: Approaches toward Green Sustainable Methodology for Preparation of Optically Active Amino Acids. *Asymmetric Synth. Appl. of-Amino Acids ACS Symp. Ser.* **2009**. b) Ma, J.-A. Recent Developments in the Catalytic Asymmetric Synthesis of α- and β-Amino Acids. *Angew. Chemie Int. Ed.* **2003**, *42* (36), 4290–4299.

[81] For reviews on applications of unnatural amino acids see: a) Lin, Y. A.; Chalker, J. M.; Davis, B. G. Olefin Metathesis for Site-Selective Protein Modification. *ChemBioChem* **2009**, *10* (6), 959–969. b) Lang, K.; W. Chin, J. Bioorthogonal Reactions for Labeling Proteins. *ACS Chem. Biol.* **2014**, *9* (1), 16–20. c)deGruyter, J. N.; R. Malins, L.; S. Baran, P. Residue-Specific Peptide Modification: A Chemist's Guide. *Biochemistry* **2017**, *56* (30), 3863–3873.

[82] A. Lin, Y.; M. Chalker, J.; Floyd, N.; J. L. Bernardes, G.; G. Davis, B. Allyl Sulfides Are Privileged Substrates in Aqueous Cross-Metathesis: Application to Site-Selective Protein Modification. *J. Am. Chem. Soc.* **2008**, *130* (30), 9642–9643.

glycopeptides,[83] or generation of peptide staples[84] and macrocycles. Noteworthy applications include construction of all-carbon analogs of disulfide-bridged macrocyclic peptides such as oxytocin,[85] and thioether-bridged lantibiotics such as nisin.[86] Disulfide bridges are important in stabilizing secondary and tertiary protein structure; however they are a reductive liabilities. Thus these "dicarba analogs" have been shown to have similar levels of activity as the parent compounds, but with longer half-life *in vivo.* Additionally, the allyl group provides a biorthogonal handle that has been shown to participate in cross-metathesis for the labeling of proteins in *in vitro* studies.[81,82]

[83] J. McGarvey, G.; E. Benedum, T.; W. Schmidtmann, F. Development of Co- and Post-Translational Synthetic Strategies to C-Neoglycopeptides. *Org. Lett.* **2002**, *4* (21), 3591–3594.

[84] For a review on peptide staples see: a) Verdine, G. L.; Hilinski, G. J. Stapled Peptides for Intracellular Drug Targets. *Methods Enzymol.* **2012**, *503*, 3–33. For a lead reference see: b) Kim, Y.-W.; Grossmann, T. N.; Verdine, G. L. Synthesis of All-Hydrocarbon Stapled α-Helical Peptides by Ring-Closing Olefin Metathesis. *Nat. Protoc.* **2011**, *6* (6), 761–771.

[85] a) L. Stymiest, J.; F. Mitchell, B.; Wong, S.; C. Vederas, J. Synthesis of Biologically Active Dicarba Analogues of the Peptide Hormone Oxytocin Using Ring-Closing Metathesis. *Org. Lett.* **2002**, *5* (1), 47–49. b) L. Stymiest, J.; F. Mitchell, B.; Wong, S.; C. Vederas, J. Synthesis of Oxytocin Analogues with Replacement of Sulfur by Carbon Gives Potent Antagonists with Increased Stability. *J. Org. Chem.* **2005**, *70* (20), 7799–7809.

[86] Ghalit, N.; Reichwein, J. F.; Hilbers, H. W.; Breukink, E.; Rijkers, D. T. S.; Liskamp, R. M. J. Synthesis of Bicyclic Alkene-/Alkane-Bridged Nisin Mimics by Ring-Closing Metathesis and Their Biochemical Evaluation as Lipid II Binders: Toward the Design of Potential Novel Antibiotics. *ChemBioChem* **2007**, *8* (13), 1540–1554.

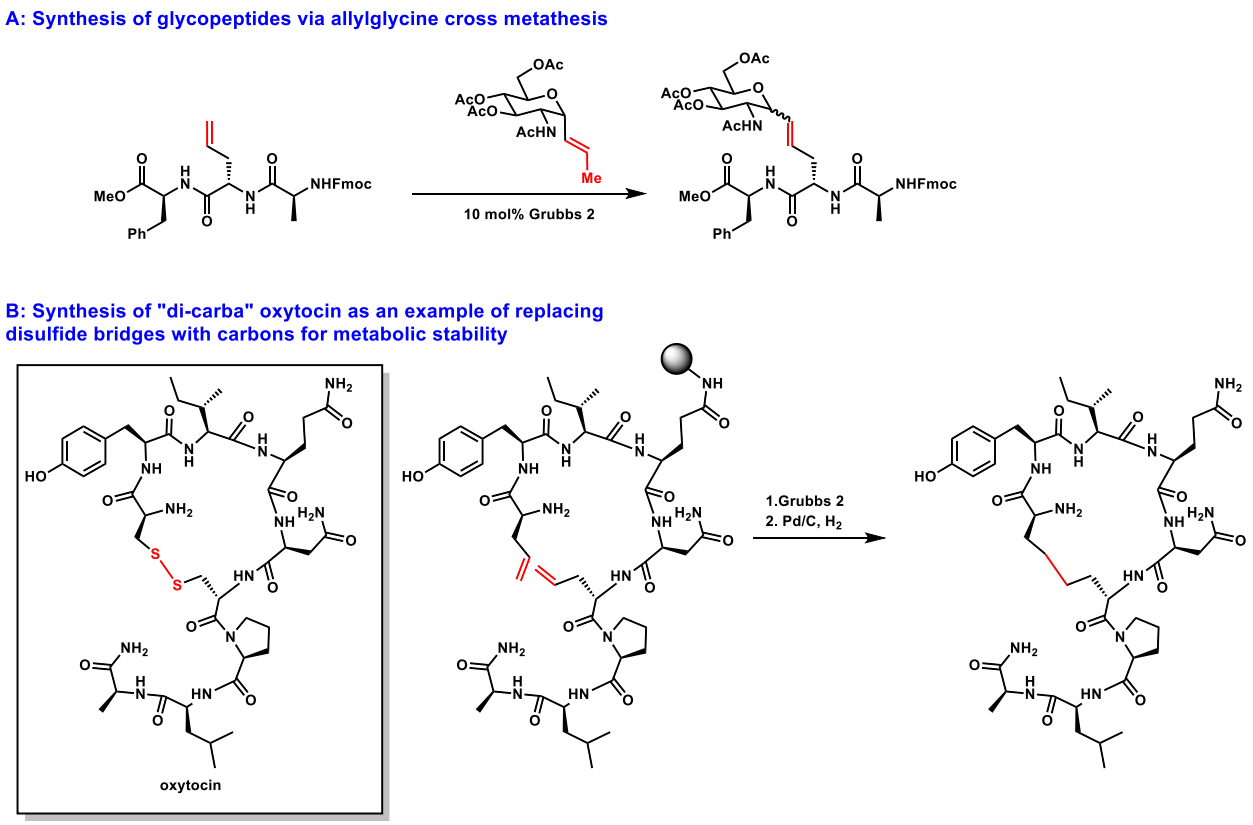

Figure 2.1 Select applications of α-allyl glycine

2.2 Methods for of the syntheses of enantioenriched α-allyl amino acids

An overview on modern methods for enantioselective syntheses of amino acids was provided in Chapter 1, so a briefly highlight of the syntheses relevant to the enantioselective synthesis of α-allyl amino acids and their strengths and weaknesses will be presented here. As a result of their broad utility, α-allyl amino acids have been targets of widespread synthetic effort in both chiral auxiliary and catalytic enantioselective contexts.

In the context of enolate alkylation (Chapter 1.5.2) the Myers auxiliary has proven to be particularly useful in the highly diastereoselective synthesis of α-allyl and in limited cases α-alkyl-α-allyl amino acids.[40] Umpolung to that approach, in the context of glycinimine additions (Chapter 1.5.3), the Ellman auxiliary has proven to be particularly useful in the highly diastereoselective synthesis of α-allyl amino acids.[53,54]

As discussed in Chapter 1.5.2, among catalytic approaches, the phase-transfer-catalyzed (PTC) allylation of Schiff base, ester enolates was pioneered by O'Donnell[41–43] (Scheme 1A) and advanced to the current state-of-the-art by Maruoka through the discovery of highly effective, C_2 symmetric, quaternary ammonium salt catalysts (Figure 2.2 A).[44,45] This methodology provides access to unbranched α-allyl amino esters, but the preparation of branched products via PTC is generally not possible. Approaches involving transition-metal π-allyl intermediates have also been developed, but preparing branched products is hampered by requiring substitution to occur on a hindered electrophilic partner, which is possible in limited cinnamyl contexts employing iridium and molybdenum catalysis.[48–50,87] More effective approaches require the preparation of glycine allyl esters, which undergo enantioselective Claisen[63–66] rearrangements that are superstoichiometric in chiral information or the preparation of allylic ammonium ylides, which undergo [2,3]-sigmatropic rearrangements to afford cinnamylated products[67–69] (Chapter 1.6).

The coupling of nucleophilic allylating agents with α-imino esters allows for the stereocontrolled construction of β-branched-α-allyl amino acid derivatives (Chapter 1.5.3). Lectka and Jørgensen simultaneously and independently published Lewis-acid-catalyzed allylations of *N*-tosyl α-imino esters using chiral copper complexes (Figure 2.2 B).[58] While these methods stand out in their ability to synthesize β-branched-α-allyl amino acids in high enantio- and diastereoselectivies, they are single reports and suffer from limited nucleophile scope, having to preform hydrolytically unstable *N*-tosyl α-imino esters, and challenging removal of tosyl amine protecting groups to unveil the amino acid products. Additions to α-hydrozono esters has also been accomplished by Kobayashi in excellent enantio- and diastereocontrol, however these methods

[87] Huo, X.; He, R.; Fu, J.; Zhang, J.; Yang, G.; Zhang, W. Stereoselective and Site-Specific Allylic Alkylation of Amino Acids and Small Peptides via a Pd/Cu Dual Catalysis. *J. Am. Chem. Soc.* **2017**, *139* (29), 9819–9822.

require superstoichiometric chiral ligand and furnish alkylhydrazine products, which are also recalcitrant to mild cleavage methods.[59]

2.3 Development of hydrogen-bond donor catalyzed synthesis of α-allyl amino esters[88]

Inspired by the enantioselective copper catalyzed synthesis of α-allyl amino esters, a new approach was envisioned, involving nucleophilic allylation of α-halo amino esters catalyzed by chiral hydrogen-bond-donor (HBD) catalysts (Figure 2.2 C).

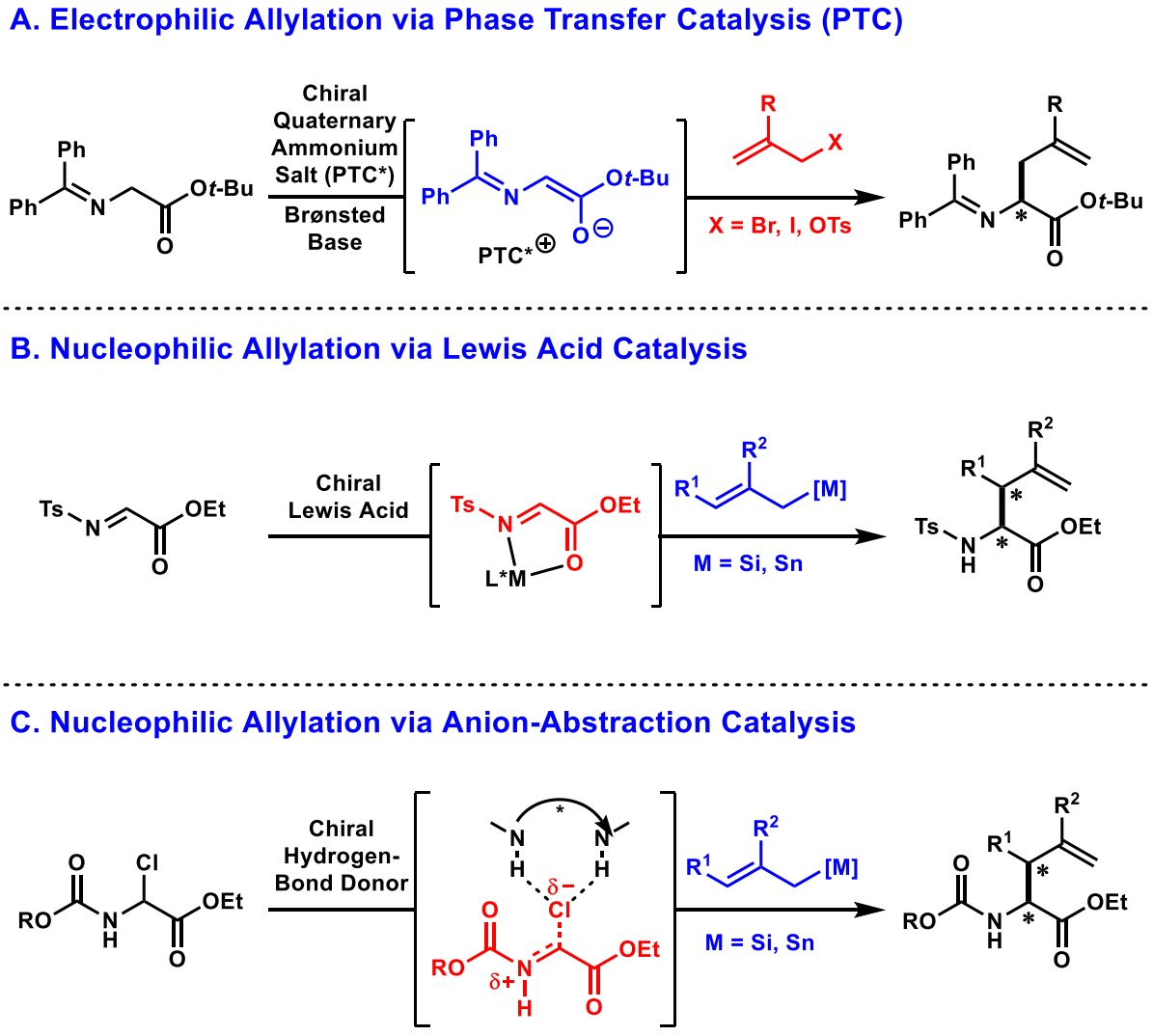

Figure 2.2 Summary of enantioselective methods for the synthesis of α-allyl amino esters

[88] Portions of this will appear in Bendelsmith, A. J.; Kim, S. C.; Wasa, M.; Roche, S. P.; Jabosen, E. N. Enantioselective Synthesis of α-Allyl Amino Esters via Hydrogen-Bond-Donor Catalysis. *J. Am. Chem. Soc. Submitted.*

The proposed strategy benefits from the ready accessibility of *N*-carbamoyl α-chloro amino esters as α-imino ester equivalents.[89,90] The Roche group has reported two simple procedures for the synthesis of ethyl 2-(((benzyloxy)carbonyl)amino)-2-chloroacetate (Figure 2.3 **1-Cbz**). The first is a one-pot, zero purification AcOH catalyzed three component coupling of benzyl carbamate, ethyl glyoxylate and acetylchloride (Figure 2.3 A). The second is a two-step procedure in which ethyl glyoxylate and benzyl carbamate are condensed with acetic acid as a catalyst to afford ethyl 2-(((benzyloxy)carbonyl)amino)-2-hydroxyacetate (**1-Cbz-OH**), which can be purified via recrystallization from 1:1 DCM:hexanes. **1-Cbz-OH** can be deoxychlorinated with 5 equivalents of thionyl chloride to afford **1-Cbz** with no further purification (Figure 2.3 B). All studies were performed with the two-step procedure for ease of purification and storage of the hemiaminal, although equivalent results are obtained through the one-step procedure.

A: 1-step procedure of the synthesis of 1-Cbz

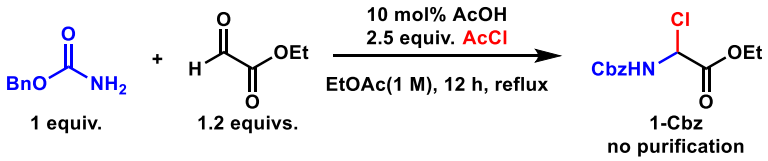

B: 2-step procedure of the synthesis of 1-Cbz

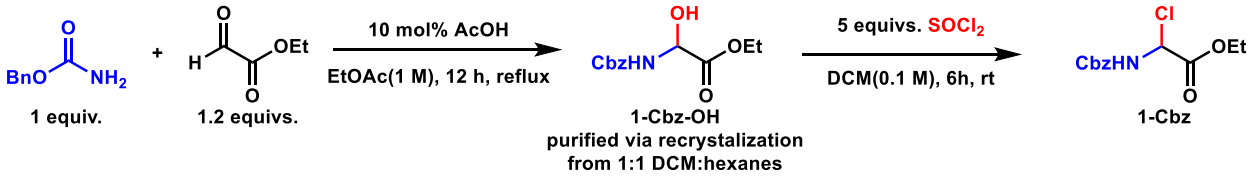

Figure 2.3 synthesis of the substrate **1-Cbz**

[89] a) Roche, S. P.; Samanta, S. S.; Gosselin, M. M. J. Autocatalytic One Pot Orchestration for the Synthesis of α-Arylated, α-Amino Esters. *Chem. Commun.* **2014**, *50* (20), 2632–2634. b) Samanta, S. S.; P. Roche, S. In Situ-Generated Glycinyl Chloroaminals for a One-Pot Synthesis of Non-Proteinogenic α-Amino Esters. *J. Org. Chem.* **2017**, *82* (16), 8514–8526.

[90] For an HBD catalyzed Mannich addition to **1-Cbz** see: Wasa, M.; Y. Liu, R.; P. Roche, S.; N. Jacobsen, E. Asymmetric Mannich Synthesis of α-Amino Esters by Anion-Binding Catalysis. *J. Am. Chem. Soc.* **2014**, *136* (37), 12872–12875.

The products resulting from the proposed nucleophilic allylation protocol would possess readily cleavable carbamate protecting groups, facilitating further synthetic manipulations.[91] In this Chapter, the highly enantioselective and diastereoselective synthesis of α-allyl amino esters via anion-abstraction catalyzed addition of allylsilane and allylstannane nucleophiles to the *N*-carbamoyl-α-chloro amino esters **1-Cbz** and **1-Fmoc** will be discussed.

2.3.1 Catalyst optimization studies

The allylation of α-chloro glycinate **1-Cbz** with 2-methallyltrimethylsilane was selected as a model reaction for catalyst optimization (Figure 2.4 B). A prior report from the Jacobsen lab detailed the highly enantioselective Mannich addition of 1,3-dicarbonyls and β-ketoesters to the same electrophile **1-Cbz**, catalyzed by Takemoto's thiourea (Figure 2.4 A).[90] When using Takemoto's thiourea in the methallylation of **1-Cbz**, only trace conversion is observed to exclusively hydrolysis product **1-Cbz-OH**.

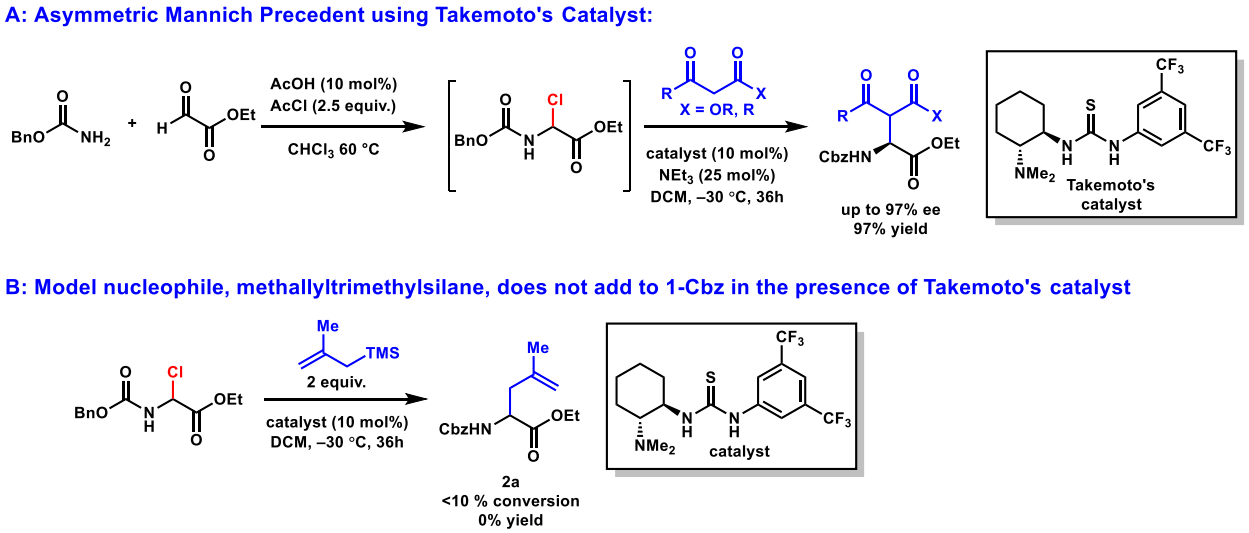

Figure 2.4 Comparison of Takemoto's catalyst in Mannich versus methallylsilane addition

[91] Wuts, P. G. M.; Greene, T. W. *Greene's Protective Groups in Organic Synthesis*; John Wiley & Sons, Inc.: Hoboken, NJ, USA, 2006.

The difference in reactivity with Takemoto's catalyst could stem from the vastly different nucleophilicities between 1,3-diketone enolates (N = 17.46 for 1,3-diphenylpropane-1,3-dione enolate)[92] and methallylsilanes (N = 4.41 for methallyltrimethylsilane), differing by 13 orders of magnitude.[93] Therefore, it was hypothesized that 3,5-bistrifluoromethylaniline (Half-Schreiner) derived squaramides, which are substantially better anion-abstractors may affect substitution with methallylsilane.[94] A comparison of different classes of half-Schreiner H-bond donors was conducted using 2-(9-phenanthryl)pyrrolidino amide catalysts, **3e-7e** as representative of the emerging privileged class of arylpyrrolidine amido catalysts. This study identified squaramides as optimal for the allylation of α-chloro amino ester **1-Cbz** (Figure 2.5).[95] Squaramide **4e** afforded the product in both higher yield and selectivity than the analogous urea **6e** and thiourea **7e**, the latter of which provided no conversion. Reactions not at full conversion at 36 hours are still cleanly producing product and thus yields are indicative of reaction rate. While squaramide hydrogen-bond donors are substantially more acidic and stronger chloride binders than ureas and thioureas,

[92] Corral-Bautista, F.; Appel, R.; Frickel, J. S.; Mayr, H. Quantification of Ion-Pairing Effects on the Nucleophilic Reactivities of Benzoyl- and Phenyl-Substituted Carbanions in Dimethylsulfoxide. *Chem. - A Eur. J.* **2015**, *21* (2), 875–884.

[93] Mayr, H.; Bug, T.; F. Gotta, M.; Hering, N.; Irrgang, B.; Janker, B.; Kempf, B.; Loos, R.; R. Ofial, A.; Remennikov, G.; et al. Reference Scales for the Characterization of Cationic Electrophiles and Neutral Nucleophiles,. *J. Am. Chem. Soc.* **2001**, *123* (39), 9500–9512.

[94] For a detailed study on the relationship between HBD arene substituents and anion-binding strength see: Rötheli, A. R. A Mechanistic Approach Towards Highly Efficient Anion-Binding Catalysts. **2016** Ph.D. Thesis, Harvard University

[95] For a chloride binding reaction using arylpyrrolidine squaramide catalysts see: Zhang, H.; Lin, S.; N. Jacobsen, E. Enantioselective Selenocyclization via Dynamic Kinetic Resolution of Seleniranium Ions by Hydrogen-Bond Donor Catalysts. *J. Am. Chem. Soc.* **2014**, *136* (47), 16485–16488.

there are limited examples of Cl-abstraction reactions in which squaramides are the optimal class of catalysts.[96]

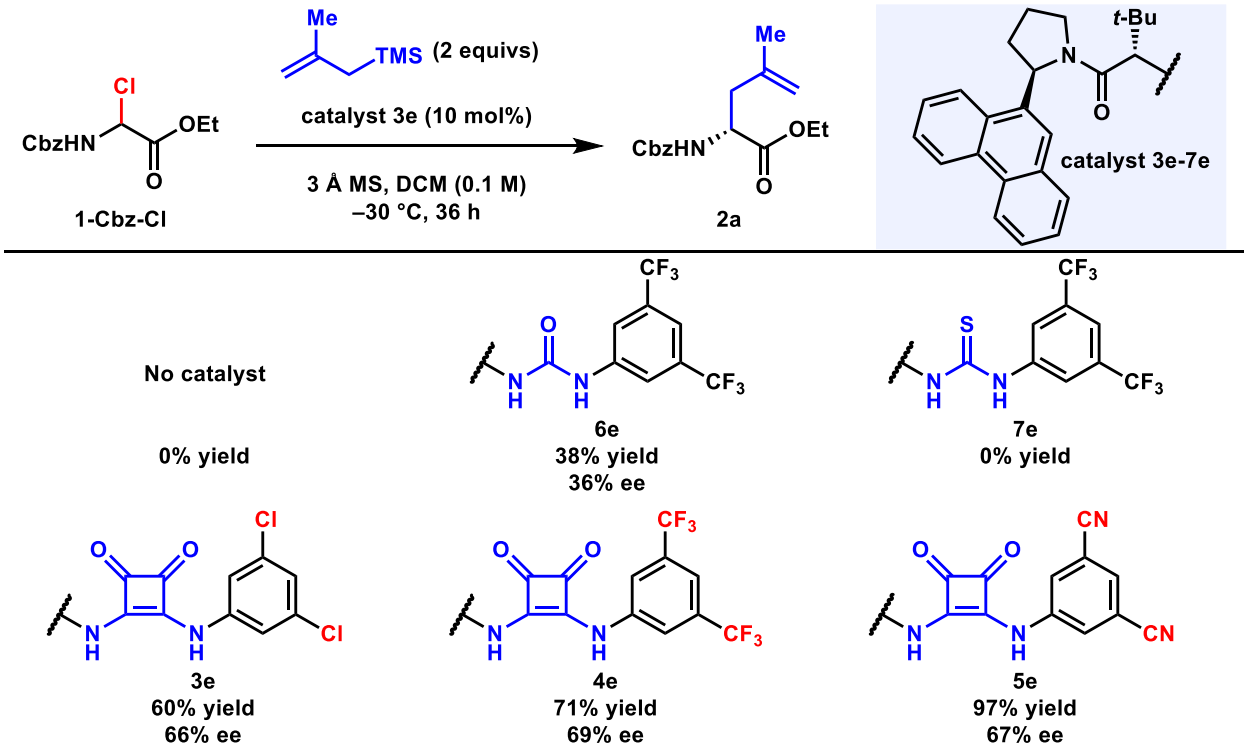

Figure 2.5 Stronger, more acidic HBDs are more effective catalysts in the allylation of **1-Cbz**

One hypothesis is that squaramides are optimal because chloride-abstraction α to an ester may require a large degree of C–Cl bond breaking to be activated sufficiently to engage in substitution with weak intermolecular allylsilane nucleophiles. To probe this line of reasoning, the reaction was performed with a series of 3,5-disubstited arylsquaramide catalysts (**3e-5e**) with a range of electron deficient substituents. Arene substitution has been shown to modulate the acidity

[96] For a series of reports on the increased strength of squaramide catalysts and their use in catalytic transformations see: a) Auvil, T. J.; Schafer, A. G.; Mattson, A. E. Design Strategies for Enhanced Hydrogen-Bond Donor Catalysts. *European J. Org. Chem.* **2014**, *2014* (13), 2633–2646. b) Alemán, J.; Parra, A.; Jiang, H.; Jørgensen, K. A. Squaramides: Bridging from Molecular Recognition to Bifunctional Organocatalysis. *Chem. - A Eur. J.* **2011**, *17* (25), 6890–6899. c) Amendola, V.; Fabbrizzi, L.; Mosca, L.; Schmidtchen, F.-P. Urea-, Squaramide-, and Sulfonamide-Based Anion Receptors: A Thermodynamic Study. *Chem. - A Eur. J.* **2011**, *17* (21), 5972–5981. d) Amendola, V.; Bergamaschi, G.; Boiocchi, M.; Fabbrizzi, L.; Milani, M. The Squaramide versus Urea Contest for Anion Recognition. *Chem. - A Eur. J.* **2010**, *16* (14), 4368–4380. e) Lu, T.; Wheeler, S. E. Origin of the Superior Performance of (Thio)Squaramides over (Thio)Ureas in Organocatalysis. *Chem. - A Eur. J.* **2013**, *19* (45), 15141–15147.

and thus the chloride-binding strength of the hydrogen-bond donor.[97] The yield of product **2a** increases from 60% with 3e (Cl: $\sigma_m = 0.37$), to 71% with 4e (CF3: $\sigma_m = 0.43$), up to 97% with 5e (CN: $\sigma_m = 0.56$), indicating this reaction is most efficiently catalyzed by potent anion-binding catalysts.[98]

An extensive survey of chiral dual-hydrogen-bond-donors revealed that arylpyrrolidinosquaramides **4a-g** (Figure 2.6 A) catalyzed the formation of **2a** with promising levels of enantiocontrol. As observed previously in reactions involving stabilized cationic intermediates, enantioselectivity was strongly responsive to the polarizability of the arene substituent on the pyrrolidine.[99] Such effects have been ascribed to stabilizing π interactions between the catalyst and positively charged intermediates and/or transition states, in which the diastereomeric transition state leading to the major product is stabilized preferentially. However, arene polarizability alone does not account for the effects on reaction enantioselectivity in the

[97] For a series of reports exploring effects of catalyst acidity and activity see: a) Hine, J.; Linden, S. M.; Kanagasabapathy, V. M. 1,8-Biphenylenediol Is a Double-Hydrogen-Bonding Catalyst for Reaction of an Epoxide with a Nucleophile. *J. Am. Chem. Soc.* **1985**, *107* (4), 1082–1083. b) Okino, T.; Hoashi, Y.; Takemoto*, Y. Enantioselective Michael Reaction of Malonates to Nitroolefins Catalyzed by Bifunctional Organocatalysts. *J. Am. Chem. Soc.* **2003**, *125* (42), 12672–12673. c) Wittkopp, A.; Schreiner, P. R. Metal-Free, Noncovalent Catalysis of Diels–Alder Reactions by Neutral Hydrogen Bond Donors in Organic Solvents and in Water. *Chem. Eur. J.* **2003**, *9* (2), 407–414. d) Jensen, K. H.; Sigman, M. S. Systematically Probing the Effect of Catalyst Acidity in a Hydrogen-Bond-Catalyzed Enantioselective Reaction. *Angew. Chemie Int. Ed.* **2007**, *46* (25), 4748–4750. e) Jensen, K. H.; Sigman, M. S. Evaluation of Catalyst Acidity and Substrate Electronic Effects in a Hydrogen Bond-Catalyzed Enantioselective Reaction. *J. Org. Chem.* **2010**, *75* (21), 7194–7201.

[98] σ_m values from Hansch, C.; Leo, A.; Taft, R. W. A Survey of Hammett Substituent Constants and Resonance and Field Parameters. *Chem. Rev.* **1991**, *91* (2), 165–195.

[99] For a review of cation-π interactions in small molecule catalysis see: a) Kennedy, C. R.; Lin, S.; Jacobsen, E. N. The Cation-π Interaction in Small-Molecule Catalysis. *Angew. Chemie Int. Ed.* **2016**, *55* (41), 12596–12624. For examples of HBD reactions characterizing a cation-π interaction see: b) Knowles, R. R.; Lin, S.; N. Jacobsen, E. Enantioselective Thiourea-Catalyzed Cationic Polycyclizations. *J. Am. Chem. Soc.* **2010**, *132* (14), 5030–5032. c) Lin, S.; Jacobsen, E. N. Thiourea-Catalysed Ring Opening of Episulfonium Ions with Indole Derivatives by Means of Stabilizing Non-Covalent Interactions. *Nat. Chem.* **2012**, *4* (10), 817–824.

allylation reaction (Figure 2.6 B).[100] The point of attachment of the arene to the pyrrolidine is also important, with arenes bearing ring-fusion ortho to the pyrrolidine group affording lower enantioselectivity. Such sensitivity to the spatial disposition of the aryl group is consistent with a highly ordered network of attractive non-covalent interactions in the enantioselectivity-determining transition state assembly. [99]

[100] Arene polarizabilites come from: Waite, J.; Papadopoulos, M. G.; Nicolaides, C. A. Calculations of Induced Moments in Large Molecules. III. Polarizabilities and Second Hyperpolarizabilities of Some Aromatics. *J. Chem. Phys.* **1982**, *77* (5), 2536–2539.

A.

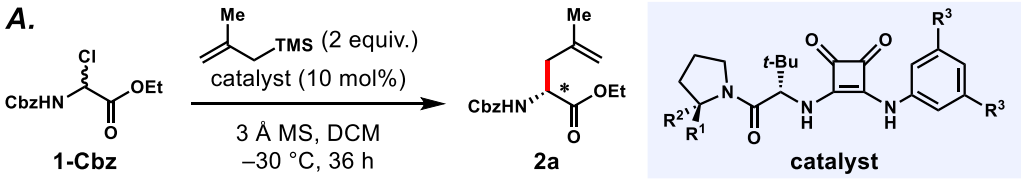

Entry	R^1	R^2	R^3	yield (%)	ee (%)
1	**Phenyl (4a)**	H	CF_3	50	52
2	**1-Naphthyl (4b)**	H	CF_3	49	56
3	**2-Naphthyl (4c)**	H	CF_3	58	71
4	**3-Phenanthryl (4d)**	H	CF_3	78	86
5	**9-Phenanthryl (4e)**	H	CF_3	73	74
6	**1-Pyrenyl (4f)**	H	CF_3	75	53
7	**4-Pyrenyl (4g)**	H	CF_3	81	74
8	**Phenyl (4a')**	Me	CF_3	71	85
9	**1-Naphthyl (4b')**	Me	CF_3	71	87
10	**2-Naphthyl (4c')**	Me	CF_3	65	92
11	**3-Phenanthryl (4d')**	Me	CF_3	74	97
12	**9-Phenanthryl (4e')**	Me	CF_3	64	94
13	**3-Phenanthryl (5d')**	Me	CN	94	97

B.

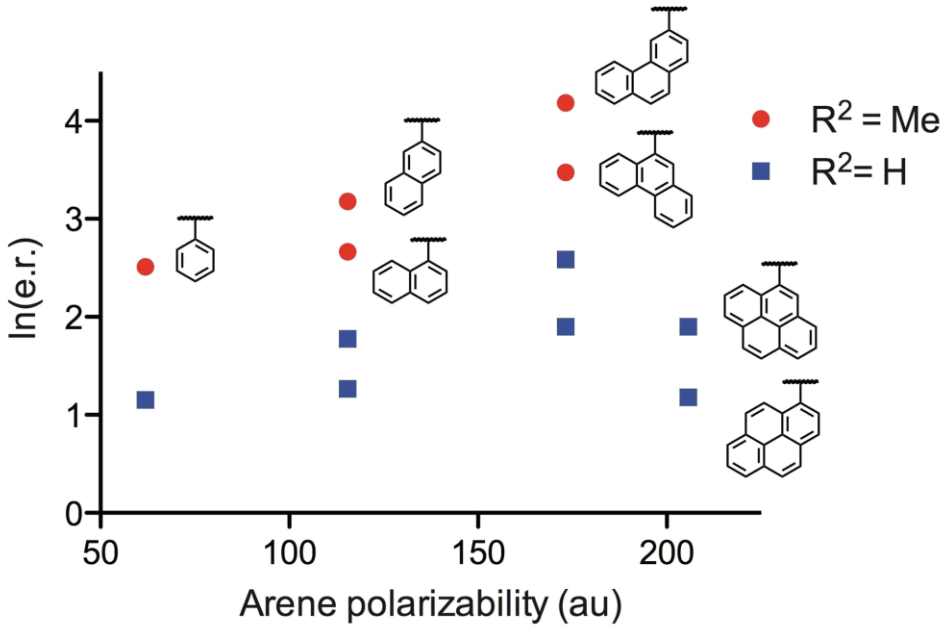

Figure 2.6 (A) Yield and enantioselectivity of **2a** for a series of 2-arylpyrrolidine- and 2-aryl-2-methylpyrrolidine-substituted catalysts. Yields were determined by ^{1}H NMR by integration against an internal standard. (B) Relationship between the enantiomeric ratio of **2a** and the polarizability of the arene substituents on the catalysts **4a**–**4g** (R^2 = H, blue series) and **4a'**–**4e'** (R^2 = Me, red series).

Further evidence for the importance of the conformational properties of the arylpyrrolidine in enantioinduction was provided through the evaluation of 2-aryl-2-methyl-substituted pyrrolidine-derived catalysts. Dual H-bond-donor catalysts bearing such fully substituted arylpyrrolidine derivatives have been found to exist predominantly as the amide (*Z*)-rotamer, whereas the unsubstituted analogs exist as rotameric mixtures (Figure 2.7, also see methods section for rotameric ratios).[101] In the model allylation reaction, catalysts bearing fully substituted arylpyrrolidines (R^2 = Me, **4a'–4e'**, Figure 2.6 B, red circles) all induce higher enantioselectivities than the corresponding un-substituted catalysts (R^2 = H **4a–4e**, Figure 2.6 B, blue squares). A dependence of ee on arene group polarizability and positioning was observed with the fully substituted arylpyrrolidine catalysts similar to that of the unsubstituted catalysts. At this stage it may be concluded that the properties of the arylpyrrolidine have a strong influence on reaction enantioselectivity, but that full elucidation of the bases for these effects and their relative importance will require a sophisticated multiparameter analysis undertaken in Chapter 3.[102] Finally, optimization of the aniline-derived portion of the catalyst optimal for enantioselectivity revealed that the more electron deficient dicyano derivative **5d'** afforded comparable enantioselectivities but substantially improved rates and product yields than the bis-trifluoromethyl derivative **4d'**, as also seen with the suboptimal catalysts **4e** and **5e** (Figure 2.5).

[101] Lehnherr, D.; D. Ford, D.; J. Bendelsmith, A.; Rose Kennedy, C.; N. Jacobsen, E. Conformational Control of Chiral Amido-Thiourea Catalysts Enables Improved Activity and Enantioselectivity. *Org. Lett.* **2016**, *18* (13), 3214–3217.

[102] For a review on multiparameter regression analyses applied to asymmetric catalysis see: Sigman, M. S.; C. Harper, K.; N. Bess, E.; Milo, A. The Development of Multidimensional Analysis Tools for Asymmetric Catalysis and Beyond. *Acc. Chem. Res.* **2016**, *49* (6), 1292–1301.

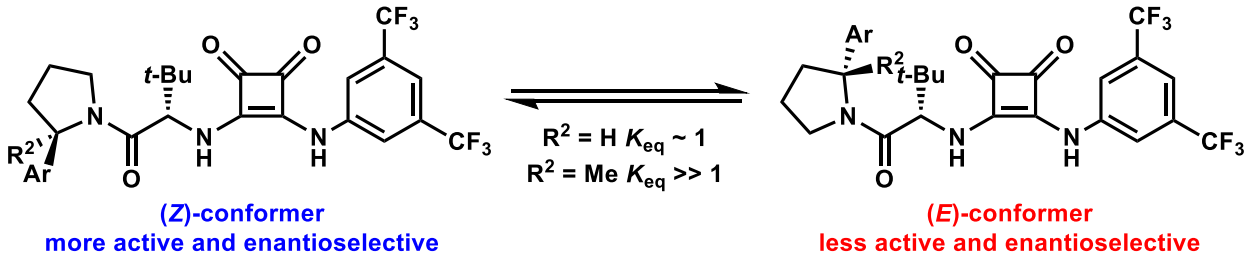

Figure 2.7 Installation of a geminal methyl substituent on the arylpyrrolidine locks the conformation into the more active and enantioselective (*Z*)-conformer

2.3.2 Reaction parameter optimization studies for the addition of methallylsilane to 1-Cbz

Although arypyrrolidine catalysts were found to be optimal in this reaction, other classes of HBD catalysts were investigated (Figure 2.8). As mentioned in section 2.3.1, Takemoto's thiourea was optimal in the Mannich addition of malonates to the same electrophile, **1-Cbz**; however in this reaction this catalyst provides no conversion, even at room temperature, indicating it shuts down an operative racemic reaction at that temperature.[90] One possibility is that the sulfur of the thiourea may be too nucleophilic, and may directly add in to the electrophile to make for an unreactive intermediate that also quenches the catalyst. Since thioureas in general provide no conversion, Takemoto's urea was evaluated and also provided no conversion. To investigate if the basic amine was inhibitory to catalysis, the variant with Ellman's sulfonamide was tested and provided modest yield and enantioselectivity. Since the stronger hydrogen-bond donors, squaramides, were optimal for both yield and enantioselectivity in the formation of **2a**, guanidinium BAr^F catalysts were investigated, which are substantially more acidic and stronger HBD catalysts.[94,103] Guanidinium catalysts provided high levels of reactivity but racemic or near racemic products.

[103] For an enantioselective reaction catalyzed by guanidinium see: a) Uyeda, C.; Jacobsen, E. N. Enantioselective Claisen Rearrangements with a Hydrogen-Bond Donor Catalyst. *J. Am. Chem. Soc.* **2008**, *130* (29), 9228–9229. b) Uyeda, C.; Jacobsen, E. N. Transition-State Charge Stabilization through Multiple Non-Covalent Interactions in the Guanidinium-Catalyzed Enantioselective Claisen Rearrangement. *J. Am. Chem. Soc.* **2011**, *133* (13), 5062–5075.

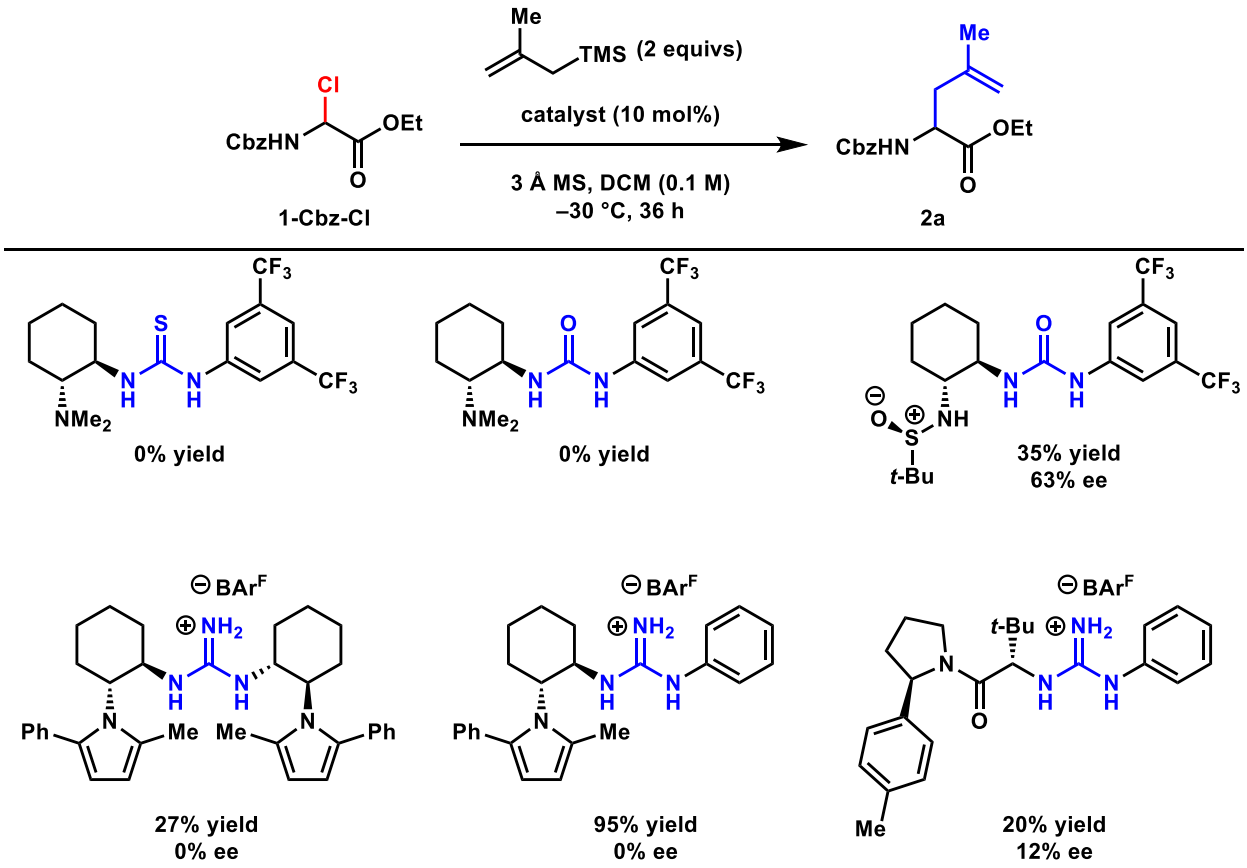

Figure 2.8 Evaluation of cyclohexyldiamine derived and guanidinium HBD catalysts

The electrophile and nucleophile both have a number of handles that can be varied to optimize enantioselectivity without any effect on the scope of the reaction, as they would not end up in the desired amino acid end products. While the optimal set of protecting groups are those reported in section 2.2.1, positions that were systematically varied include the carbamate protecting group, ester protecting group, and allylsilane silyl substituents. The order in which these were optimized predate identification of the optimal catalyst, so many are run with the optimal catalyst at the time, 9-phenanthrylpyrrolidino squaramide catalyst **4e**.

A variety of 2-methylallylsilanes were examined and trimethylsilyl (TMS) was found to be the optimal group on the allylsilane for enantioselectivity (Figure 2.9). TBS provided similar levels of reactivity and slightly diminished enantioselectivity. TES and TIPS were nearly

unreactive and the product that was recovered was the adduct in which the chloride had added into the β-silylcarbocation, rather than the standard eliminated allyl product.

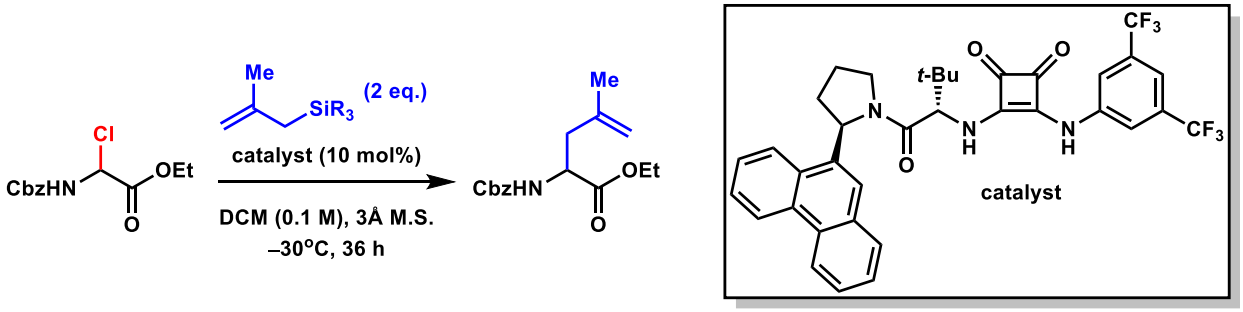

nucleophile	yield (%)	ee (%)
Me, TMS	75	70
Me, TBS	85	60
Me, TES	<10	NA
Me, TIPS	<10	NA

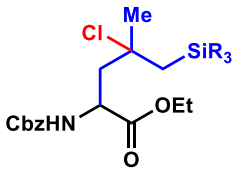

Recovered product

Figure 2.9 Effect of silyl group identity on enantioselectivity and yield in the enantioselective methallylation of **1-Cbz**

The *N*-protecting is an optimal handle for tuning enantioselectivity, as a number of carbamates are commercial varying in their steric, electronic, and arene expanse profiles. Thus an extensive range of commercial carbamates were evaluated the enantioselective glycine allylation (Figure 2.10). Carbamates are found to be optimal for reactivity, while amides are unreactive. Among carbamates, those with π-systems appear to be optimal for enantioselectivity, but beyond that there is no obvious trend among the carbamates tested. Cbz was found to be optimal for enantioselectivity by a relatively large margin and nearly optimal for reactivity.

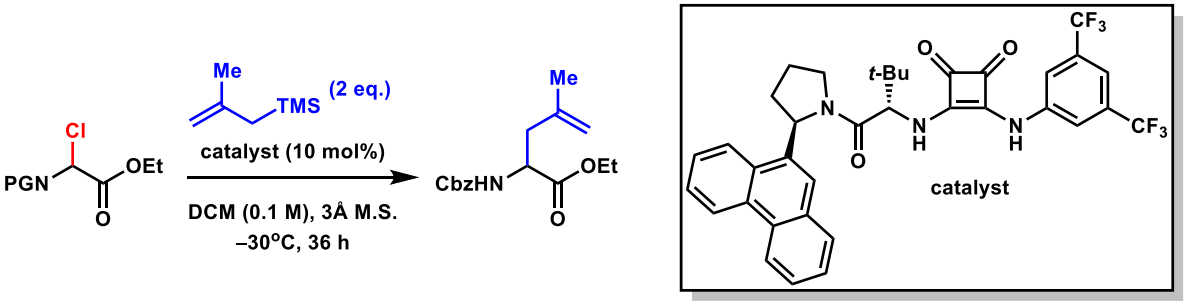

Protecting Group	yield (%)	ee (%)	Protecting Group	yield (%)	ee (%)
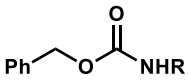	73	74	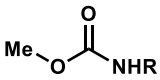	82	12
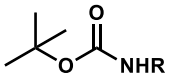	decomp	NA	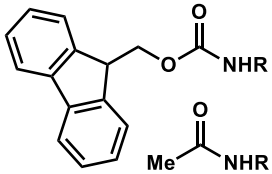	71	62
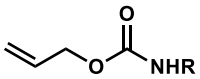	68	51		<5	NA
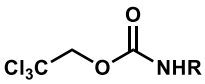	35	24	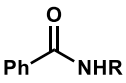	<5	NA

Figure 2.10 Effect of *N*-protecting group identity on enantioselectivity and yield in the enantioselective methallylation of **1-Cbz**

The last substrate handle is the identity of the ester protecting group of **1-Cbz** (Figure 2.11). Methyl and ethyl esters are optimal and provide minimally different results, with ethyl esters giving slightly higher enantioselectivities. Substrates bearing an isopropyl ester are slower to react and provide messier reactions and lower enantioselectivities. The thionyl chloride prep to make **1-Cbz** cleaves *t*-butyl esters, so they could not be tested. Given the sensitivity to arene groups on the catalyst as well as on the carbamate protecting group, it would be interesting to see the effect of a benzyl ester.

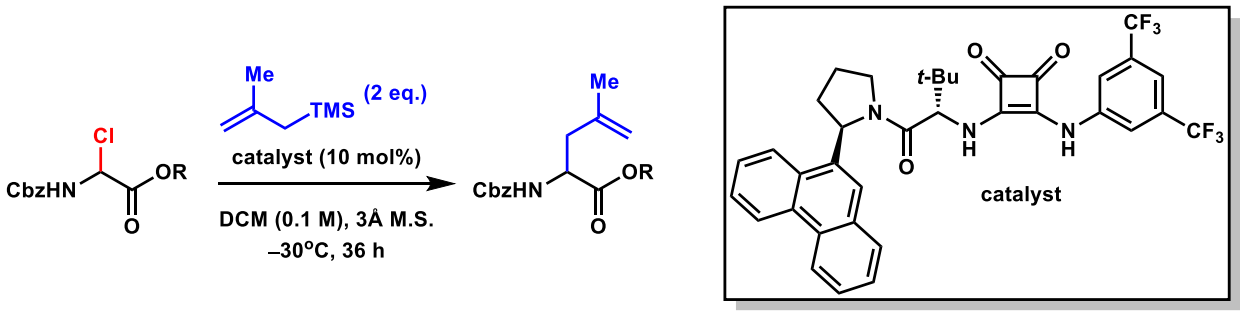

Ester group (R)	yield (%)	ee (%)
Me	75	72
Et	73	74
i-Pr	63	57
t-Bu	$SOCl_2$ prep destroys SM	NA

Figure 2.11 Effect of the ester identity on enantioselectivity and yield in the enantioselective methallylation of **1-Cbz**

Having optimized both the electrophile, nucleophile, and catalyst, the only remaining reaction parameters to optimize are the identity of solvent, molecular sieves, and substrate and catalyst concentrations. Molecular sieves are necessary in this chemistry to achieve reproducibly and consistently high yields. Molecular sieves of different pore size, macroscopic shape (i.e. rod, sphere, and powder), supplier, and activation method were evaluated. As long as molecular sieves have pore size 3 or 4Å, are powdered (as purchased or manually), and are activated in an oven overnight or heated with a propane torch under vacuum the yields and enantioselectivities were highly reproducible.

In an extensive survey of solvents (Figure 2.12), halogenated solvents are by far the best solvents for both reactivity and enantioselectivity. Substrate does not react at –30 °C in the other solvents tested, so the reaction was instead run at 0 °C, which has minimal contribution from

uncatalyzed background reactivity. Ethereal solvents provide enantioselectivities around 80% ee, with aromatic solvents providing slightly lower enantioselectivities at 70% ee. Due to the difference in temperature and differing contributions from racemic background chemistry, it is challenging to determine the most enantioselective solvent under the same conditions in this transformation.

Upon identification of DCM as an optimal solvent, substrate concentration and catalyst loading were varied (Figure. The reaction is relatively insensitive to the reaction concentration, so long as the concentration of catalyst does not drop below .005 M, which allowed the scale-up of **2i**, as discussed in section 2.6, to be run under the relatively concentrated conditions of 0.5 M with minimal catalyst loading of 1 mol%, as reflected in the bottom line of the right-hand table.

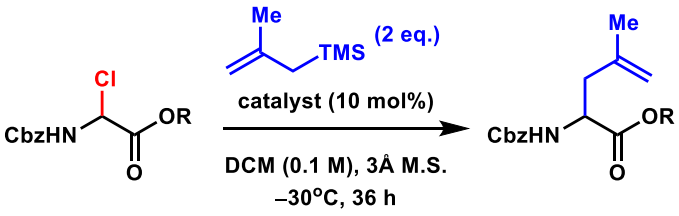

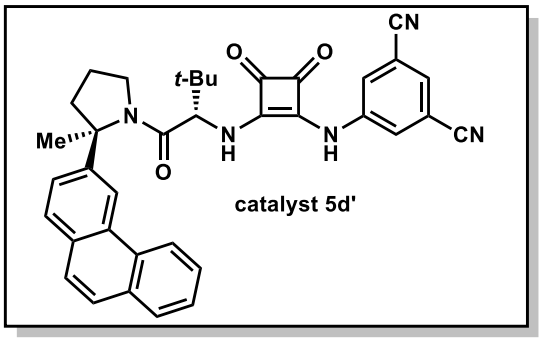

solvent	yield (%)	ee (%)
MTBE*	55	82
Et_2O*	61	78
THF*	41	71
Toluene*	50	66
Benzene*	60	69
EtOAc	12	63
DCM	**94**	**97**
$CHCl_3$	92	95
DCE	88	94

*run at 0C

DCM concentration and catalyst loading optimization

[1-Cbz]	mol% 5d'	ee (%)
0.1 M	10 mol%	97
0.1 M	5 mol%	97
0.1 M	2.5 mol%	95
0.2 M	2.5 mol%	96
0.25 M	2.5 mol%	97
0.25 M	1 mol%	93
0.5 M	2.5 mol%	97
0.5 M	1 mol%	96

Figure 2.12 Solvent and concentration of 1-Cbz and catalyst **5d'**optimization in the enantioselective methallylation of **1-Cbz**

2.4 Reaction scope in the allylation of 1-Cbz catalyzed by squaramide HBD 5d'

The scope of the α-allyl amino ester synthesis was investigated with optimal catalyst **5d'** (Figure 2.13). Relative to screening scale, the reactions were run more concentrated, at 0.25 M in DCM, which allowed the catalyst loading to be dropped to 2.5 mol percent while preserving reactivity and enantioselectivity. The product of the model reaction, **2a** was formed in 88% isolated yield and 97% ee. 2-arylallyltrimethylsilanes with electronically neutral or donating substituents furnished their corresponding products **2b–g** in 90-96% ee. Para- and meta-bromide substitution on the nucleophile rendered it minimally reactive under the standard reaction conditions; however an elevated reaction temperature of –5 °C formed para- and meta-bromide products **2f** and **2g** with high yields and enantioselectivities. Even at elevated temperatures, the ortho-bromo substituted silane was completely unreactive, potentially due to diminished nucleophilicty as a result of allylic strain forcing the ortho-substituted arene out of conjugation.

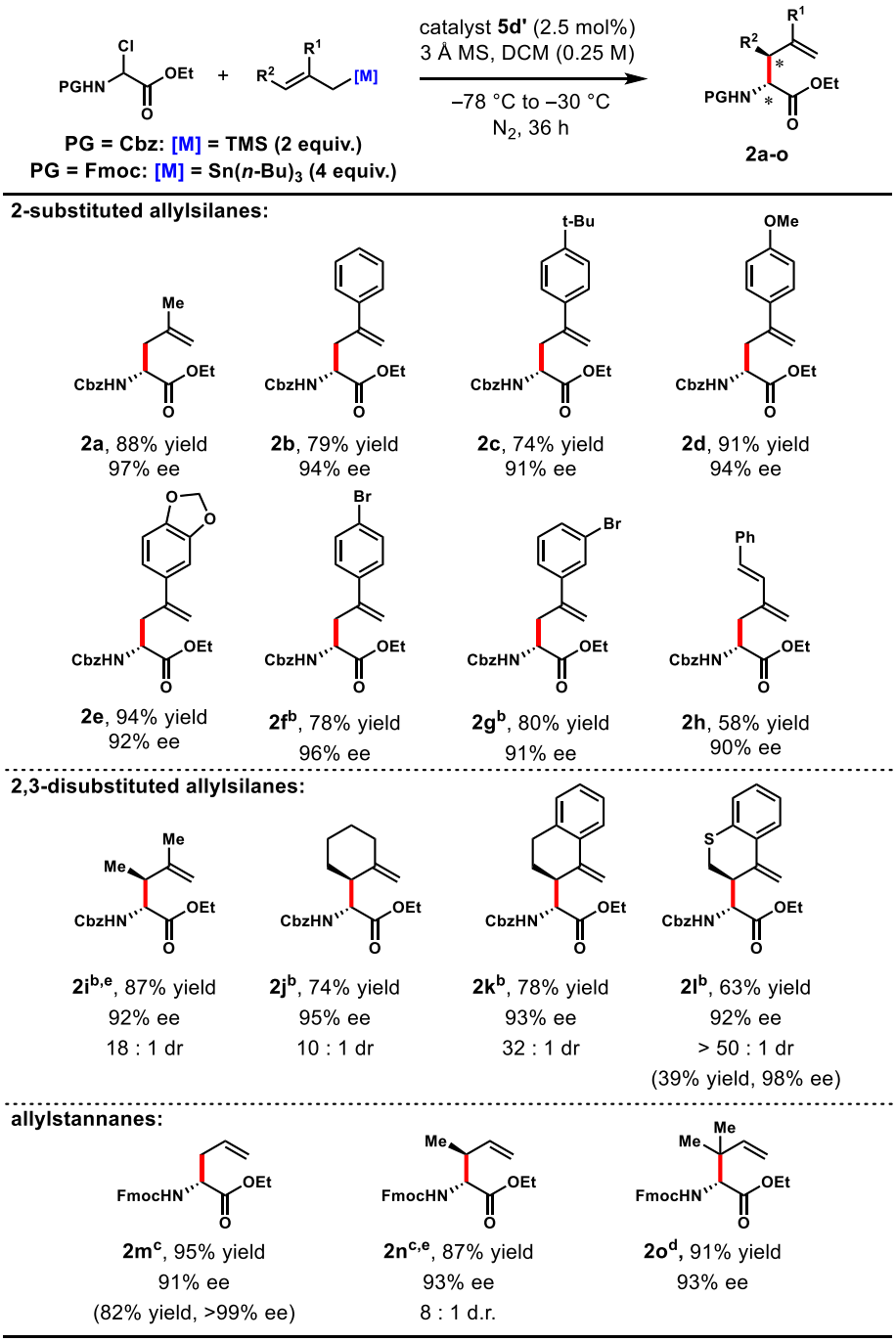

Figure 2.13 Reaction scope in the allylation of **1** with allylsilane and allylstannane nucleophiles catalyzed by squaramide **5d'**. [a] Conditions: substrate (0.5 mmol), catalyst (0.0125 mmol), nucleophile (1.0 mmol), 3 Å MS (60 mg), DCM (2 mL), under N_2, initially cooled to –78 °C and stirred at –30 °C, 36 h. Enantiomeric excess determined by HPLC. Diastereomeric ratio determined by ^{1}H NMR of the crude product, yield reflects isolation of major diasteromer. [b] –5 °C. [c] catalyst (0.05 mmol), nucleophile (2.0 mmol), DCM (5 mL), –50 °C, 72 h. [d] catalyst (0.05 mmol), nucleophile (1.5 mmol), DCM (5 mL), –30 °C, 72 h. [e] (*E*)-trimethyl(2-methylbut-2-en-1-yl)silane and (*E*)-crotylstannane employed as the nucleophiles. Yields and enantioselectivities in parentheses are of crystallized products.

β-Branched-α-allyl amino esters were produced with high diastereoselectivities and enantioselectivities using 2,3-disubstituted allylsilanes as nucleophilic reacting partners (Figure 2.13, **2i–l**). As noted above, these products are generally inaccessible using electrophilic allylation reagents in traditional enolate allylations.[41–45] The enantio- and diastereoselectivies of branched products **2i–l** and **2n** are generally higher than those obtained with previously reported catalytic asymmetric methods.[58] Additional benefits of this method include a larger range of reported nucleophiles, as well as products containing easily cleavable N-protecting groups.

In contrast, allylsilane nucleophiles lacking 2-substituents were completely unreactive under the catalytic conditions, an observation consistent with the fact that allyltrimethylsilane (*N* = 1.68)[104] is substantially less nucleophilic than 2-methylallylsilane (N = 4.41).[93] The more nucleophilic allyltributylstannanes (N = 5.46 for the parent com-pound) [93] were evaluated and found to be effective reacting partners, allowing construction of α-allyl amino esters **2m–o** with high yields and enantioselectivities.

Reoptimization of the reaction conditions and the carbamate protecting group was necessary for reactions employing stannane nucleophiles; in particular the Fmoc-protected analog of **1** was found to provide improved enantioselectivities (e.g., 93 vs 74% ee with prenylstannane nucleophile). Crotylstannanes underwent reaction to furnish the branched product **2n**. Both the (*E*)- and (*Z*)-crotyltributylstannane afforded the syn diastereomer predomi-nantly (8:1 with the (*E*)-isomer, 4:1 with the (*Z*)-isomer). A similar outcome was observed using silane nucleophiles leading to product **2i**, indicating that the allylation reactions proceed through open transition states. Reaction of prenyl tributylstan-nane with **1-Fmoc** generated the reverse-prenyl amino ester **2o** in 93% ee.

[104] Ammer, J.; Nolte, C.; Mayr, H. Free Energy Relationships for Reactions of Substituted Benzhydrylium Ions: From Enthalpy over Entropy to Diffusion Control. *J. Am. Chem. Soc.* **2012**, *134* (33), 13902–13911.

Although the nucleophiles in Figure 2.13 generally afford products with high enantio- and diastereoselectivity, there were many allyl nucleophiles that either were unreactive, provided poor yield of product, or poorly selective. Given the proposed radical mechanism in related transformations, 2-cyclopropylallylsilane was employed as a radical clock.[35,39] Interestingly the product was obtained with no ring-opened product, which does not rule out a radical mechanism, but lends additional support for generation of a β-silyl cation intermediate. This nucleophile provided product in approximately 60% ee. 2-(*m*-fluorophenyl)allylsilane provided product in just 80% ee, which is much lower than the 91% ee obtained for the analogous *m*-bromophenyl nucleophile. Last, while cyclohexenylmethylsilane afforded products in 95% ee and 10:1 d.r., the cyclpentenyl analog was much less selective, at 78% ee and 2:1 d.r. for reasons not understood.

A number of allylsilanes were not nucleophilic enough to participate in reaction with **1-Cbz** even at room temperature. Unsurprisingly, 2-bromoallylsilane was completely unreactive. Surprisingly, putting an electron withdrawing group one or two methyl units away from the olefin also rendered nucleophiles unreactive, which is surprising due to the relatively small inductive withdrawing effect. However, such a small inductive destabilization could be amplified by the necessity to form a full cation at the β-silyl carbon. As discussed above, allylsilanes lacking 2-substitution are insufficiently nucleophilic to engage in this chemistry, as the β-silyl cation would be secondary rather than tertiary. Last, 2-alkynylallylsilanes would be an ideal nucleophile as the products would bear a terminal alkyne valuable in labelling proteins with biorthogonal Click functionalizations; however, these nucleophiles decompose under the reaction conditions, yielding very little product and sideproducts resulting in allene formation. It would be interesting to use the same nucleophile with a terminal alkynylTMS group to protect allene formation and other decomposition pathways.

The only stannanes evaluated not in Figure 2.13 is (*E*) and (*Z*)-cinnamyltributylstannanes. Both stannanes provide very messy reactions with trace desired product. While this would be an interesting nucleophile, cinnamylated amino esters can be synthesized in a number of ways with π-allyl and [2,3]-rearrangement chemistry as discussed in Chapter 1 and section 2.2.[48,68,69]

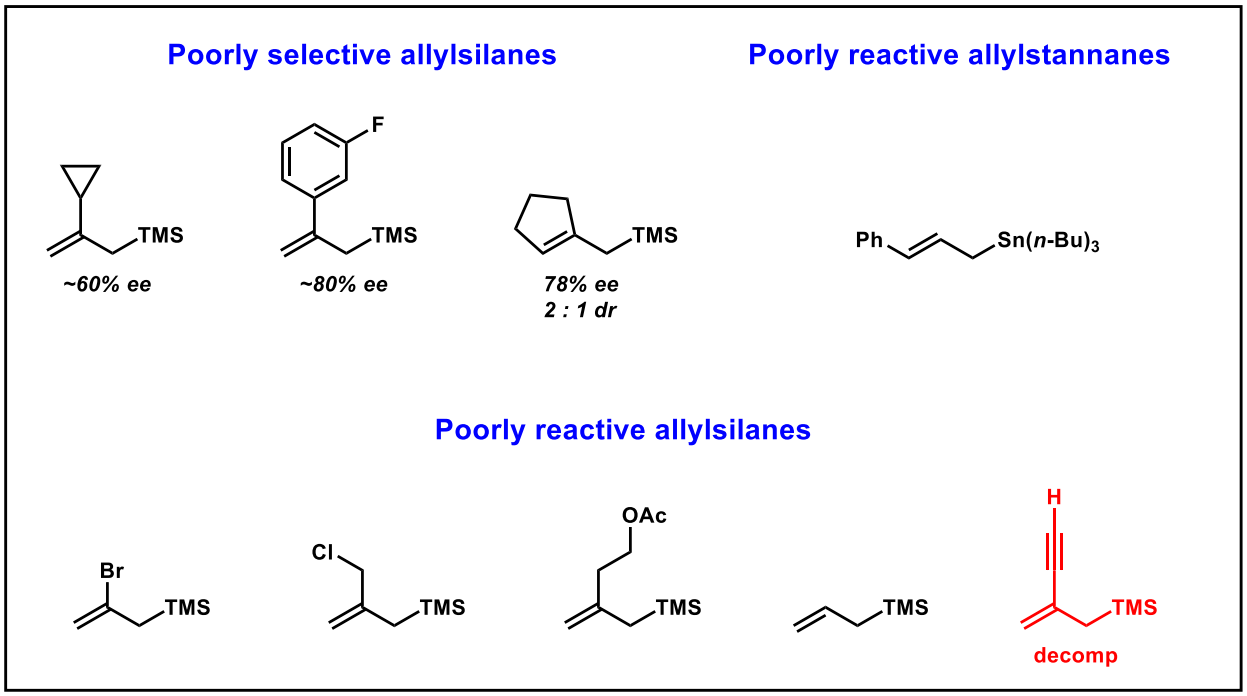

Figure 2.14 Suboptimal nucleophiles in the allylation of **1**

Products **2l** and **2m** were able to be recrystallized and upgraded to enantiopurity and 98% ee respectively. The absolute configuration of allylsilane addition products was assigned by comparison of optical rotation of **2a** to a literature value.[105] Crystal structure was solved for **2l** (provided in methods section), which confirmed the assignment of **2a** and was used to assign the major diastereomer of products setting two stereocenters by analogy. The absolute configuration of stannane addition products was assigned by independently synthesizing **2m** from (D)-allylglycine and overlaying HPLC traces.

[105] Kiyohara, H.; Nakamura, Y.; Matsubara, R.; Kobayashi, S. Enantiomerically Enriched Allylglycine Derivatives through the Catalytic Asymmetric Allylation of Iminoesters and Iminophosphonates with Allylsilanes. *Angew. Chemie Int. Ed.* **2006**, *45* (10), 1615–1617.

2.5 Reaction optimization for the addition of stannanes to 1

As discussed in section 2.3, the addition of allyl stannanes to **1** did not provide products with high levels of enantioselectivity under the same conditions employed in the addition of allylsilanes. In order to achieve satisfactory levels of enantioselectivity, *N*-carbamoyl protecting group, ester protecting group, and stannane identity were all reevaluated with allyl and prenyl stannanes. Additionally, solvent, temperature and concentration screening were all repeated for stannane nucleophiles.

N-carbamoyl protecting groups were found to have a profound effect on the levels of enantioselectivity in the addition of prenylstannane to **1** (Figure 2.15). Contrary to the allylation with methallyltrimethylsilane, the allylation with prenylstanne finds Fmoc carbamate as the optimal protecting group. The trend again implies that groups with conjugated π-systems are advantages for achieving high selectivity. Fmoc is distinct from the other protecting groups tried in that the solubility of the starting material **1-Fmoc** is substantially less soluble than the other substrates tests. Intriguingly, the more soluble analog Fmoc*, with *t*-butyl groups on the 2 and 7 positions, provides almost racemic product for reasons not understood. Once again amides are unreactive in this chemistry, and thus not depicted in Figure 2.15.

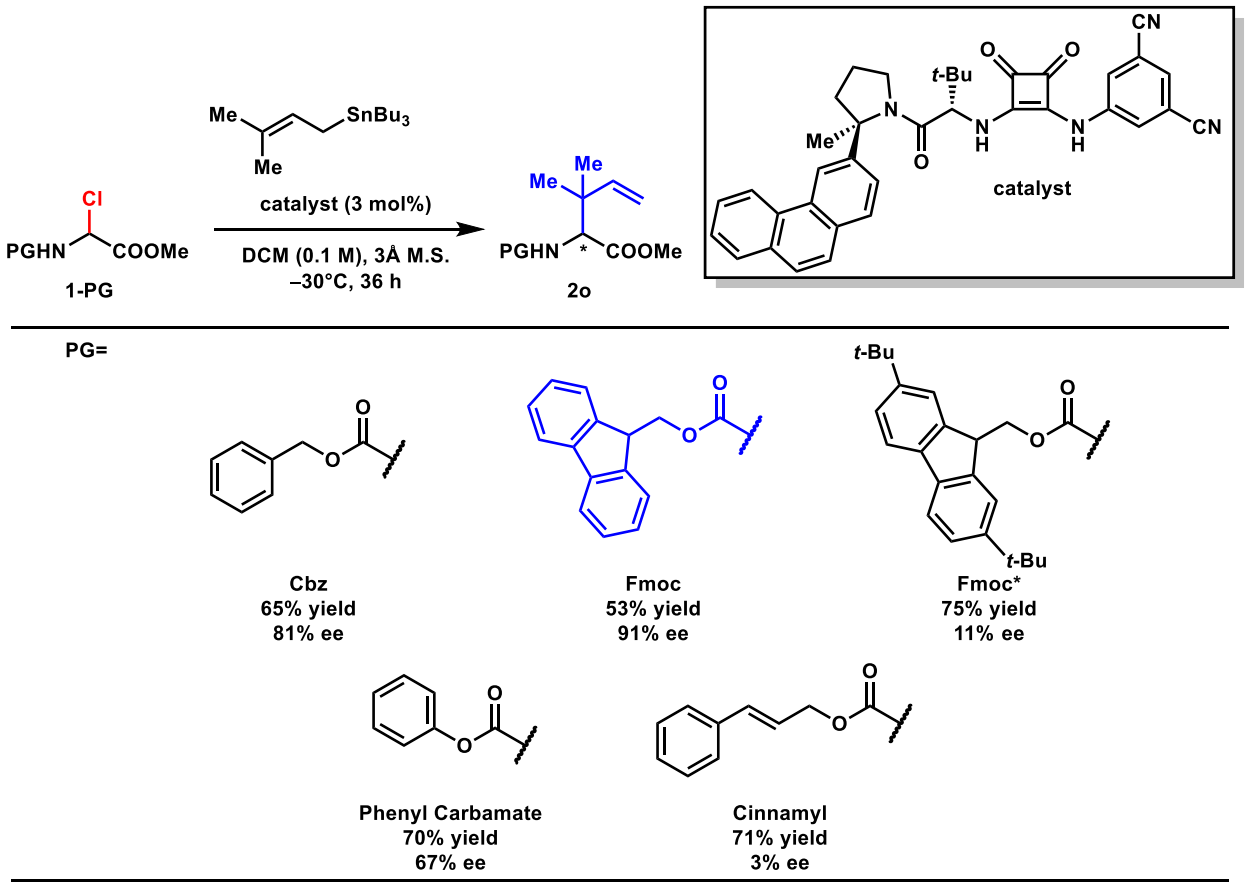

Figure 2.15 Evaluation of electrophile *N*-protecting group the addition of prenylstannane to **1**

A variety of allylstannane sources were evaluated, which revealed that allyl-tri-*n*-butylstannane is by far optimal for both selectivity and reactivity (Figure 2.16). Intriguingly tetraallyl tin and diallyl-di-*n*-butyl tin both gave complete conversion, but product was racemic in both cases. The less nucleophilic triphenyl tin was unreactive at –30 °C, and at 0 °C gave 12% ee, perhaps due to competitive racemic background at this temperature.

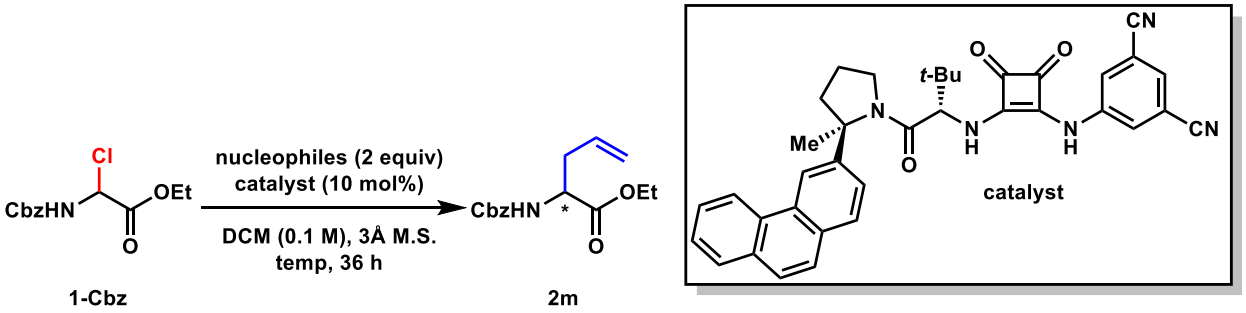

nucleophiles	temp (°C)	yield (%)	ee (%)
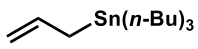	-30	97	71
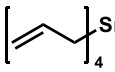	-30	98	0
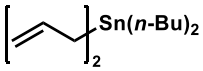	-30	102	0
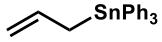	-30	0	NA
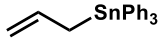	0	60	12

Figure 2.16 Evaluation of stannane substituents in addition of allylstannanes to **1**

Due to the insolubility of the **1-Fmoc** starting material require for high enantioselectivity in the addition of stannane nucleophiles, the reaction parameter optimization is somewhat distinct from the conditions for the allylsilane nucleophiles. A brief summary of many reaction parameters in the reverse-prenylation of **1-Fmoc** is provided in Figure 2.17. Ethyl ester was found to be substantially better than methyl ester for enantioselectivity and slightly better for yield, potentially due to the increased solubility of the ethyl ester. DCM and $CHCl_3$ are both optimal for conversion, however, DCM provides higher enantioselectivities. THF, while able to solubilize the starting material provides no conversion. Ideally the reaction could be run under increased the concentrations and with lower catalyst loading, as in the allylsilane reactions. However, the poor solubility of Fmoc, along with the high (3-4) equivalences of stannanes required relatively dilute reaction concentrations of 0.1 M in DCM and catalyst loading of 10 mol%. The optimal temperature is –30 °C for the reverse prenylation, whereas for allylation and crotylation –50 °C is

optimal.

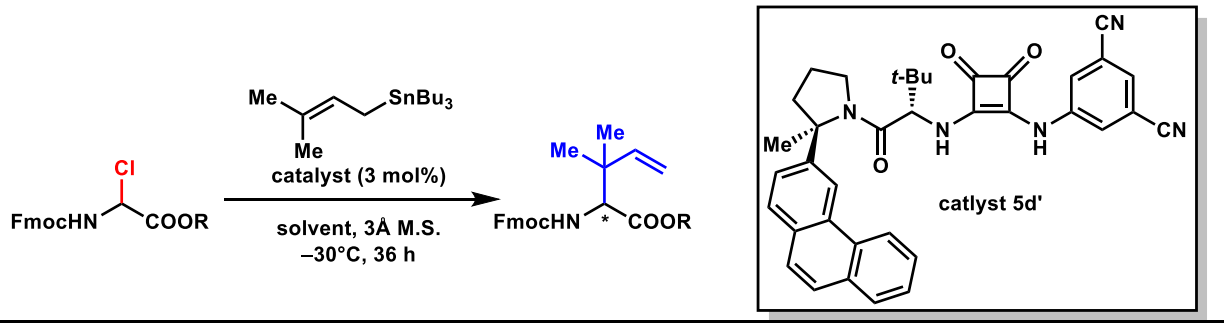

Ester group (in 0.1M DCM, 10 mol% 5d')

R	yield (%)	ee(%)
Me	75	80
Et	82	93

Solvent screening (with ethyl ester)

solvent	yield (%)	ee(%)
DCM	82	93
THF	0	NA
$CHCl_3$	97	89

Concentration and catalyst loading (with ethyl ester)

conc (M)	catalyst (mol %)	yield (%)	ee(%)
0.1	3	97	89
0.3	1	85	88

Temperature screen in DCM (with ethyl ester)

temp (°C)	yield (%)	ee (%)
0	100	50
–30	92	93
–50	38	24

Figure 2.17 Miscellaneous parameter optimization for prenylstannane addition to **1-Fmoc**

2.6 Synthetic applications of HBD catalyzed allylations of α-chloroglycine 1

The new catalytic protocol proved to be readily adaptable to the preparative-scale synthesis of α-allyl amino esters. The screening provided in Figures 2.12 and 2.17 determined the most synthetically ideal conditions for allylations run on scale. For example, using either the α-chloro amino ester **1-Cbz** or **1-Fmoc** and appropriate allylsilane or allylstannane nucleophiles, the β-branched products **2i** and **2o** were generated on gram scale (Figure 2.18). The reaction of 2,3-dimethylallylsilane with **1-Cbz** could be conducted at relatively high concentrations (0.5 M in DCM) with 1.5 equiv. of the nucleophile and 1 mol% catalyst with no compromise in enantioselectivity relative to the smaller scale reaction. The addition of prenylstannane to **1-Fmoc**

could not be conducted at higher concentration due to the limited solubility of **1-Fmoc** in DCM, but the catalyst loading could be lowered to 5 mol% while preserving the high enantioselectivity of the reaction.

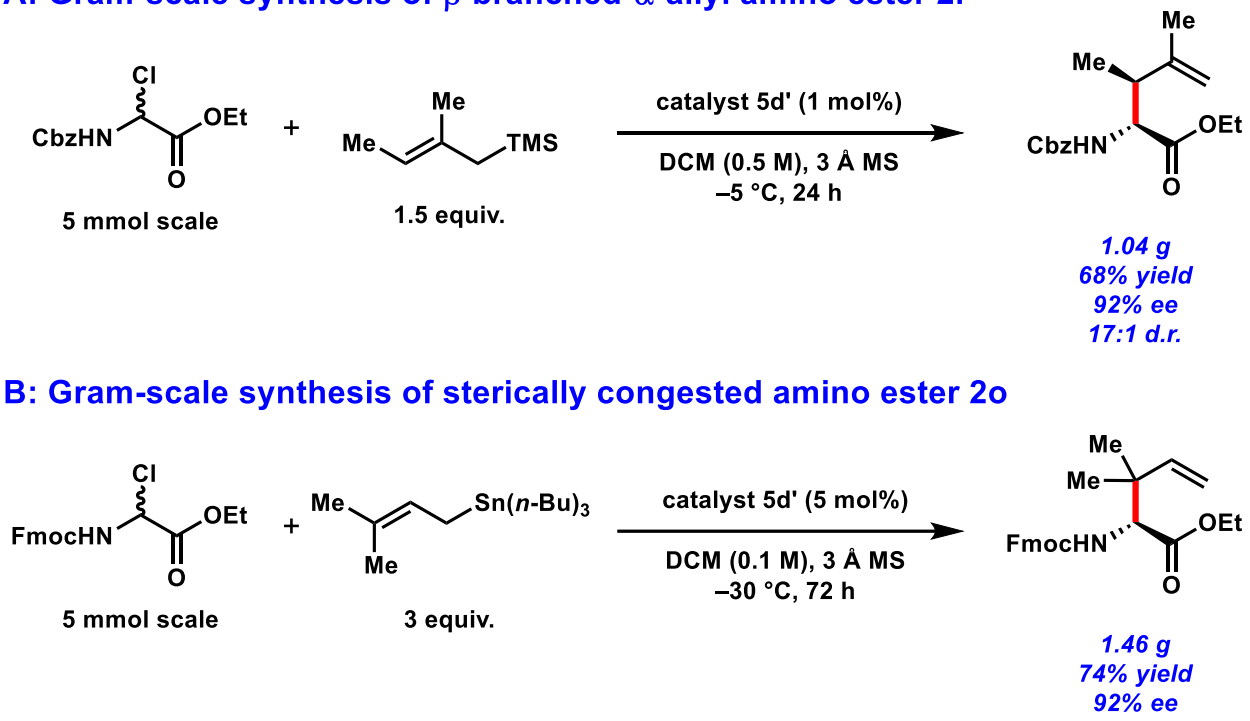

Figure 2.18 Gram scale synthesis of products **2i** and **2o**

While the direct generation of carbamate-protected amino esters provides amino acid derivatives in conveniently protected form, a natural concern is the likely incompatibility of the alkenyl group in the allylated products with typical protocols for Cbz group removal. Indeed, under standard hydrogenolysis conditions, compound **2i** underwent competitive reduction of the alkene. However, reduction with triethylsilane under $Pd(OAc)_2$ catalysis left the alkenyl group intact and afforded a mixture of TMS protected and free amine, which could be worked up with HCl to provide the corresponding amine HCl salt in 87% yield with no measurable racemization (Figure

2.19).[106]

A: Standard hydrogenolysis conditions for 2i

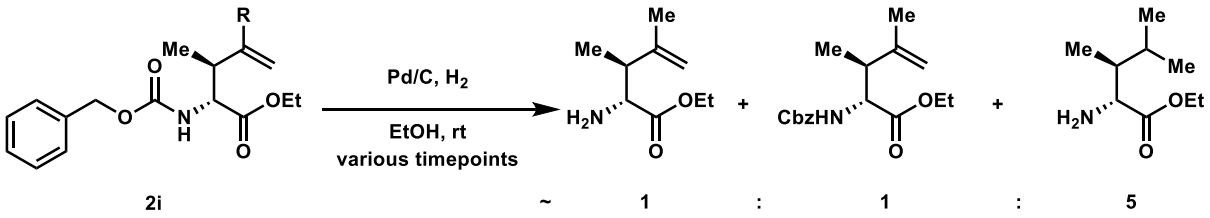

A: Pd(OAc) catalyzed TES-H reductive conditions for Cbz removal for 2i

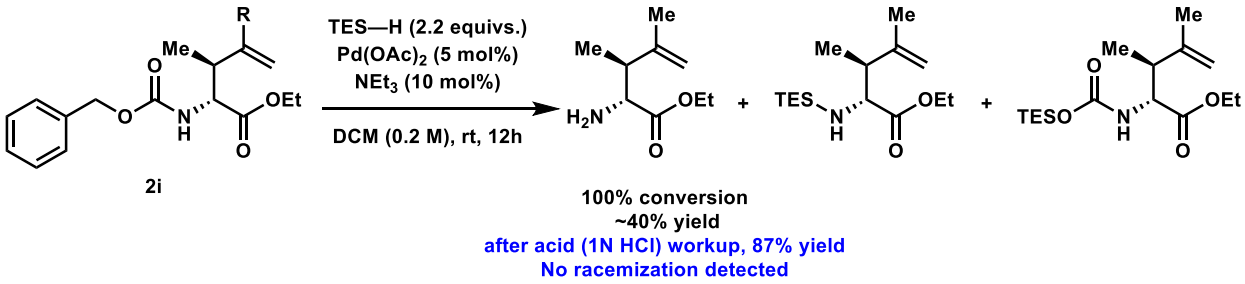

Figure 2.19 Methods for Cbz deprotection of product **2i**

2.7 Introduction: applications of α-aryl amino acids

Unnatural arenes can serve a number of biological functions, altering structural rigidity and shape, π-π stacking abilities, and solubility, allowing for wide ranges of applications, from drug discovery to nonenzymatic copying of oligonucleotides.[107] α-arylglycine derivatives have emerged

[106] For precedent using this method for Cbz removal see: a) Sakaitani, M.; Kurokawa, N.; Ohfune, Y. N-Carboxylate Ion Equivalent. II. Novel Transformations of N-Benzyloxycarbonyl (Z) Group and N-Allyloxycarbonyl Group into N-t-Butyldimethylsilyloxycarbonyl Intermediate. *Tetrahedron Lett.* **1986**, *27* (32), 3753–3754. b) Coleman, R. S. Chemoselective Cleavage of Benzyl Ethers, Esters, and Carbamates in the Presence of Other Easily Reducible Groups. *Synthesis (Stuttg).* **1999**, *1999* (S1), 1399–1400. c) Wipf, P.; Uto, Y. Total Synthesis and Revision of Stereochemistry of the Marine Metabolite Trunkamide A. *J. Org. Chem.* **2000**, *65* (4), 1037–1049.

[107] a) Kim, S. C.; O'Flaherty, D. K.; Zhou, L.; Lelyveld, V. S.; Szostak, J. W. Inosine, but none of the 8-oxo-purines, is a plausible component of a primordial version of RNA. *Proc. Natl. Acad. Sci. U. S. A.* **2018**, *115*, 13318–13323. b) Hughes, A. B. *Amino Acids, Peptides, and Proteins in Organic Chemistry*; Wiley-VCH, 2009.

as particularly useful in the context of natural product synthesis, peptide mimetics, chiral ligands, and antibiotic synthesis. Optically pure indolylglycines have been widely employed in the synthesis of marine alkaloids, including the dragmacidins[108] and hamacanthins.[109] Phenylglycine derivatives can be mapped on to the important β-lactam antibiotics cefalosporins[110] and norcarcidins,[111] as well as in the important class of glycopeptide antibiotics vancomycin and related compounds.[112]

In addition to biological and total synthesis applications, amino acids and short peptides containing arylglycine residues have emerged as chiral auxiliaries, catalysts for a variety of transformations as well as chiral ligands. Aryl amino acids have proven to be particularly useful as chiral auxiliaries in the aldol reaction and enolate alkylations.[113] The Miller group and others have used peptides as organocatalysts.[114,115] Additionally arylglycines derivatives (often the amino

---

[108] a) Kawasaki, T.; Enoki, H.; Matsumura, K.; Ohyama, M.; Inagawa, M.; Sakamoto, M. First Total Synthesis of Dragmacidin A via Indolylglycines. *Org. Lett.* **2000**, *2* (19), 3027–3029. b) Kawasaki, T.; Ohno, K.; Enoki, H.; Umemoto, Y.; Sakamoto, M. Syntheses of Bis(Indolyl)-Piperazine Alkaloids, Dragmacidin B and C, and Dihydrohamacanthin A. *Tetrahedron Lett.* **2002**, *43* (23), 4245–4248.

[109] Higuchi, K.; Takei, R.; Kouko, T.; Kawasaki, T. Total Synthesis of Marine Bisindole Alkaloid (+)- *Cis* - Dihydrohamacanthin B. *Synthesis (Stuttg).* **2007**, *2007* (5), 669–674.

[110] Spencer, J. L.; Flynn, E. H.; Roeske, R. W.; Siu, F. Y.; Chauvette, R. R. Chemistry of Cephalosporin Antibiotics. VII. Synthesis of Cephaloglycin [1] and Some Homologs. *J. Med. Chem.* **1966**, *9* (5), 746–750.

[111] Townsend, C. A.; Brown, A. M. Nocardicin A: Biosynthetic Experiments with Amino Acid Precursors. *J. Am. Chem. Soc.* **1983**, *105* (4), 913–918.

[112] For a review on the synthesis of the vancomycins see: Rao, A. V. R.; Gurjar, M. K.; Reddy, K. L.; Rao, A. S. Studies Directed toward the Synthesis of Vancomycin and Related Cyclic Peptides. *Chem. Rev.* **1995**, *95* (6), 2135–2167.

[113] For a review on amino acids as chiral auxiliaries and ligands see: Vicario, J.; Badia, D.; Carrillo, L.; Reyes, E.; Etxebarria, J. α-Amino Acids, β-Amino Alcohols and Related Compounds as Chiral Auxiliaries, Ligands and Catalysts in the Asymmetric Aldol Reaction. *Curr. Org. Chem.* **2005**, *9* (3), 219–235.

[114] For a review on amino acids and peptides as asymmetric organocatalysts see: Jarvo, E. R.; Miller, S. J. Amino Acids and Peptides as Asymmetric Organocatalysts. *Tetrahedron* **2002**, *58* (13), 2481–2495

[115] For a review on amino acids as organocatalysts in carbohydrate synthesis see: Kazmaier, U. Amino Acids — Valuable Organocatalysts in Carbohydrate Synthesis. *Angew. Chemie Int. Ed.* **2005**, *44* (15), 2186–2188.

acohol) have been employed as ligand or structural moieties in a range of transition metal and organocatalysts, including PHOX,[116] BOX,[117] and N-heterocyclic carbene catalysts.[118] arylglycines and 1,2-aminoalcohols derived from them, have multiple desirable properties as a chiral ligand or organocatalyst, namely their structural rigidity and ability to engage in secondary non-covalent attractive interactions.

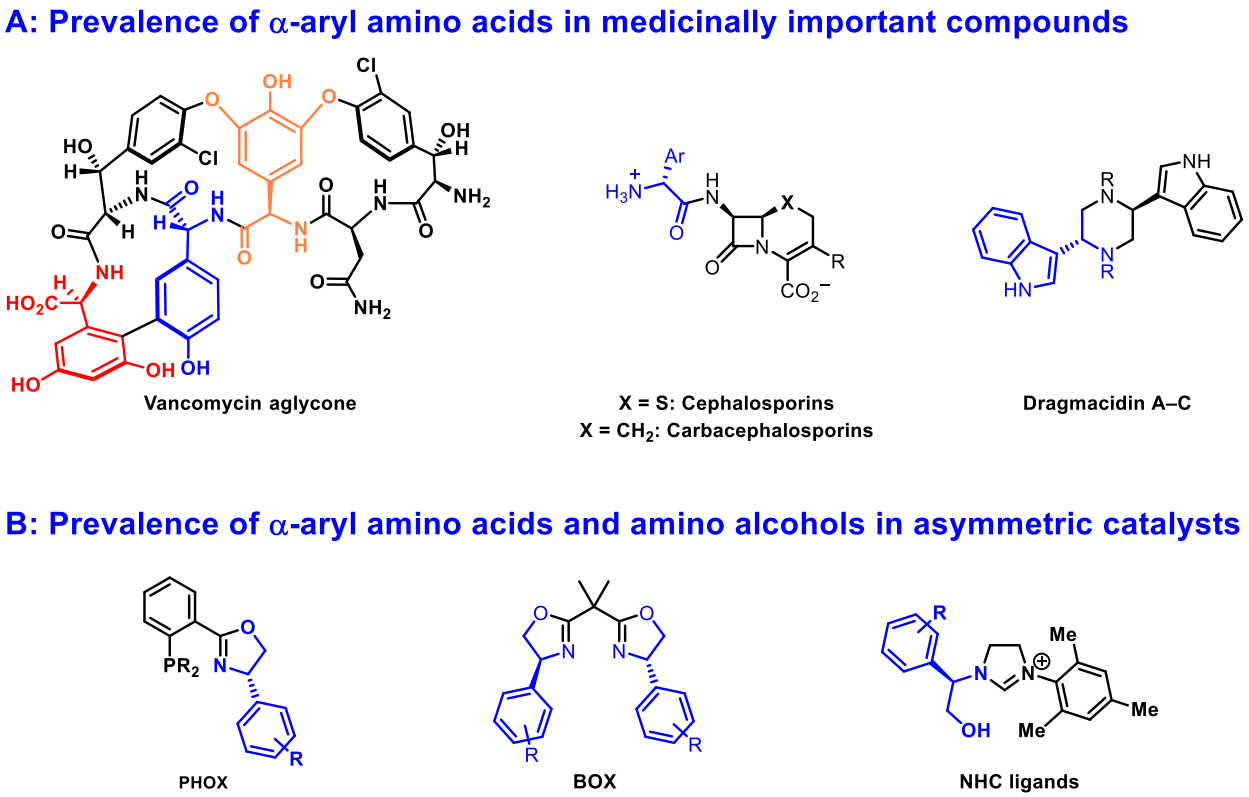

Figure 2.20 Applications of α-arylglycines in medicinally important compounds and catalysis

[116] For a review on PHOX ligands see: Pfaltz, A.; Drury, W. J. Design of Chiral Ligands for Asymmetric Catalysis: From C2-Symmetric P,P- and N,N-Ligands to Sterically and Electronically Nonsymmetrical P,N-Ligands. *Proc. Natl. Acad. Sci. U. S. A.* **2004**, *101* (16), 5723–5726.

[117] For a review on BOX ligands see: Desimoni, G.; Faita, G.; Jørgensen, K. A. C2-Symmetric Chiral Bis(Oxazoline) Ligands in Asymmetric Catalysis. *Chem. Rev.* **2006**, *106* (9), 3561–3651.

[118] For a review on amino acid containing NHC ligands see: a) Schuster, O.; Yang, L.; Raubenheimer, H. G.; Albrecht, M. Beyond Conventional *N* -Heterocyclic Carbenes: Abnormal, Remote, and Other Classes of NHC Ligands with Reduced Heteroatom Stabilization. *Chem. Rev.* **2009**, *109* (8), 3445–3478. For an early example see: b) Clavier, H.; Coutable, L.; Toupet, L.; Guillemin, J.-C.; Mauduit, M. Design and Synthesis of New Bidentate Alkoxy-NHC Ligands for Enantioselective Copper-Catalyzed Conjugate Addition. *J. Organomet. Chem.* **2005**, *690* (23), 5237–5254.

2.8 Methods for the syntheses of enantioenriched α-aryl amino acids

Given the prevalence of α-aryl amino acids in chemical biology, chemical synthesis, and methods development, methods for their enantiopure synthesis has been the subject of much research.[119] Despite the relative simplicity of the arylglycine products, their enantiopure synthesis is often hampered by base, or in some cases acid, catalyzed racemization of the acidic α-proton through equilibration to stereoablated enolate intermediates or enol tautomers. In Chapter 1, the synthesis of enantioenriched amino acids was discussed at length, so a short summary will be presented here followed by specific chiral auxiliary and enantioelective syntheses of α-furanyl, α-indolyl, and α-(2,4-dimethoxy)phenyl amino acids, relevant to the following sections.

Of the methods discussed in Chapter 1, Strecker amino acid syntheses are by far the most practical and well developed methods for the synthesis of α-aryl amino acids. [16] However, Strecker syntheses are not well suited to the synthesis of electron rich α-aryl glycinates due to the harsh acidic conditions required for subsequent nitrile hydrolysis, which will decompose electron rich arenes, especially indoles. In fact very few Strecker reactions are reported for the three classes of nucleophiles employed here, and when they are used, the nitrile hydrolysis is not reported.[120]

When employing electron rich arenes or heterocycles, the Friedel-Crafts addition to α-imino esters is the best reported disconnection to synthesize enantioenriched α-aryl glycinates, in both chiral auxiliary and enantioselective catalytic contexts. The Ellman auxiliary has proven to be the chiral auxiliary of choice for these transformations. 1,3-dimethoxybenzene and 2-methyl furan proceed with 98% and 90% de respectively in an indium (III) triflate catalyzed addition to

[119] For a review on asymmetric syntheses of arylglycines see: Williams, R. M.; Hendrix, J. A. Asymmetric Synthesis of Arylglycines. *Chem. Rev.* **1992**, *92* (5), 889–917.

[120] For a rare example in which nitrile hydrolysis is reported see: Rueping, M.; Sugiono, E.; Azap, C. A Highly Enantioselective Brønsted Acid Catalyst for the Strecker Reaction. *Angew. Chemie Int. Ed.* **2006**, *45* (16), 2617–2619.

Ellman α-imino esters.[121] The addition of N-Me, N-H indole and N-Me pyrrole to the same electrophile can be accomplished in 95%, 98%, and 97% de respectively when employing copper (II) triflate as a catalyst; however removal of the protecting group is not attempted and may present problems.[122] One notable chiral auxiliary method is the use of a chiral *syn*-diphenyl oxazoline of glyoxylate, which can be α-brominated with NBS and trapped with furan nucleophiles in the presence of zinc (II) chloride to afford products in 90-93% ee.[123]

From the chiral auxiliary methods, it is clear that the addition of arenes to α-imino esters is catalyzed by the presence of Lewis acids. Despite this, there are relatively few chiral Lewis acid enantioselective syntheses of these products. Notably, Jørgensen has been able to use the chiral Cu (I) *p*-Tol-BINAP catalysts used in the addition of allylsilanes to affect arylations of *N*-carbamoyl α-imino esters with anilines (>90% ee), furans (89% ee), and 1,3-dimethoxy benzene (79% ee).[62] Johannsen was able to adapt this catalytic system to affect indole addition to *N*-tosyl α-imino esters in 96% ee, although deprotection of the tosyl amine product is not reported and likely impossible in the presence of an indole.[61] Trost's dinuclear zinc complexes were used to affect addition of N-H indoles to *N*-paramethoxyphenyl α-imino esters in >99% ee, although again deprotection of the product is not shown.[124] In addition to Lewis acid promoted arylations of α-imino esters, chiral phosphoric acids have been employed to in the addition of 1,3-dimethoxy benzene to racemic

---

[121] Li, Y.; Ji, D.-M.; Xu, M.-H. Highly Diastereoselective Friedel–Crafts Reaction of Arenes with N-Tert-Butanesulfinylimino Ester towards the Efficient Synthesis of α-Arylglycines. *Org. Biomol. Chem.* **2011**, *9* (24), 8452.
[122] Ji, D.-M.; Xu, M.-H. Highly Diastereoselective Friedel–Crafts Reaction of Indoles with an N-Tert-Butanesulfinylimino Ester: An Efficient and Practical Approach to Enantiomerically Enriched α-(3-Indolyl)Glycines. *Chem. Commun.* **2010**, *46* (9), 1550.

[123] Williams, R. M.; Hendrix, J. A. Asymmetric Synthesis of Arylglycines. *J. Org. Chem.* **1990**, *55* (12), 3723–3728.

[124] Wang, X.-W.; Hua, Y.-Z.; Wang, M.-C. Synthesis of 3-Indolylglycine Derivatives via Dinuclear Zinc Catalytic Asymmetric Friedel–Crafts Alkylation Reaction. *J. Org. Chem.* **2016**, *81* (19), 9227–9234.

Ellman α-imino esters with 93% ee.[125] A chiral phosphoric acid catalyzed addition of indole to α-imino esters with 2-nitrophenylsulfenyl (Nps) and triphenylmethylsulfenyl (Trs) protecting groups in 88% ee, which upon mild acidic removal of the protecting group can be upgraded to >99% ee.[126] This represents the only asymmetric catalytic method for indole addition in which deprotection of the products is demonstrated.

2.9 Development of hydrogen-bond donor catalyzed synthesis of α-aryl amino esters

Given the ability of hydrogen-bond donor squaramide catalysts to affect the highly enantio- and diastereoselective addition of allylsilanes and allylstannanes to α-chloro *N*-carbamoyl glycinates, the addition of other weak π-electrophiles to the same electrophile class seemed plausible. Additionally, the racemic addition of 1,3-dimethoxybenzene, furan, pyrrole, and indole to **1-Cbz** are all racemically reported in chloroform and at cryogenic or room temperatures, which are conditions that seemed conducive to enantioselective catalysis.[89] Furthermore, Jørgensen found that the copper Lewis acid catalyzed enantioselective addition of allylsilanes to *N*-carbamoyl α-imino esters could be directly translated to enantioselective Friedel-Crafts additions with 1,3-dimethoxybenzene and 2-methylfuran. Although HBD catalyzed additions of Friedel-Crafts nucleophiles to imine or imine equivalents α-to a carbonyl, thiourea HBD catalysts have demonstrated the ability to affect highly enantioselective indole additions to both imines and α-

[125] Enders, D.; Seppelt, M.; Beck, T. Enantioselective Organocatalytic Synthesis of Arylglycines via Friedel-Crafts Alkylation of Arenes with a Glyoxylate Imine. *Adv. Synth. Catal.* **2010**, *352* (9), 1413–1418.
[126] Wanner, M. J.; Hauwert, P.; Schoemaker, H. E.; de Gelder, R.; van Maarseveen, J. H.; Hiemstra, H. Synthesis of Enantiopure (S)-Indolylglycine by Organocatalyzed Friedel–Crafts Alkylation of Indole. *European J. Org. Chem.* **2008**, *2008* (1), 180–185.

chloro-*N*-carbamoyl lactams in intermolecular and intramolecular, Pictet-Spengler contexts.[127,128] These precedents, taken together, led to the investigation of chiral HBD catalyzed additions of Friedel-Crafts nucleophiles to **1**. Due to the diversity of nucleophiles explored, model reactions were developed with 2-Me furan, *N*-H indole, *N*-Me indole, and 1,3-dimethoxybenzene, which were optimized in parallel. For the purposes of discussion the subsequent reaction optimization sections are divided by nucleophile employed, and as a result conditions and catalysts surveyed may seem arbitrary or suboptimal, but were thought to be optimal at the time the screens were conducted.

2.9.1 Reaction optimization with 2-methyl furan nucleophile

The arylation of α-chloro glycinate **1-Cbz** with 2-methylfuran was selected as a model reaction for catalyst optimization. An extensive survey of chiral dual-hydrogen-bond-donors revealed that arylpyrrolidinosquaramides were optimal, as with the allylation; however enantioselectivies were modest and without trends, with the 3,5-dibromophenylpyrrolidino half-Schriener squaramide providing 47% ee.

Inspired by the ability for substrates containing Fmoc protecting groups to provide higher enantioselectivies than the Cbz analogs with allylstannane nucleophiles, an extensive survey the carbamate protecting group was conducted with the 3,5-dibromophenylpyrrolidino squaramide catalyst (Figure 2.21).

---

[127] a) Taylor, M. S.; Jacobsen, E. N. Highly Enantioselective Catalytic Acyl-Pictet−Spengler Reactions. *J. Am. Chem. Soc.* **2004**, *126* (34), 10558–10559. b) T. Raheem, I.; S. Thiara, P.; A. Peterson, E.; N. Jacobsen, E. Enantioselective Pictet−Spengler-Type Cyclizations of Hydroxylactams: H-Bond Donor Catalysis by Anion Binding. *J. Am. Chem. Soc.* **2007**, *129* (44), 13404–13405.

[128] Wang, Y.-Q.; Song, J.; Hong, R.; Li, H.; Deng, L. Asymmetric Friedel−Crafts Reaction of Indoles with Imines by an Organic Catalyst. *J. Am. Chem. Soc.* **2006**, *128* (25), 8156–8157.

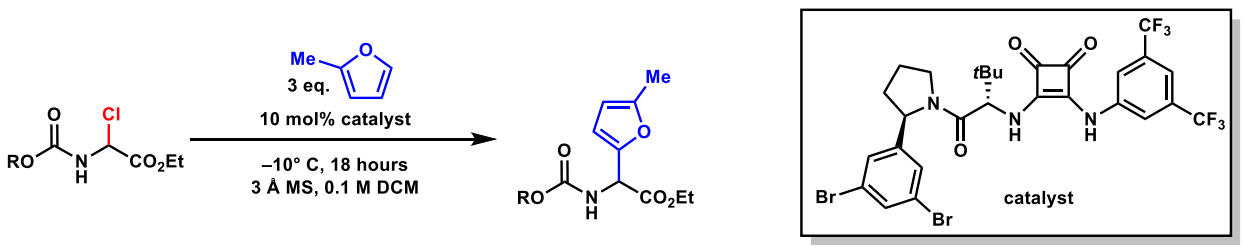

R (protecting group)	ee (%)	R (protecting group)	ee (%)
	0	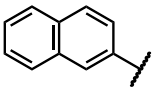	52
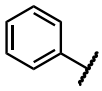	50	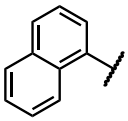	63
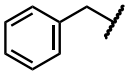	47	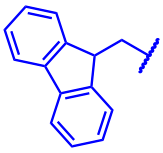	65

Figure 2.21 Carbamate protecting group studies in the 2-Me furan addition to **1**

A clear trend was observed, in which substrates bearing carbamate protecting groups fitted with aryl groups provided higher enantioselectivities. Astonishingly, the methyl carbamate protected analog of **1** provided racemic product. In the class of aryl carbamates, 2-naphthyl and phenyl gave similar levels of enantioinduction (~50% ee), however 1-naphthyl gave product in 63% ee. In the family of benzyl carbamates, Fmoc provided substantially higher levels of enantioselectivity than Cbz, with 65% ee. Despite similar results with 1-naphthylcarbamate and Fmoc, further screening was conducted exclusively with Fmoc due to its commercial nature, ease of deprotection, and higher yields of product (82% for Fmoc vs. 54% for 1-naphthyl).[91] Due to do to donation of the oxygen into the arene π system, aryl carbamates are more electron withdrawing than benzyl carbamates, which may explain the difference in reactivity.

Catalyst arylpyrrolidine optimization studies were pursued with the **1-Fmoc** substrate

(Figure 2.22). These data suggest that catalysts with larger arenes promote more enantioselective additions, where Ar = Ph provides 40% ee, Ar = 1-naphthyl provides 64% ee, and Ar = 2,3, and 9-phenanthryl provide 84, 87, and 88% ee respectively. A number of other large arenes were tested, including heteroaromatics, which revealed that as long as the arene contains a 3-ring system, the enantioselectivity is relatively flat and in the 80-90% range. One notable exception is the carbazole catalyst, which provides 32% ee. Given the ability of *N*-Me indole to add to this substrate at –60 °C it is likely that the carbazole, which should have a high effective molarity, can add in to the substrate at –10 °C, providing an alternate mode of catalysis and/or undesired functionalization of the catalyst with substrate. In the allylation, the presence of a methyl group geminal to the pyrrolidine arene, R = Me, was essential to achieving high levels of enantioselectivity. Here, in the case of Ar = Phenyl, the addition of a methyl substituent has no impact on the enantioselectivity, and in the case of Ar = 1-Naphthyl, methylation is found to be detrimental (R = H, 64% ee vs. R = Me, 42% ee). One interesting note is that the racemic reaction and reactions with poor catalysts, for example phenylpyrrolidine **4a** provide multiple regioisomers of addition, in some cases as high as 1:1 with the 4-substituted product, as depicted in the product in Figure 2.22. The connectivity of this regioisomeric product is unknown, but it is formed nearly racemically by poor catalysts and all of the catalysts that give >80% ee provide none of the side product.

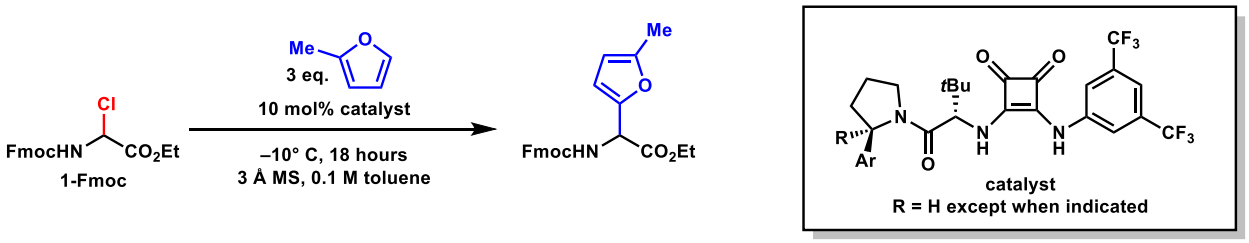

Ar (arylpyrrolidine arene)	ee (%)	Ar (arylpyrrolidine arene)	ee (%)
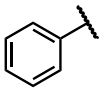	40 R = Me: 40	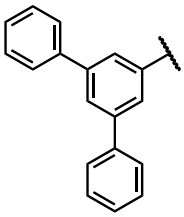	85
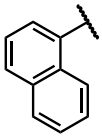	64 R = Me: 42		
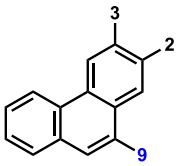	2: 84 3: 87 9: 88	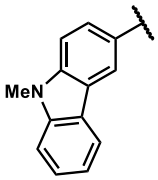	32
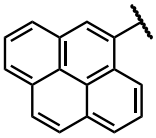	84	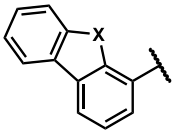	O: 85 S: 60

Figure 2.22: Survey of arylpyrrolidine catalysts on the addition of 2-Me furan to **1-Fmoc**

With optimal protecting group and catalyst in hand, a second round of conditions optimization was pursued (Figure 2.23). A broad range of solvents were tested and the reaction and the reaction was quenched at 3 hours, to observe the influence of solvent on both the rate and enantioselecivity of the transformation. Unfortunately, 3 hours was too short, so the differences in conversion are minimal and this experiment should be reevaluated. Nonetheless, the screen revealed that the reaction is able to proceed in a broad range of polar aprotic solvents. The reaction is remarkably insensitive to the identity of solvent, with most giving 80-90% ee. Notably, nitromethane gives 80% ee and acetonitrile gives 66% ee, both of which are solvents that strongly promote dissociated ion pairs and thus generally provide racemic product in enantioselective ion-

pairing catalysis.[94] This was used as evidence for the proposal that allylation and arylation of these substrates proceeds via a concerted S_N2 substitution mechanism, rather than an ion-pairing mechanism, as discussed at length in Chapter 3. The only solvent that provided racemic product was DMF, which may indeed promote iminium ion formation. Not much can be said about the rate in each solvent, although it seems that in general more polar solvents afford slightly higher conversions. Last, this screen revealed that toluene is the optimal solvent for enantioselectivity in this transformation, although at a cost to reactivity (if the reaction is run for 36 hours, it proceeds to 60% conversion with 90% ee).

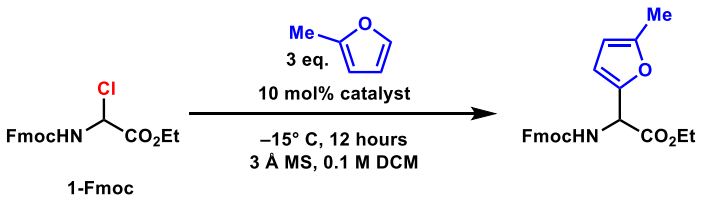

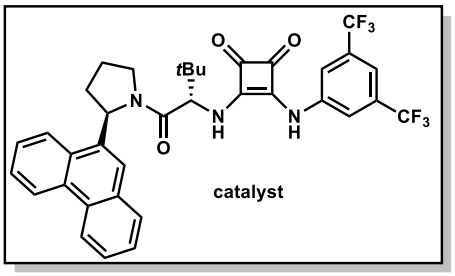

Solvent	ee (%)	yield (%)
Toluene	90	10
CCl_4	89	5
DCM	86	20
Et_2O	76	trace
THF	82	5
MeOAc	82	10
MeCN	66	20
$MeNO_2$	80	25
DMF	0	20

* reaction stopped after 3 hours

Molecular Sieves	ee (%)
3Å	90
4Å	87
5Å	86
13Å	88
None (DCM)	68
None (Toluene)	52

*all Molecular sieves stored in an oven and powdered, 60 mgs/mL

Figure 2.23 Conditions optimization in the addition of 1-methylfuran to **1-Fmoc**

Last, molecular sieve pore size was screened in this transformation and found to have a

small but not-insignificant effect on the enantioselectivity, with 3Å molecular sieves being optimal for enantioselectivity. The presence of molecular sieves is essential in reproducibly achieving high enantioselectivities, whereas in the allylation, they were only essential for conversion and did not impact enantioselectivity. One key difference between the arylation and allylation, is that HCl is produced as a stoichiometric byproduct (vs. TMSCl in the allylation). One hypothesis is that HCl is able to racemize product under the reaction conditions, through equilibration to the highly conjugated enol tautomer. HCl may be efficiently pulling HCl out of solution faster than the racemization pathway.

2.9.2 Reaction optimization with indole nucleophiles

Indole nucleophile screening was done with a variety of *N*-substituted indoles, including *N*-Me, *N*-Me, *N*-Et, *N*-Bn, *N*-allyl, *N*-TBS, as well as with electrophiles **1-Cbz** and **1-Fmoc**. Initially catalyst screening was performed on *N*-Me indole and **1-Cbz**, and the results of some of the more enantioselective catalysts are summarized in Figure 2.24. Structure activity relationships revealed almost no trend in this screening and as long as arylpyrrolidino squaramides were employed, enantioselectivities were moderate. The size of the arene and presence of a germinal methyl group are both relatively unimportant in this specific transformation. Catalyst **4d'**, which is optimal in the allylation, is also optimal here, at 78% ee.

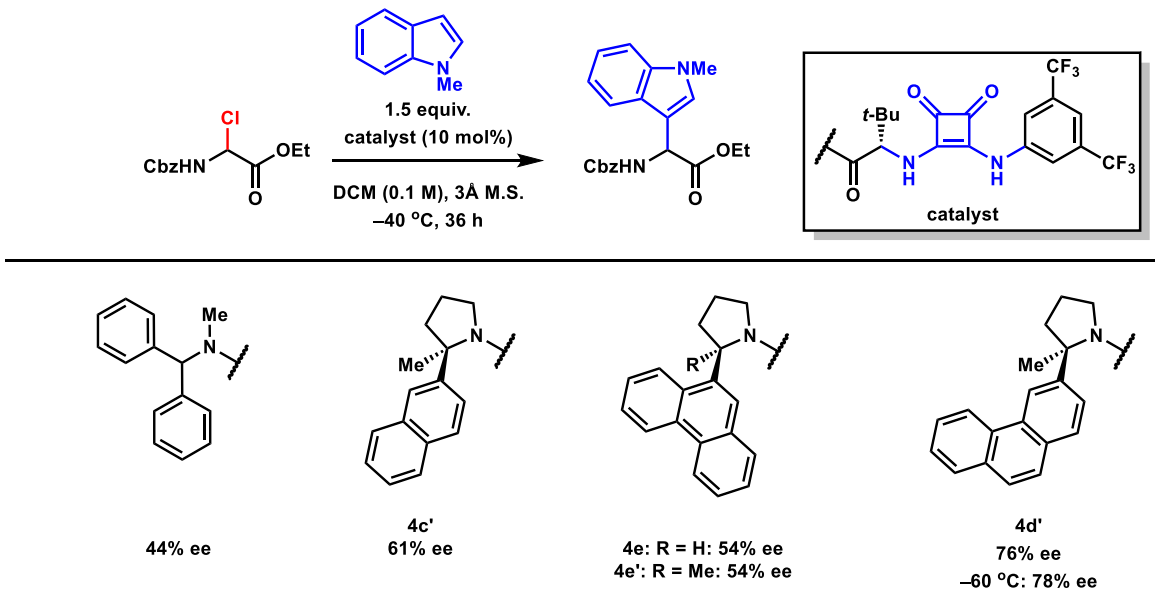

Figure 2.24 Catalyst screening in the reaction between **1-Cbz** and *N*-methyl indole

Enantioselectivities with *N*-Me indole, while promising, were unable to be optimized past the 78% ee barrier. *N*-Me indole is not an ideal substrate, as the products contain a methyl group that cannot be deprotected for further elaborations. Thus, *N*-benzyl indole was employed, as it can be deprotected under the same conditions as Cbz removal, and the additional arene may be a handle for achieving high enantioselectivity though secondary non-covalent attractive interactions.[91] Indeed, *N*-benzyl indole generally provided higher enantioselectivities than *N*-methyl indole and was a little bit slower to react, potentially as a result of a more sterically hindered nucleophile, and required he reaction to be run at –30 °C instead of –40 °C (Figure 2.25). Of the catalysts surveyed, arylpyrrolidine squaramides are optimal, with fully substituted 9-phenanthryl, **4e'** giving the best ee, at 88% ee. The arylpyrrolidine methylation has a profound impact on the enantioselectivity, which is in contrast to the *N*-methyl indole addition.

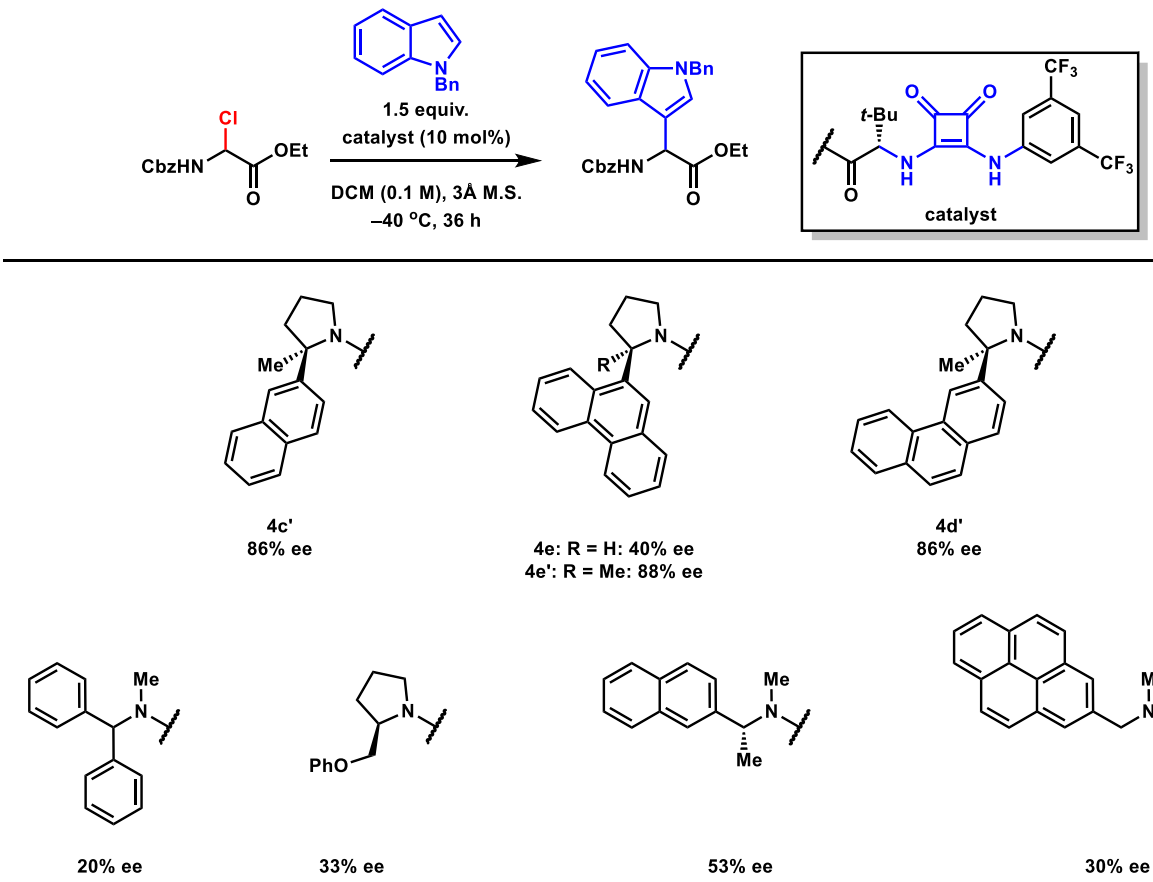

Figure 2.25 Catalyst screening in the reaction between **1-Cbz** and *N*-benzyl indole

Given the markedly improved enantioselectivities with *N*-benzyl indole, a few other protecting groups were screened, *N*-allyl and *N*-TBS; the results with two optimal catalysts and a separate class of benzhydryl amide catalyst can be found in Figure 2.26. *N*-allyl was found to give enantioselectivities intermediate to those with *N*-methyl and *N*-benzyl indoles. *N*-TBS indole decomposed under the reaction conditions to give a messy reaction, in which some *N*-H indole containing products could be detected in low ee (<30%). In conclusion, indole nucleophiles can be employed as nucleophiles with the **1-Cbz** electrophile, in which the selectivity trend is *N*-Bn > *N*-allyl > *N*-Me. Interestingly, while there are relatively few catalysts trends that can be explained by inspection, the optimal catalyst for each indole nucleophile are the fully substituted 2-naphthyl, and 3- and 9-phenanthrly squaramide catalysts (**4c'-e'**) which are also the three catalysts that provide the highest enantioselectivity in the allylation of **1**.

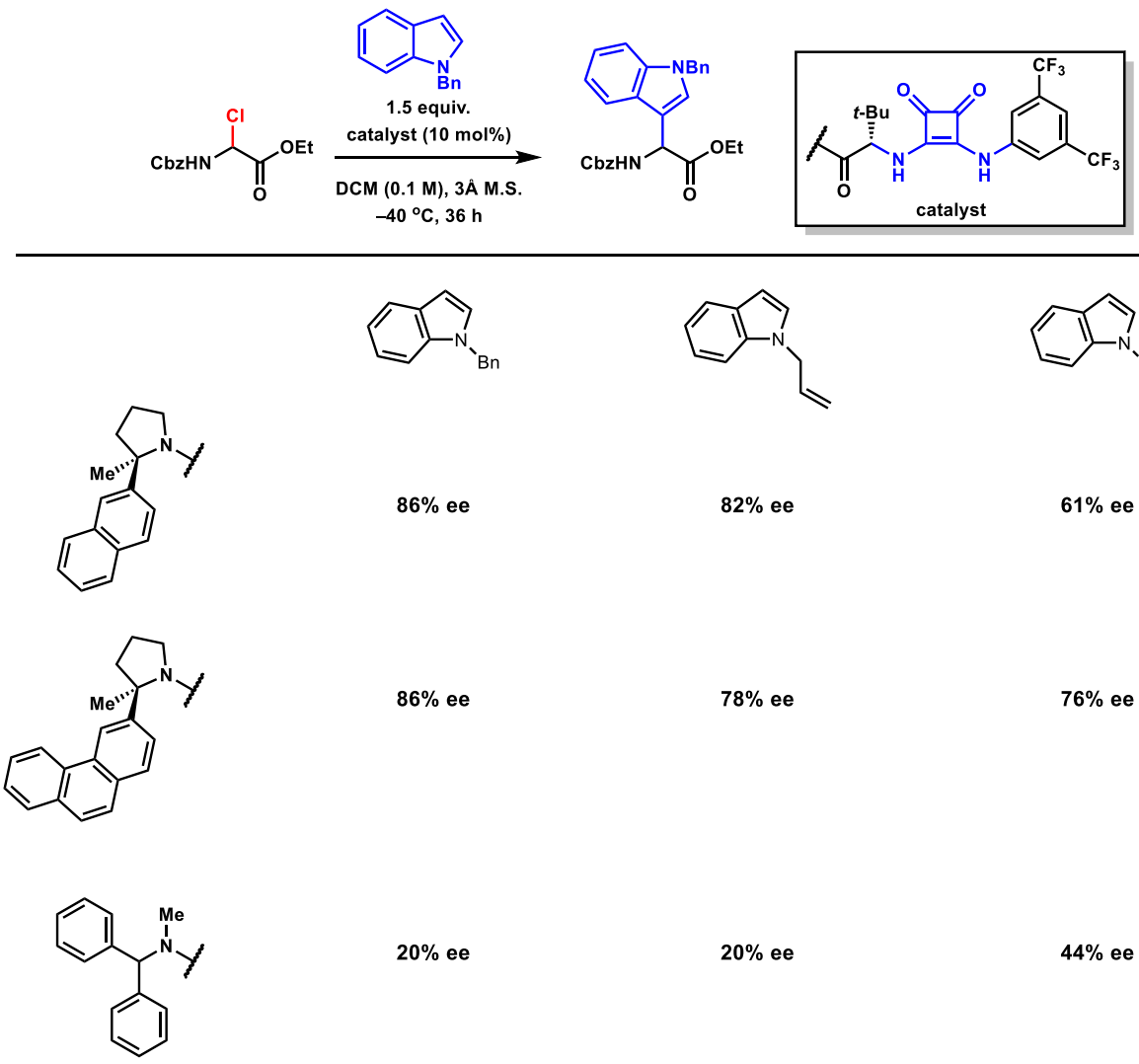

Figure 2.26 Enantioselectivities with *N*-substituted indole nucleophilic addition to **1-Cbz**

Due to the inability to optimize the enantioselectivity of the addition of indoles to **1-Cbz** beyond 88%, **1-Fmoc** was explored as an alternative electrophile. Initial catalyst screening was performed employing 2 equivalents of *N*-methyl indole at –60 °C (Figure 2.27). A comprehensive catalyst screen of amido half-Schreiner squaramides revealed that a number of catalysts are capable of inducing high levels of enantioselectivity (93-97% ee). This transformation seems completely insensitive to the size of the catalyst arene, with phenyl **4a** and 9-phenanthryl **4e** bearing catalysts both providing 94% ee. Contrary to results with other electrophile nucleophile

combinations, the conformational rigidity pyrrolidine affords is not needed, with open chain benzyl-type amides also catalyzing the reaction in 91-95% ee. Interestingly the one catalyst that affords poor enantioinduction is the open-chain 2-naphthyl catalyst where the benzylic stereocenter is mismatched with *t*-leucine (17% ee), although removal of this stereocenter altogether recovers the selectivity to 95% ee. The phenylprolinol catalyst is optimal for enantioselectivity at 97%. Interestingly, in contrast to all other electrophile nucleophile combinations, installation of the geminal methyl substituent on catalyst **4d'** substantially decreased the enantioselectivity to 81%.

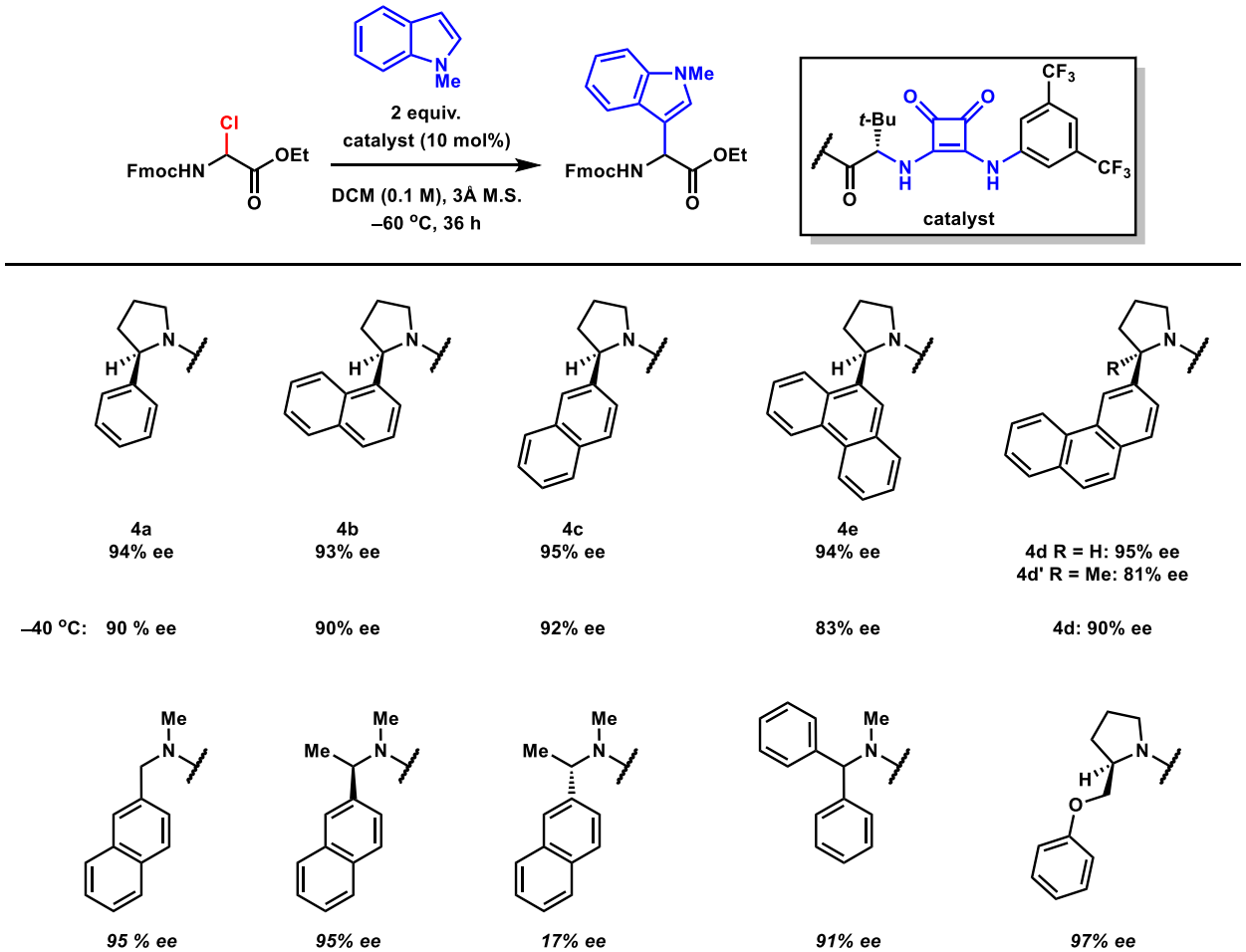

Figure 2.27 Catalyst screening in the reaction between **1-Fmoc** and *N*-methyl indole

Last, running the reaction at –40 °C provided a minor decrease in enantioselectivity for

catalysts with small arenes and a larger decrease for catalysts with large arenes. It would be interesting to follow up with an Eyring analysis to understand the enthalpic and entropic contributions to enantioselectivity from each of the catalysts to better understand the role the arene plays in achieving high enantioinduction.

Encouraged by the results with **1-Fmoc** and *N*-methyl indole, indoles with removable protecting groups were screened. Unfortunately, the reactions with *N*-allyl and *N*-benzyl indole and **1-Fmoc** did not proceed except for at extremely elevated reaction temperatures of 0 °C. It is both strange and unclear why these reactions that have a minimal steric and electronic perturbation require 60 degrees warmer reaction temperatures. The best hypothesis is that the catalyst, Fmoc and indole all have rigid large arenes that may create a congested steric pocket that rejects indoles with substitution larger than a methyl group.

Given the inability to engage indole nucleophiles with large substitution, *N*-H indole was examined as a nucleophile with electrophile **1-Fmoc** (Figure 2.28). Unfortunately, with both arylpyrroldine and open-chain catalysts, the enantioselectivity of this transformation was only moderate and unresponsive to changes to the catalyst, with phenyl catalyst **4a** and 9-phenanthryl catalyst **4e** giving the best enantioselectivities at 75% and 73% ee respectively. The enantioselectivity was relatively insensitive to catalyst parameters, with no trend with arene size, as similarly seen with *N*-methyl indole and **1-Fmoc**. For unknown reasons, 3-phenantrhryl catalyst **4d** is substantially worse than all other arylpyrrolidine catalysts. Open-chain catalysts perform relatively similarly to pyrrolidine catalysts, also as seen with *N*-methyl indole. Fully substituted aryl pyrrolidines were not tested in this context due to their poor performance with *N*-methyl indole, although for completeness should be tested.

The results and catalyst trends with **1-Fmoc** in the case of 2-methyl furan, and *N*-methyl

and *N*-benzyl indole seem divergent from the results with **1-Cbz** arylations and allylations of both **1-Fmoc** and **1-Cbz**. Specifically when **1-Fmoc** is employed in arylation, the size of the catalyst arene tends to play a small role in governing selectivity, methylation of the catalyst is detrimental or has no impact, and open chain catalysts perform similarly to pyrrolidine catalyst. One hypothesis is that Fmoc is intramolecularly stabilizing buildup of charge and thus the catalyst features governing enantioselectivity are largely steric rather than attractive stabilization of charge buildup, as will be discussed in Chapter 3.

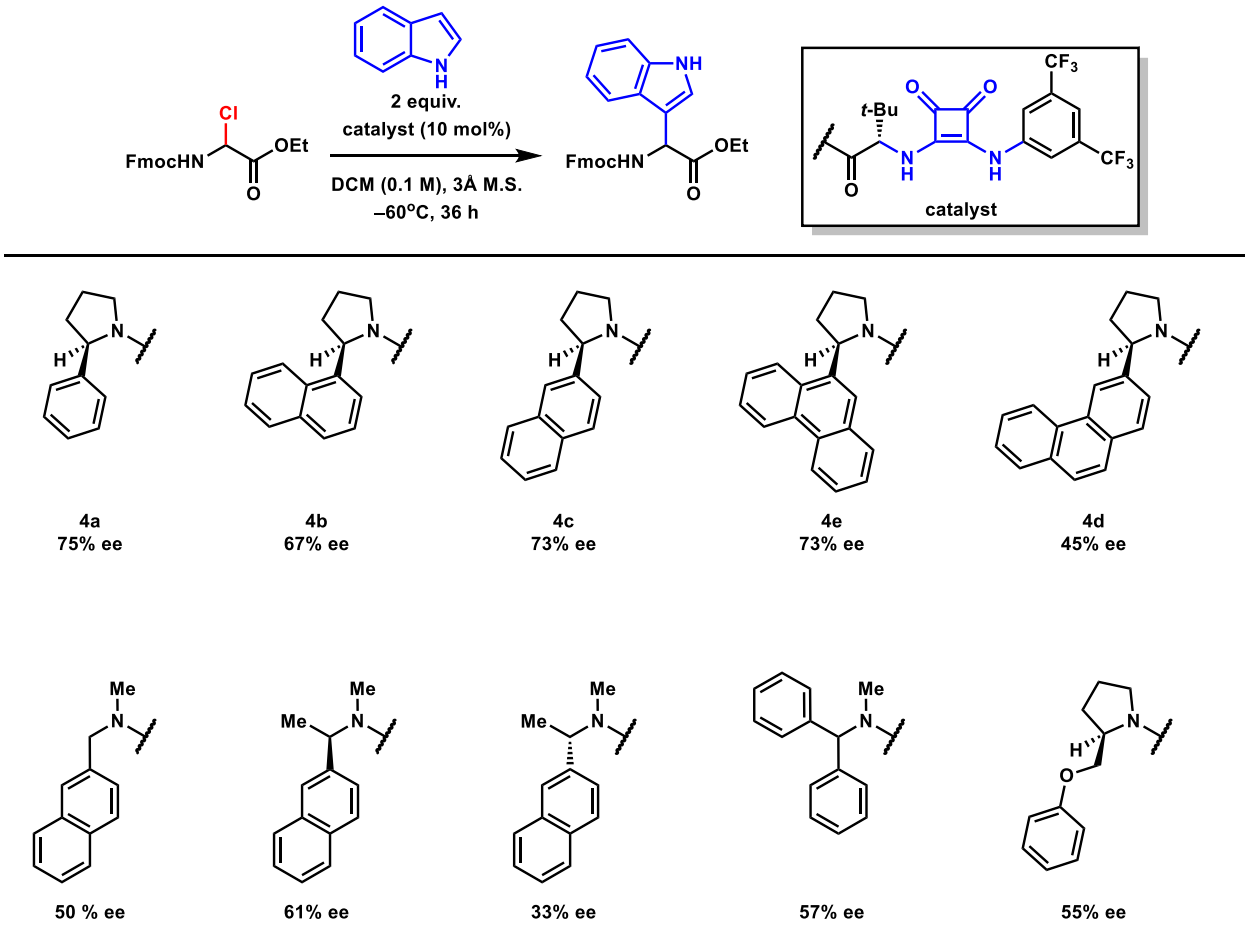

Figure 2.28 Catalyst screening in the reaction between **1-Fmoc** and *N*-H indole

2.9.3 Reaction optimization with 1,3-dimethoxybenzene as nucleophile

The optimization of nucleophilic addition of 1,3-dimethoxybenzene was underexplored relative to the optimization of other Friedel-Crafts nuclophiles. This section will onlydetail the

catalyst effects in the addition of 1,3-dimethoxybenzene to **1-Cbz** and **1-Fmoc**. Extensive screening of reaction parameters found that the optimal conditions for this transformation are similar to those for 1-methyl indole; specifically, 2 equivalents of nucleophile relative to electrophile, electrophile has 0.1 M in DCM, and the reaction is run at –15 °C, and with powdered 3Å molecular sieves (60 mgs/1mL solvent). –15 °C was chosen as racemic background does not occur at this temperature, enantioselectivity is optimal and the reaction proceeds to 60-80% conversion in 24 hours.

Initial screening was performed on the **1-Cbz** electrophile and the catalyst trends found were relatively similar to those in the allylation of **1-Cbz** (Figure **2.29**). 9-phenanthryl thioureas and ureas, **6e** and **7e**, provide minimal yields and racemic or near racemic product (<5% ee). Among squaramide catalysts, those with large arenes provide higher enantioselectivities than those with small arenes, with catalyst **4d'** being optimal at 81% ee; if the dicyano analog, which was optimal in the allylation is employed, the reaction temperature can be lowered to –25 °C, while mainting 56% yield, which provides a substantial increase to 88% ee. In addition, methylated catalysts **4a'-e'** are substantially better than non-methylated catalysts **4a-e**. The product yield was not rigorously measured but catalysts bearing large arenes provide substantially higher conversion than those with small arenes (80% for **4e'** vs. 52% with **4a'**).

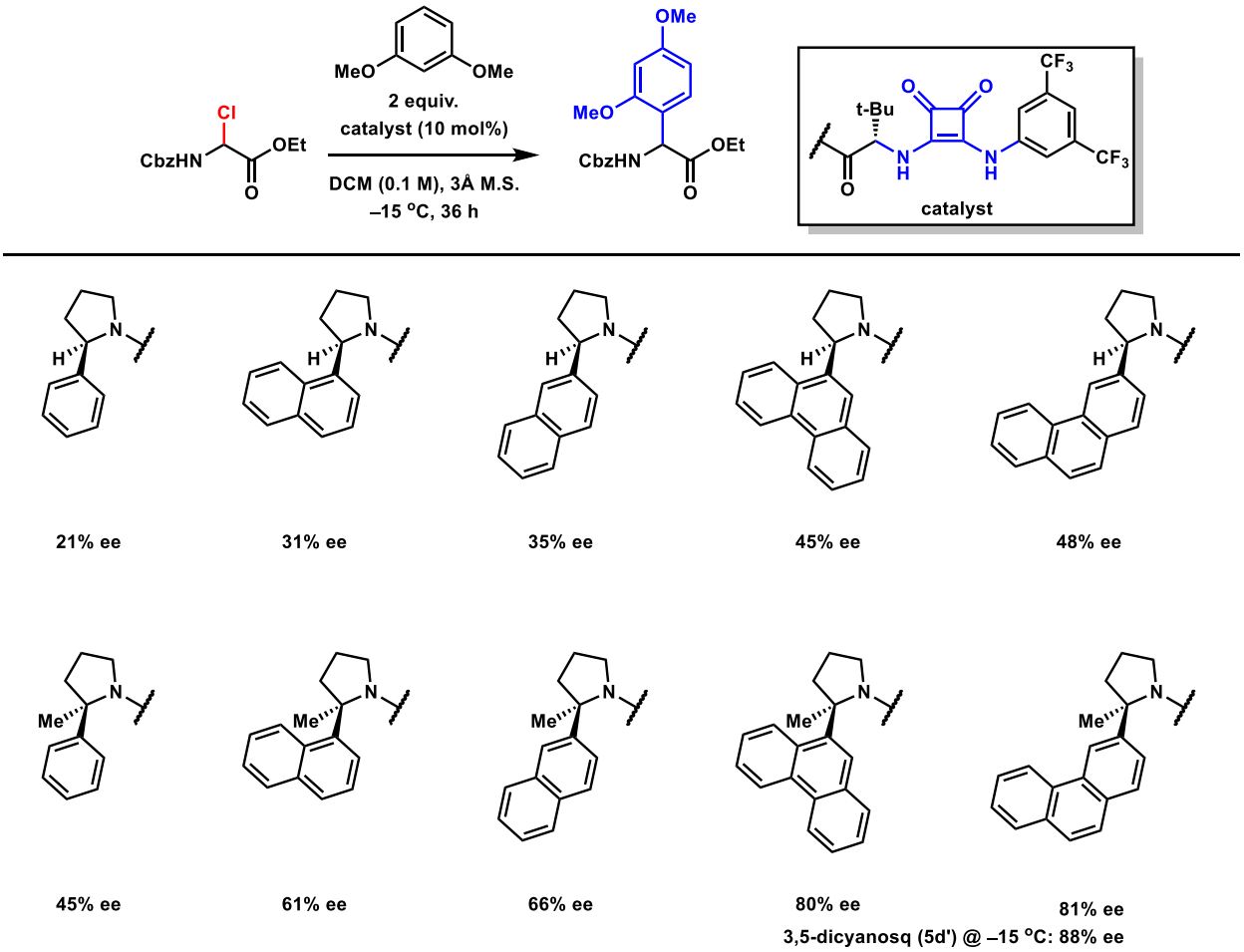

Figure 2.29 Catalyst screening in the reaction between **1-Cbz** and 1,3-dimethoxybenzene

The effect of arylpyrrolidine catalyst arene was also examined in the addition of 1,3-dimethoxybenzene with **1-Fmoc**, especially considering **1-Fmoc** tends to be an electrophile more suited to providing high enantioselectivities in Friedel-Crafts chemistry (**Figure 2.30**). The catalyst arene has a minimal effect on the enantioselectivity of this transformation, with 9-phenantrhyl catalyst being optimal at 85% ee. Other arenes (catalysts **4a-4e**) provide similar levels of selectivity, spanning 68-85% ee, with larger arenes providing somewhat higher selectivities. In this case the addition of a methyl substituent provides a huge decrease in enantioselectivity and reactivity, with yields below 50% and enantioselectivities in the 20-55% range. The effect of arene size on enantioselectivities with methylated catalysts is random in this specific transformation, given that methyl is optimal here, one hypothesis is that the poor yields and selectivity is the result

of a destabilizing steric interaction between catalyst and either the nucleophile or electrophile in the transition state.

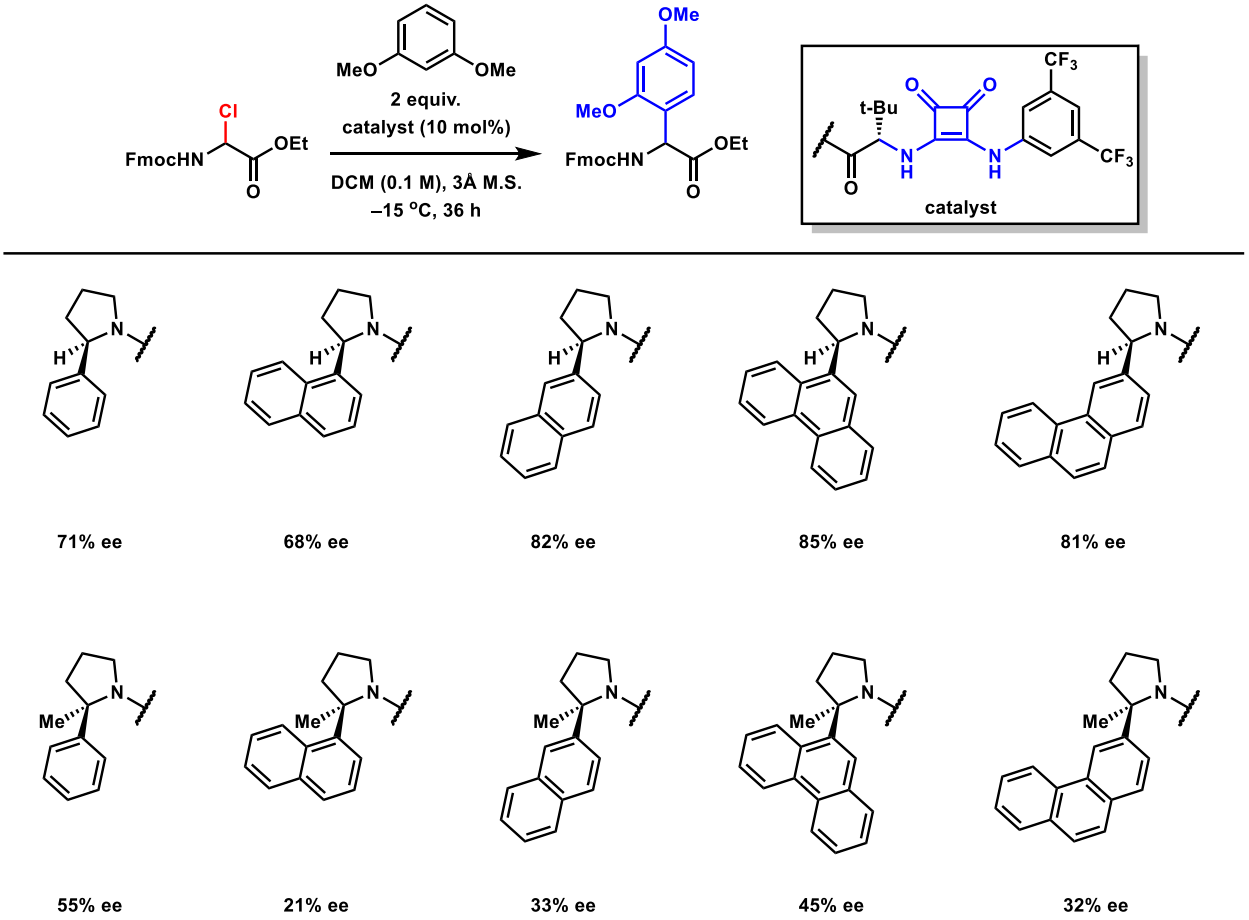

Figure 2.30 Catalyst screening in the reaction between **1-Fmoc** and 1,3-dimethoxybenzene

Last, the optimal reaction for **1-Fmoc**, employing catalyst **4e** was run in toluene, and the ee was found to be the exact same with only ~10% conversion. The substrate is poorly soluble in toluene, thus attempting this with the optimal **1-Cbz** result would be interesting. Further screening in this reaction would be beneficial. There are many arylpyrrolidines that could be screened in this transformation as well as open-chain catalysts. This has been a challenging nucleophile for enantioselectivity in Jørgensen's copper catalyzed Friedel-Crafts arylation of imines.[62]

2.10 Conclusion

An enantio- and diastereoselective synthesis of α-allyl amino esters was accomplished via

allylation of α-chloro glycine esters with a chiral squaramide hydrogen-bond donor as an anion-abstraction catalyst. Using either allylsilane or allylstannane nucleophiles, 15 representative α-allyl amino esters were constructed in high enantio- (up to 97% ee) and diastere-oselectivities (> 10:1 dr). The silane addition reaction was carried out on gram-scale at 0.5 M concentration using 1 mol% catalyst.

Using the same strategy as with allylation, an enantioselective synthesis of α-aryl amino esters was accomplished via Friedel-Crafts addition of furan, indole, and 1,3-dimethoxybenzene nucleophiles to α-chloro glycine esters with a chiral squaramide hydrogen-bond donor as an anion-abstraction catalyst. 2-methylfuran addition occurs with 90% ee to the Fmoc protected α-chloro glycine ester, *N*-methylindole addition occurs with 97% ee to the same Fmoc protected substrate, and 1,3-dimethoxybenzene addition occurs with 88% ee to the Cbz protected substrate. The full substrate scope within these classes of nucleophiles is yet to be explored.

A number of both consistent and divergent catalyst trends were observed in the addition of these diverse classes of nucleophiles. Namely, with Cbz-protected substrates, and universally in the allylation chemistry, arene size and catalyst methylation are essential to achieving high enantioinduction, and the fully substituted 3-phenanthryl squaramide **4d'** is optimal or near optimal across all nucleophiles; whereas in arylations employing Fmoc-protected substrates, all squaramide catalysts perform similarly well and without obvious trends. Understanding the mechanism of these reactions and the catalyst effects governing enantioselectivity in these transformations is of the highest interest, and will be the subject of Chapter 3.

2.11 Experimental

2.11.1 General Considerations

2.11.1.1 General Experimental Procedures

All reactions for the preparation of allylsilanes were performed in standard, dry glassware fitted with rubber septa under an inert atmosphere of nitrogen unless otherwise described. All catalytic reactions were set up at –78 °C in a dry ice acetone bath, in oven dried 2-dram vials with screw on caps fitted with septa under an inital atmosphere of nitrogen; after 30 minutes at –78 °C, nitrogen lines were removed from reactions and the vessels were moved into an immersion cooler (Neslab CC 100) at the temperature specified. Air and/or moisture sensitive liquids were transferred with stainless steel cannulae or with glass Hamilton gas-tight syringes fitted with stainless-steel needles. Reported concentrations refer to solution volumes at room temperature. Concentration of organic solutions under reduced pressure was performed using rotary evaporation under house vacuum (ca. 40 mm Hg) in a Büchi rotary evaporator at 30 °C. Reactions were monitored by thin-layer chromatography (TLC) on Silica Gel 60 F254 plates (EMD), visualized under UV light (λ_{ex} = 254 nm) or with potassium permanganate, which developed upon heating. Flash chromatography was performed using SiliaFlash P60 (230–400 mesh, SiliCycle), in 3-mL pipette on screening scale and on a 10g biotage cartridge on 0.5 mmol scale.

2.11.1.2 Materials

Reagents were purchased in reagent grade from commercial suppliers, including Sigma-Aldrich, Alfa Aesar, Strem, Oakwood, Matrix Scientific, and TCI, and were used without purification, unless otherwise indicated. Anhydrous solvents (benzene, dichloromethane, diethyl ether, *N*,*N*-dimethylformamide, tetrahydrofuran, and toluene) were prepared by passing the solvent through an activated alumina column. Triethylamine and diisopropylethylamine were distilled

over calcium hydride at atmospheric pressure or taken from Sigma-Aldrich sure/seal^{TM} bottles. Deuterated solvents — namely $CDCl_3$, CD_3OD, C_6D_6 and DMSO−d_6, (Cambridge Isotope Laboratories) — and extraction, chromatography and HPLC solvents (BDH or EMD) were used without purification. 3Å powdered molecular sieves were purchased from Sigma-Aldrich and put in an oven overnight before use (see below for more on sieves).

2.11.1.3 Instrumentation

Proton nuclear magnetic resonance (^{1}H NMR) spectra and protondecoupled carbon nuclear magnetic resonance (^{13}C {^{1}H} NMR) spectra were recorded at 25 °C (unless stated otherwise) on Inova 600 (600 MHz) or Varian Unity/Inova 500 (500 MHz) spectrometers at the Harvard University nuclear magnetic resonance facility. Chemical shifts (δ) for protons are reported in parts per million (ppm) downfield from tetramethylsilane and are referenced to residual protium in the NMR solvent. Chemical shifts for carbon are reported in parts per million downfield from tetramethylsilane and are referenced to the carbon resonances of the solvent. The solvent peak was referenced to 7.26 ppm for ^{1}H and 77.16 ppm for ^{13}C for $CDCl_3$, to 7.16 ppm for ^{1}H and 128.06 ppm for ^{13}C for C_6D_6, to 3.31 ppm for ^{1}H and 49.00 ppm for ^{13}C for CD_3OD, to 5.32 ppm for ^{1}H and 54.0 ppm for ^{13}C for CD_2Cl_2. Data are represented as follows: chemical shift, integration, multiplicity (br = broad, s = singlet, d = doublet, t = triplet, q = quartet, qn = quintet, sx = sextet, sp = septet, m = multiplet), coupling constants are reported in Hertz (Hz).

Note on nmr spectra, rotomers, and diastereomers: Products exist as a mixture of benzyl carbamate rotomers. Most protons were acquired in C_6D_6, as it was the solvent in which one rotomer was heavily favored. Carbons were taken in $CDCl_3$ due to a large residual solvent signal of C_6D_6 at 128 ppm, a peak dense region for the products. As a result, some carbamate peaks appear doubled in the ^{13}C spectra taken in $CDCl_3$. Adittionally, diastereomeric ratios were determined via relative

integration of the adjacent α, β methynyl protons, which are well resolved and presumed to have similar relaxation delays. Diastereomers were chromatographically inseperable unless subjected to preparative scale high pressure/performance liquid chromatography and thus reported ^{1}H and ^{13}C nmrs are a mixture of diastereomers when noted.

Optical rotations were measured using a 1 mL cell with a 5 cm path length on a Jasco P-2000 digital polarimeter.

High-resolution mass spectrometry (HRMS) was measured using an Agilent 6520 QTOF LC-MS.

Chiral high performance liquid chromatography (HPLC) analysis was performed using an Agilent 1200 quaternary HPLC system with commercially available AS-H, AD-H, OD-H (diacel) and (s,s)-whelk (regis tech) chiral columns, with products detected using UV absorbance at 210, 220, 230, 254, and 300 nm.

X-ray Crystallography: A crystal mounted on a diffractometer was collected data at 100 K. The intensities of the reflections were collected by means of a Bruker APEX II DUO CCD diffractometer (CuK radiation, = 1.54178 Å), and equipped with an Oxford Cryosystems nitrogen flow apparatus. The collection method involved 1.0□ scans in □ at -30□, -55□, -80□, 30□, 55□, 80□ and 115□ in 2. Data integration down to 0.84 Å resolution was carried out using SAINT V8.35 A (Bruker diffractometer, 2015) with reflection spot size optimization. Absorption corrections were made with the program SADABS (Bruker diffractometer, 2015). The structure was solved by the Intrinsic Phasing methods and refined by least-squares methods again F2 using SHELXT-2014 (Sheldrick, 2015) and SHELXL-2014 (Sheldrick, 2015) with OLEX 2 interface (Dolomanov, et al., 2009). Non-hydrogen atoms were refined anisotropically, and hydrogen atoms were allowed to ride on the respective atoms. Crystal data as well as details of data collection and

refinement are summarized in the crystallography section of the SI in Table 1, geometric parameters are shown in Table 2 and hydrogen-bond parameters are listed in Table 3. The Ortep plots produced with SHELXL-2014 program, and the other drawings were produced with Accelrys DS Visualizer 2.0 (Accelrys, 2007).

2.11.2 Catalyst Synthesis and Characterization Data

Amidopyrrolidino squaramide catalysts of the type **4a-4e, 3e, and 5e** bearing an α-secondary amide on the aryl-pyrrolidine moity are reported and were prepared following reported syntheses outlined in the Figure 2.31 below. [95,99b,129,130]

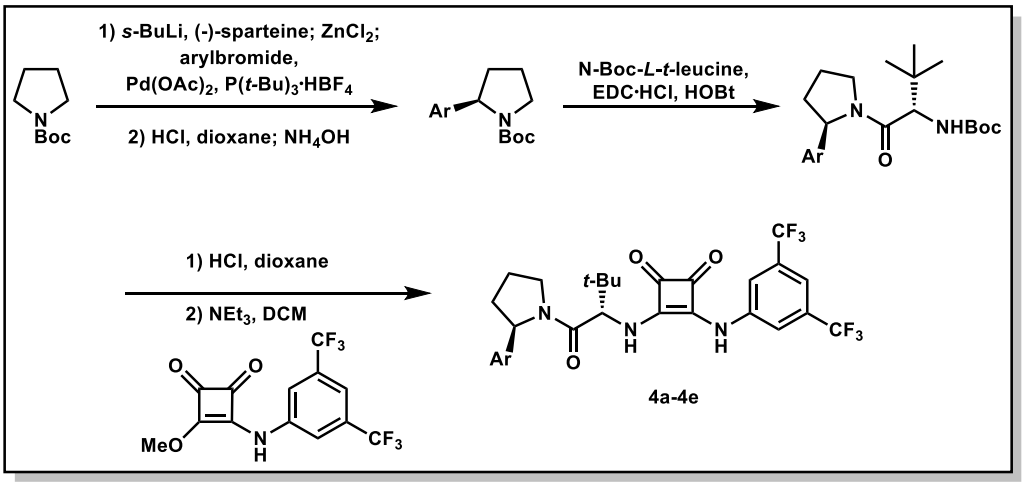

Figure 2.31: Synthesis of an α-secondary amido aryl-pyrrolidine catalysts **4a-4e**

Amidopyrrolidino squaramide catalysts of the type **4a'-4e' and 5d'** bearing an α-tertiary amide on the aryl-pyrrolidine were prepared following the synthetic route outlined in the Figure 2.32 below.

[129] Campos, K. R.; Klapars, A.; Waldman, J. H.; Dormer, P. G.; Chen, C. Enantioselective, Palladium-Catalyzed α-Arylation of N-Boc-Pyrrolidine. *J. Am. Chem. Soc.* **2006**, *128* (11), 3538–3539.

[130] Reisman, S. E.; Doyle, A. G.; Jacobsen, E. N. Enantioselective Thiourea-Catalyzed Additions to Oxocarbenium Ions. *J. Am. Chem. Soc.* **2008**, *130* (23), 7198–7199.

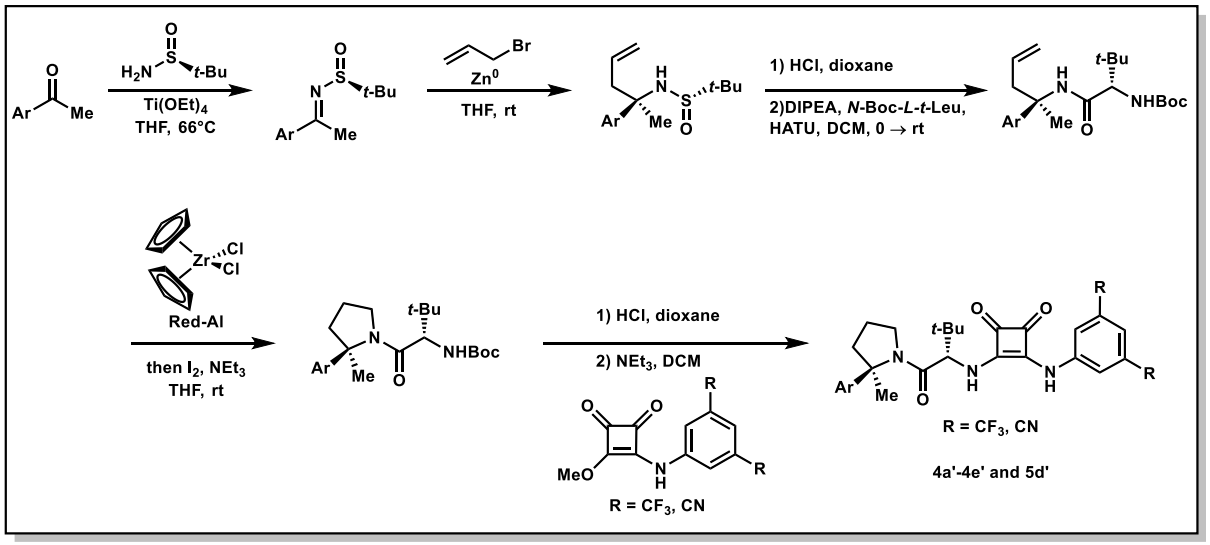

Figure 2.32: Synthesis of an α-tertiary amido aryl-pyrrolidine catalysts **4a'-4e' and 5d'**

2.11.2.1 Synthesis of catalyst 5d' and intermediates

(S,E)-2-methyl-N-(1-(phenanthren-3-yl)ethylidene)propane-2-sulfinamide (S1)

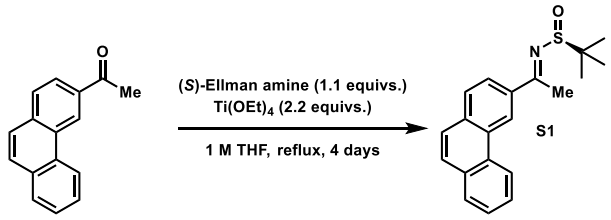

To a 50 mL flame dried flask equipped with a stir bar was added 1.99 g (9 mmol) of 3-acetylphenanthrene, 1.2 g (9.9 mmol, 1.1 equivs.) of (S)-(−)-2-Methyl-2-propanesulfinamide, and 9 mL (1 M) of THF. The flask was put under nitrogen. 4.51 g (19.8 mmol, 2.2 equivs. 4.15 mL, ρ = 1.088 g/mL) $Ti(OEt)_4$ was stored and weighed out in a glovebox and added via syringe to the reaction flask. The reaction vessel was the fitted with a reflux condenser and refluxed for 4 days. Reaction can be monitored via TLC to check for completion. (Note: many vendors sell 3-acetylphenanthrene with up to 10% 2-acetylphenanthrene contaminant, try to avoid contaminated bottles, as separations become quite challenging, cutting yields in up to half).

The reaction was quenched by dumping into 30 mLs stirring brine and diluted with 20 mL ethyl acetate. The biphasic mixture was filtered through celite into a separatory funnel. The brine

layer was washed with 2 x 20 mL of ethyl acetate. Combined organics were washed with brine and dried over Na_2SO_4, filtered and evaporated *in vacuo*.

The crude concentrate was loaded onto a packed 100g isolera biotage cartridge with ~5 mL of benzene and eluted using the following gradient and monitoring absorbance at 254 and 280 nm:

2 column volumes isocratic 90:10 Hexanes: EtOAc

10 column volumes gradient from 90:10 Hexanes: EtOAc to 40:60 Hexanes: EtOAc

2 column volumes isocratic 40:60 Hexanes: EtOAc

Product eluted from 60:40 Hexanes: EtOAc to 50:50 Hexanes: EtOAc

Yield 2.26 g (7.0 mmol, 78% yield)

^{1}H NMR (600 MHz, Chloroform-d) δ 9.19 (s, 1H), 8.70 (d, J = 7.7 Hz, 1H), 8.13 (d, J = 8.3 Hz, 1H), 7.90 (dd, J = 10.8, 8.2 Hz, 2H), 7.82 (d, J = 8.8 Hz, 1H), 7.74 (d, J = 8.8 Hz, 1H), 7.71 (ddd, J = 8.3, 7.0, 1.4 Hz, 1H), 7.64 (ddd, J = 8.0, 6.9, 1.2 Hz, 1H), 2.97 (s, 3H), 1.40 (s, 9H).

^{13}C NMR (126 MHz, cdcl$_3$) δ 176.45, 136.68, 134.20, 132.33, 130.62, 129.84, 129.20, 128.97, 128.83, 127.27, 127.19, 126.41, 124.97, 122.59, 122.40, 64.49, 57.76, 22.78.

HRMS: calculated for [$C_{20}H_{21}NOS + H^+$] 324.1422, found 324.1408.

$[\alpha]^{25.5}_D$ = 3.2° (c = 1.0, $CHCl_3$)

tert-butyl ((S)-3,3-dimethyl-1-((R)-2-methyl-2-(phenanthren-3-yl)pyrrolidin-1-yl)-1-oxobutan-2-yl)carbamate (S2)

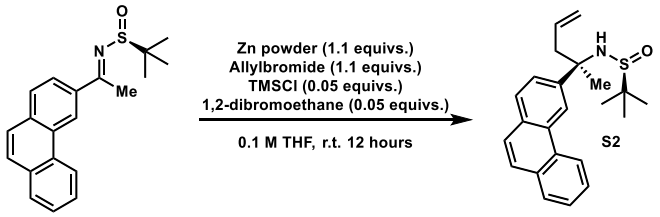

To a 200 mL flame dried Schlenk flask equipped with a stir bar was added 0.503 g (7.7 mmol) of Zn dust followed by 70 mL THF (0.1M with respect to ketimine). The flask was put

under nitrogen and 50 μL each of 1,2-dibromoethane and TMSCl were added to initiate. 0.93 g (7.7 mmol, 1.1 equivs. 0.67 mLs, ρ = 1.398 g/mL) allylbromide was added. Reaction was stirred for an hour over which the solution went from being heterogeneous and gray to homogenous and pale yellow, indicating zinc consumption. Upon complete consumption of the zinc, a solution of ketimine **S1** (2.26 g, 7.0 mmol) was added in minimal THF, ~10 mL. The reaction stirred overnight.

The reaction was quenched after 12 hours with 50 mL each saturated sodium bicarbonate and ethyl acetate. Initially an emulsion is formed and after vigorous stirring for 2 hours, two distinct layers form. The biphasic mixture was transferred to a separatory funnel and the aqueous layer was washed with 100 mL ethyl acetate. Combined organics were washed with brine and dried over sodium sulfate and concentrated *in vacuo* to yield a yellow foam. Crude NMR shows the product was formed as a single diastereomer.

The reaction was loaded in 5-7 mL DCM onto a 100g isolera biotage cartridge.

2 column volumes isocratic 60:40 hexanes:Et_2O

10 column volumes linear gradient from 60:40 hexanes:Et_2O to 100% Et_2O

4 column volumes isocratic 100% Et_2O

Remaining ketimine elutes around 50-60% ether. Product begins to elute around 70-80% Et_2O and ends 1-2 column volumes into the 100% ether fractions (pdt. Has rf 0.3 in Et_2O)

Yield 2.23 g (6.1 mmol, 87% yield)

*Note, for ortho-fused arenes, i.e. 1-naphthyl and 9-phenanthryl this reaction provided poor yields and/or selectivities, so grignard additions were performed instead of organozinc additions.

^{1}H NMR (600 MHz, Chloroform-d) δ 8.80 (d, J = 1.8 Hz, 1H), 8.67 (d, J = 7.8 Hz, 1H), 7.90 (dd, J = 7.9, 1.4 Hz, 1H), 7.88 (d, J = 8.3 Hz, 1H), 7.76 – 7.71 (m, 2H), 7.71 – 7.65 (m, 2H), 7.61 (ddd,

J = 8.0, 6.9, 1.2 Hz, 1H), 5.63 (ddt, J = 17.5, 10.2, 7.4 Hz, 1H), 5.24 (dd, J = 17.0, 2.1 Hz, 1H), 5.16 (dd, J = 10.2, 2.1 Hz, 1H), 3.93 (s, 1H), 2.84 (dd, J = 7.4, 2.9 Hz, 2H), 1.98 (s, 3H), 1.29 (s, 9H).

^{13}C NMR (126 MHz, cdcl3) δ 143.52, 133.15, 132.27, 130.97, 130.40, 129.88, 128.75, 128.60, 127.17, 126.69, 126.66, 126.42, 125.26, 122.44, 120.56, 120.46, 77.41, 77.16, 76.90, 60.51, 56.34, 49.41, 28.01, 22.97.

HRMS: calculated for [$C_{23}H_{27}NOS + H^+$] 366.1892, found 366.1871.

$[\alpha]^{25.4}_D$ = 24.0° (c = 1.0, $CHCl_3$)

tert-butyl ((S)-3,3-dimethyl-1-oxo-1-(((R)-2-(phenanthren-3-yl)pent-4-en-2-yl)amino)butan-2-yl)carbamate (S3)

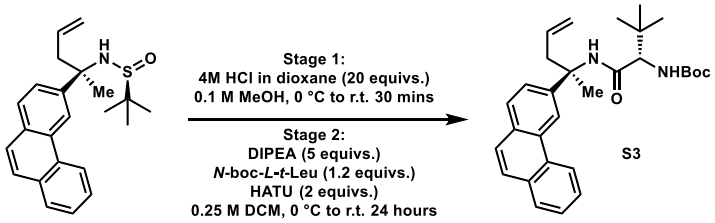

Stage 1: To a flame dried 100 mL round bottom flask equipped with a stir bar was added 1.0 g (2.7 mmol) of the sulfinamide starting material **S2** and the flask was equipped with a septum and put under nitrogen. 27 mL of anhydrous methanol was added via syringe and the reaction vessel was cooled to 0 °C in an ice water bath. 13.6 mL of 4 M HCl in dioxane was added over the course of approx. 3 minutes. The ice bath was removed and the reaction stirred for 30 minutes, after which the reaction was complete by TLC analysis. The reaction was sparged with nitrogen for 30 minutes to remove dissolved HCl and then solvent was removed *in vacuo*. The reaction flask was put under high vacuum (0.5 Torr) overnight to remove residual dioxane.

Stage 2: Assume 100% yield in stage 1. The ammonium chloride salt was redissolved in 10.8 mL DCM (0.25 M) and the reaction vessel was fitted with a stir bar, rubber septum and put

under nitrogen. The solution was cooled to 0 °C in an ice water bath and 2.35 mL DIPEA (5 equivs.) were added over 2 minutes, the reaction vessel may cloud a bit. After 15 minutes, 0.75 g *N*-boc-*L*-*tert*-leucine (1.2 equivs.) and 2.05 g HATU (2 equivs.) were added. The reaction was stirred overnight, and the ice bath was allowed to melt over the first couple hours of the reaction.

The reaction was quenched via dilution with 20 mL DCM and the addition of 25 mL of 1 M HCl in water. The biphasic mixture was poured into a separatory funnel and the organic layer was washed with 25 mL saturated aqueous sodium bicarbonate and 25 mL brine, successively. The organic layer was dried over Na_2SO_4, filtered, and concentrated *in vacuo* to yield a beige foam.

The reaction was loaded in 5 mL DCM onto a 100g isolera biotage cartridge packed with silica gel. The reaction was purified with the following eluent system.

2 column volumes isocratic 90:10 hexanes:Et_2O

8 column volumes linear gradient from 90:10 hexanes:Et_2O to 60:40 hexanes:Et_2O

4 column volumes isocratic 60:40 hexanes:Et_2O

Pdt elutes around 30% ether and is generally the first peak to elute

Yield 0.94 g (2.0 mmol, 73% yield)

^{1}H NMR (600 MHz, Chloroform-d) δ 8.75 (d, J = 8.3 Hz, 1H), 8.70 (d, J = 1.8 Hz, 1H), 7.88 (dd, J = 7.9, 1.4 Hz, 1H), 7.82 (d, J = 8.4 Hz, 1H), 7.70 (s, 2H), 7.66 (ddd, J = 8.3, 6.8, 1.4 Hz, 1H), 7.64 – 7.57 (m, 2H), 6.52 (s, 1H), 5.66 (ddt, J = 17.3, 10.2, 7.3 Hz, 1H), 5.42 (d, J = 9.5 Hz, 1H), 5.23 – 5.14 (m, 2H), 4.05 (d, J = 9.5 Hz, 1H), 2.88 (dd, J = 13.8, 7.5 Hz, 1H), 2.66 (dd, J = 13.9, 7.2 Hz, 1H), 1.94 (s, 3H), 1.52 (s, 9H), 1.10 (s, 9H).

^{13}C NMR (126 MHz, cdcl3) δ 169.96, 156.05, 143.44, 132.98, 132.10, 130.63, 130.34, 129.93, 128.51, 128.44, 126.59, 126.35, 126.30, 123.94, 122.57, 119.60, 118.78, 79.45, 77.41, 77.16, 76.90, 62.59, 58.24, 47.47, 34.27, 28.29, 26.68, 25.34.

HRMS: calculated for [$C_{30}H_{38}N_2O_3$ + H^+] 475.2961, found 475.2974.

$[\alpha]^{23.6}_D$ = –7.0° (c = 1.0, $CHCl_3$)

tert-butyl ((S)-3,3-dimethyl-1-((R)-2-methyl-2-(phenanthren-3-yl)pyrrolidin-1-yl)-1-oxobutan-2-yl)carbamate (S4)

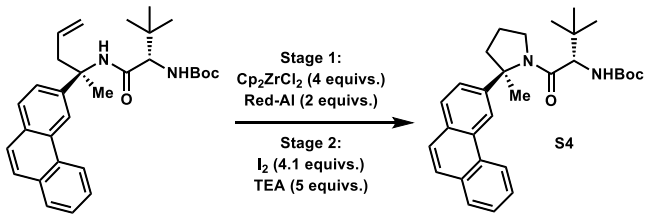

Stage 1: to a flame dried Schlenk flask equipped with a stir bar and fitted with a nitrogen/vacuum line was added 2.34 g zirconocene dichloride (8.0 mmol, 4 equivs.). Vacuum and nitrogen were cycled twice and the reaction left under nitrogen. 16 mLs of dry dioxane (0.125 M wrt allylamine) was then added via syringe and the suspension stirred at room temperature. 1.3 mLs of a solution of >60 wt% Red-Al in toluene (4.0 mmol, 2 equivs.) was added dropwise and the resulting off-white suspension was allowed to stir for 2.5 hours. The suspension was then cooled to 0 °C in an ice water bath and a solution of allyl amide **S3** (0.96 g, 2.0 mmol, 1 equiv.) in 16 mLs DCM (0.125 M) was added dropwise. The ice bath was then removed, and the resulting solution was allowed to stir overnight at room temperature.

Stage 2: The following day, the solution was again cooled to 0 °C and 2.08 g of I_2 (4.1 eq.) and 1.4 mL TEA (5 eq.) were added simultaneously. The ice bath was then removed, and the solution was allowed to stir at room temperature for 3 hours.

The solution was then diluted with additional DCM and passed through a silica plug eluting with ethyl acetate. The resulting filtrate was washed with saturated aqueous sodium thiosulfate and the organic layer was removed. The aqueous layer was extracted 2x with Et_2O and then the combined organic layers were washed with brine, dried over $MgSO_4$, filtered, and concentrated.

The reaction was loaded in 5 mL DCM onto a 100g isolera biotage cartridge packed with silica gel. The reaction was purified with the following eluent system.

2 column volumes isocratic 90:10 hexanes:Et_2O

8 column volumes linear gradient from 90:10 hexanes:Et_2O to 60:40 hexanes:Et_2O

4 column volumes isocratic 60:40 hexanes:Et_2O

Pdt elutes around 30% ether and is generally the first peak to elute, note: exact same column conditions as the previous reaction, due to complete conversion, this is not an issue.

Yield 0.59 g (1.24 mmol, 62% yield)

^{1}H NMR (600 MHz, Chloroform-d) δ 8.24 (d, J = 8.2 Hz, 1H), 8.11 (s, 1H), 7.44 (dd, J = 7.8, 1.4 Hz, 1H), 7.34 (d, J = 8.3 Hz, 1H), 7.20 (ddd, J = 8.4, 6.9, 1.5 Hz, 1H), 7.15 (ddd, J = 8.0, 7.0, 1.2 Hz, 1H), 6.99 (dd, J = 8.4, 1.9 Hz, 1H), 4.78 (d, J = 10.0 Hz, 1H), 4.03 (d, J = 10.1 Hz, 1H), 3.97 – 3.84 (m, 1H), 3.51 (dt, J = 10.0, 7.5 Hz, 1H), 1.79 – 1.71 (m, 2H), 1.68 (s, 3H), 1.60 – 1.49 (m, 2H), 1.08 (s, 9H), 0.64 (s, 9H).

^{13}C NMR (126 MHz, cdcl$_3$) δ 170.14, 156.48, 144.81, 132.32, 130.58, 130.54, 130.18, 128.62, 128.58, 126.66, 126.48, 126.40, 123.99, 122.72, 118.32, 79.59, 67.70, 58.93, 50.27, 44.86, 35.17, 28.57, 26.59, 25.36, 22.81.

HRMS: calculated for [$C_{30}H_{38}N_2O_3 + H^+$] 475.2961, found 475.2956.

$[\alpha]^{22.5}_D$ = 12.4° (c = 1.0, $CHCl_3$)

5-((2-methoxy-3,4-dioxocyclobut-1-en-1-yl)amino)isophthalonitrile (S5)

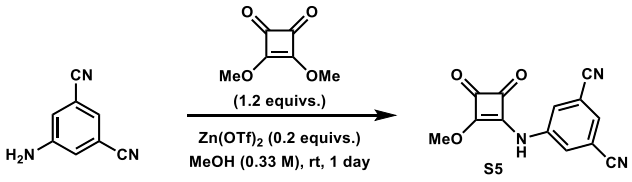

The procedure is adapted from the literature.[131] To a flame dried 50 mL round bottom flask equipped with a stir bar was added 1 g of 3,5-dicyanoaniline (7 mmol, 1 equiv.) and 1.9 g of dimethyl squarate (8.4 mmol, 1.2 equivs.). The reaction flask was capped with a rubber septum and put under nitrogen, after which 21 mL of anhydrous methanol were added via syringe. 0.51 g of $Zn(OTf)_2$ (1.4 mmol, 0.2 equivs.) were weighed out in a glovebox and quickly added as a solid to the reaction vessel. After stirring for a couple hours the reaction seizes and becomes a bright yellow sludge and it will remain that way the rest of the reaction.

The reaction was transferred with ~20 mLs methanol into a 50 mL falcon tube and centrifuged and decanted. The remaining pellet was added ~20 mL methanol and it was recentrifuged and decanted. This procedure was repeated 3 times. The product was a bright yellow solid that was still impure and was used without further purification.

Yield 1.24 g (4.9 mmol, 70% yield)

[131] Rostami, A.; Colin, A.; Li, X. Y.; Chudzinski, M. G.; Lough, A. J.; Taylor, M. S. *N* , *N′* -Diarylsquaramides: General, High-Yielding Synthesis and Applications in Colorimetric Anion Sensing. *J. Org. Chem.* **2010**, *75* (12), 3983–3992.

5-((2-(((S)-3,3-dimethyl-1-((R)-2-methyl-2-(phenanthren-3-yl)pyrrolidin-1-yl)-1-oxobutan-2-yl)amino)-3,4-dioxocyclobut-1-en-1-yl)amino)isophthalonitrile (5d')

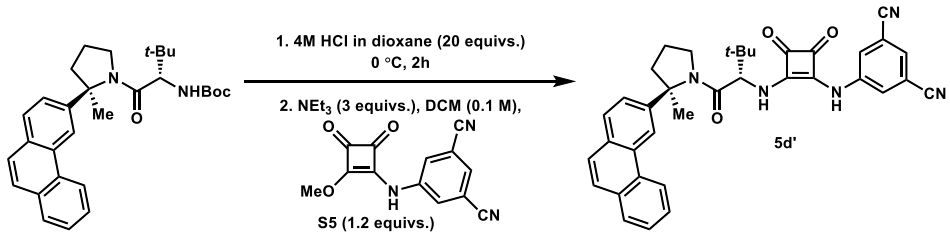

Stage 1: 0.5 g of Boc-amine **S4** (1.05 mmol, 1 equiv.) was added to a flame dried scintillation vial, which was put under nitrogen and cooled to 0 °C in an ice water bath. 4M HCl in dioxane (5.25 mL, 21.01 mmol, 20 equivs.) was added dropwise and the solution stirred at room temperature for 2 hours, after which the reaction mixture was concentrated to yield a yellow foam.

Stage 2: Assume 100% yield in stage one; the vial was put under nitrogen and DCM (10 mL, 0.1 M) was added. The vial was cooled to 0 °C in an ice water bath and triethylamine was added (0.44 mL, 3.15 mmol, 3 equivs.). After 15 minutes, 0.319 g of squaric ester **S5** was added (1.26 mmol, 1.2 equivs), the ice bath was allowed to melt and the reaction was stirred for 4 days.

The reaction mixture was concentrated and loaded in 3 mL DCM onto a 100g isolera biotage cartridge packed with silica gel. The reaction was purified with the following eluent system.

2 column volumes isocratic 50:50 hexanes:Et_2O

8 column volumes linear gradient from 50:50 hexanes:Et_2O to 100% Et_2O

2 column volumes isocratic 100% Et_2O

Pdt elutes around 80-90% ether

Product was subjected to a second column. Product was loaded in 3 mL DCM onto a 100g isolera biotage cartridge packed with silica gel and was purified with the following eluent system.

2 column volumes isocratic 100% DCM

8 column volumes linear gradient from 100% DCM to 90:10 DCM:MeOH

Pdt elutes around 5% MeOH and is a yellow/orange solid.

Yield: 0.400 g (0.672 mmol, 64% yield)

^{1}H NMR (600 MHz, DMSO-d6) δ 10.24 (s, 1H), 8.55 (d, J = 9.1 Hz, 1H), 8.39 (s, 1H), 8.36 (d, J = 10.0 Hz, 1H), 8.02 (dd, J = 31.4, 1.3 Hz, 2H), 7.89 – 7.84 (m, 2H), 7.79 – 7.71 (m, 2H), 7.56 (dd, J = 8.4, 1.8 Hz, 1H), 7.37 (tt, J = 7.1, 5.2 Hz, 2H), 5.14 (d, J = 9.9 Hz, 1H), 4.27 (ddd, J = 10.1, 7.6, 5.1 Hz, 1H), 3.93 (dt, J = 10.0, 7.3 Hz, 1H), 2.17 (ddd, J = 12.8, 8.7, 6.5 Hz, 1H), 2.11 (dt, J = 12.4, 6.1 Hz, 1H), 2.06 – 1.93 (overlapping s, 3H and m, 1H), 1.91 – 1.81 (m, 1H), 1.05 (s, 9H).

^{13}C NMR (126 MHz, dmso) δ 184.65, 180.51, 169.10, 167.50, 162.41, 144.62, 140.54, 131.64, 129.79, 129.59, 129.09, 128.78, 128.38, 128.25, 126.29, 126.16, 125.25, 124.23, 122.30, 118.18, 117.02, 113.57, 67.28, 61.59, 49.71, 43.96, 40.02, 39.85, 39.69, 39.52, 39.35, 39.19, 39.02, 35.63, 25.80, 24.57, 22.35.

HRMS: calculated for [$C_{37}H_{33}N_5O_3$ + H^+] 596.2662, found 596.2665.

$[\alpha]^{25.5}_D$ = 158.6° (c = 1.0, $CHCl_3$)

2.11.2.3 Characterization data for all novel catalysts in Chapter 2

3-((3,5-dichlorophenyl)amino)-4-(((S)-3,3-dimethyl-1-oxo-1-((R)-2-(phenanthren-9-yl)pyrrolidin-1-yl)butan-2-yl)amino)cyclobut-3-ene-1,2-dione (3e)

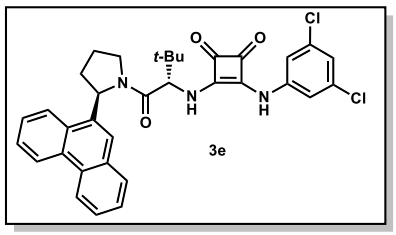

3e

Compound exists as a 6:1 mixture of rotomers, resonances correspond to the major rotomer. ^{1}H NMR (600 MHz, DMSO-d6) δ 10.31 (s, 1H), 8.86 – 8.79 (m, 1H), 8.71 (d, J = 8.3 Hz, 1H), 8.20 – 8.10 (m, 2H), 8.05 – 8.00 (m, 2H), 7.75 – 7.65 (m, 4H), 7.63 – 7.51 (m, 1H), 7.24 (s, 1H), 7.31 – 7.25 (m, 1H), 5.86 (d, J = 8.1 Hz, 1H), 5.13 (d, J = 10.0

Hz, 1H), 4.21 (t, J = 8.5 Hz, 1H), 3.85 (m, 1H), 2.51 – 2.42 (m, 1H), 2.01 – 1.93 (m, 1H), 1.84 – 1.78 (m, 1H), 1.75 (dd, J = 11.7, 5.8 Hz, 1H), 1.05 (s, 9H). ^{13}C NMR (126 MHz, dmso) δ 185.11, 181.43, 170.08, 168.05, 164.28, 139.99, 137.16, 132.28, 132.13, 130.00, 129.81, 129.63, 128.64, 128.38, 127.16, 127.08, 124.51, 124.42, 124.06, 123.63, 123.37, 123.10, 118.24, 62.37, 58.24, 48.72, 35.73, 32.66, 26.49, 23.87. HRMS: calculated for [$C_{34}H_{31}Cl_2N_3O_3$ + H^+] 600.1821, found 600.1820. $[\alpha]^{22.3}_D$ = 106.4° (c = 1.0, $CHCl_3$).

5-((2-(((S)-3,3-dimethyl-1-oxo-1-((R)-2-(phenanthren-9-yl)pyrrolidin-1-yl)butan-2-yl)amino)-3,4-dioxocyclobut-1-en-1-yl)amino)isophthalonitrile (5e)

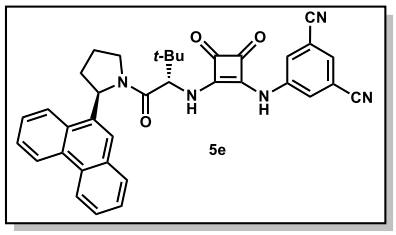

5e

Compound exists as a 7.5:1 mixture of rotomers, resonances correspond to the major rotomer. ^{1}H NMR (600 MHz, DMSO-d6) δ 10.42 (s, 1H), 8.89 – 8.82 (m, 1H), 8.74 (d, J = 8.3 Hz, 1H), 8.25 – 8.15 (m, 2H), 8.05 – 8.00 (m, 2H), 7.77 – 7.65 (m, 4H), 7.60 – 7.48 (m, 1H), 7.32 (s, 1H), 7.25 – 7.19 (m, 1H), 5.91 (d, J = 8.1 Hz, 1H), 5.15 (d, J = 10.0 Hz, 1H), 4.28 (ddd, J = 10.0, 7.3, 5.2 Hz, 1H), 3.91 (dt, J = 10.0, 7.3 Hz, 1H), 2.41 – 2.27 (m, 1H), 2.05 – 1.94 (m, 1H), 1.86 – 1.78 (m, 1H), 1.75 (m, 1H), 1.06 (s, 9H). ^{13}C NMR (126 MHz, dmso) δ 185.53, 181.47, 170.20, 168.88, 163.51, 139.47, 137.55, 132.51, 132.39, 130.66, 129.64, 129.61, 128.87, 128.08, 127.59, 127.00, 125.65, 124.42, 123.63, 123.60, 123.27, 123.21, 119.18, 79.26, 62.48, 58.44, 48.67, 35.88, 32.64, 26.37, 24.25. HRMS: calculated for [$C_{36}H_{31}N_5O_3$ + H^+] 582.2505, found 582.2497. $[\alpha]^{23.4}_D$ = 142.2° (c = 1.0, $CHCl_3$).

3-((3,5-bis(trifluoromethyl)phenyl)amino)-4-(((S)-3,3-dimethyl-1-((R)-2-(naphthalen-1-yl)pyrrolidin-1-yl)-1-oxobutan-2-yl)amino)cyclobut-3-ene-1,2-dione (4b)

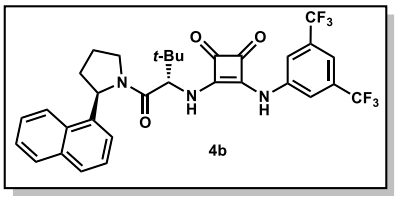

Compound exists as a 4.5:1 mixture of rotomers, resonances correspond to the major rotomer. ^{1}H NMR (600 MHz, DMSO-d_6) δ 10.42 (s, 1H), 8.27 (d, J = 10.0 Hz, 1H), 8.11 (d, J = 8.5 Hz, 1H), 8.06 (s, 2H), 7.89 (d, J = 8.0 Hz, 1H), 7.71 (d, J = 8.2 Hz, 1H), 7.61 (s, 1H), 7.54 (t, J = 7.7 Hz, 1H), 7.49 (t, J = 7.4 Hz, 1H), 7.31 (t, J = 7.7 Hz, 1H), 7.08 (d, J = 7.1 Hz, 1H), 5.86 (d, J = 8.1 Hz, 1H), 5.11 (d, J = 10.0 Hz, 1H), 4.14 (t, J = 8.5 Hz, 1H), 3.82 (td, J = 9.8, 7.1 Hz, 1H), 2.43 (tt, J = 12.1, 7.6 Hz, 1H), 1.98 (dq, J = 12.6, 5.9 Hz, 1H), 1.83 (tdd, J = 16.2, 14.1, 11.9, 7.9 Hz, 1H), 1.75 (dd, J = 12.1, 6.4 Hz, 1H), 1.04 (s, 9H). ^{13}C NMR (126 MHz, dmso) δ 184.54, 180.54, 169.15, 167.89, 162.62, 141.11, 137.76, 133.52, 131.52, 129.69, 128.64, 126.79, 125.95, 125.51, 125.22, 124.24, 123.46, 122.07, 121.33, 117.99, 114.73, 61.30, 57.69, 48.06, 35.81, 32.58, 25.79, 23.18. HRMS: calculated for [$C_{32}H_{29}F_6N_3O_3$ + H^+] 618.2191, found 618.2195. $[\alpha]^{22.1}_D$ = –251.0° (c = 1.0, $CHCl_3$).

3-((3,5-bis(trifluoromethyl)phenyl)amino)-4-(((S)-3,3-dimethyl-1-oxo-1-((R)-2-(phenanthren-3-yl)pyrrolidin-1-yl)butan-2-yl)amino)cyclobut-3-ene-1,2-dione (4d)

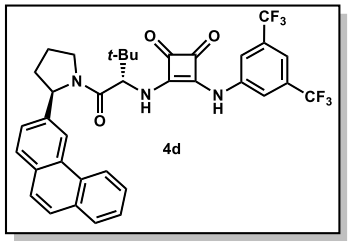

Compound exists as a 3:1 mixture of rotomers, resonances correspond to the major rotomer. ^{1}H NMR (600 MHz, DMSO-d_6) δ 10.32 (s, 1H), 8.54 (d, J = 8.3 Hz, 1H), 8.28 (d, J = 10.0 Hz, 1H), 8.12 (d, J = 12.2 Hz, 1H), 8.01 (dd, J = 17.5, 8.0 Hz, 1H), 7.94 (s, 2H), 7.88 (d, J = 8.1 Hz, 1H), 7.85 – 7.81 (m, 1H), 7.76 – 7.71 (m, 1H), 7.67 (d, J = 8.6 Hz, 1H), 7.49 (dd, J = 8.2, 1.6 Hz, 1H), 7.37 (t, J = 7.4 Hz, 1H), 7.30 (t, J = 7.4 Hz, 1H), 5.36 (dd, J = 8.2, 2.9 Hz, 1H), 5.13 (d, J = 10.0 Hz, 1H), 4.27 (dt, J = 11.1, 6.0 Hz, 1H), 3.87 – 3.80 (m, 1H), 2.40

(dq, J = 12.3, 8.4 Hz, 1H), 2.07 – 1.89 (m, 3H), 1.06 (s, 9H). ^{13}C NMR (126 MHz, dmso) δ 184.46, 180.58, 169.07, 167.97, 162.83, 142.64, 141.82, 140.90, 131.62, 131.47, 131.20, 130.27, 129.45, 129.35, 128.52, 128.35, 126.95, 126.46, 126.21, 125.19, 122.30, 118.17, 117.88, 114.80, 61.57, 60.63, 48.15, 35.35, 33.94, 25.81, 23.22.^{19}F NMR (376 MHz, DMSO-d_6) δ -61.88. HRMS: calculated for [$C_{36}H_{31}F_6N_3O_3$ + H^+] 668.2348, found 668.2345. $[\alpha]^{21.7}_D = -86°$ (c = 1.0, $CHCl_3$).

3-((3,5-bis(trifluoromethyl)phenyl)amino)-4-(((S)-3,3-dimethyl-1-((R)-2-methyl-2-phenylpyrrolidin-1-yl)-1-oxobutan-2-yl)amino)cyclobut-3-ene-1,2-dione (4a')

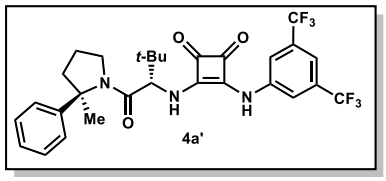

^{1}H NMR (600 MHz, DMSO-d_6) δ 10.47 (s, 1H), 8.25 (d, *J* = 10.0 Hz, 1H), 8.08 (s, 2H), 7.63 (s, 1H), 7.22 (dd, *J* = 8.4, 7.0 Hz, 2H), 7.20 – 7.16 (m, 2H), 7.13 – 7.09 (m, 1H), 5.03 (d, *J* = 9.9 Hz, 1H), 4.03 (ddd, *J* = 9.5, 7.5, 4.0 Hz, 1H), 3.82 (ddd, *J* = 9.9, 8.3, 6.8 Hz, 1H), 2.04 (ddd, *J* = 12.0, 9.8, 6.1 Hz, 1H), 1.95 – 1.86 (m, 2H), 1.84 (s, 3H), 1.76 – 1.66 (m, 1H), 1.02 (s, 9H). ^{13}C NMR (126 MHz, DMSO-d_6) δ 184.53, 180.44, 169.11, 167.39, 162.48, 146.04, 141.14, 131.38 (q, *J* = 33.0 Hz), 127.84, 125.70, 124.76, 123.15 (q, *J* = 272.9 Hz), 117.94 (d, *J* = 4.0 Hz), 114.68, 66.95, 61.35, 49.63, 43.97, 36.01, 25.74, 24.57, 21.99. ^{19}F NMR (376 MHz, DMSO-d_6) δ -61.87. HRMS calculated for [$C_{29}H_{30}F_6N_3O_3$ + H^+] 582.2186, found 582.2185. $[\alpha]_D = 6.2°$ (c = 1.0, $CHCl_3$).

3-((3,5-bis(trifluoromethyl)phenyl)amino)-4-(((S)-3,3-dimethyl-1-((R)-2-methyl-2-(naphthalen-1-yl)pyrrolidin-1-yl)-1-oxobutan-2-yl)amino)cyclobut-3-ene-1,2-dione (4b')

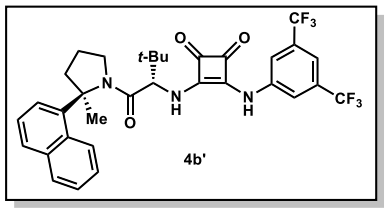

^{1}H NMR (600 MHz, DMSO-d_6) δ 10.09 (s, 1H), 7.99 (s, 2H), 7.90 – 7.76 (m, 3H), 7.71 (d, *J* = 8.1 Hz, 1H), 7.66 (s, 1H), 7.56 – 7.47 (m, 1H), 7.40 (t, *J* = 7.8 Hz, 1H), 7.21 – 7.12 (m, 2H), 4.92 (d, *J* = 10.1 Hz, 1H), 4.24 (q, *J* = 9.1 Hz, 1H), 4.11 – 4.03 (m, 1H), 2.50 – 2.42 (m, 1H), 2.32 – 2.21 (m, 1H), 2.16 – 2.04 (m, 1H), 2.01 – 1.91 (s, 4H), 0.99 (s, 9H). ^{13}C NMR (126 MHz, DMSO-d_6) δ

184.63, 180.53, 168.91, 166.98, 162.89, 140.98, 140.27, 134.41, 131.51 (q, J = 33.0 Hz), 129.37, 129.04, 127.52, 125.04, 124.43, 124.30, 123.71, 123.12 (q, J = 272.8 Hz), 117.73 (d, J = 4.1 Hz), 115.25 – 114.37 (m), 67.33, 61.22, 48.12, 40.35, 35.21, 25.69, 24.79, 23.04. ^{19}F NMR (376 MHz, DMSO-d_6) δ -61.93. HRMS calculated for [$C_{33}H_{32}F_6N_3O_3$ + H^+] 632.2342, found 632.2335. $[\alpha]_D$ = −107º (c = 1.0, $CHCl_3$).

3-((3,5-bis(trifluoromethyl)phenyl)amino)-4-(((S)-3,3-dimethyl-1-((R)-2-methyl-2-(naphthalen-2-yl)pyrrolidin-1-yl)-1-oxobutan-2-yl)amino)cyclobut-3-ene-1,2-dione (4c')

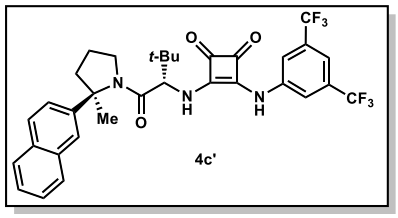

4c'

^{1}H NMR (600 MHz, DMSO-d_6) δ 10.44 (s, 1H), 8.20 (d, J = 10.0 Hz, 1H), 8.08 (s, 2H), 7.82 – 7.71 (m, 3H), 7.71 – 7.57 (m, 2H), 7.44 – 7.33 (m, 2H), 7.30 (ddd, J = 8.1, 6.7, 1.3 Hz, 1H), 5.07 (d, J = 9.9 Hz, 1H), 4.15 (ddd, J = 9.9, 7.5, 5.1 Hz, 1H), 3.89 (dt, J = 9.9, 7.2 Hz, 1H), 2.09 (ddd, J = 12.5, 8.5, 6.4 Hz, 1H), 2.03 (dt, J = 12.3, 6.0 Hz, 1H), 2.00 – 1.91 (m, 4H), 1.83 (tdd, J = 14.1, 11.7, 5.5 Hz, 1H), 1.03 (s, 9H). ^{13}C NMR (126 MHz, DMSO-d_6) δ 184.64, 180.57, 169.29, 167.51, 162.66, 143.73, 141.19, 132.70, 131.49, 131.45 (q, J = 33.0 Hz), 127.76, 127.47, 127.06, 125.62, 125.30, 123.81, 123.15 (q, J = 272.8 Hz), 123.07, 117.87 (d, J = 4.7 Hz), 115.04 – 114.12 (m), 66.98, 61.50, 49.67, 43.73, 35.78, 25.75, 24.25, 22.33. ^{19}F NMR (376 MHz, DMSO-d_6) δ -61.95. HRMS calculated for [$C_{33}H_{32}F_6N_3O_3$ + H^+] 632.2342, found 632.2344. $[\alpha]_D$ = 49.8º (c = 1.0, $CHCl_3$).

3-((3,5-bis(trifluoromethyl)phenyl)amino)-4-(((S)-3,3-dimethyl-1-((R)-2-methyl-2-(phenanthren-3-yl)pyrrolidin-1-yl)-1-oxobutan-2-yl)amino)cyclobut-3-ene-1,2-dione (4d')

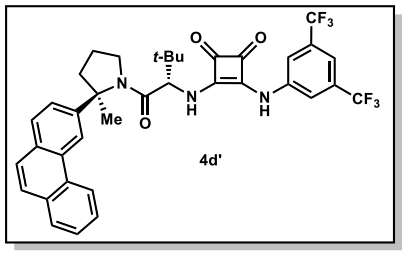

^{1}H NMR (600 MHz, DMSO-d_6) δ 10.29 (s, 1H), 8.56 (d, J = 8.3 Hz, 1H), 8.39 (d, J = 1.8 Hz, 1H), 8.24 (d, J = 10.0 Hz, 1H), 7.96 (s, 2H), 7.86 (d, J = 8.4 Hz, 1H), 7.79 (dd, J = 8.0, 1.3 Hz, 1H), 7.73 (d, J = 8.9 Hz, 1H), 7.69 (d, J = 8.9 Hz, 1H), 7.65 (s, 1H), 7.56 (dd, J = 8.4, 1.8 Hz, 1H), 7.33 (t, J = 7.0 Hz, 1H), 7.23 (t, J = 7.4 Hz, 1H), 5.15 (d, J = 10.0 Hz, 1H), 4.31 (ddd, J = 10.1, 7.5, 5.1 Hz, 1H), 3.93 (dt, J = 10.0, 7.3 Hz, 1H), 2.20 – 2.05 (m, 2H), 2.05 – 1.92 (overlapping s, 3H and m, 1H), 1.91 – 1.80 (m, 1H), 1.05 (s, 9H). ^{13}C NMR (126 MHz, dmso) δ 184.95, 181.02, 169.58, 168.01, 163.16, 145.05, 141.46, 132.07, 132.01, 130.26, 130.08, 129.59, 128.69, 126.83, 126.73, 126.57, 126.43, 124.64, 122.76, 122.49, 120.32, 118.66, 118.20, 115.12, 79.63, 67.70, 62.06, 50.15, 44.40, 36.01, 26.18, 24.99, 22.80. HRMS: calculated for [$C_{37}H_{33}F_6N_3O_3$ + H^+] 682.2504, found 682.2499. $[\alpha]^{21.8}_D$ = 119.0° (c = 1.0, $CHCl_3$).

3-((3,5-bis(trifluoromethyl)phenyl)amino)-4-(((S)-3,3-dimethyl-1-((R)-2-methyl-2-(phenanthren-9-yl)pyrrolidin-1-yl)-1-oxobutan-2-yl)amino)cyclobut-3-ene-1,2-dione (4e')

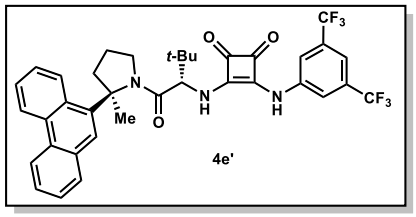

^{1}H NMR (600 MHz, DMSO-d_6) δ 10.06 (s, 1H), 8.76 (d, *J* = 8.2 Hz, 1H), 8.69 (d, *J* = 8.4 Hz, 1H), 7.99 (s, 2H), 7.97 – 7.72 (m, 4H), 7.70 (s, 1H), 7.61 (ddd, *J* = 8.3, 6.8, 1.5 Hz, 1H), 7.55 (s, 1H), 7.42 – 7.18 (m, 2H), 5.00 – 4.83 (m, 1H), 4.30 (q, *J* = 9.3 Hz, 1H), 4.16 – 4.03 (m, 1H), 2.57 (q, *J* = 10.9 Hz, 1H), 2.46 – 2.12 (m, 2H), 2.10 – 1.93 (m, 4H), 0.99 (s, 9H). ^{13}C NMR (126 MHz, DMSO-d_6) δ 184.68, 180.56, 168.94, 167.18, 162.88, 140.97, 138.20, 131.52 (q, *J* = 33.0 Hz), 131.01, 130.92, 129.28, 128.69, 128.56, 126.69, 126.65, 125.23, 125.16, 124.36, 123.81, 123.12 (q, *J* = 273.5 Hz), 122.26, 117.74 (d, *J* = 4.1 Hz), 115.18 – 114.31 (m), 67.25, 61.23, 48.09, 35.11,

25.70, 24.96, 22.95. ^{19}F NMR (376 MHz, DMSO-d_6) δ -61.82 ppm. HRMS calculated for [$C_{37}H_{34}F_6N_3O_3$ + H^+] 682.2499, found 682.2493; $[\alpha]_D = -127.2^o$ (c = 1.0, $CHCl_3$).

2.11.3 Synthesis of electrophiles, nucleophiles, and their intermediates

2.11.3.1 Synthesis of α-hydroxy and α-chloroamino esters

General Procedure for the Preparation of Ethyl 2-(((Benzyloxy)carbonyl)amino)-2-chloroacetate (1-Cbz)

Ethyl 2-(((benzyloxy)carbonyl)amino)-2-chloroacetate (1-Cbz) can be prepared by two methods as described by Roche.[89,90] Due to ability to purify and store material at the α-hydroxy amino ester, **1-Cbz** was made using the two step Roche procedure below.

Ethyl 2-(((benzyloxy)carbonyl)amino)-2-hydroxyacetate (1-Cbz-OH)

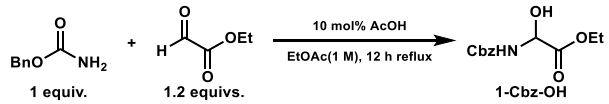

In a 250 mL round-bottom flask equipped with a reflux condenser, acetic acid (6 mmol, 0.34 mL, ρ = 1.05 g/mL) was added to a vigorously stirring solution of benzyl carbamate (60 mmol, 9.07 g) and ethyl 2-oxoacetate (72 mmol, 14.3 mL of ~ 50% w/w solution in toluene) in ethyl acetate (60 mL). The reaction mixture was heated to reflux and stirred overnight, then concentrated *in vacuo* to yield an off-white slurry. The crude mixture was dissolved in minimal DCM heated to 35 °C (approximately 100 mLs of DCM). An equal volume of rt hexanes was added while swirling the flask. The mixture was allowed to sit at rt for 2 hours, after which crystals started to form in the solution. The mixture was then put in a freezer overnight. The resulting solid was filtered, washed with hexanes and dried under reduced pressure to give ethyl 2-(((benzyloxy)carbonyl)amino)-2-hydroxyacetate **1-Cbz-OH** (11.85 g, 78% yield) as a white solid with water as the only impurity. The NMR spectroscopic data were in agreement with those reported in the literature.[89a]

Ethyl 2-(((benzyloxy)carbonyl)amino)-2-chloroacetate (1-Cbz)

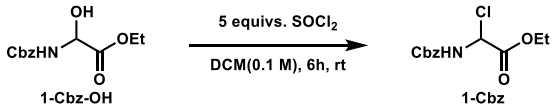

Treatment of ethyl 2-(((benzyloxy)carbonyl)amino)-2- hydroxyacetate (0.75 mmol, 189.9 mgs) with $SOCl_2$ (3.75 mmol, 0.27 mL) in DCM (7.5 mL) at room temperature under nitrogen atmosphere for 6h, followed by removal of residual $SOCl_2$ and DCM under reduced pressure gave ethyl 2-(((benzyloxy)carbonyl)amino)-2-chloroacetate **1-Cbz** as a white solid in quantitative yield. The compound, without further purification, was then transferred as a solid and used immediately in the catalytic allylation, due to slow hydrolysis when not kept under vacuum. The product can be transferred as a stock solution to give identical results, but one must account for the water in **1-Cbz-OH** to have an accurate titre. The spectroscopic data of **1-Cbz** matched those reported by Roche.[89a]

General Procedure for the Preparation of Ethyl 2-((((9H-Fluoren-9-yl)methoxy)carbonyl)-amino)-2-hydroxyacetate (1-Fmoc-OH) and the related α-chloroamino ester **1-Fmoc**, can be prepared via the same method as **1-Cbz**, with slight condition modifications due to the poor solubility of Fmoc-containing compounds.

Ethyl 2-((((9H-Fluoren-9-yl)methoxy)carbonyl)amino)-2-hydroxyacetate (1-Fmoc-OH)

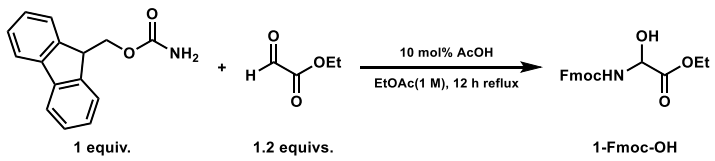

In a 500 mL round-bottom flask equipped with a reflux condenser, acetic acid (14.2 mmol, 0.8 mL, ρ = 1.05 g/mL) was added to a vigorously stirring solution of 9-Fluorenylmethyl carbamate (14.2 mmol, 3.4 g) and ethyl 2-oxoacetate (20.1 mmol, 4.0 mL of ~ 50% w/w solution in toluene) in ethyl acetate (200 mL). The reaction mixture was heated to reflux and stirred

overnight. It is imperative that one monitor the reaction by TLC, as 9-Fluorenylmethyl carbamate and the product are challenging to separate. Upon completion, the reaction mixture concentrated *in vacuo* to yield a white powder. The crude mixture was dissolved in minimal DCM heated to 35 °C (approximately 100–200 mLs of DCM). An equal volume of rt hexanes was added while swirling the flask. The mixture was allowed to sit at rt for 2 hours, after which crystals started to form in the solution. The mixture was then put in a freezer overnight. The resulting solid was filtered, washed with hexanes and dried under reduced pressure to give ethyl 2-((((9H-fluoren-9-yl)methoxy)carbonyl)amino)-2-hydroxyacetate **1-Fmoc-OH** (4.12 g, 85% yield) as a white solid with water as the only impurity. The spectroscopic data of **1-Fmoc-OH** matched those reported in the literature.[132]

Ethyl 2-((((9H-Fluoren-9-yl)methoxy)carbonyl)amino)-2-chloroacetate (1-Fmoc)

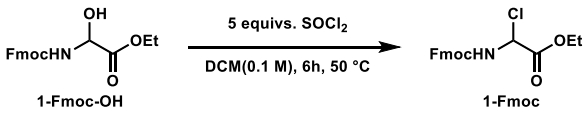

In a 10 mL pressure resistant microwave vial equipped with a rubber septum, $SOCl_2$ (3.0 mmol, 0.22 mL) was added to a solution of ethyl 2-((((9H-fluoren-9-yl)methoxy)carbonyl)amino)-2-hydroxyacetate (0.6 mmol, 204.8 mgs) in DCM (6 mL) at room temperature and under nitrogen. The reaction vessel was then sealed, put in an oil bath heated to 50 °C for 6h. If the reaction is run longer than the recommended time, the product will begin to decompose, as compared to **1-Cbz-Cl**, which can be run for >24 hours without decomposing. Removal of residual $SOCl_2$ and DCM under reduced pressure gave ethyl 2-((((9H-fluoren-9-yl)methoxy)carbonyl)amino)-2-chloroacetate **1-Fmoc** as a white to off-white solid in quantitative yield. The compound, without further purification, was then transferred as a solid and used immediately in the catalytic allylation,

[132] Zhang, Y.; Dai, Y.; Li, G.; Cheng, X. The Catalytic Synthesis of Carboniolamide: The Role of Sp 3 Hybridized Oxygen. *Synlett* **2014**, *25* (18), 2644–2648.

due to slow hydrolysis when not kept under vacuum. The product can be transferred as a stock solution to give identical results, however one must account for the water in **1-Fmoc-OH** to have an accurate titre. The spectroscopic data of **1-Fmoc** is reported below.

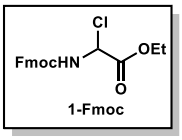

^{1}H NMR (600 MHz, Chloroform-d) δ 7.78 (d, J = 7.5 Hz, 2H), 7.59 (q, J = 7.3, 6.8 Hz, 2H), 7.42 (t, J = 7.4 Hz, 2H), 7.33 (t, J = 7.4 Hz, 2H), 6.23 (d, J = 10.6 Hz, 1H), 6.18 (d, J = 10.4 Hz, 1H), 4.50 (h, J = 10.1, 8.7 Hz, 2H), 4.34 (qd, J = 7.2, 2.8 Hz, 2H), 4.24 (t, J = 7.0 Hz, 1H), 1.36 (t, J = 7.2 Hz, 3H). ^{13}C NMR (126 MHz, cdcl3) δ 166.06, 153.95, 143.45, 141.43, 128.01, 127.29, 125.10, 120.21, 68.09, 63.34, 46.99, 13.99. HRMS: calculated for [$C_{19}H_{18}ClNO_4$ + H^+] 360.1003, found 356.1502, which matches formula for [$C_{20}H_{21}NO_5$ + H^+] 356.1498, indicating rapid methanolysis.

2.11.3.2 Synthesis of allylsilanes

All previously reported allylsilanes were synthesized according to the procedures in Sodeoka *et al*. and all allylsilanes reported for the first time here adapt one of two procedures from the same article.[133] Synthesized allylsilanes were stored in vials at 3 °C and could be kept for up to a month, after which decomposition may occur. Methallyltrimethylsilane was purchased from Sigma Aldrich and was run neat through a silica plug upon opening and then stored for up to 4 months, although identical results were obtained under optimal reaction conditions, when using methallyltrimethylsilane directly from the Sigma Aldrich bottle.

Trimethyl(2-phenylallyl)silane (3b)

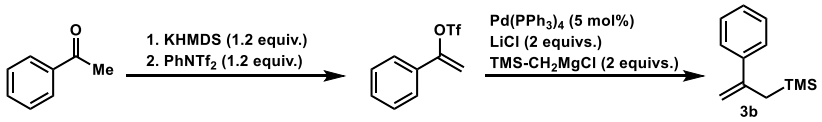

[133] Shimizu, R.; Egami, H.; Hamashima, Y.; Sodeoka, M. Copper-Catalyzed Trifluoromethylation of Allylsilanes. *Angew. Chemie Int. Ed.* **2012**, *51* (19), 4577–4580.

Trimethyl(2-phenylallyl)silane **3b** was prepared according to the two step literature procedure from Sodeoka at the 10 mmol scale. The two step sequence gave **3b** as a clear oil (1.56 g, 8.2 mmol, 82% yield). The NMR spectroscopic data were in agreement with those reported in the literature.[133]

(2-(4-(tert-butyl)phenyl)allyl)trimethylsilane (3c)

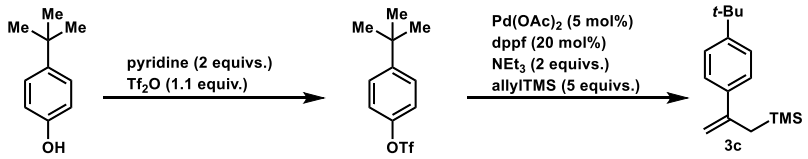

(2-(4-(tert-butyl)phenyl)allyl)trimethylsilane **3c** was prepared according to the two step literature procedure from Sodeoka at the 10 mmol scale. The two step sequence gave **3c** as a clear oil (1.30 g, 5.3 mmol, 53% yield). The NMR spectroscopic data were in agreement with those reported in the literature.[133] Note: half the time we ran this reaction we got an inseparable ~10:1 mixture of the branched to linear regioisomer. Due to the low nucleophilicity of the *p*-(*t*-bu)cinnamyl silane the impurity need not be separated before running the catalytic allylation.

(2-(4-methoxyphenyl)allyl)trimethylsilane (3d)

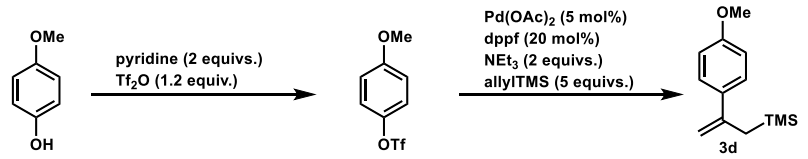

(2-(4-methoxyphenyl)allyl)trimethylsilane **3d** was prepared according to the two step literature procedure from Sodeoka at the 10 mmol scale. The two step sequence gave **3d** as a clear oil (1.05 g, 4.8 mmol, 48% yield). Similarly to **3c**, **3d** was often obtained as a 2:1 to 10:1 mixture of branched:linear isomers. Due to the low nucleophilicity of cinnamyl type silanes the reaction can be run with a mixture of isomers with identical results, recovering the linear silane at the end of the reaction. The NMR spectroscopic data were in agreement with those reported in the

literature.[133]

(2-(benzo[d][1,3]dioxol-5-yl)allyl)trimethylsilane (3e)

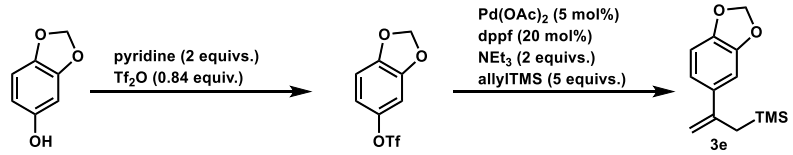

(2-(benzo[d][1,3]dioxol-5-yl)allyl)trimethylsilane **3e** was prepared according to the two step literature procedure from Sodeoka at the 10 mmol scale. The two step sequence gave **3e** as a clear oil (1.24 g, 5.3 mmol, 53% yield). The NMR spectroscopic data were in agreement with those reported in the literature.[133]

(2-(4-bromophenyl)allyl)trimethylsilane (3f)

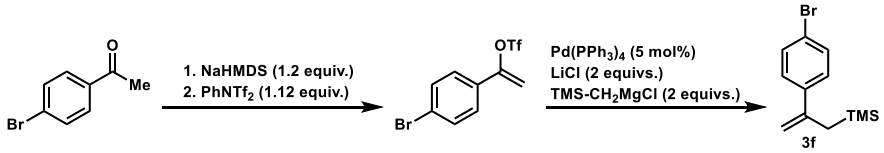

(2-(4-bromophenyl)allyl)trimethylsilane **3f** was prepared by adapting the two step literature procedure from Sodeoka at the 10 mmol scale. The two step sequence gave **3f** as a clear oil (2.34 g, 8.7 mmol, 87% yield). The NMR spectroscopic data were in agreement with those reported in the literature.[133]

(2-(3-bromophenyl)allyl)trimethylsilane (3g)

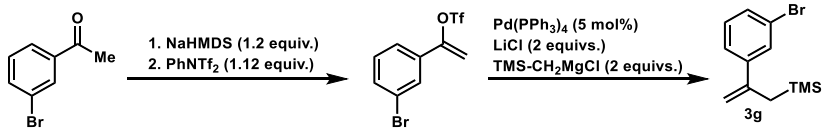

(2-(3-bromophenyl)allyl)trimethylsilane **3g** was prepared according to the two step literature procedure from Sodeoka at the 10 mmol scale. The two step sequence gave **3g** as a clear oil (1.91 g, 7.1 mmol, 71% yield). The NMR spectroscopic data were in agreement with those reported in the literature.[133]

(*E*)-trimethyl(2-methylene-4-phenylbut-3-en-1-yl)silane (3h)

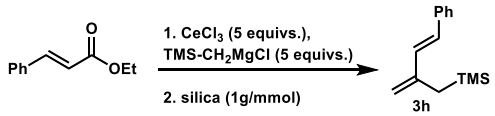

(*E*)-trimethyl(2-methylene-4-phenylbut-3-en-1-yl)silane **3h** was prepared according to the literature procedure from Gouverneur at the 10 mmol scale. The two step sequence gave **3h** as a clear oil (1.97 g, 9.1 mmol, 91% yield). The NMR spectroscopic data were in agreement with those reported in the literature.[134]

(*E*)-trimethyl(2-methylbut-2-en-1-yl)silane (3i-(*E*))

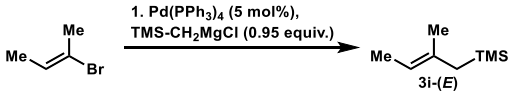

(*E*)-trimethyl(2-methylbut-2-en-1-yl)silane **3i-(*E*)** was prepared according to the literature procedure at the 20 mmol scale. **3i-(*E*)** was isolated as a clear oil in 100% diastereomeric purity by NMR (1.91 g, 13.4 mmol, 67% yield). The NMR spectroscopic data were in agreement with those reported in the literature.[135] Note: We used diastereomerically pure (*E*)-2-bromobut-2-ene; however, according to the literature procedure this is unncessessary and a diastereomeric mixture of vinyl bromides will selectively cross couple to give diastereomerically pure **3i-(*E*)**.

(*Z*)-trimethyl(2-methylbut-2-en-1-yl)silane (3i-(*Z*))

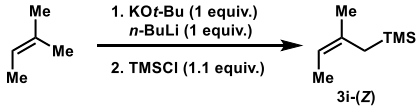

(*Z*)-trimethyl(2-methylbut-2-en-1-yl)silane **3i-(*Z*)** was prepared according to the literature

[134] a) Lam, Y.; Bobbio, C.; Cooper, I. R.; Gouverneur, V. A Concise Synthesis of Enantioenriched Fluorinated Carbocycles. *Angew. Chemie Int. Ed.* **2007**, *46* (27), 5106–5110. b) Walkowiak, J.; del Campo, T.; Ameduri, B.; Gouverneur, V. Syntheses of Mono-, Di-, and Trifluorinated Styrenic Monomers. *Synthesis (Stuttg).* **2010**, *2010* (11), 1883–1890.

[135] Andreini, B. P.; Carpita, A.; Rossi, R.; Scamuzzi, B. Palladium-Catalyzed Diastereoselective Syntheses of (E)-1-Trimethylsilyl-2-Alkenes, (E)-1-Trimethylsilyl-1-Alken-3-Ynes, (1E,5E)-1-Trimethylsilyl-1,5-Alkadien-3-Ynes, (1E,3Z)- and (1E,3E)-1-Trimethylsilyl- 1,3-Alkadienes. *Tetrahedron* **1989**, *45* (17), 5621–5640.

procedure at the 10 mmol scale.[105] **3i-(*Z*)** was isolated as a clear oil in 100% diastereomeric purity by NMR (0.71 g, 5.0 mmol, 50% yield). The NMR spectroscopic data were in agreement with those reported in the literature.[136]

(cyclohex-1-en-1-ylmethyl)trimethylsilane (3j)

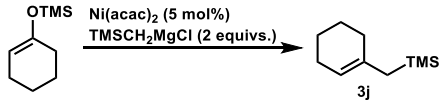

(cyclohex-1-en-1-ylmethyl)trimethylsilane **3j** was prepared according to the literature procedure at the 10 mmol scale.[137] **3j** was isolated as a clear oil (1.23 g, 7.3 mmol, 73% yield). The NMR spectroscopic data were in agreement with those reported in the literature.[138]

((3,4-dihydronaphthalen-1-yl)methyl)trimethylsilane (3k)

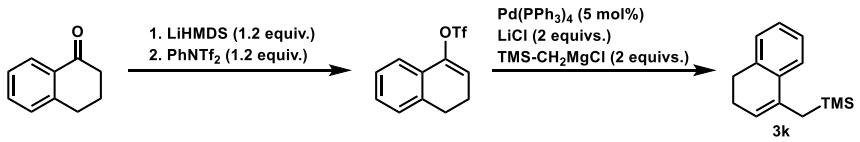

((3,4-dihydronaphthalen-1-yl)methyl)trimethylsilane **3k** was prepared according to the two step literature procedure from Sodeoka at the 10 mmol scale. The two step sequence gave **3k** as a clear oil (2.01 g, 9.3 mmol, 93% yield). The NMR spectroscopic data were in agreement with those reported in the literature.[133]

---

[136] Alberts, V.; Cuthbertson, M. J.; Hawker, D. W.; Wells, P. R. 1H,13C And29Si NMR Spectra of Allylic Trimethylsilanes. *Org. Magn. Reson.* **1984**, *22* (9), 556–560.

[137] Hayashi, T.; Katsuro, Y.; Kumada, M. Nickel-Catalyzed Cross-Coupling of Silyl Enol Ethers with Grignard Reagents. Regio- and Stereocontrolled Synthesis of Olefins. *Tetrahedron Lett.* **1980**, *21* (40), 3915–3918.

[138] Carey, F. A.; Toler, J. R. Formation of Vinylsilanes and Allylsilanes in Thermal Elimination Reactions of Esters of .Beta.-Hydroxyalkyltrimethylsilanes. *J. Org. Chem.* **1976**, *41* (11), 1966–1971.

((2H-thiochromen-4-yl)methyl)trimethylsilane (3l)

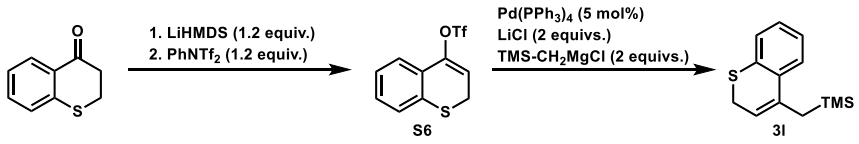

((2H-thiochromen-4-yl)methyl)trimethylsilane **3l** was prepared by adapting the two step literature procedure from Sodeoka at the 10 mmol scale.[133] The two step sequence gave **3l** as a pale yellow to clear oil (2.02 g, 8.6 mmol, 86% yield).

2H-thiochromen-4-yl trifluoromethanesulfonate (S6)

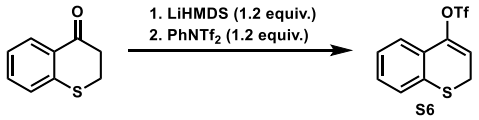

To a flame dried flask equipped with a stir bar was added 1.65 g (10 mmol) thiochromanone and 50 mL of THF. The flask was put under a flow of nitrogen and cooled in a dry ice acetone bath at –78 °C, after which 12 mL of 1M solution of NaHMDS (12 mmol, 1.2 equivs.) was added. The reaction was allowed to stir at –78 °C for an hour, after which a solution of 4.2 g (12 mmol, 1.2 equivs.) of N-phenyl bistriflimide in minimal (~10 mL) THF was added via syringe. The reaction was warmed to 0 °C in an ice water bath and stirred for 4 hours.

Reaction was worked up via addition of 50 mL saturated sodium bicarbonate solution and the biphasic mixture was extracted with 2x 50 mL of diethyl ether. Combined organics were washed with brine and evaporated *in vacuo*. The concentrate was a brown oil and loaded onto 100g isolera biotage cartridge packed with silica and run using the following eluent system:

2 column volumes isocratic 100% hexanes

8 column volumes linear gradient 100:0 hexanes:Et_2O to 70:30 hexanes:Et_2O

Product varies when it comes out and is difficult to separate from an aromatic impurity. Product used in the next step with impurity present in ~10-20%.

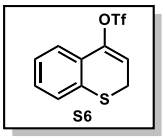

^{1}H NMR (600 MHz, Chloroform-d) δ 7.42 (dd, J = 7.7, 1.3 Hz, 1H), 7.28 (dd, J = 7.4, 1.4 Hz, 1H), 7.23 (td, J = 7.5, 1.5 Hz, 1H), 7.20 (td, J = 7.5, 1.4 Hz, 1H), 6.02 (t, J = 5.6 Hz, 1H), 3.61 (d, J = 5.6 Hz, 2H). ^{13}C NMR (126 MHz, cdcl3) δ 147.48, 134.07, 132.23, 131.10, 130.12, 127.51, 126.19, 123.67, 112.89, 24.58. HRMS: calculated for [$C_{10}H_7F_3O_3S_2 + H^+$] 296.9867, found 296.9867.

((2H-thiochromen-4-yl)methyl)trimethylsilane (3l)

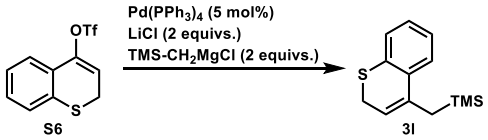

To a flame dried round bottom flask or Schlenk flask equipped with a stir bar was added 2.96 g (10 mmol) vinyl triflate and 50 mL of THF. The flask was closed with a rubber septum and put under a flow of nitrogen. In a glovebox, 568 mgs (0.5 mmol, 5 mol%) of $Pd(PPh_3)_4$ and 844 mgs (20 mmol, 2 equivs.) of dried LiCl were weighed into a vial. The vial of solids was dumped into the flask under positive flow of nitrogen, the reaction was recapped. Finally, 20 mL of 1 M solution of (trimethylsilylmethyl)magnesium chloride in Et_2O (20 mmol, 2 equivs.) was added dropwise over the course of 10 minutes. After stirring for 12 hours, the reaction was quenched with ~50 mL aqueous NH_4Cl, extracted with 2 x 50 mL of Et_2O. The combined organics were washed with brine and dried over Na_2SO_4. A short silica plug was run with ~250 mL of pentane, to give pure product as a colorless oil in 86% yield (8.6 mmol, 2.02 g).

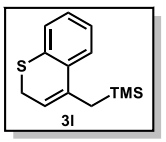

^{1}H NMR (600 MHz, Chloroform-d) δ 7.31 (dd, J = 7.4, 1.7 Hz, 1H), 7.28 (dd, J = 7.4, 1.8 Hz, 1H), 7.10 (pd, J = 7.3, 1.6 Hz, 2H), 5.70 (t, J = 5.6 Hz, 1H), 3.28 (d, J = 5.6 Hz, 2H), 1.97 (s, 2H), -0.05 (s, 9H). ^{13}C NMR (126 MHz, cdcl3) δ 136.74, 135.04, 133.91, 127.67, 127.20, 125.84, 125.23, 116.57, 25.16, 24.26, -1.03. HRMS: calculated for [$C_{13}H_{18}SSi + H^+$] 235.0977, found 235.0979.

2.11.3.3 Synthesis of allylstannanes

Allyltributylstannane was purchased from Sigma Aldrich and prenyltributylstannane was purchased from Alfa Aesar. Both were used directly from the bottle and stored at 3 °C for up to a year. Both the E and Z crotylstannanes were synthesized from the corresponding E or Z crotyl chloride. Crotylstannanes were stored in vials at 3 °C and could be kept for up to a year, after which decomposition may occur.

(*E*)-but-2-en-1-yltributylstannane (3n-(*E*))

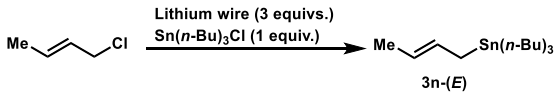

(*E*)-but-2-en-1-yltributylstannane **3n-(*E*)** was prepared according to a literature procedure.[139] (*E*)-crotyl chloride can be purchased from Sigma Aldrich in a > 19 : 1 mixture of *E* : *Z* isomers. **3n-(*E*)** was isolated as a clear oil (2.04 g, 5.9 mmol, 59% yield). The NMR spectroscopic data were in agreement with those reported in the literature.[139]

(*Z*)-but-2-en-1-yltributylstannane (3n-(*Z*))

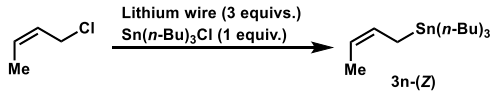

(*Z*)-but-2-en-1-yltributylstannane **3n-(*Z*)** was prepared according to a literature procedure.[139] (*Z*)-crotyl chloride can be synthesized in two steps from 2-butyn-1-ol via a Lindlar hydrogenation followed by a deoxychlorination of *Z*-crotyl alcohol with hexachloroacetone and triphenylphosphine. **3n-(*Z*)** was isolated as a clear oil (2.08 g, 6.0 mmol, 60% yield). The NMR spectroscopic data were in agreement with those reported in the literature.[139]

2.11.4 Enantioselective Glycine Allylation

[139] Balduzzi, S.; Brook, M. A.; McGlinchey, M.J. Diastereoselective Addition of Allyl- and Crotylstannanes to Dicobalt-Complexed Acetylenic Aldehydes. *Organometallics* **2005**, *24* (11), 2617–2627.

2.11.4.1 General procedures for the synthesis of allyl glycine substrates

General procedure for reaction parameter and catalyst optimization (0.10 mmol scale)

1 dram vials equipped with a flea stir bar are put in an oven kept at 120 °C overnight. To a rt 1 dram vial is added squaramide catalyst (0.01 mmol catalyst, 10 mol%) and 60 mgs (60 mgs/mL of solvent) of powdered 3Å molecular sieves that had been kept in an oven at 120 °C for a minimum of 24 hours.* At this point solid **1-Cbz/Fmoc** (0.10 mmol) is weighed out into the vial, the vial is capped with a screw top fitted with a septum, an inlet of N_2 is added to the vial, and 1 mL of the DCM is added. Alternately, 1mL of 0.1 M solution of **1-Cbz/Fmoc** in DCM can be added to a capped vial containing catalyst, molecular sieves, and a N_2 inlet. The vials are then put in a dry ice acetone bath kept at –78 °C for 10 minutes, after which silane or stannane nucleophile is added via syringe (0.20 mmol, 2 equivs. for silanes and 0.40 mmol, 4 equivs. For stannanes). After 10 minutes, the nitrogen inlet is removed, the top of the cap is covered with electrical tape and transferred to a cryocool maintained at –30 °C, unless another temperature is specified and stirred for 36 hours.

The reactions are quenched with 0.2 mL of 0.5 M NaOAc (1 equiv.) in MeOH at the reaction temperature (generally –30 °C) and allowed to stir for an hour to ensure the electrophile is entirely quenched. The reaction is then warmed to rt, opened, and filtered through a celite plug with excess DCM and concentrated *in vacuo*. The product is purified either via a pipette column (~10:1 hexanes:ethyl acetate) or PTLC (~1.5:1 hexanes:ethyl acetate) optimal eluent conditions will vary slightly depending on the product. NMRs are integrated against dibromomethane standard to determine yield. Enantiomeric excess is determined via chiral normal phase HPLC against a racemic standard, column conditions provided in the product characterization section.

*Note about molecular sieves: We observed that the source of molecular sieves, both

company and type (powdered, rods, spheres), and the activation method did not affect the results as long as the sieves were 3 or 4 Å and in powdered form (either purchased or via mortar and pestle from rods or spheres). We hypothesize the molecular sieves capture HCl and water.

General procedure for racemic standard synthesis (0.10 mmol scale)

The synthesis of racemic standards use the same conditions as for reaction parameter and catalyst optimization with the exception of the following. The catalyst used is 1,3-bis(3,5-bis(trifluoromethyl)phenyl)urea, commonly called Schreiner's urea (4.8 mgs, 0.01 mmol, 10 mol%). The reactions are set up and stirred at rt for 36 hours and quenched, purified and analyzed analogously to the optimization screening procedure. Racemic standards are generally messier reactions than the catalytic enantioselective method.

General procedure for enantioselective glycine allylation (0.5 mmol, Figure 2.13)

Powdered 3Å molecular sieves and a 2 dram vial equipped with a magnetic stir bar were separately put in an oven kept at 120 °C overnight. To the cooled to rt 2 dram vial was added 3-phenanthryl squaramide catalyst **5c** (7.4 mgs, 0.0125 mmol catalyst, 2.5 mol%) and 100 mgs of powdered 3Å molecular sieves. At this point solid **1-Cl** (136 mgs, 0.5 mmol, made via general procedure for **1-Cl** on 0.75 mmol scale) was weighed out into the vial, the vial was capped with a screw top fit with a septum, an inlet of N_2 was added to the vial, and 2 mLs of DCM were added. The vial was then put in a dry ice acetone bath kept at –78 °C for 10 minutes, after which silane nucleophile was added via Hamilton syringe (1.0 mmol, 2 equivs.). After 10 minutes, the nitrogen inlet was removed, the top of the cap was covered with electrical tape and transferred to a cryocool at –30 °C (or the indicated temperature) and stirred for 36 hours.

The reaction was quenched with 1.0 mL of 0.5 mmol NaOAc (1 equiv.) in MeOH at –30 °C and allowed to stir for an hour to ensure the electrophile was all quenched. The reaction was

then warmed to rt, opened, and filtered through a celite plug with excess DCM and concentrated *in vacuo*. The concentrate was loaded on to a 25g isolera biotage silica cartridge using 1 mL of benzene and run with a gradient of:

2 column volumes 100:0 hexanes:Et_2O

8 column volumes from 100:0 to 60:40 hexanes:Et_2O

2 column volumes 60:40 hexanes:Et_2O

Remaining allylsilanes elute at the solvent front or very early, and products elute near and may elute before or after quenched starting material, ethyl 2-acetoxy-2-(((benzyloxy)carbonyl)amino)acetate depending on the nucleophile.

Enantiomeric excess is determined via chiral normal phase HPLC against a racemic standard, column conditions provided in the product characterization section.

Modification for allylstannane nucleophiles:

The reaction set-up is the same as for the allylsilane nucleophiles performed on the same scale. Notable differences from the reactions employing allylsilanes as nucleophiles include: the reaction is run at 0.1 M in DCM (5 mL), with 10 mol% catalyst (0.05 mmol), and 4 equivalents of nucleophile (2 mmol). Due to the high toxicity of tetraalkyl stannanes and their tendency to streak on silica, crude reaction mixtures were quenched at the reaction temperatures with 1.0 mL of 0.5 mmol NaOAc (1 equiv.) in MeOH at and allowed to stir for an hour to ensure the electrophile was all quenched. Vials were brought to room temperature and diluted into 10 mL of acetonitrile. The acetonitrile was washed with 3x15 mL of pentane. Pentane was exposed of as tin waste and the acetonitrile layer was dried over Na_2SO_4 filtered and concentrated. The concentrate was loaded on to a 25g isolera biotage silica cartridge using 1 mL of benzene and run with a gradient of:

2 column volumes 100:0 hexanes:Et_2O

8 column volumes from 100:0 to 60:40 hexanes:Et_2O

2 column volumes 60:40 hexanes:Et_2O

Due to incomplete partitioning into pentane and the tendency of tin to streak on silica, there are often trace triallyl stannane peaks in the nmr spectra. Serial silica column chromatography can increase purity or products can easily be separated once deprotected at the carbamate or ester.

2.11.4.2 Characterization data for products

Ethyl (R)-2-(((benzyloxy)carbonyl)amino)-4-methylpent-4-enoate (2a)

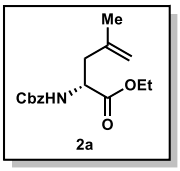

128 mgs, 88% yield. $[\alpha]^{24.1}_D = -23.6°$ (c = 1.0, $CHCl_3$); absolute stereochemistry assigned via comparison to the literature[105] and analogy to the crystal structure of **2l**. The NMR spectroscopic data were in agreement with those reported in the literature.[105]

HPLC (ChiralPak AS-H, 10% IPA/hexanes, 1 mL/min, 210 nm)

Racemic sample: retention times (10.0, 12.0 mins) Enantioenriched sample: retention times (9.9, 11.9 mins) **ee = 96.9%**

Ethyl (R)-2-(((benzyloxy)carbonyl)amino)-4-phenylpent-4-enoate (2b)

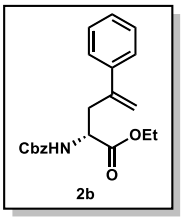

140 mgs, 79% yield. $[\alpha]^{23.6}_D = -21°$ (c = 1.0, $CHCl_3$); ^{1}H NMR (600 MHz, Benzene-d6) δ 7.26 (d, J = 7.6 Hz, 2H), 7.18 (d, J = 7.4 Hz, 2H), 7.06 (m, 6H), 5.17 (s, 1H), 5.11 (d, J = 8.2 Hz, 1H), 5.01 (q, J = 12.3 Hz, 2H), 4.91 (s, 1H), 4.60 (q, J = 7.0 Hz, 1H), 3.76 – 3.65 (m, 2H), 2.92 (dd, J = 14.3, 5.9 Hz, 1H), 2.76 (dd, J = 14.3, 7.1 Hz, 1H), 0.80 (t, J = 7.1 Hz, 3H); ^{13}C NMR (126 MHz, cdcl3) δ 171.65, 155.51, 143.64, 139.99, 136.34, 128.44, 128.35, 128.07, 128.01, 127.79, 126.31, 116.43, 66.78, 61.29, 52.95, 38.08, 14.00. HRMS: calculated for $[C_{21}H_{23}NO_4 + H^+]$ 354.1705, found 354.1713.

HPLC (ChiralPak OD-H, 20% IPA/hexanes, 1 mL/min, 210 nm)

Racemic sample: retention times (8.5, 11.3 mins) Enantioenriched sample: retention times (7.9, 11.3 mins) **ee = 94.3%**

Ethyl (R)-2-(((benzyloxy)carbonyl)amino)-4-(4-(tert-butyl)phenyl)pent-4-enoate (2c)

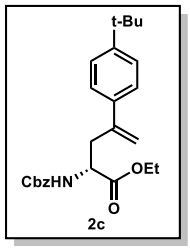

152 mgs, 74% yield. $[\alpha]^{23.7}_D$ = –8° (c = 1.0, $CHCl_3$); ^{1}H NMR (600 MHz, Benzene-d_6) δ 7.31 (d, *J* = 8.5 Hz, 2H), 7.19 (d, *J* = 8.5 Hz, 4H), 7.10 (t, *J* = 7.5 Hz, 2H), 7.05 (t, *J* = 7.3 Hz, 1H), 5.25 (d, *J* = 1.4 Hz, 1H), 5.18 (d, *J* = 8.3 Hz, 1H), 5.02 (s, 2H), 4.93 (d, *J* = 1.4 Hz, 1H), 4.65 (q, *J* = 7.1 Hz, 1H), 3.78 – 3.65 (m, 2H), 2.96 (dd, *J* = 14.2, 6.0 Hz, 1H), 2.83 (dd, *J* = 14.2, 7.1 Hz, 1H), 1.18 (s, 9H), 0.81 (t, *J* = 7.1 Hz, 3H); ^{13}C NMR (126 MHz, cdcl3) δ 171.82, 155.67, 150.98, 143.40, 137.07, 136.45, 128.63, 128.27, 128.18, 126.17, 125.42, 116.01, 67.01, 61.44, 53.09, 38.28, 34.65, 31.41, 14.16. HRMS: calculated for [$C_{25}H_{31}NO_4$ + H^+] 410.2331, found 410.2334.

HPLC (ChiralPak OD-H, 20% IPA/hexanes, 1 mL/min, 210 nm)

Racemic sample: retention times (6.6, 8.4 mins) Enantioenriched sample: retention times (6.3, 9.0 mins) **ee = 90.9%**

Ethyl (R)-2-(((benzyloxy)carbonyl)amino)-4-(4-methoxyphenyl)pent-4-enoate (2d)

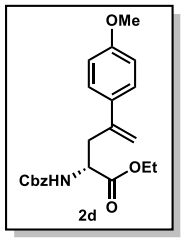

174 mgs, 91% yield. $[\alpha]^{25.3}_D$ = –7.3° (c = 1.0, $CHCl_3$); ^{1}H NMR (600 MHz, Benzene-d6) δ 7.24 (d, J = 8.4 Hz, 2H), 7.18 (d, J = 7.5 Hz, 2H), 7.10 (t, J = 7.4 Hz, 2H), 7.04 (t, J = 7.4 Hz, 1H), 6.69 (d, J = 8.4 Hz, 2H), 5.17 (s, 1H), 5.15 (d, J = 8.3 Hz, 1H), 5.02 (dd, J = 12.4 Hz, 2H), 4.88 (s, 1H), 4.65 (q, J = 7.1 Hz, 1H), 3.84 – 3.69 (m, 2H), 3.27 (s, 3H), 2.94 (dd, J = 14.2, 6.0 Hz, 1H), 2.77 (dd, J = 14.2, 7.1 Hz, 1H), 0.83 (t, J = 7.1 Hz, 3H); ^{13}C NMR (126 MHz, cdcl3) δ 171.83, 159.50, 155.62, 143.04, 136.44, 132.45, 128.62, 128.26, 128.18, 127.59, 115.13, 113.89, 66.99, 61.47, 55.39, 53.09, 38.41, 14.19. HRMS: calculated for [$C_{22}H_{25}NO_5$ + H^+] 384.1811, found 384.1802.

HPLC (ChiralPak OD-H, 20% IPA/hexanes, 1 mL/min, 210 nm)

Racemic sample: retention times (9.5, 12.9 mins) Enantioenriched sample: retention times (9.7, 14.0 mins) **ee = 94.0%**

Ethyl (R)-4-(benzo[d][1,3]dioxol-5-yl)-2-(((benzyloxy)carbonyl)amino)pent-4-enoate (2e)

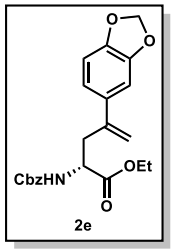

187 mgs, 94% yield. $[\alpha]^{23.8}_D$ = –4.0° (c = 1.0, $CHCl_3$); ^{1}H NMR (600 MHz, Benzene-d6) δ 7.18 (d, J = 7.0 Hz, 2H), 7.10 (t, J = 7.5 Hz, 2H), 7.04 (t, J = 7.3 Hz, 1H), 6.87 (d, J = 1.8 Hz, 1H), 6.73 (dd, J = 8.1, 1.8 Hz, 1H), 6.55 (d, J = 8.0 Hz, 1H), 5.26 (s, 2H), 5.09 (d, J = 8.0 Hz, 1H), 5.07 (s, 1H), 5.02 (q, J = 63.6, 12.3, 11.3, 1.2, 0.0 Hz, 2H), 4.81 (s, 1H), 4.61 (td, J = 7.6, 6.1 Hz, 1H), 3.77 (qq, J = 7.2, 3.8 Hz, 2H), 2.86 (dd, J = 14.3, 5.9 Hz, 1H), 2.66 (dd, J = 14.3, 7.2 Hz, 1H), 0.83 (t, J = 7.2 Hz, 3H); ^{13}C NMR (126 MHz, cdcl3) δ 171.77, 155.60, 147.88, 147.45, 143.19, 136.42, 134.22, 128.60, 128.24, 128.14, 119.98, 115.67, 108.21, 107.04, 101.21, 66.98, 61.50, 53.05, 38.52, 14.19. HRMS: calculated for [$C_{22}H_{23}NO_6$ + H^+] 398.1604, found 398.1600.

HPLC (Regis Tech (s,s)-whelk, 10% IPA/hexanes, 1 mL/min, 210 nm)

Racemic sample: retention times (24.2, 28.3 mins) Enantioenriched sample: retention times (23.0, 27.7 mins) **ee = 92%**

Ethyl (R)-2-(((benzyloxy)carbonyl)amino)-4-(4-bromophenyl)pent-4-enoate (2f)

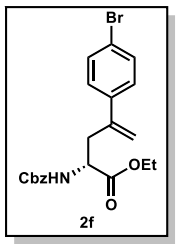

168 mgs, 78% yield. $[\alpha]^{23.6}_D$ = –7.3° (c = 1.0, $CHCl_3$); ^{1}H NMR (600 MHz, Benzene-d6) δ 7.21 – 7.16 (m, 4H), 7.11 (t, J = 7.5 Hz, 2H), 7.05 (t, J = 7.4 Hz, 1H), 6.88 (d, J = 8.2 Hz, 2H), 5.06 – 4.95 (m, 4H), 4.84 (s, 1H), 4.49 (q, J = 7.0 Hz, 1H), 3.79 – 3.63 (m, 2H), 2.80 (dd, J = 14.3, 5.9 Hz, 1H), 2.61 (dd, J = 14.4, 7.0 Hz, 1H), 0.79 (t, J = 7.1 Hz, 3H); ^{13}C NMR (126 MHz, cdcl3) δ 171.61, 155.59, 142.82, 139.10, 136.31, 131.66, 128.69, 128.37, 128.25, 128.12, 122.02, 117.27, 67.13, 61.66, 53.10, 38.30, 14.21.

HRMS: calculated for [$C_{21}H_{22}BrNO_4 + H^+$] 432.0810, found 432.0817.

HPLC (ChiralPak OD-H, 10% IPA/hexanes, 1 mL/min, 210 nm)

Racemic sample: retention times (14.2, 20.6 mins) Enantioenriched sample: retention times (14.3, 21.0 mins) **ee = 95.5%**

Ethyl (R)-2-(((benzyloxy)carbonyl)amino)-4-(3-bromophenyl)pent-4-enoate (2g)

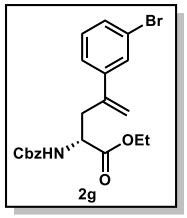

172 mgs, 80% yield. $[\alpha]^{23.6}_D$ = –43.2° (c = 1.0, $CHCl_3$); ^{1}H NMR (600 MHz, Benzene-d6) δ 7.50 (t, J = 1.9 Hz, 1H), 7.19 (d, J = 7.6 Hz, 2H), 7.14 (s, 1H), 7.10 (t, J = 7.4 Hz, 2H), 7.06 (d, J = 7.4 Hz, 1H), 7.01 (d, J = 7.9 Hz, 1H), 6.68 (t, J = 7.9 Hz, 1H), 5.08 (d, J = 8.1 Hz, 1H), 5.02 (dd, J = 28.6, 12.2 Hz, 2H), 4.83 (s, 1H), 4.49 (dt, J = 8.1, 6.4 Hz, 1H), 3.75 – 3.61 (m, 2H), 2.77 (dd, J = 14.4, 6.0 Hz, 1H), 2.61 (dd, J = 14.4, 6.7 Hz, 1H), 0.80 (t, J = 7.1 Hz, 3H); 13C NMR (126 MHz, cdcl3) δ 171.53, 155.54, 142.57, 142.44, 136.36, 135.92, 130.89, 130.06, 129.57, 128.63, 128.30, 128.21, 125.13, 122.67, 117.89, 67.08, 61.65, 53.02, 38.13, 14.17. HRMS: calculated for [$C_{21}H_{22}BrNO_4 + H^+$] 432.0810, found 432.0810.

HPLC (ChiralPak OD-H, 20% IPA/hexanes, 1 mL/min, 210 nm)

Racemic sample: retention times (8.0, 11.5 mins) Enantioenriched sample: retention times (8.2, 11.9 mins) **ee = 91.1%**

Ethyl (R,E)-2-(((benzyloxy)carbonyl)amino)-4-methylene-6-phenylhex-5-enoate (2h)

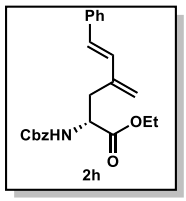

110 mgs, 79% yield. $[\alpha]^{23.6}_D$ = –6.7° (c = 1.0, $CHCl_3$); ^{13}C NMR (126 MHz, cdcl3) δ 172.01, 155.78, 140.97, 137.04, 136.36, 129.97, 129.30, 128.77, 128.64, 128.29, 128.25, 127.89, 126.72, 119.40, 67.13, 61.68, 53.29, 35.29, 29.85, 14.31; ^{1}H NMR (600 MHz, Benzene-d6) δ 7.26 (d, J = 7.6 Hz, 2H), 7.18 (d, J = 7.0 Hz, 2H), 7.13 – 7.06 (m, 4H), 7.04 (t, J = 7.3 Hz, 2H), 6.77 (d, J = 16.4 Hz, 1H), 6.66 (d, J = 16.4 Hz, 1H), 5.18 (d, J = 8.3 Hz,

1H), 5.05 (s, 2H), 5.03 (s, 1H), 4.91 (s, 1H), 4.78 (q, J = 6.7 Hz, 1H), 3.86 (q, J = 7.1 Hz, 2H), 2.75 (dd, J = 14.3, 6.2 Hz, 1H), 2.58 (dd, J = 14.2, 6.9 Hz, 1H), 0.85 (t, J = 7.1 Hz, 3H). HRMS: calculated for [$C_{23}H_{25}NO_4$ + H^+] 380.1862, found 380.1866.

HPLC (ChiralPak OD-H, 10% IPA/hexanes, 1 mL/min, 210 nm)

Racemic sample: retention times (10.2, 16.7 mins) Enantioenriched sample: retention times (10.2, 16.4 mins) **ee = 90.2%**

Ethyl (2R,3S)-2-(((benzyloxy)carbonyl)amino)-3,4-dimethylpent-4-enoate (2i)

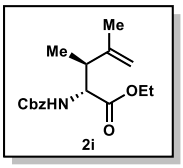

133 mgs, 87% yield. $[\alpha]^{23.6}_D$ = –12.2° (c = 1.0, $CHCl_3$); ^{1}H NMR (600 MHz, Benzene-d6) δ 7.19 (d, J = 7.1 Hz, 2H), 7.09 (t, J = 7.4 Hz, 2H), 7.04 (t, J = 7.2 Hz, 1H), 5.10 (d, J = 9.1 Hz, 1H), 5.08 – 5.00 (m, 2H), 4.74 (t, 1H), 4.73 (s, 1H), 4.64 (s, 1H), 3.92 – 3.79 (m, 2H), 2.48 (p, J = 7.0 Hz, 1H), 1.67 (s, 3H), 0.85 (t, J = 7.0 Hz, 6H); ^{13}C NMR (126 MHz, cdcl3) δ 172.01, 156.17, 145.30, 136.39, 128.56, 128.20, 128.12, 112.76, 67.04, 61.30, 56.60, 43.73, 20.35, 14.33, 14.21. HRMS: calculated for [$C_{17}H_{23}NO_4$ + H^+] 306.1705, found 306.1706.

HPLC (Regis Tech (s,s)-whelk, 3% IPA/hexanes, 1 mL/min, 210 nm)

Racemic sample: retention times (19.3, 20.6, 23.0 mins) Enantioenriched sample: retention times (19.7, 20.5, 23.8 mins) **ee = 92%**

Ethyl (R)-2-(((benzyloxy)carbonyl)amino)-2-((S)-2-methylenecyclohexyl)acetate (2j)

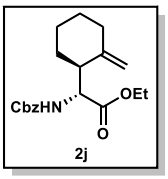

123 mgs, 74% yield. $[\alpha]^{23.6}_D$ = 21.6° (c = 1.0, $CHCl_3$); ^{1}H NMR (600 MHz, Benzene-d6) δ 7.19 (d, J = 7.0 Hz, 2H), 7.09 (t, J = 7.4 Hz, 2H), 7.04 (t, J = 7.6 Hz, 1H), 5.05 (m, 3H), 4.94 (t, J = 9.4 Hz, 1H), 4.76 (s, 1H), 4.65 (s, 1H), 3.94 – 3.79 (m, 2H), 2.28 (dt, J = 9.3, 4.6 Hz, 1H), 2.22 – 2.14 (m, 1H), 1.93 (dt, J = 13.6, 4.9 Hz, 1H), 1.66 – 1.49 (m, 2H), 1.47 – 1.39 (m, 1H), 1.35 – 1.18 (m, 3H), 0.87 (t, J = 7.1 Hz, 3H).; ^{13}C NMR (126

MHz, cdcl3) δ 172.57, 156.20, 147.92, 136.36, 128.64, 128.29, 128.23, 109.59, 67.20, 61.08, 54.81, 47.03, 33.39, 28.38, 27.95, 22.53, 14.20. HRMS: calculated for [$C_{19}H_{25}NO_4$ + H^+] 332.1862, found 332.1861.

HPLC (Regis Tech (s,s)-whelk, 3% IPA/hexanes, 1 mL/min, 210 nm)

Racemic sample: retention times (13.3, 14.5, 15.7, 18.1 mins) Enantioenriched sample: retention times (13.4, 14.9, 16.1, 18.6 mins) **ee = 95%**

Ethyl (R)-2-(((benzyloxy)carbonyl)amino)-2-((S)-1-methylene-1,2,3,4-tetrahydronaphthalen-2-yl)acetate (2k)

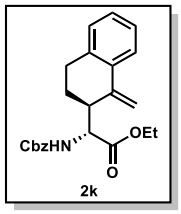

148 mgs, 78% yield. $[\alpha]^{27.1}_D$ = 38.1° (c = 1.0, $CHCl_3$); ^{1}H NMR (500 MHz, Chloroform-d) δ 7.51 (d, J = 8.2 Hz, 1H), 7.41 – 7.28 (m, 5H), 7.24 – 7.08 (m, 3H), 5.45 (s, 1H), 5.25 (d, J = 9.6 Hz, 1H), 5.10 (s, 2H), 4.99 (s, 1H), 4.49 (t, J = 9.4 Hz, 1H), 4.16 – 3.98 (m, 2H), 3.06 (ddd, J = 16.6, 10.3, 5.7 Hz, 1H), 2.90 – 2.73 (m, 2H), 2.10 – 1.88 (m, 2H), 1.17 (t, J = 7.1 Hz, 3H); ^{13}C NMR (126 MHz, cdcl3) δ 172.48, 156.11, 143.06, 136.31, 136.15, 133.90, 129.12, 128.65, 128.32, 128.22, 128.11, 126.29, 125.09, 111.11, 67.21, 61.04, 55.12, 45.43, 26.07, 24.42, 14.15. HRMS: calculated for [$C_{23}H_{25}NO_4$ + H^+] 380.1862, found 380.1855.

HPLC (Regis Tech (s,s)-whelk, 5% IPA/hexanes, 1 mL/min, 210 nm)

Racemic sample: retention times (18.7, 22.6 mins) Enantioenriched sample: retention times (20.0, 23.5 mins) **ee = 92.5%**

Ethyl (R)-2-(((benzyloxy)carbonyl)amino)-2-((S)-4-methylenethiochroman-3-yl)acetate (2l)

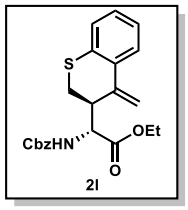

125 mgs, 63% yield. After crystalization 78 mgs, 39% yield. $[\alpha]^{24.3}_D$ = 47.2° (c = 1.0, $CHCl_3$); ^{1}H NMR (600 MHz, Chloroform-d) δ 7.43 (d, J = 8.0 Hz, 1H), 7.39 – 7.29 (m, 5H), 7.13 (p, J = 7.6 Hz, 2H), 7.04 (t, J = 8.0 Hz, 1H), 5.48 (s, 1H),

5.33 (d, J = 34.1 Hz, 1H), 5.09 (s, 2H), 5.03 (s, 1H), 4.77 (s, 1H), 4.06 (dd, J = 13.6, 7.0 Hz, 2H), 3.41 – 3.25 (m, 1H), 3.06 (dd, J = 13.6, 3.5 Hz, 2H), 1.15 (t, J = 7.3 Hz, 3H). ^{13}C NMR (126 MHz, cdcl$_3$) δ 172.14, 155.99, 141.19, 136.22, 132.61, 128.66, 128.53, 128.40, 128.36, 127.24, 127.13, 126.88, 124.81, 114.77, 67.37, 61.28, 55.09, 44.43, 29.86, 28.97. HRMS: calculated for [$C_{22}H_{23}NO_4S$ + H^+] 398.1426, found 398.1429.

HPLC (ChiralPak AS-H, 20% IPA/hexanes, 1 mL/min, 210 nm)

Racemic sample: retention times (26.7, 27.2 mins) Enantioenriched sample: retention times (25.0, 26.5 mins) **ee = 92.0%**. Crystalized sample: retention times (23.6, 25.2 mins) **ee = 98.3%**.

Ethyl (R)-2-((((9H-fluoren-9-yl)methoxy)carbonyl)amino)pent-4-enoate (2m)

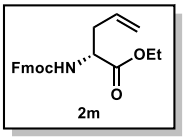

173 mgs, 95% yield, after recrystalization 149 mgs, 82% yield. $[\alpha]^{26.8}_D$ = 0.33° (c = 1.0, $CHCl_3$). ^{1}H NMR (600 MHz, Benzene-d6) δ 7.55 (d, J = 7.5 Hz, 2H), 7.38 (dd, J = 7.7, 4.8 Hz, 2H), 7.20 (ddt, J = 7.8, 4.3, 2.4 Hz, 2H), 7.13 (tdd, J = 7.4, 4.0, 1.2 Hz, 2H), 5.76 (d, J = 9.7 Hz, 1H), 5.50 (d, J = 9.6 Hz, 1H), 4.37 (dd, J = 10.7, 6.9 Hz, 1H), 4.27 (dd, J = 10.8, 6.8 Hz, 1H), 4.04 – 3.89 (m, 1H), 3.86 – 3.77 (m, 2H), 3.23 (s, 3H), 0.82 (t, J = 7.1 Hz, 3H). ^{13}C NMR (126 MHz, cdcl3) δ 167.69, 155.84, 143.75, 143.62, 141.43, 127.89, 127.21, 125.07, 120.13, 80.80, 67.38, 62.35, 56.32, 47.17, 29.80, 14.16. HRMS: calculated for [$C_{22}H_{23}NO_4$ + H^+] 366.1705, found 366.1704.

Absolute stereochemistry assigned by synthesis of ethyl (R)-2-(((benzyloxy)carbonyl)amino)pent-4-enoate from (D)-allylglycine via sequential Fmoc protection with Fmoc-OSu and ethyl esterification with iodoethane. Absolute stereochemistry additionally matches that found in the crystal structure of **2l**.

HPLC (ChiralPak AS-H, 10% IPA/hexanes, 1 mL/min, 210 nm)

Racemic sample: retention times (13.3, 16.0 mins) Enantioenriched sample: retention times (13.6

mins) **ee > 99.9%**

Authentic standard Ethyl (R)-2-((((9H-fluoren-9-yl)methoxy)carbonyl)amino)pent-4-enoate rt = (13.7 mins)

Ethyl (2R,3S)-2-((((9H-fluoren-9-yl)methoxy)carbonyl)amino)-3-methylpent-4-enoate (2n)

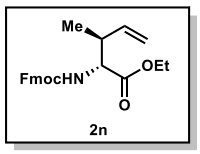

165 mgs, 87% yield. $[\alpha]^{23.4}_D$ = 23.4° (c = 1.0, $CHCl_3$); ^{1}H NMR (600 MHz, Benzene-d6) δ 7.56 (d, J = 7.5 Hz, 2H), 7.45 (dd, J = 12.6, 7.5 Hz, 2H), 7.21 (t, J = 7.4 Hz, 2H), 7.14 (d, J = 7.5 Hz, 2H), 5.65 (dt, J = 17.6, 8.6 Hz, 1H), 5.14 (d, J = 9.2 Hz, 1H), 4.99 – 4.78 (m, 2H), 4.56 (dd, J = 9.2, 5.4 Hz, 1H), 4.50 – 4.33 (m, 2H), 4.06 (t, J = 6.9 Hz, 1H), 3.93 – 3.77 (m, 2H), 2.46 (q, J = 6.8 Hz, 1H), 0.85 (t, J = 7.2 Hz, 3H); ^{13}C NMR (126 MHz, cdcl3) δ 171.48, 156.05, 144.05, 143.93, 141.45, 138.66, 127.84, 127.20, 125.25, 120.13, 116.46, 67.21, 61.49, 57.94, 47.34, 41.07, 34.27, 22.49, 15.58, 14.40, 14.21. HRMS: calculated for [$C_{23}H_{25}NO_4$ + H^+] 380.1862, found 380.1872.

HPLC (ChiralPak AS-H, 10% IPA/hexanes, 1 mL/min, 210 nm)

Racemic sample: retention times (8.7, 9.2 mins) Enantioenriched sample: retention times (8.8, 9.3 mins) **ee = 93.4%.**

Ethyl (R)-2-((((9H-fluoren-9-yl)methoxy)carbonyl)amino)-3,3-dimethylpent-4-enoate (2o)

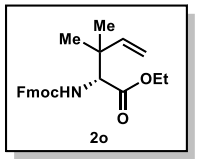

179 mgs, 91% yield. $[\alpha]^{23.8}_D$ = 7.6° (c = 1.0, $CHCl_3$); ^{1}H NMR (600 MHz, Benzene-d6) δ 7.55 (d, J = 7.5 Hz, 2H), 7.48 – 7.40 (m, 2H), 7.20 (t, J = 7.2 Hz, 2H), 7.14 (t, J = 7.5 Hz, 2H), 5.79 (dd, J = 17.4, 10.7 Hz, 1H), 5.27 (d, J = 9.6 Hz, 1H), 4.95 – 4.81 (m, 2H), 4.49 (d, J = 9.6 Hz, 1H), 4.41 (dd, J = 10.8, 7.1 Hz, 1H), 4.34 (dd, J = 10.8, 6.7 Hz, 1H), 4.06 (t, J = 6.9 Hz, 1H), 3.97 – 3.75 (m, 2H), 0.98 (s, 3H), 0.96 (s, 3H), 0.86 (t, J = 7.1 Hz, 3H).^{13}C NMR (126 MHz, cdcl3) δ 171.25, 156.16, 144.03, 143.94, 143.02, 141.45, 127.84, 127.19, 125.25, 125.22, 120.13, 120.11, 114.12, 67.20, 61.41, 61.25, 47.35, 40.66, 34.28,

24.51, 23.55, 22.49, 14.38. HRMS: calculated for [$C_{24}H_{27}NO_4 + H^+$] 394.2018, found 394.2011. HPLC (ChiralPak OD-H, 10% IPA/hexanes, 1 mL/min, 210 nm)

Racemic sample: retention times (10.2, 12.1 mins) Enantioenriched sample: retention times (9.3, 10.9 mins) **ee = 92.9%**

2.11.5 X-Ray crystallographic information and data

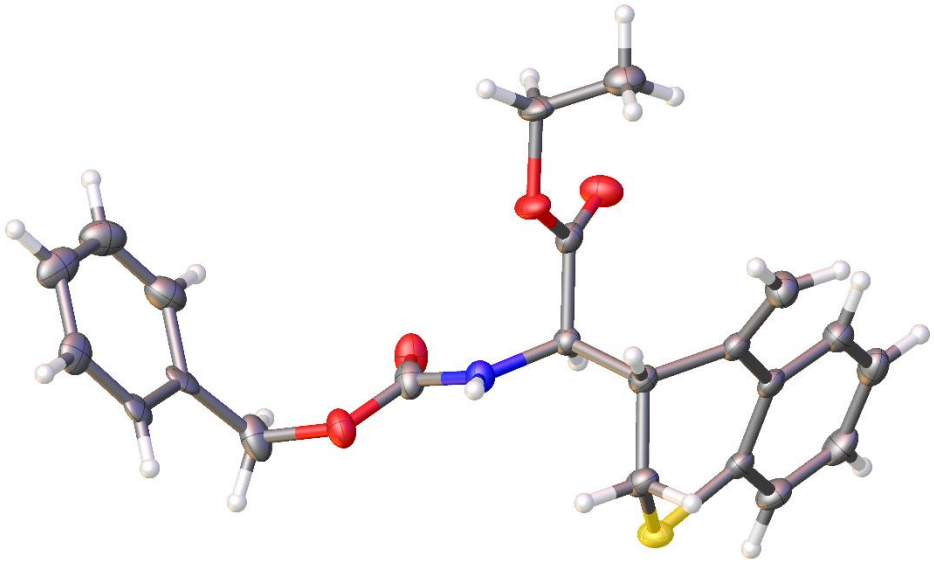

Figure 2.33 Crystal structure of 2l for absolute stereochemistry determination

X-ray Crystallography: A crystal mounted on a diffractometer was collected data at 100 K. The intensities of the reflections were collected by means of a Bruker APEX II DUO CCD diffractometer ($Cu_{K\alpha}$ radiation, λ=1.54178 Å), and equipped with an Oxford Cryosystems nitrogen flow apparatus. The collection method involved 1.0° scans in ω at -30°, -55°, -80°, 30°, 55°, 80° and 115° in 2θ. Data integration down to 0.84 Å resolution was carried out using SAINT V8.35 A (Bruker diffractometer, 2015) with reflection spot size optimization. Absorption corrections were made with the program SADABS (Bruker diffractometer, 2015). The structure was solved by the Intrinsic Phasing methods and refined by least-squares methods again F^2 using SHELXT-2014 (Sheldrick, 2015) and SHELXL-2014 (Sheldrick, 2015) with OLEX 2 interface (Dolomanov,

et al., 2009). Non-hydrogen atoms were refined anisotropically, and hydrogen atoms were allowed to ride on the respective atoms. Crystal data as well as details of data collection and refinement are summarized in Table 1, geometric parameters are shown in Table 2 and hydrogen-bond parameters are listed in Table 3. The Ortep plots produced with SHELXL-2014 program, and the other drawings were produced with Accelrys DS Visualizer 2.0 (Accelrys, 2007).

Table 1. Experimental details

	(80909535)
Crystal data	
Chemical formula	$C_{22}H_{23}NO_4S$
M_r	397.47
Crystal system, space group	Orthorhombic, $P2_12_12_1$
Temperature (K)	100
a, b, c (Å)	5.1729 (2), 10.5450 (4), 35.9696 (11)
V (Å^3)	1962.08 (12)
Z	4
Radiation type	Cu $K\alpha$
μ (mm^{-1})	1.70
Crystal size (mm)	0.22 × 0.12 × 0.10
Data collection	
Diffractometer	Bruker D8 goniometer with CCD area detector
Absorption correction	Multi-scan *SADABS*
T_{min}, T_{max}	0.633, 0.753
No. of measured, independent and observed [$I > 2\sigma(I)$] reflections	35289, 3382, 3263
R_{int}	0.051
$(\sin \theta/\lambda)_{max}$ (Å^{-1})	0.595
Refinement	
$R[F^2 > 2\sigma(F^2)]$, $wR(F^2)$, S	0.037, 0.086, 1.10

No. of reflections	3382
No. of parameters	256
No. of restraints	51
H-atom treatment	H-atom parameters constrained
$\Delta\rho_{max}$, $\Delta\rho_{min}$ (e Å^{-3})	0.23, -0.23
Absolute structure	Flack x determined using 1265 quotients [(I+)-(I-)]/[(I+)+(I-)] (Parsons, Flack and Wagner, Acta Cryst. B69 (2013) 249-259).
Absolute structure parameter	0.006 (8)

Computer programs: *APEX3* v2016.1-0 (Bruker-AXS, 2016), *SAINT* 8.35A (Bruker-AXS, 2015), *SHELXT2014* (Sheldrick, 2015), *SHELXL2014* (Sheldrick, 2015), Bruker *SHELXTL* (Sheldrick, 2015).

Table 2. Geometric parameters (Å, º)

S1—C1	1.767 (3)	C14—H14B	0.9800
S1—C9	1.802 (3)	C14—H14C	0.9800
O1—C12	1.339 (4)	C15—O4A	1.344 (13)
O1—C13	1.456 (3)	C15—O4	1.392 (9)
O2—C12	1.204 (4)	O4—C16	1.469 (10)
O3—C15	1.206 (4)	C16—C17	1.527 (10)
N1—C15	1.345 (4)	C16—H16A	0.9900
N1—C11	1.451 (4)	C16—H16B	0.9900
N1—H1	0.7508	C17—C18	1.3900
C1—C2	1.393 (4)	C17—C22	1.3900
C1—C6	1.410 (4)	C18—C19	1.3900
C2—C3	1.377 (5)	C18—H18	0.9500
C2—H2	0.9500	C19—C20	1.3900
C3—C4	1.384 (5)	C19—H19	0.9500
C3—H3	0.9500	C20—C21	1.3900
C4—C5	1.375 (5)	C20—H20	0.9500
C4—H4	0.9500	C21—C22	1.3900
C5—C6	1.404 (4)	C21—H21	0.9500
C5—H5	0.9500	C22—H22	0.9500
C6—C7	1.481 (4)	O4A—C16A	1.463 (15)
C7—C10	1.326 (4)	C16A—C17A	1.495 (15)
C7—C8	1.523 (4)	C16A—H16C	0.9900
C8—C9	1.525 (4)	C16A—H16D	0.9900

C8—C11	1.541 (4)	C17A—C18A	1.3900
C8—H8	1.0000	C17A—C22A	1.3900
C9—H9A	0.9900	C18A—C19A	1.3900
C9—H9B	0.9900	C18A—H18A	0.9500
C10—H10A	0.9500	C19A—C20A	1.3900
C10—H10B	0.9500	C19A—H19A	0.9500
C11—C12	1.521 (4)	C20A—C21A	1.3900
C11—H11	1.0000	C20A—H20A	0.9500
C13—C14	1.498 (5)	C21A—C22A	1.3900
C13—H13A	0.9900	C21A—H21A	0.9500
C13—H13B	0.9900	C22A—H22A	0.9500
C14—H14A	0.9800		
C1—S1—C9	101.62 (15)	C13—C14—H14C	109.5
C12—O1—C13	116.1 (3)	H14A—C14—H14C	109.5
C15—N1—C11	120.9 (3)	H14B—C14—H14C	109.5
C15—N1—H1	120.8	O3—C15—O4A	122.6 (8)
C11—N1—H1	118.1	O3—C15—N1	125.4 (3)
C2—C1—C6	120.1 (3)	O4A—C15—N1	110.8 (8)
C2—C1—S1	115.8 (2)	O3—C15—O4	126.7 (5)
C6—C1—S1	124.1 (2)	N1—C15—O4	107.2 (5)
C3—C2—C1	121.3 (3)	C15—O4—C16	116.6 (8)
C3—C2—H2	119.3	O4—C16—C17	109.7 (9)
C1—C2—H2	119.3	O4—C16—H16A	109.7
C2—C3—C4	119.5 (3)	C17—C16—H16A	109.7
C2—C3—H3	120.2	O4—C16—H16B	109.7
C4—C3—H3	120.2	C17—C16—H16B	109.7
C5—C4—C3	119.5 (3)	H16A—C16—H16B	108.2
C5—C4—H4	120.2	C18—C17—C22	120.0
C3—C4—H4	120.2	C18—C17—C16	118.8 (7)
C4—C5—C6	122.8 (3)	C22—C17—C16	121.1 (7)
C4—C5—H5	118.6	C19—C18—C17	120.0
C6—C5—H5	118.6	C19—C18—H18	120.0
C5—C6—C1	116.7 (3)	C17—C18—H18	120.0
C5—C6—C7	120.3 (3)	C18—C19—C20	120.0

C1—C6—C7	123.0 (3)	C18—C19—H19	120.0
C10—C7—C6	123.0 (3)	C20—C19—H19	120.0
C10—C7—C8	119.5 (3)	C19—C20—C21	120.0
C6—C7—C8	117.4 (3)	C19—C20—H20	120.0
C7—C8—C9	109.4 (2)	C21—C20—H20	120.0
C7—C8—C11	111.8 (3)	C22—C21—C20	120.0
C9—C8—C11	111.9 (2)	C22—C21—H21	120.0
C7—C8—H8	107.8	C20—C21—H21	120.0
C9—C8—H8	107.8	C21—C22—C17	120.0
C11—C8—H8	107.8	C21—C22—H22	120.0
C8—C9—S1	113.3 (2)	C17—C22—H22	120.0
C8—C9—H9A	108.9	C15—O4A—C16A	117.5 (13)
S1—C9—H9A	108.9	O4A—C16A—C17A	105.4 (14)
C8—C9—H9B	108.9	O4A—C16A—H16C	110.7
S1—C9—H9B	108.9	C17A—C16A—H16C	110.7
H9A—C9—H9B	107.7	O4A—C16A—H16D	110.7
C7—C10—H10A	120.0	C17A—C16A—H16D	110.7
C7—C10—H10B	120.0	H16C—C16A—H16D	108.8
H10A—C10—H10B	120.0	C18A—C17A—C22A	120.0
N1—C11—C12	112.2 (2)	C18A—C17A—C16A	122.9 (12)
N1—C11—C8	110.3 (2)	C22A—C17A—C16A	117.1 (12)
C12—C11—C8	109.3 (2)	C19A—C18A—C17A	120.0
N1—C11—H11	108.3	C19A—C18A—H18A	120.0
C12—C11—H11	108.3	C17A—C18A—H18A	120.0
C8—C11—H11	108.3	C18A—C19A—C20A	120.0
O2—C12—O1	124.2 (3)	C18A—C19A—H19A	120.0
O2—C12—C11	124.5 (3)	C20A—C19A—H19A	120.0
O1—C12—C11	111.3 (2)	C21A—C20A—C19A	120.0
O1—C13—C14	111.1 (3)	C21A—C20A—H20A	120.0
O1—C13—H13A	109.4	C19A—C20A—H20A	120.0
C14—C13—H13A	109.4	C20A—C21A—C22A	120.0
O1—C13—H13B	109.4	C20A—C21A—H21A	120.0
C14—C13—H13B	109.4	C22A—C21A—H21A	120.0
H13A—C13—H13B	108.0	C21A—C22A—C17A	120.0
C13—C14—H14A	109.5	C21A—C22A—H22A	120.0

C13—C14—H14B	109.5	C17A—C22A—H22A	120.0
H14A—C14—H14B	109.5		
C9—S1—C1—C2	172.3 (2)	C8—C11—C12—O2	100.7 (3)
C9—S1—C1—C6	-8.9 (3)	N1—C11—C12—O1	44.8 (3)
C6—C1—C2—C3	1.2 (5)	C8—C11—C12—O1	-78.0 (3)
S1—C1—C2—C3	180.0 (3)	C12—O1—C13—C14	-85.6 (4)
C1—C2—C3—C4	0.3 (5)	C11—N1—C15—O3	1.3 (5)
C2—C3—C4—C5	-1.8 (5)	C11—N1—C15—O4A	-166.5 (6)
C3—C4—C5—C6	1.9 (5)	C11—N1—C15—O4	172.1 (5)
C4—C5—C6—C1	-0.5 (5)	O3—C15—O4—C16	-11.3 (9)
C4—C5—C6—C7	-179.5 (3)	N1—C15—O4—C16	178.1 (5)
C2—C1—C6—C5	-1.1 (4)	C15—O4—C16—C17	-109.0 (10)
S1—C1—C6—C5	-179.8 (2)	O4—C16—C17—C18	96.6 (10)
C2—C1—C6—C7	177.9 (3)	O4—C16—C17—C22	-79.8 (9)
S1—C1—C6—C7	-0.8 (4)	C22—C17—C18—C19	0.0
C5—C6—C7—C10	-23.7 (5)	C16—C17—C18—C19	-176.5 (10)
C1—C6—C7—C10	157.3 (3)	C17—C18—C19—C20	0.0
C5—C6—C7—C8	158.2 (3)	C18—C19—C20—C21	0.0
C1—C6—C7—C8	-20.8 (4)	C19—C20—C21—C22	0.0
C10—C7—C8—C9	-124.2 (3)	C20—C21—C22—C17	0.0
C6—C7—C8—C9	54.0 (4)	C18—C17—C22—C21	0.0
C10—C7—C8—C11	111.2 (3)	C16—C17—C22—C21	176.4 (10)
C6—C7—C8—C11	-70.6 (3)	O3—C15—O4A—C16A	12.2 (12)
C7—C8—C9—S1	-64.9 (3)	N1—C15—O4A—C16A	-179.6 (8)
C11—C8—C9—S1	59.6 (3)	C15—O4A—C16A—C17A	-140.1 (11)
C1—S1—C9—C8	41.2 (2)	O4A—C16A—C17A—C18A	108.7 (15)
C15—N1—C11—C12	81.0 (3)	O4A—C16A—C17A—C22A	-72.5 (13)
C15—N1—C11—C8	-156.7 (3)	C22A—C17A—C18A—C19A	0.0
C7—C8—C11—N1	177.3 (2)	C16A—C17A—C18A—C19A	178.7 (16)
C9—C8—C11—N1	54.1 (3)	C17A—C18A—C19A—C20A	0.0

C7—C8—C11—C12	-58.8 (3)	C18A—C19A—C20A—C21A	0.0
C9—C8—C11—C12	178.0 (2)	C19A—C20A—C21A—C22A	0.0
C13—O1—C12—O2	-2.4 (4)	C20A—C21A—C22A—C17A	0.0
C13—O1—C12—C11	176.3 (2)	C18A—C17A—C22A—C21A	0.0
N1—C11—C12—O2	-136.6 (3)	C16A—C17A—C22A—C21A	-178.8 (15)

Table 3. Hydrogen-bond parameters

D—H···*A*	*D*—H (Å)	H···*A* (Å)	*D*···*A* (Å)	*D*—H···*A* (°)
N1—H1···O3^{i}	0.75	2.32	3.065 (4)	170.2

Symmetry code(s): (i) *x*+1, *y*, *z*.

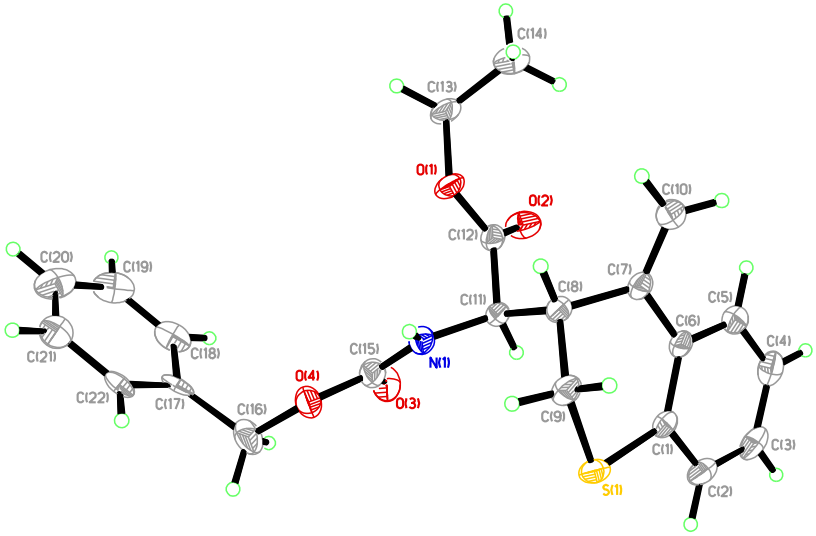

Figure 2.34. Perspective views showing 50% probability displacement

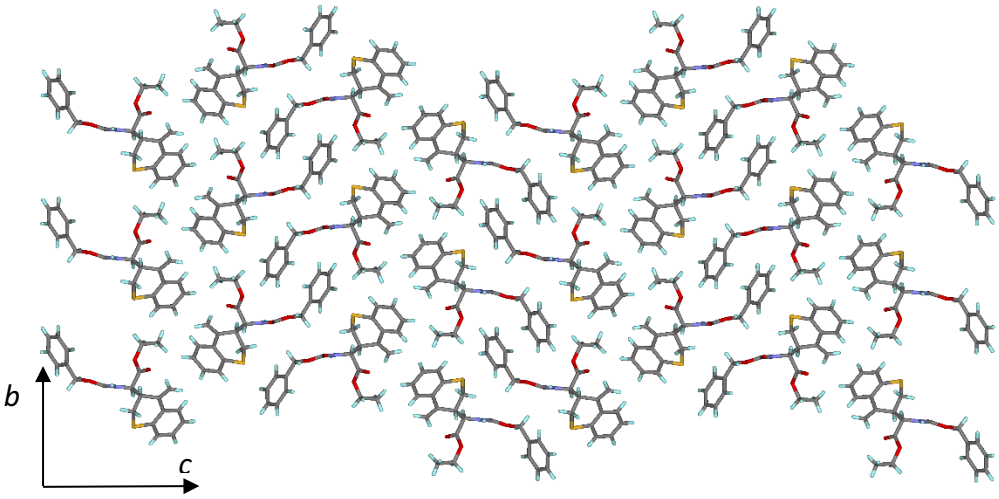

Figure 2.35. Three-dimensional supramolecular architecture viewed along the *a*-axis direction.

Chapter 3

Mechanistic Investigation of the Hydrogen-Bond Donor Catalyzed Allylation of α-Chloroglycines

3.1 Introduction

In introductory organic chemistry, the two mechanisms for substitution reactions, unimolecular S_N1 and bimolecular S_N2 are taught as two discrete possibilities. Based on the kinetic definition this is true. However, the hallmark of an S_N1 is the presence of a cationic intermediate that generally loses the stereochemical information of the starting material, due to bond breaking preceding bond formation. Whereas the hallmark of an S_N2 is a stereospecific concerted reaction in which bond breaking and formation occur in the same step. When using these definitions of S_N1 and S_N2, which are the definitions that will be used in this chapter, they are no longer discrete possibilities, but rather on a spectrum that is depicted in the More O'Ferrall–Jencks plot in Figure 3.1.[140]

Reactivity on the edge of S_N1 and S_N2 are often hard to distinguish from each other. If the ionization of the substrate is rate determining the process, is by definition S_N1. However, if nucleophilic addition is rate determining, addition to an ionized intermediate versus direct

[140] For seminal reports see: a) O'Ferrall, R. A. M. Relationships between E2 and E1cB Mechanisms of β-Elimination. *J. Chem. Soc. B* **1970**, *0* (0), 274–277. b) Jencks, W. P. General Acid-Base Catalysis of Complex Reactions in Water. *Chem. Rev.* **1972**, *72* (6), 705–718. Applications to substitution mechanisms: c) Harris, J. M.; Shafer, S. G.; Moffatt, J. R.; Becker, A. R. Prediction of SN2 Transition State Variation by the Use of More O'Ferrall Plots. *J. Am. Chem. Soc.* **1979**, *101* (12), 3295–3300.

displacement of the starting material are kinetically identical. Due to the difference in transition state pictures, the mechanistic chemist's toolbox has ways of distinguishing these two scenarios, specifically linear free energy relationships (LFERs) to determine the buildup of charge in a transition state, and kinetic isotope effects (KIEs), which can directly inform bond-breaking and formation in the transition state, as well as transition state hybridization geometries. However, these tools are not always applicable or diagnostic.

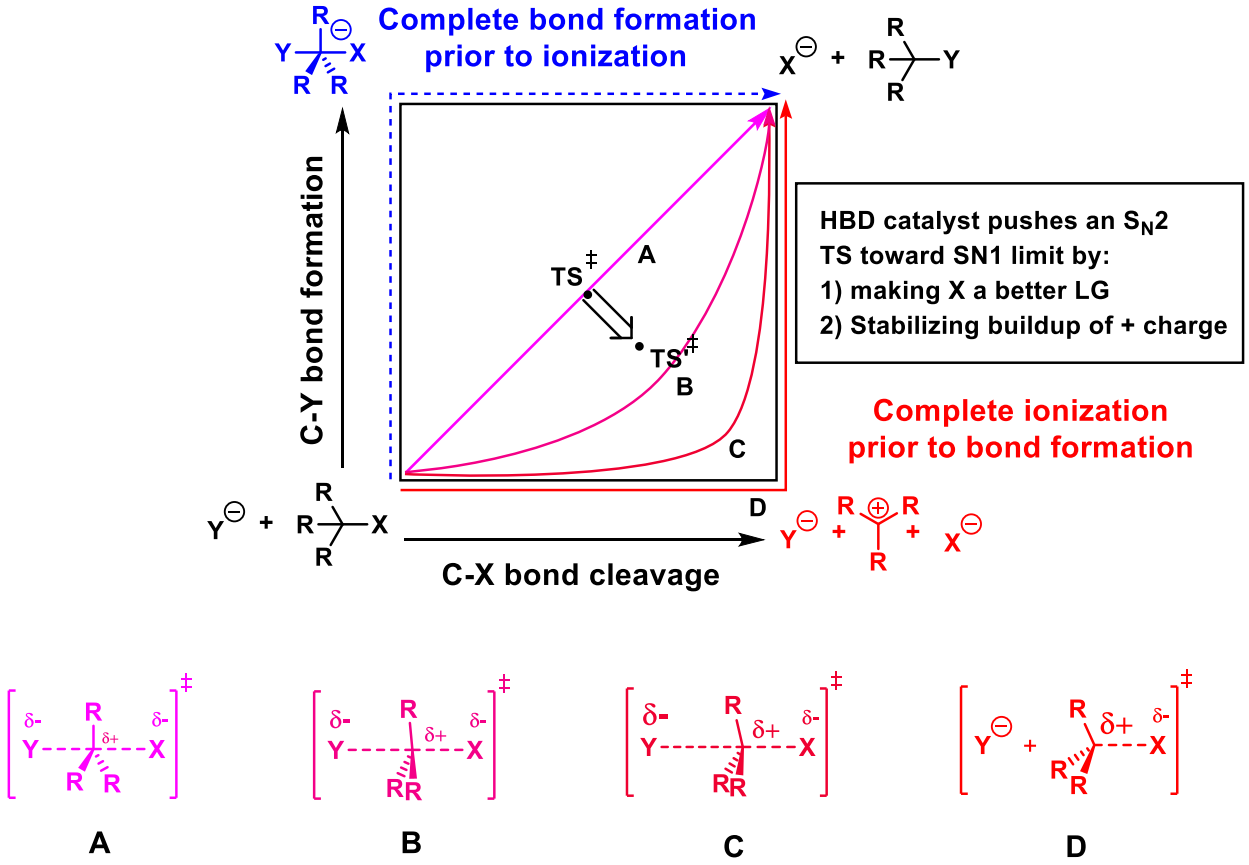

Figure 3.1 More O'Ferrall–Jencks plot for S_N1 and S_N2 reactions

Hydrogen-bond donor catalysis, and in particular anion-abstraction catalysis has mostly been applied to S_N1 reactions, yet it has a high potential to catalyze reactions on the S_N1 S_N2 interface. This is because leaving groups are often chloride or other halide or pseudohalide anions, which dual hydrogen-bond donor catalysts have been shown to bind and thus stabilize the buildup

of negative charge.[141] Additionally, chiral hydrogen bond-donors are able to stabilize the buildup of positive charge on the electrophile through secondary non-covalent attractive interactions; namely C-H- and cation-π interactions. The ability to stabilize the electrophile in the S_N2 transition state should advance bond breaking relative to bond formation, which at the limit would push this to a dissociative S_N1 mechanism. In fact, recently, hydrogen-bond donors have been shown to be exquisite catalysts for highly dissociative S_N2 glycosylation reactions rather than preceding through the intermediacy of an oxocarbenium intermediate.[142]

The squaramide hydrogen-bond donor catalyzed allylation of *N*-carbamoyl α-chloroglycinates developed in Chapter 2 is a reaction that is hypothesized to exist on the edge of the S_N1 S_N2 continuum. The primary feature that puts it in the S_N1 camp is the prior ability to hydrogen bond-donor catalysts to engage weak neutral π nucleophiles, such as allylsilanes and Friedel-Crafts arenes, with *N*-acyliminium ions generated via an S_N1 mechanism.[99b,127b,143] Features that would suggest that the reaction mechanism is S_N2 include an iminium
that would require carbocationic character α-to a carbonyl,[144] as well as optimal enantioselectivity in DCM, a solvent known to promote dissociated ion-pairs.[94]

---

[141] For a review on ion-pairing catalysis: Brak, K.; Jacobsen, E. N. Asymmetric Ion-Pairing Catalysis. *Angew. Chemie Int. Ed.* **2013**, *52* (2), 534–561.

[142] a) Park, Y.; Harper, K. C.; Kuhl, N.; Kwan, E. E.; Liu, R. Y.; Jacobsen, E. N. Macrocyclic Bis-Thioureas Catalyze Stereospecific Glycosylation Reactions. *Science* **2017**, *355* (6321), 162–166. b) Kwan, E. E.; Park, Y.; Besser, H. A.; Anderson, T. L.; Jacobsen, E. N. Sensitive and Accurate ^{13} C Kinetic Isotope Effect Measurements Enabled by Polarization Transfer. *J. Am. Chem. Soc.* **2017**, *139* (1), 43–46.

[143] For HBD catalyzed reactions with *N*-acyliminium ion intermediates see: a) T. Raheem, I.; S. Thiara, P.; N. Jacobsen, E. Regio- and Enantioselective Catalytic Cyclization of Pyrroles onto N-Acyliminium Ions. *Org. Lett.* **2008**, *10* (8), 1577–1580. b) Peterson, E. A.; Jacobsen, E. N. Enantioselective, Thiourea-Catalyzed Intermolecular Addition of Indoles to Cyclic N-Acyl Iminium Ions. *Angew. Chemie Int. Ed.* **2009**, *48* (34), 6328–6331. c) Park, Y.; S. Schindler, C.; N. Jacobsen, E. Enantioselective Aza-Sakurai Cyclizations: Dual Role of Thiourea as H-Bond Donor and Lewis Base. *J. Am. Chem. Soc.* **2016**, *138* (45), 14848–14851.

[144] For key references in substitution next to carbonyls see: a) Conant, J. B.; Kirner, W. R.; Hussey, R. E. The Relation Between the Structure of Organic Halides and the Speeds of Their Reaction with Inorganic Iodides. III. The Influence of Unsaturated Groups. *J. Am. Chem. Soc.* **1925**, *47*, 488-501. b) Paddon-Row, M. N.; Santiago, C.; Houk, K. N. Possibility of .pi.-electron donation by the electron-withdrawing substituents CN, CHO, CF3, and +NH3. *J. Am. Chem.*

3.1.1 *N*-acyliminium ions in anion-abstraction hydrogen-bond donor catalysis

N-acyl iminium ion has been extensively studied in chiral hydrogen-bond donor catalyzed anion-abstraction transformations.[99b,127b,143] In each of these examples, an α-hydroxylactam is activated to deoxychlorination with a Lewis or Brønsted acid/chlorinating agent (e.g. HCl, AcCl, TMSCl, and BCl_3). These α-choro amines do not undergo autoheterolysis because the nitrogen is either *N*-acyl or *N*-cabamoyl. This *N*-acyl α-chloro electrophile can undergo chloride abstraction by a dual hydrogen-bond donor catalysts to form a chiral ion pair with chloride anion bound to catalyst (Figure 3.2).

This approach has allowed access to a diverse array of chiral amines and alkaloid natural products, such as harmicine and epilupinine.[127b,143c] Various weak π nucleophiles such as indoles,[127b] olefins,[99b] and allyltrimethylsilanes[143c] have been shown to be suitable in intramolecular nucleophilic substitutions to furnish complex heterocycles. Additionally, intermolecular nucleophilic attack via indole[143b] have been demonstrated, increasing the generality of chiral hydrogen bond donor catalysis with α-chloro lactam derived *N*-Acyl iminium electrophiles.

Soc. **1980**, *102*, 6561-6563. c) Kost, D.; Aviram, K. SN2 transition state. 4. Effect of .alpha.-substituents on SN2 reactivity and the SN2-SN1 borderline problem. A molecular orbital approach. *J. Am. Chem. Soc.* **1986**, *108*, 2006-2013. d) Bach, R. D.; Coddens, B. A.; Wolber, G. J. Origin of the reactivity of allyl chloride and .alpha.-chloroacetaldehyde in SN2 nucleophilic substitution reactions: a theoretical comparison. *J. Org. Chem.* **1989**, *51*, 1030-1033.

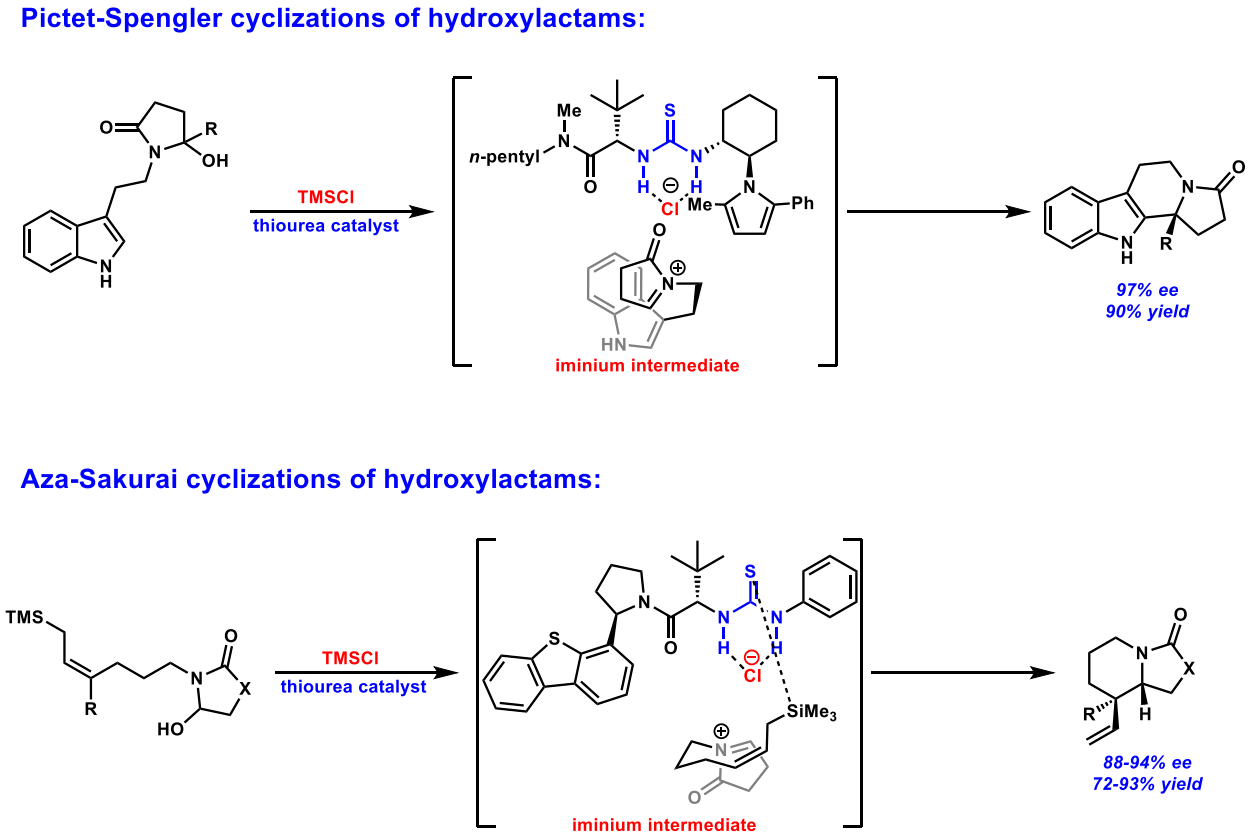

Figure 3.2 Two examples of enantioselective nucleophilic additions to chiral *N*-acyl iminium ion pairs generated by hydrogen-bond donor chloride-abstraction

One could consider two plausible mechanisms of hydrogen-bond donor catalyzed, nucleophilic attack to *N*-acyl iminium ions: S_N1 and S_N2. A wealth of mechanistic evidence has strongly suggested an S_N1-pathway for these hydrogen-bond donor catalyzed nucleophilic additions to *N*-acyliminium ions. NMR studies of 5-Hydroxy-1-[2-(1H-indol-3-yl)-ethyl]-pyrrolidin2-one with TMSCl have shown a rapid, irreversible conversion to the corresponding chloride via dehydration. Presumably this proceeds through the intermediacy of an iminium intermediate, showing that these substrates are unstable and that they can easily form an ion-pair. Additionally, NMR studies of hydrogen bond donor catalysts with tetrabutylammonium halides (halides = Cl/ Br/ I) have shown a significant downfield shift of two N-Hs of up to 0.56 ppm, with a clear decreasing trend of chloride, bromide to iodide in chemical shifts. The observed trend is consistent with the coordinating ability of the counter ions.[127b] Despite the intermediacy of the

same or highly related iminium ion in each case, the rate determining step is not preserved across reactions. In the polycyclization, a secondary KIE experiment suggested that the ionization of the starting material to the iminium is rate determining, indicating a true kinetic S_N1. However, in the aza-Sakurai addition of allylsilanes, a strong inverse secondary KIE of 0.83- 0.85 was observed on the vinyl proton of the nucleophile, indicating the rate-limiting step is nucleophilic attack. Overall, the wealth of precedent demonstrate that the C-Cl bond α to an N-acyl group is very labile and that chiral hydrogen-bond donor catalysts can abstract the chloride to form an ion pair to promote these transformations that precede through an iminium ion.

Additionally, many hydrogen-bond donor catalyzed iminium ion transformations both in the anion-binding and anion-abstraction contexts have complete mechanistic pictures with well understood methods of enantioinduction.[34,99a,141,145] Generally the primary mode of catalysis over background reactivity is hydrogen-bonding to chloride making for a more naked and electrophilic iminium, while also holding together a chiral ion-pair. This chiral ion-pair is able to achieve enantioinduction by preferentially stabilizing one diastereomeric transition state by secondary non-covalent attractive interactions to catalyst, including cation-π interactions, π-π interactions, substrate and catalyst hydrogen-bonding networks. The modes of achieving enantioselectivity are relatively well-understood in the context of ion-pairing catalysis.

Given the *N*-acyl iminium ion precedent and mechanistic studies above, one could assume that allylation of **Cbz-1** in Chapter 1 occurs via an S_N1 pathway, where **Cbz-1** undergoes a catalyst promoted ionization equilibrium to *N*-carbamoyl iminium ester cation and catalyst bound chloride ion-pair. Given the weaker electron withdrawing ability of *N*-carbamoyl, one could postulate that

[145] Klausen, R. S.; Kennedy, C. R.; Hyde, A. M.; Jacobsen, E. N. Chiral Thioureas Promote Enantioselective Pictet–Spengler Cyclization by Stabilizing Every Intermediate and Transition State in the Carboxylic Acid-Catalyzed Reaction. *J. Am. Chem. Soc.* **2017**, *139* (35), 12299–12309.

the equilibrium of iminium ions would be even more stabilized than the corresponding *N*-acyliminium ions. However, as briefly mentioned in section 1, several experimental results suggest that the allylation may not operate via S_N1 pathway, such as the virtue of it being α-to a carbonyl and the ability to achieve 97% ee in DCM, a solvent known to promote dissociated ion-pairs. The mechanisms by which hydrogen-bond donors can promote rate acceleration and enantioselectivity in transformations in which the transition state and intermediates leading up to the transition state are covalent rather than charged species is not understood and worthy of further study.

3.1.2 Substitution α-to carbonyls

In 1925, Conant published a seminal report, which measured the relative rates of Finkelstein reactions and found that α-chloro acetone undergoes substitution at 35,700 times the rate of substitution on primary propyl chloride (Figure 3.3).[144a] Since then, chemists have attempted to explain this dramatic rate acceleration phenomenon and arrived at two differing schools of thought. Traditional thought is that the productive molecular orbital mixing allows the C-X σ* to engage in productive overlap with the LUMO of the carbonyl, creating a new lower energy delocalized LUMO. This is reflected in the transition state by being able to delocalize the net negative charge of the incoming nucleophile and outgoing leaving group into the carbonyl.[144b,c,d] A more modern interpretation of the rate acceleration from an α-carbonyl compound is a stabilizing electrostatic interaction between the partially anionic incoming nucleophile and outgoing leaving group and the partially cationic carbon of the carbonyl.[146] Likely both explanations are valid.

[146] a) Galabov, B.; Nikolova, V.; Wilke, J. J.; Schaefer, H. F.; Allen, W. D. Origin of the S_N2 Benzylic Effect. *J. Am. Chem. Soc.* **2008**, *130* (30), 9887–9896. b) Wu, C.-H.; Galabov, B.; Wu, J. I.-C.; Ilieva, S.; von R. Schleyer, P.; Allen, W. D. Do π-Conjugative Effects Facilitate S_N2 Reactions? *J. Am. Chem. Soc.* **2014**, *136* (8), 3118–3126.

Additionally, Houk has computed that the destabilizing effect of putting a cation next to a formyl group ranges from 13-19 kcal/mol depending on the degree of conjugation from the π system of the formyl group. So not only do carbonyls stabilize S_N2 transition states, they also strongly destabilize S_N1 cationic intermediates. Thus, α-acyl carbenium ions are exceedingly high in energy and have only rarely been invoked in S_N1 chemistry in the presence of super-acids and in the presence of strong activation in a non-classical norbornyl system, in which the rate retardation due to the presence of the ketone is $10^{7.3}$.[147,148]

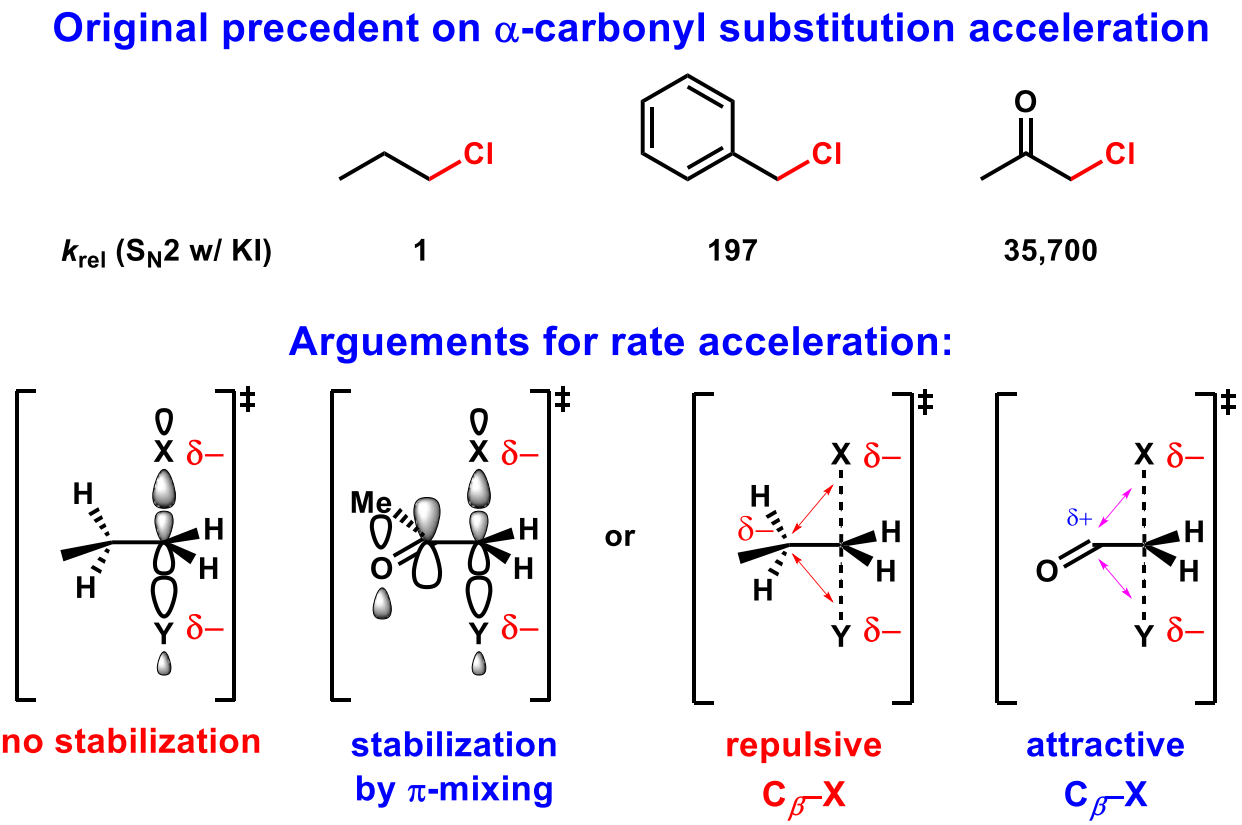

Figure 3.3 α-carbonyls dramatically accelerate S_N2 reactions via orbital overlap or electrostatic stabilization in the S_N2 transition state

[147] Creary, X. Generation of .Alpha.-Keto Cations. Quantitative Aspects. *J. Org. Chem.* **1979**, *44* (22), 3938–3945.

[148] Begue, J. P.; Charpentier-Morize, M. ..Alpha.-Acylcarbenium Ions. *Acc. Chem. Res.* **1980**, *13* (7), 207–212.

3.2 Kinetic analysis of the squaramide catalyzed allylation of α-chloroglycinates

As discussed in the introduction, 3.1 the hydrogen-bond donor catalyzed allylation of α-chloroglycinates has a number of features that place it on the border of S_N1 and S_N2. A thorough literature review suggests that except in rare highly activated cases, which do not describe the conditions for this transformation, there are no examples of α-carbonyl S_N1 additions. On the other hand the weak π allylsilane and Friedel-Crafts nucleophiles are canonically S_N2 nucleophiles or nucleophiles to activated planar π-systems such as carbonyls and imines in Lewis and Brønsted acid contexts. No examples could be found in which they stereoinvertively add to an sp^3 hybridized carbon. Thus, it is surprising that this transformation occurs via any mechanism, and the substitution mechanism of carbon-carbon bond formation and the mode of catalyst activation and enantioinduction are of the highest interest.

To probe the substitution mechanism of C-C bond formation, a kinetic analysis was conducted to determine if the C-C bond forming step was rate and selectivity determining in this reaction. If the reaction were to obey a first order rate law, ionization of the substrate would likely be rate determining. If the reaction were to display a second order rate law, the C-C bond forming step would likely be rate and selectivity determining.

Initially full reaction course kinetics were performed in order to determine that the reaction is well-behaved (Figure 3.4, for details and conditions, see experimental section). The concentration [**2a**] vs. time plot appears to have a second order profile. To rigorously determine this, the plot was linearized using equation (7) for a second order reaction in which the initial reagent stoichiometry is not 1:1, derived in the experimental section of this chapter. Indeed, the data fit a second-order linearized integrated rate law quite well with $R^2 = 0.982$. Deviation from linearity occurs at the end of the reaction due to the inability to measure integrals well and that as

the concentration of [**1-Cbz**] nears 0, the linearized data get more sensitive to small deviations in [**1-Cbz**]. The ability to fit a second-order rate law to these data indicate that it is well-behaved, without catalyst decomposition, product inhibition, or a significant induction period. Furthermore, the data go through the (0,0) point, as necessitated by the equation and the rate constant can be extracted to give $k = 0.62\ M^{-1}h^{-1}$. Last, the data fit both a simulated second-order and first-order reaction with this rate constant quite well, due to the excess in nucleophile, as found in the experimental section of this chapter. This indicates that orders in components should be determined given the ambiguity as a result of unequal stoichiometry.

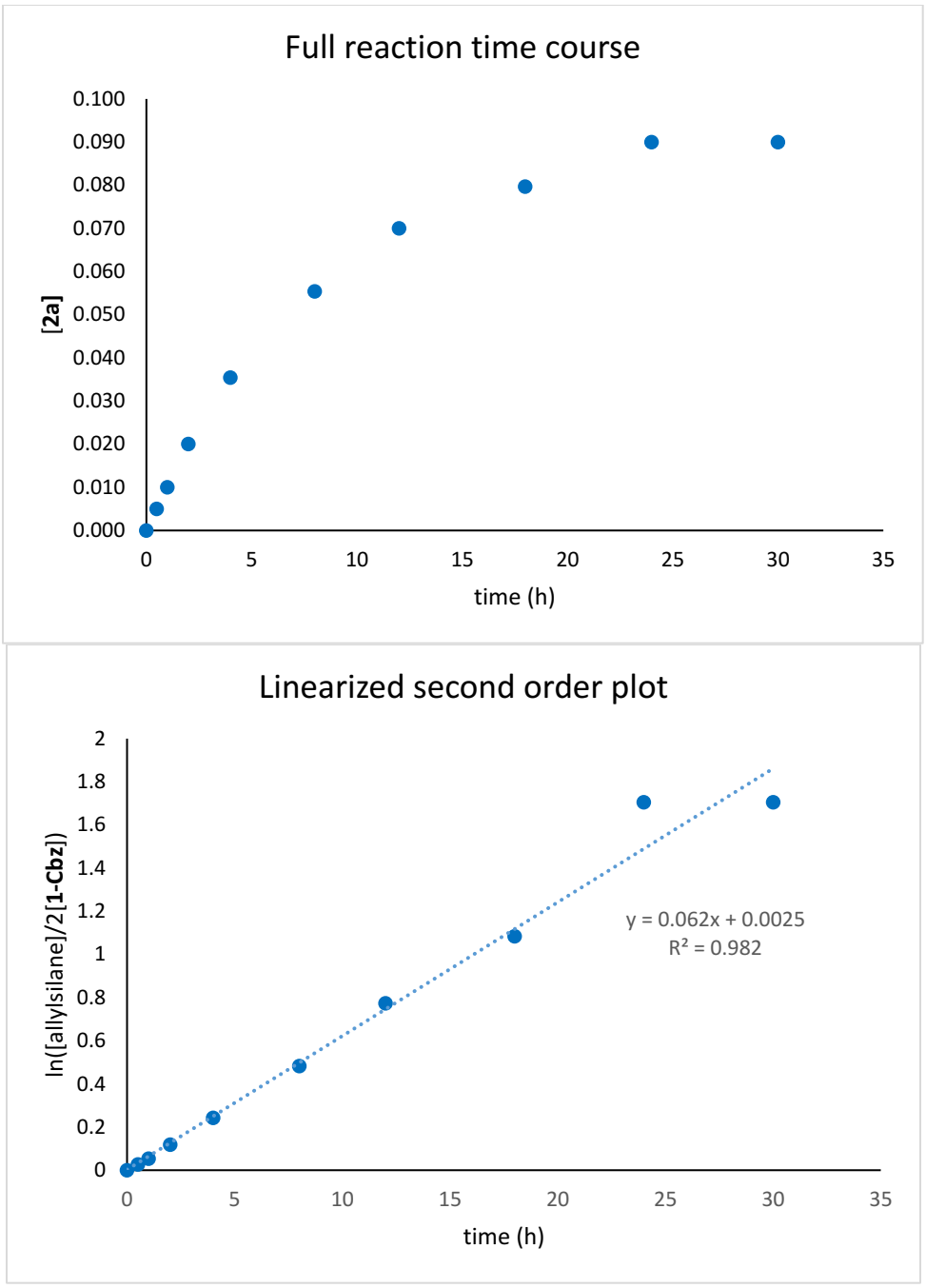

Figure 3.4 Full reaction profile (top) and linearized second order integrated rate law plot (bottom) in the squaramide **5d'** catalyzed allylation of **1-Cbz**

Given the good fit to the second-order rate law with [**1-Cbz**] = 0.1 M and [2-methallylsilane] = 0.2, one could surmise that the reaction has a first-order kinetic dependence on the concentration of each reagent. To ensure this is the case, initial rate kinetics were conducted to

determine the order in each reacting partner and the catalyst, **5d'** (Figure 3.5, for experimental conditions, see experimental).

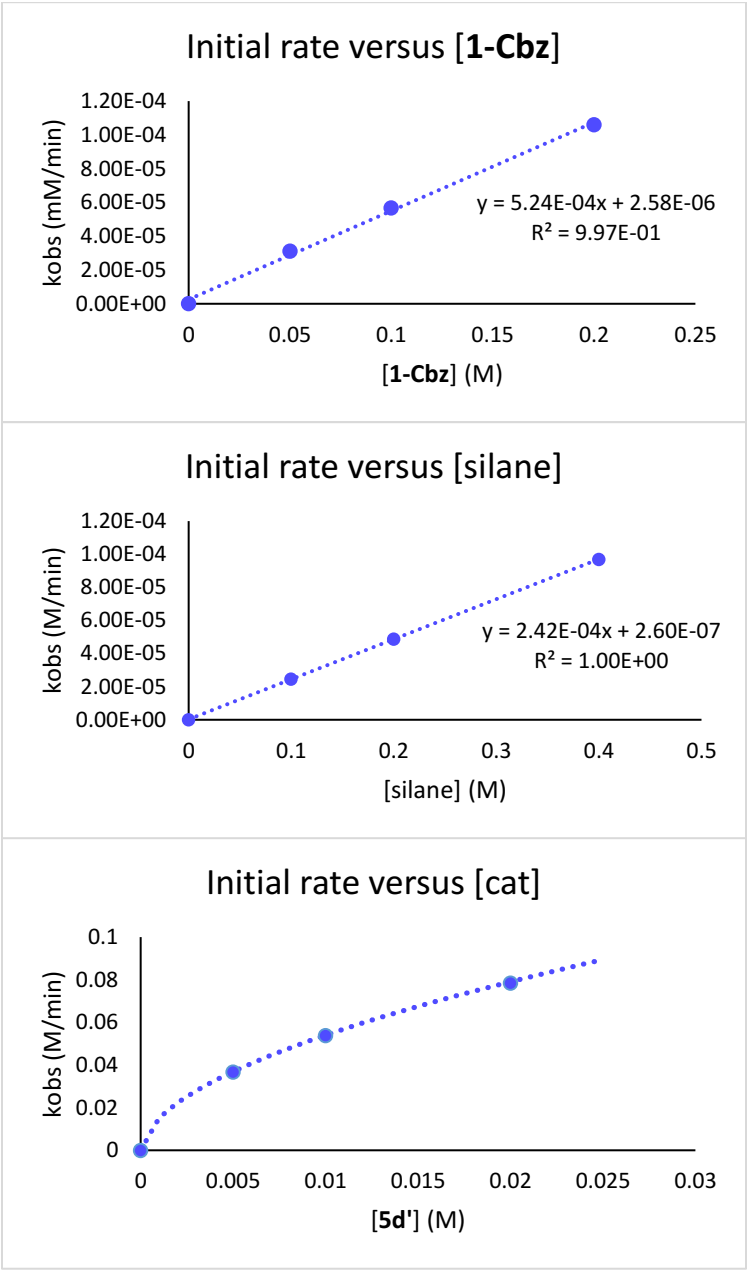

Figure 3.5 Observed rate, k_{obs} versus concentration of a varied reaction component in the initial rate kinetics of the **5d'** catalyzed addition of allylsilane to **1-Cbz**. In each plot, standard reaction conditions, halved concentration, and doubled concentration in one component are represented. Top: varying [**1-Cbz**], Middle: varying [silane], Bottom: varying [**5d'**]

Based on the good linear fits in the top two graphs in Figure 3.5, the catalytic reaction was determined to obey a second-order rate law, with first-order dependence on both the α-chloro glycinate and allylsilane concentrations, consistent with either a concerted S_N2 mechanism or rate-determining allylation of an iminium intermediate in an S_N1 pathway. Interestingly, the k_{obs} versus catalyst **5d'** concentration is not linear. The catalyst was found to have an observed 0.55 order (see experimental), consistent with off-cycle catalyst dimerization and one catalyst in the rate determining transition state. Off-cycle catalyst dimerization has been observed in multiple contexts before and is standard for this class of hydrogen-bond donor catalysts, via the equilibrium presented in Figure 3.6.[94,149]

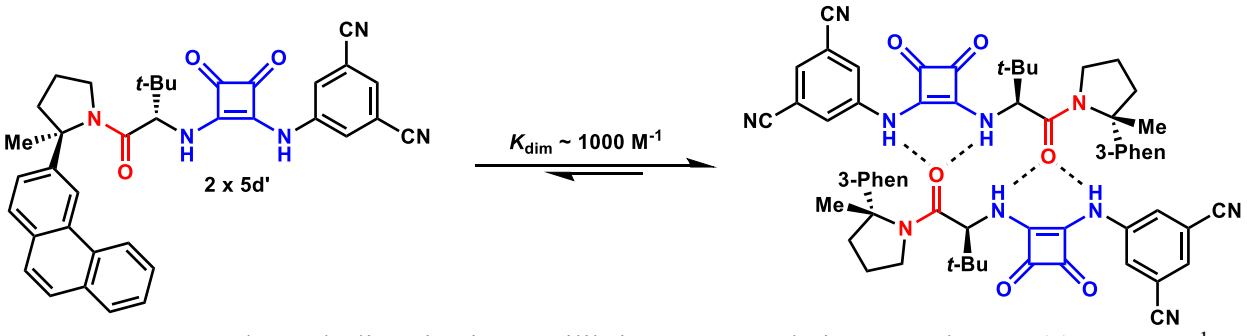

Figure 3.6 Catalyst 5d' dimerization equilibrium measured via ITC to be roughly 1000 M^{-1}

Off-cycle dimerization is an equilibrium process; if the equilibrium (K_{dim}) lies completely toward dimerized catalyst, the observed order would be 0.5; whereas if the dimerization is irrelevant, the observed order would be 1. To determine the strength of off-cycle dimerization, isothermal calorimetry (ITC) dilution experiments were conducted in DCM at room temperature, and it was found K_{dim} ~ 1000 M^{-1}. Unfortunately, due to poor data quality the dimerization constant cannot be determined more precisely; however this number is in line with what has been seen for squaramide catalysts in other studies (two half-Schriner arylpyrrolidine squaramides have been

[149] Kennedy, C. R.; Lehnherr, D.; Rajapaksa, N. S.; Ford, D. D.; Park, Y.; Jacobsen, E. N. Mechanism-Guided Development of a Highly Active Bis-Thiourea Catalyst for Anion-Abstraction Catalysis. *J. Am. Chem. Soc.* **2016**, *138* (41), 13525–13528.

characterized to have K_{dim} = 1710 and 1210 M^{-1} in DCM at room temperature).[94] If one fits an off-cycle catalyst dimerization equilibrium of 1000 M^{-1} and one catalyst in the rate determining transition state, one would expect to see an observed 0.57 order in catalyst, consistent with the value of 0.55 (see experimental for discussion).

Given the kinetic dependence on concentration of electrophile and nucleophile, as well as the 0.55 observed order in catalyst, which as confirmed by ITC measurements supports an off-cycle dimerization and a rate determining transition state, one can advance the simplified catalytic cycle below in Figure 3.7.

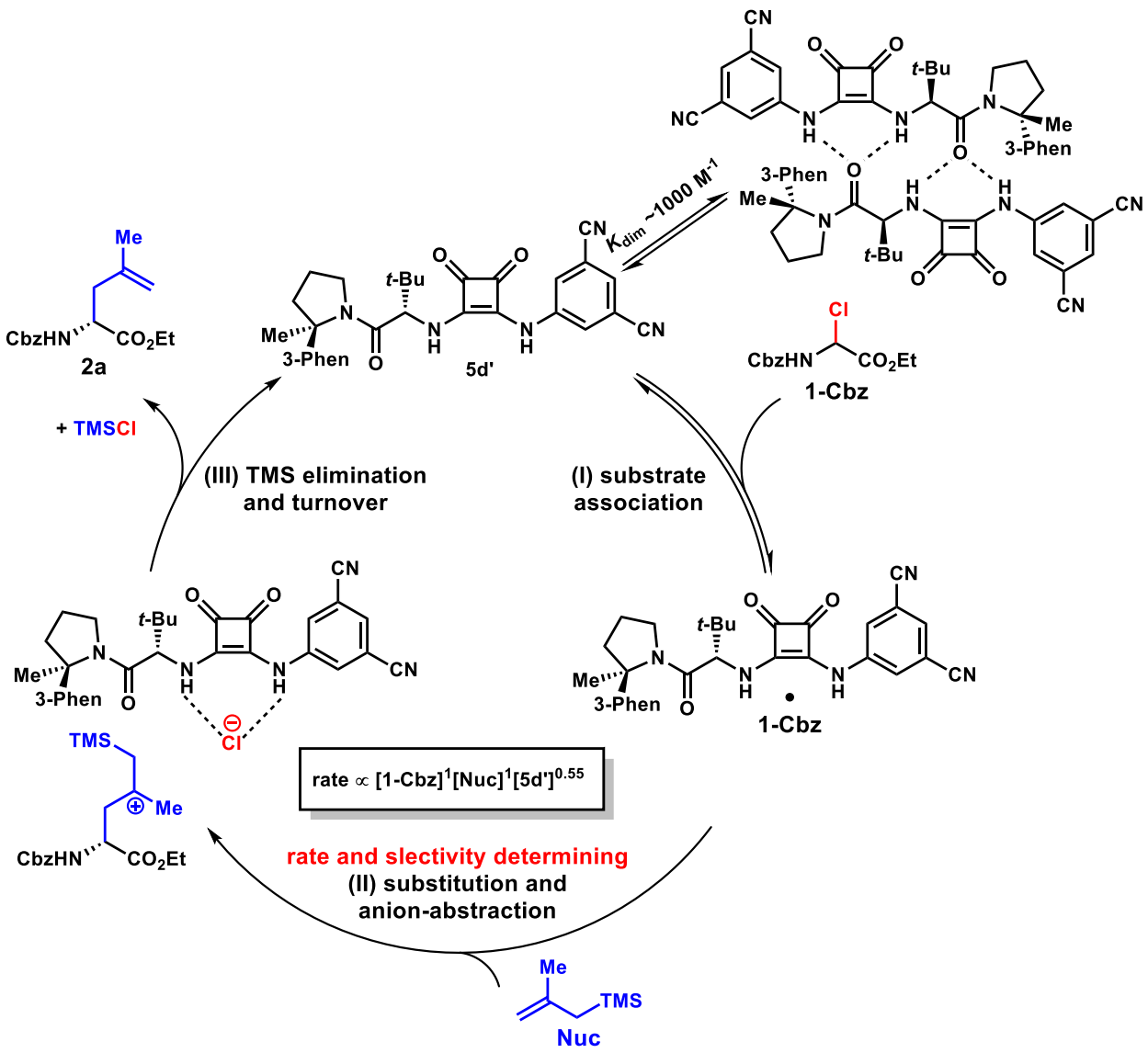

Figure 3.7 Simplified catalytic cycle for the **5d'** catalyzed allylation of **1-Cbz**

A simplified catalytic cycle for the allylation reaction is outlined in Figure 3.7. The catalytic mechanism is proposed to involve three fundamental steps: 1) complexation of the electrophile, **1-Cbz** to catalyst **5d'**, 2) substitution involving C–Cl bond breaking and C–C bond formation, and 3) trimethylsilyl elimination from the β-silyl cation to form product **2a** and TMSCl. Additionally the catalyst undergoes off-cycle dimerization. While the kinetic analysis reveal that the substitution step must be rate and selectivity determining, it reveals nothing about the mechanism of that step. As discussed above, the detailed mechanism of the substitution step and

the role of the catalyst in promoting it are of greatest interest, since that process results in formation of the new C–C bond and is enantiodetermining.

3.3 Mechanism of the C-C bond forming substitution step and racemization mechanism

As discussed in the introduction, enantioselective anion-binding catalysis has been applied successfully to many reactions proceeding via *N*-acyliminium intermediates;[99b,12b,143] however, several considerations led us to question whether such species are involved in the system under consideration here. α-Chloro carbonyl compounds such as **1** are generally activated toward S_N2 substitution pathways and deactivated toward dissociative S_N1 mechanisms.[144] Optimal enantioselectivities are obtained using DCM as solvent in the allylations of **1** (Figure S7). In contrast, nonpolar ethereal or aromatic solvents are generally required to achieve high enantioselectivities in ion-pairing catalysis promoted by chiral H-bond donors. Indeed, DCM has been found to promote solvent separation of ion pairs in these systems, resulting in severe diminution of enantioinduction.[94]

Two plausible mechanisms for the substitution step are outlined in Figure 3.8. If a stepwise S_N1 is operant, anion abstraction would precede C–C bond formation with the intermediacy of a discrete, highly electrophilic iminium ion intermediate. The unexpected solvent effect noted above might be reconciled with a secondary attractive interaction holding the ion-pair together, such as the iminium–Cl H-bond depicted in Figure 3.8 (right). These mechanisms require very different roles for the catalyst and have divergent modes of enantioinduction; thus knowing which the catalyst promotes is of interest in adapting this methodology for future reaction development, especially if the concerted stereospecific mechanism is operative, which is unprecedented as a mode of catalysis and enantioinduction in anion-binding catalysis.

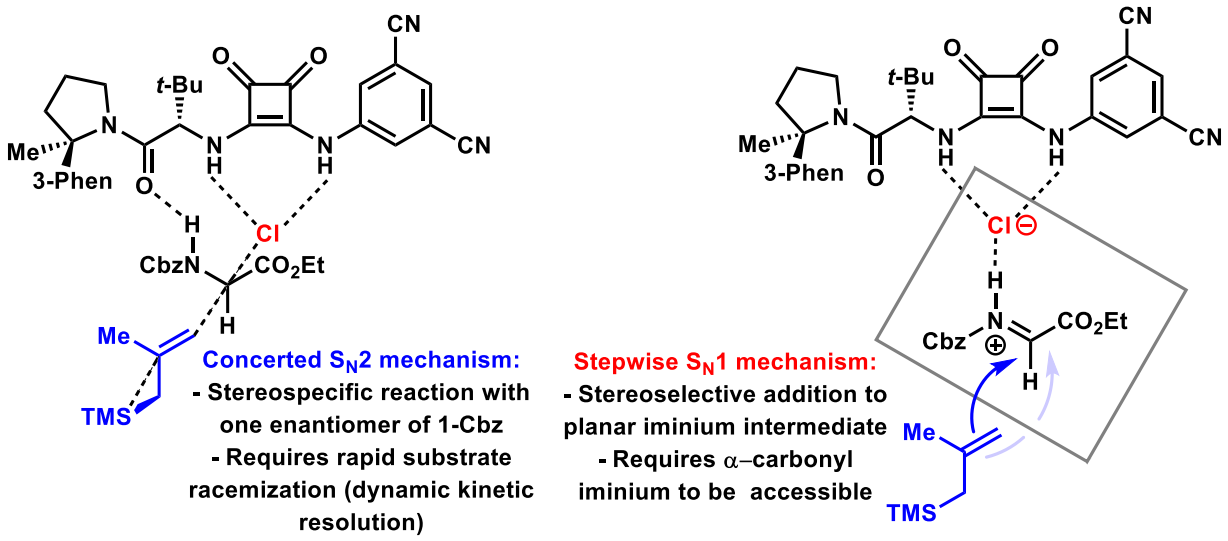

Figure 3.8 Two mechanistic scenarios (S_N2 vs. S_N1) for **5d'** catalyzed allylation of **1-Cbz**

If the reaction proceeds through a concerted, stereospecific nucleophilic displacement, a dynamic kinetic resolution with rapid racemization of the α-chloro glycinate would be required to account for the observed high yields and enantioselectivies. Such a racemization could occur via bimolecular chloride displacement (S_N2, Figure 3.9 A), chloride dissociation (S_N1, Figure 3.9 B), or sequential tautomerization pathways (Figure 3.9 C). Whether or not the racemization is catalyzed by the hydrogen-bond donor **5d'** is also of interest.

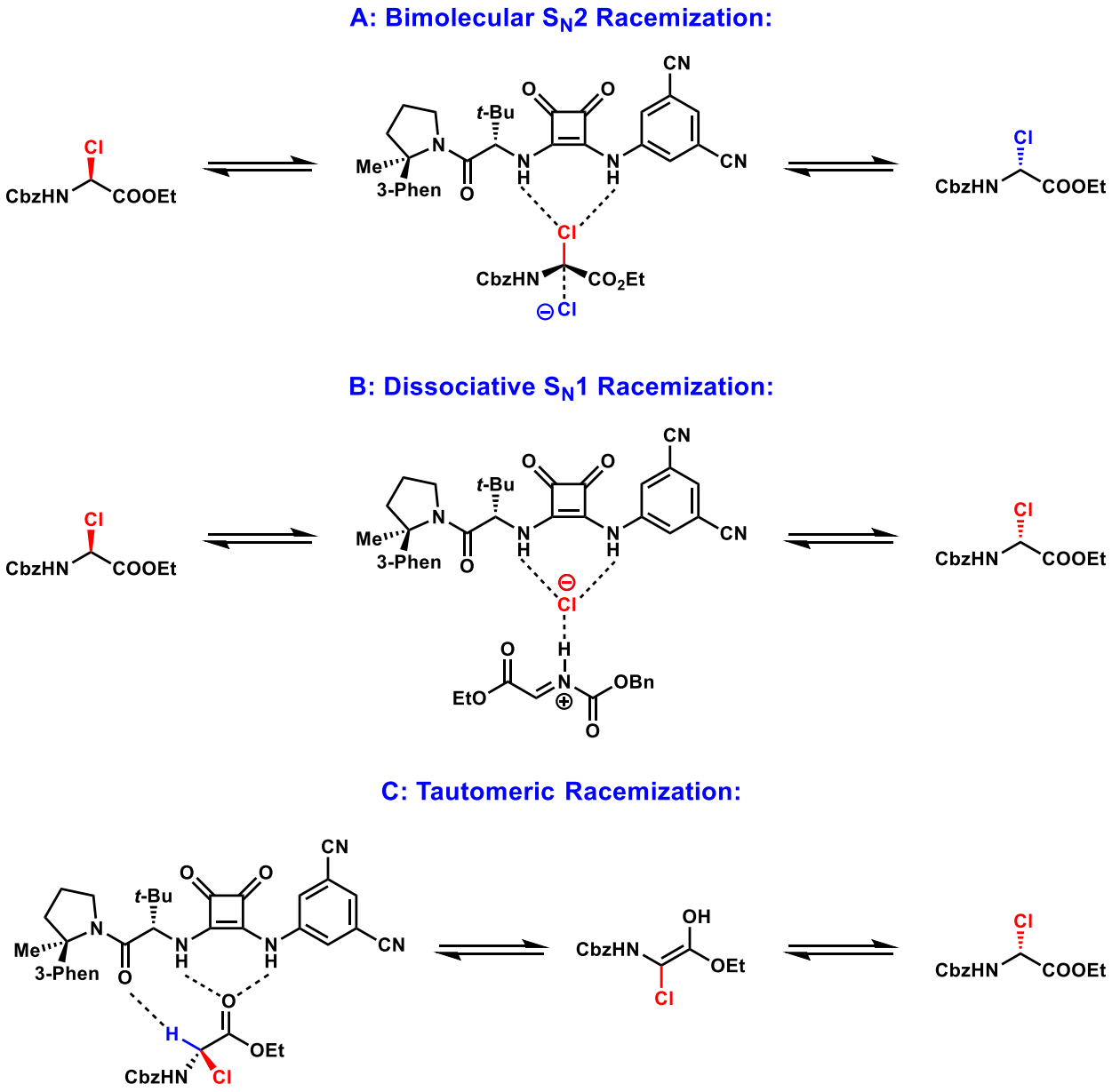

Figure 3.9 Mechanistic possibilities for squaramide **5d'** promoted racemization of **1-Cbz**

3.3.1 Substrate racemization studies

To probe the racemization the simplest experiment would be to generate the substrate, **1-Cbz**, enantioenriched. Racemic α-hydroxy glycinate precursor, **1-Cbz-OH** was subjected to preparatory chiral HPLC to obtain enantiopure **1-Cbz-OH**. The compound was then subjected to deoxychlorination under a variety of conditions and with a variety of deoxychlorinating reagents

(e.g. $SOCl_2$ and PCl_3) and subsequently quenched with sodium methoxide and sodium acetate to look for enantioenrichment. Both $SOCl_2$ and PCl_3 have been used to perform stereospecific deoxychlorinations of secondary benzylic alcohols to generate enantioenriched chlorides.[150] Unfortunately, quenched material was always racemic, implying the substrate was not being generated in enantioenriched fashion or the quench was racemizing the substrate faster than addition. The inability to generate enantioenriched substrate in DCM at 0 °C may point to a facile racemization even in the absence of catalyst.

Next, an NMR method was devised to determine the rate of racemization. In the thiourea promoted addition of silyl ketene acetals to oxocarbenium ions generated from an α-chloro ether, a selective inversion recovery NMR experiment was conducted to measure the rate of exchange (racemization) of the starting material, which determined that catalyst promotes a dissociative, S_N1 type racemization.[151]

An analogous experiment was attempted here. First, a synthesis of a substrate mono-deuterated at the benzylic position was synthesized in order to generate a second stereogeneic center in which the diastereomeric protons have different shift due to being *syn* or *anti* to the α-chloride. Additionally, this simplifies the benzyl carbamate region of the spectrum from two sets of doublets to two resolved singlets so that clean peak shapes and estimations of FWHM can be determined. The Bloch-McConnell equations were then used to simulate Lorentzian peaks with an exchange term and the NMR experimental peaks were fit in order to determine the rate of exchange at a given temperature.[152] Temperatures were arrayed and fit to the exponential or linearized Eyring

[150] Huy, P. H.; Motsch, S.; Kappler, S. M. Formamides as Lewis Base Catalysts in S_N Reactions-Efficient Transformation of Alcohols into Chlorides, Amines, and Ethers. *Angew. Chemie Int. Ed.* **2016**, *55* (34), 10145–10149.

[151] Ford, D. D.; Lehnherr, D.; Kennedy, C. R.; Jacobsen, E. N. On- and Off-Cycle Catalyst Cooperativity in Anion-Binding Catalysis. *J. Am. Chem. Soc.* **2016**, *138* (25), 7860–7863.

[152] McConnell, H. M. Reaction Rates by Nuclear Magnetic Resonance. *J. Chem. Phys.* **1958**, *28* (3), 430–431.

equation to get k_{rac} at a given temperature and to be able to extrapolate outside this window (see experimental for details). Unfortunately, due to the conformational flexibility of this system, multiple exchange processes occurred in the –80 to 80 °C window, which were unable to be ruled out from the exchange process associated with substrate racemization. Thus, the rate of racemization and the ability of the squaramide catalyst **5d'** to promote the racemization is still unknown. To determine that racemization is indeed occurring, a mono-deuterated benzylcarbamate substrate enantiopure at the benzylic position will be subjected to the reaction conditions and monitored via NMR. If the ratio of the two peaks stay the same, that scenario implies that racemization is rapid or both enantiomers of substrate are being consumed by catalyst at the same rate.

Despite the inability to accurately measure racemization rate, given the yield and enantioselectivity observed, plus the observation that nucleophilic addition is rate determining, implies that racemization must be occurring regardless of the substitution mechanism. For example, to achieve 97% ee and 88% yield in an S_N2 mechanism there must be racemization. In an S_N1 reaction, since nucleophile addition is rate determining, ionization must be reversible, and except in the unlikely case where chloride is dissociating and reassociating to the same face of iminium with perfect fidelity, racemization must occur in this case as well.

The most common methods of determining S_N1 with rate determining nucleophilic addition versus S_N2, which are kinetically indistinguishable are KIE and Hammett studies.[142] Unfortunately, the allylation of **1-Cbz** is well suited to neither method. As will be discussed in the next section, the inability to compute an S_N1 transition state, combined with the loose dissociated S_N2 transition state that is found renders a KIE as inconclusive. In principle, a Hammett study would be useful in principle to determine the amount of positive charge buildup in the transition

state, which should be substantially larger in an S_N1 manifold. However, the α-aryl-α-chloro glycine substrates are not stable, as discussed in Chapter 4, thus there is no appropriate place to install an arene for a Hammett study. Thus, computational studies of the background and catalyzed reaction pathways were pursued, as well as a multivariate regression analysis, to determine the mechanism of substitution, and will be the focus of the rest of this chapter.

3.3.2 Uncatalyzed reaction coordinate favors an S_N2 mechanism

The uncatalyzed reaction coordinate was probed in an effort to better understand the energies and geometries of relevant stationary points (i.e. ground states and transition states) in order to determine the mechanism of the C-C bond forming step, namely allylsilane addition to an iminium ion (S_N1) or direct addition to the α-chloro glycinate starting material (S_N2). All computations were conducted at the B3LYP level of theory using the Pople basis set 6-311+g(d,p).[153] The polarization continuum model (PCM) was employed, with the DCM dielectric.[154] Last, given that hydrogen-bond donor catalysis has demonstrated to achieve selectivity through secondary non-covalent attractive interactions, it is necessary to use Grimme's dispersion correction with Becke-Johnson damping (GD3BJ) to be able to accurately pick up on electrostatic interactions.[155] Ground states were identified by conducting a frequency analysis and observing no imaginary frequencies. Transition states were identified by applying tight

[153] a) Ditchfield, R.; Hehre, W. J.; Pople, J. A. Self-Consistent Molecular-Orbital Methods. IX. An Extended Gaussian-Type Basis for Molecular-Orbital Studies of Organic Molecules. *J. Chem. Phys.* **1971**, *54* (2), 724–728. b) Hehre, W. J.; Ditchfield, R.; Pople, J. A. Self—Consistent Molecular Orbital Methods. XII. Further Extensions of Gaussian—Type Basis Sets for Use in Molecular Orbital Studies of Organic Molecules. *J. Chem. Phys.* **1972**, *56* (5), 2257–2261. c) Hariharan, P. C.; Pople, J. A. The Influence of Polarization Functions on Molecular Orbital Hydrogenation Energies. *Theor. Chim. Acta* **1973**, *28* (3), 213–222.

[154] Scalmani, G.; Frisch, M. J. Continuous Surface Charge Polarizable Continuum Models of Solvation. I. General Formalism. *J. Chem. Phys.* **2010**, *132* (11), 114110.

[155] a) Grimme, S.; Antony, J.; Ehrlich, S.; Krieg, H. A Consistent and Accurate *Ab Initio* Parametrization of Density Functional Dispersion Correction (DFT-D) for the 94 Elements H-Pu. *J. Chem. Phys.* **2010**, *132* (15), 154104. b) Grimme, S.; Ehrlich, S.; Goerigk, L. Effect of the Damping Function in Dispersion Corrected Density Functional Theory. *J. Comput. Chem.* **2011**, *32* (7), 1456–1465.

convergence constraints, conducting a frequency analysis and observing one imaginary frequency associated with the step of interest. Furthermore, an intrinsic reaction coordinate (IRC) scan was performed for transition states to ensure the transition states were the relevant saddle point on the potential energy surface.

The uncatalyzed computations suggest that the reaction is relatively exothermic at ΔE_{rxn} = –24.5 kcal/mol, consistent with breaking a weak C-Cl bond and C-Si bond in favor of a new C-C and Si-Cl bond, both of which are stronger than the bonds in the reagents. 4 S_N2 transition states are found with the lowest at $\Delta E_{SN2}^{\ddagger}$ = 12.7 kcal/mol. No S_N1 transition states could be located because *in silico* addition of chloride or 2-methallylsilane are both barrierless. The iminium intermediate 31.6 kcal/mol above the ground state, making this the lower bound to the barrier to addition to an iminium at $\Delta E_{SN1}^{\ddagger} \geq 31.6$ kcal/mol. Therefore, computationally the S_N2 pathway is expected to be favored by at least 18.9 kcal/mol. The summary of the reaction coordinate is provided in Figure 3.10.

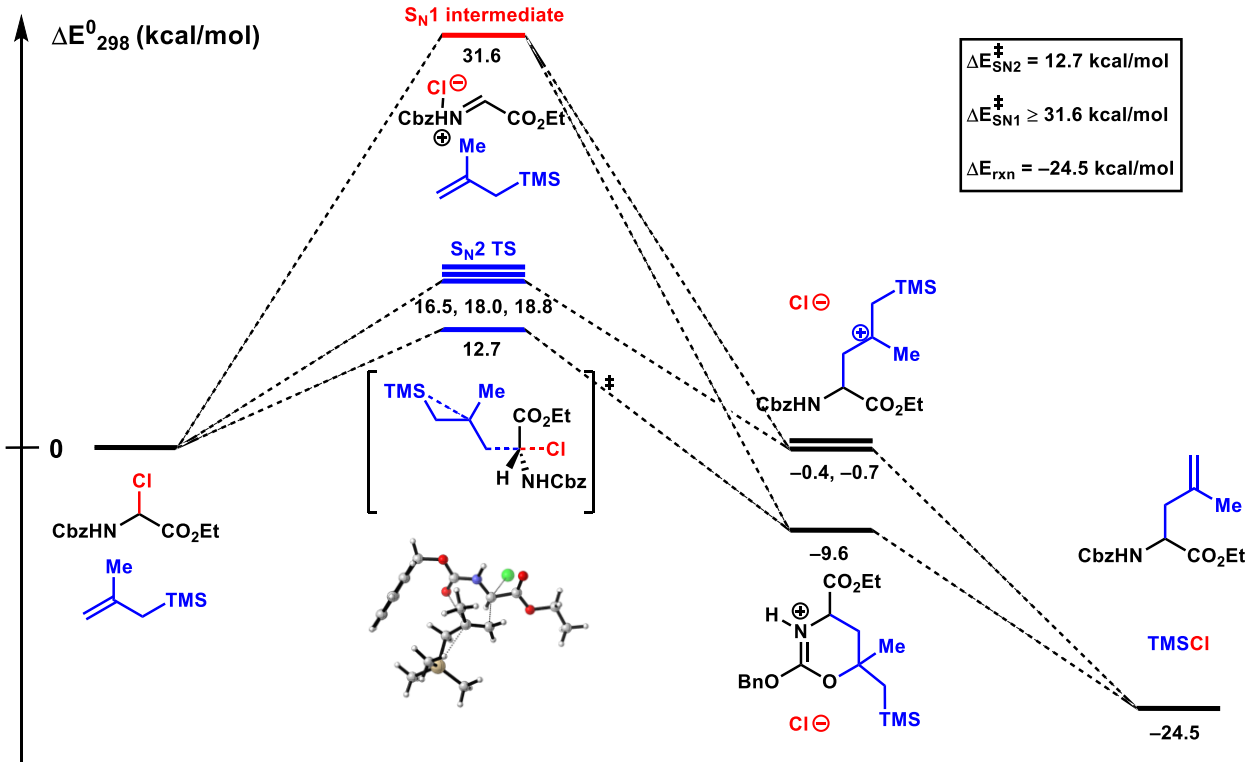

Figure 3.10 Computational evaluation of the uncatalyzed reaction predicts that the S_N1 pathway is much higher in energy than the S_N2 pathway. For a fuller discussion of the conformational landscape at each stationary point, see experimental section

The reactant ensemble global ground state was identified as a dipole-dipole interaction complex between **1-Cbz** and nucleophile, which was located from an IRC from the lowest energy S_N2 transition state, and is depicted in Figure 3.11. A few notable features of this ground state, are that the C-Cl bond orients itself such that the σ* is lined up with both the ester and the carbamate π-systems. The C-Cl bond length is found to be elongated at 1.90 Å. This is also true in the geometry of just **1-Cbz**, which has a C-Cl bond length of 1.89 Å.

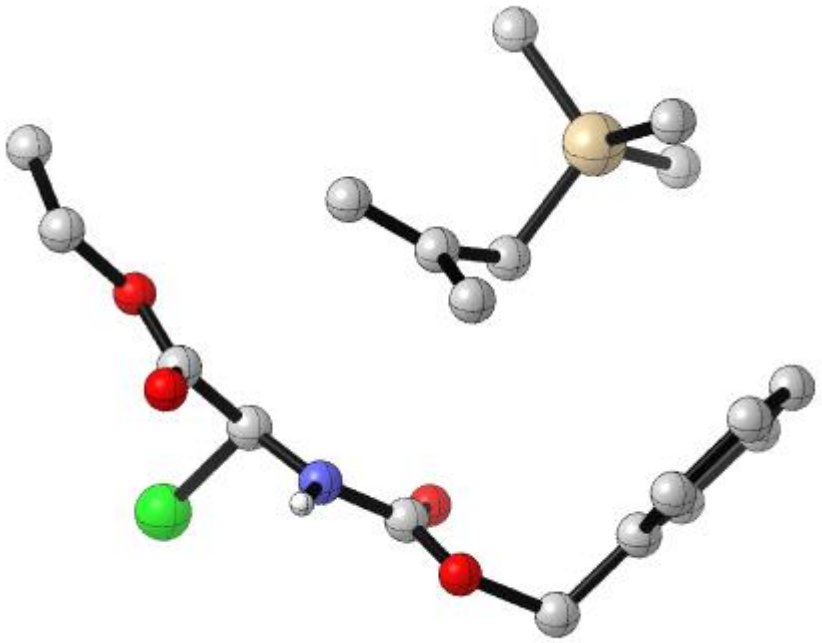

Figure 3.11 Global reactant ground state is dipole-dipole interaction between reacting partners

The ground state iminium geometry is the linear iminium with the dissociated chloride H-bonding to the iminium with H-Cl = 1.78 Å, depicted in Figure 3.12; for a fuller discussion of the conformational landscape of the iminium intermediate see the experimental section. In the SN1 iminium intermediate pathway, *in silico*, there is barrierless addition of both chloride and methallylsilane to the iminium intermediate. Therefore, the energy of the intermediate was computed and set as a lower bound on the energy of the transition state. In reality this step cannot be barrierless, since there is observed first-order in methallylsilane concentration. Thus, the SN1 barrier is an energetically inaccessible > 31.6 kcal/mol uphill from the starting materials.

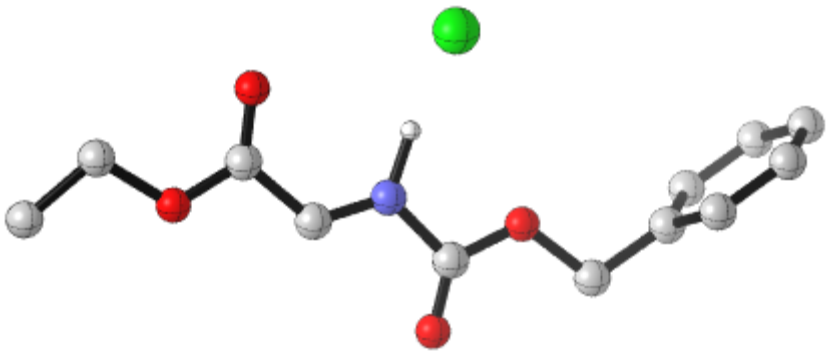

Figure 3.12 Iminium ground state is linear and with Cl-H-N iminium H-bonding

In the S_N2 concerted displacement of chloride, one can imagine 6 low energy nucleophile trajectories. The three incoming gauche trajectories, with two distinct facial additions with respect to the nucleophile. 4 of the 6 low energy transition states were able to be located and find they have energies of 12.7, 16.5, 18.0, and 18.8 kcal/mol above starting material. The lowest energy S_N2 transition state is able to pick up a Cbz arene stabilization of β-silyl carbocationic buildup of charge, which is not present in the other transition states (an energetic comparison of two nucleophile trajectories is compared in Figure 3.13). These transition states are relatively dissociative, with an extremely long C-Cl bond at 2.9 Å. This is consistent with the hypothesis that this reaction is on the edge of S_N1 and S_N2, and in Figure 3.1, this would most resemble C, where a large amount of iminium character and chloride character are built up in the transition state.

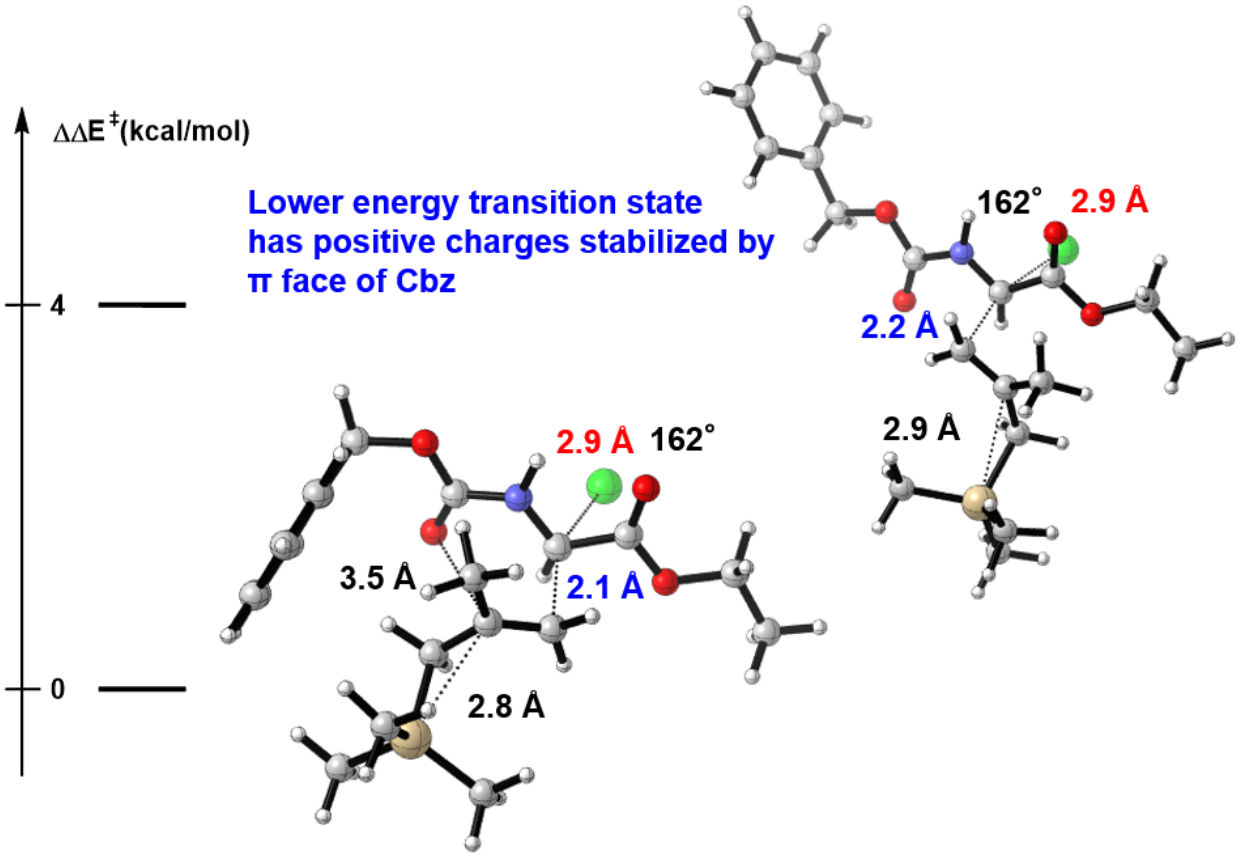

Figure 3.13 Lowest energy S_N2 transition state has a cation-π interaction with the nearby Cbz

All S_N2 transition states located are much lower than the pathway proceding through an iminium intermediate, thus suggesting that the S_N2 should be favored. In general computations overpredicts the barrier to ionization in the gas phase or organic solvent continuum models; however, the observed 18.9 kcal/mol is a difference larger than what one would expect from systematic computational error. To delve into this further, the iminium and S_N2 transition state energies were recalculated in a water PCM at the B3LYP/6-31g(d), which would penalize charged intermediates less. We find that in this case, the predicted energy difference is even larger, with the S_N2 being favored by at least 22.7 kcal/mol versus the 18.9 in DCM PCM.

The β-silyl cations are found to be roughly thermoneutral with respect to the starting materials. However, there is one conformer of β-silyl cation, in which the pendant carbamate can trap down to form a 6-membered ring intermediate, which is 10 kcal/mol downhill in energy

relative to the starting materials (Figure 3.14). This intermediate would be the product of a [4 + 2] cycloaddition as depicted in Figure 3.14. It is unclear if this intermediate is on-cycle and able to eliminate directly to product or a low-energy off-cycle intermediate.

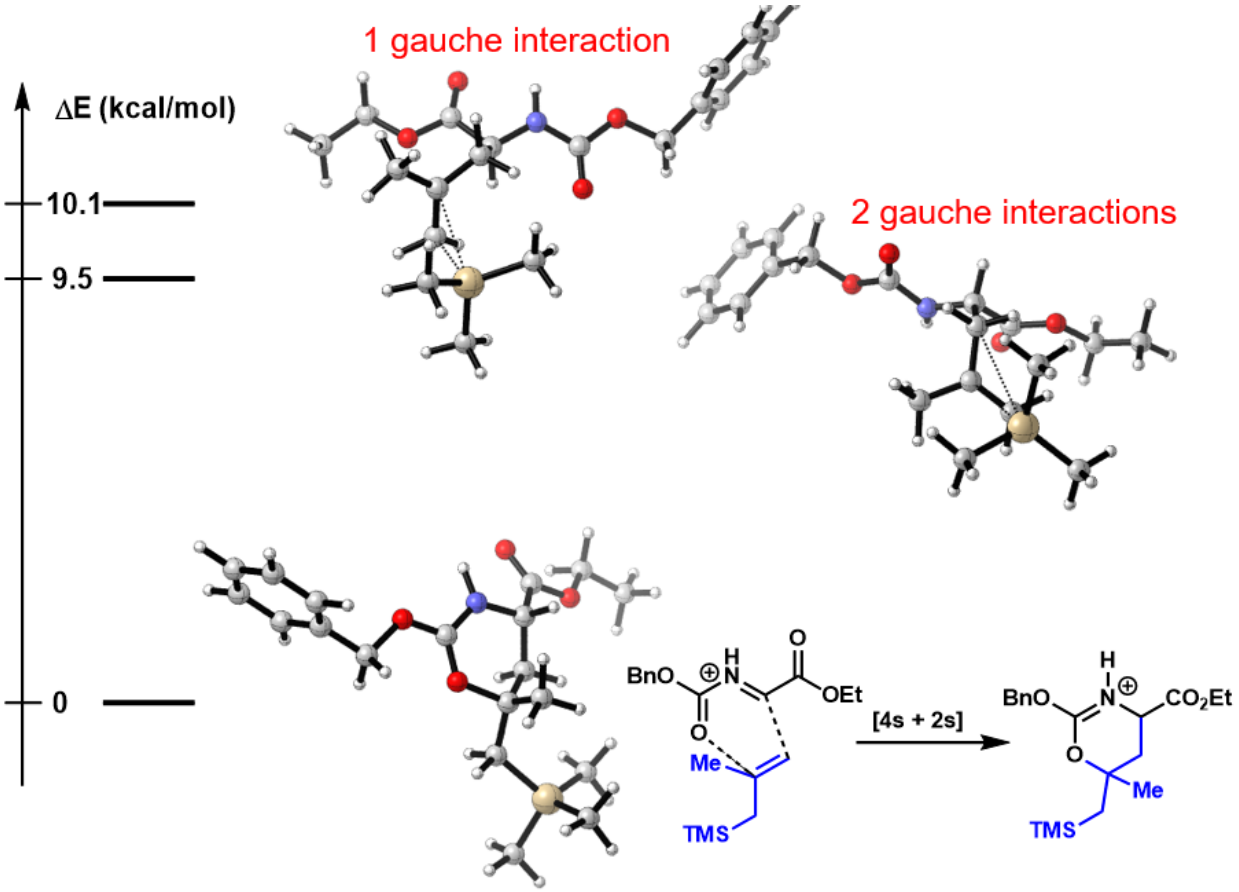

Figure 3.14 Ground state for β-silylcation is carbamate trapping to for a 6-membered ring

3.4 Catalyzed S_N2 reaction coordinate accurately predicts experimental enantioselectivity

Squaramide **5d'** catalyzed S_N1 and S_N2 transition states were pursued in order to understand how the hydrogen-bond donor catalyzes this reaction and the mechanism of enantioinduction, including the secondary interactions responsible for differnentiation of diasteromeric transition states leading to major and minor enantiomers of product. Just as in the uncatalyzed reaction pathway, S_N1 transition states were not able to be located due to barrierless

addition of chloride or 2-methallylsilane to the iminium intermediate. Thus, only the S_N2 pathway will be discussed in this section.

3.4.1 Catalyst substrate ground state binding computational studies

Given the large number of Lewis basic sites on the substrate, specifically, ester, carbamate, and chloride, it is unclear which functionality catalyst is hydrogen-bonding to in both the ground and transition states. To get at ground state binding, molecular mechanics were initially conducted. Due to the large number of rotatable bonds in the substrate and catalyst, 934 ground states were found via molecular mechanics conformational searching. Of these, all those that were more than 25 kcal/mol above the lowest energy were rejected and those 0-25 kcal/mol within the ground state were subjected to geometry optimization and frequency analysis using B3LYP/6-31g(d). 103 distinct binding modes were found this way, with a roughly equal distribution of chloride (N = 33), ester (N = 32), and carbamate (N = 38) binding modes; see Figure 3.15 for a histogram of **5d'**·**1-Cbz** complexes. The global ground state was found to be carbamate binding, with chloride binding modes generally being the least favorable.

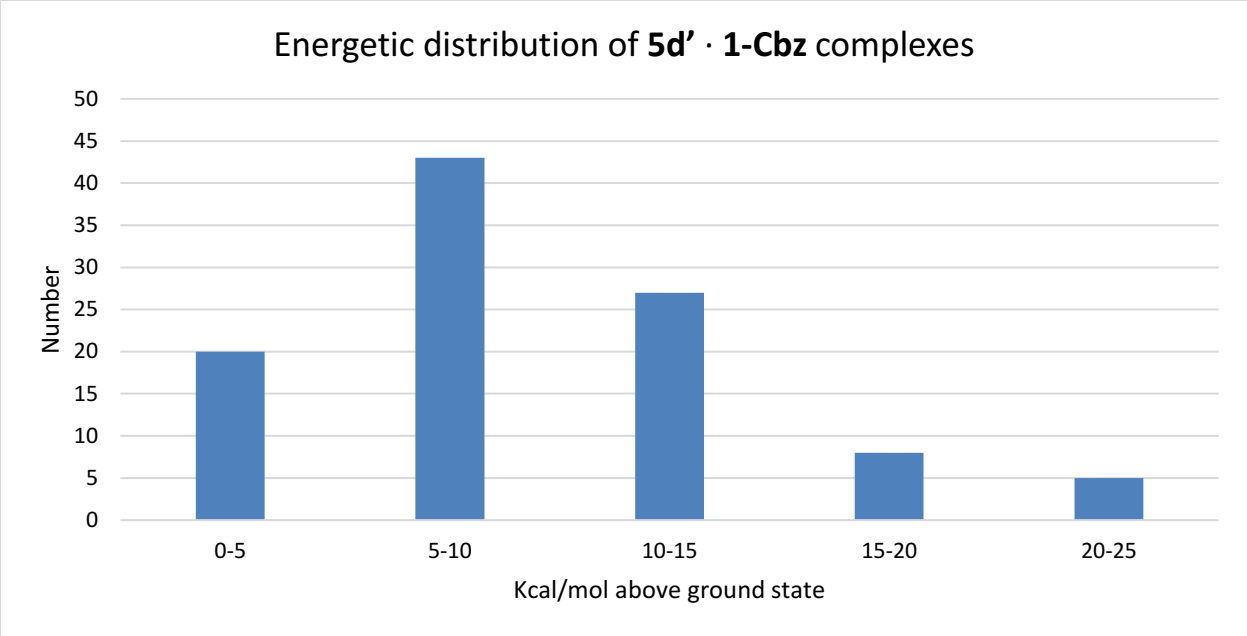

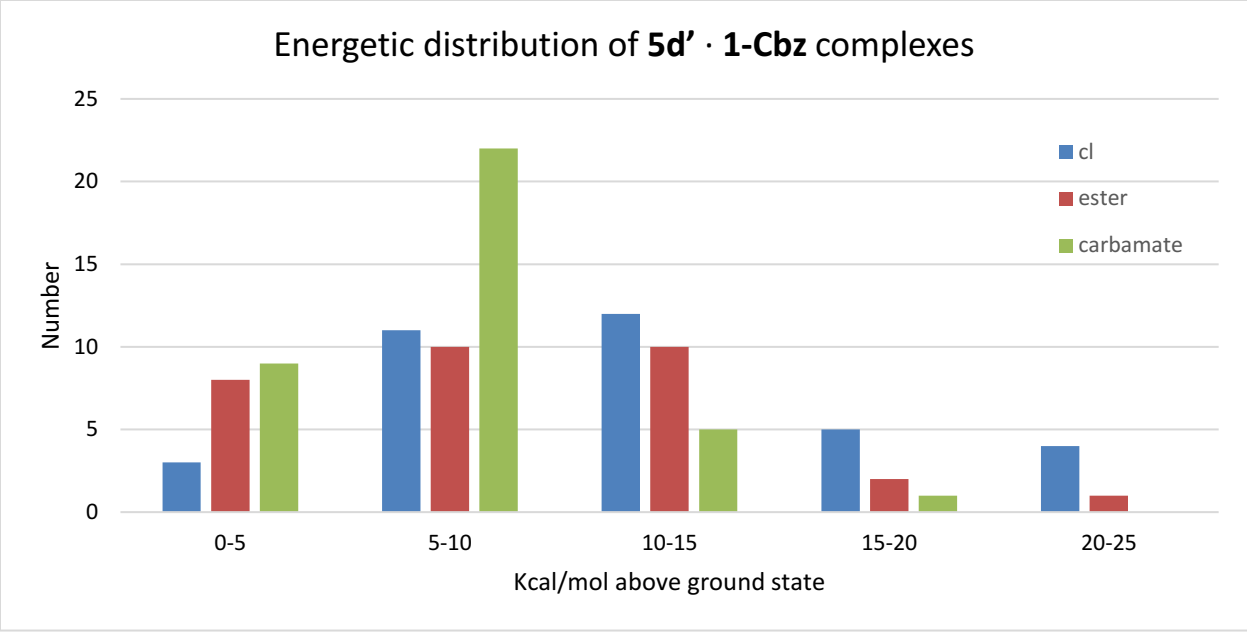

Figure 3.15 Distribution of **5d'** and **1-Cbz** ground states, reveal carbamate binding is favored

The global ground state is depicted in Figure 3.16 and has a few notable features. First, the Cbz group and 3,5-bis(trifluoromethylaniline) are engaged in a slip-stacked π-π interaction. The amide of catalyst is hydrogen bonding to the α-proton of the substrate, with the O-H distance 2.50 Å. Last, it appears that the catalyst arene is sitting over the most polarizable section of the molecule, potentially engaging in a C-H-π interaction with the α-proton of substrate.

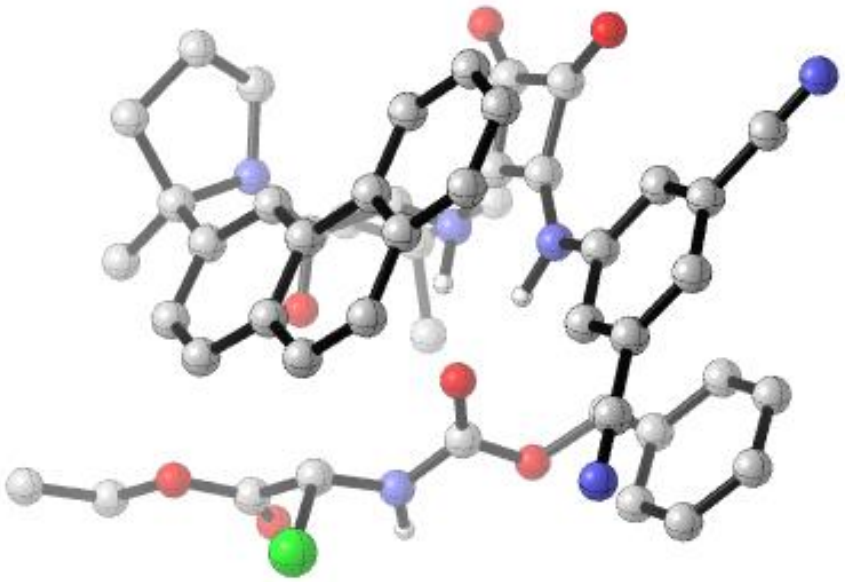

Figure 3.16 Global **5d'** · **1-Cbz** ground state is carbamate binding

To confirm that this finding makes chemical sense, an electrostatic potential map of the substrate was conducted to find the sites of electron density. Based on the large red bulb around carbamate in Figure 3.17, one can see that indeed carbamate is the site of most electron density, followed by ester, followed by chloride. This is exactly in line with the ground state binding computational studies.

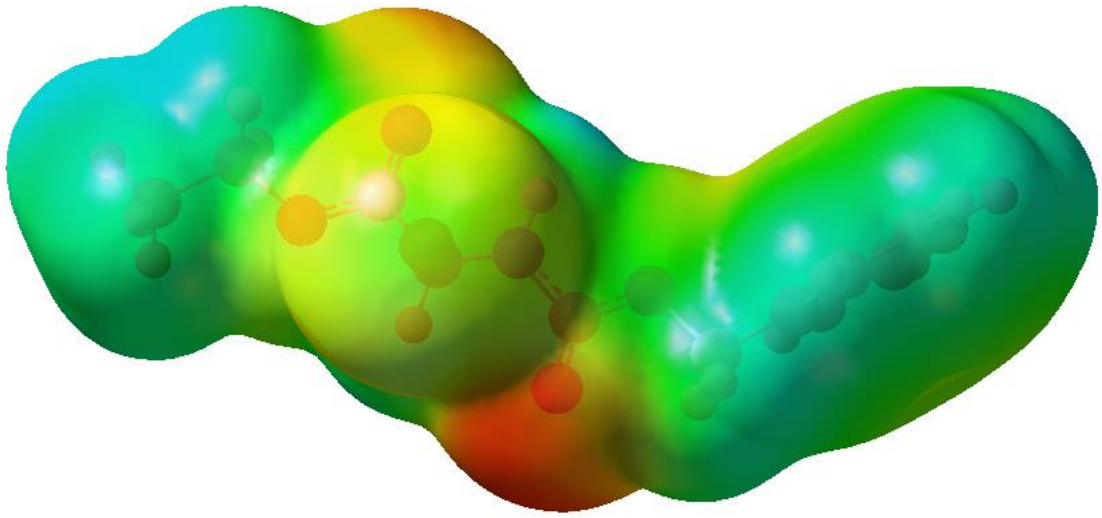

Figure 3.17 Electrostatic potential map of **1-Cbz** reveals electron density on carbamate

3.4.2 Catalyzed S_N2 transition state studies

As carbamate binding was found to be the lowest energy binding mode in the ground state, carbamate, ester, and chloride binding modes were also surveyed in the transition state searching. It seems unlikely that carbamate binding would lead to productive catalysis, but ester binding could potentially facilitate an α-S_N2 reaction and somewhat more obvious, partial abstraction of chloride via catalyst could facilitate an S_N2 reaction.

In contrast to the ground state studies, chloride binding modes were found to have substantially lower energies in the S_N2 reaction between **1-Cbz** and 2-methallylsilane. 28 unique transition states were found, and of those 9 were chloride binding, 17 were ester binding, and only 2 were carbamate binding; the distribution can be found in the histogram in Figure 3.18.

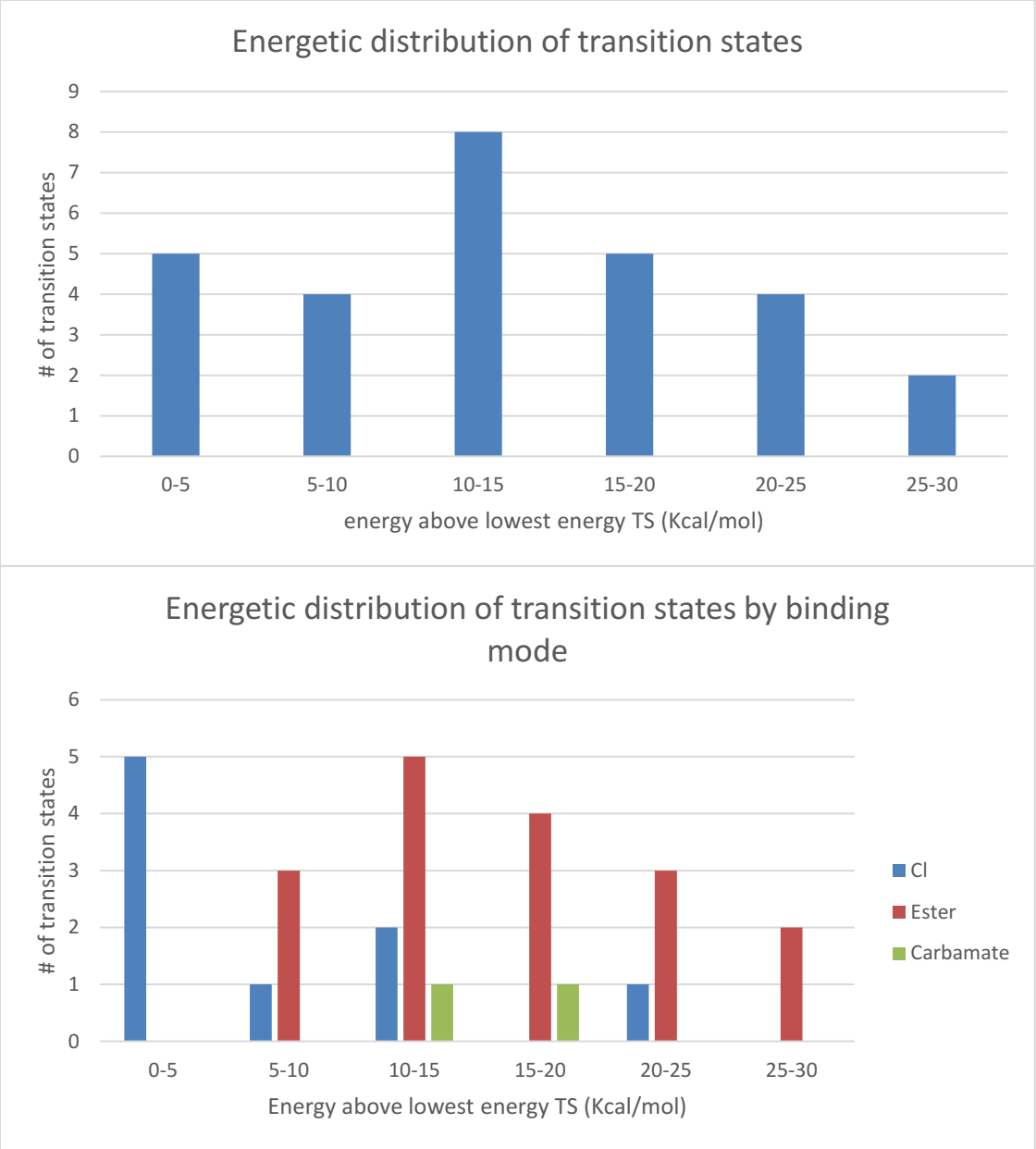

Figure 3.18 Distribution of **5d'** binding modes in the transition state geometries of the S_N2 between **1-Cbz** and 2-methallylsilane

Again, an electrostatic potential map was calculated to determine if a chloride binding mode of catalysis made sense as the lowest energy transition state. This electrostatic potential map was generated by calculating nbo charges for the lowest energy uncatalyzed transition state and generating density and polarization cubes to map those nbo charges onto the transition state. Due to difficulty to see all parts of the electrostatic potential map in one figure, the side and back view

are both provided (Figure 3.19). This electrostatic potential map clearly shows that the chloride is building up an immense amount of electron density, which is consistent with the formation of a chloride anion in a very dissociative transition state. In addition, one can see in the back view (Figure 3.19 right) that there is strong iminium character in the transition state. This is seen by a lobe of blue associated with the N-H bearing iminium ion character.

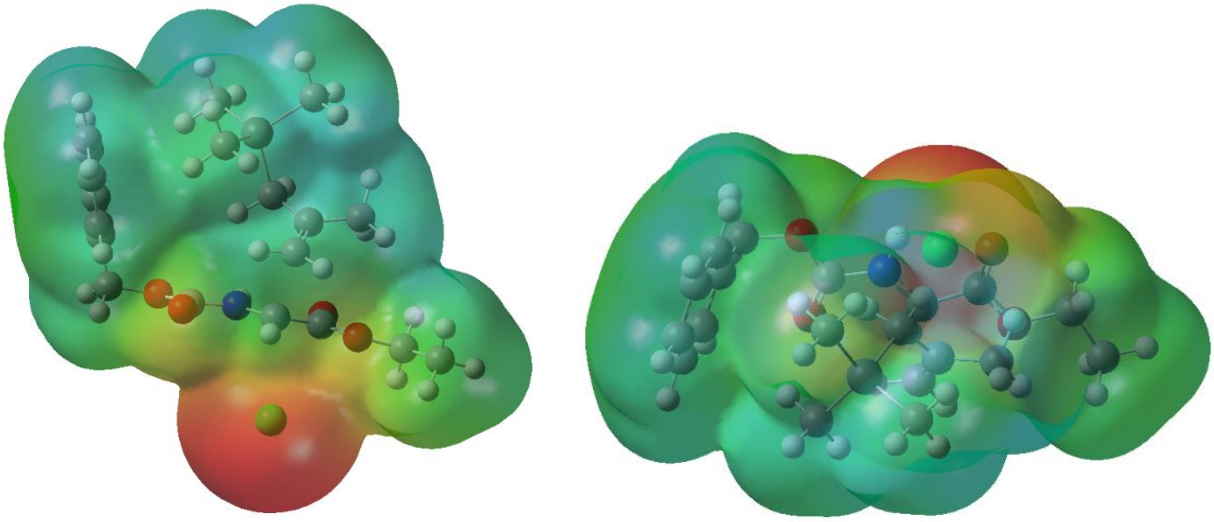

Figure 3.19 Electrostatic potential map for the lowest energy uncatalyzed S_N2 transition state in the addition of methallylsilane to **1-Cbz**. Electrostatic potential map is shown from two angles

Given the electrostatic potential map, one could envision that the lowest energy transition states would stem from catalyst dual N-H binding to the incipient chloride anion, while catalyst amide makes contact with the acidic N-H bearing iminium ion character. In fact, of the chloride binding transition states, only 2 contain these two interactions, and these are the lowest energy transition state leading to the major and minor enantiomers of product (Figure 3.20).

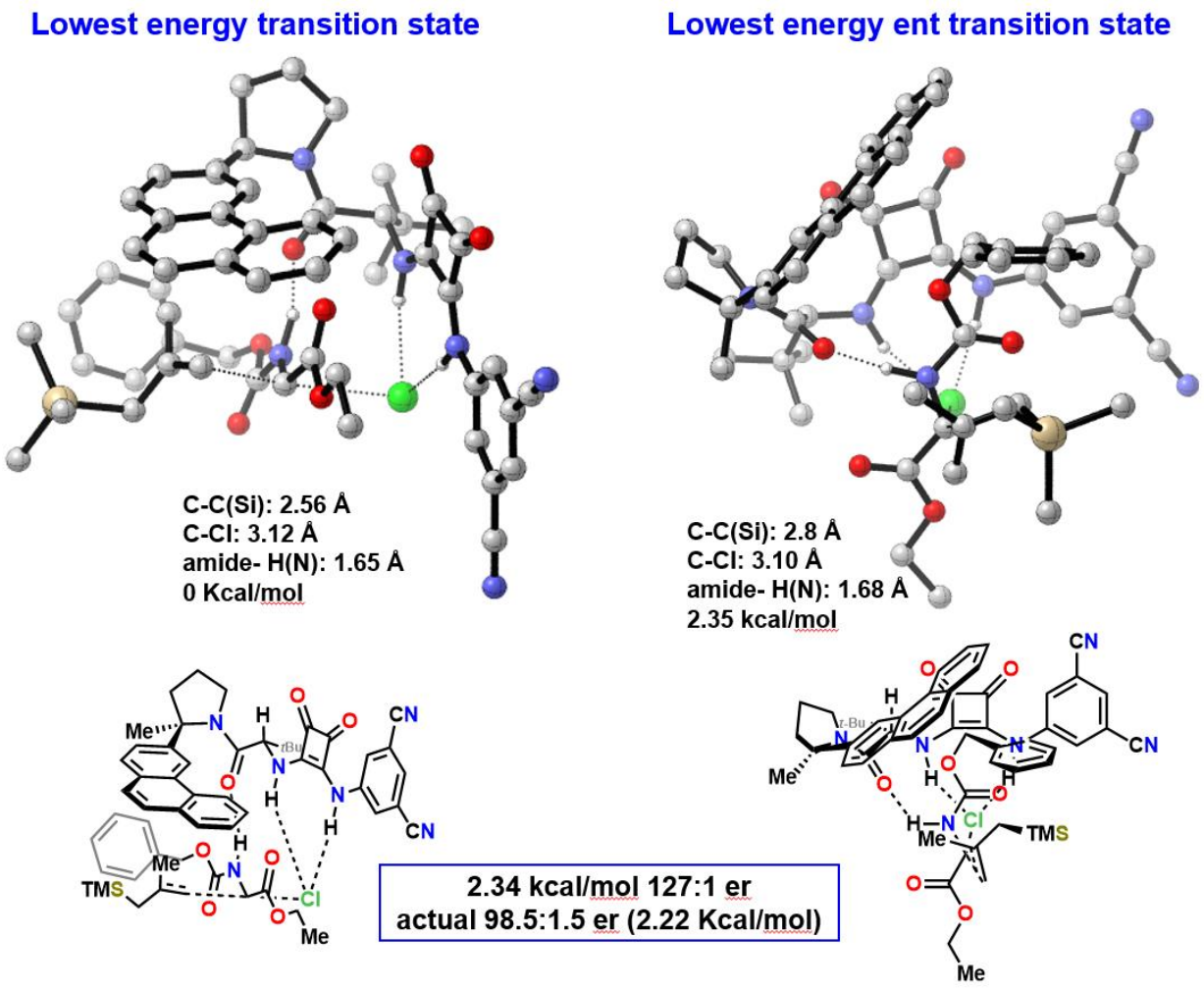

Figure 3.20 Lowest energy **5d'** catalyzed **1-Cbz** and 2-methallylsilane S_N2 transition states, leading to the major (left) and minor (right) enantiomers of product

In the substitution reaction between 2-methallylsilane and **1-Cbz**, there is a unique low energy catalyzed S_N2 reaction for each of the two diastereomeric pathways leading to the major and minor enantiomers of product. In order for a transition state to be near the global minimum, a couple of features must be preserved. Specifically, the two features shown in the electrostatic potential map: squaramide N-H abstraction of the chloride of 1-Cbz, while the *t*-leucine amide oxygen engages in a hydrogen bonding interaction with the N-H of substrate bearing large partial positive charge. These two features essentially dock substrate to catalyst, which determines the position of the conformationally rigid arylpyrrolidine component of the catalyst.

In the major transition state, the pyrrolidine arene sits directly over the methallylsilane and bond forming coordinate. It is thus hypothesized that in the transition state leading to the major enantiomer of product, the catalyst 3-phenanthrene is engaging in a stabilizing cation-π or C-H-π with the nascent β-silyl carbocation or its α-protons. Whereas in the transition state leading to the minor enantiomer of product, these catalyst substrate docking constraints force the arene to point off into empty space. The substrate therefore rotates in order to pick up a T shaped π-π stacking interaction between the Cbz group of substrate and the catalyst 3-phenanthrene.[156] The Cbz group appears to be engaging in a cation-π or C-H-π with the nascent β-silyl carbocation or its α-protons. Therefore the major difference between these two transition states is the ability to directly engage with the allylsilane partial positive charge versus engaging indirectly through an intermediate Cbz arene.

The transition state model put forward in Figure 3.20 correctly predicts the major enantiomer of product. Furthermore, it predicts the enantioselectivity remarkable closely; experimental enantioselectivity is 97%, which corresponds to $\Delta\Delta G^{\ddagger}$ = 2.22 kcal/mol, whereas the computationally predicted enantioselectivity is 98% ee and to $\Delta\Delta G^{\ddagger}$ = 2.34 kcal/mol. The ability to match the experimental result so closely, puts some confidence in these computations as being representative of the true lowest energy transition states. External secondary validation of these computations would be ideal, traditionally the ability to accurately predict multiple ^{13}C KIE would

[156] For lead references on π stacking geometries and their relative stabilities see: a) Sinnokrot, M. O..; Sherrill, C. D. Substituent Effects in Π−π Interactions: Sandwich and T-Shaped Configurations. *J. Am. Chem. Soc.* **2004**, *126* (24), 7690–7697. b) Wheeler, S. E.; Houk, K. N. Substituent Effects in the Benzene Dimer Are Due to Direct Interactions of the Substituents with the Unsubstituted Benzene. *J. Am. Chem. Soc.* **2008**, *130* (33), 10854–10855. c) Martinez, C. R.; Iverson, B. L. Rethinking the Term "Pi-Stacking." *Chem. Sci.* **2012**, *3* (7), 2191.

be a method of validation.[157] Often S_N2 transition states have large primary KIEs, while S_N1 transition states have KIEs near 1.00.[142] However, in this case the inability to find an S_N1 transition transition state, coupled with a very low energy imaginary frequency associated with the highly dissociative computed transition state leads to a computationally predicted KIE of 1.001 at the α-carbon, rendering this method not at all conclusive. The ability to accurately predict the experimental enantioselectivity with a range of arylpyrroldine squaramide catalsts would be another form of external validation; however, computations with catalysts bearing suboptimal arenes tend not to converge to the desired transition state.

In addition to further experimental validation of the computational model, future computational work is also ongoing. Specifically, the current model uses 2-methallylsilane as the nucleophile, which does not allow the model to account for the high diastereoselectivity observed in the reaction. A model with 2,3-dimethallylsilane is underway. A catalyst fragment approach to decompose the energetic contributions to $\Delta\Delta G^{\ddagger}$ from each component of the catalyst is also underway to better understand the mode enantioinduction; this method has been used extensively by Houk, in what is called the ActivationStrain-Distortion/InteractionModel.[158] Additionally, the addition of indole nucleophiles to **1-Cbz** is being investigated computationally and similarly finds a low-lying S_N2 mechanism and the inability to find an S_N1 mechanism due to barrierless addition.

---

[157] For lead references on KIEs as computational validation see: Beno, B. R.; Houk, K. N.; Singleton, D. A. Synchronous or Asynchronous? An "Experimental" Transition State from a Direct Comparison of Experimental and Theoretical Kinetic Isotope Effects for a Diels−Alder Reaction. *J. Am. Chem. Soc.* **1996**, *118* (41), 9984–9985. b) DelMonte, A. J.; Haller, J.; Houk, K. N.; Sharpless, B.; Singleton, D. A.; Thomas, A. A. Experimental and Theoretical Kinetic Isotope Effects for Asymmetric Dihydroxylation. Evidence Supporting a Rate-Limiting "(3 + 2)" Cycloaddition. *J. Am. Chem. Soc* **1997**, *199* (41), 9907–9908.

[158] For reviews on distortion analyses see: a) Fernández, I.; Bickelhaupt, F. M. The Activation Strain Model and Molecular Orbital Theory: Understanding and Designing Chemical Reactions. *Chem. Soc. Rev.* **2014**, *43* (14), 4953–4967. b) Bickelhaupt, F. M.; Houk, K. N. Analyzing Reaction Rates with the Distortion/Interaction-Activation Strain Model. *Angew. Chemie Int. Ed.* **2017**, *56* (34), 10070–10086.

3.5 Effect of arylpyrrolidine on enantioselectivity and multiparameter regression modelling

An alternate method to validate the computational model and gain complementary mechanistic insight is to use a multivariate regression model LFER regression model. Sigman has pioneered using computationally derived parameters to construct multivariate correlations, which has led to development of catalysts with improved selectivities as well as increased mechanistic understanding in a number of transformations.[102,159] Sigman has been able to rapidly generate steric,[160] vibrational frequency,[161] and electronic descriptors for non-covalent attractive (generally π) interactions.[162]

In each of these models, an experimental parameter or parameter is being varied. Then, computationally a large number of molecular descriptors are predicted for the parameter that is being experimentally varied. Then an experimental result or output, in this case enantioselectivity, is modeled as a function of the predicted molecular descriptor parameters to arrive at a multiparameter computationally derived LFER. Often, mechanistic insight can be gleaned from the parameters that are essential in the model, and in numerous cases the models have been able to predict a more selective catalysis; notably this was applied to a chiral phosphoric acid catalyzed reaction that led to two new optimal catalysts.[159]

---

[159] Milo, A.; Neel, A. J.; Dean Toste, F.; Sigman, M. S. A Data-Intensive Approach to Mechanistic Elucidation Applied to Chiral Anion Catalysis. *Science* **2015**, *347* (6223), 737-743.

[160] a) Harper, K. C.; Sigman, M. S. Three-Dimensional Correlation of Steric and Electronic Free Energy Relationships Guides Asymmetric Propargylation. *Science* **2011**, *333* (6051), 1875–1878. b) Harper, K. C.; Bess, E. N.; Sigman, M. S. Multidimensional Steric Parameters in the Analysis of Asymmetric Catalytic Reactions. *Nat. Chem.* **2012**, *4* (5), 366–374.

[161] Milo, A.; Bess, E. N.; Sigman, M. S. Interrogating Selectivity in Catalysis Using Molecular Vibrations. *Nature* **2014**, *507* (7491), 210–214.

[162] a) Neel, A. J.; Hilton, M. J.; Sigman, M. S.; Toste, F. D. Exploiting Non-Covalent π Interactions for Catalyst Design. *Nature* **2017**, *543* (7647), 637–646. b) Orlandi, M.; Coelho, J. A. S.; Hilton, M. J.; Toste, F. D.; Sigman, M. S. Parametrization of Non-Covalent Interactions for Transition State Interrogation Applied to Asymmetric Catalysis. *J. Am. Chem. Soc.* **2017**, *139* (20), 6803–6806.

In this system, there is a clear dependence of the enantioselectivity on the size and spatial disposition of the arene of the arylpyrrolidine catalyst, as discussed in Chapter 2. Simply fitting the enantioselectivity data to an LFER model, in which $\Delta\Delta G^{\ddagger}$ was correlated with pyrrolidine arene polarizability, which does not take into account spatial orientation and connectivity, did not produce a meaningful correlation, when it has been shown to do so in other contexts.[99b] Therefore, the effect of the pyrrolidine arene seems to be subtle yet complicated and a suitable system for Sigman's multiparameter regression models. Additionally, if the modeled parameters are in line with the computational model, then it would provide some external validation.

In the multiparameter regression studies, the mechanistic question that is being posed is, what is the role of the pyrrolidine arene in influencing enantioselectivity in the α-chloroglycine allylation? To answer this, 30 catalysts were synthesized and evaluated in the methallylation of **1-Cbz** (Figure 3.21). The catalysts span an enantioselectivity range from 4% to 97% ee, indicating a $\Delta\Delta G^{\ddagger}$ span of 2.21 kcal/mol. Interestingly, all catalysts give the same absolute sense of enantioselectivity. At this point, the catalyst were truncate as an arylpyrrolidine formamide and were computationally parameterized with Sterimol parameters (B_1, B_5, L), vibrational frequencies and intensities corresponding to the one aromatic ring stretch and the amide carbonyl stretching frequency, various NBO charges, isotropic and anisotropic arene polarizabilities, and SAPT interaction energies with probe molecules (see experimental for parameterization).[163]

[163] For references and key references on SAPT analyses see: a) Jeziorski, B.; Moszynski, R.; Szalewicz, K. Perturbation Theory Approach to Intermolecular Potential Energy Surfaces of van Der Waals Complexes. *Chem. Rev.* **1994**, *94* (7), 1887–1930. b) Parker, T. M.; Burns, L. A.; Parrish, R. M.; Ryno, A. G.; Sherrill, C. D. Levels of Symmetry Adapted Perturbation Theory (SAPT). I. Efficiency and Performance for Interaction Energies. *J. Chem. Phys.* **2014**, *140* (9), 094106.

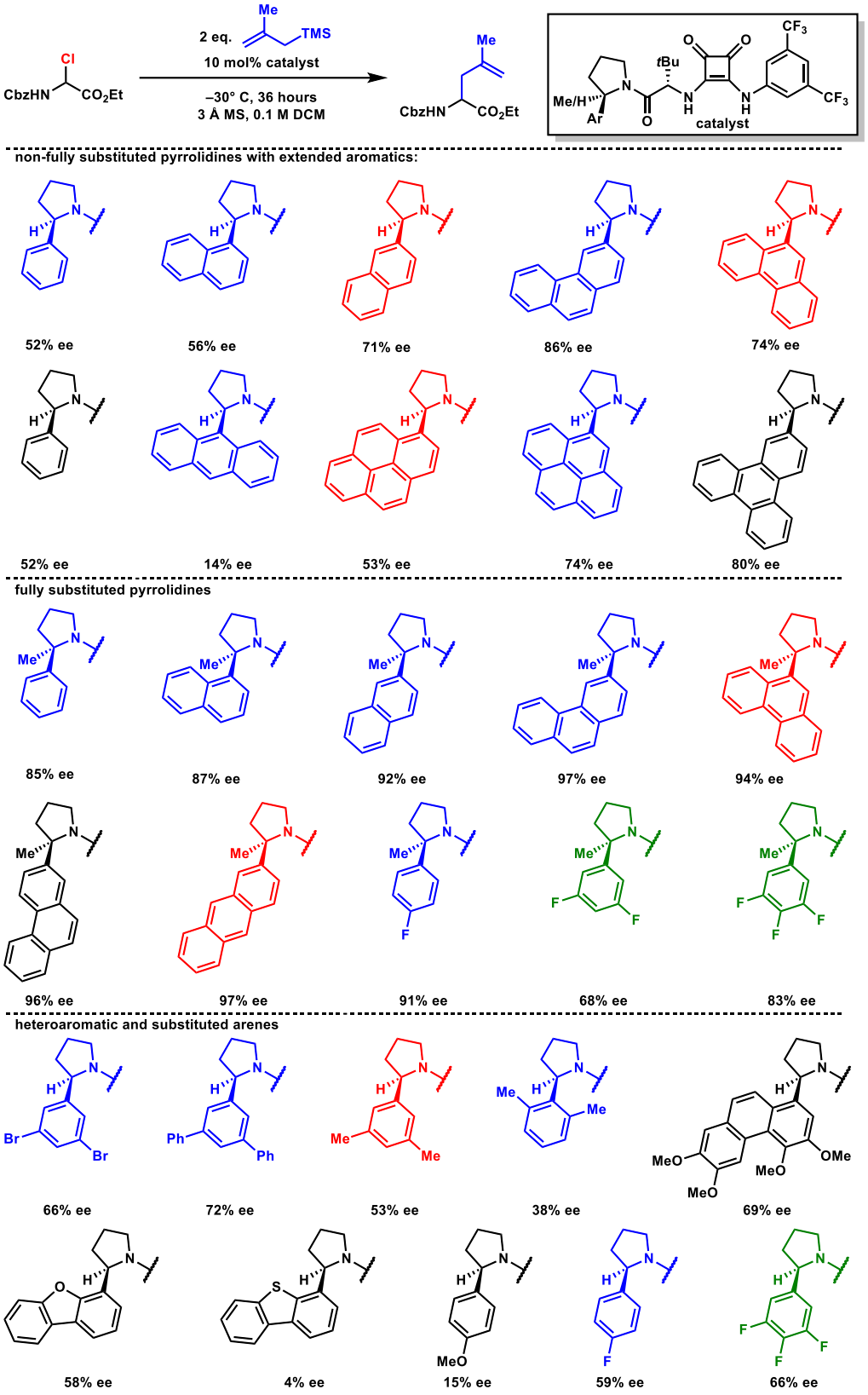

Figure 3.21 Aryl pyrrolidine variations for multiparameter regression modelling. Training set are in blue, validation set are in red, and a secondary validation set that fails in green

After parameters were collected, a training set of 14 catalysts was randomly chosen of the 30 catalysts evaluated (Figures 3.21 and 3.22 in blue). Regression models were formed using the collection of parameters described above and $R^2_{adjusted}$ was maximized in order to avoid overfitting. The resulting model is: $\Delta\Delta G^{\ddagger}$ = 0.96 + 0.32(B_1 Me vs. H) + 0.37(B_5 arene) +0.29(L arene) + 0.42(SAPT dispersion interaction between arene and methane probe). The plot of predicted versus actual $\Delta\Delta G^{\ddagger}$ has a high R^2 and slope close to unity and y-intercept close to 0, indicating that this is a relatively good model. For the regression model with a chemical depiction of each term for the phenylpyrrolidine as example, see Figure 3.22.

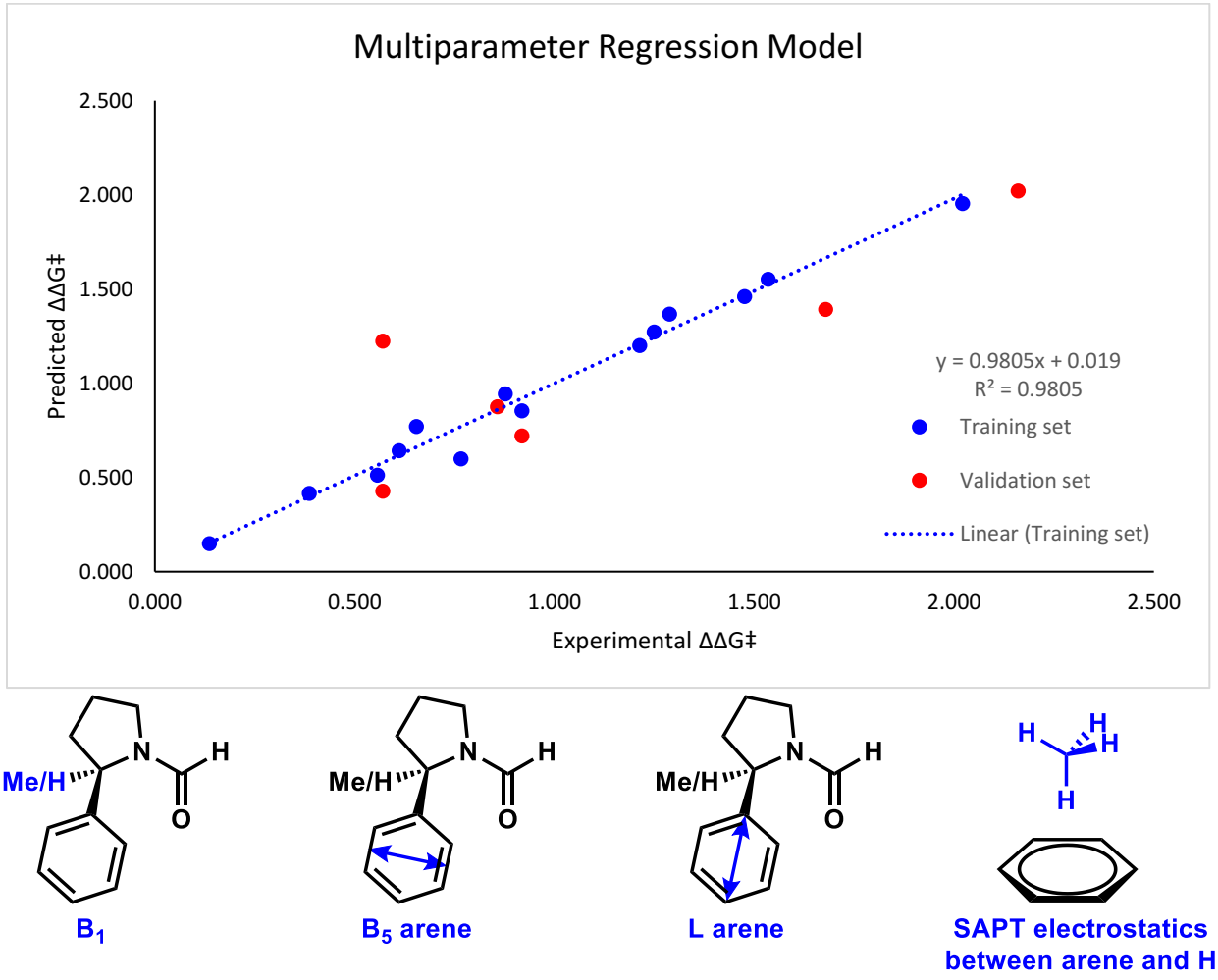

Figure 3.22 Multiparameter regression model of predicted versus experimental $\Delta\Delta G^{\ddagger}$ with a description of each term in the model to arrive at the predicted $\Delta\Delta G^{\ddagger}$

To make intuitive sense of this model, each term will be described. The B_1 (Me vs. H) term describes the steric difference between the geminal methyl or hydrogen substituent to the arene and is a binary term that serves to allow comparison between fully substituted and non-fully substituted catalysts. The B_5 (arene) term is the maximum perpendicular distance relative to the point of connection to the pyrrolidine, it explains the width of each arene. The L (arene) term describes the maximum length of the arene along the axis defined by the point of substitution to the pyrrolidine. The SAPT dispersion term describes the symmetry adapted perturbation theory dispersion decomposition component in the interaction between a given arene and a methane probe molecule placed at the energetic minimum over the face of the arene (Figure 3.23).

Multiple probe molecules were tested in the SAPT analysis, including parallel and perpendicular iminium geometries, parallel and perpendicular *t*-butyl carbocation geometries, and methane (Figure 3.23). Models incorporating iminium probe SAPT energies universally fail to correlate well. The models with the parallel orientation of the *t*-butyl carbocation as a probe are decent and one can get correlations but models have poor predictive power. Models using methane as a probe are the optimal models to date and validate moderately well. The inability for models containing iminium probe SAPT energies to correlate well, indicates that it is unlikely that the catalyst arene is interacting with an iminium, consistent with the mechanistic picture arrived at through DFT. The ability for models containing *t*-butyl cation and methane SAPT arene interaction energies to correlate well suggests that the catalyst arene may be picking up a cation-π or C-H-π leading to differential stabilization of diastereomeric transition states. This is consistent with the DFT picture in which catalyst in the major transition state is directly interacting with the β-silyl cation. The interpretation of the steric terms in the model are that the catalyst needs a certain length and width to be able to position itself in order to stabilize buildup of positive charge.

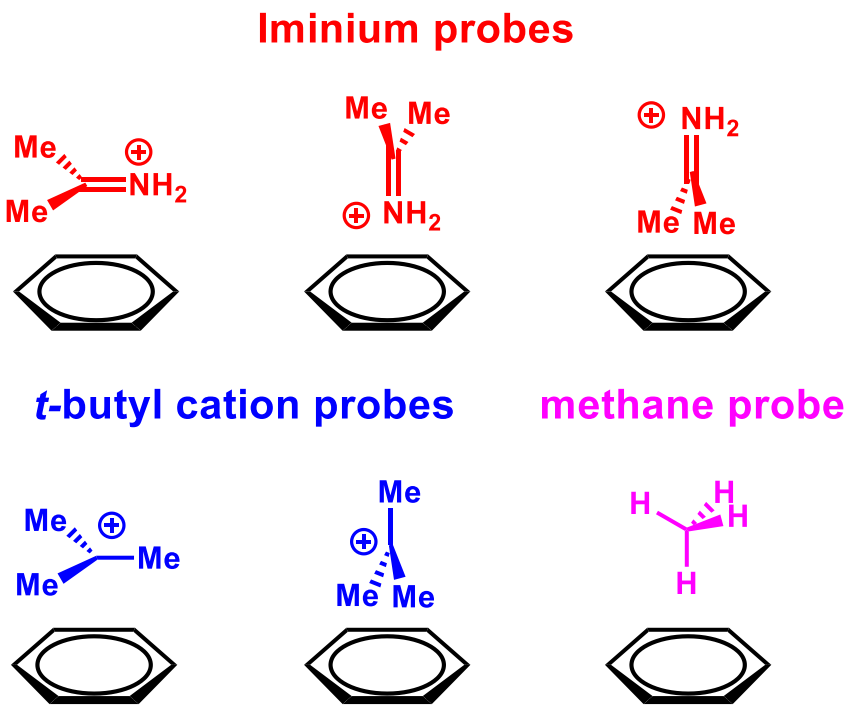

Figure 3.23 Small molecule probes for SAPT interaction energies with pyrrolidine arene

Next, the model needed to be validated, thus 6 catalyst were chosen at random to validate the model and are depicted in red in Figures 3.21 and 3.22. Overall, the validation set matches the model relatively well, with one notable outlier. Importantly, the model can predict a second optimal catalyst, the fully substituted 2-anthracenyl pyrrolidine quite well. The only outlier is the 1-pyrenyl catalyst, which is predicted to have much higher enantioselectivity than it does. This indicates that although the model is relatively validated it may still not be able to fully explain the arene size and positioning effects.

Last, polyfluorinated catalysts (green in both Figures 3.21 and 3.24) were synthesized in order to knock-out a cation-π interaction. The model does not handle these catalysts well and consistently overpredicts the enantioselectivity, which may be the result of only being trained on two mono-fluorinated catalysts. Thus, these polyfluorinated catalysts do not represent the training set. This indicates that the model probably does not have the exact non-covalent stabilizing energetic component correct yet. However, the ability for polyfluorinated catalysts to still give

decent to high enantioselectivities is consistent with the absence of a strong cation-π, which would be substantially perturbed here. Future modeling will attempt to fit these fluorinated catalysts to improve correlation and mechanistic understanding.

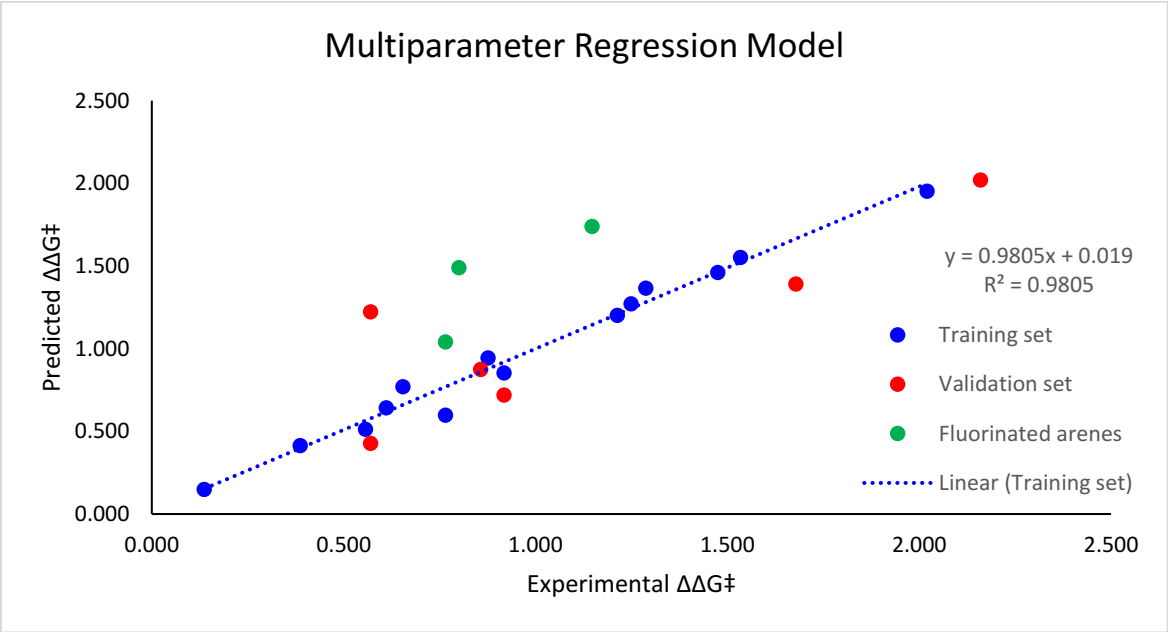

Figure 3.24 Additional validation set with polyfluorinated arylpyrrolidines fails to validate

3.6 Conclusion and outlook

In conclusion, the squaramide **5d'** catalyzed methallylsilane addition into **1-Cbz** was studied via kinetics, DFT computations, and regression modeling. The kinetics demonstrate that the reaction is well-behaved and overall second-order, with a first order dependence on the concentration of each of the reaction components. Additionally, it is an observed 0.55 order in catalyst **5d'**, indicative of a strong off-cycle catalyst dimerization equilibrium and one catalyst in the transition state. This finding is corroborated by ITC measurements of the catalyst dimerization equilibrium, which is found to be ~1000 M^{-1}.

The kinetics determine that the C-C bond formation is rate and selectivity determining. A solvent screen revealed that the allylation is optimal in DCM and proceeds with moderate enantioselectivity in acetonitrile, both solvents that should promote dissociated ion-pairs and thus

provide racemic product. Additionally, the iminium intermediate would be substantially destabilized by an α-carbonyl. Thus, contrary to precedent with other *N*-acyl iminium ion chemistry, the possibility of an S_N2 mechanism was investigated.

Uncatalyzed DFT computations predict that the iminium intermediate is indeed inaccessible at 31.6 kcal/mol above the ground state and that there is a relatively low-lying S_N2 pathway, just 12.7 kcal/mol above the ground state, confirming the likelihood of an S_N2 pathway. To reconcile high yields and enantioselectivities with an S_N2 pathway, a dynamic kinetic resolution must be occurring, in which the starting material is racemizing. NMR studies were carried out to confirm rapid racemization and determine if it is catalyzed by squaramide **5d'** or independent of catalyst. Unfortunately, conformational flexibility of the starting material prevented clean analysis and this is still an open question.

Catalyzed DFT calculations were then pursued, which provide a transition state picture for unique low energy transition states leading to major and minor enantiomers of product **2a**. The dual-hydrogen-bond donor partial abstraction of chloride and catalyst amide hydrogen-bonding to a nascent iminium ion are preserved in both pathways. These effects serve to dock catalyst and substrate and in the major pathway the pyrrolidine arene is well situated to directly stabilize buildup of positive charge in the nucleophile β-silyl cation, whereas in the minor pathway, it is positioned such that it cannot engage directly with nucleophile and instead engages with the Cbz of substrate in a π-π stacking interaction.

A multivariate regression analysis was carried out to better understand the role of the pyrrolidine arene and the fundamental interactions responsible for enantioselectivity. The model is relatively predictive and validates well except for with poly-fluorinated arenes. The model

independently predicts a cation or C-H π interaction between catalyst and the substitution transition state, somewhat validating the computational model.

In summary, this reaction provides a new mode of enantioselective anion-binding catalysis, in which a concerted S_N2 can be promoted. This is significant because there are a number of C-X bonds that hydrogen-bond donors do not have the ability to heterolyze via anion-abstraction. Thus, the ability to affect highly enantioselective S_N2 reaction manifolds could be enabling in expanding the scope of hydrogen-bond donor chemistry in systems in which the cationic intermediates are too high in energy to be accessible. Understanding the elements of this α-chloroglycine allylation necessary for reactivity and efficient enantioinduction could shed light on other systems that may be amenable to S_N2 activation by anion-binding hydrogen bond donor catalysts. Indeed, recently, the ability to affect S_N2 reactions in glycoside couplings has allowed for the synthesis of β-glycosides from α-chloro and α-phosphate donors in an S_N2 reaction.[142a,164] Additionally, two unpublished projects, specifically a desymmetrizing opening of oxetanes by bromide, and an enantioselective neryl chloride terpene cyclization are both predicted to go through S_N2 reactions demonstrating hydrogen-bond donor induced S_N2 reactivity may be more prevalent than initially thought, and thus worthy of further mechanistic investigation.

3.7 Experimental

3.7.1 Kinetic analyses of the catalytic allylation of α-chloroglycinates 1-Cbz

In order to shed light on the mechanism of the substitution reaction, the order in the concentration of the electrophile, **1-Cbz**, and the nucleophile, 2-methallyltrimethylsilane was determined. Due to the heterogeneity, time scale, and temperature of the reaction the optimal method to monitor the reaction was via initial rate quench kinetics, in which the reaction was

[164] Levi, S. M.; Li, Q.; Rötheli, A. R.; Jacobsen, E. N. Catalytic Activation of Glycosyl Phosphates for Stereoselective Coupling Reactions. *Proc. Natl. Acad. Sci. U. S. A.* **2019**, *116* (1), 35–39.

aliquoted at time points and diluted into benzene-d6, which stopped the reaction. The initial time points are uniformly 0% conversion, which indicates with a high level of confidence that the reaction does not warm up in the needle or proceed post quench.

In order to conduct initial rate kinetics, it must first be determined that the reaction is well-behaved and that the initial reaction is representative of the overall reaction. Thus a full reaction course was conducted by quenching the reaction using the method described above. Time points were taken at times (h): 0.5, 1, 2, 4, 8, 12, 18, 24, and 30 and concentration of product **2a** was detected. Conversion was measured by monitoring the appearance of the two incoming allyl protons at 2.1 and 2.3 and integrated relative to the methyne peak of triphenylmethane at 5.35 ppm as an internal standard added before the reaction. Peaks were chosen because they were the cleanest and far away from the DCM region, which provides poor integrals in the 4-5 ppm window. The conditions for the full reaction course kinetics were as follows: [electrophile **1-Cbz**]$_0$ = 0.1 M, [nucleophile]$_0$ = 0.2 M, [catalyst **5d'**]$_0$ = 0.005 M in DCM with 30 mgs/mL 3Å molecular sieves, kept at –30 °C. Conversion was measured to between 3 and 4 half-lives, 90% conversion. Due to the messiness of crude reaction mixtures, NMR integrals were determined to the nearest 0.005 M. The raw data for the full reaction course are presented in Table 3.1 below. As shown in Figure 3.4 of the main text, the reaction appears to have second order behavior. In order to determine this, the data were linearized using equation 1 derived below. The data fit the linearization equation quite well, with R^2 = 0.982.

Table 3.1 Full reaction time course product concentration in the squaramide **5d'** catalyzed allylation of **1-Cbz**

time (h)	product **2a** (M)
0	0.000
0.5	0.005
1	0.010
2	0.020
4	0.035
8	0.055
12	0.070
18	0.080
24	0.090
30	0.090

To linearize the data, imagine the second order reaction below, where **1-Cbz** is *A*, 2-methallyltrimethylsilane is *B*, and **2a** is *P*.

$$\frac{d[P]}{dt} = k[A][B] \text{ (1)}$$

Now, if the two concentrations are not equal, then call the initial amount of $A = [A]_0$ and the initial amount of $B = [B]_0$, also define a new variable $P = x$, which is the amount of each reactant depleted at time *t*. We can rewrite (1) as:

$$\frac{dx}{dt} = k([A]_0 - x)([B]_0 - x) \text{ (2)}$$

Rearranging (2) provides:

$$\frac{dx}{([A]_0 - x)([B]_0 - x)} = kdt \text{ (3)}$$

Now, integrate (3) from $t = 0$ to $t = t$, an arbitrary point in time:

$$\int_0^x \frac{dx}{([A]_0 - x)([B]_0 - x)} = k\int_0^t dt \text{ (4)}$$

Solving this integral using the method of partial fractions provides:

$$\frac{1}{[B]_0 - [A]_0}\left(\ln\frac{[A]_0}{[A]_0 - x} - \ln\frac{[B]_0}{[B]_0 - x}\right) = kt \text{ (5)}$$

Applying the rules of logarithms, (5) can be simplified:

$$\frac{1}{[B]_0 - [A]_0} \ln \frac{[B][A]_0}{[A][B]_0} = kt \quad (6)$$

Which, plugging in the relevant values for $[A]_0 = 0.1$ and $[B]_0 = 0.2$ into (6) gives:

$$\ln \frac{[B]}{2[A]} = 0.1kt \ (7)$$

Equation (7) is used to linearize the data in Figure 3.4, in which ln([2-methallylsilane]/2[**1-Cbz**] is plotted against t, to find a rate constant of $k = 0.62\ M^{-1}h^{-1}$.

Additionally, due to noise at high conversion, which is also the most diagnostic regime for differing first and second order rate laws, the data was fit to a simulated reaction course in mathematica for both first an second order reactions given the initial starting conditions and a floating rate constant, which is provided in Figure 3.25 (first-order fit in red and second-order fit in blue). Note that due to the 2:1 stoichiometry, both models fit nearly perfectly, indicating that determining order in both reacting components in necessary.

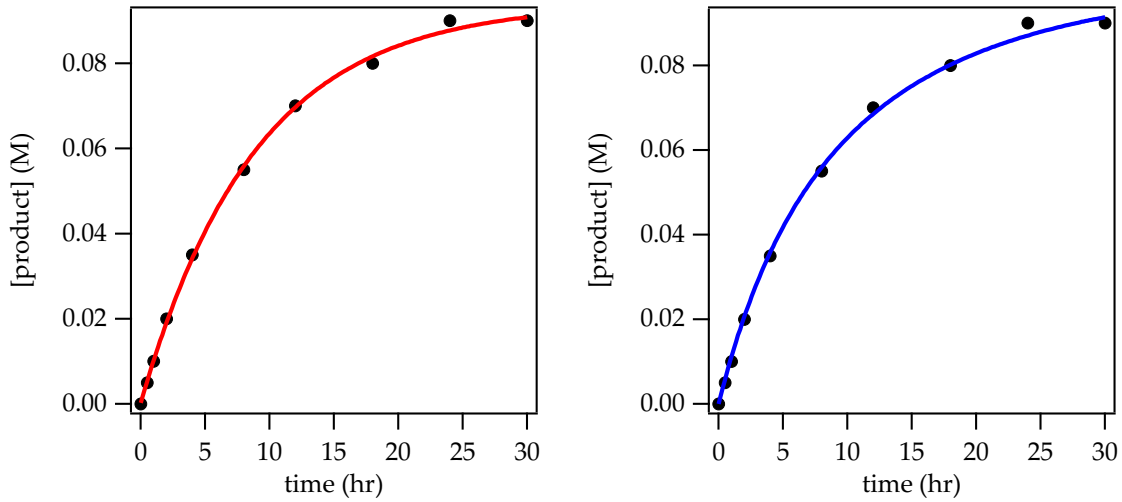

Figure 3.25 Simulated full reaction course for first-order kinetics (red, left) and second order kinetics (blue,right). Both models fit, indicate further kinetic analysis must be performed

In the initial rate kinetics, the reaction parameters were all the same as in the full-reaction time course, with one key difference being a temperature of T = –35 °C, which was chosen to slow

down the reaction to get more accurate time points and to be able to space them out slightly. Product was detected and conversion measured out to 20%, with minimal deviation from linearity. Below is a representative example of the NMR kinetics time course (Figure 3.26), with the following time points 30, 60, 90, 120, 180, 240, 300, 360 minutes (from bottom to top):

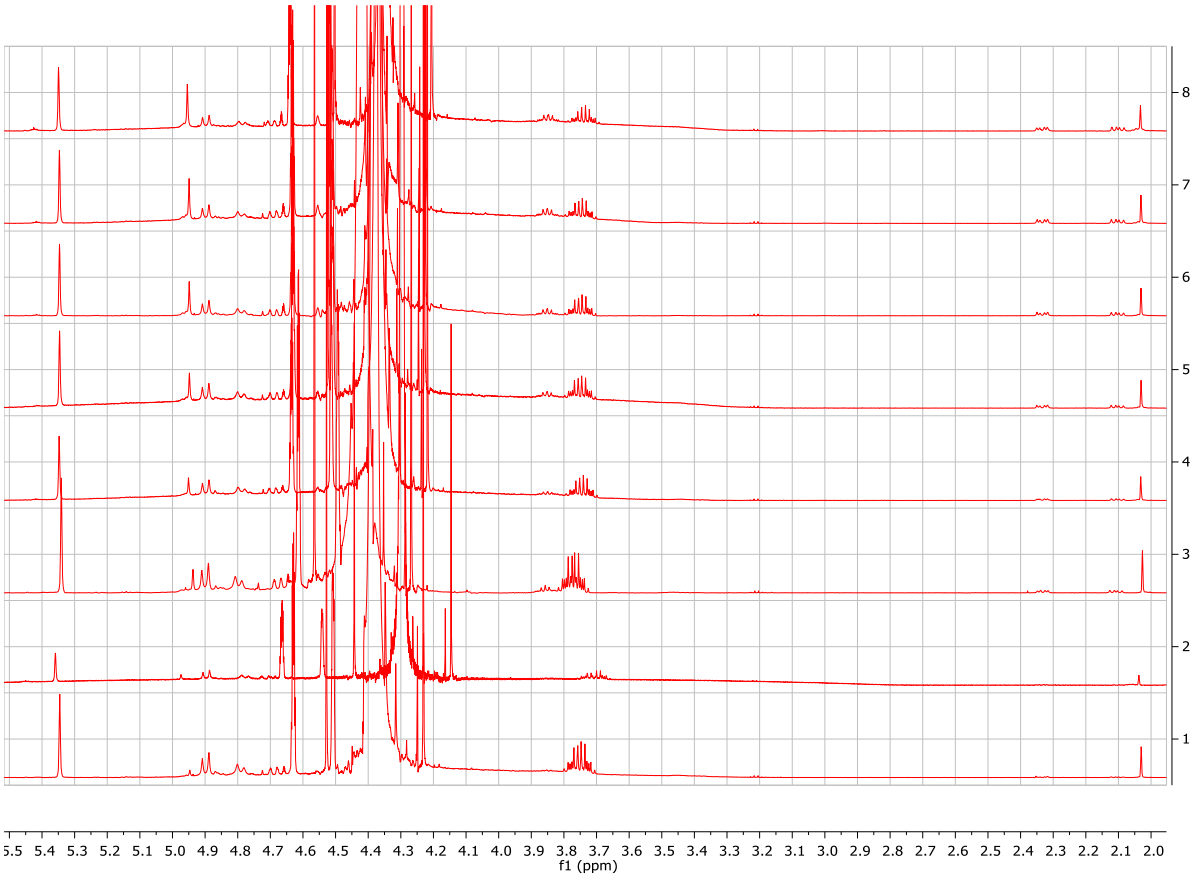

Figure 3.26 Representative NMR spectra for monitoring product concentration for kinetic analyses of the squaramide **5d'** catalyzed allylation of **1-Cbz**

The NMRs reflect 4 scans, with T1 = 15 seconds, and no steady-state pulsing. Spectra were autophased and baseline correceted using the Whittaker Smoother algorithm. Integrals were converted into yield by comparing to internal standard. [Product] versus time was plotted for standard reaction conditions and for reaction conditions under which each reacting partner or catalyst was doubled and halved to determine order in the reaction component. Standard reaction conditions are at –35 °C, in DCM, 0.1 M [1-Cbz], 0.2 M [methallylsilane], 0.01 M [4d'], 30

mgs/mL 3Å molecular sieves. Data were collected in triplicate for nucleophile and electrophile concentrations and as a single run for catalyst concentrations. The raw concentration versus time data and plots can be found in Table 3.2 and Figure 3.27 below.

Table 3.2 product concentration in initial rate kinetics of the squaramide **5d'** catalyzed allylation of **1-Cbz**. Top: varying [**1-Cbz**], Middle: varying [silane], Bottom: varying [**5d'**]

time	[**1-Cbz**] = 0.05 M	[**1-Cbz**] = 0.1 M	[**1-Cbz**] = 0.2 M
0	0	0	0
30	0.001	0.002	0.004
60	0.002	0.004	0.008
90	0.003	0.006	0.01
120	0.004	0.008	0.014
180	0.006	0.011	0.019
240	0.008	0.014	0.024
300	0.009	0.017	0.029
0	0	0	0
30	0.001	0.003	0.004
60	0.002	0.004	0.007
90	0.003	0.006	0.01
120	0.004	0.008	0.013
180	0.005	0.011	0.019
240	0.007	0.015	0.023
300	0.009	0.018	0.028
0	0	0	0
30	0.001	0.002	0.004
60	0.002	0.004	0.008
90	0.003	0.006	0.011
120	0.004	0.007	0.014
180	0.006	0.011	0.02
240	0.008	0.013	0.025
300	0.01	0.017	0.03

time	[silane] = 0.1 M	[silane] = 0.2 M	[silane] = 0.4 M
0	0	0	0
30	0.001	0.001	0.003
67	0.001	0.003	0.006
94	0.002	0.004	0.009
122	0.003	0.006	0.012
181	0.004	0.009	0.017
240	0.006	0.011	0.021
300	0.007	0.014	0.025

360	0.009	0.017	0.029
0	0	0	0
30	0	0.001	0.003
60	0.001	0.002	0.007
90	0.002	0.004	0.01
120	0.003	0.005	0.014
180	0.004	0.008	0.019
240	0.005	0.011	0.023
300	0.007	0.014	0.026
360	0.008	0.016	0.031
0	0	0	0
30	0.001	0.001	0.002
63	0.001	0.003	0.006
92	0.002	0.004	0.008
124	0.003	0.007	0.011
183	0.004	0.009	0.016
241	0.006	0.012	0.02
300	0.008	0.015	0.025
360	0.009	0.019	0.028

time	[**5d'**] = 0.005 M	[**5d'**] = 0.01 M	[**5d'**] = 0.02 M
0	0	0	0
30	0.001	0.002	0.003
60	0.002	0.004	0.006
90	0.003	0.006	0.008
120	0.005	0.008	0.011
180	0.007	0.011	0.015
240	0.009	0.014	0.019
300	0.011	0.016	0.022
360	0.013	0.02	0.025

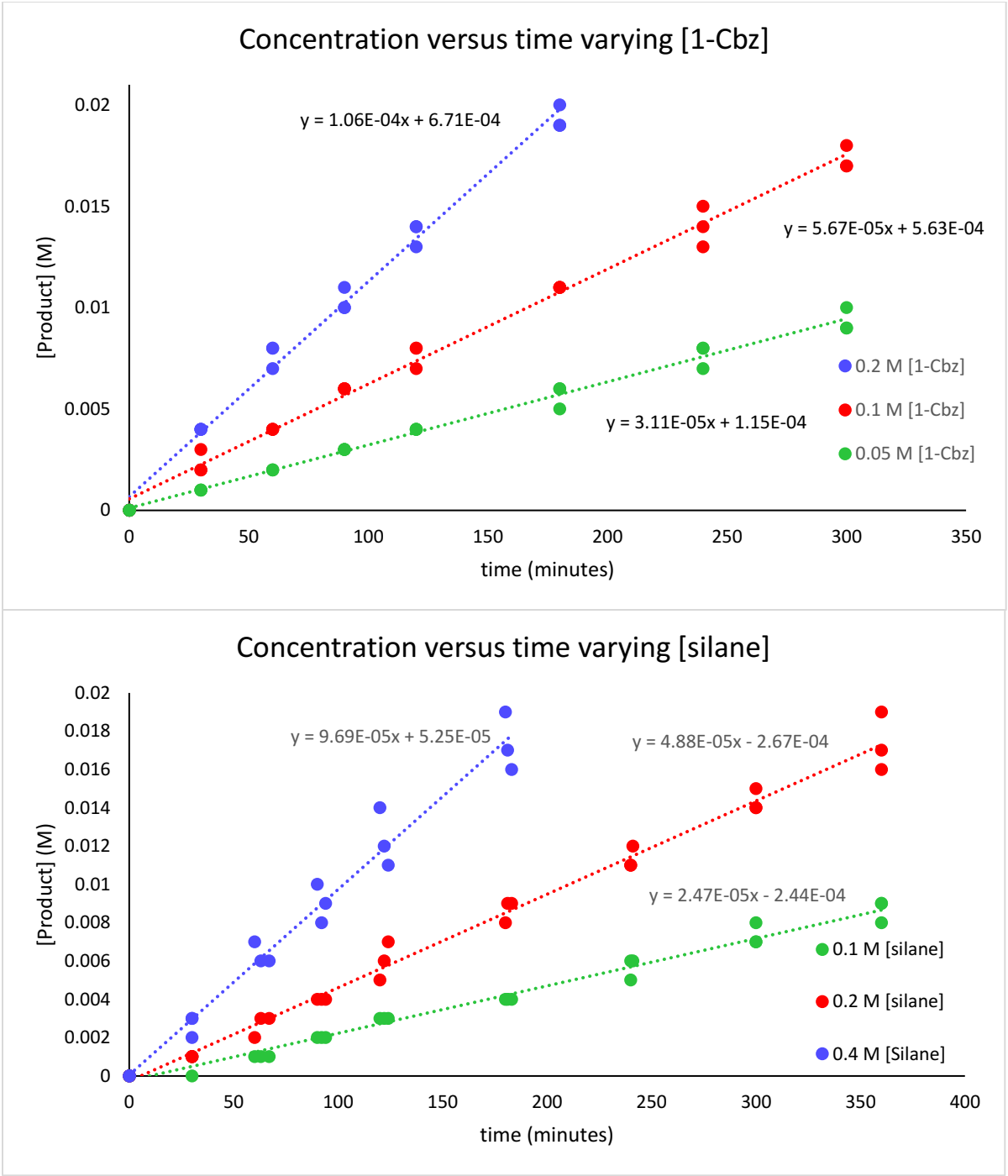
Concentration versus time varying [1-Cbz]
y = 1.06E-04x + 6.71E-04
y = 5.67E-05x + 5.63E-04
y = 3.11E-05x + 1.15E-04
0.2 M [1-Cbz]
0.1 M [1-Cbz]
0.05 M [1-Cbz]
[Product] (M)
time (minutes)
0.02
0.015
0.01
0.005
0
0
50
100
150
200
250
300
350
Concentration versus time varying [silane]
y = 9.69E-05x + 5.25E-05
y = 4.88E-05x - 2.67E-04
y = 2.47E-05x - 2.44E-04
0.1 M [silane]
0.2 M [silane]
0.4 M [Silane]
[Product] (M)
time (minutes)
0.02
0.018
0.016
0.014
0.012
0.01
0.008
0.006
0.004
0.002
0
0
50
100
150
200
250
300
350
400

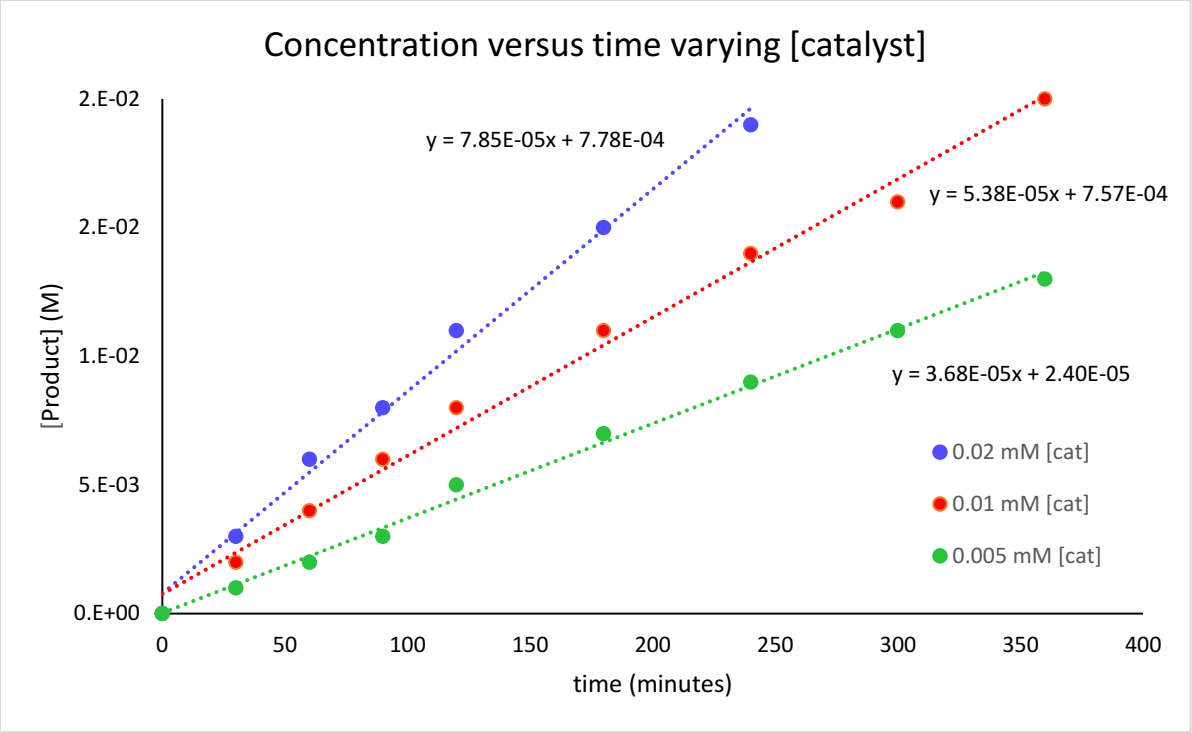

Figure 3.27 Concentration of product **2a** versus time plots in the initial rate kinetics of the **5d'** catalyzed addition of allylsilane to **1-Cbz**. In each plot, standard reaction conditions are represented in red, with green representing a halved concentration in one component and blue representing doubled concentration in one component. Top: varying [**1-Cbz**], Middle: varying [silane], Bottom: varying [**5d'**]

The slopes of each of the graphs above were plotted against the concentration of the reagent or catalyst that was varied (Figure 3.5). The k_{obs} vs. [**1-Cbz**] and k_{obs} vs. [methallylsilane] plots were both linear with R^2=0.997 and R^2=1.00 respectively, indicating that the reaction is cleanly first order both reacting partners. Data is slightly sub linear, due to the initial rate approximation.

The k_{obs} vs. [**5d'**] graph was not linear, thus a least squares fit to a function of the form $k_{obs} = a*[\mathbf{5d'}]^b$ found $b = 0.55$, which is the dashed line in the bottom plot. This indicates the observed kinetic dependence on concentration of catalyst is 0.55 order. ITC was subsequently used to determine the mechanistic significance of this observed order.

3.7.2 Determination of catalyst dimerization equilibrium

ITC was used to determine the dimerization constant of the catalyst **5d'**. To conduct this experiment, a 0.010 M solution of **5d'** in DCM was prepared and successively injected into a

reservoir of blank DCM and the heat output was measured for each successive injection. The heat profile as a function of injection can be found in Figure 3.28. These data can be fit according to the procedure in Andreas Rötheli's thesis to give a dimerization constant of ~1000 M^{-1}.[94] Unfortunately there is baseline drift during the course of this experiment, potentially due to DCM evaporation in the injection needle, however a rough number can still be extracted.

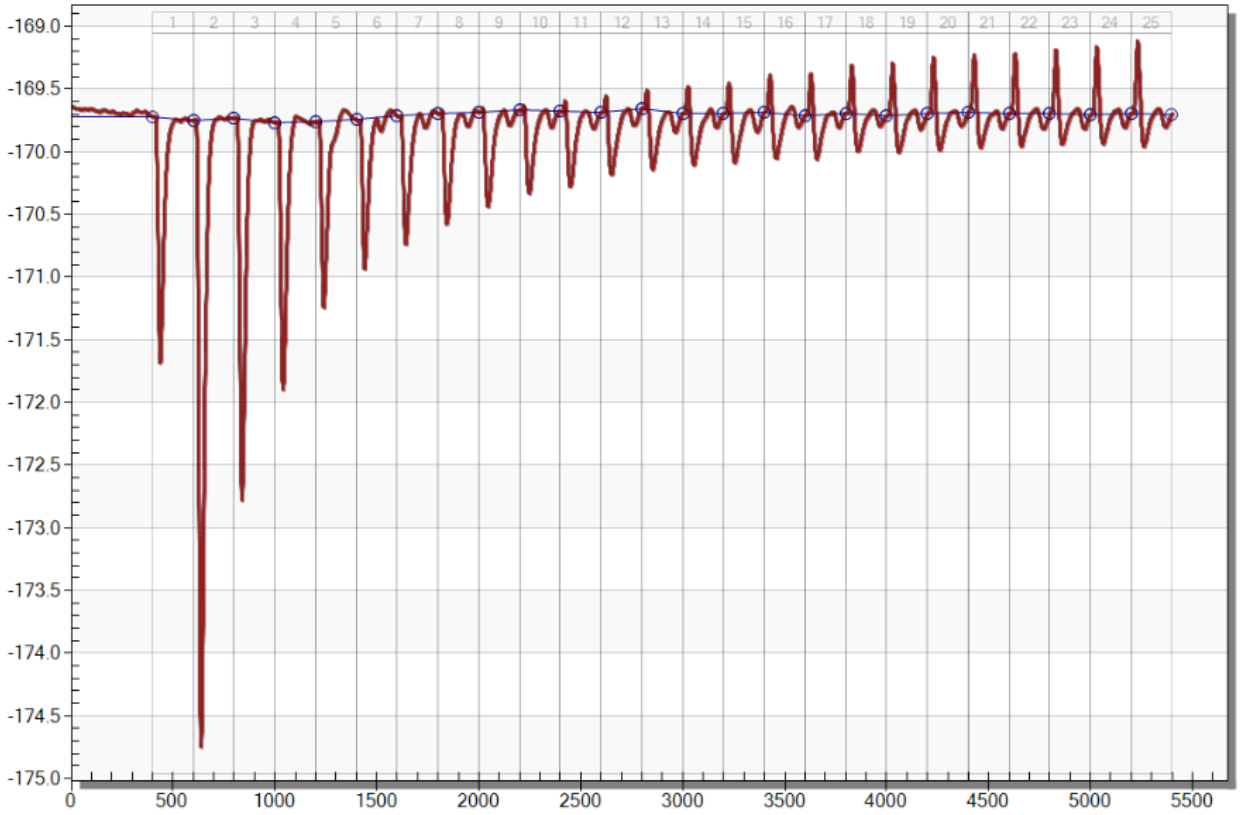

Figure 3.28 Raw heat data for the ITC catalyst **5d'** dilution, first data point intentionally not fit

This dimerization can be used to back-calculate an observed order in catalyst for a reaction that is monomeric in catalyst in the transition state using the following derivation:

Start by assuming a catalytic cycle, wherein C is a catalyst that undergoes off-cycle dimerization and catalyzes the reaction of A to B:

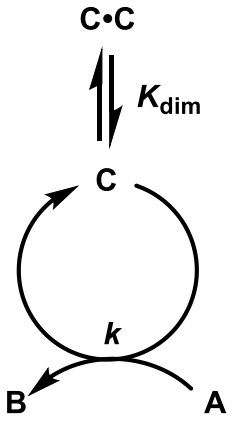

The dimerization equilibrium, K_{dim} is defined as:

$$K_{dim} = \frac{[C \cdot C]}{[C]^2} \quad (8)$$

For a transition state monomeric in catalyst, the rate of this transformation is:

$$rate = k[A][C] \quad (9)$$

Writing out the speciation of catalyst, where C_0 is the initial amount of catalyst added:

$$C_0 = [C] + 2[C \cdot C] = C + 2K_{dim}[C]^2 \quad (10)$$

Solving the quadratic equation for $[C]$ gives:

$$[C] = \frac{-1 \pm \sqrt{1 + 8K_{dim}[C]_0}}{4K_{dim}} \quad (11)$$

Plugging (11) into rate equation (9) gives:

$$rate = k[A]\frac{-1 \pm \sqrt{1+8K_{dim}[C]_0}}{4K_{dim}} \quad (12)$$

Then for a given K_{dim} one can find a fit this function (12) to an arbitrary power function of the the form:

$$rate = k[A][C]_0^b \quad (13)$$

Fitting function (12) to the function (13) gives an apparent catalyst order, which for K_{dim} = 1000 M^{-1} gives an apparent order of 0.575 in catalyst. Moreover this can be done generally for any K_{dim} and the plot is provided below, in Figure 3.29.

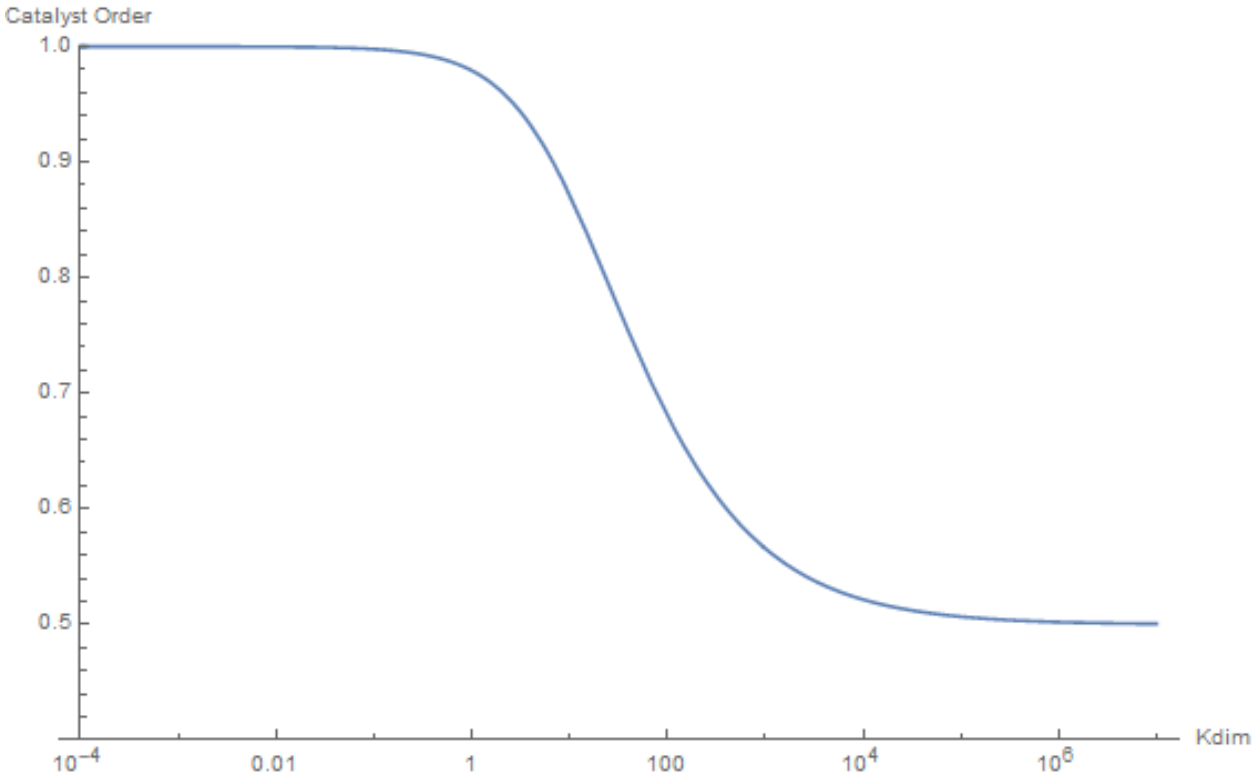

Figure 3.29 Observed order in catalyst given a catalyst dimerization constant

3.7.3 NMR racemization studies

To probe the racemization of starting material, the following synthetic route, figure 3.30, was carried out to synthesize the mono-deuterated staring material **1-Cbz-*d***. The NMR of **1-Cbz-*d*** in CD_2Cl_2 at –30 °C is provided below in Figure 3.31. Note that the substrate exists as two carbamate rotomers ~10:1 and only the major one is integrated, thus all integrals are off by a constant factor of roughly 1.1. One can clearly see that, as desired the benzylic singlets are well resolved in CD_2Cl_2 at –30 °C.

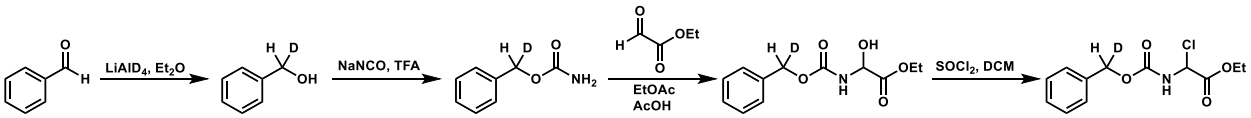

Figure 3.30 Synthesis of mono-deuterated **1-Cbz-*d*** for NMR racemization studies

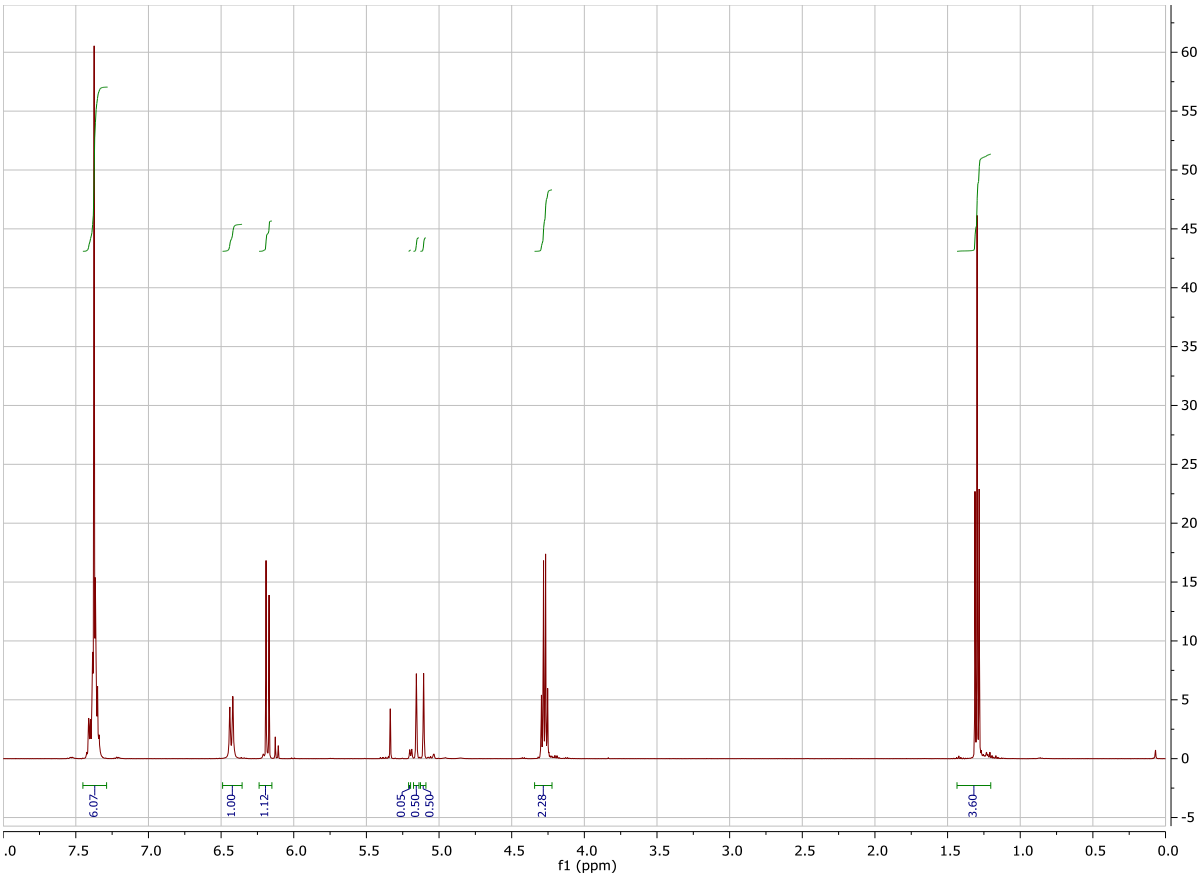

Figure 3.31 NMR spectrum of **1-Cbz-*d*** in CD_2Cl_2 at –30 °C

10 mol% Catalyst **5d'** and **1-Cbz-*d*** were mixed in an NMR tube and NMRs were taken with the temperature arrayed and from 30 °C to –80 °C in ten degree increments. One can see that the benzyl peaks are broad at 30 °C and sharpen around –30 °C and then rebroaden again below this temperature (Figure 3.32) This is indicative of two dynamic processes, one at low temperature and one at high. The high temperature one seems to effect the benzyl group while the low temperature one seems to effect the ethyl group more.

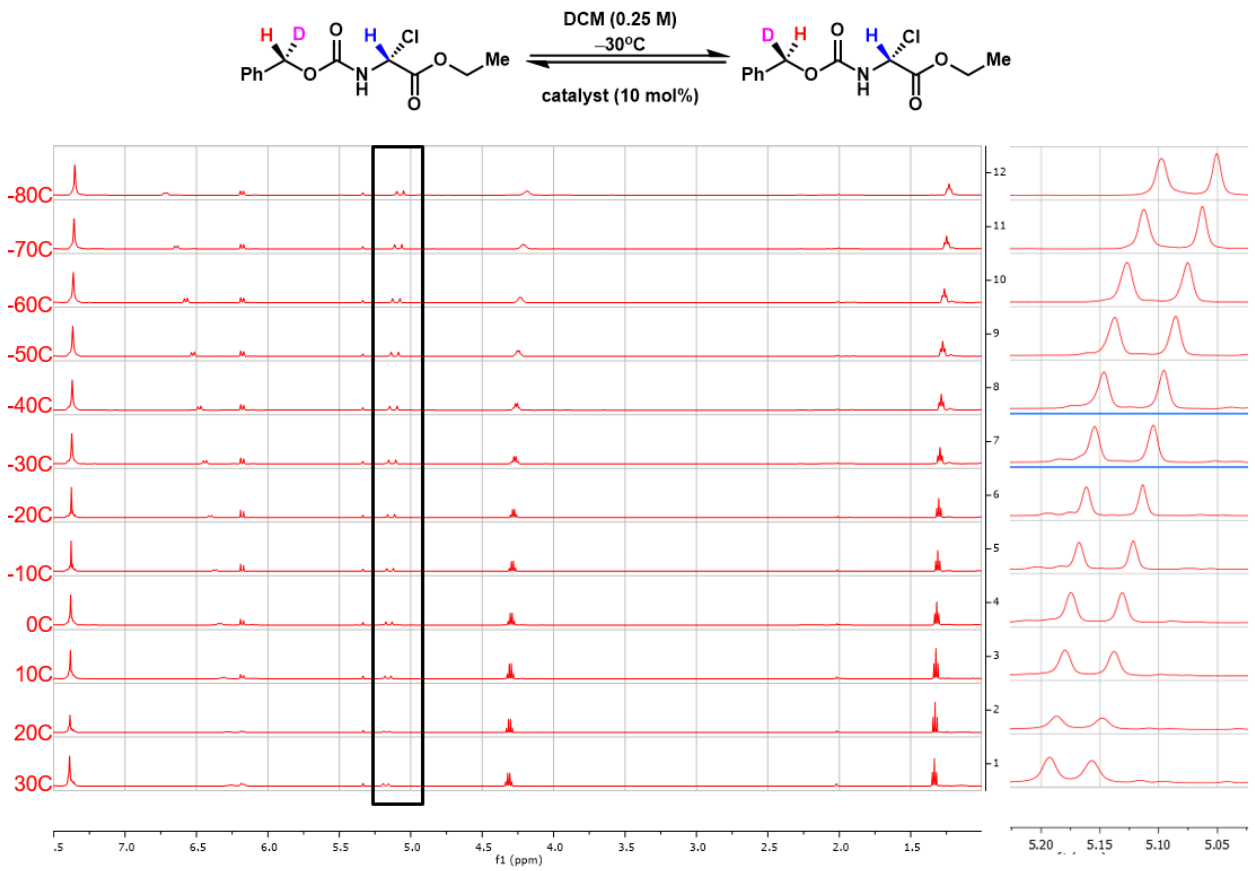

Figure 3.32 Temperature array in the NMR spectrum of 10 mol% Catalyst **5d'** and **1-Cbz-*d***

The spectra were then simulated using the Bloch-McConnell equations and fit to the data to obtain an exchange rate, with simulated spectra in blue and actual spectra in black (Figure 3.33).[152] The data for the catalyzed and uncatalyzed exchange process were then fit to the Eyring and linearized Eyring equations. Data deviate at low temperature do to broadening preventing determination of an intrinsic line width. The exchange process observed here appears to not be catalyzed by the squaramide **5d'**.

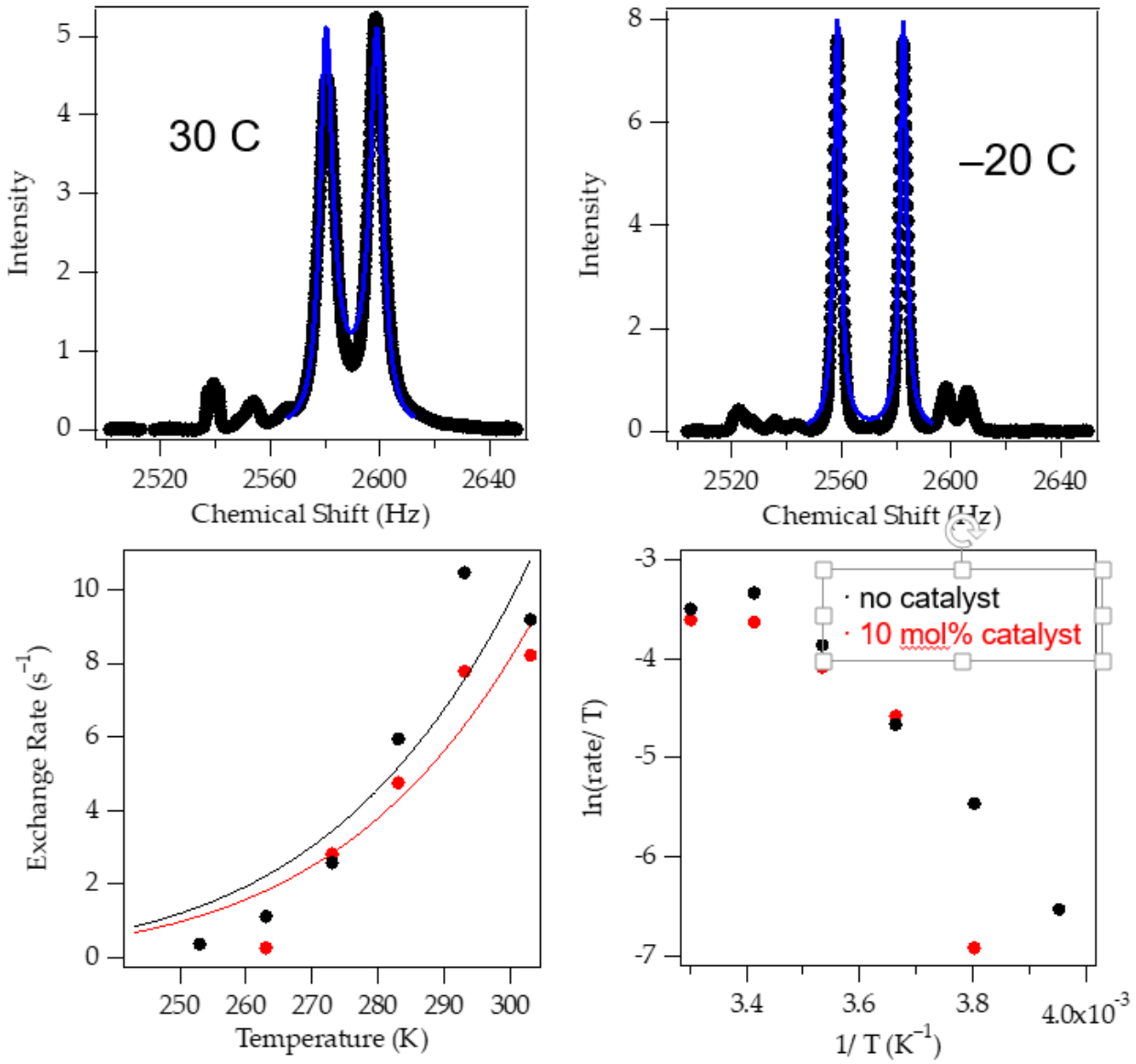

Figure 3.33 Simulated and experimental NMR spectra of **1-Cbz-*d*** at 30 °C and –20 °C as representative examples. Exchange rates obtained from fitting line widths and plotted against exponential and linearized Eyring equations

While the process observed in Figure 3.33 appears to be racemization and would give a racemization rate of ~1s^{-1}, much faster than reaction rate, further analysis reveals that this is unlikely to be the actual racemization mechanism, but is rather another dynamic process, perhaps carbamate rotomeric exchange. This was determined because, although DCM's boiling point prevents surveying temperatures higher than 30 °C, when the same procedure is done in

chloroform or dichloroethane up to 50 and 70 °C respectively, rather than observing complete coalescence of these peaks, what occurs instead is a rebroadening, indicative of yet another dynamic process that is undetermined (Figure 3.34).

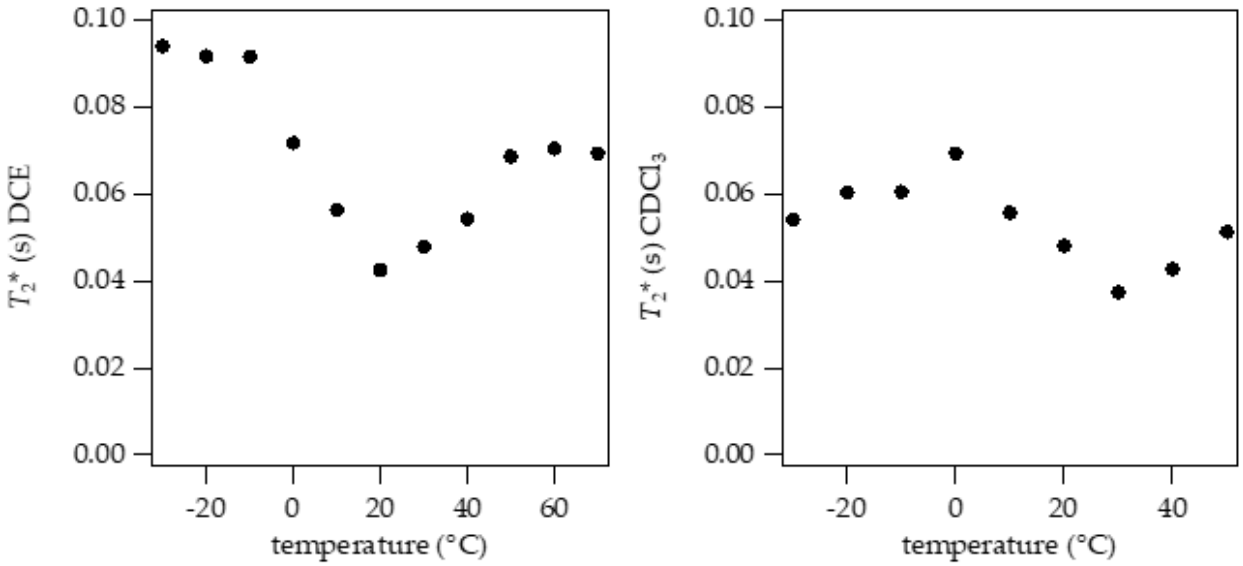

Figure 3.34 T_2* as a function of temperature for the uncatalyzed NMR exchange process of **1-Cbz-*d*** in dichloroethane and chloroform.

Given the conformational flexibility of the substrate, the ability to determine the exchange rate via NMR seems unlikely or impossible. It is possible one of the exchange processes observed is the relevant one, but that cannot be stated with any confidence. Thus, this method of determining the rate of racemization was abandoned.

3.7.4 Computations

Calculations were executed at Harvard University on the Odyssey research computing cluster using the Gaussian 16.[165] The B3LYP density functional was employed with the 6-311+G(d,p) basis sets of Pople, and co-workers were used as specified.[153] The PCM continuous surface charge polarizable continuum models of solvation for both DCM and H2O were employed.[154] The D3 version of Grimme's dispersion with Becke-Johnson damping was employed as a dispersion correction.[155] Default optimization convergence criteria, tight SCF convergence criteria, and default integration settings were used. All stationary points were verified by frequency calculations using the rigid-rotor/harmonic-oscillator assumption. Transition structures were characterized by the existence of a single imaginary frequency corresponding to the process of interest, and local minima were characterized by the absence of any imaginary frequencies. Uncorrected electronic energies are included for all stationary points. Energies are reported in units of hartrees and relative energies are in units of kcal mol^{-1}. Distances are reported in units of angstroms (Å). Computational pictures rendered in Cylview.[166]

A thorough discussion of the conformational landscape was discussed in section 3.3, however iminium geometries were not discussed. Iminium geometries were calculated and the

[165] Gaussian 16, Revision B.01, Frisch, M. J.; Trucks, G. W.; Schlegel, H. B.; Scuseria, G. E.; Robb, M. A.; Cheeseman, J. R.; Scalmani, G.; Barone, V.; Petersson, G. A.; Nakatsuji, H.; Li, X.; Caricato, M.; Marenich, A. V.; Bloino, J.; Janesko, B. G.; Gomperts, R.; Mennucci, B.; Hratchian, H. P.; Ortiz, J. V.; Izmaylov, A. F.; Sonnenberg, J. L.; Williams-Young, D.; Ding, F.; Lipparini, F.; Egidi, F.; Goings, J.; Peng, B.; Petrone, A.; Henderson, T.; Ranasinghe, D.; Zakrzewski, V. G.; Gao, J.; Rega, N.; Zheng, G.; Liang, W.; Hada, M.; Ehara, M.; Toyota, K.; Fukuda, R.; Hasegawa, J.; Ishida, M.; Nakajima, T.; Honda, Y.; Kitao, O.; Nakai, H.; Vreven, T.; Throssell, K.; Montgomery, J. A., Jr.; Peralta, J. E.; Ogliaro, F.; Bearpark, M. J.; Heyd, J. J.; Brothers, E. N.; Kudin, K. N.; Staroverov, V. N.; Keith, T. A.; Kobayashi, R.; Normand, J.; Raghavachari, K.; Rendell, A. P.; Burant, J. C.; Iyengar, S. S.; Tomasi, J.; Cossi, M.; Millam, J. M.; Klene, M.; Adamo, C.; Cammi, R.; Ochterski, J. W.; Martin, R. L.; Morokuma, K.; Farkas, O.; Foresman, J. B.; Fox, D. J. Gaussian, Inc., Wallingford CT, 2016.

[166] CYLview, 1.0b; Legault, C. Y., Université de Sherbrooke, 2009 (http://www.cylview.org)

linear iminium was found to be the ground state; higher energy iminium intermediates are depicted in Figure 3.35.

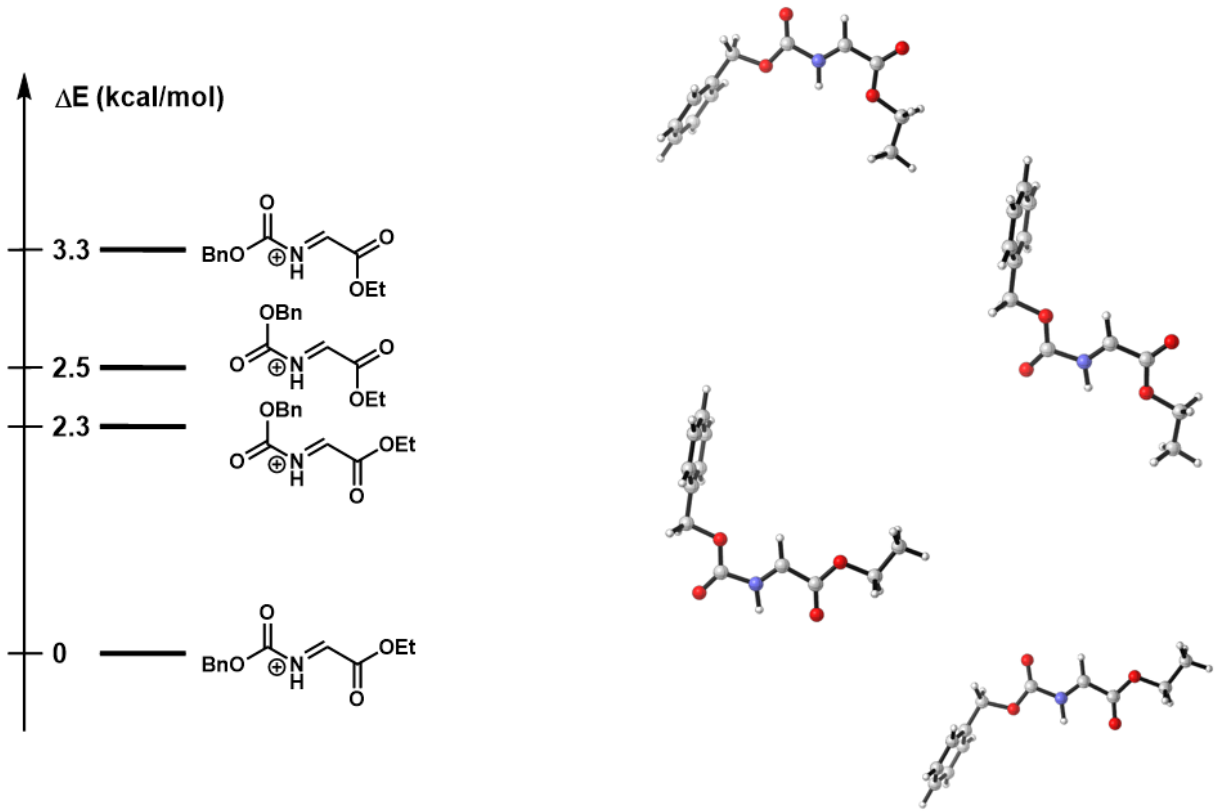

Figure 3.35 Iminium conformational landscape

Below are computational structures and energies for all stationary states discussed in section 3.3 with relevant keycards displayed and cartesian coordinates provided:

1-Cbz·methallylsilane: E(RB3LYP) -1847.995695

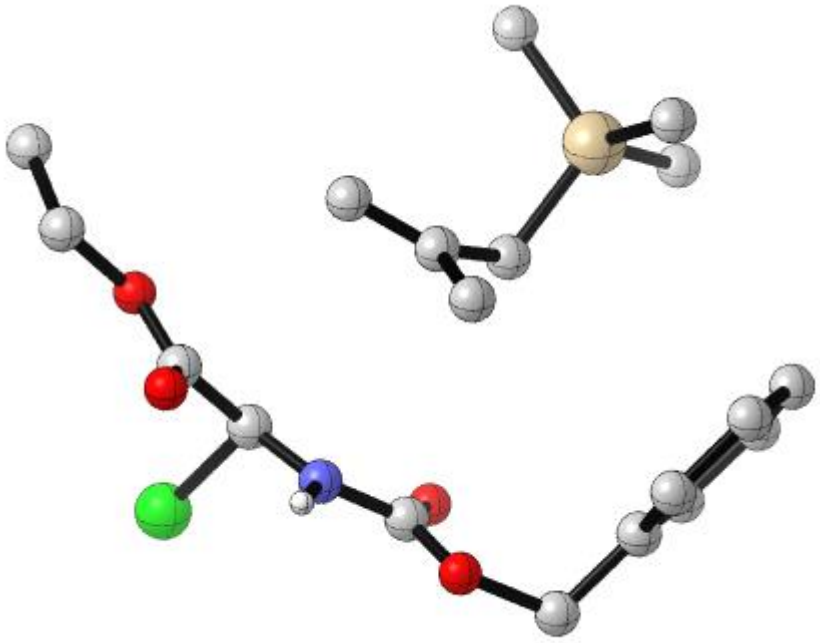

Keycard: opt freq=noraman b3lyp/6-311+g(d,p) scrf=(solvent=dichloromethane,pcm) empiricaldispersion=gd3bj

0 1

C	-2.49485100	-1.04890800	-0.41938300
H	-2.05460500	-0.44994200	-1.20690600
C	-3.39377500	-0.25028800	0.51524000
O	-4.00667600	0.72488800	-0.13424200
O	-3.52315800	-0.52146700	1.68642500
C	-4.92712000	1.55746000	0.63361100
H	-5.73879800	0.92046700	0.98845400
H	-4.38735700	1.94915200	1.49652500
C	-5.41304000	2.65375800	-0.28550100
H	-5.93412200	2.23788400	-1.15004400
H	-6.10794400	3.29766800	0.25840000
H	-4.57935200	3.26551200	-0.63600700
Cl	-3.67886500	-2.19091200	-1.36182800
N	-1.54045400	-1.75623100	0.30814100
C	-0.40998700	-2.26425400	-0.28077700
O	-0.10796300	-2.10329200	-1.44289800
O	0.29907700	-2.95607200	0.62811600
C	1.57499200	-3.49730300	0.17746100
H	1.77928900	-4.28899200	0.89629100
H	1.44482200	-3.92877000	-0.81340900
C	2.65710300	-2.45256500	0.18403700
C	3.07569200	-1.88290500	1.39061300

C	3.25520300	-2.04126100	-1.00808600
C	4.07200800	-0.91160600	1.40335700
H	2.61469000	-2.19728300	2.32030200
C	4.26532800	-1.08135400	-0.99555800
H	2.92346200	-2.46843300	-1.94702900
C	4.67181400	-0.51190300	0.20904700
H	4.38361900	-0.46996700	2.34261100
H	4.72583700	-0.77295000	-1.92653100
H	5.44913700	0.24312900	0.21807300
H	-1.76419600	-2.01194200	1.26129100
C	-1.16302400	1.95446200	0.75934200
H	-1.80449900	2.04702900	1.62845600
H	-1.50163200	2.42315300	-0.15781300
C	-0.00048600	1.29448000	0.82366300
C	0.93518900	1.19471900	-0.34994800
H	0.37510200	1.13101000	-1.28831800
H	1.55463400	0.29608200	-0.28356600
Si	2.07964500	2.70899800	-0.51749100
C	3.07937900	2.96976500	1.05876900
H	3.76935100	3.81063600	0.93727400
H	2.42629300	3.19452700	1.90675900
H	3.66714000	2.08285500	1.30732400
C	3.23527200	2.43538100	-1.98068200
H	2.66630400	2.25510200	-2.89783900
H	3.86544600	3.31524200	-2.14353500
H	3.88773500	1.57603100	-1.81502300
C	0.45776100	0.63601700	2.09710300
H	0.55227100	-0.44423100	1.95318700
H	1.44964000	0.99393500	2.38811300
H	-0.23709900	0.81862800	2.91866900
C	1.03033100	4.23968300	-0.84451600
H	0.43938800	4.12372000	-1.75826200
H	0.34005900	4.42974600	-0.01885200
H	1.66725800	5.12142900	-0.96559500

Imminium^{+}Cl^{-}: E(RB3LYP) -1281.892736

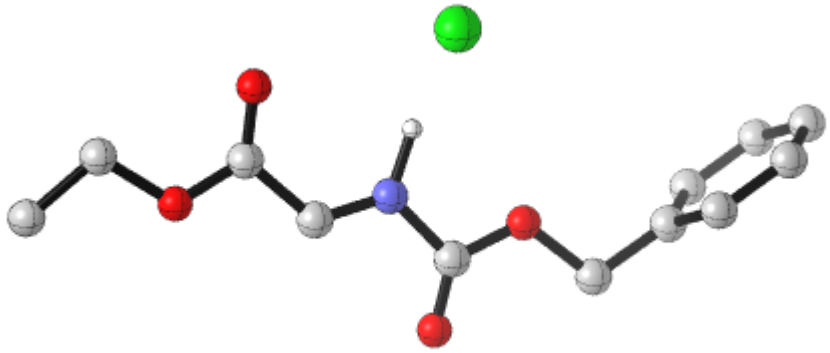

Keycard: opt freq=noraman b3lyp/6-311+g(d,p) scrf=(solvent=dichloromethane,pcm) empiricaldispersion=gd3bj

0 1

C	-2.28770900	-0.65036500	-0.00053900
H	-2.50850600	-1.71447800	-0.00050700
C	-3.43591300	0.32840400	-0.00049900
N	-1.07021700	-0.27297900	-0.00055800
H	-0.72573300	0.81314200	-0.00046400
O	-3.31155600	1.52383100	-0.00153600
C	-0.03343800	-1.31351200	-0.00053500
O	-0.30286000	-2.48169800	-0.00100200
O	1.13317200	-0.73189300	-0.00071100
O	-4.56517600	-0.36494300	0.00065400
C	-5.81108300	0.40738500	0.00091400
H	-5.80221900	1.04303300	0.88728800
H	-5.80287700	1.04262200	-0.88575500
C	-6.95528700	-0.57729700	0.00156100
H	-7.89764200	-0.02493700	0.00179400
H	-6.92863500	-1.21047400	-0.88720100
H	-6.92797400	-1.21009800	0.89057000
C	2.31025000	-1.63112800	-0.00113600
H	2.23532000	-2.25355500	-0.89183600
H	2.23500400	-2.25489900	0.88859500
C	3.53253900	-0.77195100	-0.00027400
C	4.10487400	-0.36095700	-1.20689400
C	4.10428500	-0.36264200	1.20719900
C	5.23470800	0.45286200	-1.20678500
H	3.66513000	-0.67877700	-2.14570900
C	5.23411900	0.45117000	1.20879300
H	3.66409300	-0.68180000	2.14534800
C	5.79993900	0.85957900	0.00142700
H	5.67380400	0.76770700	-2.14588500
H	5.67276100	0.76468500	2.14854900

H	6.68011300	1.49175600	0.00208700
Cl	-0.00902700	2.43913400	-0.00009400

methallylTMS: E(RB3LYP) -566.052592

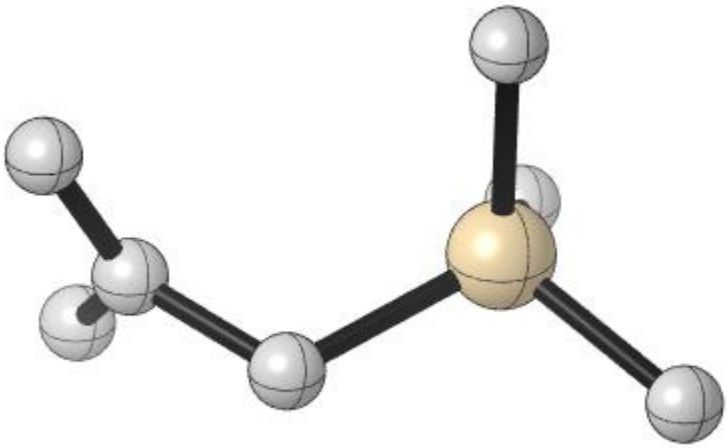

Keycard: opt freq=noraman b3lyp/6-311+g(d,p) scrf=(solvent=dichloromethane,pcm) empiricaldispersion=gd3bj

0 1

C	2.36228800	1.29211300	0.05654500
H	1.90141200	2.24067100	-0.19838200
H	3.28138700	1.32830400	0.63128800
C	1.82081400	0.12780100	-0.32050900
C	0.52717700	0.04808900	-1.08488200
H	0.51913100	-0.83366200	-1.73503700
H	0.40554800	0.92453100	-1.73027600
Si	-1.02749000	-0.01150000	0.01697300
C	-1.20874800	1.64300700	0.89744100
H	-2.08977000	1.64332500	1.54638600
H	-0.33193700	1.85409200	1.51551300
H	-1.31881900	2.46064200	0.17865800
C	-2.51633400	-0.31198500	-1.10001500
H	-2.43462000	-1.27477100	-1.61358000
H	-3.44446900	-0.31816800	-0.52036100
H	-2.60125900	0.46947300	-1.86119800
C	2.46958800	-1.18952500	0.01770000
H	1.77686000	-1.84469900	0.55377100
H	2.75298800	-1.71857900	-0.89915500
H	3.36350800	-1.05526700	0.62934200
C	-0.90843200	-1.39086000	1.29555800
H	-0.76671100	-2.36646700	0.82153300
H	-0.07766700	-1.22400700	1.98673800
H	-1.82883300	-1.43625400	1.88611600

SN2 Transition state 1: E(RB3LYP) -1847.969337

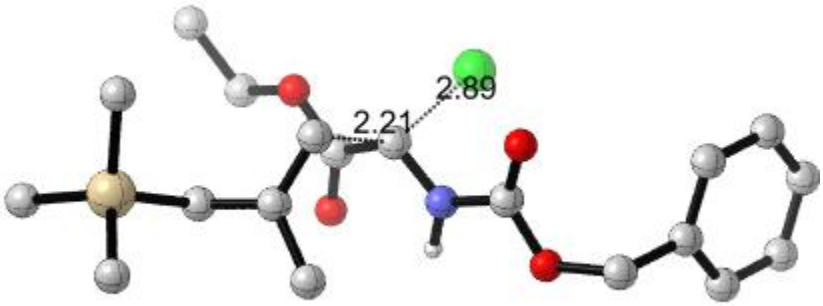

Keycard: opt=(calcfc,ts,noeigentest) freq=noraman b3lyp/6-311+g(d,p) scrf=(solvent=dichloromethane,pcm) empiricaldispersion=gd3bj

0 1

C	-0.01703600	0.65452700	0.23307200
H	0.20284300	0.90784200	1.25542100
C	-0.87943500	1.53714400	-0.61740100
O	-1.68743700	2.28787800	0.11262200
O	-0.85620100	1.46871300	-1.82714800
C	-2.50351900	3.26556000	-0.60051000
H	-1.82636900	4.02733200	-0.98983700
H	-2.98822500	2.76436200	-1.43846000
C	-3.49712600	3.82945800	0.38834200
H	-2.98654700	4.30203400	1.22928800
H	-4.11081100	4.58331300	-0.10995300
H	-4.15792300	3.04816200	0.77072300
Cl	1.56625600	3.06999000	0.26432300
N	0.85676700	-0.10201400	-0.44218500
C	1.85271600	-0.84646700	0.19460700
O	1.94073700	-0.93726500	1.39499200
O	2.61877500	-1.42625900	-0.72286400
C	3.76901600	-2.20205600	-0.23556100
H	3.47962100	-2.68966900	0.69305800
H	3.91886600	-2.94447500	-1.01561200
C	4.97200700	-1.32123000	-0.06363600
C	5.25415700	-0.73359700	1.17320800
C	5.81046400	-1.06292300	-1.15235900
C	6.35836600	0.10315400	1.31750100
H	4.60262300	-0.92654700	2.01672800
C	6.91367700	-0.22540200	-1.00932200
H	5.59818500	-1.51972200	-2.11292600
C	7.18812400	0.35945000	0.22673600
H	6.56918000	0.55648900	2.27883500
H	7.55833400	-0.03071100	-1.85829100
H	8.04614900	1.01183500	0.33932300
H	0.82796000	-0.07329800	-1.45650700

C	-1.56501900	-0.64287800	1.12385300
H	-2.04545500	0.11146100	1.73440800
H	-0.80695400	-1.25071900	1.60226100
C	-2.16645400	-1.07582200	-0.03571200
C	-3.39895900	-0.46677200	-0.54512100
H	-3.46217900	-0.51611100	-1.63498800
H	-3.50816400	0.56729900	-0.21214800
Si	-4.99209100	-1.32882100	0.14431500
C	-5.03580700	-1.06408300	2.00190300
H	-5.95004300	-1.49467700	2.42111600
H	-4.18471100	-1.53971400	2.49621600
H	-5.02187600	0.00086700	2.25071100
C	-6.42986600	-0.46398600	-0.69877800
H	-6.38729700	-0.59348900	-1.78376300
H	-7.37984700	-0.87657200	-0.34629500
H	-6.42701400	0.60798300	-0.48240000
C	-1.54382700	-2.16885500	-0.83932600
H	-2.30155100	-2.85933900	-1.21465300
H	-1.06933600	-1.72761500	-1.72566700
H	-0.79176200	-2.72469600	-0.28156200
C	-4.96953900	-3.15999600	-0.26973700
H	-4.87335900	-3.32763100	-1.34608400
H	-4.15103300	-3.68036400	0.23452800
H	-5.90638500	-3.62177600	0.05654400

SN2 Transition state 2: E(RB3LYP) -1847.966979

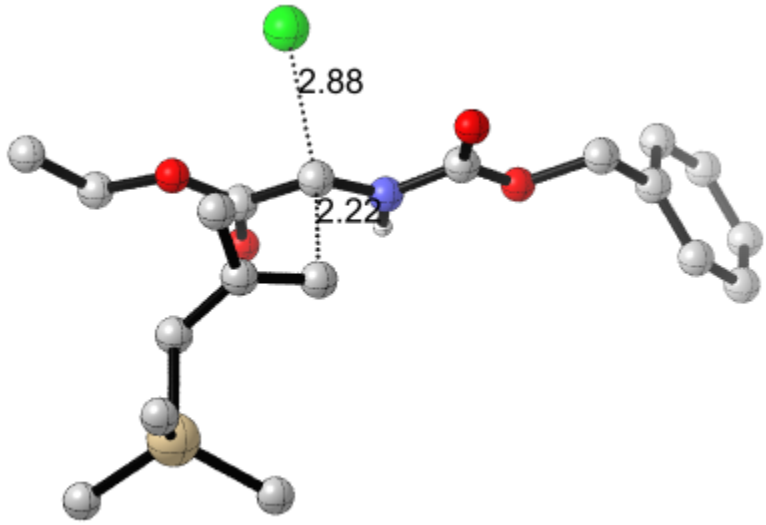

Keycard: p opt=(calcfc,ts,noeigentest) freq=noraman b3lyp/6-311+g(d,p) scrf=(solvent=dichloromethane,pcm) empiricaldispersion=gd3bj

0 1

C	-0.24015400	1.06081200	0.35005800

H	-0.40087300	1.39482900	1.35980300
C	-1.07372800	1.57465100	-0.78503200
O	-2.16876300	2.17803800	-0.35741500
O	-0.76406500	1.37983000	-1.94036700
C	-3.00805200	2.80854900	-1.37018500
H	-2.39965500	3.55718300	-1.87931900
H	-3.30572300	2.04689500	-2.09161200
C	-4.19007400	3.42211900	-0.65700100
H	-3.86095100	4.15992600	0.07669700
H	-4.82890500	3.92316300	-1.38777600
H	-4.78472900	2.66033800	-0.14853600
Cl	0.59524600	3.82039900	0.41457000
N	0.96868700	0.60109600	0.01105700
C	1.93691300	0.27633300	0.96445000
O	1.72977100	0.30448800	2.15350500
O	3.06381800	-0.06403000	0.35039300
C	4.19206300	-0.40733100	1.22561200
H	4.40536500	0.46420800	1.84392700
H	3.88139200	-1.23398200	1.86366600
C	5.34645700	-0.77561700	0.34650500
C	6.18645700	0.21689500	-0.16665100
C	5.58336700	-2.11217100	0.01576700
C	7.24676100	-0.12245800	-1.00316000
H	6.00880500	1.25524900	0.09066300
C	6.64517300	-2.45405400	-0.81918400
H	4.93714100	-2.88583000	0.41590400
C	7.47704300	-1.45882900	-1.33049000
H	7.89432700	0.65257100	-1.39568700
H	6.82424100	-3.49344400	-1.06783500
H	8.30452100	-1.72348300	-1.97833100
H	1.19384000	0.52692500	-0.97637200
C	-1.30363000	-0.85581500	0.72689300
H	-0.70244200	-0.98851900	1.61784200
H	-0.96881000	-1.35717300	-0.17293800
C	-2.61782300	-0.46619100	0.84282300
C	-3.56152000	-0.60554300	-0.26972900
H	-3.06284200	-0.56636900	-1.24220000
H	-4.35787500	0.14089100	-0.23096500
Si	-4.44045800	-2.33476500	-0.27144800
C	-5.31179900	-2.61702800	1.36787300
H	-5.87722400	-3.55302000	1.32671900
H	-4.60215900	-2.69512600	2.19577000
H	-6.01705000	-1.81230500	1.59353400
C	-5.67332400	-2.26639100	-1.68601200
H	-5.17138800	-2.07209700	-2.63785600
H	-6.20375200	-3.21936600	-1.77233000

H	-6.41586700	-1.48017100	-1.52430900
C	-3.11612900	0.14692800	2.11045900
H	-3.25491700	1.22139100	1.94480900
H	-4.09423000	-0.25704800	2.38004500
H	-2.42353200	0.00737500	2.94001200
C	-3.13790500	-3.65313500	-0.56744500
H	-2.59462000	-3.47114600	-1.49900000
H	-2.41219200	-3.68927900	0.24917600
H	-3.61015000	-4.63729600	-0.64055400

SN2 Transition state 3: E(RB3LYP) -1847.975459

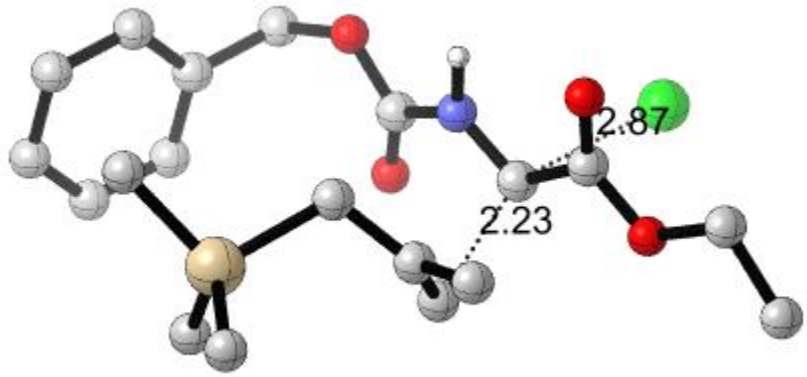

Keycard: opt=(calcfc,ts,noeigentest) freq=noraman b3lyp/6-311+g(d,p) scrf=(solvent=dichloromethane,pcm) empiricaldispersion=gd3bj

0 1

C	1.91767700	-0.81593000	0.25739600
H	2.04191400	-1.18184600	1.26114100
C	3.06074600	-0.21725700	-0.50223400
O	4.01378800	0.21521800	0.30436400
O	3.02763000	-0.09827200	-1.70845900
C	5.22104100	0.73818400	-0.32579100
H	5.66905500	-0.07515300	-0.89857300
H	4.93274900	1.53473300	-1.01237900
C	6.12658800	1.23019100	0.77891800
H	6.38426200	0.41868000	1.46182100
H	7.04905900	1.61823000	0.34093400
H	5.65140300	2.03300700	1.34669600
Cl	3.65170300	-3.09989700	0.13664600
N	0.92782200	-1.31264400	-0.49011800
C	-0.12858500	-2.04496500	0.06166600
O	-0.26650500	-2.20744000	1.24888300
O	-0.91556600	-2.48146300	-0.91496900
C	-2.14579000	-3.17264500	-0.50599800
H	-2.39532200	-3.77009300	-1.37940900

H	-1.90952300	-3.82320100	0.33331900
C	-3.22979900	-2.18819000	-0.17054200
C	-3.93616000	-1.54888800	-1.19490200
C	-3.54286000	-1.89818000	1.16012000
C	-4.93882800	-0.63156300	-0.89302100
H	-3.70249900	-1.77479900	-2.22963200
C	-4.54986400	-0.98358900	1.46274800
H	-2.99320000	-2.38640500	1.95562300
C	-5.24709200	-0.34784800	0.43733600
H	-5.48262800	-0.14298300	-1.69273600
H	-4.78610600	-0.76512500	2.49741900
H	-6.02757700	0.36605900	0.67279500
H	0.97826100	-1.18657500	-1.49654200
C	1.12117800	1.00469200	1.26334300
H	1.95134700	1.18952900	1.93308300
H	0.29874200	0.41608900	1.65147300
C	0.94648900	1.78705400	0.14724100
C	-0.24936000	1.66537500	-0.69056700
H	-0.66714400	0.65444400	-0.66714100
H	-0.05487100	1.95773300	-1.72518300
Si	-1.72256700	2.75865200	-0.06303400
C	-1.15918700	4.54025700	0.12379300
H	-2.00985200	5.16687200	0.40884300
H	-0.39701200	4.64370100	0.90081300
H	-0.75425400	4.93545100	-0.81198100
C	-3.05275000	2.60779100	-1.37765500
H	-3.34024700	1.56428800	-1.52455600
H	-3.94642400	3.16358000	-1.07853000
H	-2.70751400	3.01062000	-2.33391700
C	1.98717000	2.77687900	-0.26970700
H	2.38418700	2.50238000	-1.25289900
H	1.53471700	3.76532400	-0.38626800
H	2.80506700	2.84441200	0.44579400
C	-2.29561000	2.06344000	1.58153400
H	-2.57153300	1.01014000	1.49099700
H	-1.52068600	2.15424600	2.34703600
H	-3.17695100	2.60910800	1.93165700

SN2 Transition state 4: E(RB3LYP) -1847.965746

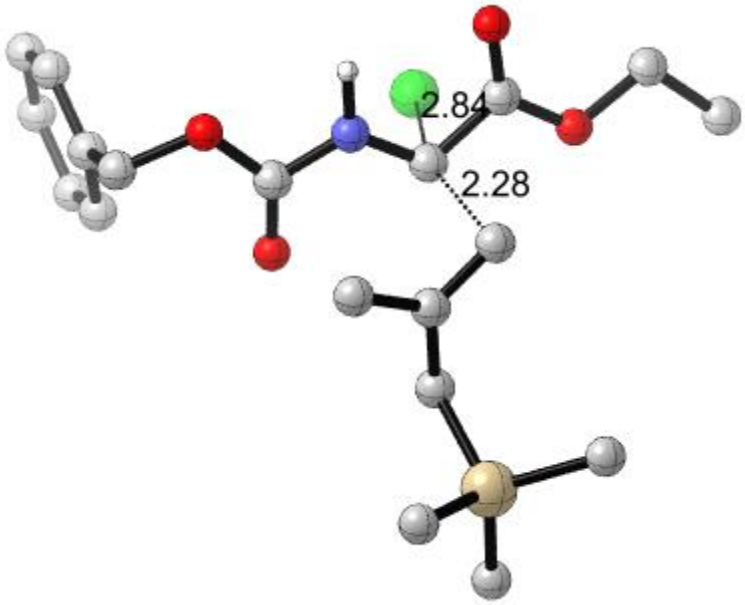

Keycard: opt=(calcfc,ts,noeigentest) freq=noraman b3lyp/6-311+g(d,p) scrf=(solvent=dichloromethane,pcm) empiricaldispersion=gd3bj

0 1

C	-0.29963500	1.26850000	-0.31587000
H	-0.45601300	0.87578100	0.67244600
C	-0.72367400	2.66067600	-0.69707500
O	-1.61884200	3.15349700	0.14015000
O	-0.30495200	3.19382100	-1.70149700
C	-2.04854600	4.52722300	-0.09413400
H	-1.16458500	5.16393500	-0.03618900
H	-2.46045600	4.58760200	-1.10262200
C	-3.06991100	4.86464900	0.96693900
H	-2.63653400	4.78006800	1.96518300
H	-3.40934000	5.89321000	0.82455000
H	-3.93722600	4.20438300	0.90010000
Cl	1.42181400	2.75917500	1.38650800
N	0.66432100	0.74672500	-1.07774000
C	1.35408900	-0.41540700	-0.71464700
O	1.05040800	-1.08754600	0.23930000
O	2.32991900	-0.63633300	-1.58783200
C	3.19483200	-1.79719300	-1.33042700
H	2.57048000	-2.61030600	-0.96533300
H	3.58245900	-2.03961200	-2.31692600
C	4.29249100	-1.45040200	-0.36727100
C	5.44419800	-0.80215800	-0.82436000
C	4.16860700	-1.75019500	0.99209000
C	6.45624000	-0.45328700	0.06572100

H	5.54664700	-0.57071700	-1.87902000
C	5.18245200	-1.40498700	1.88293700
H	3.27309000	-2.24339000	1.34971100
C	6.32581800	-0.75452800	1.42148600
H	7.34502400	0.04982400	-0.29641900
H	5.07806100	-1.63921000	2.93572700
H	7.11304400	-0.48340600	2.11520300
H	0.97347700	1.28102900	-1.88465100
C	-2.31723200	0.46531900	-1.00374600
H	-2.24822500	0.84641200	-2.01629500
H	-2.88940500	1.04669100	-0.29325300
C	-2.04299300	-0.85487900	-0.74746000
C	-2.35760900	-1.46824700	0.54878900
H	-2.44052000	-0.71902700	1.34089900
H	-1.61149600	-2.21329600	0.83364300
Si	-4.06690200	-2.37381200	0.55812300
C	-4.04692800	-3.79966600	-0.66586200
H	-3.19299300	-4.46031700	-0.49191800
H	-4.95881000	-4.39436200	-0.55500500
H	-4.00383600	-3.45170700	-1.70083000
C	-4.29402200	-3.01004500	2.31070800
H	-4.28154200	-2.18894000	3.03274300
H	-5.25244700	-3.52922600	2.40509300
H	-3.50105100	-3.71308900	2.58047100
C	-1.43343100	-1.70252700	-1.82080700
H	-0.91864000	-2.57258900	-1.41607000
H	-2.22114800	-2.05680300	-2.49449100
H	-0.74490800	-1.11846900	-2.43686300
C	-5.39534800	-1.12445700	0.11114200
H	-5.39324800	-0.28167800	0.80835200
H	-5.24862800	-0.72971700	-0.89787400
H	-6.38430900	-1.59059900	0.14958800

Betasilylcation 1: E(RB3LYP) -1847.996848

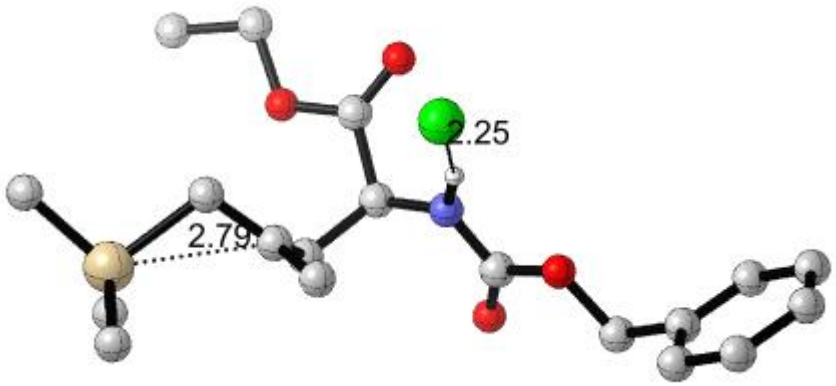

Keycard: opt freq=noraman b3lyp/6-311+g(d,p) scrf=(solvent=dichloromethane,pcm) empiricaldispersion=gd3bj

0 1

C	-0.64723800	1.26040800	-0.86448300
H	-0.56009900	1.76304600	-1.83242600
C	-1.30818300	2.28021600	0.06428100
O	-2.62757200	2.33987800	-0.15303400
O	-0.71050800	2.97486200	0.84603400
C	-3.37692300	3.33609900	0.60583400
H	-3.21607900	3.14419400	1.66729900
H	-2.97104200	4.31950100	0.36560800
C	-4.83031100	3.20432300	0.21044600
H	-5.22155400	2.21562200	0.46089300
H	-5.41904700	3.94873100	0.75124100
H	-4.96203700	3.37412900	-0.86009800
N	0.67630000	0.94962300	-0.41350300
C	1.64208900	0.64588300	-1.31632700
O	1.48794200	0.64773600	-2.52944400
O	2.79797300	0.33837900	-0.69703500
C	3.90803900	-0.02295200	-1.56552200
H	3.62088100	-0.89972900	-2.14749700
H	4.10004000	0.80499200	-2.24842800
C	5.09234800	-0.30318600	-0.68878900
C	5.29882100	-1.58259200	-0.16600700
C	5.98915600	0.71811200	-0.36517100
C	6.38350200	-1.83765200	0.66991000
H	4.60632400	-2.37971100	-0.41380100
C	7.07548200	0.46632300	0.47014100
H	5.83428200	1.71301200	-0.76825900
C	7.27347300	-0.81248600	0.98951200
H	6.53475100	-2.83310000	1.07076200
H	7.76561300	1.26527700	0.71479700
H	8.11827400	-1.00992200	1.63910400

H	0.86584600	0.83109800	0.58797600
C	-1.53797400	0.00303000	-1.18507400
H	-2.47637700	0.37405400	-1.59011500
H	-1.00156800	-0.54900500	-1.95763000
C	-1.77753300	-0.86825500	-0.00544200
C	-0.73933500	-1.80436900	0.40598100
H	-0.11171600	-2.15340100	-0.41220000
H	-0.08834700	-1.20647000	1.10016800
H	-1.11842500	-2.62503700	1.01402400
C	-2.97575700	-0.75459600	0.72399200
H	-2.93759200	-1.14596100	1.74073200
H	-3.48812600	0.20044100	0.62291700
Si	-4.32550600	-1.99836700	-0.11549500
C	-4.57889900	-1.48867600	-1.89484000
H	-3.69742600	-1.67776800	-2.51146900
H	-5.40544100	-2.07424700	-2.30938000
H	-4.84685000	-0.43257100	-1.98006800
C	-3.68259000	-3.74307700	0.05331000
H	-4.45770700	-4.43741300	-0.28582400
H	-2.79236400	-3.91472100	-0.55584000
H	-3.44743800	-3.98842800	1.09207000
C	-5.83452600	-1.67240500	0.93897500
H	-6.66141600	-2.29224600	0.57893400
H	-5.65225500	-1.92313400	1.98636400
H	-6.14234200	-0.62591600	0.87829300
Cl	0.89574700	0.05839500	2.69981100

Betasilylcation 2: E(RB3LYP) -1847.996283

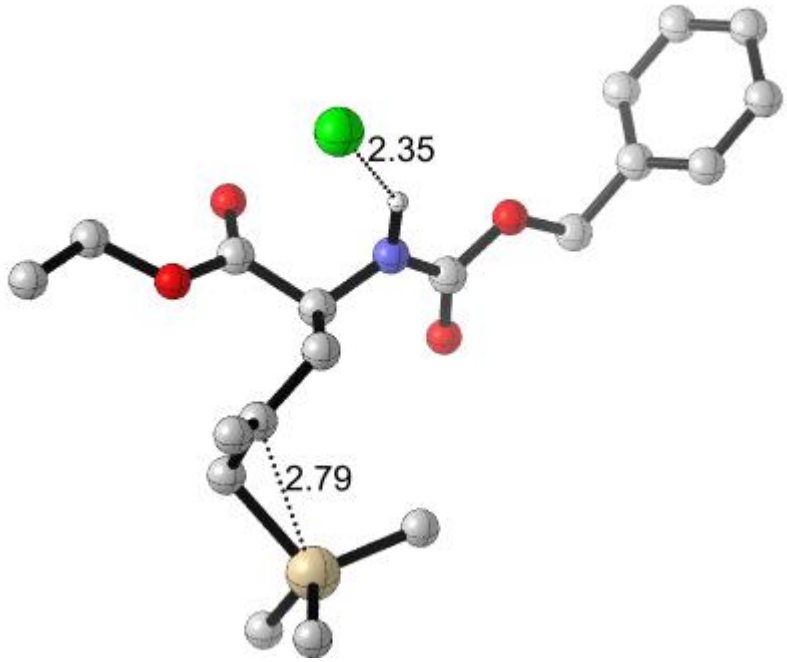

Keycard: opt freq=noraman b3lyp/6-311+g(d,p) scrf=(solvent=dichloromethane,pcm) empiricaldispersion=gd3bj

Title Card Required

0 1

C	0.80506700	-0.52852900	-0.35641900
H	0.99890300	0.23971000	-1.10843900
C	1.20820000	-1.86282700	-1.00161100
O	2.42995000	-2.23644500	-0.60796000
O	0.53252400	-2.45801600	-1.80358900
C	2.96574100	-3.47118600	-1.16359900
H	2.28593800	-4.28072000	-0.89566400
H	2.98481900	-3.37514500	-2.25020300
C	4.34681400	-3.66264200	-0.57920600
H	4.30089800	-3.75407200	0.50787100
H	4.78699300	-4.57808800	-0.98093700
H	4.99998500	-2.82594200	-0.83711400
N	-0.61171700	-0.50043800	-0.11457200
C	-1.40410400	0.44682900	-0.66503900
O	-1.01993900	1.35658100	-1.38778800
O	-2.69132400	0.26225700	-0.30135400
C	-3.64295800	1.22725500	-0.82956000
H	-3.36058300	2.22128000	-0.48056600
H	-3.58908500	1.20826100	-1.91847000
C	-5.00390200	0.83410700	-0.33618900
C	-5.49071700	1.33600700	0.87364400

C	-5.79120800	-0.05706500	-1.07018100
C	-6.74415900	0.95160800	1.34525400
H	-4.88538600	2.02981500	1.44695400
C	-7.04484000	-0.44373600	-0.60149600
H	-5.41940700	-0.44883800	-2.01071000
C	-7.52288800	0.06018400	0.60790500
H	-7.11306000	1.34723900	2.28436000
H	-7.64789500	-1.13495300	-1.17857000
H	-8.49865300	-0.23871200	0.97285400
H	-0.99151400	-1.22757000	0.49176100
C	1.58859400	-0.23776900	0.93256900
H	1.15716600	0.65688500	1.40227500
H	1.41573400	-1.04629300	1.64822000
C	3.04073500	0.03624000	0.81039100
C	3.86680000	-0.29642900	1.99016400
H	3.35305400	-0.03914600	2.91988400
H	3.95845600	-1.39144800	1.99058500
H	4.86395900	0.13715100	1.95774100
C	3.61387900	0.64855100	-0.30881200
H	4.69523500	0.55294400	-0.39383000
H	3.08988100	0.55501600	-1.25578400
Si	3.46431600	2.66720600	-0.00259100
C	1.67279900	3.13265000	0.22671600
H	1.30718600	2.90607000	1.23050600
H	1.59873000	4.21736500	0.09431500
H	1.00715000	2.66663900	-0.50366000
C	4.52554400	3.09410500	1.47123700
H	4.55669700	4.18375100	1.57037800
H	4.12416700	2.68945400	2.40266800
H	5.55210700	2.74123200	1.34821400
C	4.17067600	3.28495600	-1.61850400
H	4.19954400	4.37861300	-1.59105100
H	5.18789200	2.92025800	-1.77704800
H	3.55121400	2.98253200	-2.46578300
Cl	-0.33286100	-2.96941000	1.92114500

Betasilylcation 3: E(RB3LYP) -1848.010925

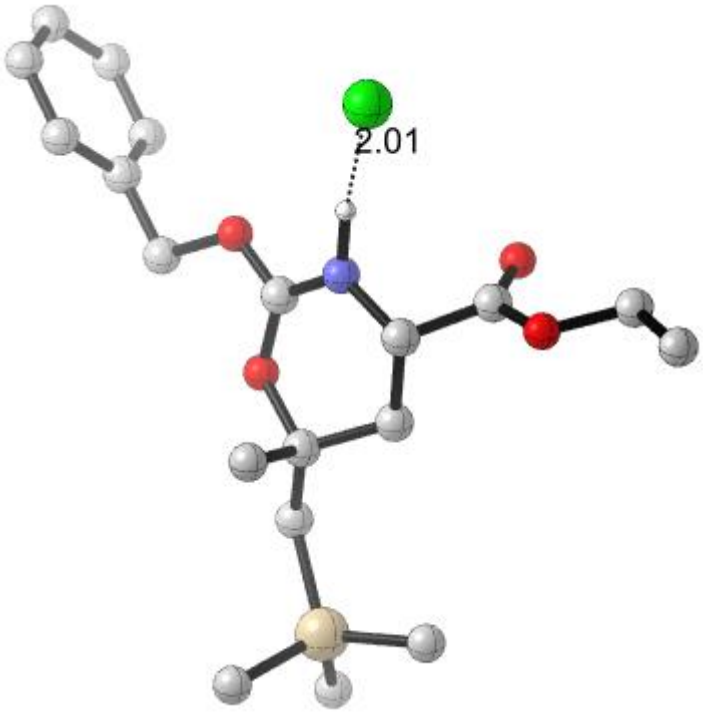

Keycard: opt freq=noraman b3lyp/6-311+g(d,p) scrf=(solvent=dichloromethane,pcm) empiricaldispersion=gd3bj

0 1

C	1.06621500	1.37734700	0.28372400
H	1.35445600	1.59708100	1.31242500
C	1.41788900	2.58735400	-0.58376400
O	2.46098200	3.23070900	-0.06494500
O	0.86178800	2.86912000	-1.61677600
C	2.97442500	4.37090100	-0.81827900
H	3.26785200	4.01744200	-1.80801000
H	2.16287300	5.09038900	-0.93137600
C	4.14047200	4.93765900	-0.04173800
H	4.93407200	4.19603700	0.07173000
H	4.54767300	5.79676100	-0.58001900
H	3.82453500	5.27156100	0.94856100
N	-0.36933900	1.14528900	0.22916400
C	-0.90300400	-0.03353900	0.04802400
O	-0.23244900	-1.14267000	-0.03587400
O	-2.20172600	-0.09746400	-0.05932700
C	-2.84374700	-1.43090300	-0.14520700
H	-2.46627400	-1.91892700	-1.04164900
H	-2.54412900	-1.99407000	0.73699900
C	-4.31954600	-1.20218500	-0.20211900
C	-4.96647300	-1.08794400	-1.43520800

C	-5.05973800	-1.08102600	0.97717100
C	-6.33838000	-0.85403500	-1.48981800
H	-4.39495300	-1.18241200	-2.35189300
C	-6.43101200	-0.84602300	0.92408500
H	-4.56118100	-1.16940900	1.93611900
C	-7.07117900	-0.73193300	-0.30987100
H	-6.83399000	-0.76749200	-2.44937600
H	-6.99914100	-0.75281200	1.84188300
H	-8.13869900	-0.55027600	-0.35144600
H	-0.99094300	1.96633900	0.44073200
C	1.81814100	0.15286500	-0.24759600
H	1.74248500	0.12057400	-1.33673600
H	2.87042100	0.24123300	0.01283900
C	1.25507500	-1.14599900	0.31823500
C	1.31362800	-1.23757300	1.83613700
H	2.35144600	-1.16327900	2.16479200
H	0.75351800	-0.43492800	2.31768000
H	0.91026000	-2.19261200	2.17333200
C	1.78598600	-2.37284100	-0.39201500
H	1.14360600	-3.22107700	-0.13094100
H	1.68277700	-2.22527800	-1.47168800
Si	3.57474100	-2.97566500	-0.07003300
C	4.82953300	-1.57127800	-0.09062300
H	4.71352600	-0.89140500	0.75796800
H	5.83784000	-1.99282000	-0.03219600
H	4.76852500	-0.98611500	-1.01233200
C	3.66730200	-3.89050300	1.57253600
H	4.65557500	-4.34607800	1.68788500
H	3.50345400	-3.23256200	2.42893400
H	2.92335400	-4.69135300	1.61522600
C	3.94257000	-4.17236900	-1.47407100
H	4.93050700	-4.62403100	-1.34534800
H	3.20580300	-4.98046900	-1.50635200
H	3.92810300	-3.66294700	-2.44196300
Cl	-1.72482700	3.69645900	1.15048700

Product 2a: E(RB3LYP) -978.391801

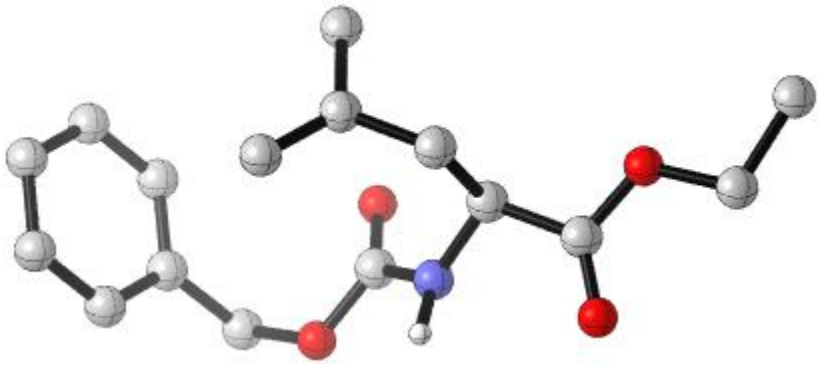

Keycard: opt freq=noraman b3lyp/6-311+g(d,p) scrf=(solvent=dichloromethane,pcm) empiricaldispersion=gd3bj

0 1

C	-1.76757800	-0.10428500	0.01873700
H	-1.76261900	0.08963600	1.09021900
C	-3.15552400	-0.57202300	-0.38766600
O	-4.09744200	0.16976600	0.20004600
O	-3.37636400	-1.46409000	-1.17593000
C	-5.48137900	-0.10358000	-0.16521800
H	-5.58008200	0.02259900	-1.24462300
H	-5.69989500	-1.14331000	0.08276400
C	-6.35230700	0.86259100	0.60537700
H	-6.11039100	1.89656200	0.35055200
H	-7.40057900	0.68324100	0.35488500
H	-6.22872700	0.72742500	1.68190500
N	-0.80402000	-1.15047300	-0.24306900
C	0.28555200	-1.30609100	0.55275700
O	0.41408000	-0.84078100	1.67099900
O	1.20656400	-2.09193600	-0.05727200
C	2.51243300	-2.15274400	0.58113000
H	2.37931300	-2.27751800	1.65434300
H	2.96415000	-3.04984900	0.16139200
C	3.32521400	-0.92556900	0.26348300
C	3.48054400	0.09321000	1.20612700
C	3.90653700	-0.77829500	-0.99992200
C	4.20533400	1.24150700	0.89257100
H	3.01680000	-0.00980300	2.17930600
C	4.62699000	0.36982600	-1.31784500
H	3.79068600	-1.56555800	-1.73717800
C	4.77761800	1.38303500	-0.37045800
H	4.31735900	2.02703800	1.63090400
H	5.07216800	0.47436300	-2.30049100
H	5.33828600	2.27742400	-0.61648300
H	-0.73781000	-1.50358800	-1.18686700

C	-1.43158900	1.20807200	-0.75223200
H	-1.50191100	1.00015600	-1.82348700
H	-2.19882400	1.94675300	-0.50348500
C	-0.05834200	1.73462800	-0.41608200
C	0.96539100	1.56192500	-1.25439000
H	0.83601100	1.06008300	-2.20735000
H	1.96522400	1.89900500	-1.00754200
C	0.09552200	2.41379000	0.91758300
H	-0.57351400	3.27792100	0.99241200
H	-0.16008800	1.72968300	1.73185500
H	1.12137300	2.75138800	1.07199800

TMSCl: E(RB3LYP) -869.643001

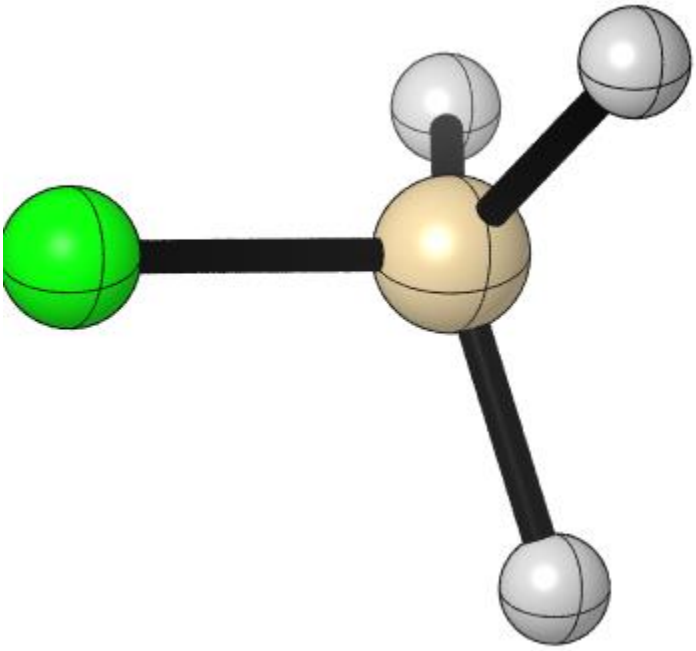

Keycard: opt freq=noraman b3lyp/6-311+g(d,p) scrf=(solvent=dichloromethane,pcm) empiricaldispersion=gd3bj

0 1

Si	0.36275400	-0.00005600	0.00003800
C	0.88761500	0.73082900	-1.63699800
H	0.51453000	1.75173800	-1.74957500
H	1.98029800	0.75821200	-1.69620200
H	0.51595500	0.13216100	-2.47215500
C	0.88674100	1.05285800	1.45137300
H	0.51267000	2.07466500	1.35101600
H	0.51512100	0.63878900	2.39189100
H	1.97933400	1.09299300	1.50410400
C	0.88796200	-1.78307200	0.18606600

H	0.51483000	-2.20748700	1.12134100
H	0.51646000	-2.39081700	-0.64262300
H	1.98066200	-1.84758300	0.19375300
Cl	-1.76954900	-0.00032800	-0.00027800

Selected computations performed in water PCM:

Imminium^{+}Cl^{-} (H_2O PCM): E(RB3LYP) -1281.628517

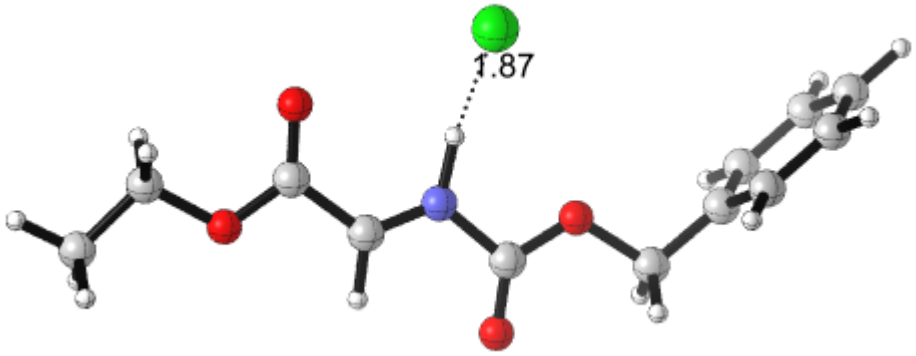

Keycard: opt freq=noraman b3lyp/6-31g(d) scrf=(solvent=water,pcm) empiricaldispersion=gd3bj

0 1

C	-2.30041300	-0.67892700	-0.00187700
H	-2.51878500	-1.74428700	-0.00218400
C	-3.43444100	0.31409800	-0.00132700
N	-1.07698400	-0.30564700	-0.00191800
H	-0.74738500	0.75214900	-0.00165300
O	-3.28283800	1.51383600	-0.00268400
C	-0.03600600	-1.34210800	-0.00232200
O	-0.30620400	-2.51516300	-0.00350400
O	1.13003800	-0.75061400	-0.00115200
O	-4.57555300	-0.35895500	0.00083700
C	-5.79915200	0.44354900	0.00194200
H	-5.77432900	1.08134800	0.88918900
H	-5.77663100	1.08030000	-0.88611500
C	-6.96710900	-0.51646500	0.00401600
H	-7.89955500	0.05639600	0.00487300
H	-6.95257400	-1.15237900	-0.88596700
H	-6.95028900	-1.15133000	0.89470700
C	2.30600500	-1.64860700	-0.00130700
H	2.23027000	-2.27323900	-0.89297000
H	2.22911400	-2.27510500	0.88894700
C	3.52446400	-0.78116100	0.00040300
C	4.09125200	-0.35992100	-1.20817400
C	4.08992000	-0.36289000	1.21063000
C	5.21113100	0.47115300	-1.20717600

H	3.65452800	-0.68528300	-2.14848400
C	5.20980700	0.46817000	1.21291900
H	3.65215700	-0.69057300	2.14964900
C	5.77079200	0.88589700	0.00369300
H	5.64791200	0.79188300	-2.14811900
H	5.64555400	0.78657700	2.15513100
H	6.64480300	1.53060200	0.00496800
Cl	0.04312100	2.44487800	-0.00147300

MethallylTMS (H_2O PCM): E(RB3LYP) -565.940591

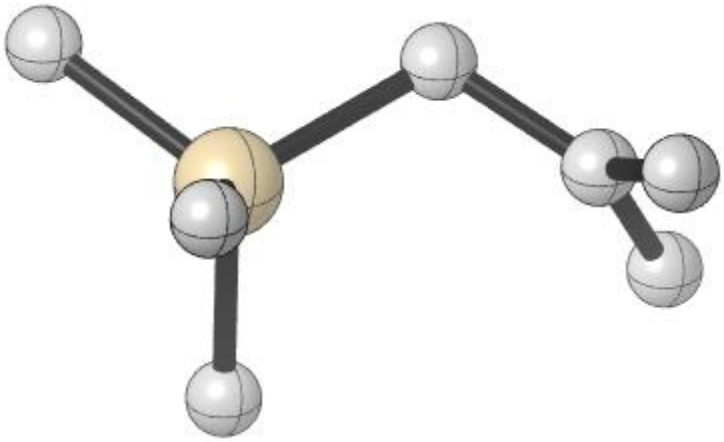

Keycard: opt freq=noraman b3lyp/6-31g(d) scrf=(solvent=water,pcm) empiricaldispersion=gd3bj

0 1

C	2.35767900	1.29257900	0.05634900
H	1.89959000	2.24447700	-0.20205500
H	3.27668700	1.33207100	0.63581500
C	1.81754800	0.12656700	-0.32462700
C	0.52436300	0.04617500	-1.09514300
H	0.51871800	-0.83507800	-1.75026800
H	0.40405800	0.92545200	-1.74132400
Si	-1.02745500	-0.01167700	0.01648400
C	-1.21439300	1.66094300	0.87235800
H	-2.07598700	1.66386000	1.55055400
H	-0.32019700	1.89951300	1.45902300
H	-1.35906200	2.46526900	0.14112000
C	-2.52583200	-0.34576500	-1.08646000
H	-2.43957500	-1.31846800	-1.58542400
H	-3.45328500	-0.35065400	-0.50123800
H	-2.62434400	0.42176900	-1.86340300
C	2.46875000	-1.19115600	0.01538000
H	1.77668400	-1.84986300	0.55345900
H	2.75507000	-1.72495100	-0.90107300
H	3.36459500	-1.05687500	0.62925500

C	-0.88644900	-1.37138400	1.32116400
H	-0.73745800	-2.35646700	0.86367500
H	-0.04916000	-1.18600100	2.00358200
H	-1.80196000	-1.41833100	1.92339900

SN2 Transition state 1 (H_2O PCM): E(RB3LYP) -1847.598219

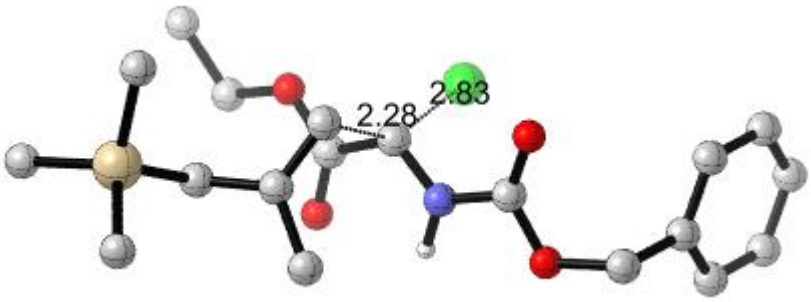

Keycard: opt=(calcfc,ts,noeigentest) freq=noraman b3lyp/6-31g(d) scrf=(solvent=water,pcm) empiricaldispersion=gd3bj

0 1

C	0.04403600	0.64494100	0.19629900
H	0.25855700	0.84357700	1.23256500
C	-0.85476900	1.51985100	-0.61766100
O	-1.62672400	2.28394600	0.14229400
O	-0.88339000	1.43854300	-1.83266700
C	-2.49642700	3.22231100	-0.55582100
H	-1.85677800	3.98051400	-1.01616600
H	-3.02444400	2.68371700	-1.34542100
C	-3.43747500	3.80929600	0.47330200
H	-2.88154000	4.31635700	1.26748800
H	-4.09382100	4.53883400	-0.01113500
H	-4.06126600	3.03048400	0.92382400
Cl	1.63172000	2.99072700	0.22389100
N	0.88682900	-0.11893200	-0.50256700
C	1.89393600	-0.87222700	0.11480600
O	2.00826300	-0.94842400	1.32001200
O	2.63165600	-1.46388400	-0.81801700
C	3.78503700	-2.23470000	-0.33599300
H	3.48011600	-2.77892200	0.55821900
H	3.97190600	-2.93328000	-1.15094900
C	4.95985900	-1.33312000	-0.08143000
C	5.25812100	-0.89855600	1.21541400
C	5.75143100	-0.89703900	-1.15146800
C	6.33564500	-0.04086400	1.43959300
H	4.63938900	-1.22867700	2.04371000
C	6.82568600	-0.03646700	-0.92918000
H	5.52454400	-1.23517500	-2.15924600

C	7.11914100	0.39242200	0.36796400
H	6.56257100	0.28911500	2.44910400
H	7.43556400	0.29534700	-1.76426100
H	7.95786800	1.06008600	0.54263200
H	0.82260300	-0.09505100	-1.51735700
C	-1.52508400	-0.74183800	1.08786400
H	-1.95086300	-0.04762900	1.80613100
H	-0.72667800	-1.38550800	1.44353000
C	-2.19347800	-1.02820900	-0.07799300
C	-3.44967800	-0.34877400	-0.43992700
H	-3.55525100	-0.23544500	-1.52456200
H	-3.52570300	0.63249000	0.03824300
Si	-5.01917500	-1.28812100	0.19346700
C	-4.95355000	-1.31421100	2.07442100
H	-5.84924400	-1.79616900	2.48341000
H	-4.07960400	-1.86776700	2.43533000
H	-4.90234000	-0.29811700	2.48245500
C	-6.48671700	-0.28220700	-0.42451300
H	-6.50833300	-0.24636200	-1.51966000
H	-7.42927300	-0.72573200	-0.08273500
H	-6.44385300	0.74774500	-0.05200800
C	-1.63574900	-2.02024200	-1.05039600
H	-2.41527300	-2.70273700	-1.40335200
H	-1.27634200	-1.48068400	-1.93839200
H	-0.81299000	-2.60406600	-0.63365500
C	-5.06208800	-3.03918800	-0.49865700
H	-4.99976100	-3.04265900	-1.59294600
H	-4.24162600	-3.65069900	-0.10699900
H	-6.00241500	-3.52823300	-0.21724400

SN2 Transition state 2 (H_2O PCM): E(RB3LYP) -1847.594245

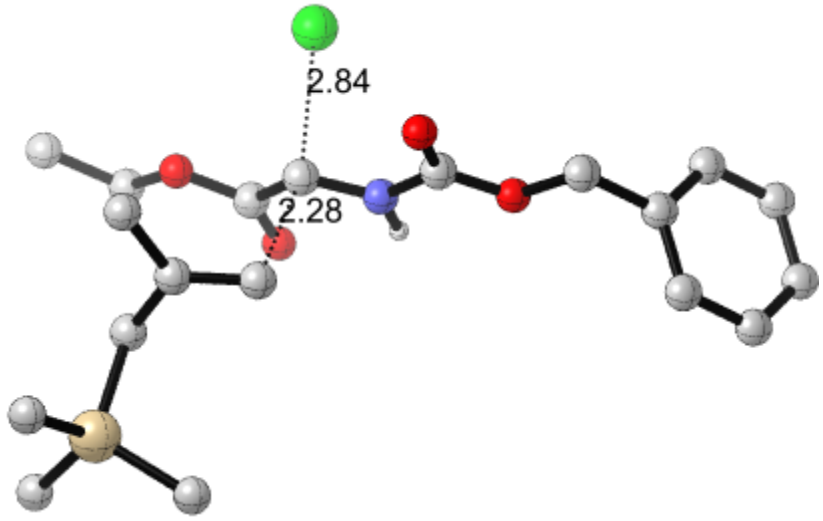

Keycard: opt=(calcfc,ts,noeigentest) freq=noraman b3lyp/6-31g(d) scrf=(solvent=water,pcm) empiricaldispersion=gd3bj

0 1

C	-0.24155100	1.18196500	0.34759000
H	-0.40531500	1.52417400	1.35518700
C	-1.11824800	1.59589700	-0.79350000
O	-2.23573400	2.17671500	-0.38026800
O	-0.81697500	1.34744400	-1.94647100
C	-3.12207100	2.67922800	-1.42072500
H	-2.56953700	3.43017600	-1.99166800
H	-3.37717500	1.85227500	-2.08725400
C	-4.33568700	3.26224500	-0.73081100
H	-4.04600800	4.06626500	-0.04778200
H	-5.01653200	3.67342100	-1.48251400
H	-4.87257700	2.49573500	-0.16316100
Cl	0.46015600	3.93339800	0.30036300
N	0.96698200	0.72907100	0.00683400
C	1.95191700	0.44256200	0.96054000
O	1.75576900	0.52206300	2.15507700
O	3.07027300	0.07865000	0.34310800
C	4.19094000	-0.26763700	1.22452200
H	4.44908000	0.62493400	1.79819800
H	3.84652800	-1.04425700	1.91026000
C	5.31834300	-0.73321700	0.35411800
C	6.26437900	0.17946000	-0.12633000
C	5.41946500	-2.08192700	-0.00699100
C	7.29931100	-0.24998900	-0.95731000
H	6.18942000	1.22682500	0.15380900
C	6.45307900	-2.51339700	-0.83814900
H	4.68760100	-2.79331800	0.36660500

C	7.39409200	-1.59711900	-1.31422200
H	8.03146700	0.46380800	-1.32299900
H	6.52664100	-3.56197000	-1.11089200
H	8.20138600	-1.93287000	-1.95859300
H	1.16383600	0.59676800	-0.98257600
C	-1.23929200	-0.80734300	0.82376800
H	-0.64095500	-0.85309600	1.72836800
H	-0.85140700	-1.32558600	-0.04762700
C	-2.56728900	-0.46092000	0.88306400
C	-3.47191500	-0.67492300	-0.25986300
H	-2.93677600	-0.64029500	-1.21617100
H	-4.28981100	0.05274800	-0.27631500
Si	-4.29412700	-2.42913300	-0.23212000
C	-5.21553900	-2.68688000	1.39033100
H	-5.75496600	-3.64131300	1.36557300
H	-4.53106000	-2.71560000	2.24540600
H	-5.95098700	-1.89361500	1.56709100
C	-5.48516700	-2.45069400	-1.69108900
H	-4.95798200	-2.26928400	-2.63460800
H	-5.98512200	-3.42359100	-1.76543200
H	-6.25826200	-1.68171000	-1.58065100
C	-3.13413300	0.18122100	2.11147100
H	-3.36016100	1.23218500	1.88985600
H	-4.08068900	-0.29062600	2.39452200
H	-2.44511400	0.14053400	2.95823000
C	-2.93658400	-3.71666200	-0.43871600
H	-2.37369700	-3.55510100	-1.36530000
H	-2.22870500	-3.68738700	0.39693000
H	-3.36782800	-4.72383400	-0.47858300

SN2 Transition state 3 (H_2O PCM): E(RB3LYP) -1847.605382

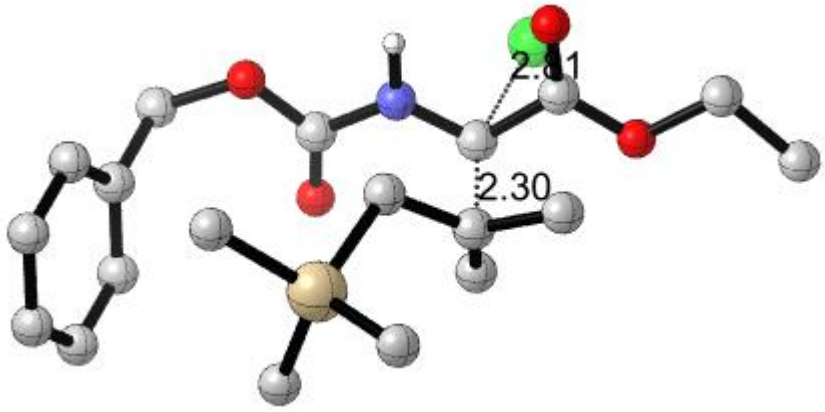

Keycard: opt=(calcfc,ts,noeigentest) freq=noraman b3lyp/6-31g(d) scrf=(solvent=water,pcm) empiricaldispersion=gd3bj

0 1

C	1.93860400	-0.87562200	0.22278900
H	2.01286200	-1.24939300	1.22945000
C	3.07916000	-0.20660000	-0.47430100
O	4.00142200	0.21628300	0.37798000
O	3.06822000	-0.02930000	-1.67953900
C	5.18705000	0.82901100	-0.20466300
H	5.67921100	0.07545200	-0.82561800
H	4.87089800	1.65582900	-0.84473400
C	6.05880900	1.29002300	0.94276900
H	6.34489900	0.44675100	1.57845500
H	6.96917300	1.74876100	0.54452300
H	5.53720600	2.03193500	1.55539300
Cl	3.67782000	-3.07897300	0.07241000
N	0.96000000	-1.32372600	-0.56423500
C	-0.11801800	-2.06773500	-0.06257200
O	-0.23524700	-2.33994600	1.11301200
O	-0.93821300	-2.37389800	-1.06165500
C	-2.16664800	-3.08713200	-0.69036100
H	-2.45918300	-3.57113300	-1.62158300
H	-1.90981100	-3.84052600	0.05459400
C	-3.21994200	-2.13626500	-0.19467200
C	-3.97029500	-1.38455900	-1.10800600
C	-3.46309600	-1.99156800	1.17646400
C	-4.95217900	-0.50248000	-0.65717200
H	-3.78864200	-1.49772700	-2.17356000
C	-4.44866000	-1.11261400	1.62787900
H	-2.87665100	-2.56694800	1.88552500
C	-5.19299300	-0.36632400	0.71209200
H	-5.53206300	0.07303100	-1.37224700
H	-4.63303100	-1.00889000	2.69297200
H	-5.95857300	0.31903600	1.06345300
H	1.01893700	-1.12182600	-1.55981400
C	1.07118600	0.96582600	1.28551900
H	1.88452800	1.14094300	1.98212300
H	0.25528700	0.33839600	1.63185400
C	0.92368000	1.75425700	0.17204500
C	-0.24500100	1.62855400	-0.71511800
H	-0.65398600	0.61097100	-0.72041000
H	-0.00791800	1.92417800	-1.74280100
Si	-1.74112900	2.71163500	-0.13034400
C	-1.19631300	4.50309600	0.07702100
H	-2.06040700	5.12858100	0.33152600
H	-0.46036800	4.61234200	0.88146300
H	-0.75784600	4.90180100	-0.84502800
C	-3.03720600	2.56123000	-1.48681000
H	-3.30545700	1.51402300	-1.65846200

H	-3.95060700	3.10016100	-1.20843000
H	-2.66952600	2.98252200	-2.42942800
C	1.96716100	2.76338300	-0.20302800
H	2.41519300	2.48742700	-1.16624800
H	1.50720100	3.74728900	-0.34534800
H	2.75412200	2.84644900	0.54905000
C	-2.35071200	2.00796000	1.50396200
H	-2.58993500	0.94322000	1.41548000
H	-1.59877400	2.12700200	2.29191500
H	-3.26084800	2.52630100	1.82801300

SN2 Transition state 4 (H_2O PCM): E(RB3LYP) -1847.594310

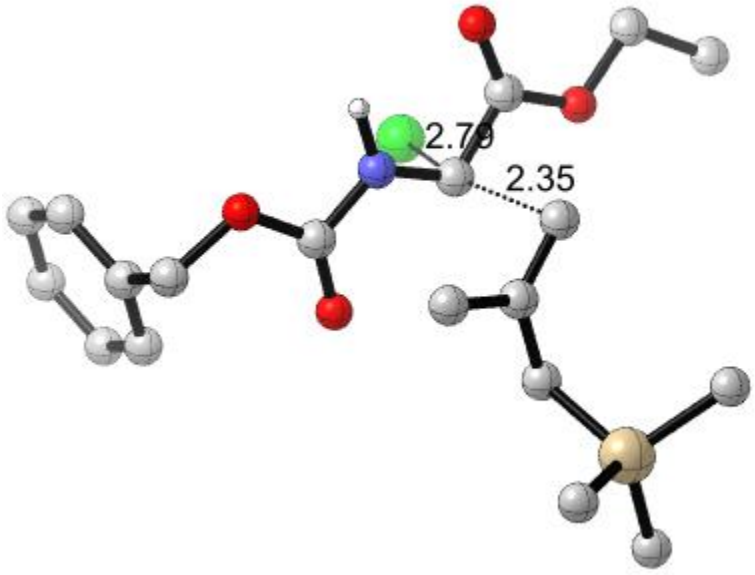

Keycard: opt=(calcfc,ts,noeigentest) freq=noraman b3lyp/6-31g(d) scrf=(solvent=water,pcm) empiricaldispersion=gd3bj

0 1

C	-0.27338200	1.31568700	-0.28380800
H	-0.44699500	0.88267000	0.68557800
C	-0.73569800	2.69419400	-0.65883700
O	-1.63958800	3.16553500	0.18717100
O	-0.32967000	3.24194200	-1.66698900
C	-2.12431100	4.51257700	-0.07563000
H	-1.26928500	5.19224000	-0.02301800
H	-2.52887600	4.53946600	-1.09070900
C	-3.17130400	4.82112100	0.97223200
H	-2.74324900	4.76977800	1.97786300
H	-3.55820400	5.83222100	0.81144200
H	-4.00642900	4.11677600	0.90809200
Cl	1.41224000	2.75163400	1.42155600
N	0.67330900	0.80427600	-1.06910400

C	1.36491700	-0.36774100	-0.73068400
O	1.07939200	-1.03828800	0.23829000
O	2.31349700	-0.59259300	-1.63217900
C	3.17046000	-1.75956100	-1.38642400
H	2.53738300	-2.57996000	-1.04697600
H	3.56902300	-1.98259200	-2.37565100
C	4.25444200	-1.43080500	-0.39909600
C	5.37725000	-0.70197100	-0.81142500
C	4.14447500	-1.82430100	0.93954800
C	6.37600200	-0.36873100	0.10245200
H	5.46678200	-0.39731200	-1.85092400
C	5.14605100	-1.49606600	1.85396400
H	3.26986000	-2.38033700	1.26179200
C	6.26145500	-0.76675000	1.43711500
H	7.24412400	0.19527300	-0.22569300
H	5.05497700	-1.80811300	2.89020500
H	7.04089100	-0.51093100	2.14899100
H	0.95336900	1.34341100	-1.88580100
C	-2.34715600	0.49077900	-1.01536300
H	-2.26137300	0.88734500	-2.02325900
H	-2.92410000	1.07036300	-0.30327400
C	-2.03055000	-0.81631600	-0.75178400
C	-2.33194300	-1.43768400	0.55302600
H	-2.46380500	-0.68109000	1.33545600
H	-1.53910300	-2.12820700	0.85895100
Si	-3.98635100	-2.43710800	0.54557700
C	-3.85903700	-3.90457700	-0.63025000
H	-2.97319500	-4.51289100	-0.41493600
H	-4.74100000	-4.54728800	-0.52192200
H	-3.80755000	-3.58952400	-1.67792000
C	-4.23494400	-3.03380900	2.31572400
H	-4.29121000	-2.19095500	3.01395400
H	-5.16597600	-3.60637200	2.40197200
H	-3.41033300	-3.68248700	2.63287200
C	-1.38780500	-1.65682600	-1.81724400
H	-0.79974400	-2.47410200	-1.39441800
H	-2.16387500	-2.09851100	-2.45524800
H	-0.75402200	-1.05084600	-2.47316200
C	-5.36823600	-1.27222000	0.01693800
H	-5.43429000	-0.40766700	0.68765600
H	-5.20290700	-0.89711300	-0.99928300
H	-6.33638500	-1.78618400	0.03349500

Ground and transition states involving catalyst **5d'** are found below. They were found under all the same conditions as background uncatalyzed computations, with the exception that

computations were conducted at B3LYP/6-31g(d) rather than with 6-311+g(d,p), as at that basis set, zero to one optimization steps were completed in a week:

Lowest energy binding mode between 1-Cbz and 5d': E(RB3LYP) -3211.179331

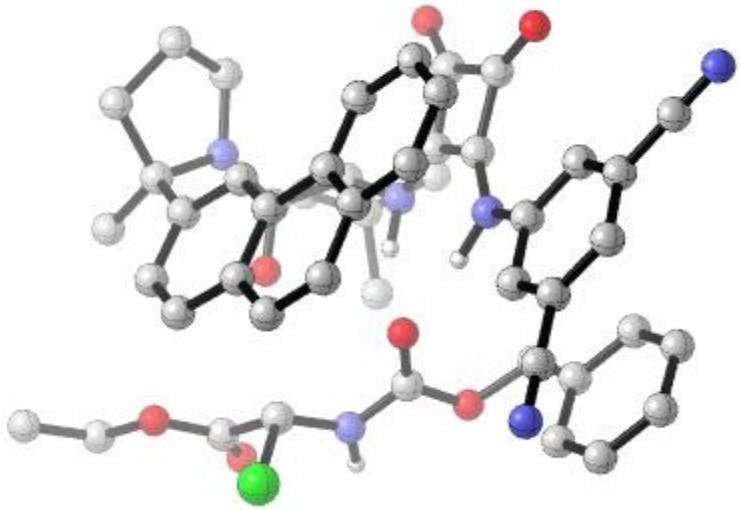

Keycard: opt freq=noraman b3lyp/6-31g(d) scrf=(solvent=dichloromethane,pcm) empiricaldispersion=gd3bj

0 1

C	-3.28965800	0.32488900	0.19155000
C	-3.41704200	-0.95401000	-0.36096200
C	-4.65221100	-1.38213600	-0.85045200
C	-5.77585600	-0.54958800	-0.80178700
C	-5.62646000	0.72912400	-0.25281100
C	-4.39583000	1.17778300	0.24422100
H	-2.55889000	-1.61369200	-0.40651800
H	-6.73285300	-0.88350800	-1.18198100
H	-4.29768600	2.18499400	0.63329400
C	-6.75606100	1.61001500	-0.21151300
N	-7.67350200	2.32401700	-0.18235100
C	-4.75839200	-2.69408200	-1.41393600
N	-4.83749400	-3.75902500	-1.87419400
N	-2.03618400	0.67150400	0.68907900
C	-1.54578500	1.88763200	1.00762500
C	-0.24646900	2.21404800	1.44237000
C	-1.97552600	3.31123600	1.01702800
C	-0.54072700	3.66395600	1.44312300
H	-1.36308400	-0.09662700	0.72487100
O	-3.00000700	3.93230600	0.78211400
O	0.11256900	4.67803100	1.63685600
N	0.82399900	1.47518700	1.74288600
H	0.80319800	0.49682500	1.46102100

C	2.17273100	2.04592100	1.87448800
H	2.06796700	3.12529800	1.79277400
C	2.82583300	1.75699600	3.25356200
C	2.02045300	2.53104400	4.31114800
H	2.00553400	3.60557100	4.09467300
H	0.98386400	2.17899000	4.34774600
H	2.46121800	2.38844900	5.30377400
C	2.83272300	0.26352200	3.61934200
H	1.81440100	-0.13700200	3.67059800
H	3.39774900	-0.33266900	2.90124400
H	3.27954600	0.13674400	4.61195800
C	4.26806100	2.28901500	3.20285400
H	4.29158800	3.35260900	2.93609100
H	4.74756700	2.17890700	4.18133400
H	4.87048400	1.73858600	2.47139000
C	2.92382400	1.44943800	0.67878100
O	3.04716000	0.21633800	0.62265300
C	3.19592900	3.72897000	-0.39501500
C	3.76217700	1.65277900	-1.62052700
C	3.13892900	4.02259600	-1.89701700
H	4.08020400	4.18454300	0.06670200
H	2.31000200	4.09289500	0.12735800
C	3.98758400	2.90657200	-2.51422200
H	2.10581000	3.97206500	-2.25270200
H	3.52102800	5.01962700	-2.12966900
H	3.73602300	2.69871100	-3.55650000
H	5.04688600	3.18286600	-2.47390700
N	3.30057000	2.25805500	-0.33233800
C	2.63745300	0.76124300	-2.16653700
C	2.89588400	-0.51272300	-2.71338800
C	1.32395400	1.21134700	-2.13724000
C	1.85945500	-1.30224900	-3.17234700
H	3.90475800	-0.90260100	-2.74164000
C	0.24788100	0.45348600	-2.64352700
H	1.11524600	2.17244100	-1.68745500
C	0.52251600	-0.85073100	-3.14566200
H	2.06730100	-2.29629700	-3.55661300
C	-1.11631100	0.95990600	-2.69616400
C	-0.55191400	-1.67565900	-3.61720300
C	-2.14444200	0.12376000	-3.22283300
C	-1.46935600	2.26327100	-2.27797300
C	-1.82990300	-1.21026200	-3.64959700
H	-0.31931300	-2.68178200	-3.95525600
C	-3.46424800	0.62125700	-3.32632700
C	-2.77007400	2.72291100	-2.37262500
H	-0.71174800	2.92775500	-1.87883100

H	-2.63897100	-1.83940800	-4.01110800
C	-3.77744000	1.89849500	-2.90929900
H	-4.23412900	-0.02983400	-3.73107900
H	-3.01380000	3.71947600	-2.02042200
H	-4.79670800	2.26479700	-2.98272100
C	5.09012600	0.91176100	-1.42609300
H	5.52199500	0.64913500	-2.39727900
H	5.79578800	1.57333100	-0.91479000
H	4.95580600	0.00904900	-0.83316900
Cl	1.87412500	-4.03440700	-0.90108000
C	3.87937400	-2.74209500	0.45667800
O	4.57039900	-2.57196600	-0.66136400
O	4.34639600	-2.97052500	1.55400100
C	6.01808500	-2.70171300	-0.55232100
H	6.38286400	-1.88528900	0.07677500
H	6.23779900	-3.64855700	-0.05331500
C	6.58167700	-2.64680900	-1.95550000
H	6.35827600	-1.68870500	-2.43338200
H	7.66918900	-2.76391700	-1.91356100
H	6.16987800	-3.45190400	-2.57129100
N	1.70341500	-2.69914300	1.45095300
C	0.57375100	-2.00124900	1.70779200
O	0.03623300	-1.24595100	0.89597500
O	0.14696000	-2.22696400	2.95741300
C	-1.00579800	-1.48541400	3.41364500
H	-0.94656000	-1.57630500	4.50041000
H	-0.87993700	-0.43055800	3.15622100
C	-2.31876100	-2.02337400	2.89513700
C	-3.47610600	-1.26377000	3.10582100
C	-2.41896500	-3.26151100	2.25645400
C	-4.71871500	-1.74208800	2.69589400
H	-3.40237300	-0.29144600	3.58651900
C	-3.66369000	-3.73481400	1.83403100
H	-1.52948900	-3.86052300	2.09067300
C	-4.81544900	-2.98063000	2.05778200
H	-5.60756600	-1.13967300	2.85673600
H	-3.73004200	-4.69215000	1.32618900
H	-5.78086400	-3.34852800	1.72405500
H	2.14651800	-3.21794700	2.20058000
C	2.37455900	-2.63094300	0.21531700
H	2.12147200	-1.72688700	-0.33144500

Lowest energy major transition state: E(RB3LYP) -3777.132231

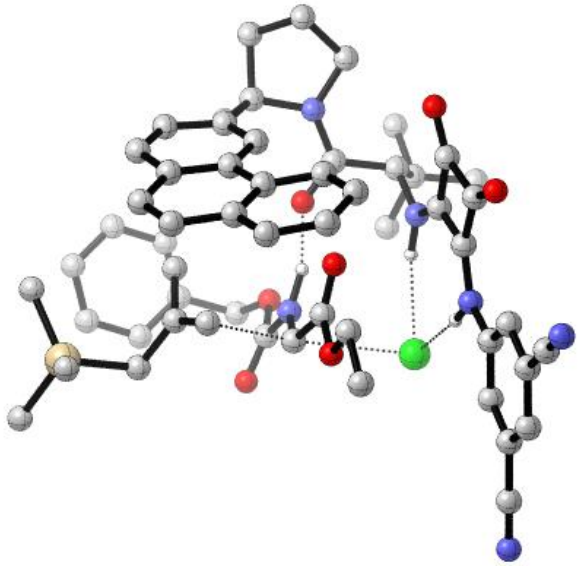

Keycard: opt=(calcfc,ts,noeigentest) freq=noraman b3lyp/6-31g(d) scrf=(solvent=dichloromethane,pcm) empiricaldispersion=gd3bj

0 1

C	-0.14058100	-1.14563900	-1.66494700
H	-0.17604400	-2.00848000	-2.31545200
C	0.94098400	-0.99021400	-0.64284300
O	1.75378200	-2.04165300	-0.66425800
O	0.99789000	-0.04249100	0.11180400
C	2.66408600	-2.15530400	0.47059700
H	3.21419700	-1.22127500	0.57182500
H	2.05116400	-2.28524600	1.36373000
C	3.56890600	-3.33908900	0.22110900
H	4.15584400	-3.20245200	-0.69066300
H	4.25865600	-3.44111600	1.06471500
H	2.99075100	-4.26398900	0.13283800
N	-0.91805400	-0.12880100	-1.92457000
C	-1.89672500	-0.22718000	-2.94583600
O	-2.11165800	-1.25036000	-3.55451700
O	-2.50653600	0.94260800	-3.07226600
C	-3.75272700	0.93530900	-3.84894100
H	-3.88710800	1.98377900	-4.11198800
H	-3.60040100	0.33865600	-4.74816300
C	-4.85997100	0.40700500	-2.98066500
C	-5.37007600	1.20603000	-1.94859900
C	-5.32341400	-0.90557200	-3.12675300
C	-6.32112000	0.69680100	-1.06667800
H	-5.01047900	2.22445800	-1.83301900
C	-6.28455500	-1.41315200	-2.25002700
H	-4.92070500	-1.53001300	-3.91801500

C	-6.77988000	-0.61491100	-1.21720900
H	-6.70528200	1.32117700	-0.26572700
H	-6.64126400	-2.43175000	-2.37029200
H	-7.52539300	-1.01119600	-0.53415600
H	-0.86148700	0.76178100	-1.37276800
C	-1.10736500	-2.55769900	0.23514300
H	-0.67164200	-1.88554000	0.96485800
H	-0.60422600	-3.50459500	0.06428200
C	-2.35971400	-2.32452800	-0.24875200
C	-3.11578700	-3.34334100	-1.01651300
H	-2.44294100	-4.03892200	-1.53189000
H	-3.77194800	-2.87904000	-1.75858300
Si	-4.20038000	-4.43152400	0.14389300
C	-5.33740000	-3.36655400	1.20965500
H	-6.07066200	-3.99988700	1.72334100
H	-4.77471200	-2.82506900	1.97803800
H	-5.88734300	-2.63352400	0.61007800
C	-5.22232900	-5.55249800	-0.97703000
H	-4.58034100	-6.16713800	-1.61845900
H	-5.85345800	-6.22635900	-0.38593200
H	-5.87830000	-4.96030400	-1.62586100
C	-3.03502600	-1.01687800	0.01865200
H	-3.43861400	-0.59343900	-0.90680600
H	-3.90092100	-1.15645600	0.67212500
H	-2.37089100	-0.28982300	0.48534200
C	-3.04718600	-5.42772000	1.25407400
H	-2.36154800	-6.04730600	0.66444100
H	-2.44422000	-4.76518100	1.88618600
H	-3.61885100	-6.09223800	1.91253000
C	4.96512100	-0.26499600	-1.28677600
C	5.03114300	-1.05244600	-2.44773200
C	6.00751200	-2.04717500	-2.56242200
C	6.92722000	-2.28342700	-1.53219300
C	6.84381700	-1.49056400	-0.38201700
C	5.87949600	-0.48318800	-0.24703500
H	4.31267400	-0.89204700	-3.24470400
H	7.67694900	-3.05908400	-1.62198400
H	5.83978300	0.11738300	0.65691100
C	7.76100000	-1.72051600	0.69632300
N	8.50137900	-1.91284900	1.57192200
C	6.05938400	-2.84788100	-3.75058800
N	6.10427100	-3.50133000	-4.71116800
N	3.95275900	0.68787100	-1.22730300
C	3.63202500	1.53206900	-0.22348100
C	2.52624700	2.41185600	-0.12053500
C	4.13958100	1.91446200	1.11410400

C	2.93877500	2.84007400	1.23627200
H	3.29766800	0.67776200	-2.02892100
O	5.07376100	1.60378800	1.84559100
O	2.47590900	3.57042600	2.10351600
N	1.49921800	2.70718700	-0.90849300
H	1.36374300	2.14434000	-1.75177400
C	0.50578100	3.71986800	-0.55216000
H	0.99050200	4.38327100	0.16141600
C	0.11656500	4.58536100	-1.79516200
C	1.40206600	5.23360800	-2.33868100
H	1.90709400	5.82324400	-1.56436600
H	2.10521400	4.48149400	-2.70773200
H	1.15608600	5.90404100	-3.16908200
C	-0.54786300	3.75027300	-2.90326300
H	0.09718800	2.94012400	-3.26067200
H	-1.48665200	3.30617700	-2.56760900
H	-0.75845900	4.39904100	-3.76097500
C	-0.85258400	5.69219000	-1.34553000
H	-0.39592100	6.34064200	-0.58965900
H	-1.11992500	6.31828900	-2.20309700
H	-1.77980000	5.28100600	-0.93289100
C	-0.71728100	3.05238700	0.10027700
O	-1.24638600	2.06262400	-0.43563900
C	-0.60633000	4.66561700	2.03626700
C	-2.47600900	3.05792200	1.85174300
C	-1.31730200	4.54457700	3.38423700
H	-0.81082900	5.63730000	1.57387000
H	0.47055200	4.51827400	2.11534200
C	-2.71921500	4.09061500	2.98294900
H	-0.82774200	3.78296000	4.00026200
H	-1.30965900	5.48781200	3.93561100
H	-3.29503100	3.65220400	3.80115100
H	-3.28820300	4.93665600	2.57933600
N	-1.21992200	3.58300600	1.23074200
C	-2.25860000	1.66399000	2.44965500
C	-3.37870500	0.90400300	2.85810600
C	-0.99330600	1.13223400	2.63691800
C	-3.21747300	-0.37202400	3.35512900
H	-4.37929100	1.30972300	2.75480900
C	-0.79157000	-0.15948100	3.17188800
H	-0.13456800	1.71193800	2.32890400
C	-1.93472200	-0.94694600	3.49109000
H	-4.08776300	-0.96178200	3.63164700
C	0.53509300	-0.71349900	3.40004300
C	-1.76919100	-2.30385900	3.92521500
C	0.65307400	-2.06895100	3.83090900

C	1.71965600	0.04264100	3.24507700
C	-0.52988300	-2.84889200	4.06192700
H	-2.65839900	-2.89263300	4.13477700
C	1.93680600	-2.61922200	4.05806400
C	2.96361200	-0.51021700	3.49049600
H	1.66242100	1.08416000	2.95360500
H	-0.41227300	-3.88152900	4.37932600
C	3.07644900	-1.85534200	3.89264700
H	2.00909800	-3.65482500	4.38002000
H	3.85302800	0.09780000	3.36151300
H	4.05591500	-2.28671200	4.07744300
C	-3.64001500	3.07875800	0.84702100
H	-4.59274400	2.97462600	1.37393900
H	-3.65362500	4.04286700	0.32857000
H	-3.55124700	2.28130800	0.11127200
Cl	1.78841800	0.52520100	-3.46284700

Lowest energy minor transition state: E(RB3LYP) -3777.128509

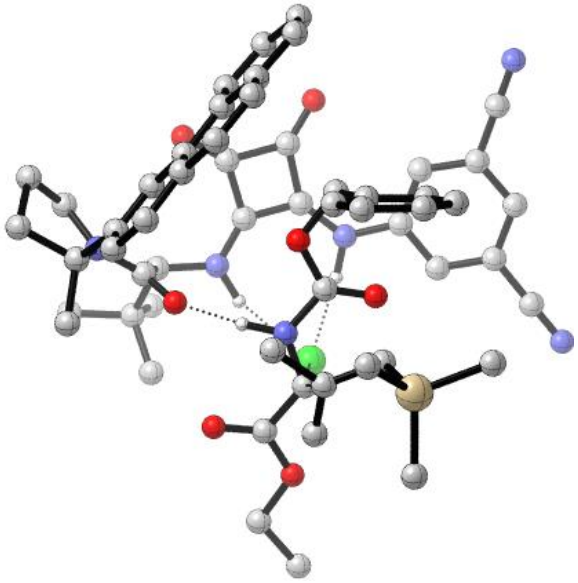

Keycard: opt=(calcfc,ts,noeigentest) freq=noraman b3lyp/6-31g(d) scrf=(solvent=dichloromethane,pcm) empiricaldispersion=gd3bj

0 1

C	0.68008200	2.78050100	-0.89359500
H	1.67639400	3.00436400	-0.54292400
C	-0.22539300	3.88460800	-1.34550100
O	0.42588800	5.04360300	-1.33188800
O	-1.36892600	3.70455100	-1.70663200
C	-0.34306200	6.21069800	-1.73601400
H	-1.19355500	6.30513400	-1.05563900
H	-0.72598900	6.03460800	-2.74525600

C	0.58590100	7.40311200	-1.66711500
H	0.96420000	7.54174300	-0.65001300
H	0.04115000	8.30589100	-1.96090600
H	1.43581000	7.27567100	-2.34458800
Cl	0.03470300	3.83205600	1.94932000
N	0.13695100	1.63905200	-0.49456100
C	0.96442000	0.69330300	0.14752100
O	2.11730700	0.91918000	0.44164700
O	0.29874600	-0.44239100	0.33585700
C	1.11275000	-1.54323800	0.86295200
H	0.37005100	-2.29910200	1.10977600
H	1.60890000	-1.20446900	1.77095600
C	2.10692800	-2.02813300	-0.15416300
C	1.66641200	-2.49576700	-1.39661400
C	3.47549400	-2.02513000	0.13362200
C	2.58083000	-2.97200100	-2.33436200
H	0.60832100	-2.48899400	-1.62740800
C	4.39219300	-2.50531400	-0.80237300
H	3.82071800	-1.64109200	1.08927600
C	3.94568900	-2.98258500	-2.03743600
H	2.22258400	-3.35020200	-3.28667300
H	5.45304400	-2.50231700	-0.57048200
H	4.65805500	-3.36022700	-2.76510700
H	-0.88972300	1.46025600	-0.57966400
C	1.49616900	2.70337300	-3.06633200
H	0.59756400	3.07297600	-3.54820700
H	2.29445700	3.41974400	-2.89821700
C	1.75178400	1.35215500	-3.05135400
C	3.06850600	0.81065300	-2.67994300
H	3.62392000	1.49901900	-2.03498100
H	2.99458500	-0.16301200	-2.18821500
Si	4.19727700	0.55669300	-4.23387800
C	3.42577900	-0.71980200	-5.38492800
H	4.10613000	-0.93710600	-6.21695100
H	2.48350200	-0.36075700	-5.81348500
H	3.22663000	-1.66003600	-4.86030500
C	5.85716100	-0.03585200	-3.57214700
H	6.30783300	0.71522800	-2.91347500
H	6.55539100	-0.22469500	-4.39608400
H	5.74389700	-0.96236000	-3.00067300
C	0.64748400	0.39038800	-3.35239200
H	0.17636300	0.08687900	-2.40350600
H	1.01809500	-0.52745000	-3.81478300
H	-0.13593300	0.83340900	-3.97172200
C	4.37234100	2.21350300	-5.11159600
H	4.78305400	2.97795200	-4.44190200

H	3.40576200	2.57319800	-5.48110900
H	5.04784800	2.12352200	-5.97048000
C	1.93968800	0.72975100	3.67412700
C	2.91622500	1.69608000	3.38892300
C	4.26123900	1.42799400	3.65628100
C	4.66136800	0.20356900	4.20845700
C	3.67254700	-0.74401400	4.49445300
C	2.31630600	-0.49460000	4.24023700
H	2.62262100	2.63711800	2.93702200
H	5.70544900	-0.00318600	4.40616700
H	1.57184900	-1.25215800	4.46622600
C	4.05304200	-2.00853000	5.05373100
N	4.36477400	-3.03477100	5.50262500
C	5.25000100	2.41704900	3.34098500
N	6.05486000	3.21547500	3.08302400
N	0.62600400	1.03871200	3.32774100
C	-0.45593100	0.22865900	3.30090000
C	-1.71622200	0.46339200	2.70193200
C	-0.84151200	-1.14446400	3.71571500
C	-2.19506000	-0.89010900	3.05978800
H	0.48812100	1.98149600	2.92466900
O	-0.31590800	-2.08810600	4.29174400
O	-3.21700600	-1.53407900	2.85510300
N	-2.25436100	1.47660200	2.03737000
H	-1.68080900	2.30841800	1.86255000
C	-3.59090200	1.38181100	1.45213400
H	-4.17312700	0.72764300	2.10108100
C	-4.28799500	2.78473300	1.44927600
C	-4.26279000	3.32667800	2.89052800
H	-4.72491100	2.61874200	3.58865900
H	-3.24340300	3.52773000	3.23132000
H	-4.82462800	4.26579000	2.93839000
C	-3.57961500	3.77312800	0.51103400
H	-2.53550100	3.93963300	0.79007100
H	-3.59380400	3.43124200	-0.52530700
H	-4.09022700	4.74167900	0.56137200
C	-5.75238300	2.63954400	1.00572700
H	-6.31703400	1.99464500	1.68750400
H	-6.23036500	3.62466000	1.01069500
H	-5.83402700	2.23657900	-0.00850400
C	-3.47264500	0.74651100	0.05379400
O	-2.50162300	1.00811200	-0.67542900
C	-5.51176800	-0.68060500	0.47623100
C	-4.50190600	-0.55176100	-1.78105800
C	-6.04710900	-1.82000600	-0.39464200
H	-6.30138800	0.04503700	0.68615800

H	-5.08304500	-1.02927100	1.41733400
C	-5.87800900	-1.27027300	-1.81024400
H	-5.44070000	-2.72045200	-0.25869400
H	-7.08328800	-2.06533800	-0.14982200
H	-5.90781600	-2.03627400	-2.58833000
H	-6.66054600	-0.53273300	-2.02535800
N	-4.45919500	-0.06768300	-0.36902100
C	-3.39480400	-1.57327400	-2.05728900
C	-3.04072900	-1.87749200	-3.39169500
C	-2.79987800	-2.29326100	-1.03285400
C	-2.13577200	-2.88093600	-3.66751100
H	-3.48405800	-1.32562300	-4.21282500
C	-1.88430500	-3.34073500	-1.28088400
H	-3.04145500	-2.03588300	-0.00981800
C	-1.54735600	-3.64097100	-2.63274800
H	-1.86838100	-3.10439400	-4.69711600
C	-1.26521900	-4.11055700	-0.21209200
C	-0.61415300	-4.69018800	-2.92333200
C	-0.30835500	-5.11442100	-0.54648500
C	-1.55046700	-3.88977200	1.15529900
C	-0.01526800	-5.39069500	-1.92303000
H	-0.38424800	-4.90234000	-3.96412900
C	0.35174100	-5.81839300	0.48651400
C	-0.88749200	-4.58798200	2.14954300
H	-2.29174400	-3.15808200	1.45101100
H	0.70796300	-6.16937100	-2.14912800
C	0.08015400	-5.55412500	1.81489100
H	1.08749300	-6.57064600	0.21412900
H	-1.10074400	-4.36180600	3.18876400
H	0.60537000	-6.09233700	2.59834600
C	-4.49172100	0.62657000	-2.76648400
H	-4.82862200	0.29528600	-3.75278900
H	-5.19283200	1.39157200	-2.41914200
H	-3.50058300	1.07087900	-2.85566900

3.7.5 Parametrization for regression modeling

Parameterization for regression modeling was done by Jen Crawford in the Sigman group at the University of Utah. Excess of 50 parameters were calculated for 30 catalysts. For ease of viewing, only those parameters included in the model depicted in Figures 3.22 and 3.24 are provided below in Table 3.3.

Table 3.3 Catalyst arene parameterization for regression modelling, where Aryl is the pyrrolidine substituent, X is the geminal subsituent which can take on H or Me, and the parameters B1X, B5Ar, LAr, and Dispersion tps CH4 are as depicted in Figure 3.22

Aryl	X	B1X	B5Ar	LAr	Dispersion tps CH4
1-Nap	H	1.17	5.644362	6.446433	-2.5728
1-Nap	Me	1.7	5.642304	6.606454	-2.5728
1-Pyr	H	1.17	6.970264	8.813096	-3.009
2-Nap	H	1.17	4.380319	8.536736	-2.5759
2-Nap	Me	1.7	4.320308	8.58592	-2.5759
26MePh	H	1.17	4.565468	6.424986	-2.4961
3-Phen	H	1.17	6.906513	8.599444	-2.8885
3-Phen	Me	1.7	6.920126	8.590804	-2.8885
35BrPh	H	1.17	4.807128	6.423601	-2.3858
35MePh	H	1.17	4.602674	6.39425	-2.4862
35PhPh	H	1.17	6.937469	8.115592	-3.0785
4-Pyr	H	1.17	5.816817	8.586153	-2.9933
4FPh	H	1.17	3.184886	7.123077	-1.9779
4FPh	Me	1.7	3.203766	7.14131	-1.9779
9-Phen	H	1.17	5.637178	8.528647	-3.0565
9-Phen	Me	1.7	5.639268	8.501889	-3.0565
Anth	H	1.17	5.802341	6.679247	-3.1461
Ph	H	1.17	3.193849	6.416201	-2.0353
Ph	Me	1.7	3.20579	6.435232	-2.0353
2Anth	Me	1.7	5.479569	10.74705	-2.9929
35FPh	Me	1.7	3.842318	6.449808	-1.9198
345FPh	H	1.17	3.85179	7.135976	-1.8981
345FPh	Me	1.7	3.842734	7.159518	-1.8981

Chapter 4

Cooperative Lewis Acid and Hydrogen Bond Donor Catalysis: Synthesis of α,α-Disubstituted Amino Acids with Squaramides and Boron Trifluoride Etherate

4.1 Introduction

Chiral Lewis acid catalysts have proven to promote an immense range of transformations due to the highly modular nature of the Lewis acidic element employed, as well as the broad range of chiral ligand scaffolds that have been developed.[167] Specific tailoring of the ligand employed has allowed for high enantioselectivity, while the ability to tune the strength of the Lewis acidity and specific atom affinity (i.e. halo-, oxo-, aza-, and thiophilicity) has allowed for astonishing chemoselectivity in diverse reactions.

Chiral ligand design has been a combined effort and a few privileged C_2 chiral scaffolds have emerged in Lewis acid catalysis (Figure 4.1), notable examples include BOX,[117,168]

[167] For reviews on Enantioselective Lewis acid catalysis and privileged ligands: a) *Lewis Acids in Organic Synthesis*; Yamamoto, H., Ed.; Wiley, 2000. b) Yoon, T. P.; Jacobsen, E. N. Privileged Chiral Catalysts. *Science* **2003**, *299* (5613), 1691–1693. c) *Privileged Chiral Ligands and Catalysts*; Zhou, Q.-L., Ed.; Wiley-VCH Verlag GmbH & Co. KGaA: Weinheim, Germany, 2011. d) *Comprehensive Asymmetric Catalysis I - III. Ed.* Jacobsen, E. N.; Pfaltz, A.; Yamamoto, H. Springer-Verlag Berlin An, 2015.

[168] For a review see: Johnson, J. S..; Evans, D. A. Chiral Bis(Oxazoline) Copper(II) Complexes: Versatile Catalysts for Enantioselective Cycloaddition, Aldol, Michael, and Carbonyl Ene Reactions. *Acc. Chem. Res.* **2000**, *33* (6), 325–335.

PyBOX,[169] BINAP,[170] BINOL,[171] Salen,[172] and TADDOL.[173] Lewis acids have primarily been used in two contexts, to lower the LUMO of π-systems, such as carbonyls and imines, to activate them toward nucleophilic additions, Michael additions, or cycloadditions,[174] and to abstract leaving groups to generate a highly electrophilic species that can be trapped by nucleophiles.[175]

[169] For a review see: Desimoni, G.; Faita, G.; Quadrelli, P. Pyridine-2,6-Bis(Oxazolines), Helpful Ligands for Asymmetric Catalysts. *Chem. Rev.* **2003**, *103* (8), 3119–3154.

[170] Miyashita, A.; Yasuda, A.; Takaya, H.; Toriumi, K.; Ito, T.; Souchi, T.; Noyori, R. Synthesis of 2,2'-Bis(Diphenylphosphino)-1,1'-Binaphthyl (BINAP), an Atropisomeric Chiral Bis(Triaryl)Phosphine, and Its Use in the Rhodium(I)-Catalyzed Asymmetric Hydrogenation of .Alpha.-(Acylamino)Acrylic Acids. *J. Am. Chem. Soc.* **1980**, *102* (27), 7932–7934.

[171] For reviews see: a) Chen, Y.; Yekta, S. Yudin, A. K. Modified BINOL Ligands in Asymmetric Catalysis. *Chem Rev.* **2003**, *103* (8) 3155–3212. b) Brunel, J. M. BINOL: A Versatile Chiral Reagent. *Chem. Rev.* **2005**, *105* (3),857–898.

[172] For reviews see: a) Atwood, D. A.; Harvey, M. J. Group 13 Compounds Incorporating Salen Ligands. *Chem. Rev.* **2000**, *101* (1), 37–52. b) Cozzi, P. G. Metal–Salen Schiff Base Complexes in Catalysis: Practical Aspects. *Chem. Soc. Rev.* **2004**, *33* (7), 410–421. c) Baleizao, C.; Hermenegildo Garcia. Chiral Salen Complexes: An Overview to Recoverable and Reusable Homogeneous and Heterogeneous Catalysts. *Chem. Rev.* **2006**, *106* (9), 3987–4043. For key reference see: d) Jacobsen, E. N.; Zhang, W.; Muci, A. R.; Ecker, J. R.; Deng, L. Highly Enantioselective Epoxidation Catalysts Derived from 1,2-Diaminocyclohexane. *J. Am. Chem. Soc.* **1991**, *113* (18), 7063–7064.

[173]For reviews see: a) Haase, C.; Sarko, C. R.; DiMare, M. TADDOL-Based Titanium Catalysts and Their Adducts: Understanding Asymmetric Catalysis of Diels-Alder Reactions. *J. Org. Chem.* **1995**, *60* (6), 1777–1787. b) Seebach, D.; Beck, A. K.; Heckel, A. TADDOLs, Their Derivatives, and TADDOL Analogues: Versatile Chiral Auxiliaries. *Angew. Chemie Int. Ed.* **2001**, *40* (1), 92–138.

[174] Yates, P.; Eaton, P. Acceleration of the Diels-Alder Reaction by Aluminum Chloride. *J. Am. Chem. Soc.* **1960**, *82* (16), 4436–4437.

[175] *Friedel-Crafts and Related Reactions*; Olah, G. A., Ed.; Wiley: New York, 1964.

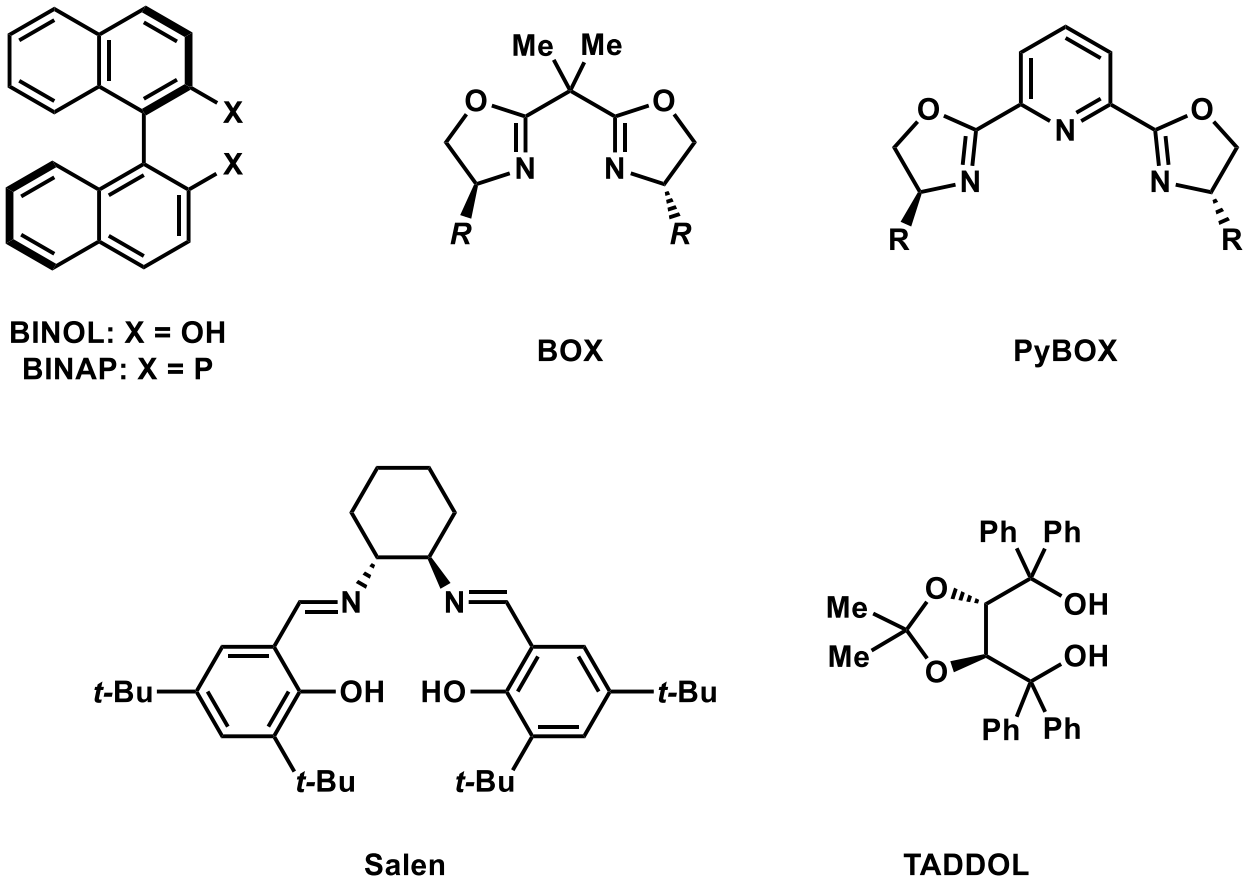

Figure 4.1 Privileged C_2 symmetric ligand scaffolds in asymmetric Lewis acid catalysis

While chiral Lewis acids have been demonstrated to catalyze a wide range of reactions, including Friedel-Crafts additions, Mannich reactions, ene reactions, conjugate additions, Nazarov cyclizations, Diels-Alder reactions, and Mukaiyama aldol reactions, among many others, this catalytic strategy has a few downsides.[167a] The most potent Lewis acids are generally transition metal or main-group inorganics with halide or triflate ligands. Fitting these Lewis acids with chiral ligands necessarily replaces these extremely withdrawing halide or triflate ligands with more donating ligands, which decreases the acidity of the complex relative to the parent Lewis acid. This therefore requires prior synthesis of these Lewis acid ligand complexes and requires the ligand stay on during the course of the reaction in order to outcompete racemic background processes. Last, often these reactions have products that are more Lewis basic than the starting

material, resulting in product inhibition and thus requiring the use of high loadings of precious chiral catalysts.[176] One solution to the deactivating effect of chiral ligands is the addition of a second Lewis or Brønsted acid, a strategy pioneered by Yamamoto, in what he calls combined acid catalysis or Brønsted assisted Lewis acid catalysis.[177] One elegant solution to these problem would be to employ a transient activating ligand (i.e. reversible binding) for a Lewis acid that could activate the Lewis acid to make it more potent. This strategy would have a few distinct advantages over traditional chiral Lewis acid catalysis. It would allow the use of off the shelf inorganic halides/triflates, expand the scope of Lewis acid chemistry by generation of stronger Lewis acids, and potentially allow for lower loadings of chiral information. The advantages of ligand accelerated enantioselective catalysis have been demonstrated previously, most notably in the Sharpless asymmetric dihydroxylation.[178]

4.1.1 Hydrogen-bond donors in Lewis acid catalysis

Dual hydrogen-bond donors (HBDs) catalytically function as soft Brønsted or Lewis acids. Analogously to Lewis acids, HBDs primarily engage in two modes of catalysis, π-electrophile activation and anion-abstraction/binding, in which the dual N-H's can bind leaving groups to generate reactive chiral ion-pairs, which can be intercepted by nucleophiles to form a variety of

[176] For two examples that discuss product inhibition in Lewis acid chemistry see: a) Evans, D. A.; Miller, S. J.; Lectka, T.; von Matt, P. Chiral Bis(Oxazoline)Copper(II) Complexes as Lewis Acid Catalysts for the Enantioselective Diels−Alder Reaction. *J. Am. Chem. Soc.* **1999**, *121* (33), 7559–7573. b) Gatzenmeier, T.; van Gemmeren, M.; Xie, Y.; Höfler, D.; Leutzsch, M.; List, B. Asymmetric Lewis Acid Organocatalysis of the Diels-Alder Reaction by a Silylated C-H Acid. *Science* **2016**, *351* (6276), 949–952.

[177] For reviews on combined acid catalysis see: a) Yamamoto, H.; Payette, J. N. Brønsted Acids, H-Bond Donors, and Combined Acid Systems in Asymmetric Catalysis. In *Hydrogen Bonding in Organic Synthesis*; Wiley-VCH Verlag GmbH & Co. KGaA: Weinheim, Germany; pp 73–140. b) Yamamoto, H. From Designer Lewis Acid to Designer Brønsted Acid towards More Reactive and Selective Acid Catalysis. *Proc. Jpn. Acad. Ser. B. Phys. Biol. Sci.* **2008**, *84* (5), 134–146. c) Yamamoto, H.; Futatsugi, K. "Designer Acids": Combined Acid Catalysis for Asymmetric Synthesis. *Angew. Chemie Int. Ed.* **2005**, *44* (13), 1924–1942.

[178] Jacobsen, E. N.; Marko, I.; Mungall, W. S.; Schroeder, G.; Sharpless, K. B. Asymmetric Dihydroxylation via Ligand-Accelerated Catalysis. *J. Am. Chem. Soc.* **1988**, *110* (6), 1968–1970.

products.[141,179] HBDs have been proven to be highly selective catalysts in a broad range of transformations. However, due to the relatively weak nature of hydrogen bonds, the range of substrates that catalysts can engage is extremely limited. HBD catalysts almost exclusively activate halide, specifically chloride, leaving groups. Additionally HBDs generally only heterolyze weak C-Cl bonds that result in heteroatom stabilized cations, such as N-acyl iminium ions,[99b,127b,143] oxocarbeniums,[130] and 3-membered onium intermediates.[95,99c] These two requirements result in a very narrow range of substrates that can both be activated and are also bench stable and do not undergo auto-heterolysis. Additionally, the requirement of heteroatom carbocation stabilization precludes the formation of many interesting products, such as those bearing tertiary and quaternary stereocenters.

In 2017, the Jacobsen group discovered cooperative activity between squaramide HBDs and trimethylsilyl triflate (TMSOTf), which was applied to two reactions preceding through oxocarbenium ion intermediates (Figure 4.2 B).[180] NMR titration and computational studies suggest that the HBD is able to abstract triflate from TMSOTf, generating a "super Lewis acid" with enhanced Lewis acidity relative to TMSOTf that is capable of activating acetals with high enantioselectivity (Figure 4.2 A). A follow-up study demonstrated the utility of this method in expanding the substrate scope of HBD catalysis by synthesizing quaternary stereocenters via a true carbocationic intermediate (Figure 4.3 C).[181]

[179] For a review on HBD catalysis see: Doyle, A. G..; Jacobsen, E. N. Small-Molecule H-Bond Donors in Asymmetric Catalysis. *Chem. Rev.* **2007**, *107* (12), 5713–5743.

[180] Banik, S. M.; Levina, A.; Hyde, A. M.; Jacobsen, E. N. Lewis Acid Enhancement by Hydrogen-Bond Donors for Asymmetric Catalysis. *Science* **2017**, *358* (6364), 761–764.

[181] Wendlandt, A. E.; Vangal, P.; Jacobsen, E. N. Quaternary Stereocentres via an Enantioconvergent Catalytic SN1 Reaction. *Nature* **2018**, *556* (7702), 447–451.

The central strategy behind this mode of catalysis is to engage anion-abstraction catalysts in an interaction with the Lewis acid rather than with the substrate directly. The Lewis acid provides a baseline level of activity and the HBD can enhance the Lewis Acidity by partially or completely abstracting a halide or triflate ligand, to render the Lewis acid more electron deficient and/or coordinatively unsaturated. This would create either a new chiral Lewis acid HBD complex, or if abstraction is complete, a chiral ion-paired complex with an extraordinarily activated cationic Lewis acid. If this concept could be extended beyond silylium chemistry to the entire suite of Lewis acid chemistry it could enable enantioinduction in a large number of transformations that have been recalcitrant to asymmetric catalysis.

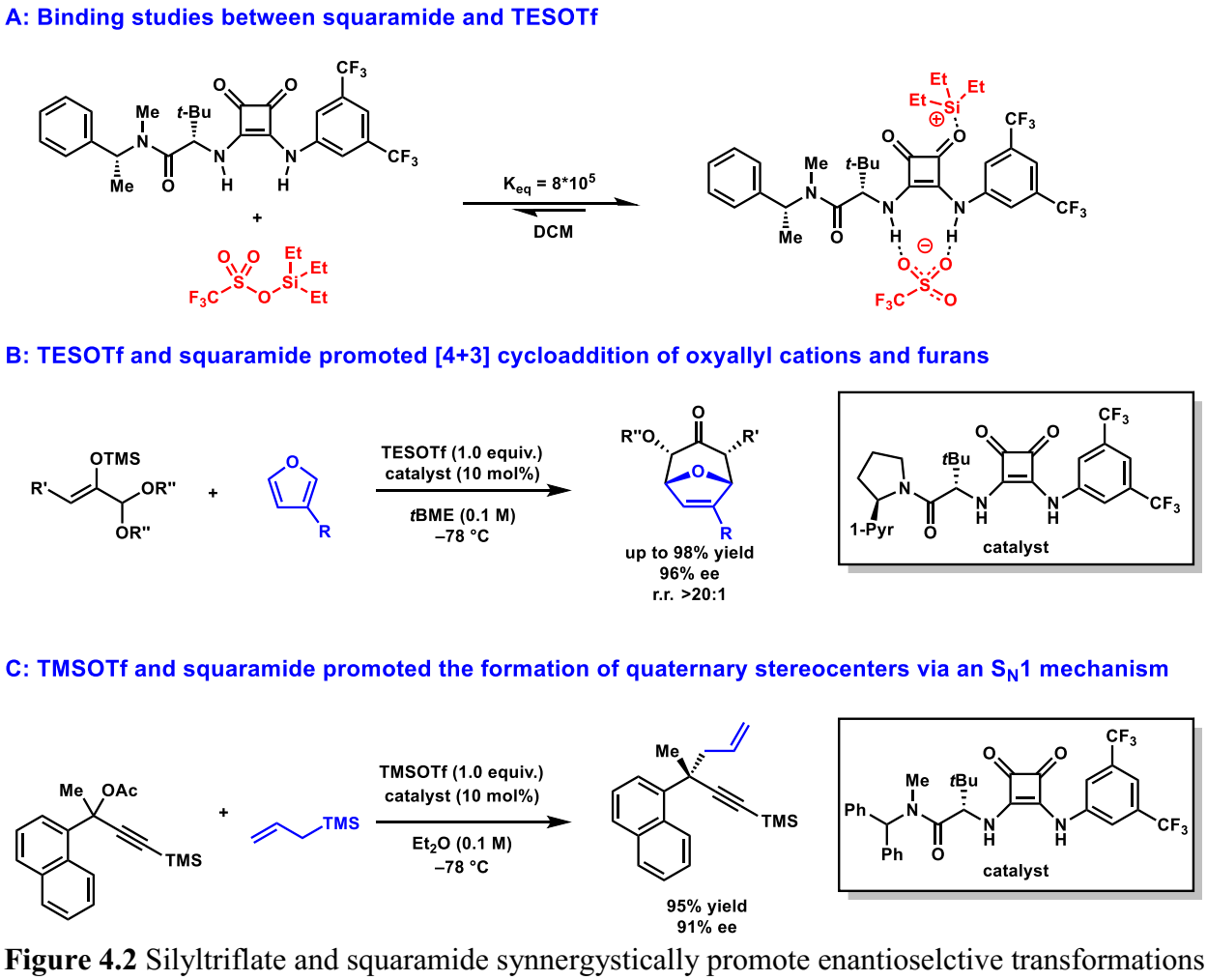

Figure 4.2 Silyltriflate and squaramide synnergystically promote enantioselctive transformations

4.1.2 Chiral boron Lewis acid chemistry

The suite of boron Lewis acids, including boron trifluoride etherate ($BF_3 \cdot OEt_2$), borontrichloride (BCl_3), borontibromide (BBr_3), and tris-polyfluorinated aryl boron complexes (BCF) are among the strongest Lewis acids and thus catalyze many transformations, including reduction of carbonyls and imines, aldol reactions, and Diels-Alder cycloadditions.[182] In particular $BF_3 \cdot OEt_2$ has emerged as the boron Lewis acid of choice due to the extremely withdrawing nature of fluoride ligands, and strength of the boron fluoride bond in BF_3 (1.291 Å and 154 kcal/mol), allowing for high levels of Lewis acidity and inability to hydrolyze to produce HF (in contrast to BCl_3: BDE of 109 kcal/mol and BBr_3: BDE of 90 kcal/mol, which easily hydrolize to generate HCl and HBr respectively due to having bond strengths less than $B(OR)_3$: BDE of 128 kcal/mol).[183,184]

Boron Lewis acids have been rendered chiral through the use of chiral ligands, most notably through the use of 1,2-amino alcohols, especially in oxazaborolidine catalysts, and BINOL scaffolds; these complexes have primarily been used to enantioselectively catalyze reduction of carbonyls and imines, Diels-Alder cycloadditions, and aldol reactions.[185]

---

[182] For a review on boron lewis acids see: Hatano, M.; Ishihara, K. Lewis Acids; 2016; pp 27–66.

[183] Bond dissociation energies taken from: Cottrell, T. L. *The Strengths Of Chemical Bonds*; Butterworths: London, 1958.

[184] For a compendium of BF_3 catalyzed reactions see: Cornel, V.; Lovely, C. J. Boron Trifluoride Etherate. In *Encyclopedia of Reagents for Organic Synthesis*; John Wiley & Sons, Ltd: Chichester, UK, 2007.

[185] For reviews on enantioselective boron Lewis acid catalysis see: a) Deloux, L.; Srebnik, M. Asymmetric Boron-Catalyzed Reactions. *Chem. Rev.* **1993**, *93* (2), 763–784. b) Yamamoto, H.; Maruoka, K.; Furuta, K. Chiral Lewis Acid Catalysts Organoaluminum and Boron Reagent. In *Selectivities in Lewis Acid Promoted Reactions*; Springer Netherlands: Dordrecht, 1989; pp 281–294.

Notably, boron Lewis acids, in particular BCF[186] and BF_3,[187] have demonstrated the ability to abstract alkyl leaving groups, especially benzylic and tertiary fluorides to generate carbocations. These processes have not been rendered enantioselective through the use of chiral boron complexes because the chiral ligands are substantially more donating than fluorides, and even if they could catalyze these transformations turnover would be challenging as the resulting BF_4^- is relatively chemically inert. While the presence of chiral ligands prevent accessing the full reactivity of boron Lewis acids, the problem has been mitigated through the use of combined acid systems. Challenging Diels-Alder cycloadditions have been promoted through Brønsted acid assisted chiral Lewis acid catalysis as demonstrated by Yamamoto (Figure 4.3 A),[188] and more recently Lewis acid activated Brønsted acid assisted chiral Lewis acid catalysis as demonstrated by Corey (Figure 4.3 B).[189] While these solutions enable Diels-Alder reactions with α,β-unsaturated aldehydes that would otherwise not proceed with chiral boron Lewis acids alone, they are only a marginal improvement and a range of boron chemistry is still not amenable to enantioselective catalysis. Although envisioning a mechanism for turnover is challenging, an

[186] Caputo, C. B.; Stephan, D. W. Activation of Alkyl C–F Bonds by $B(C_6F_5)_3$: Stoichiometric and Catalytic Transformations. *Organometallics* **2012**, *31* (1), 27–30.

[187] a) Hirano, K.; Fujita, K.; Yorimitsu, H.; Shinokubo, H.; Oshima, K. Boron Trifluoride-Catalyzed Reaction of Alkyl Fluoride with Silyl Enolate, Allylsilane, and Hydrosilane. *Tetrahedron Lett.* **2004**, *45* (12), 2555–2557. b) Hirano, K.; Yorimitsu, H.; Oshima, K. Boron Trifluoride-Mediated Alkylation of Diphenylphosphine with Tert-Alkyl Fluoride. *Org. Lett.* **2004**, *6* (24), 4873–4875.

[188] a) Furuta, K.; Shimizu, S.; Miwa, Y.; Yamamoto, H. Chiral (Acyloxy)Borane (CAB): A Powerful and Practical Catalyst for Asymmetric Diels-Alder Reactions. *J. Org. Chem.* **1989**, *54* (7), 1481–1483. b) Ishihara, K.; Yamamoto, H. Bronsted Acid Assisted Chiral Lewis Acid (BLA) Catalyst for Asymmetric Diels-Alder Reaction. *J. Am. Chem. Soc.* **1994**, *116* (4), 1561–1562.

[189] a) Corey, E. J.; Shibata, T.; Lee, T. W. Asymmetric Diels−Alder Reactions Catalyzed by a Triflic Acid Activated Chiral Oxazaborolidine. *J. Am. Chem. Soc.* **2002**, *124* (15), 3808–3809. b) Ryu D. H.; Lee, T. W.; Corey, E. J. Broad-Spectrum Enantioselective Diels−Alder Catalysis by Chiral, Cationic Oxazaborolidines. *J. Am. Chem. Soc.* **2002**, *124* (34), 9992–9993. c) Ryu D. H.; Corey, E. J. Triflimide Activation of a Chiral Oxazaborolidine Leads to a More General Catalytic System for Enantioselective Diels−Alder Addition. *J. Am. Chem. Soc.* **2003**, *125* (21), 6388–6390. d) Thirupathi, B.; Breitler, S.; Mahender Reddy, K.; Corey, E. J. Acceleration of Enantioselective Cycloadditions Catalyzed by Second-Generation Chiral Oxazaborolidinium Triflimidates by Biscoordinating Lewis Acids. *J. Am. Chem. Soc.* **2016**, *138* (34), 10842–10845.

alternative solution would be to partially or completely abstract a fluoride from BF_3 to generate a highly electrophilic borenium ion Lewis acid, which has been accomplished with silylium Lewis acids and silver salts, but rarely applied to enantioselective catalysis.[190]

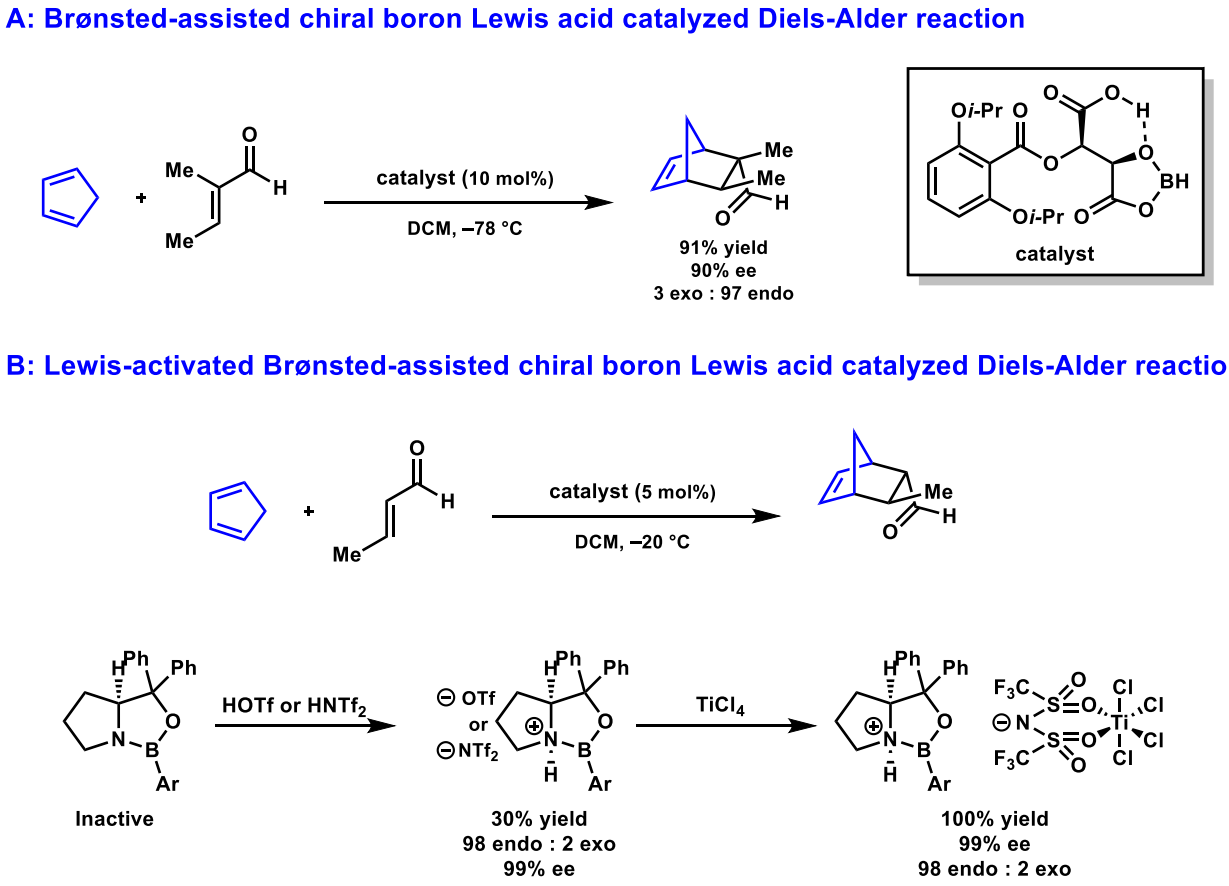

Figure 4.3 Combined acid systems enable challenging Diels-Alder reactions

4.1.3 Enantioselective synthesis of α,α-disubstituted amino acids

In Chapter 1, the synthesis of α,α-disubstituted amino acids is discussed at length, and thus a short summary is provided here, with a focus on α-alkyl-α-aryl amino acids. α,α-disubstituted amino acids have been the target of much synthetic interest, as they have a number of desirable

[190] For discussion of chiral borenium catalysis see: a) Chen, J.; Lalancette, R. A.; Jäkle, F. Synthesis and Lewis Acid Properties of a Ferrocene-Based Planar-Chiral Borenium Cation. *Chem. Commun.* **2013**, *49* (43), 4893. b) Lam, J.; Günther, B. A. R.; Farrell, J. M.; Eisenberger, P.; Bestvater, B. P.; Newman, P. D.; Melen, R. L.; Crudden, C. M.; Stephan, D. W. Chiral Carbene–Borane Adducts: Precursors for Borenium Catalysts for Asymmetric FLP Hydrogenations. *Dalt. Trans.* **2016**, *45* (39), 15303–15316. c) Eisenberger, P.; Crudden, C. M. Borocation Catalysis. *Dalt. Trans.* **2017**, *46* (15), 4874–4887.

conformational and metabolic properties in the synthesis of oligomeric peptides, inlcluding: increased chemical stability and hydrophobicity, restriction of conformational freedom of amino acid momomers, side chains, and entire peptides, and increased metabolic stability.[191]

Given the biological interest in α,α-disubstituted amino acid and their lack of natural sources, there exist many synthetic strategies for their construction.[192] When both substituents are alkyl, especially when one is methyl, many strategies discussed in Chapter 1 can be used for making disubstituted amino acids, including Strecker reactions in both auxiliary[193] and enantioselective catalytic[194] contexts, enolate alkylations in auxiliary,[195] PTC,[47,196] and metal π-allyl contexts,[49,50] side chain additions to Ellman ketimines,[57,197] and C-H activations.[79]

---

[191] For reviews on properties of α,α-disubstituted amino acid and their peptides: a) Venkataram Prasad, B. V.; Balaram, P.; Benedetti, E. The Stereochemistry of Peptides Containing α-Aminoisobutyric Aci. *Crit. Rev. Biochem.* **1984**, *16* (4), 307–348. b) Karle, I. L.; Balaram, P. Structural Characteristics of .Alpha.-Helical Peptide Molecules Containing Aib Residues. *Biochemistry* **1990**, *29* (29), 6747–6756.

[192] For a review on asymmetric syntheses of α,α-disubstituted amino acids see: Vogt, H.; Bräse, S. Recent Approaches towards the Asymmetric Synthesis of α,α-Disubstituted α-Amino Acids. *Org. Biomol. Chem.* **2007**, *5* (3), 406–430.

[193] a) Davis, F. A.; Lee, S.; Zhang, H.; Fanelli, D. L. Applications of the Sulfinimine-Mediated Asymmetric Strecker Synthesis to the Synthesis of α-Alkyl α-Amino Acids. *J. Org. Chem.* **2000**, *65* (25), 8704–8708. b) Borg, G.; Chino, M.; Ellman, J. A. Asymmetric Synthesis of Pre-Protected α,α-Disubstituted Amino Acids from Tert-Butanesulfinyl Ketimines. *Tetrahedron Lett.* **2001**, *42* (8), 1433–1435.

[194] a) Vachal, P..; Jacobsen, E. N. Enantioselective Catalytic Addition of HCN to Ketoimines. Catalytic Synthesis of Quaternary Amino Acids. *Org. Lett.* **2000**, *2* (6), 867–870. b) Masumoto, S.; Usuda, H.; Suzuki, M.; Kanai, M.; Shibasaki, M. Catalytic Enantioselective Strecker Reaction of Ketoimines. *J. Am. Chem. Soc.* **2003**, *125* (19), 5634–5645. c) Chavarot, M.; Byrne, J. J.; Chavant, P. Y.; Vallée, Y. Sc(BINOL)2Li: A New Heterobimetallic Catalyst for the Asymmetric Strecker Reaction. *Tetrahedron: Asymmetry* **2001**, *12* (8), 1147–1150.

[195] a) Ma, D.; Ding, K. Synthesis of Enantiopure α,α-Disubstituted Amino Acids from the Asymmetric Strecker Reaction Products of Aldehydes. *Org. Lett.* **2000**, *2* (16), 2515–2517. b) Hugelshofer, C. L.; Mellem, K. T.; Myers, A. G. Synthesis of Quaternary α-Methyl α-Amino Acids by Asymmetric Alkylation of Pseudoephenamine Alaninamide Pivaldimine. *Org. Lett.* **2013**, *15* (12), 3134–3137.

[196] a) Ooi, T.; Tayama, E.; Maruoka, K. Highly Stereoselective N-Terminal Functionalization of Small Peptides by Chiral Phase-Transfer Catalysis. *Angew. Chemie Int. Ed.* **2003**, *42* (5), 579–582. b) Ooi, T.; Takeuchi, M.; Kato, D.; Uematsu, Y.; Tayama, E.; Sakai, D.; Maruoka, K. Highly Enantioselective Phase-Transfer-Catalyzed Alkylation of Protected α-Amino Acid Amides toward Practical Asymmetric Synthesis of Vicinal Diamines, α-Amino Ketones, and α-Amino Alcohols. *J. Am. Chem. Soc.* **2005**, *127* (14), 5073–5083.

[197] Reeves, J. T.; Tan, Z.; Herbage, M. A.; Han, Z. S.; Marsini, M. A.; Li, Z.; Li, G.; Xu, Y.; Fandrick, K. R.; Gonnella, N. C.; et al. Carbamoyl Anion Addition to *N* -Sulfinyl Imines: Highly Diastereoselective Synthesis of α-Amino Amides. *J. Am. Chem. Soc.* **2013**, *135* (15), 5565–5568.

While many solutions exist for the synthesis of α,α-dialkyl amino acids, many of these methods cannot be extended to α-alkyl-α-aryl amino acids as the aryl group cannot be added via enolate addition, except in one report by Maruoka, in which an enolate performs S_NAr on fluorinated chromium arene complexes.[47] Additionally, in enolate chemistry, the alkyl group must be added first, as α-arylglycines do not readily alkylate due to the substantial $A_{1,3}$ strain built up between the planar α-aryl enol and the *N*-protecting group, as well as the diminished nucleophilicity of the sterically encumbered and conjugated enolate. Trost π-allyl additions to azalactones ease enolate formation sterically and electronically and can allow for the synthesis of α-alkyl-α-aryl amino acids in limited contexts and moderate enantioselectivities.[198] The Strecker addition to aryl alkyl ketones is the best way to make the these products, however syntheses are often hampered by requiring catalysts to distinguish aryl from alkyl groups, which is more challenging that distinguishing aryl groups and hydrogen. Additional complications include competitive retro-Strecker reactions, as well as challenge in hydrolyzing neopentyl-like nitriles.[194a] Alkyl additions to iminophenylglycinates would be an ideal way to synthesize these compounds, and this has been achieved in the context of Ellman and Davis sulfinamide auxiliary chemistry, albeit with lower enantioselectivities due to incomplete control over (*E*)- and (*Z*)-imine formation. Translating this into asymmetric catalysis would provide a useful entry to the synthesis of α-alkyl-α-aryl amino acids, however the low reactivity of ketimines requires the use of hard, basic organometallic nucleophiles, which has prevented this methodology from being adapted to asymmetric catalysis.

---

[198] Serra, M.; Bernardi, E.; Marrubini, G.; De Lorenzi, E.; Colombo, L. Palladium-Catalyzed Asymmetric Decarboxylative Allylation of Azlactone Enol Carbonates: Fast Access to Enantioenriched α-Allyl Quaternary Amino Acids. *European J. Org. Chem.* **2019**, *2019* (4), 732–741.

4.2 Development an asymmetric α,α-disubstituted amino acid synthesis: squaramide catalyzed and $BF_3 \cdot OEt_2$ promoted allylation of α-methoxy-α-phenyl glycinates

Given the ability of squaramide catalysts to promote the addition of allylsilane nucleophiles to α-chloroglycinates in high yields and enantioselectivities as discussed in Chapters 1 and 2, the analogous synthesis of α,α-disubstituted amino esters from α-chloro-α-substituted amino esters seemed plausible (Figure 4.4 A). However, efforts were stymied by the complete inability to form the requisite α-chloro-α-substituted amino ester substrates. In the case of α-chloro-alanine, the substrate rapidly eliminates to form the enamine as depicted in Figure 4.4 B. In the case of α-chloro-α-phenyl glycine the necessary alpha hydroxyl compound is inaccessible due to the thermodynamics of ketoaminal formation, which favors either the phenylglyoxylate starting material or over condensation to the imine (Figure 4.4 B). Attempts to affect radical benzylic C-H chlorination of α-phenyl glycine with NCS and analogous reagents either provided no conversion, complete conversion to the imine, or complete decomposition depending on the conditions employed.

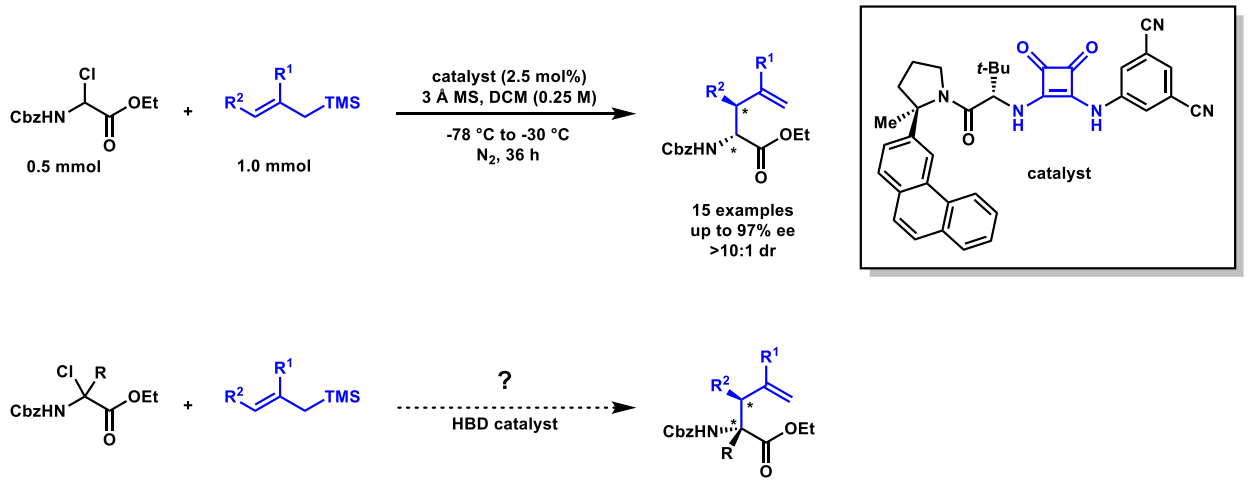

Figure 4.4 Inability to form the substrate prevents direct extension of HBD catalyzed allylation of α-chloroglycinates to the synthesis of α,α-disubstituted amino acids

Given the high synthetic value and dearth of methods for the synthesis of α,α-disubstituted amino acids, there exist other imino phenylglyoxylate equivalents that are shelf and solution stable. Notably Shono was able to perform an anodic oxidation of the methyl carbamate of α-phenyl glycine methyl ester, among other amino esters, in methanol to form bis-protected α-methoxy-α-phenyl glycine (Figure 4.5 A).[199] Additionally, it has been shown that this exact substrate can undergo deoxy allylation with allylsilane in the presence of superstoichiometric $BF_3 \cdot OEt_2$ and that

[199] Shono, T.; Matsumura, Y.; Inoue, K. Electroorganic Chemistry. 71. Anodic .Alpha.-Methoxylation of N-Carbomethoxylated or N-Acylated .Alpha.-Amino Acid Esters and .Alpha.-Amino-.Beta.-Lactams. *J. Org. Chem.* **1983**, *48* (8), 1388–1389.

TMSOTf can catalyze a very similar transformation (Figure 4.5 B).[200] These reactions are run in DCM at cryogenic to room temperatures, conditions remarkably similar to the allylation discussed in Chapter 2.

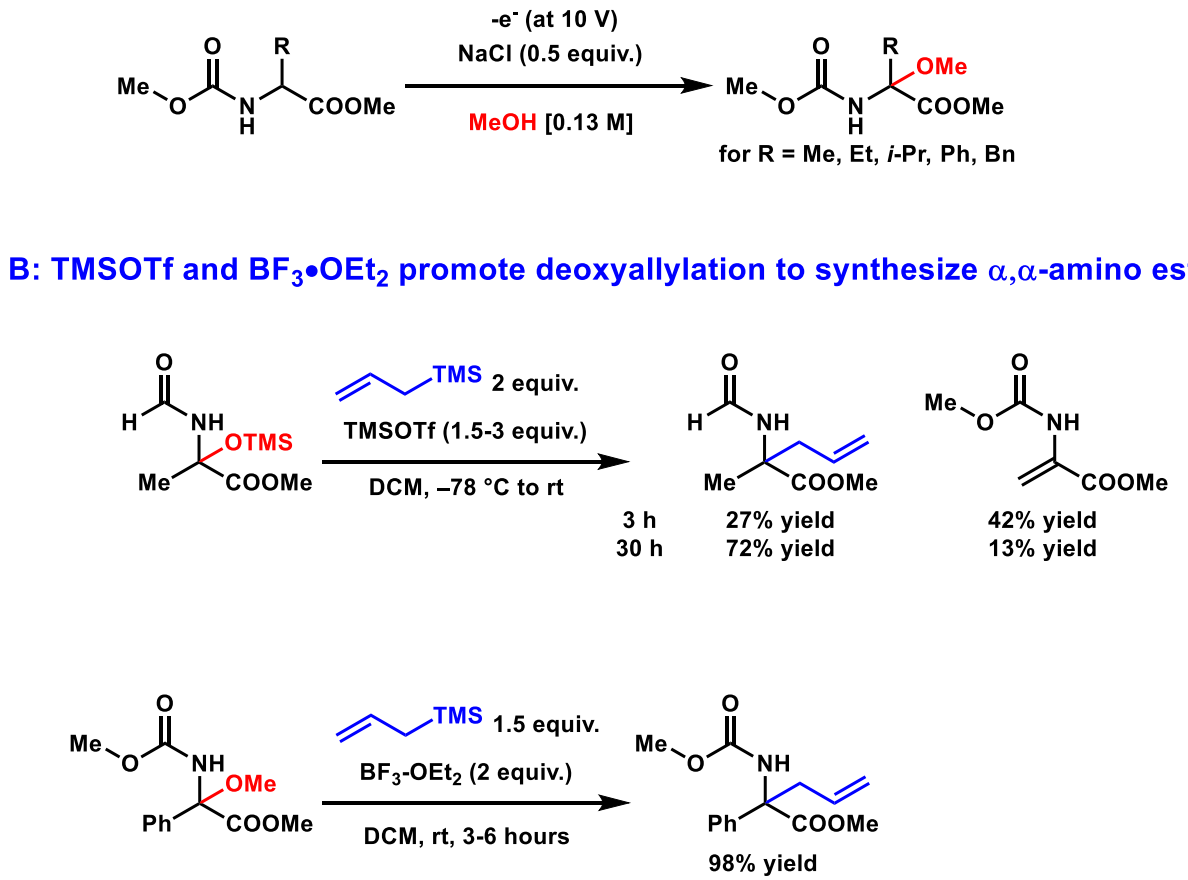

Figure 4.5 Racemic precedent for the preparation and allylation of α-methoxy-α-phenyl glycine

4.2.1 Optimization of the squaramide catalyzed and BF_3 promoted allylation of α-methoxy-α-phenyl glycine

The ability for the Jacobsen group to merge enantioselective HBD catalysis and silylium Lewis acid catalysis while achieving high levels of enantioinduction made plausible the ability to

[200] Roos, E. C.; Lopez, M. C.; Brook, M. A.; Hiemstra, H.; Speckamp, W. N.; Kaptein, B.; Kamphuis, J.; Schoemaker, H. E. Synthesis of .Alpha.-Substituted .Alpha.-Amino Acids via Cationic Intermediates. *J. Org. Chem.* **1993**, *58* (12), 3259–3268.

enantioselectively catalyze the addition of allylsilanes to α-methoxy-α-phenyl glycine made via the Shono procedure. In this context, the Jacobsen group has demonstrated the ability to abstract methoxide and acetate to generate oxocarbeniums and non-heteroatom stabilized carbocations and engage these electrophiles with furans and allylsilanes respectively, thus extending this methodology to *N*-acyliminium ion allylations, reactions prevalent in HBD catalysis is not a stretch.[180,181]

The Shono anodic oxidation was applied to *N*-Cbz α-phenyl glycine methyl ester under the exact conditions reported for the methyl carbamate substrate, synthesizing starting material **8-Cbz** in 76% yield. Initial screening was conducted with a one equivalent of TMSOTf and 10 mol% 9-phenanthryl squaramide **4e**, which provided 11% ee and 23% yield of methallylated **9a** and 20% ee and 27% yield of **9b** (Figure 4.6). Unfortunately, the rate of TMSOTf catalyzed background reaction is the exact same as the rate of the HBD co-catalyzed process. This prompted the exploration of other Lewis acids in this chemistry; however, for completeness this system should be investigated further, at least with a catalyst screen to see the range of possible enantioselectivities and effect of other hydrogen-bond donor scaffolds, including ureas and thioureas.

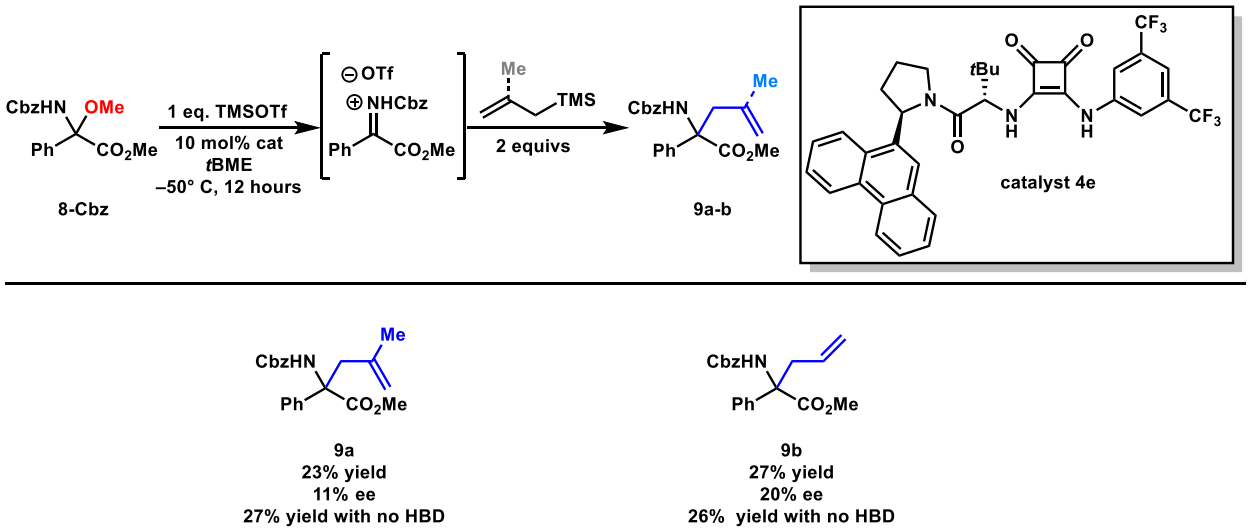

Figure 4.6 Initial survey of TMSOTf squaramide catalyzed deoxyallylation of **8**

Given the ability of TMSOTf and $BF_3 \cdot OEt_2$ to promote this transformation in DCM, alternate conditions were screened for TMSOTf and boron Lewis acids in DCM (Figure 4.7). In DCM at –78 °C, TMSOTf does not promote the reaction, whereas at 4 °C, complete decomposition occurs; intermediate temperatures should be screened. $BF_3 \cdot OEt_2$ and 4-pyrenylpyrrolidine squaramide catalyst **4g** promotes the allylation of **8-Cbz** in 50% ee with 70% conversion. BCF does not promote the reaction, while BCl_3 provides 15% conversion and 6% yield. Thus subsequent studies were performed with $BF_3 \cdot OEt_2$.

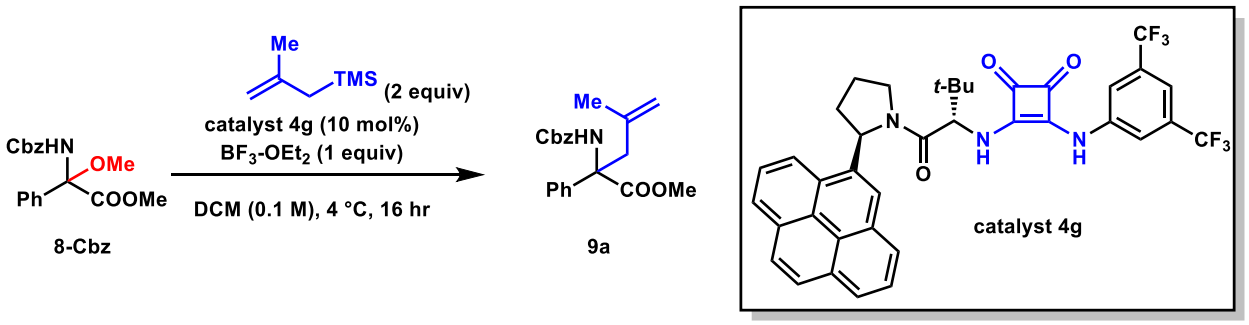

lewis acid	conversion	ee
TMSOTf (–78 °C)	0	-
TMSOTf (4 °C)	decomp	-
BF_3-OEt_2	71	50
$B(C_6F_5)_3$	0	-
BCl_3	15	6

Figure 4.7 Lewis acid screening in the HBD **4g** catalyzed methallylation of **8-Cbz**

Since boron Lewis acids have never been explored in the context of HBD chemistry, logically the next step would be the determination that squaramides are the optimal class of HBD for this transformation (Figure 4.8). Indeed squaramide **4g** provide substantially higher levels of enantioselectivity than the corresponding urea **6g** and thiourea **7g**. Interestingly, all three classes of HBD catalysts provide essentially the same conversion, raising the question of whether or not the catalyst is involved in the rate determining step, a question that will be revisited. To determine if the catalyst is even acting as an H-bond donor, the squaramide catalyst **4g** N-H's were replaced with N-Me, and the product was racemic, but the conversion remained the same, at 68% ee.

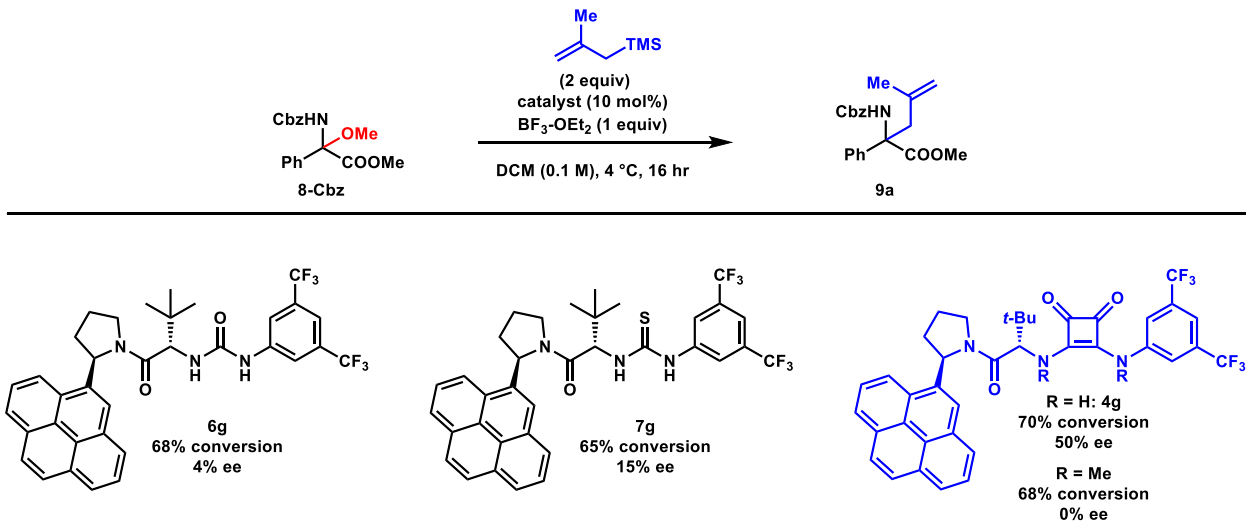

Figure 4.8 Effect of HBD class on the enantioselectivity and conversion of the $BF_3 \cdot OEt_2$ promoted methallylation of **8-Cbz**

Having identified squaramides and $BF_3 \cdot OEt_2$ as the optimal combination of HBD and Lewis acids for this transformation, an extensive squaramide screen was conducted (Figure 4.9). This screen reveals that arylpyrrolidine catalysts are uniquely enantioselective in the methallylation of **8-Cbz**. The enantioselectivity landscape is extremely flat with respect to the pyrrolidine arene, with all examined catalysts **4a-g** providing between 40 and 53% ee. The addition of a methyl substituent geminal to the arene (**4a'**) proves to be disastrous to the enantioselectivity of this transformation, reducing the ee from 45% to 3%. Rarely does the addition of this methyl group reduce the ee by such a drastic amount; this effect is almost certainly mechanistically interesting. Other catalyst amide substituents that are optimal in other transformations provide very low levels of enantioselectivity (<12% ee) here.

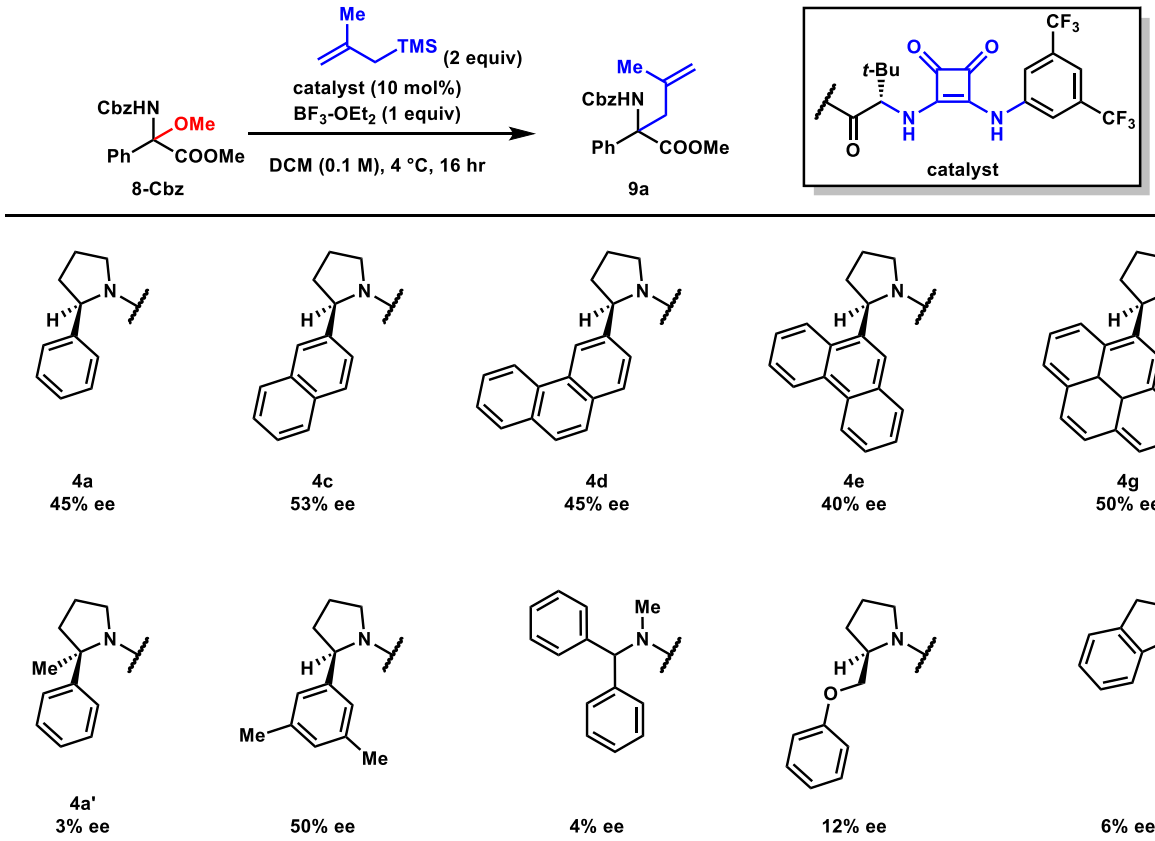

Figure 4.9 Squaramide catalyst screen in the $BF_3 \cdot OEt_2$ promoted methallylation of 8-Cbz

The flat enantioselectivity with respect to arylpyrrolidine leaves little room for catalyst optimization. Thus, the next position that was varied was the arene directly attached to the squaramide portion of the 9-phenanthryl pyrrolidine catalyst (Figure 4.10). Traditionally this portion of the catalyst modulates the HBD acidity and thus the anion-binding strength of the catalyst and has a minimal impact on the enantioselectivity but may have a large impact on the rate of the reaction, as seen in Chapter 2.[94] In this case, we see a clear and significant trend of the HBD aniline substituents on the enantioselectivity of the allylation of **8-Cbz**. The optimal catalyst in this series is the 3,5-dinitro catalyst, which is the most withdrawing substiuent, with $\sigma_m = 0.71$ (43% ee), followed by 3,5-bis(trifluoromethyl), with $\sigma_m = 0.43$ (40% ee); the least selective catalyst is the 3,5-dimethyl catalyst, with $\sigma_m = -0.07$ (–5% ee).[98] Interestingly, the sign of enantioselectivity flips for the phenyl and 3,5-dimethyl phenyl catalysts. Furthermore, the yield is

completely independent of the anion-binding strength of the catalyst, and if anything the more electron rich, weaker anion-binding catalysts provide slightly higher yields. These data suggest that a catalyst anion-binding step is not rate determining, which is consistent with the same yield provided by thioureas, ureas, squaramides, and *N,N*-dimethylsquaramides. This will be revisited in the next section, in which the mechanism is discussed in more detail.

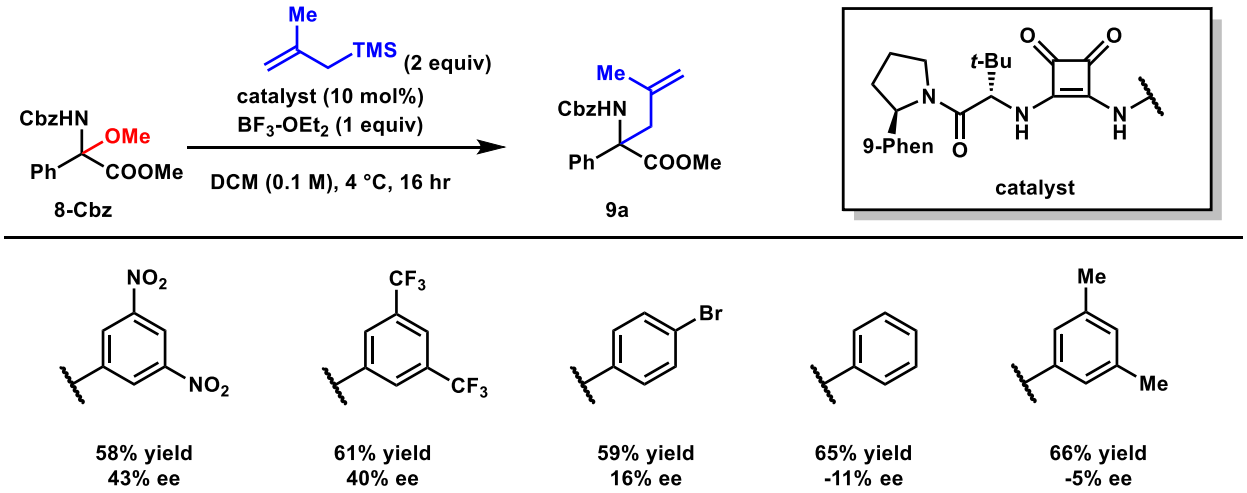

Figure 4.10 Effect of squaramide electronic tuning on the enantioselectivity and yield of **9a**

Having exhausted tunable catalyst parameters, the next steps to optimize the methallylation of **8-Cbz**, involve substrate engineering in order to find a substrate more amenable to enantioselective catalysis. Since the amide has had a profound effect on the enantioselectivity of related transformations, as discussed in Chapter 2, and is ultimately not incorporated into the amino acid end product, it is the natural choice to vary. A protecting group screen was conducted with substrates that were tolerated in the anodic oxidation, namely Cbz, Boc, methyl carbamate, alloc, and Ac (Figure 4.11). As in Chapter 2, substrates bearing acetamide protecting groups were completely unreactive in this chemistry. Among the carbamate protecting groups examined, all provided very similar enantioselectivies ranging from 30% with Boc to 50% with Cbz, potentially indicating that the Cbz arene is playing a role in enantioinduction, although this is far from conclusive and Alloc provides a very similar 47% ee.

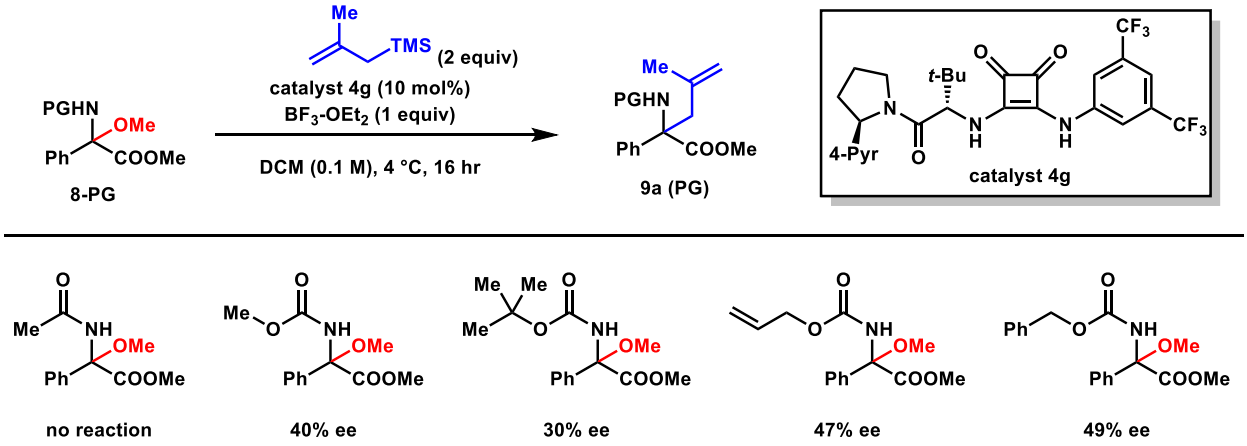

Figure 4.11 Protecting group screen in the squaramide and BF_3 promoted methallylation of **8**

Varying the ester group was attempted, however transesterification to the methyl ester occurred under the electrochemical oxidation conditions. Initial attempts to transesterify the methyl ester of **8-Cbz** failed, and so this was deemed a poor choice of substrate modification. In a last attempt to boost the enantioselectivity of this transformation, the side chain of the amino ester was varied and the results are presented in Figure 4.12. Unfortunately, many of the substrates tested were not suited to the anodic oxidation, with substrates bearing large and electron rich arenes completely decomposing. Of the substrates that were able to be synthesized, all provided substantially lower enantioselectivities than the initially tested substrate **8-Cbz**. The structurally related *p*-tolyl substrate provided high conversion to 73% but low enantioselectivity at 26% ee. Substrates bearing *p*-CF_3-phenyl and α-CF_3 groups provided no conversion, which is unsurprising if ionization of the substrate is rate determining, as formation of an α-CF_3 iminium would be very uphill energetically. In the related HBD and silylium catalyzed anion-abstraction chemistry acetoxy groups are abstracted substantially better than methoxy groups, thus α-methoxy-α-trifluoromethyl substrate was tested, which was also provided no conversion.[181] Aliphatic substrates bearing an α-methyl and an α-isopropyl group were tested and the methyl substrate proceeded cleanly to full conversion but provided product in just 5% ee. The isopropyl substrate

was both sluggish and provided low enantioselectivity. Last, the glycine derived substrate was tested and provided both low conversion and racemic product.

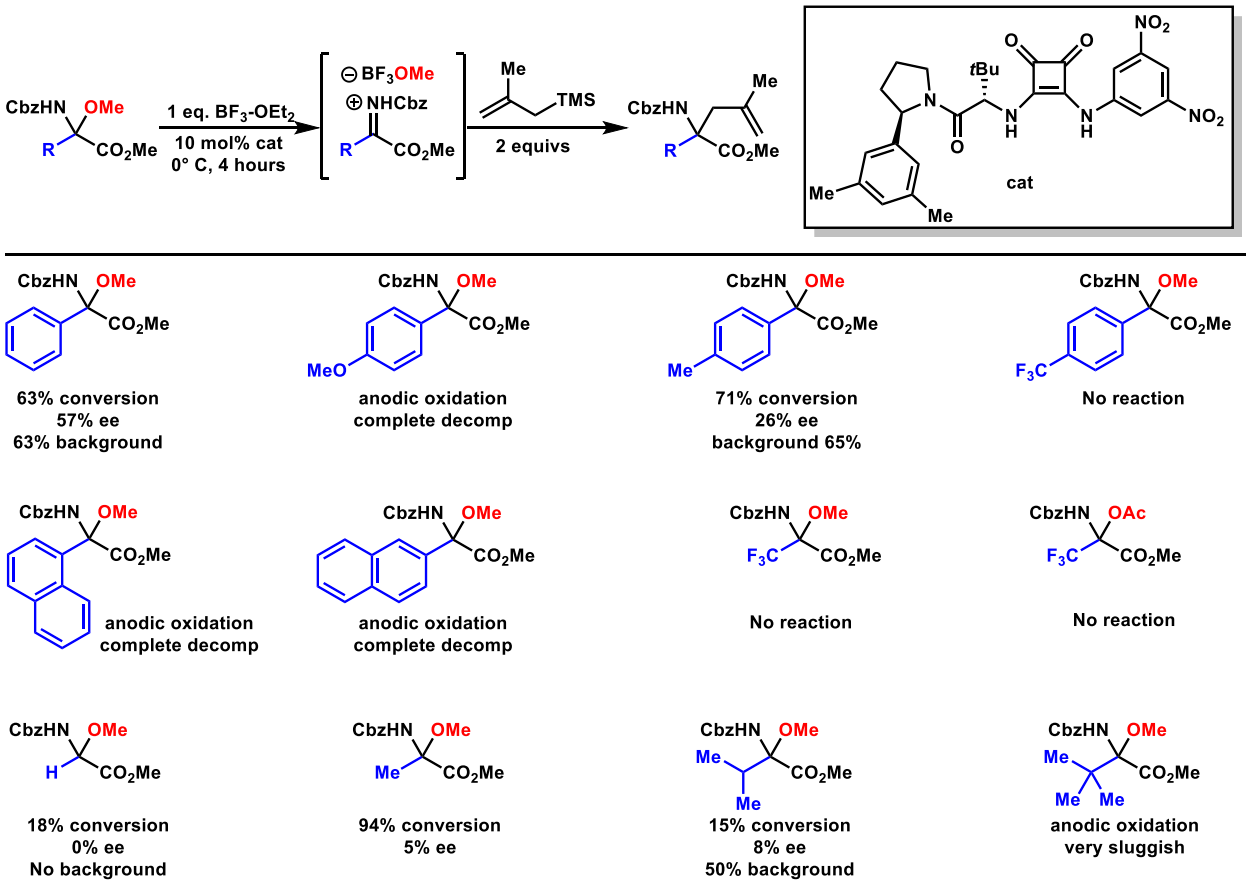

Figure 4.12 Amino ester side-chain screen in the squaramide and BF_3 promoted methallylation of disubstituted amino esters

At this point, optimization of reaction parameters had been exhauseted and the transformation seemed unlikely to be optimized past the 57% ee result with the 3,5-dimethylphenylpyrrolidine substituted 3,5-dinitrophenyl squaramide shown in Figure 4.12. Given the lack of catalysis over background, it seemed likely that the mechanism of the transformation is was preventing further optimization, so mechanistic investigations were pursued for further optimization.

4.2.2 Mechanistic investigation into the squaramide catalyzed and BF_3 promoted allylation of α-methoxy-α-phenyl glycine

In the course of optimization of the methallylation of **8-Cbz**, a few pieces of evidence suggested that the squaramide is not catalyzing the rate determining step. Separate pieces of evidence include the same conversion observed in the absence of HBD catalyst, with different classes of HBDs (thiourea, urea, and squaramde), and with *N*,*N*-dimethyl squaramide, which has the hydrogen-bond donor functionality knocked out. To confirm that this is the case, and to distinguish from the scenario in which reactions are stalling out at the same conversion in the presence and absence of HBD catalyst, early reaction time points were taken to better determine the rate in the presence and absence of HBD, as well as to determine if enantioselectivity is constant over the course of the reaction (Figure 4.13). The conversion at early time points is identical in the presence and absence of HBD catalyst and the ee is found to be relatively flat, with slightly lower enantioselectivity at very early time points, which may be the result of poor temperature control, analytical challenges at precisely determining ee at low conversions, or product inhibition of BF_3 changing the relative loadings of BF_3 and catalyst over the course of the reaction. Additionally, this revealed the reaction goes to completion in a couple hours, rather than the previously expected reaction time of 12+ hours.

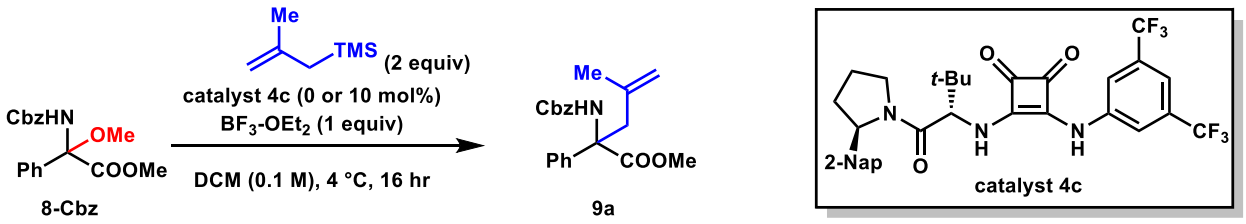

time (min)	background conversion	HBD catalyzed conversion	ee
10	11	11	49
30	33	31	52
60	51	50	53

Figure 4.13 Effect of HBD on conversion and ee of the allylation of **8-Cbz** at early time points

These data, as well as wealth of other data, implied that there may be a competitive racemic background reaction, which is preventing optimization of the reaction. Thus, the reaction was run with 100 mol% of squaramide HBD catalyst **4g**, which revealed that increasing the catalyst loading from 10 to 100 mol% increased the enantioselectivity from 50% to 67% (Figure 4.14). Given that the reaction went to 50% conversion in one hours at 4 °C, the reaction was run at –25 °C, which decreased the yield to 42% and ee to 33%.

In an attempt to increase the enantioselectivity by decreasing the BF_3 to HBD ratio without increasing the amount of HBD, lowering the loadings of BF_3 was attempted (Figure 4.14). However, it was found that substoichiometric loadings of BF_3 provide low conversion, and furthermore the conversion never exceeds the amount of BF_3 added, implying that BF_3 may be consumed in this reaction, as the presumed BF_3OMe anion and TMS cation almost certainly react or disproportionate, potentially in a way the renders the products catalytically inactive. In a last attempt to increase the enantioselectivity, slow addition of BF_3 was attempted, but this had no impact on the enantioselectivity.

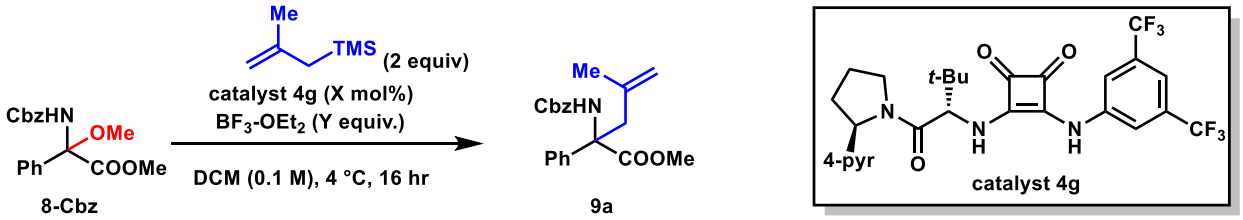

Effect of catalyst loading and temperature on conversion and ee

catalyst loading (X mol%)	BF_3-OEt_2	temp (°C)	conversion	ee
10	1 equiv.	4	64	50
100	1 equiv.	4	66	67
10	1 equiv.	–25	42	33

Effect of BF_3•OEt_2 loading on conversion and ee

catalyst loading (X mol%)	BF_3-OEt_2	temp (°C)	conversion	ee
10	0.1 equiv.	4	trace	ND
10	0.5 equiv.	4	15	ND
10	1.0 equiv.	4	64	50
10	1.0 slow addition	4	70	50

Figure 4.14 Effect of squaramide and $BF_3 \cdot OEt_2$ loadings on conversion and enantioselectivity in the allylation of **8-Cbz**

The data point to the catalytic cycle depicted in Figure 4.15. The proposal is that the rate determining step is the ionization of the substrate, which is performed by BF_3 alone to create a high energy *N*-acyl phenylglyoxylate iminium ion pair, with some boron anion that may or may not be BF_3OMe. This iminium ion-pair can either directly react with methallylsilane or to form a beta-silyl cation, which can be eliminated to product. Alternately, the HBD catalyst can intercept and bind the iminium ion-pair and direct the facial addition of methallylsilane, in what is likely the selectivity determining step.

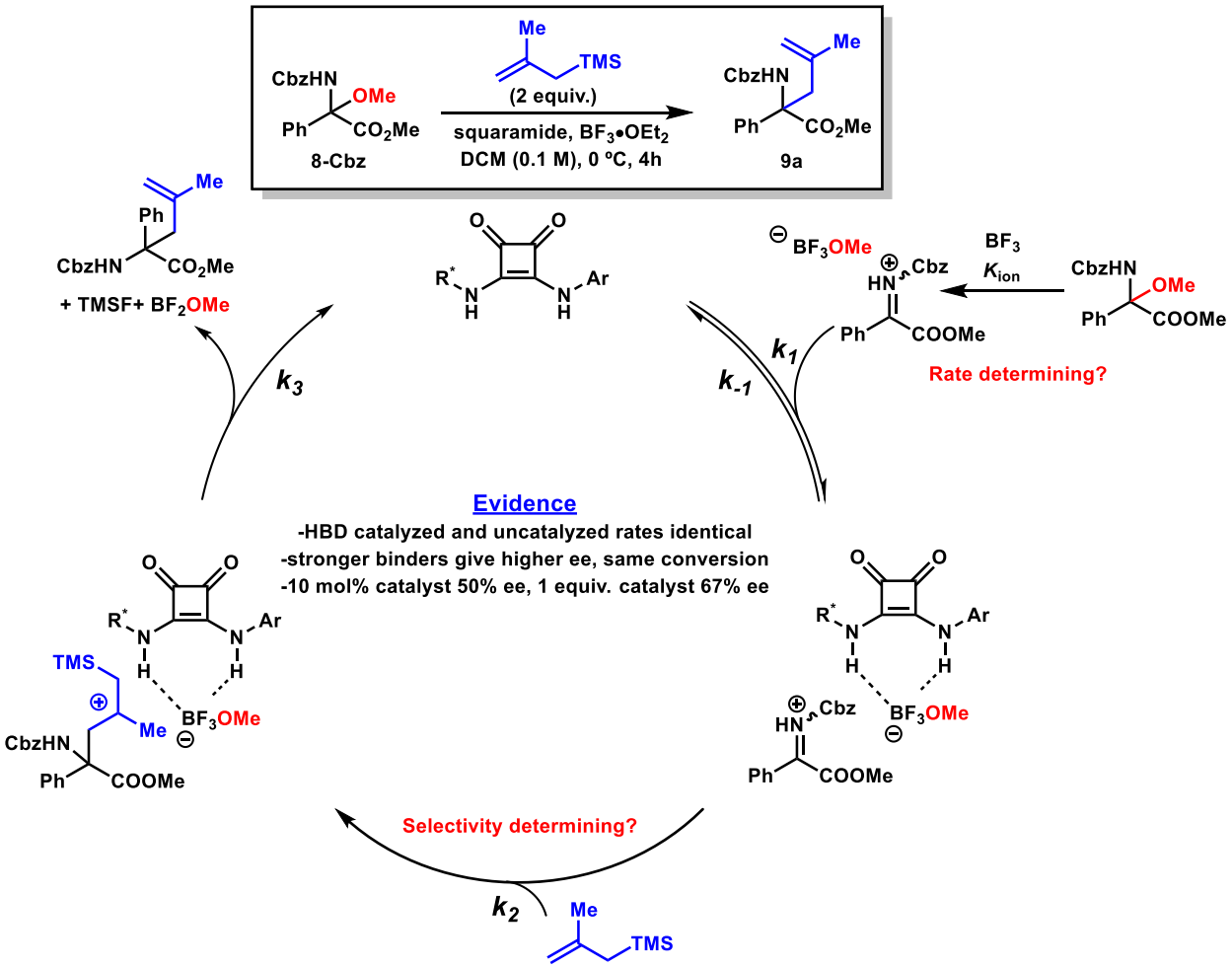

Figure 4.15 Proposed catalytic cycle for the squaramide catalyzed and BF_3 promoted methallylation of **8-Cbz**

Evidence for this mechanistic cycle includes that the rates in the absence and presence of HBD catalyst are identical, while also being heavily dependent on the loading of BF_3, implying BF_3 alone catalyzes the rate determining step, which is likely ionization. Evidence for competing catalyzed and uncatalyzed post-rate determining selectivity determining pathways are the dependence of ee on the loading of HBD and on the strength of the anion-binding properties of the HBD catalyst. When the concentration of catalyst is higher or the anion-binding properties are stronger, this biases the iminium catalyst association equilibrium, providing higher enantioselectivities. Not much is known about HBD binding of BF_3OMe or related borate anions, thus *in situ* ^{19}F NMR studies were conducted to determine the nature of the anion and anion-

binding. However, these results were inconclusive, as over 20 ^{19}F peaks were observed, indicating that there may be more than one viable anion, especially given the known ability of mixed fluoroborate species to disproportionate.[201] In fact, even mixing BF_3 and methallylsilane produced around 10 peaks in the ^{19}F NMR spectrum, indicating that studying the anion and anion-binding in this chemistry is likely intractable.

4.2.3 Outlook on HBD and BF_3 co-catalysis

From section 4.2, it is clear that BF_3 and HBD catalysts can be combined to promote an enantioselective reaction. With respect to reaction optimization, it seems unlikely that HBD and BF_3 can be optimized to give high enantioselectivities in this transformation. Given the high synthetic interest in the reaction, one should reinvestigate the better studied TMSOTf and HBD co-catalysis systems explored briefly in Figure 4.6, especially with acetate leaving groups.

Given the lack of rate acceleration, it is unclear if there is any interaction between BF_3 and a squaramide hydrogen bond-donor catalyst that is productive to enantioselective catalysis or if the two catalysts are operating completely independently. It is not clear what the interaction would be, but it is unlikely to impossible that a squaramide would have the ability to abstract a fluoride from BF_3. To further explore if HBD and BF_3 can be combined productively to affect an enantioselective transformation, the methallylation of 4 different classes of electrophiles were tested, all of which are not suited to TMSOTf catalysis (Figure 4.16). Whether or not the catalyst provides rate acceleration seems to be highly dependent on the transformation. However, universally the products formed were racemic, even when HBD increases the rate of reaction, indicating that borate anions may not be well recognized by the catalyst, and that the interaction allowing for enantioselectivity in the amino acid synthesis is a different substrate catalyst

[201] Moor, J. E. d.; van der Kelen, G. P. Studies on Trivalent Boron Compounds : I. The Boron and Proton Magnetic Resonance Spectra of Some Trivalent Boron Compounds. *J. Organomet. Chem.* **1966**, *6* (3), 235–241.

interaction, perhaps ester or carbamate binding. Further elucidation of BF_3 and HBD co-catalysis will be the subject of the next section, 4.3.

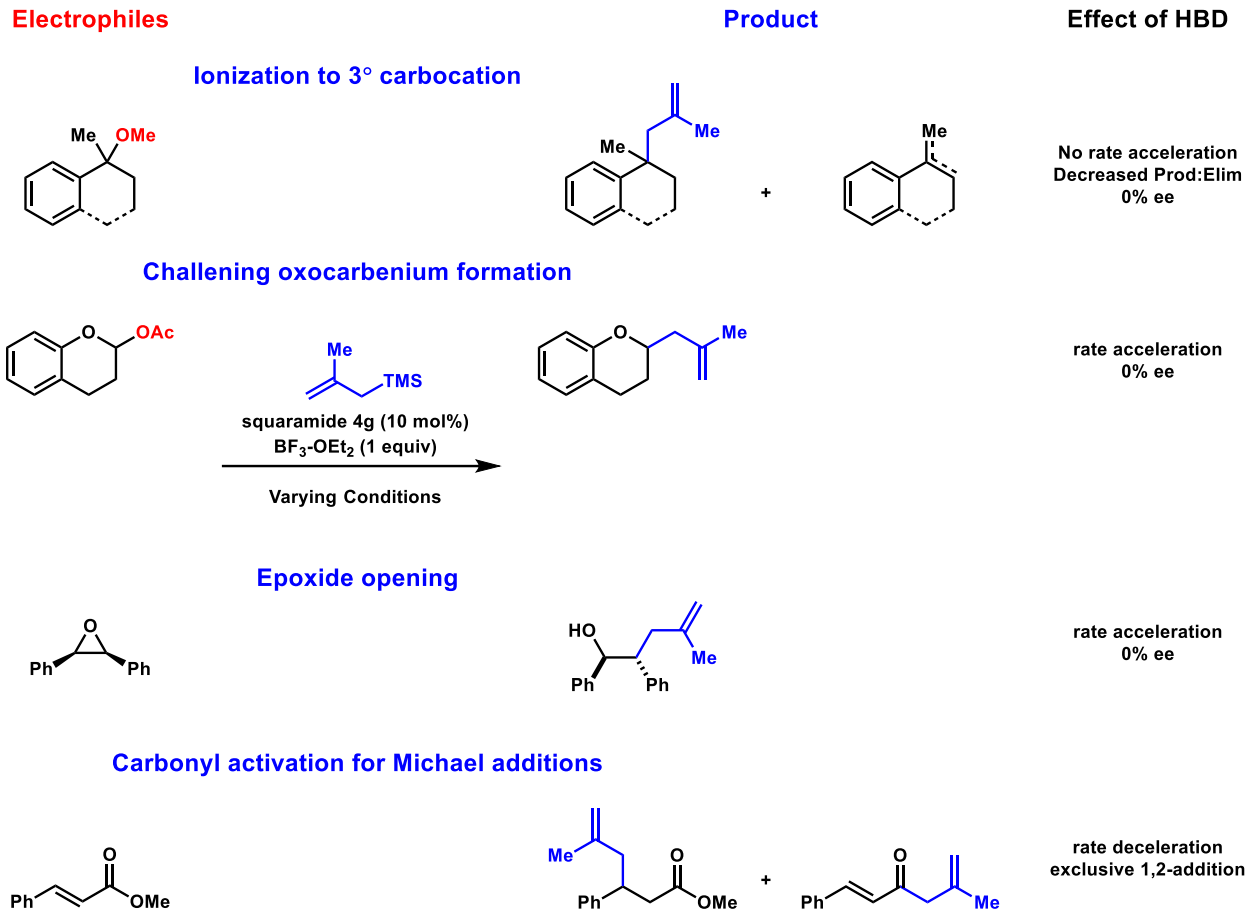

Figure 4.16 $BF_3 \cdot OEt_2$ and squaramide HBD co-catalysis provides racemic reactivity in 4 unrelated transformations and divergent rate acceleration in the presence of a squaramide catalyst

4.3 Development of a screening method and Gutmann-Beckett NMR method for identification of enantioselective Lewis acid and hydrogen-bond donor co-catalytic systems

The ability to combine HBD and silylium Lewis acid catalysis has already proven to be incredibly enabling in expanding the range of electrophiles amenable to enantioselective anion-abstraction catalysis. Specifically it has allowed for the use of acetals and 3° benzylic acetates, which are far more shelf stable than the corresponding α-chloro ethers and 3° benzylic chlorides, which undergo auto-heterolysis and hydrolysis in air.[180,181] Additionally, this co-catalytic strategy has allowed hydrogen-bond donor ion-pairing catalysis access to extremely electrophilic

intermediates that strong silyl Lewis acids can generate by heterolyzing bonds that would be inert to HBD catalysts. Central to achieving enantioselectivity in these transformations is the ability to generate a hotter Lewis acid via HBD abstraction of triflate from silyltriflates, creating a more naked silylium, which allows for enantioselective catalysis over racemic background catalysis by the Lewis acid alone (Figure 4.17 A). The BF_3 catalyzed allylation of α-methoxy-α-phenyl glycinates further demonstrates the enabling ability for HBD and Lewis acid co-catalysis to promote processes that HBDs alone cannot catalyze. However, this reaction never surpassed 53% ee largely because of the inability for an HBD co-catalyzed process to outcompete a racemic BF_3 catalyzed background reaction. Attempts to study the effect of HBDs on BF_3 catalysis was challenging due to the complicated nature of the reaction.

A mechanistically simple model reaction and an NMR method were designed to rapidly assess combinations of Lewis acids and HBD catalysts capable of giving enantioselectivity and rate enhancement over racemic Lewis acid catalysis, which will be the focus of this section. Identification of set of Lewis acid and HBD co-catalytic systems viable in enantioselective catalysis would be incredibly enabling and have a few distinct advantages over the traditional strategy of enantioselective Lewis acid catalysis, in which a preformed Lewis acid fitted with chiral ligands is employed. First, it would allow the use of off the shelf inorganic halides/triflates. Second as discussed in the intro, BOX (and other traditional) ligands require either replacing extremely withdrawing ligands, such as halides or triflates with somewhat donating ligands (such as oxazolines) or coordinative saturating the transition metal. Central to this HBD Lewis acid co-catalytic concept is the hypothesis that the Lewis acid will provide a baseline level of activity and that the HBD will enhance the Lewis acidity by partially or completely abstracting a halide or triflate ligand, to render the Lewis acid more electron deficient and/or coordinatively unsaturated,

opening doors to achieving enantioselectivity in extremely challenging contexts (Figure 4.17 B and C).

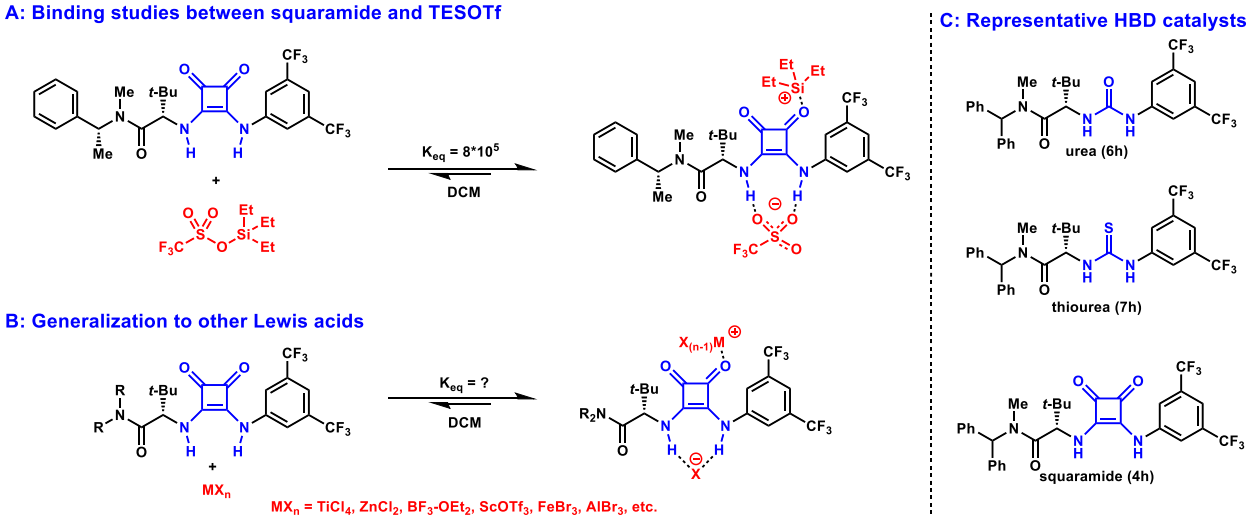

Figure 4.17 Generalization of HBD enhancement of silylium Lewis acidity allowing for enantioselective co-catalytic HBD Lewis acid systems

4.3.1 Addition of methallylsilane to benzaldehyde and benzaldehyde dimethylacetal as a model reaction for assessing HBD Lewis acid co-catalytic systems

To identify new synergistic LA and HBD combinations, the Hosomi-Sakurai reaction between benzaldehyde or benzaldehyde dimethyl acetal and 2-methallyltrimethylsilane was chosen as a model reaction. These two reactions were chosen because they are well precedented in the literature to be catalyzed by a number of Lewis acids,[202] they served as a model reaction in the initial report of HBD TMSOTf co-catalysis, and they represent the two primary forms of activation that both HBD and Lewis acids catalyze. Specifically, in the context of benzaldehyde, Lewis acids and HBDs catalyze additions by coordinating the carbonyl, thus lowering the LUMO

[202] For reviews on catalytic Hosomi-Sakurai reactions see: a) Zhu, L.; Hu, Y.; Sun, F.; Huang, Y. Recent Developments in the Catalyzed Hosomi-Sakurai Reactions. *Adv. Sci. Focus* **2014**, *2* (2), 97–105. b) Lade, J. J.; Pardeshi, S. D.; Vadagaonkar, K. S.; Murugan, K.; Chaskar, A. C. The Remarkable Journey of Catalysts from Stoichiometric to Catalytic Quantity for Allyltrimethylsilane Inspired Allylation of Acetals, Ketals, Aldehydes and Ketones. *RSC Adv.* **2017**, *7* (13), 8011–8033.

and facilitating addition of nucleophiles, while in the context of benzaldehyde dimethyl acetal, a Lewis acid abstracts an alkoxide to generate an oxocarbenium and a HBD is inert but can abstract a chloride an α-chloroether to generate an oxocarbenium.

In this reaction, conversion and enantioselectivity were planned to be used as readouts of success for any given combination. However, the reaction was too facile at –78, thus conversion was consistently 100% even at early time points, so conversion could not be used. In the future initial rate kinetics should be explored to study HBD co-catalyst acceleration over LA background rate, but in these initial studies, enantioselectivity was used as a binary readout for acceleration over background. This is possible because in the absence of HBD rate acceleration, the enantioselectivity should not exceed the ratio of HBD to LA.

For any given Lewis acid, 18 reaction were screened, a 3x3x2 array of co-catalysis with 3 classes of HBD: urea **6h**, thiourea **7h**, and squaramide **4h**, 3 solvents: toluene, diethyl ether/tBME, and dichloromethane using 2 electrophiles: benzaldehyde and benzaldehyde dimethylacetal. Differing classes of HBDs often give drastically different enantioselectivites, have differing anion-binding strengths, and different potential coordination sites to a Lewis acid.[141,179] This specific benzhydryl amide catalyst was chosen due to the ease of synthesis of large quantities as well as its ability to give medium to high levels of enantioselectivity in a number of transformations.[33,181] Studies have shown the importance of solvent in both the rate and enantioselectivity of ion-pairing catalysis.[94] As mentioned above, the two different electrophiles were chosen as they have divergent modes of activation; benzaldehyde would be activated via direct LA or HBD coordination, whereas the benzaldehyde dimethylacetal would undergo anion-abstraction by the LA to form an oxocarbenium ion-paired intermediate.

The reported TMSOTf HBD combination was run as a control experiment with 50 mol% of TMSOTf and 10 mol% of HBD. The combination with squaramide **4h** gave modest enantioselectivity (Figure 4.18) of –44% and –51% in tBME and toluene respectively, while nearly racemic results were obtained with the urea and thiourea (**6-7h**) and truly racemic results were obtained in DCM. This suggests that silyl triflate is activated by squaramides in this model reaction, and may or may not be activated by ureas and thioureas, as expected. Interestingly until this point, ethereal solvents had always been presumed optimal for enantioselectivity in TMSOTf cocatalysis due to the ability of ethereal solvents to buffer TMSOTf via solvent coordination.

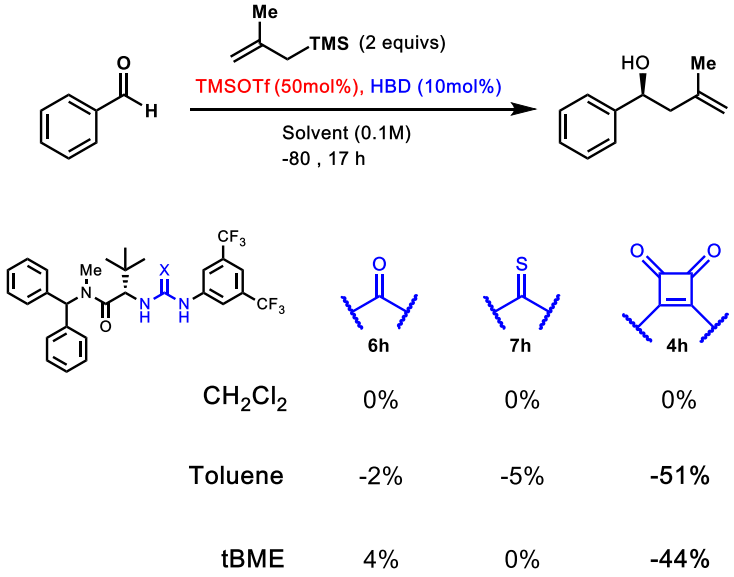

Figure 4.18 Benzaldehyde methallylation with TMSOTf and HBD catalysts

A variety of commonly Lewis acids were screened with this set up were examined in the aldehyde allylation. The Lewis acids can be classified into three classes: 1) boron Lewis acids (BF_3-Et_2O, BCl_3, BBr_3, BCF), 2) lanthanide triflates ($Yb(OTf)_3$, $Gd(OTf)_3$, $Ce(OTf)_3$), and 3) first row and miscellaneous metal halides/triflates ($Bi(OTf)_3$, $AlCl_3$, $TiCl_4$, $Sc(OTf)_3$, $NaBAr_F$, Na(OTf), $In(OTf)_3$, $Mg(OTf)_2$, $Fe(OTf)_3$, $FeBr_3$).

The summary of the results with boron Lewis acids is presented in Figure 4.19. For boron Lewis acids, ethereal solvents were optimal for enantioselectivity. Interestingly with BF_3, all three

HBD catalysts give some level of enantioselectivity and the urea is slightly better than the squaramide (21 vs. 19% ee). This is in contrast to the results in the amino acid synthesis, in which squaramides were far superior to ureas and thioureas. This is another example of a reaction in which BF_3 and HBDs provide enantioselectivity, in contrast to the reactions tested in Figure 4.16, which were all racemic. Additionally, these levels of enantioselectivity indicate that HBD promoted rate acceleration is likely. For BCl_3, thiourea in ether was uniquely effective relative to the other combinations with BCl_3 and also indicates rate acceleration. It is possible that since thioureas are more nucleophilic than the other catalysts, the thiourea could abstract a chloride and add into the boron with the sulfur to create a new chiral adduct. Last, interestingly, the optimal results for BF_3 and BCl_3 give differing senses of absolute stereochemistry. BCF provided complete conversion but racemic product in all 9 reactions. This is expected, as BCF has no abstractable ligands so there is no opportunity for productive catalyst-catalyst interactions as envisioned in Figure 4.17.

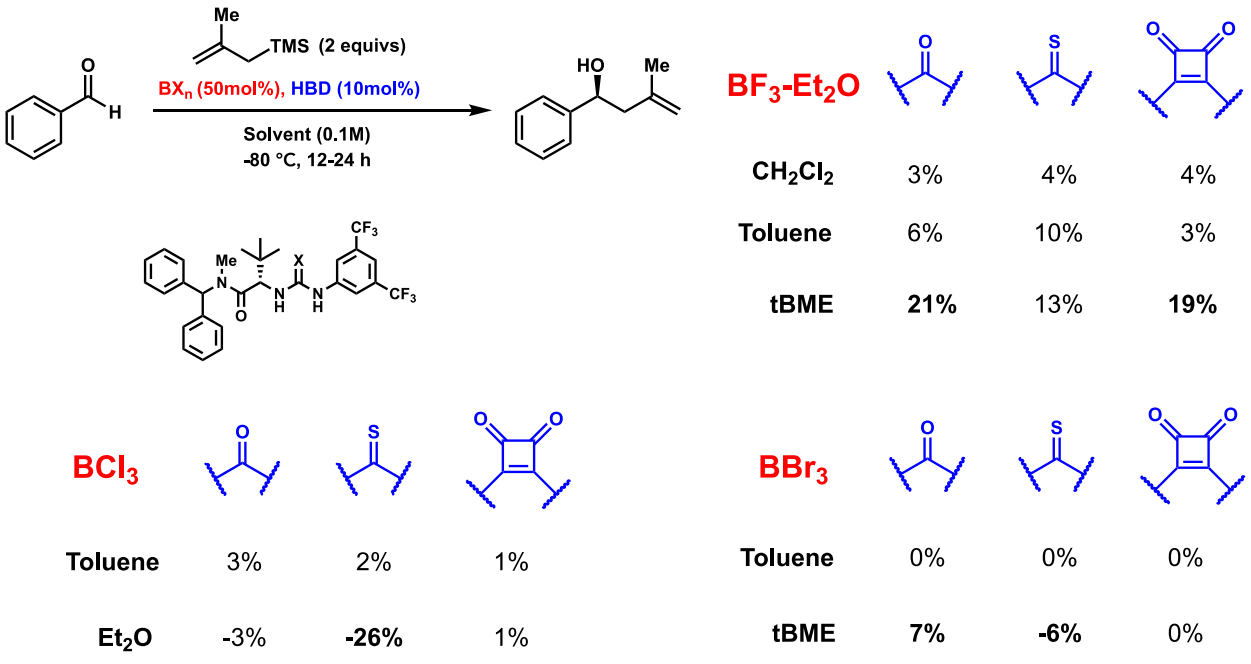

Figure 4.19 Benzaldehyde methallylation with boron Lewis acids and HBD catalysts

The analogous screen was performed with the lanthanide (III) triflates, $Yb(OTf)_3$, $Gd(OTf)_3$, $Ce(OTf)_3$, and pseudolanthanide triflate, $Yb(OTf)_3$. These Lewis acids are generally less active than boron and silyl triflate Lewis acids. Additionally, all four Lewis acids were sparingly soluble in ethereal and aromatic solvents, which raises the possibility for HBD to act as a phase transfer catalyst. As a result of weak Lewis acidity and poor solubility these reactions were much less clean and often did not proceed to high conversion. Optimal results for bismuth and ytterbium triflate in tBME with squaramide catalyst, although enantioselectivities are low. Toluene was optimal for the cerium squaramide combination and the gadolinium urea combination, providing –39 and –36% ee respectively, although at low conversion. This is another case where HBD rate acceleration or phase-transfer catalysis seems likely.

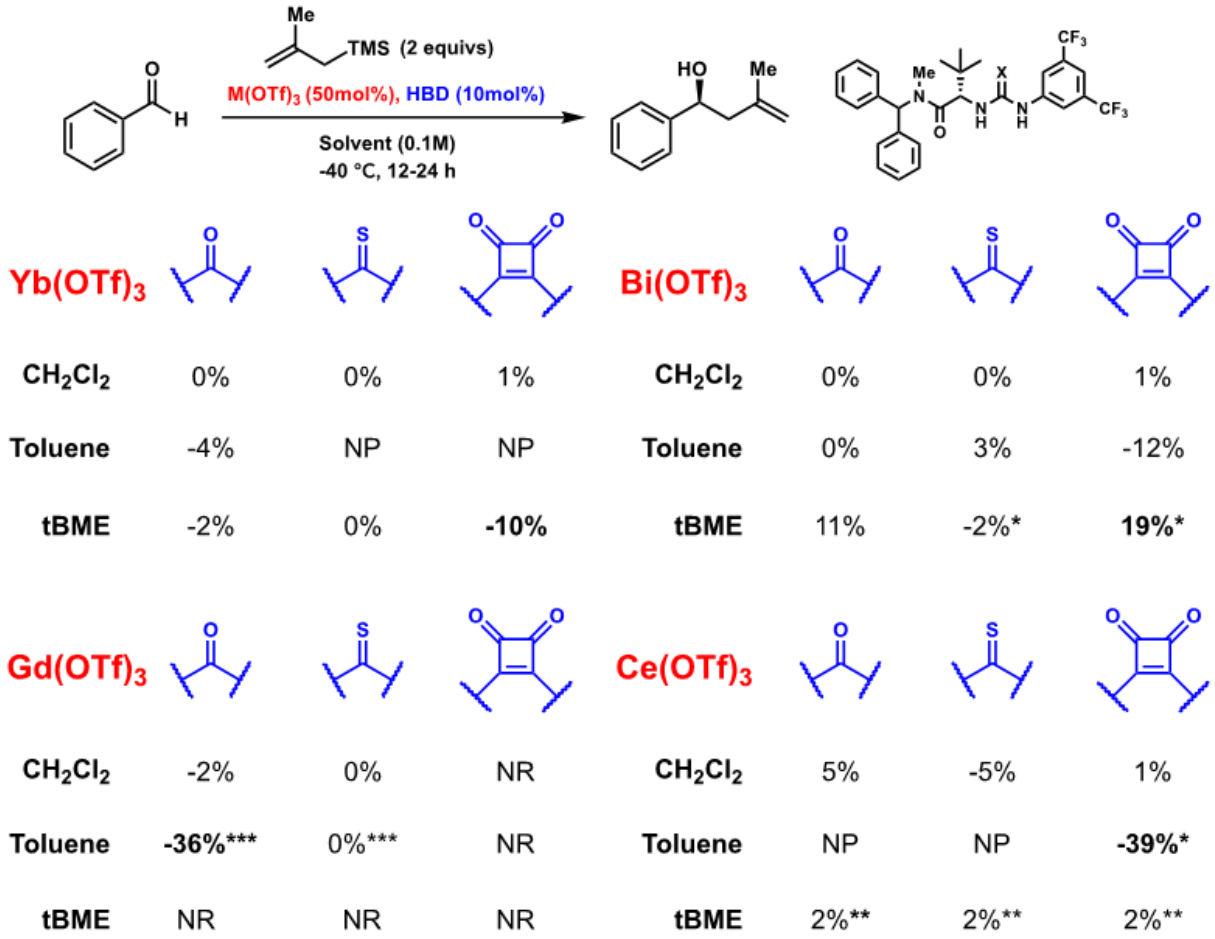

Figure 4.20 Benzaldehyde methallylation with Lanthanide (III) triflates and HBD catalysts

Last, this screen was performed on select first row transition metal and miscellaneous triflates or halides Figure 4.21. Selection of Lewis acids in this last set may seem arbitrary, but were chosen due to a combination of redox innocence and precedent in ability to catalyze racemic Sakurai reactions. Iron Lewis acids provided low levels of enantioselectivity, while all other Lewis acids in this category either do not catalyze the reaction or catalyze it a racemic fashion. Many of these poorly selective or unselective Lewis acids are highly active first row transition metals complexes, suggesting that either there is no rate acceleration over the robust background in the

presence of HBD or the HBD is not strong enough to dissociate a ligand from an already electron deficient metal.

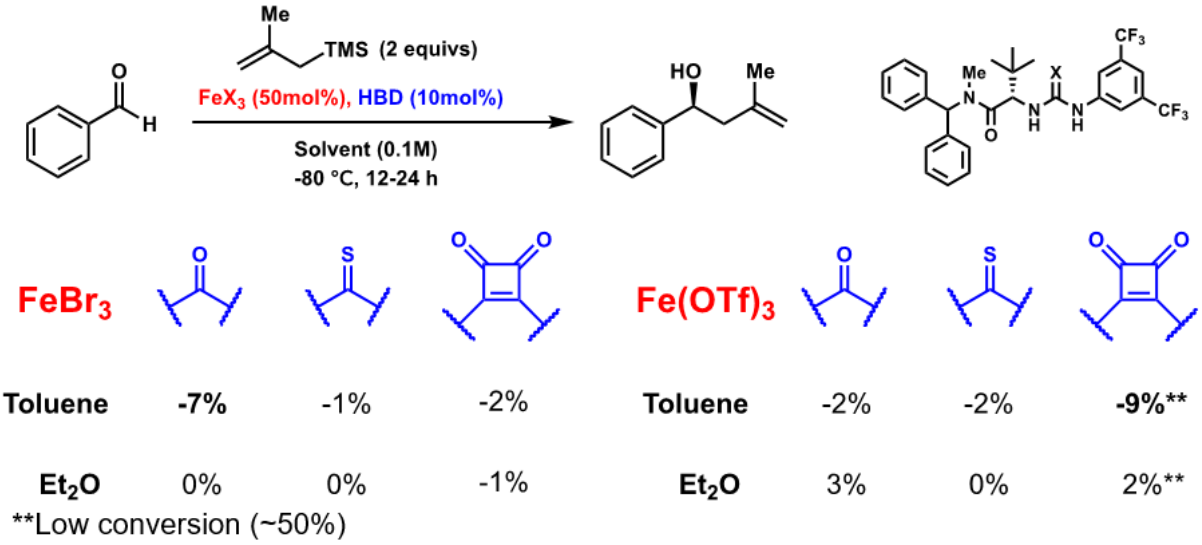

Figure 4.21 Benzaldehyde methallylation with miscellaneous Lewis acids and HBD catalysts

Lewis acid catalysts that had enantioselectivities high enough to indicate the possibility of rate acceleration in the presence of hydrogen-bond donors were subsequently tested in the Sakurai methallyltrimethylsilane addition to benzaldehyde dimethyl acetal, and the results are presented in Figure 4.22. In general enantioselectivities were low in this reaction. Interestingly the optimal HBD catalyst for TMSOTf was thiourea, when all previous TMSOTf catalyzed reactions have found squaramides to be optimal. BF_3 universally gave low but non-zero enantioselectivies. $Bi(OTf)_3$ provided low reactivity (~50% conversion) at –80 °C but 22% ee with squaramide in ether. The same combination was optimal for BCl_3, which also provided 22% ee.

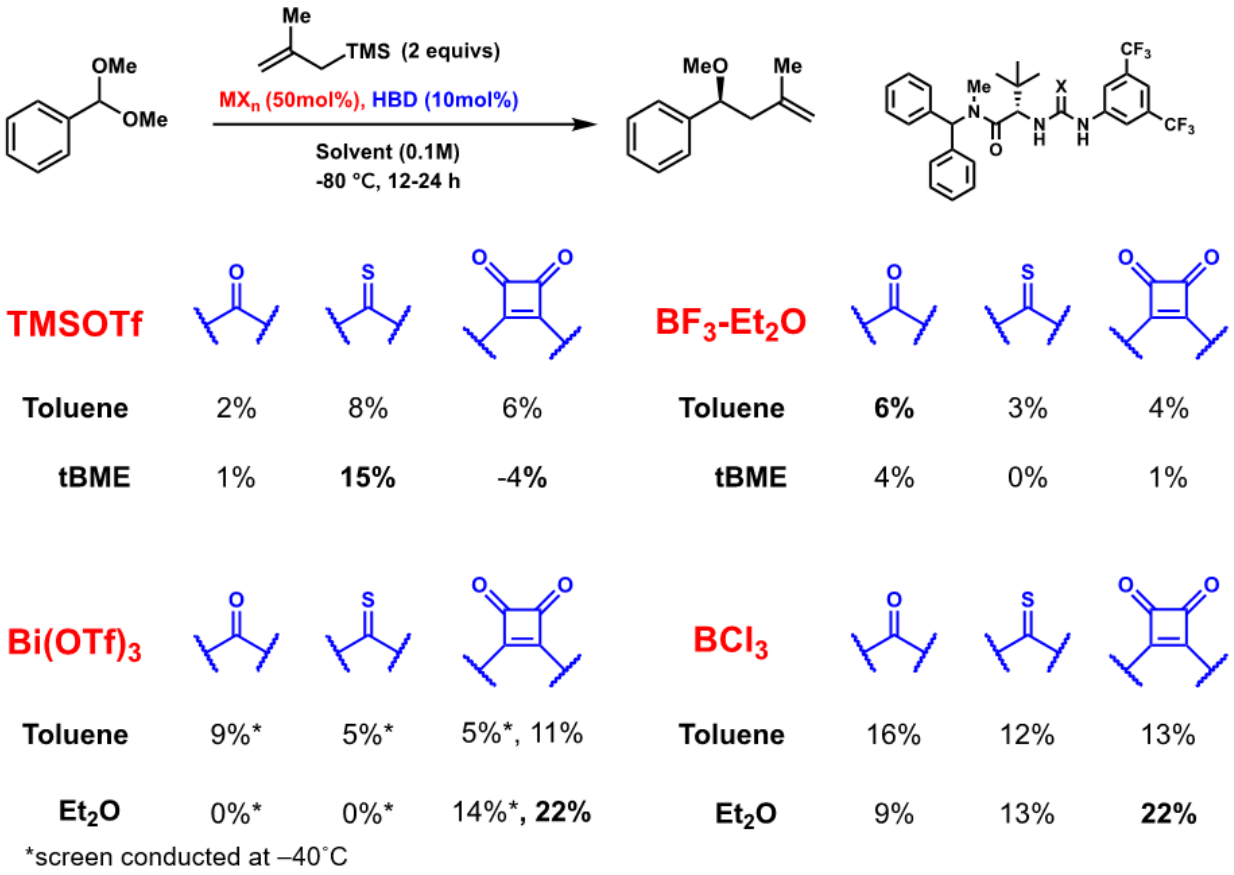

Figure 4.22 Benzaldehyde dimethyl acetal methallylation with Lewis acids and HBD catalysts

TMSOTf and 1-pyrenylpyrrolidine squaramide **4f** have demonstrated the ability to induce 88% ee in the methallylsilane addition to *p*-bromobenzaldehyde dibenzyl acetal,[180] thus something about this choice of catalyst and/or substrate must be quite poor for enantioselectivity, given that analogous conditions gives 4% ee here. Therefore, the 22% ee provided by BCl_3 and squaramide catalyst **4h** was encouraging. Given the ability of arylpyrrolidines to catalyze the related transformation in the 2017 Science report in high ee, a small screen of arylpyrrolidines was conducted to see if the reaction was responsive to this catalyst structure (Figure 4.23). In an initial screen of arylpyrrolidines there is a clear trend between the size of the arene and the enantioselectivity of the transformation, with 4-pyrenyl catalyst **4g** giving the highest ee at 68%. Interestingly, methylation of catalyst **4e** provides substantially lower selectivity. Last,

heteroaromatics provide substantially different enantioselectivities than aromatics, with 4-dibenzofuran giving 20% ee and 4-dibenzothiophene giving –66% ee. These data are consistent with a cation-π or π-π interactions at play in the mechanism of enantiodiscrimination.

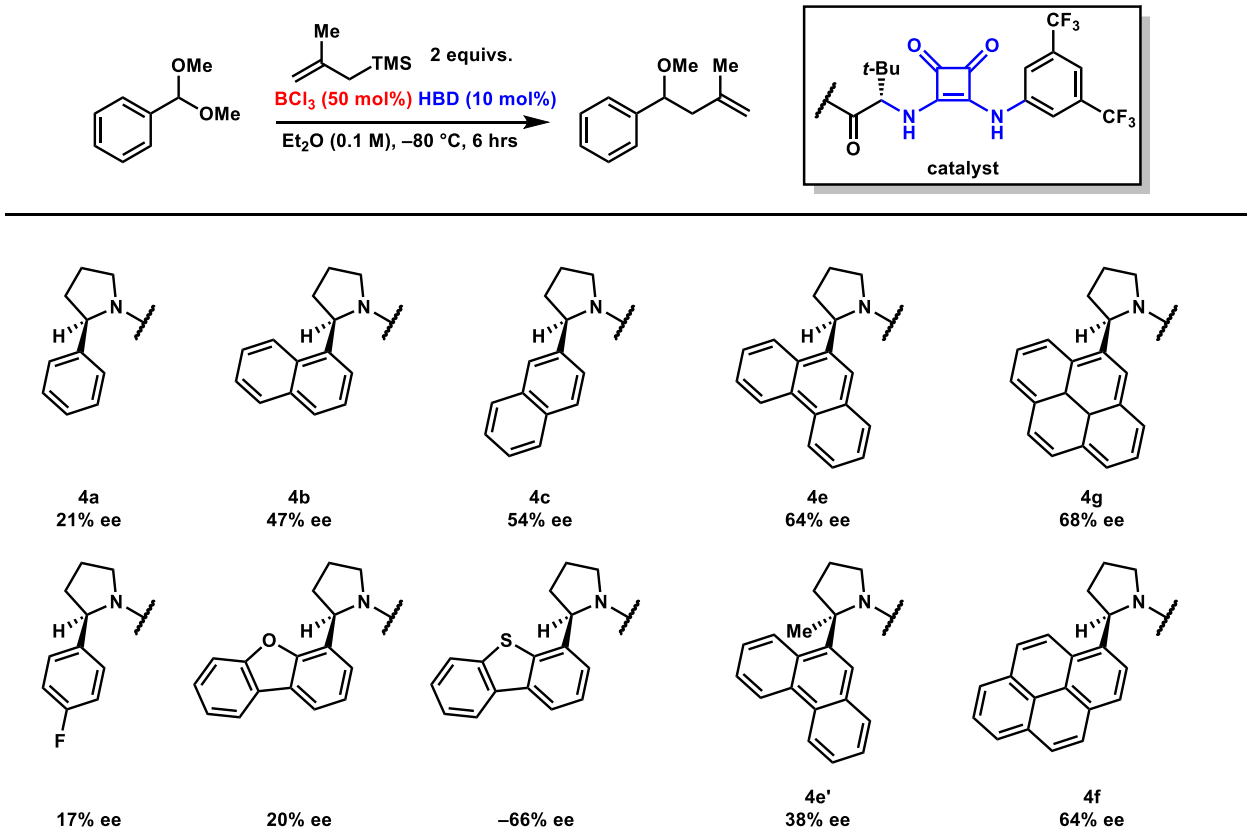

Figure 4.23 Arylpyrrolidine screen in the BCl_3 and squaramide catalyzed benzaldehyde dimethyl acetal methallylation

No further reactions were run in the optimization of this reaction and there are many remaining parameters that could lead to reaction optimization, including: temperature, solvent, relative loadings of BCl_3, more extensive catalyst screening, and more extensive substrate screening, especially dibenzylacetal substrates. The electronic properties of the phenyl ring of the benzaldehyde acetal could be tuned by adding electron-withdrawing or electron-donating groups. In doing so, a relationship between the electronic properties of the benzaldehyde and the enantioselectivity can be investigated in Hammett studies. Additionally it would be extremely

synthetically interesting if this methodology could be extended to the allylation of acetophenone ketals for the synthesis of chiral 3° alcohols.

4.3.2 Gutmann-Beckett quantification of Lewis acidity enhancement by hydrogen-bond donor catalysts.

The Sakurai screening revealed a number of Lewis acids capable of being activated by hydrogen-bond donor catalysts. The Gutmann-Beckett method was used to confirm that this is the case and to quantify the degree of Lewis acidity enhancement in the presence of HBD catalysts. The Gutmann-Beckett method, is an NMR study in which the ^{31}P shift of triethylphosphine oxide is measured to determine the strength of a Brønsted or Lewis acid.[203] In this case, the ^{31}P shift was measured in the presence and absence of Lewis acid, each class of HBD catalyst (**4h**, **6h**, and **7h**), and both Lewis acid and HBD catalyst (Figure 4.24). In theory this can be benchmarked against acceptor numbers, known values in the literature for various Lewis acids to quantify the relative Lewis acidity of any co-catalytic combination. Although in reality, acceptor numbers are only valuable under equivalent conditions, which are not standardized for the Gutmann-Beckett method, as shifts vary drastically as a result of equivalencies, solvent, and to a lesser extent temperature.

[203] For derivation of the Gutmann-Beckett method see: a) Mayer, U.; Gutmann, V.; Gerger, W. The Acceptor Number ? A Quantitative Empirical Parameter for the Electrophilic Properties of Solvents. *Monatshefte fur Chemie* **1975**, *106* (6), 1235–1257. b) Beckett, M. A.; Strickland, G. C.; Holland, J. R.; Sukumar Varma, K. A Convenient n.m.r. Method for the Measurement of Lewis Acidity at Boron Centres: Correlation of Reaction Rates of Lewis Acid Initiated Epoxide Polymerizations with Lewis Acidity. *Polymer (Guildf).* **1996**, *37* (20), 4629–4631. For application of the method to Hydrogen-bonding see c) Diemoz, K. M.; Franz, A. K. NMR Quantification of Hydrogen-Bond-Activating Effects for Organocatalysts Including Boronic Acids. *J. Org. Chem.* **2019**, *84* (3), 1126–1138.

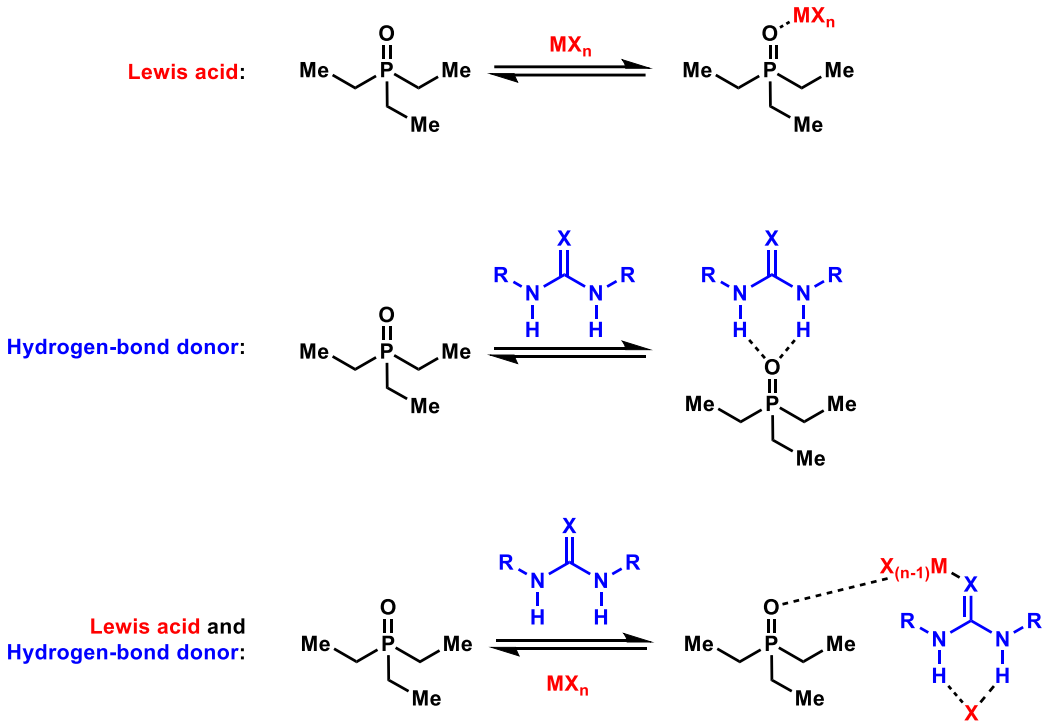

Figure 4.24 Relevant equilibria in the Gutmann-Beckett study between Lewis acids and HBDs

A few of the Lewis acids that provided enantioselectivities and were fully soluble in toluene and ether under the relevant concentrations were investigated using the Gutmann-Beckett method. This study found that the co-catalytic system is indeed synergistic and results in drastically increased Lewis acidity for TMSOTf. In diethyl ether, upon addition of just 10 mol% squaramide **4h**, $\Delta\delta^{31}P = 1.63$ ppm; just 50 mol% TMSOTf, $\Delta\delta^{31}P = 3.46$ ppm; whereas the addition of both 50 mol% squaramide and 50 mol% TMSOTf results in $\Delta\delta^{31}P = 19.99$ ppm, indicating a much more Lewis acidic combined species, consistent with the hypothesis in the 2017 study from the Jacobsen group (Figure 4.25).[180] Given the presence of only one peak for each spectrum despite substoichiometric loadings indicates that the on/off mechanism between catalysts and $Et_3P{=}O$ must be rapid on the NMR time scale, with broad peaks indicating that the dynamic process is slowing down near coalescence on the NMR time scale. In toluene, some peaks are coalesced and in the baseline (see methods section).

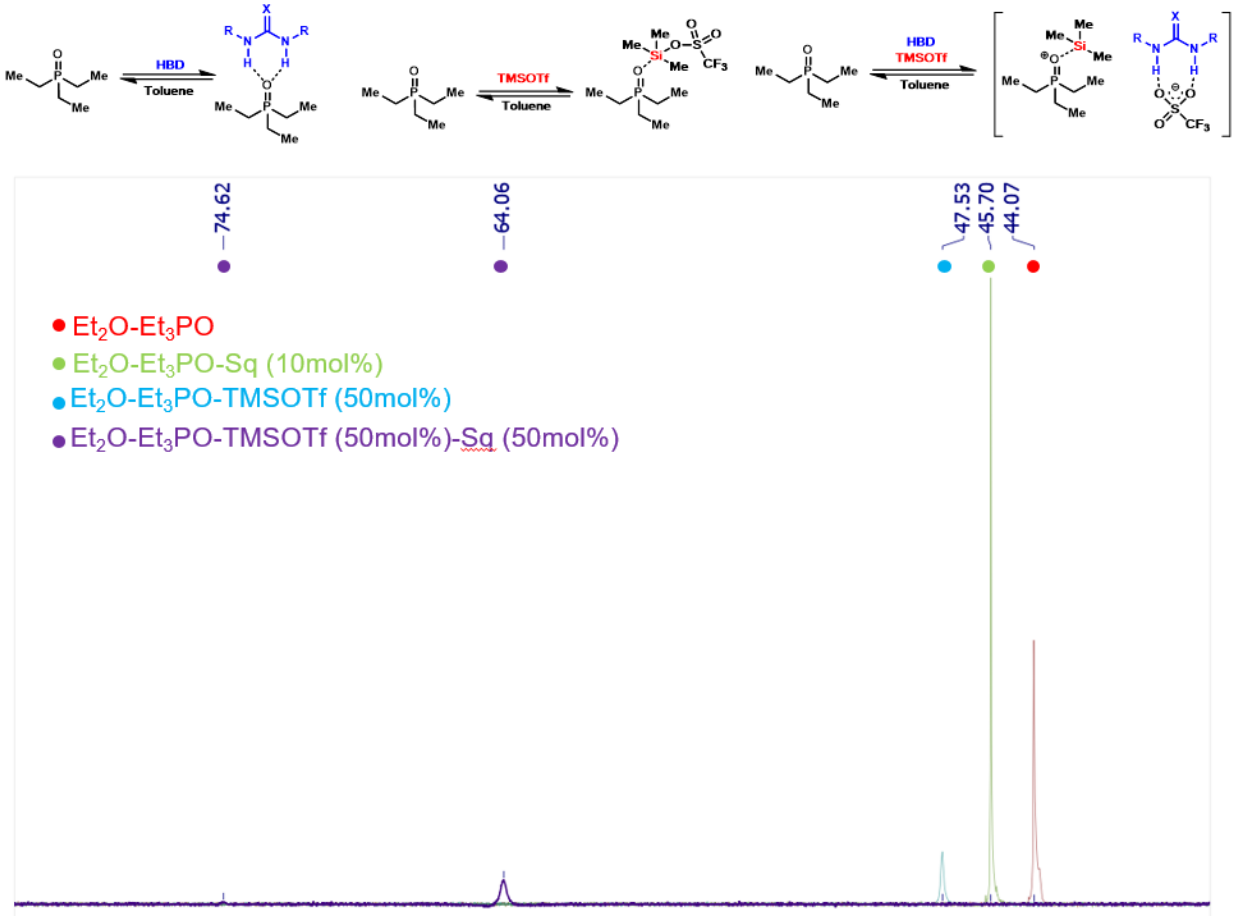

Figure 4.25 Gutmann-Beckett investigation of squaramide **4h** and TMSOTf in Et_2O

For BF_3 multiple peaks were observed upon substoichometric addition, potentially indicating slow exchange or irreversible binding of the triethylphosphine oxide to BF_3 (see methods), thus a full equivalent was employed and the results are displayed in Figure 4.25. In toluene, upon addition of 50 mol% squaramide **4h**, $\Delta\delta^{31}P$ = 6.89 ppm; just 100 mol% $BF_3{\cdot}OEt_2$, $\Delta\delta^{31}P$ = 30.94 ppm; whereas the addition of both 100 mol% squaramide **4h** and 100 mol% $BF_3{\cdot}OEt_2$ results in $\Delta\delta^{31}P$ = 31.73 ppm, indicating that the hydrogen-bond donor plays a minimal role in enhancing the Lewis acidity of $BF_3{\cdot}OEt_2$, consistent with the results observed in the amino acid synthesis (Figure 4.26).

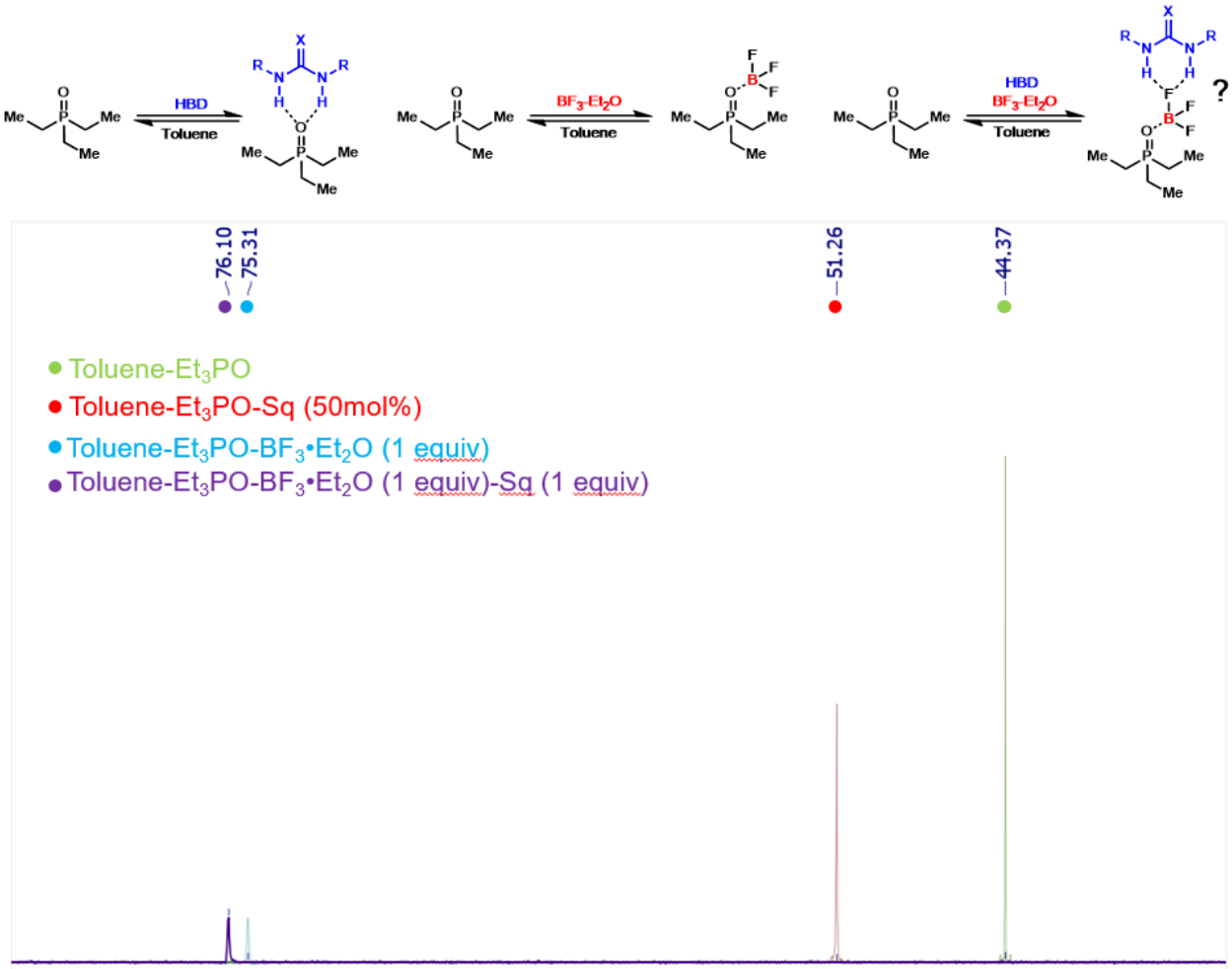

Figure 4.26 Gutmann-Beckett investigation of squaramide **4h** and $BF_3 \cdot OEt_2$

The results with BCl_3 are the most complicated and potentially most interesting; thus the co-catalytic effect was tested with urea **6h**, thiourea **7h** and squaramide **4h**. . In toluene, upon addition of 50 mol% squaramide **4h**, $\Delta\delta^{31}P$ = 6.88 ppm; and just 100 mol% BCl_3, $\Delta\delta^{31}P$ = 38.14 ppm. Upon addition of 100 mol% BCl_3 and 100 mol% thiourea **7h**, $\Delta\delta^{31}P$ = 38.19 ppm; urea **6h**, $\Delta\delta^{31}P$ = 38.32 ppm, indicating minimal to no synergistic HBD activation. When 100 mol% BCl_3 and 100 mol% squaramide **4h** were added, multiple species were formed at $\Delta\delta^{31}P$ = 39.09, 42.81, and 43.38 ppm in a roughly 1:1:1 ratio, potentially consistent with multiple modes of activation, including the possibility of fully abstracting a chloride from BCl_3, generating a highly acidic cationic BCl_2 borenium Lewis acid as depicted in Figure 4.27. These results may explain the ability

to achieve moderate enantioselectivity with BCl_3 and squaramides as depicted in Figures 4.21 and 4.22. Attempts to crystallize the adduct to determine the structure failed. To further understanding the nature of interactions, titrimetric NMR studies should be conducted get binding constants and stoichiometry, and NOESY and ^1H NMR studies to probe binding geometries. Additionally DFT could be used to predict the most energetically favorable co-catalyst interactions and co-catalyst substrate interactions allowing for enantioinduction with BCl_3.

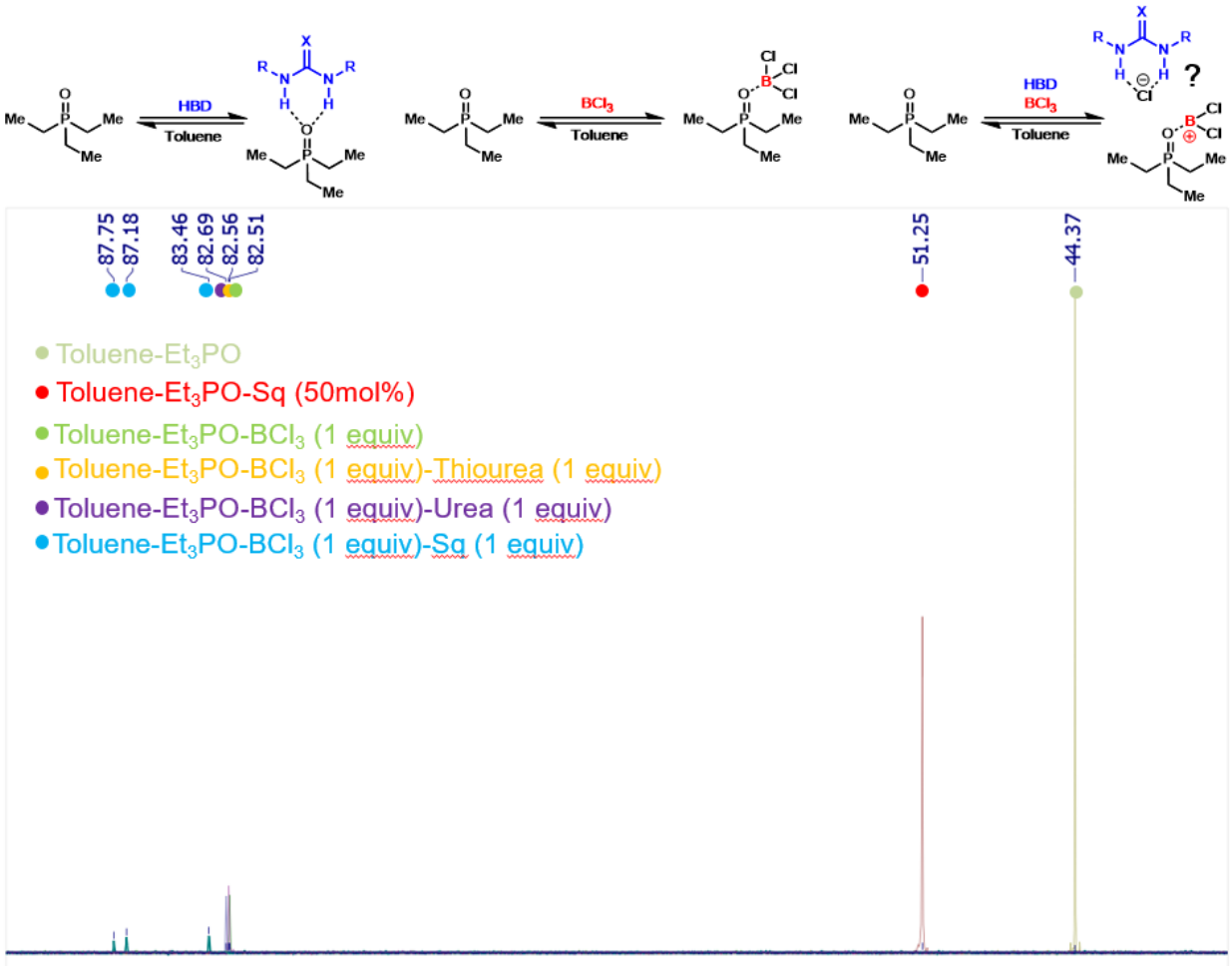

Figure 4.27 Gutmann-Beckett investigation of classes of hydrogen-bond donors **4h**, **6h**, and **7h** with BCl_3

4.4 Conclusion and outlook

In conclusion, the ability for hydrogen bond-donors, specifically squaramides, and $BF_3{\cdot}OEt$ to work in concert to provide moderate levels (up to 53%) of enantioselectivity in the

addition of allylsilanes to α-methoxy-α-phenyl glycinates was demonstrated. Preliminary mechanistic investigations revealed that the squaramide hydrogen-bond donor does not catalyze the rate determining step and it is proposed that it is inefficiently intercepting an iminium ion-pair to which methallylsilane is being added, along with the competitive racemic addition. While this reaction was unable to be optimized past 53% ee without employing stoichiometric amounts of squaramide catalyst, it nonetheless demonstrated that hydrogen-bond donors and Lewis acids can affect enantioselectivities beyond the reported silylium chemistry.

This led to a systematic investigation of the ability for HBD catalysts to accelerate the rate of Lewis acid catalyzed processes, a feature highly desirable in achieving high enantioinduction. This investigation was performed using the enantioselectivity in the Hosomi-Sakurai methallylation of benzaldehyde and benzaldehyde dimethyl acetal as readouts for rate enhancement, which revealed that boron Lewis acids and some lanthanide Lewis acids are capable of giving enantioselectivities and rate enhancement in the presence of HBDs. In particular squaramide and BCl_3 was able to give up to 68% ee in an unoptimized reaction.

A Gutmann-Beckett study was carried out with TMSOTf and boron Lewis acids in the presence of HBDs in order to quantify the Lewis acidity enhancement. HBDs seem to strongly enhance the strength of TMSOTf and mildly enhance the strength of $BF_3{\cdot}OEt_2$ and BCl_3. Squaramide and BCl_3 form multiple downfield species, indicating that the combination produces multiple highly electrophilic species worthy of further study, especially in the context of the 68% ee result in the Sakurai reaction.

The ability to find combinations of Lewis acids and HBD catalysts would enable enantioinduction in challenging reactions involving high energy intermediates, greatly expanding the scope of anion-abstraction chemistry that hydrogen-bond donors can perform. Further

investigations into BCl_3, BF_3, and lanthanide Lewis acid catalyzed processes should be the focus of future studies.

4.5 Experimental

4.5.1 Procedures for synthesis and allylation of α-methoxy-α-phenyl glycinate 8-Cbz

Preparation of 8-Cbz

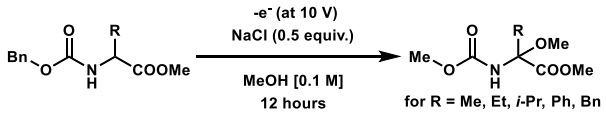

8-Cbz was prepared by adapting the procedure from Shono.[199] 1 mmol, 0.299 g of *N*-Cbz phenylglyoxylate methyl ester was weighed out into a scintillation vial along with 0.5 mmol, 29 mgs of NaCl. To this solution was added 10 mL of methanol. The reaction was placed in an ice water bath and bulk electrolysis was done in an undivided cell performed by a potentiostat set to constant current at 10 V. The working electrode was a platinum rod, the counter electrode was a platinum mesh, and the reference electrode was a silver rod. The ice bath was allowed to melt over the course of the first hour and the reaction was run overnight for approximately 12 hours. Note, this potential is well outside the solvent window for methanol, yet at lower potentials the reaction did not proceed well. If the reaction does not go to completion it is challenging to separate the starting material from the product.

The reaction was worked up by removal of the solvent under reduced pressure and the residue was subjected to column chromatography with hexanes:ethyl acetate 10:1 to 1:1 over the course of 8 column volumes. Product was generally isolated in 50-60% yield, 165-197 mgs.

General procedure for the catalytic reaction 8-Cbz:

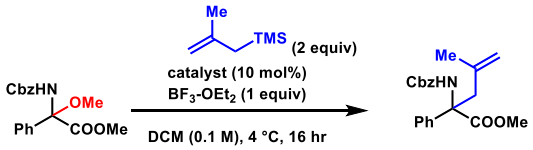

The reactions run on screening scale are conducted at the 0.05 mmol scale. 2 dram scintillation vials equipped with a flea stir bar are put in an oven kept at 120 °C overnight. To a rt 2 dram vial is added squaramide catalyst (0.005 mmol catalyst, 10 mol%) and solid **8-Cbz** (0.05 mmol, 16.5 mgs) is weighed out into the vial, the vial is capped with a screw top fitted with a septum, an inlet of N_2 is added to the vial, and 0.5 mL of DCM is added. The vials are then put in an ice water bath for 10 minutes, after which silane nucleophile is added via syringe (0.10 mmol, 2 equivs. for methallylsilanes 17.5 µL) followed by 0.05 mol of $BF_3 \cdot OEt_2$ 6 µL. Alternately, a 1M solution of $BF_3 \cdot OEt_2$ can be prepared in DCM and added. After 10 minutes, the nitrogen inlet is removed, the top of the cap is covered with electrical tape and transferred to a fridge maintained at 4 °C, unless another temperature is specified and stirred for 12-16 hours.

The reactions are quenched with 0.5 mL of 6:1 MeOH:NEt_3 at the reaction temperature (generally 4 °C) and allowed to stir for an hour to ensure the Lewis acid is entirely quenched. The reaction is then warmed to rt, opened, and filtered through a celite plug with excess DCM and concentrated *in vacuo*. The product is purified either via a pipette column (~10:1 hexanes:ethyl acetate) or PTLC (~1.5:1 hexanes:ethyl acetate) optimal eluent conditions will vary slightly depending on the product. NMRs are integrated against dibromomethane standard to determine yield. Enantiomeric excess is determined via chiral normal phase HPLC against a racemic standard, which is prepared via the exact same method except the omission of squaramide catalyst.

4.5.2 NMR spectral data for 8-Cbz and 9a-9b

methyl 2-(((benzyloxy)carbonyl)amino)-2-methoxy-2-phenylacetate (8-Cbz):

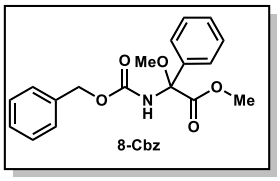

^{1}H NMR (600 MHz, Chloroform-*d*) δ 7.59 (d, *J* = 7.3 Hz, 2H), 7.53 – 7.27 (m, 8H), 6.52 (s, 1H), 5.10 (d, *J* = 12.2 Hz, 1H), 5.03 (d, *J* = 12.4 Hz, 1H), 3.70 (s, 3H), 3.34 (s, 3H).

methyl 2-(((benzyloxy)carbonyl)amino)-4-methyl-2-phenylpent-4-enoate (9a):

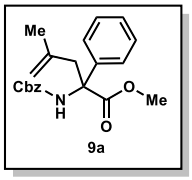

^{1}H NMR (600 MHz, Chloroform-*d*) δ 7.44 (d, *J* = 7.8 Hz, 2H), 7.39 – 7.28 (m, 8H), 6.48 (s, 1H), 5.07 (d, *J* = 12.3 Hz, 1H), 4.95 (d, *J* = 12.3 Hz, 1H), 4.85 (s, 1H), 4.70 (s, 1H), 3.66 (s, 3H), 3.51 (d, *J* = 13.9 Hz, 1H), 3.23 (d, *J* = 13.3 Hz, 1H), 1.63 (s, 3H).

methyl 2-(((benzyloxy)carbonyl)amino)-2-phenylpent-4-enoate (9b):

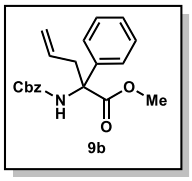

^{1}H NMR (600 MHz, Chloroform-*d*) δ 7.44 (d, *J* = 7.7 Hz, 2H), 7.40 – 7.27 (m, 8H), 6.36 (s, 1H), 5.66 (dq, *J* = 16.6, 7.7 Hz, 1H), 5.18 – 5.09 (m, 2H), 5.09 – 4.91 (m, 2H), 3.67 (s, 3H), 3.52 (s, 1H), 3.19 (dd, *J* = 13.5, 7.5 Hz, 1H).

4.4.2 General procedure for Lewis acid and hydrogen bond donor screening

All reagents for this project were commercially available and purchased from Sigma-Aldrich and used without further purification. 10 1/2-dram vials were equipped with flea stir bars

and placed in an oven overnight. The oven-dried vials were allowed to cool to room temperature after which 0.01 mmol of squaramide **4h** (6.2 mgs, 0.1 equiv.) was added to three vials, 0.01 mmol of urea **6h** (5.7 mgs, 0.1 equiv.) was added to another three vials, and 0.01 mmol of thiourea **7h** (5.8 mgs, 0.1 equiv.) was added to another three vials, with the 10th vial empty as racemic standard. In the event the Lewis acid was a solid, 0.05 mmol (0.5 equiv.) was weighed out into each vial. The vials were then put under nitrogen atmosphere. Then 1 mL of DCM, *t*BME or Ether, and toluene were dispensed from a solvent purification system (as described in the experimental section in Chapter 2), and added to the vials such that each vial contains a unique combination of catalyst and solvent. 1mL of DCM was added to the 10th racemic standard vial. Next, 0.1 mmol (10.2 μL, 1.0 equiv.) of benzaldehyde or 0.1 mmol (15 μL, 1.0 equiv.) of benzaldehyde dimethyl acetal was added. The reaction was then cooled to –78 °C in a dry ice/acetone bath (this step is done before the addition of electrophile if the Lewis acid is solid). After temperature equilibration for 10 minutes, 0.2 mmol (35.215 μL, 2.0 equiv.) of methallyltrimethylsilane was added via syringe. In the event that the Lewis acid is a liquid or a solution, 0.05 mmol (0.5 equiv.) was added via syringe. After 10 minutes, nitrogen lines were removed, reactions were sealed with electrical tape and moved to a –80 °C freezer (stirring was shown to not affect the ee of this transformation). Reactions were generally run overnight, for 12-16 hours.

To quench the reaction, 0.5 mL of a 1:1 mixture of methanol and trimethylamine was added at –80 °C and kept at that temperature for 1 hour to ensure all Lewis acid had been quenched. After which, the reactions were brought to room temperature and evaporated to dryness under rotary evaporation. For dimethyl acetal products, no further purification was needed and ^{1}H NMR and chiral HPLC was conducted to assess conversion and enantioselectivity. For benzaldehyde products, crude reaction mixtures generally exist as a mixture of TMS protected and free alcohol.

To ease analysis, 0.5 mL of 0.1 M HCl in Et_2O was added to each reaction vessel and the crude material was allowed to stir neat in HCl solution at room temperature until TLC revealed that complete TMS deprotection had occurred, generally 30-60 minutes. At this point, ^1H NMR and chiral HPLC was conducted to assess conversion and enantioselectivity.

4.5.3 General procedure for Gutmann-Beckett method and additional NMR spectra

Triethylphosphine oxide (TEPO) was purchased from Sigma Aldrich and used without purification. NMR tubes, catalysts, solvents, and TEPO were rigorously dried and stored in a glovebox. An external capillary standard was added to each NMR tube in order to lock given that solvents are non-deuterated and to reference the phosphorous NMR shifts. 0.1 M triphenylphosphine in benzene-d_6 was flame sealed in a capillary tube and used as a standard for locking and peak referencing. For each ^{31}P NMR evaluations, amounts of HBD and Lewis acid were varied and should be added according to the equivalences written on the spectrum.

Procedure for just TEPO: In a glovebox, weigh out 2.3 mgs of triethylphosphine oxide and add 0.6 mL solvent (0.017 mmol triethylphosphine oxide, 0.0285 M). Seal with an NMR tube septum.

Procedure for just HBD and TEPO assuming 1:1 molarity: In a glovebox weigh out 0.017 mmol of catalyst and triethylphospine each into a vial and add solvent. Seal with an NMR tube septum

Procedure for just Lewis acid and TEPO assuming 1:1 molarity: If the Lewis acid is a solid, bring it into the glovebox and follow the same procedure as for HBD. If the Lewis acid is a liquid follow the same procedure for just TEPO, and after outside the glovebox add 0.017 mmol of Lewis acid through the septum using a syringe.

Procedure for Lewis acid, HBD and TEPO assuming 1:1:1 molarity. Since HBD is varied, 0.017 mmol of each HBD is weighed into a separate NMR tube; a 0.0285 M stock solution of Lewis acid and TEPO is made and 0.6 mL is dispensed into each NMR tube and capped with a septum.

Procedure for taking NMR: NMRs were taken on a 400 MHz spectrometer, which is 162 MHz for ^{31}P detection. Generally 256 scans were collected at room temperature with 5 second relaxation delays, which was determined to be long enough to let the ^{31}P fully relax. NMR data were autophased and baseline corrected in mnova and referenced to triphenylphosphine $\delta^{31}P = 6.00$ ppm.

Figure 4.27 shows the Gutmann-Beckett NMR spectrum upon addition of squaramide and TMSOTf in toluene. As one can see, the exchange of TMSOTf association with TEPO is dynamic and coalesced on the NMR time scale, making peaks broaden into the baseline. If one analyzes the peaks, it appears that the TMSOTf and squaramide combination produces a far downfield shift relative to TMSOTf alone, indicating Lewis acidity enhancement. However, there could be additional peaks in the baseline that are not observable, so this does not serve as definitive proof. One could raise or lower the temperature to resolve or coalesce the peaks, but that was not explored here.

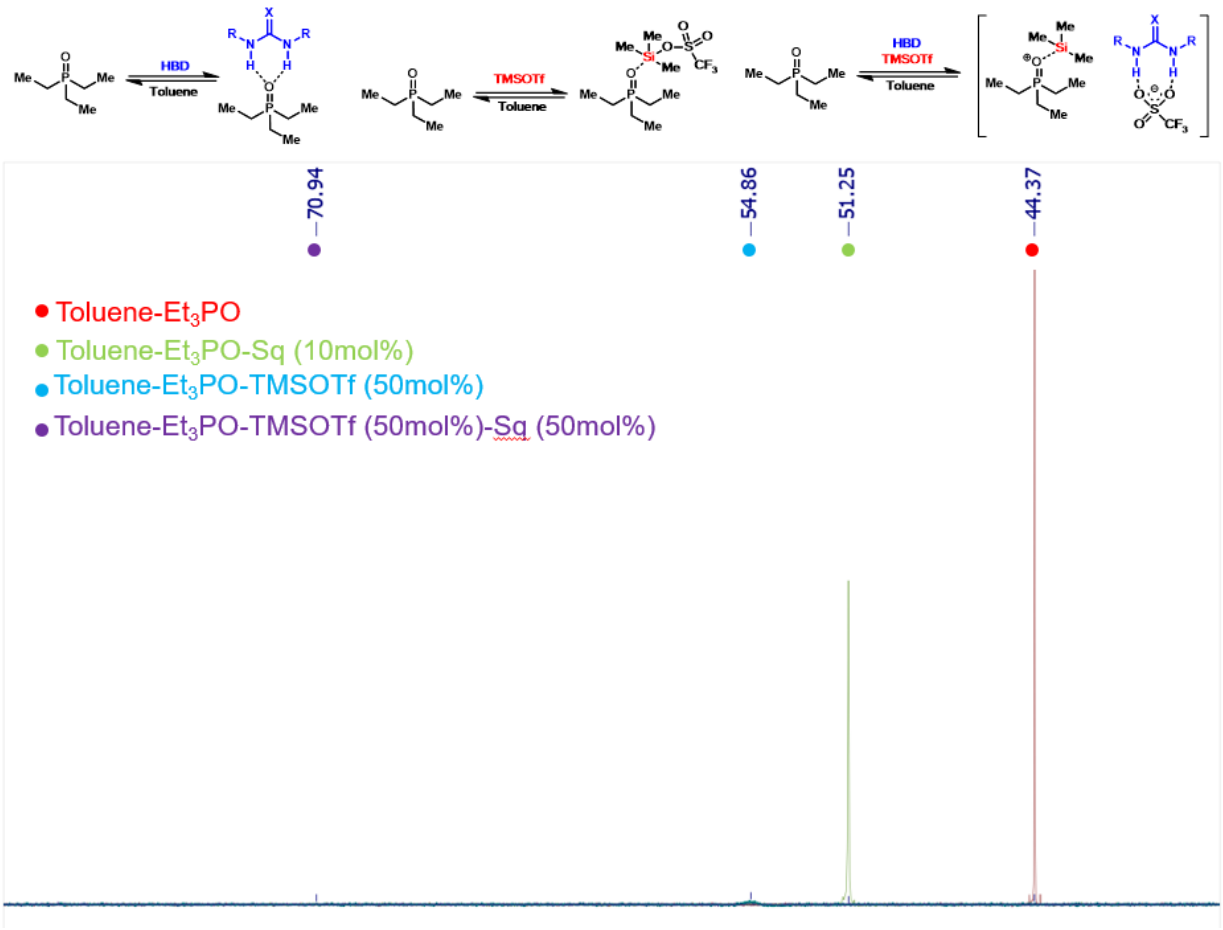

Figure 4.28 Gutmann-Beckett investigation of squaramide **4h** and TMSOTf in toluene

Figure 4.28 shows the Gutmann-Beckett NMR spectrum upon addition of squaramide and BF_3OEt_2 in toluene. The addition of just 50 mol% BF_3 produces two new shifts in the spectrum, one that is just downfield of TEPO alone, $\Delta\delta^{31}P$ = 1.15 ppm and one at $\Delta\delta^{31}P$ = 31.71 ppm in a roughly 1:1 ratio. This indicates that binding of TEPO to BF_3 is strong and perhaps irreversible, or at least slow on the NMR time scale. The subsequent addition of squaramide produces a large downfield shift in the first peak, an additional $\Delta\delta^{31}P$ = 13.76 ppm, but no shift in the second peak, indicating that squaramide prefers to bind the free TEPO over the one that is already associated with BF_3. Since this spectrum does not accurately probe the potential Lewis acidity enhancement, the 1:1:1 stoichiometry was examined and the results are presented in Figure 4.25. Attempts to

study BF_3 HBD co-catalysis in Et_2O was attempted, however the product of BF_3 and TEPO, presumably the zwitterionic adduct, is not soluble in Et_2O, making the analysis impossible.

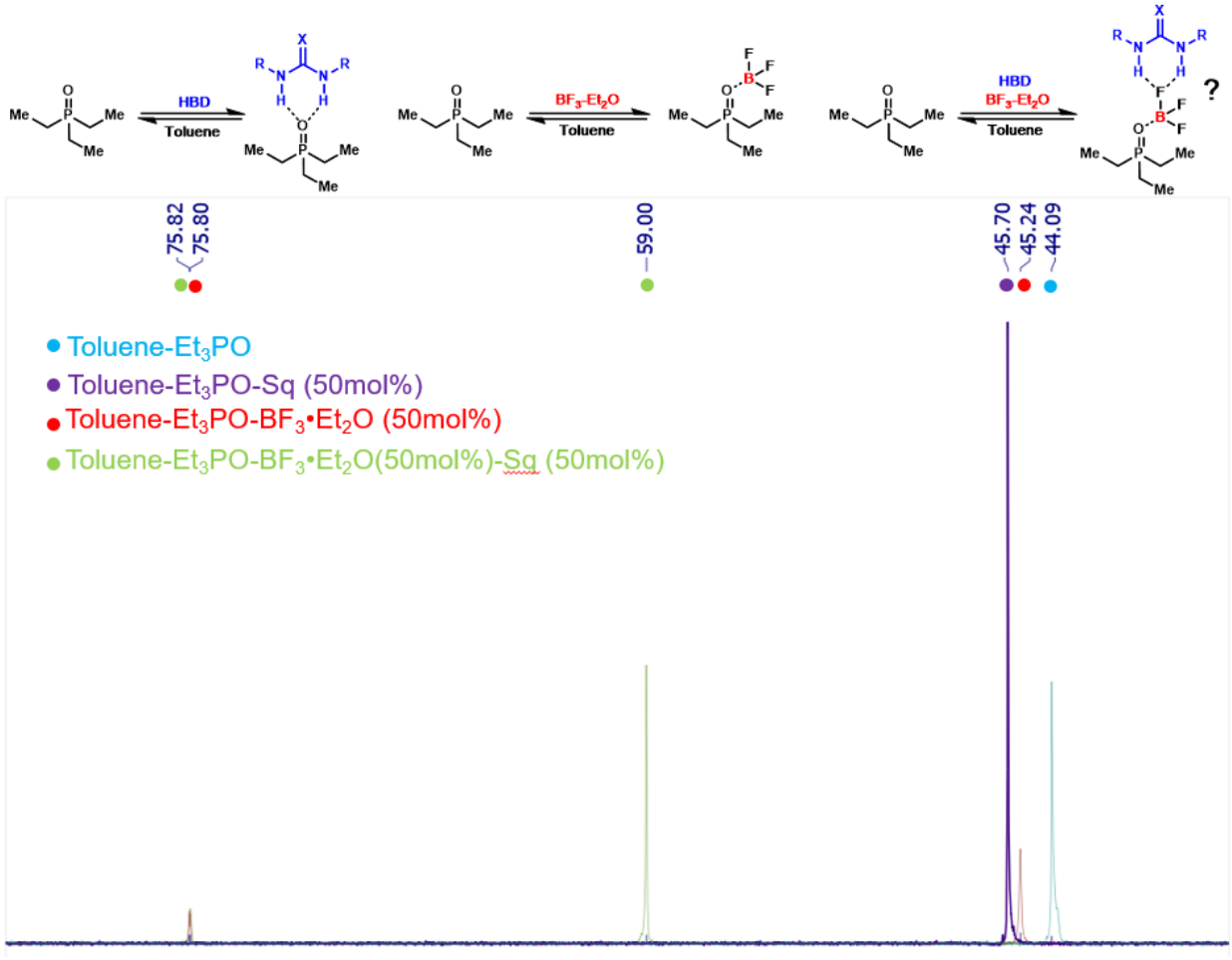

Figure 4.29 Gutmann-Beckett investigation of squaramide **4h** and $BF_3{\cdot}OEt_2$ in toluene

Chapter 5

Development of an HCl and Hydrogen-Bond Donor Co-Catalyzed Enantioselective Semi-Pinacol Rearrangement

5.1 Introduction

The proton, or H+, is arguably the most ubiquitous catalyst in all of chemistry. Therefore, the development of chiral Brønsted acids for enantioselective catalysis has been the subject of much research over the last 20 years.[204] In 2004, Terada and Akiyama both reported highly enantioselective Mannich additions of silyl ketene acetals and malonates to benzaledehyde derived imines, the first transformations catalyzed by BINOL derived phosphoric acid catalysts.[205]

While the initial Mannich reports are effectively catalyzed by BINOL phosphoric acids, many other transformations are not. A phosphoric acid is acidic enough to protonate an imine; however, it is generally not acidic enough to protonate carbonyls, olefins, and C-X bonds that can

[204] For select reviews in chiral Brønsted acid catalysis see: a) Akiyama, T. Stronger Brønsted Acids. *Chem Rev.* **2007**, *107* (12), 5744–5758. b) Terada, M. Chiral Phosphoric Acids as Versatile Catalysts for Enantioselective Transformations. *Synthesis (Stuttg).* **2010**, *2010* (12), 1929–1982. c) Kampen, D.; Reisinger, C. M.; List, B. Chiral Brønsted Acids for Asymmetric Organocatalysis; Springer, Berlin, Heidelberg, 2010; pp 1–37. d) Cheon, C. H.; Yamamoto, H. Super Brønsted Acid Catalysis. *Chem. Commun.* **2011**, *47* (11), 3043. e) Parmar, D.; Sugiono, E.; Raja, S.; Rueping, M. Complete Field Guide to Asymmetric BINOL-Phosphate Derived Brønsted Acid and Metal Catalysis: History and Classification by Mode of Activation; Brønsted Acidity, Hydrogen Bonding, Ion Pairing, and Metal Phosphates. *Chem. Rev.* **2014**, *114* (18), 9047–9153. f) Akiyama, T.; Mori, K. Stronger Brønsted Acids: Recent Progress. *Chem. Rev.* **2015**, *115* (17), 9277–9306. g) Min, C.; Seidel, D. Asymmetric Brønsted Acid Catalysis with Chiral Carboxylic Acids. *Chem. Soc. Rev.* **2017**, *46* (19), 5889–5902.

[205] a) Uraguchi, D.; Terada, M. Chiral Brønsted Acid-Catalyzed Direct Mannich Reactions via Electrophilic Activation. *J. Am. Chem. Soc.* **2004**, *126* (17) 5356–5357. b) Akiyama, T.; Itoh, J.; Yokota, K.; Fuchibe, K. Enantioselective Mannich-Type Reaction Catalyzed by a Chiral Brønsted Acid. *Angew. Chemie Int. Ed.* **2004**, *43* (12), 1566–1568.

undergo subsequent heterolysis. Strong Brønsted acids, such as HCl, H_2SO_4, or TfOH are sufficiently acidic to promote all of the above reactions. Thus, the ability to develop new, more acidic catalysts around the BINOL scaffold that approach the acidity of HCl has been an active research area (Figure 5.1).[204f,206] These stronger Brønsted acid catalysts have promoted hundreds of C-C and C-X bond forming reactions, including imine additions, (hetero)-Diels-Alder cycloadditions, Nazarov cyclizations, semi-pinacol rearrangements, Michael additions, Aldol reactions, and many others.[204e] BINOL derived chiral acids have reached shockingly low acidities, in some cases exceeding the acidity of HCl (pKa of –2.0 in DMSO) and approaching the acidity of TfOH (pKa of –14.3 in DMSO).[206] Yet some of the most synthetically interesting HCl and TfOH catalyzed processes are still challenging in this context. These challenges include olefin protonation and C-X bond protonation and heterolysis, which allow access to tertiary carbocations, an ideal intermediate for the synthesis of quaternary stereocenters.[181] An alternative strategy would be to use the preexisting acidity of HCl or TfOH and to design a catalyst that could somehow act as a chiral ligand without reducing its acidity.

[206] Acidity data taken from: Trummal, A.; Lipping, L.; Kaljurand, I.; Koppel, I. A.; Leito, I. Acidity of Strong Acids in Water and Dimethyl Sulfoxide. *J. Phys. Chem. A* **2016**, *120* (20), 3663–3669.

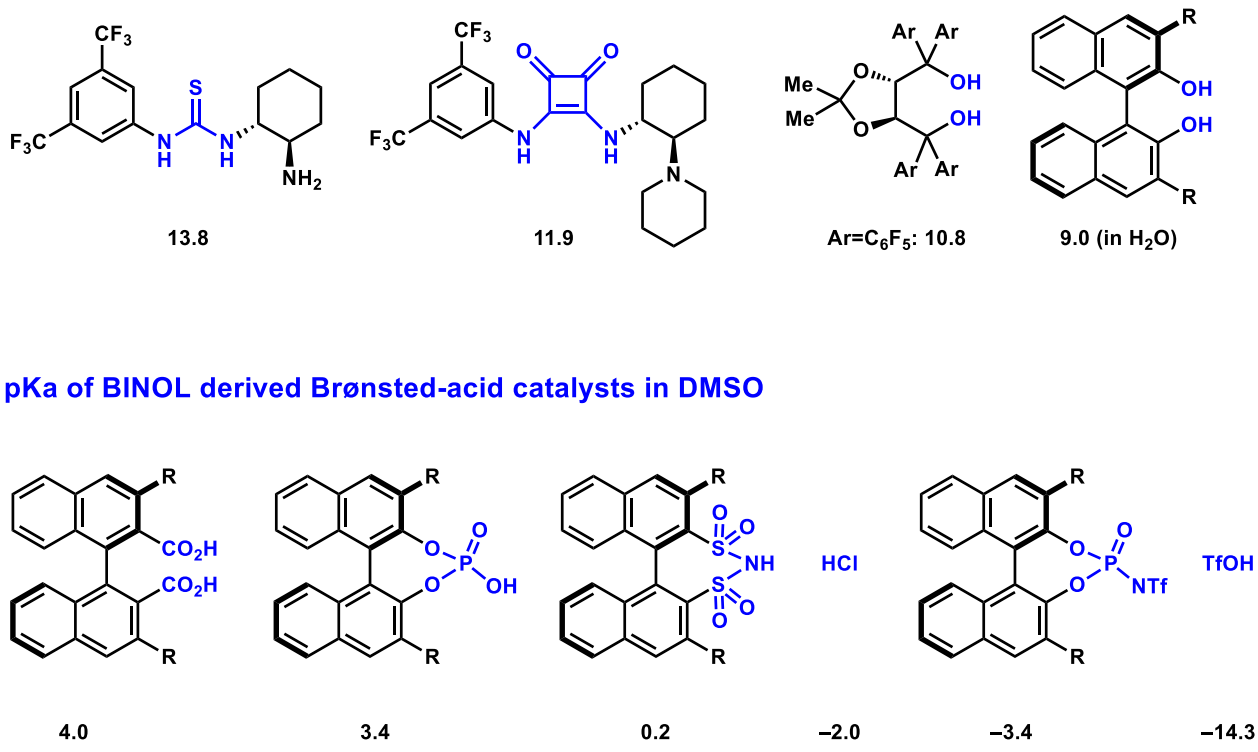

Figure 5.1 Acidities of common HBD and chiral BINOL Bronsted acid catalysts in DMSO

5.1.1 Hydrogen-bond donors in Lewis acid catalysis

Every Brønsted acid, H-X, has a dissociation constant, K_a, which is a measure of the strength of an acid and determines to what extent the acid dissociates in solution to release H+. In organic solvent, due to the poor ability to stabilize charged species, acid dissociation is attenuated relative to in water. If one were able to stabilize the negative charge of X^-, then one could influence the acid dissociation constant, K_a, and increase the acidity of that acid. Given the demonstrated ability of hydrogen-bond donors to engage anions in ion-pairing catalysis, one could imagine that anion-abstraction from H-X could bias K_a to increase the acidity and form a new activated chiral-acid (Figure 5.2). If the HBD is competent at stabilizing the anion, or in other words, the association between X^- and HBD is strong, this would allow for catalysis over racemic chemistry promoted by H-X alone. Additionally, H^+ could be associated with the catalyst via ion-pairing or

via coordination to a Lewis basic site on the catalyst, which may render it more or less acidic than H-X, depending on the degree of buffering.

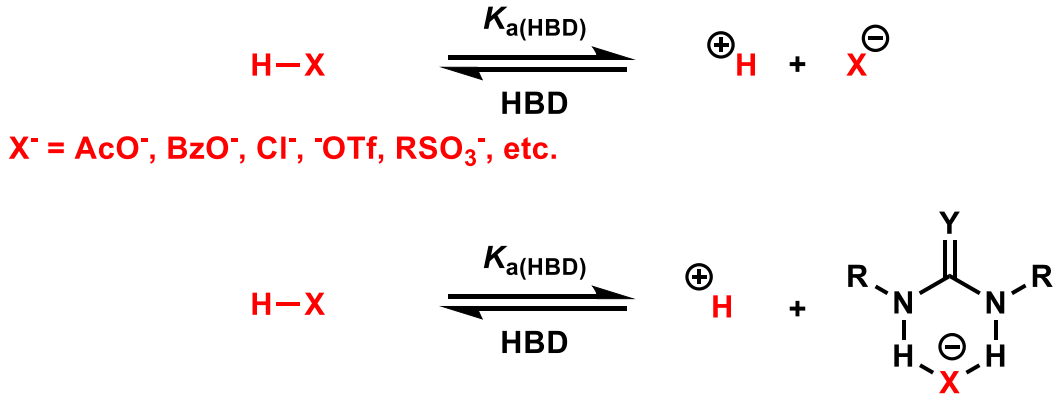

Figure 5.2 HBD anion-binding properties can influence K_a for an acid H-X via X^- stabilization

The Jacobsen group has demonstrated the ability to engage HBD catalysts and weak or strong Brønsted acids in a number of contexts. Initial reports of HBD catalyzed reactions involving Brønsted acids is in the Strecker reaction, involving the addition of weak acid HCN across an imine.[31–34] HBD catalyzed enantioselective Strecker reactions were discussed at length in Chapter 1. In the first generation of asymmetric Strecker reactions the role of catalyst and HCN is undetermined, whereas in the second generation, the HBD functionality has been shown to bind cyanide while the protonated iminium is stabilized via non-covalent attractive interactions to a catalyst arene and amide, allowing for enantioselective ion-pair collapse.

A protio-Pictet-Spengler report demonstrates the ability to HBDs and a weak Brønsted acid, benzoic acid to work in concert to achieve enantioselectivity (Figure 5.3 A).[207] An in-depth mechanistic study revealed that catalyst binds the benzoic acid in every step on-cycle and that enantioselective catalysis is achieved by the ability of thioureas to stabilize every intermediate and

[207] Klausen, R. S.; Jacobsen, E. N. Weak Brønsted Acid−Thiourea Co-Catalysis: Enantioselective, Catalytic Protio-Pictet−Spengler Reactions. *Org. Lett.* **2009**, *11* (4), 887–890.

transition state on-cycle, including the rate and enantiodetermining deprotonation rearomatization/benzoic acid turnover event.[145]

In the context of strong acids, an asymmetric Povarov cycloaddition demonstrates the ability to achieve cooperative catalysis of strong Brønsted Acids, namely *o*-nitrobenzenesulfonic acid and chiral ureas (Figure 5.3 B).[208] Enantioselectivity is achieved here by the ability of the catalyst to engage in a network of hydrogen-bonds that stabilize the iminium sulfonate ion-pair, shifting the resting state to catalyst bound a catalyst bound complex, which can undergo subsequent cycloaddition. Another example of cooperative catalysis between a benzenesulfonic acid and a chiral thiourea is in the addition of indoles to episulfonium ions.[99c] Here, the sulfonic acid is able to protonate a trichloroacetimidate to generate a sulfonium sulfonate bound to catalyst with rate and enantiodeterming indole addition to the chiral ion-pair.

An example of the ability to engage HBD catalysts with stoichiometric strong acid is in the hydrochlorination of aziridines promoted by a bifunctional phosphino thiourea catalyst (Figure 5.3 C).[209] In this transformation, catalyst phospine and aziridine substrate form a bridging hydrogen-bond while the thiourea functionality holds the chloride anion. This enantioselective ion-pair collapse can then delivere chloride to one of the carbons of a meso aziridine.

All of these strong acid co-catalyzed reactions share a couple common features. First, the substrate has an amine that is being protonated. Ammoniums are substantially less acidic than the starting acid, implying the substrate is buffering the acid. Second, enantioselectivity in each case is the result of the dual hydrogen-bonding functionality holding on to the conjugate base of the

[208] Xu, H.; Zuend, S. J.; Woll, M. G.; Tao, Y.; Jacobsen, E. N. Asymmetric Cooperative Catalysis of Strong Brønsted Acid-Promoted Reactions Using Chiral Ureas. *Science* **2010**, *327* (5968), 986–990.

[209] Mita, T.; Jacobsen, E. Bifunctional Asymmetric Catalysis with Hydrogen Chloride: Enantioselective Ring Opening of Aziridines Catalyzed by a Phosphinothiourea. *Synlett* **2009**, *2009* (10), 1680–1684.

anion and a network of non-covalent attractive interactions providing for selectivity. It would be interesting to extend this methodology beyond substrates with amine bases to substrates that are not easily protonated, such as olefins and carbonyls. This would leverage the proposed ability of an HBD to increase Brønsted acidity via binding of the conjugate anion of a strong acid, as well as enable new and challenging transformations that BINOL derived chiral acid catalysts are not strong enough to catalyze.

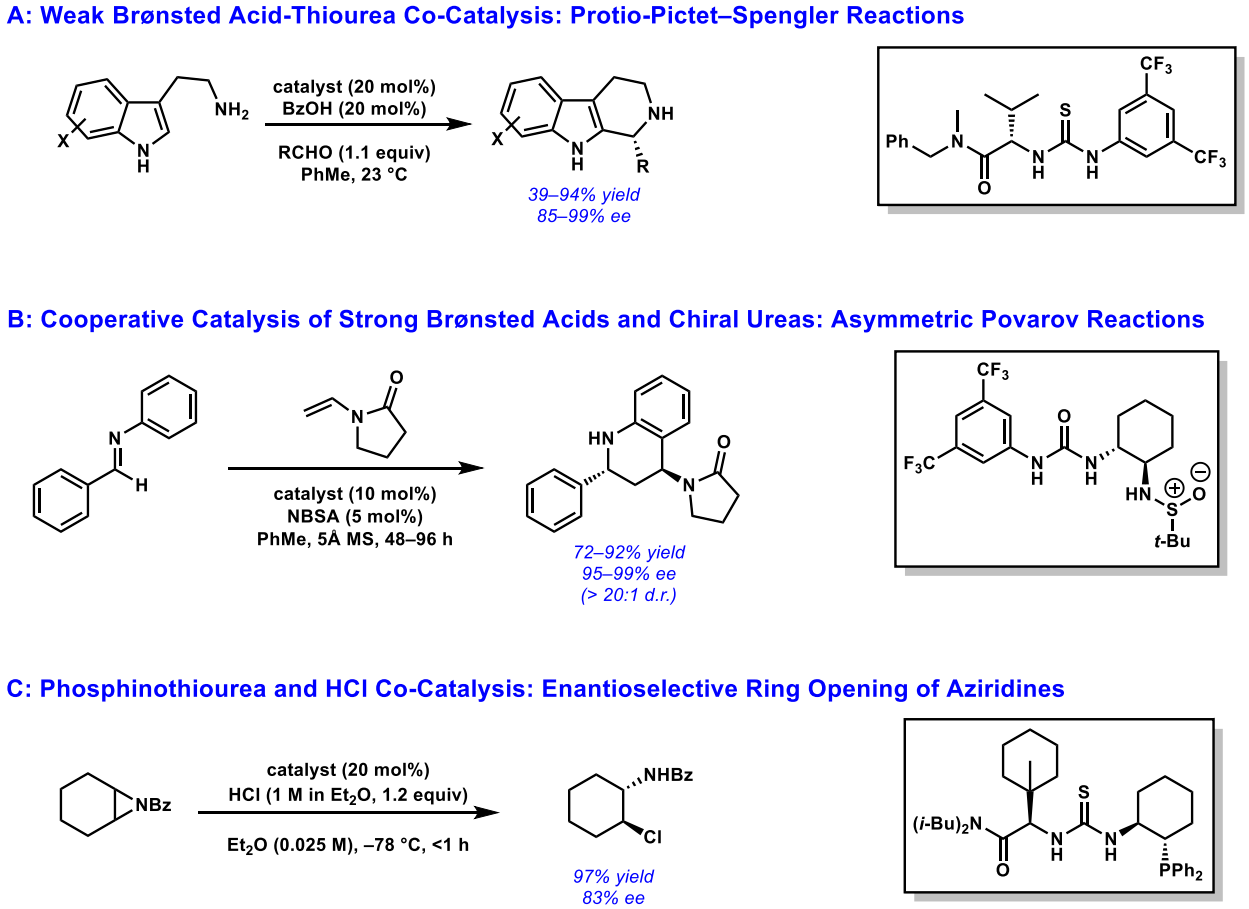

Figure 5.3 Precedent for enantioselective co-catalysis between HBDs and Brønsted acids

5.1.2 Enantioselective semi-pinacol rearrangements

The pinacol rearrangement (Figure 5.4 A) is one of the oldest known reaction, discovered in 1860 by Fittig, and involves an acid promoted ionization of a tertiary diol to form an α-hydroxy cation, which can undergo tetrahedral intermediate collapse with a 1,2-Wagner-Meerwein

rearrangement to give an α-quaternary carbonyl.[210] In recent years, the pinacol rearrangement has received considerable attention due to the ability to set congested quaternary stereocenters.[211] In fact, it has been the key step in a number of syntheses of natural products (Figure 5.4 C); most notably a vinologous epoxide semipinacol was used in multiple syntheses of ingenol to set the infamously challenging "inside-outside" circled stereocenter.[212]

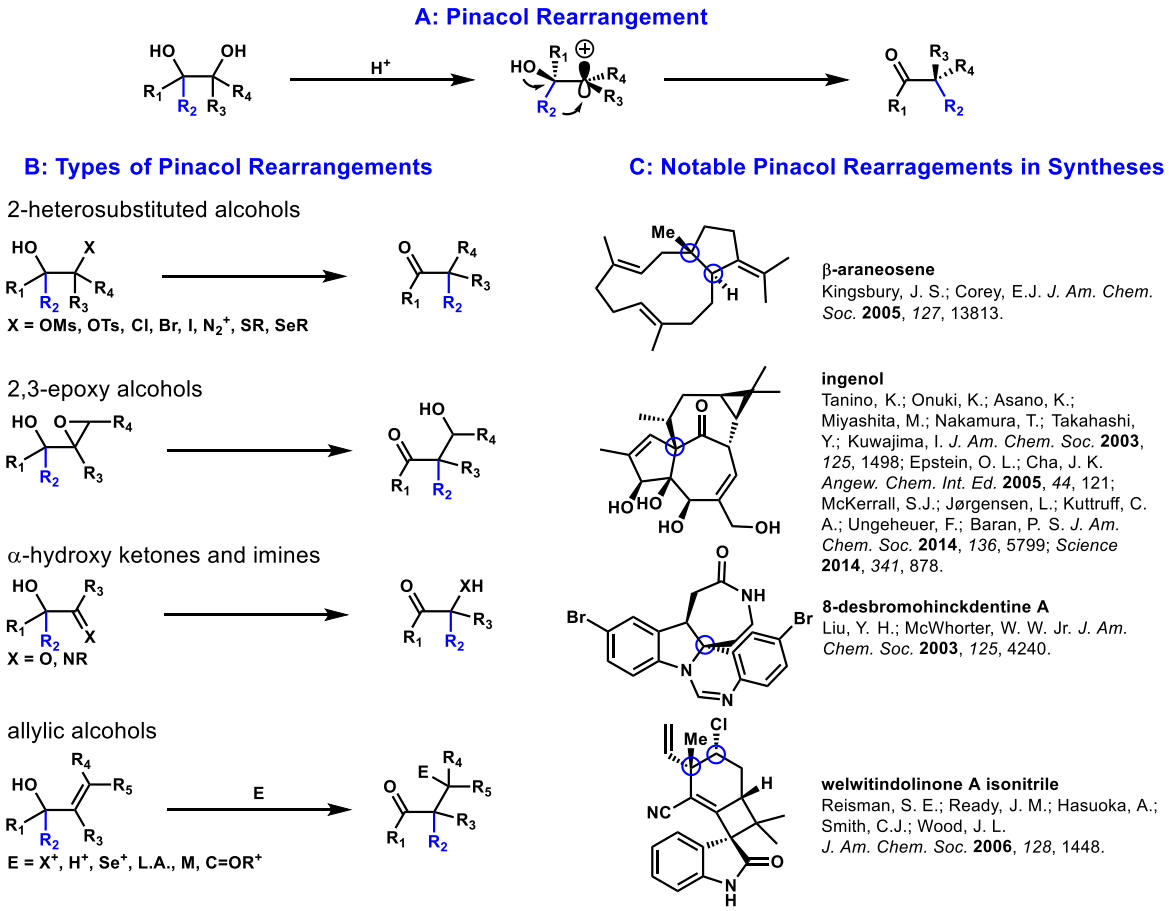

Figure 5.4 Overview on the pinacol and semi-pinacol rearrangements

[210] Fittig, R. 41. Ueber Einige Derivate Des Acetons. *Ann. der Chemie und Pharm.* **1860**, *114* (1), 54–63.

[211] Song, Z.-L.; Fan, C.-A.; Tu, Y.-Q. Semipinacol Rearrangement in Natural Product Synthesis. *Chem. Rev.* **2011**, *111* (11), 7523–7556.

[212] a) Tanino, K.; Onuki, K.; Asano, K.; Miyashita, M.; Nakamura, T; Takahashi, Y.; Kuwajima, I. Total Synthesis of Ingenol. *J. Am. Chem. Soc.* **2003**, *125* (6), 1498–1500. b) Epstein, O. L.; Cha, J. K. Rapid Access to the "In,out"-Tetracyclic Core of Ingenol. *Angew. Chemie Int. Ed.* **2005**, *44* (1), 121–123. c) Jorgensen, L.; McKerrall, S. J.; Kuttruff, C. A.; Ungeheuer, F.; Felding, J.; Baran, P. S. 14-Step Synthesis of (+)-Ingenol from (+)-3-Carene. *Science* **2013**, *341* (6148), 878–882. d) McKerrall, S. J.; Jørgensen, L.; Kuttruff, C. A.; Ungeheuer, F.; Baran, P. S. Development of a Concise Synthesis of (+)-Ingenol. *J. Am. Chem. Soc.* **2014**, *136* (15), 5799–5810.

The true pinacol rearrangement must start from a 1,2-diol; however there are many semi-pinacol variants (Figure 5.4 B). Specifically, stereospecific or stereoablative rearrangement of alcohols with an α-leaving group can occur. 2,3-epoxy alcohols can undergo stereospecific rearrangements, which is enabling given the ease of synthesis of 2,3-epoxy alcohols via Sharpless asymmetric epoxidation.[213] α-hydroxyketones or imines can undergo α-ketol rearrangements to give isomeric products. Finally, allylic alcohols can undergo electrophilic activation to generate an α-cation or α,β-three membered onium intermediate, which can undergo semipinacol rearrangement.

This last strategy has proven to be particularly adaptable to enantioselective catalysis via transition metal, electrophilic halogenation, and Brønsted acid catalysis.[214] Trost and Toste have been able to use enantioselective Pd π-allyl and Au π-acid catalysis respectively to induce ring-expansion semipinacol rearrangements of allylic cyclopropanols and cyclobutanols.[215] Alexakis and Tu have been able to perform enantioselective electrophilic halogenative semipinacol rearrangements in ring-expansion and open chain contexts.[216]

There are three examples of enantioselective protio-semi-pinacol rearrangements, one of which is an allylic alcohol. The first example, from Tu, is a cinchona alkaloid and acid co-catalyzed

---

[213] Katsuki, T.; Sharpless, K. B. The First Practical Method for Asymmetric Epoxidation. *J. Am. Chem. Soc.* **1980**, *102* (18), 5974–5976.

[214] For a review on asymmetric semi-pinacol rearrangements see: Wang, S.-H.; Li, B.-S.; Tu, Y.-Q. Catalytic Asymmetric Semipinacol Rearrangements. *Chem. Commun.* **2014**, *50* (19), 2393–2408.

[215] a)Trost, B. M.; Yasukata, T. A Catalytic Asymmetric Wagner−Meerwein Shift. *J. Am. Chem. Soc.* **2001**, *123* (29), 7162–7163. b) Kleinbeck, F.; Toste, F. D. Gold(I)-Catalyzed Enantioselective Ring Expansion of Allenylcyclopropanols. *J. Am. Chem. Soc.* **2009**, *131* (26), 9178–9179.

[216] a) Chen, Z.-M.; Zhang, Q.-W.; Chen, Z.-H.; Li, H.; Tu, Y.-Q.; Zhang, F.-M.; Tian, J.-M. Organocatalytic Asymmetric Halogenation/Semipinacol Rearrangement: Highly Efficient Synthesis of Chiral α-Oxa-Quaternary β-Haloketones. *J. Am. Chem. Soc.* **2011**, *133* (23), 8818–8821.b) Romanov-Michailidis, F.; Guénée, L.; Alexakis, A. Enantioselective Organocatalytic Fluorination-Induced Wagner-Meerwein Rearrangement. *Angew. Chemie Int. Ed.* **2013**, *52* (35), 9266–9270.

vinylogous α-ketol rearrangement in which the two catalysts promote formation of a chiral iminium intermediate, which can undergo a ring-expansion semi-pinacol rearrangement to α-quaternary spirocyclic cyclopentanone products in high yields and enantioselectivities (Figure 5.5).[217] The second example is a TRIP phosphoric acid catalyzed protio-semi-pinacol rearrangement of a dihydropyran, which is protonated to form an oxocarbenium ion (Figure 5.6).[218] This oxocarbenium chiral ion pair can undergo ring-expansion to for an α-spirocyclic cyclopentanone. Last, a chiral phosphoric acid can also catalyze a pinacol rearrangement by protonolysis of an alcohol to generate an indole stabilized carbocation, which can undergo rearrangement to an α-tertiary ketone in high yields and enantioselectivities.[219] These examples demonstrate the ability to perform semi-pinacol rearrangements, but all precede through the intermediacy of a heteroatom stabilized carbocation. If one could use a strong Brønsted acid catalyst, one may be able to protonate olefins to form non-heteroatom stabilized carbocations to expand the scope of these transformations.

[217] Zhang, E.; Fan, C.-A.; Tu, Y.-Q.; Zhang, F.-M.; Song, Y.-L. Organocatalytic Asymmetric Vinylogous α-Ketol Rearrangement: Enantioselective Construction of Chiral All-Carbon Quaternary Stereocenters in Spirocyclic Diketones via Semipinacol-Type 1,2-Carbon Migration. *J. Am. Chem. Soc.* **2009**, *131* (41), 14626–14627.

[218] Zhang, Q.-W.; Fan, C.-A.; Zhang, H.-J.; Tu, Y.-Q.; Zhao, Y.-M.; Gu, P.; Chen, Z.-M. Brønsted Acid Catalyzed Enantioselective Semipinacol Rearrangement for the Synthesis of Chiral Spiroethers. *Angew. Chemie Int. Ed.* **2009**, *48* (45), 8572–8574.

[219] Liang, T.; Zhang, Z.; Antilla, J. C. Chiral Brønsted Acid Catalyzed Pinacol Rearrangement. *Angew. Chemie Int. Ed.* **2010**, *49* (50), 9734–9736.

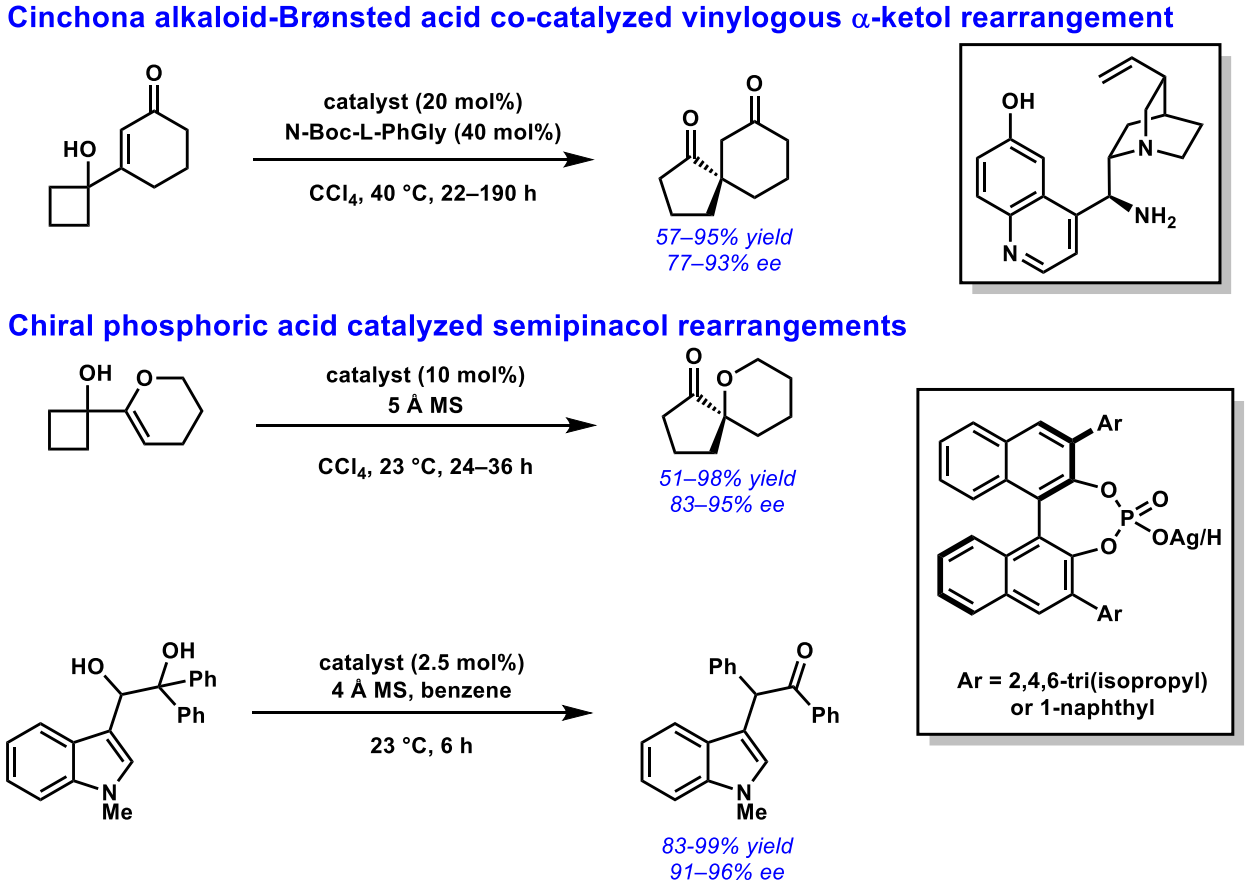

Figure 5.5 Precedent in enantioselective Brønsted acid catalyzed semi-pinacol rearrangements

5.2 Development of an HCl and HBD co-catalyzed enantioselective ring-expansion semi-pinacol rearrangement

In order to test the ability to test the ability for HBD to enhance the Brønsted acidity of an already strong acid (e.g. HCl, TfOH) a reaction involving protonation of an α-alkylstyrene olefin seemed ideal, as the intermediate would be a tertiary benzylic carbocation and products would be fully substituted carbons, including stereocenters. Until recently, no BINOL acids were sufficiently acidic to protonate 1,1-disubstituted olefins; however in 2018 List published an in hydroetherification using a highly acidic and sterically congested designer

imidodiphosphorimidate (IDPi) catalyst to make tetrahydrofurans in 95% ee and 91% yield.[220] Given the high reversibility of the protonation of styrenes through elimination of highly acidic protons α to a carbocation (estimated to have a Hammett acidity $H_0 = -17$),[221] an intramolecular reaction seemed ideal. Thus, the ring-expansion semi-pinacol depicted in Figure 5.6 was chosen as a model reaction to test the ability of HCl and HBD catalyst to afford high ee in a reaction where substrate does not buffer a strong Brønsted acid catalyst. It was chosen due to the inability for a phosphoric acid to catalyze it, the ability of the carbocationic intermediate to react faster than reelimination to starting material, and because products are synthetically interesting α-quaternary cyclic carbonyls.

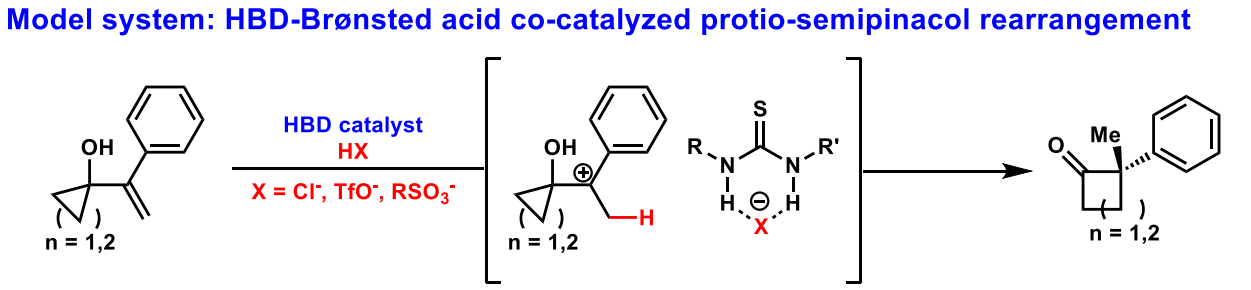

Figure 5.6 Model system for testing the ability to achieve enantioselectivity in unbuffered strong acid hydrogen-bond donor co-catalysis

5.2.1 Optimization of the cyclobutanol to cyclopentanone rearrangement

Initially the n = 2 cyclobutanol substrate depicted in Figure 5.6 was tested with an array of squaramide, urea, and thiourea HBD catalysts, hydrohalogenic acids and sulfonic acids in ethereal, halogenated and aromatic solvents at room temperature. Unfortunately, only triflic acid with or without squaramide in DCM catalyzed this reaction racemically, while thioureas and ureas

[220] Tsuji, N.; Kennemur, J. L.; Buyck, T.; Lee, S.; Prévost, S.; Kaib, P. S. J.; Bykov, D.; Farès, C.; List, B. Activation of Olefins via Asymmetric Brønsted Acid Catalysis. *Science* **2018**, *359* (6383), 1501–1505.

[221] Reed, C. A. Carborane Acids. New "Strong yet Gentle" Acids for Organic and Inorganic Chemistry. *Chem. Commun.* **2005**, No. 13, 1669–1677.

shutdown a background reaction that went to low conversion (< 20%) in their absence. All combinations with hydroiodic acid decomposed the starting material.

Thus preliminary screening was carried out with the *p*-OMe-styrene analog as depicted in Figure 5.7. This substrate was chosen because it has a more easily protonated styrene due to a paraquinonemethide resonace contributor, as depicted in the intermediate in carbocation in Figure 5.7. Initially background reactivity in the presence of acid catalyst alone was tested, which revealed that tosic and dinitrobenzenesulfonic acids catalyze the reaction extremely well, ethereal 1M HCl provides trace conversion, benzoic acid provides no conversion and triflic acid provides complete decomposition. When a thiourea hydrogen-bond donor **7a** is added the yield of the HCl catalyzed reaction increases to 33% with 27% enantioselectivity. Interestingly, the sulfonic acids, which alone provide complete conversion provide no conversion in the presence of a thiourea catalyst. This is potentially indicative that thiourea can activate HCl and buffer sulfonic acids. When the weaker anion-binding dialkylthioureas were tested with 5 mol% HCl, both Schiff base and pyrrole catalysts provided no conversion.

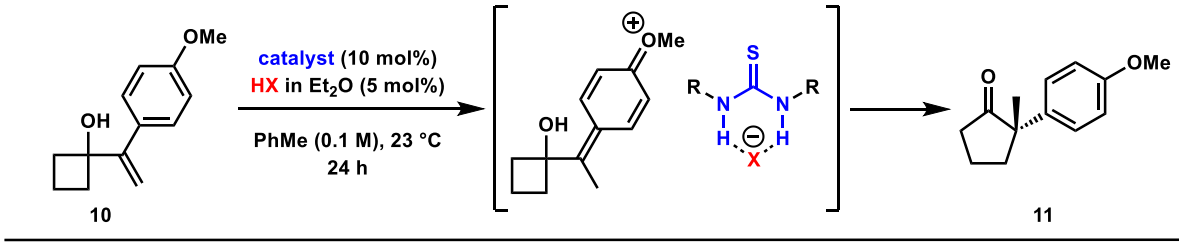

acid screen in absence of H-bond catalyst

acid (5 mol%)	yield
BzOH	0%
HCl in Ether	7%
p-TsOH	98%
2,4-DNBSA	97%
TfOH	0%*

*decomposition

acid screen in presence of H-bond catalyst 7a

acid (5 mol%)	yield	ee
HCl in Ether	33%	27%
p-TsOH	0%	ND
2,4-DNBSA	0%	ND

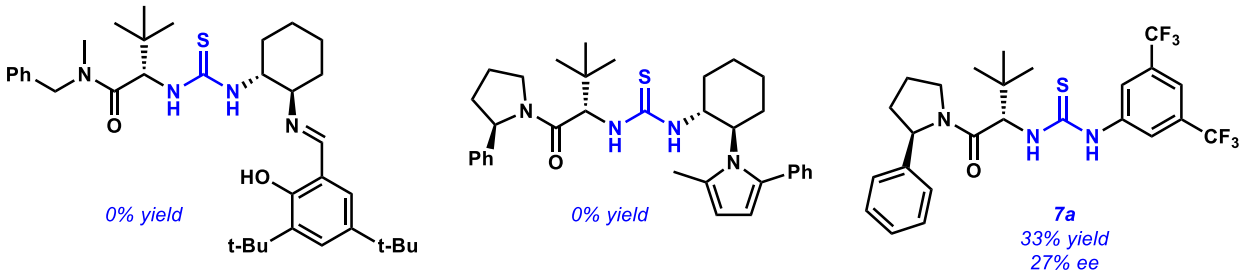

Figure 5.7 Initial acid and thiourea screening in the semi-pinacol rearrangement of **10**

Given the initial promising result that arylpyrrolidine half-Schreiner thioureas and HCl can provide some level of enantioselectivity and rate enhancement over HCl catalysis alone, a catalyst screen was conducted with arylpyrroldine thioureas and squaramides (Figure 5.8). For thioureas, phenyl catalyst **7a** seems to be uniquely bad for conversion, yet it gave substantially higher enantioselectivity than the 1-naphthyl and 9-phenanthryl analogs, which were near racemic. The 1-naphthyl and 9-phenanthryl squaramide analogs provided better, enantioselectivities than the corresponding thioureas, although ee's were still quite low. Interestingly these two catalyst give opposite senses of enantioinduction. Neither ureas nor fully-subsittuted arylpyrrolidine catalyst were screened and should be for completeness. Additionally, given what is now known about

squaramides and triflate anions in the context of TMSOTf catalysis, the combination of sulfonic acids and squaramides should be evaluated in this reaction.[180,181]

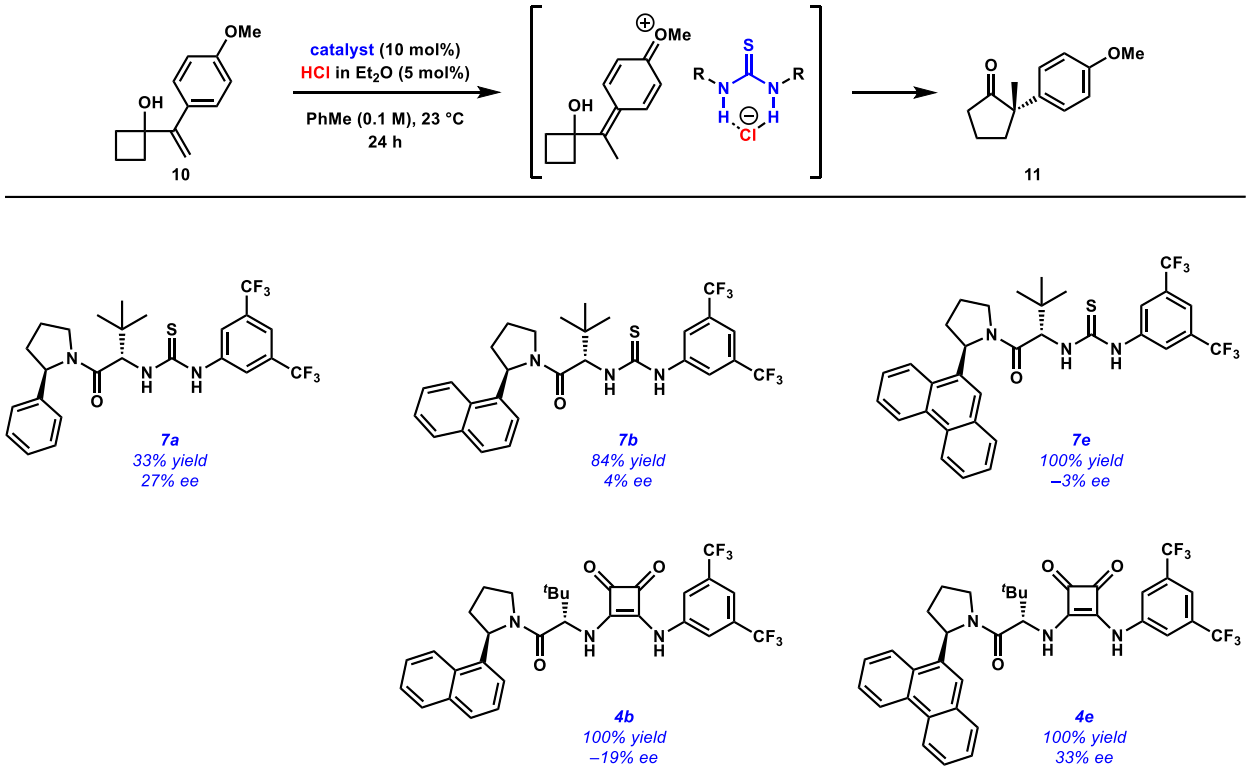

Figure 5.8 Initial thiourea and squaramide pyrroldine screening in the HCl co-catalyzed semi-pinacol rearrangement of **10**

Since enantioselectivies were generally low with arylpyrroldine catalysts, open chain amide catalysts were screened in this reaction Figure 5.9. The benzhydryl methyl amine thiourea **7h** provided compete conversion and 46% ee, which is the optimal enantioselectivity under these conditions. The urea **6h** and squaramide **4h** were tested and provided 40% ee and –5% ee respectively, thus thioureas were deemed optimal in this transformation. In attempt to probe a cation-π interaction, electronic tuning of the benzhydryl arenes was performed by adding *p*-F and *p*-OMe substituents, although both catalyst performed worse than the parent catalyst. To understand if the enantioselectivity with the benzhydryl catalyst is the result of sterics or electronics, the dicyclohexyl anolog was tested and provided somewhat worse ee at 31%. Benzhydryl groups are somewhat non-planar, thus the effect of planarization was tested with the

9-fluorenyl and 9-antrhyl catalysts while the effect of further deplanarizing with the bis-(2-naphthyl) was examined. All catalysts were worse, with the 9-anthryl catalyst being substantially worse. Last, the effect of excising one of the phenyl groups was tested by use of the benzyl amide catalysts in the bottom row of Figure 5.9. Removing a benzyl had a large impact on the conversion, and a moderate impact on the enantioselectivity; furthermore, there is a matched mismatched effect between the benzylic stereocenter and the *t*-leucine stereocenter, as the matched catalyst gives twice the ee of the mismatched catalyst (35% vs 17% ee). In conclusion, all changes to the parent benzhydryl catalyst provided a small decrease in enantioselectivity.

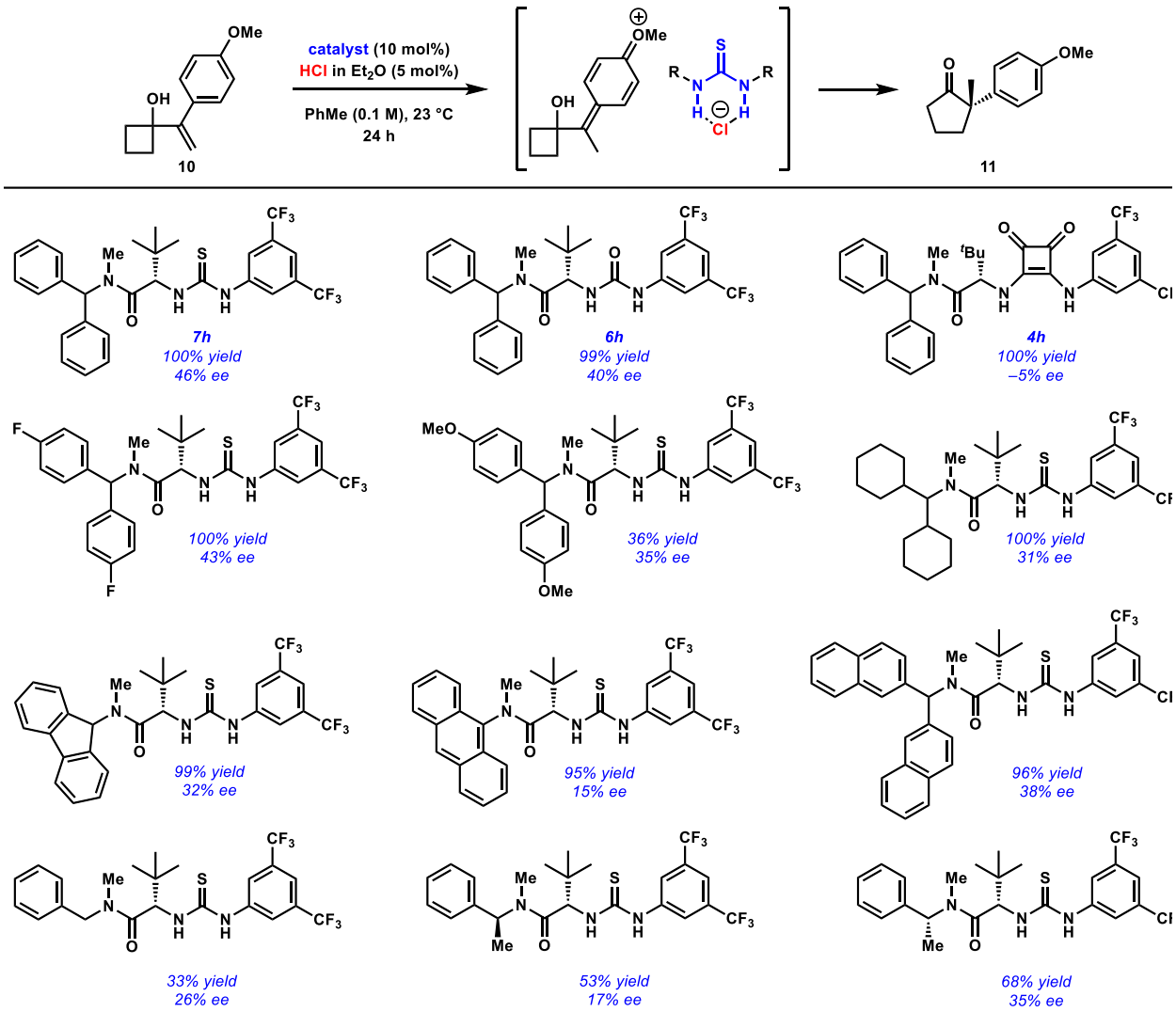

Figure 5.9 Effect of hydrogen-bond donor structure and perturbations to the catalyst benzhydryl amide on enenatioselectivity and yield in the HCl co-catalyzed semi-pinacol rearrangement of **10**

One possibility for the inability to surpass 46% ee is the presence of a more robust background reaction than anticipated. To evaluate this, HBD and HCl loadings were systematically varied to see the effect on enantioselectivity (Figure 5.10). First, the acid loading was fixed at 5 mol% and the thiourea **7h** loading was varied from 1-100 mol%. It was found that as long as there is a 1:1 ratio of thiourea and HCl, the enantioselectivity was flat at 46% ee. Knowing this, the HCl to thiourea ratio was held at 1:1 and their loading was tested at 1, 2.5, 5, and 100 mol% and it was discovered that the enantioselectivity of the transformation increased as the combined loading was

increased, with a full equivalent of each giving a marginally improved 49% ee. Last, the thiourea loading was fixed at 5 mol% and the acid loading was varied from 1 to 100 mol%. Interestingly, the enantioselectivity of the transformation did not begin to suffer until the acid loading surpassed 20 mol%, and even at 100 mol%, a 20 fold excess with respect to catalyst, the enantioselectivity is a minimally diminished 36%. These data indicate that HCl background is not that relevant in the observed low enantioselectivity and additionally, the thiourea is either providing rate enhancement over HCl background or aggregation leads to a complicated network of HCl associated with catalyst, allowing it to tie up many equivalents.

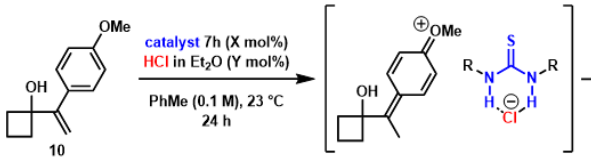

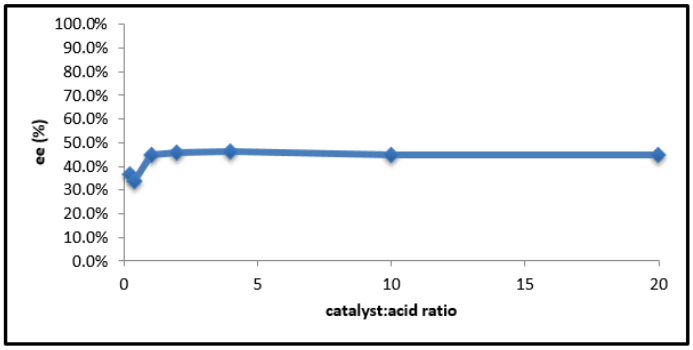

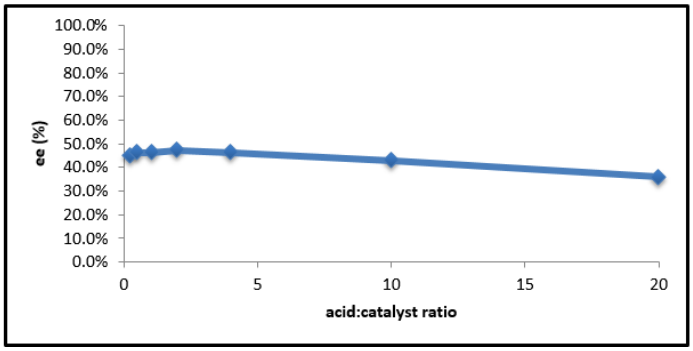

Effect of catalyst loading at fixed 5 mol% HCl in Et_2O

catalyst mol%	acid mol%	catalyst:acid ratio	ee (%)
1	5	0.2	36%
2	5	0.4	34%
5	5	1	45%
10	5	2	46%
20	5	4	46%
50	5	10	44%
100	5	20	44%

Effect of catalyst and acid loading (preserving 1:1 ratio)

catalyst mol%	acid mol%	catalyst:acid ratio	ee (%)
1	1	1	27%*
2.5	2.5	1	43%
5	5	1	45%
100	100	1	49%

Effect of acid concentration at fixed 5 mol% catalyst

catalyst mol%	acid mol%	acid:catalyst ratio	ee (%)
5	1	0.2	45%*
5	2.5	0.5	46%
5	5	1	46%
5	10	2	47%
5	20	4	46%
5	50	10	43%
5	100	20	36%

Figure 5.10 Systematic variation of HCl and thiourea loadings in the co-catalyzed semipinacol rearrangement of **10**. *indicates low conversion under the conditions

In a final effort to increase the enantioselectivity of the transformation, a solvent screen was conducted. It was found that alkane solvents provided a substantial boost in selectivity, with

all giving 60-65% ee holding all other parameters constant; heptane and cyclohexane at 0 °C both provided the optimal 65% enantioselectivity (see experimental section for more details). Many parameters were retested in alkane solvents, but none provided higher than 65% ee.

To get a sense of what was preventing high enantioinduction in this transformation, a computational study was performed on the simplified phenyl substrate using the Truhlar M06-2X functional and the Pople 6-31G(d) basis set (Figure 5.11).[153,222] Simple background computations revealed that by design, the reaction is highly exothermic at $\Delta G = -37.4$ kcal/mol due to relief of ring strain. Additionally. The intrinsic reaction barrier is quite low, also by design to outcompete deprotonation, at $\Delta G^{\ddagger} = 1.56$ kcal/mol. However, it seems the barrier is likely too low for effective enantioinduction. Unless the method of enantioinduction is minor transition state destabilization, which is an unlikely mode of enantioinduction in this case, achieving high ee seems impossible. Imagine the major pathway is made so favorable that it has no barrier; unless there is destabilization of the minor pathway, the maximum possible enantioselectivity would be 86.6%. Thus, a model reaction must be found that has a higher activation to facilitate high enantioinduction.

[222] Zhao, Y.; Truhlar, D. G. The M06 Suite of Density Functionals for Main Group Thermochemistry, Thermochemical Kinetics, Noncovalent Interactions, Excited States, and Transition Elements: Two New Functionals and Systematic Testing of Four M06-Class Functionals and 12 Other Functionals. *Theor. Chem. Acc.* **2008**, *120* (1–3), 215–241.

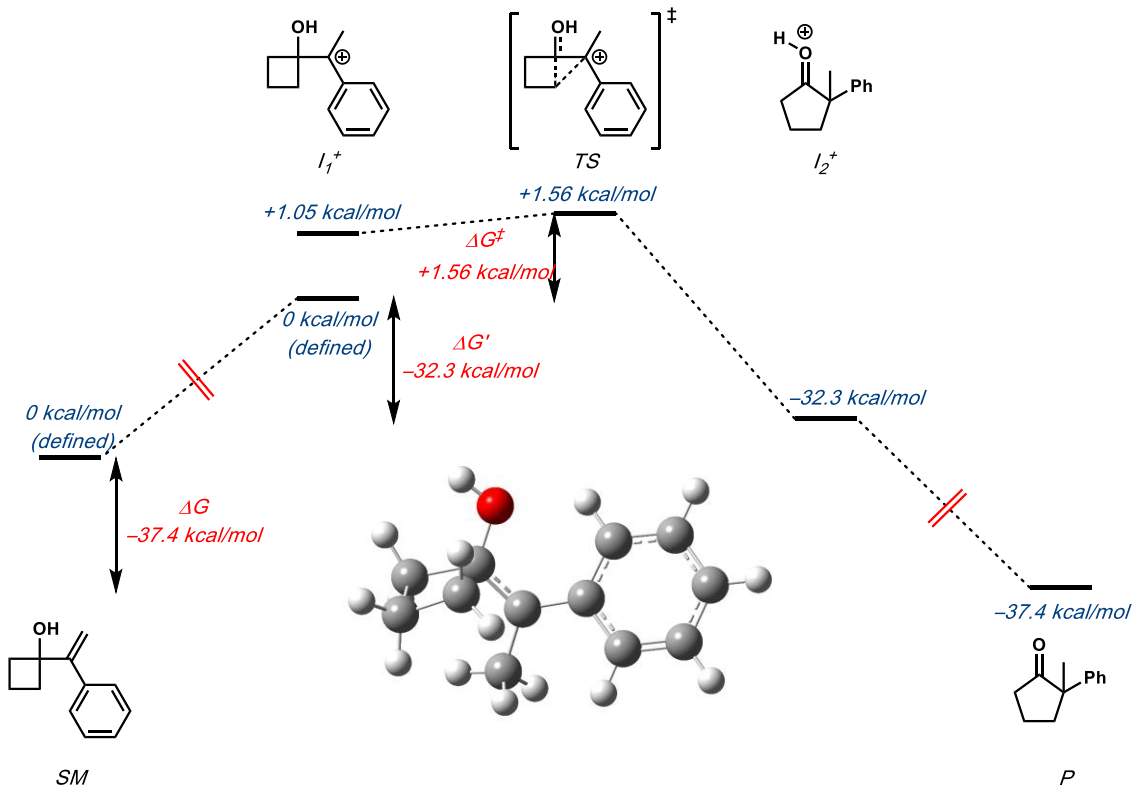

Calculations performed using M06-2X/6-31G(d)

Figure 5.11 Uncatalyzed ground state and transition state geometries and reaction thermochemistry and activation barriers for the semipinacol rearrangement of a cyclobutanol

5.2.2 Optimization of the cyclopropanol to cyclobutanone rearrangement

The ring expansion from a cyclobutane to a cyclopentane is known to be highly exothermic, relieving 20.1 kcal/mol of ring strain; however, the ring expansion from a cyclopropane to a cyclobutane only relieves 1.2 kcal/mol of ring strain.[223] This is due to the ability of the cyclopropane to adopt pseudo sp^2 Walsh orbitals, which allow for more energetically favorable bonding overlap. It was hypothesized that a less exothermic ring expansion may also have a higher activation barrier, thus the same computational picture was generated, which can be found in Figure 5.12.

[223] Ring strain values taken from: a) Wiberg, K. B. The Concept of Strain in Organic Chemistry. *Angew. Chemie Int. Ed. English* **1986**, *25* (4), 312–322. b) Anslyn, E. V.; Dougherty, D. A. *Modern Physical Organic Chemistry*; University Science: Sausalito, CA, 2006.

The thermochemical prediction at the M06-2X level of theory, with the 6-31g(d) basis set still gives a relatively exothermic at ΔG = –21.4 kcal/mol, which is 16.0 kcal/mol less exothermic than the cyclobutane to cyclopentanone expansion, which is relatively close to the 19.9 kcal/mol difference that would be predicted from just comparing the strain of cyclic alkanes, which obviously should not perfectly match here due to the presence of an exocyclic double bond in the product. The predicted reaction barrier here is 4.44 kcal/mol, which may still be a low energy barrier for effective stabilization of one diastereomeric transition state over the other diastereomeric transition state. However, importantly, $\Delta G^{\ddagger}$ = 4.44 kcal/mol is not sufficiently small to guarantee that enantioselectivities cannot break the 90% barrier; in fact 4.44 kcal/mol corresponds to 99.9% ee at room temperature (versus 86.6% ee for 1.55 kcal/mol).

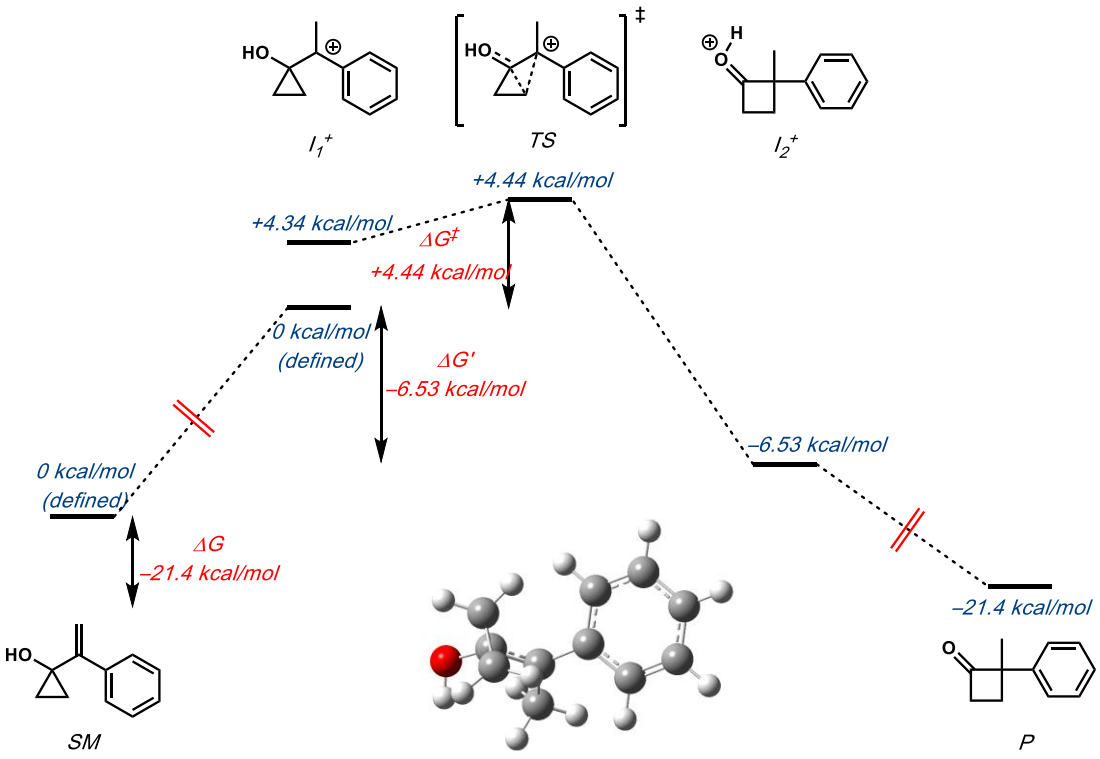

Calculations performed using M06-2X/6-31G(d)

Figure 5.12 Uncatalyzed ground state and transition state geometries and reaction thermochemistry and activation barriers for the semipinacol rearrangement of a cyclopropanol

The reaction was rescreened with the cyclopropanol substrate **12**, and much of the reaction conditions optimization was the same as in the cyclobutanol substrate, optimal parameters include: HCl as acid, thioureas provide higher selectivities than other classes of hydrogen bond donors, cyclohexane as solvent, 0.1 M as reaction concentration, and room temperature. Interestingly, for the cyclopropanol substrate **12**, the presence of a *p*-methoxystyrene is not needed. From a synthetic point of view, this is ideal, as it allows for the possibility of a greater substrate scope, which is important given the high value of the synthesis of α-quaternary stereocenters. Presumably the parent styrene works here because of the stability of cyclopropylcarbinyl carbocations though donation from a cyclpropyl pseudo sp^2 Walsh orbital, making this cation pseudo-benzhydryl rather than just benzylic as in the cyclobutanol substrate **10**.

Once optimal conditions had been found, thiourea screening was performed. An extensive screen was conducted and the most interesting results from catalysts that provided the highest levels of enantioselectivity are presented in Figure 5.13, a more comprehensive catalyst screen can be found in the experimental section 5.4. One notable difference between substrates **10** and **12**, is that while substrate **10** has a negligible background in the presence of HCl alone, substrate **12** proceeds to 40% ee in the presence of HCl alone and thiourea catalyzed reactions stall out at 60-70% conversion, indicating the potential for minimal acceleration of background HCl catalysis.

The previously optimal benzhydryl thiourea catalyst **7h** provides just –22% ee in the transformation of **12** to **13**. Extensive screening revealed that fully substituted arylpyrrolidine catalysts with cyclohexyldiaminepyrrole components were uniquely good at providing enantioselectivity in this transformation, giving 72% yield and up to 78% ee, which is the optimal ee thus far. Reverse engineering of this catalyst was performed to determine which components were necessary in providing enantioselectivity. The half-Schreiner cyclohexylamopyrrole gave

very low enantioselectivity of 8%, and the catalyst truncated after the *t*-leucine with a methyl ester gave 43% ee. Investigation of the effect of the *t*-leucineamide substituent on the thiourea pyrrole catalysts reveals the benzhydryl amide provides 55% ee. Interesting the non-fully substituted version of the optimal catalyst gives no conversion at all, for reasons that are baffling. When a 1:1 mixture of the fully substituted and non-fully substituted catalyst are added, the reaction still proceeds to 70% conversion with 78% ee. Fully substituted aryl pyrrolidine effects were investigated and the *p*-F-phenyl and 2-naphthyl catalyst gave nearly identical enantioselectivities to the phenyl catalyst. Pyrrole modifications were made as well and found in the experimental section. It seems all components of the catalyst are needed for 78% and that no structural modifications to this family of catalyst can further improve the ee. Last, structural modifications to the product were made to identify a substrate that could provide high enantioselectivity. In an attempt to differentiate diastereomeric transition states through sterics, *p*-*t*-butylstyrene substrate was tested, and through differential catalyst arene stabilization, 2-napththylstyrene substrate was tested. Both substrates provided no increase in enantioselectivity, with *p*-*t*-butylstyrene giving 78% ee and 2-naphthyl giving 75% ee. Given the inability to improve the enantioelectivity via catalyst or substrate modifications, no further reactions were run.

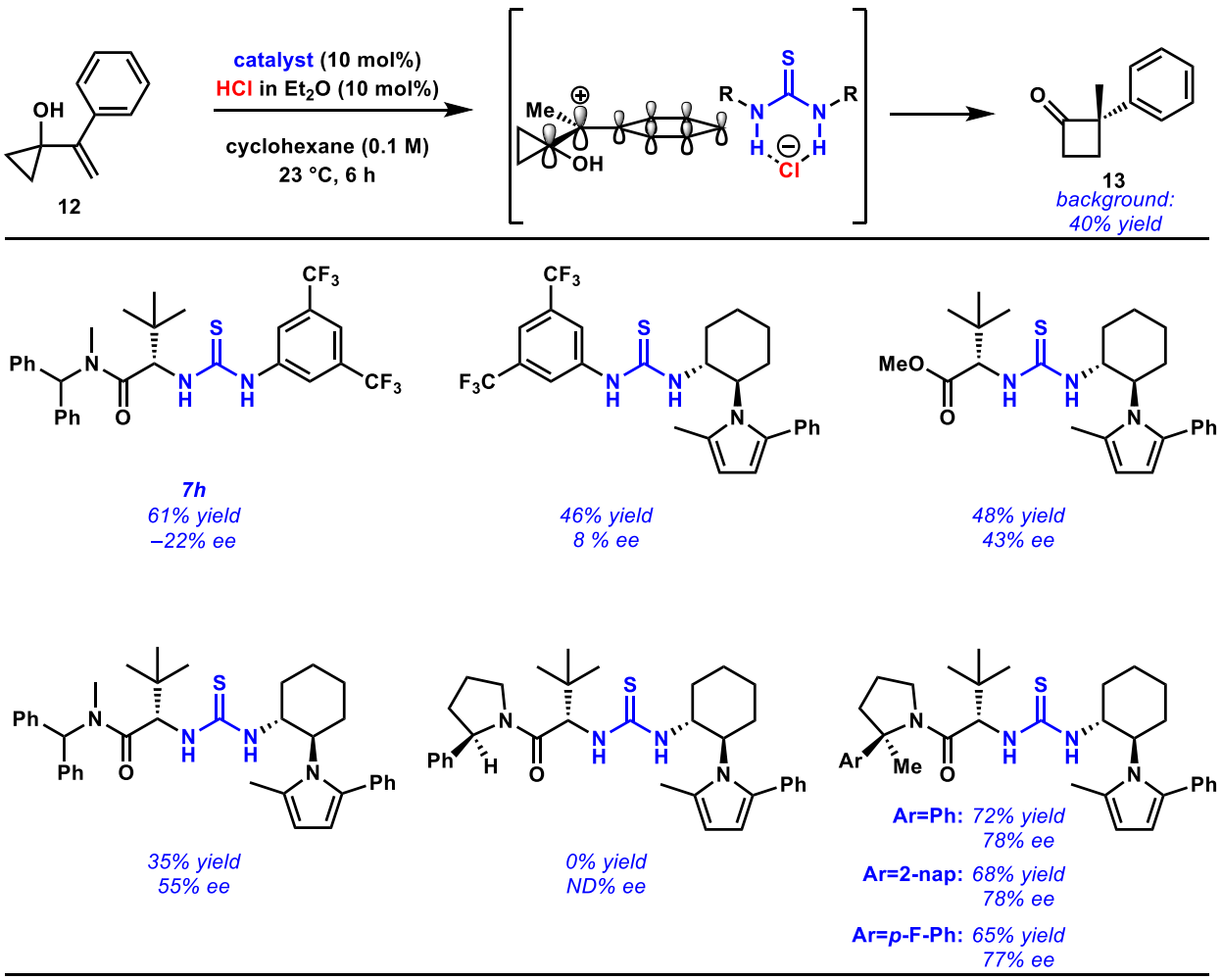

Figure 5.13 Effect of structural perturbations to the optimal arylpyrrolidine cyclohexylaminopyrrole thiourea catalyst on enenatioselectivity and yield in the HCl co-catalyzed semi-pinacol rearrangement of cyclopropanol **12**

5.3 Mechanistic hypotheses in the HCl and thiourea co-catalyzed semi-pinacol rearrangement

The central hypothesis in the co-catalysis between HCl and a thiourea is that they will associate to form an HCl·thiourea adduct with increased acidity, allowing for asymmetric catalysis over racemic background acid catalysis. Specifically in the context of the protio-semipinacol rearrangement, the catalystic cycle is envisioned as follows Figure 5.14. The HCl·thiourea adduct is hypothesized to form in an equilibrium event, which can then protonate the *p*-methoxystyrene to generate the benzylic carbocation that is stabilized by donation from the methoxy group. This

carbocation can then undergo the semi-pincaol, 1,2-rearrangement, to ring expand the cyclobutanol to a protonated cyclopentanone. This protonated cyclopentanone can then be deprotonated by the catalyst·Cl^- adduct to turn over the cycle and release product.

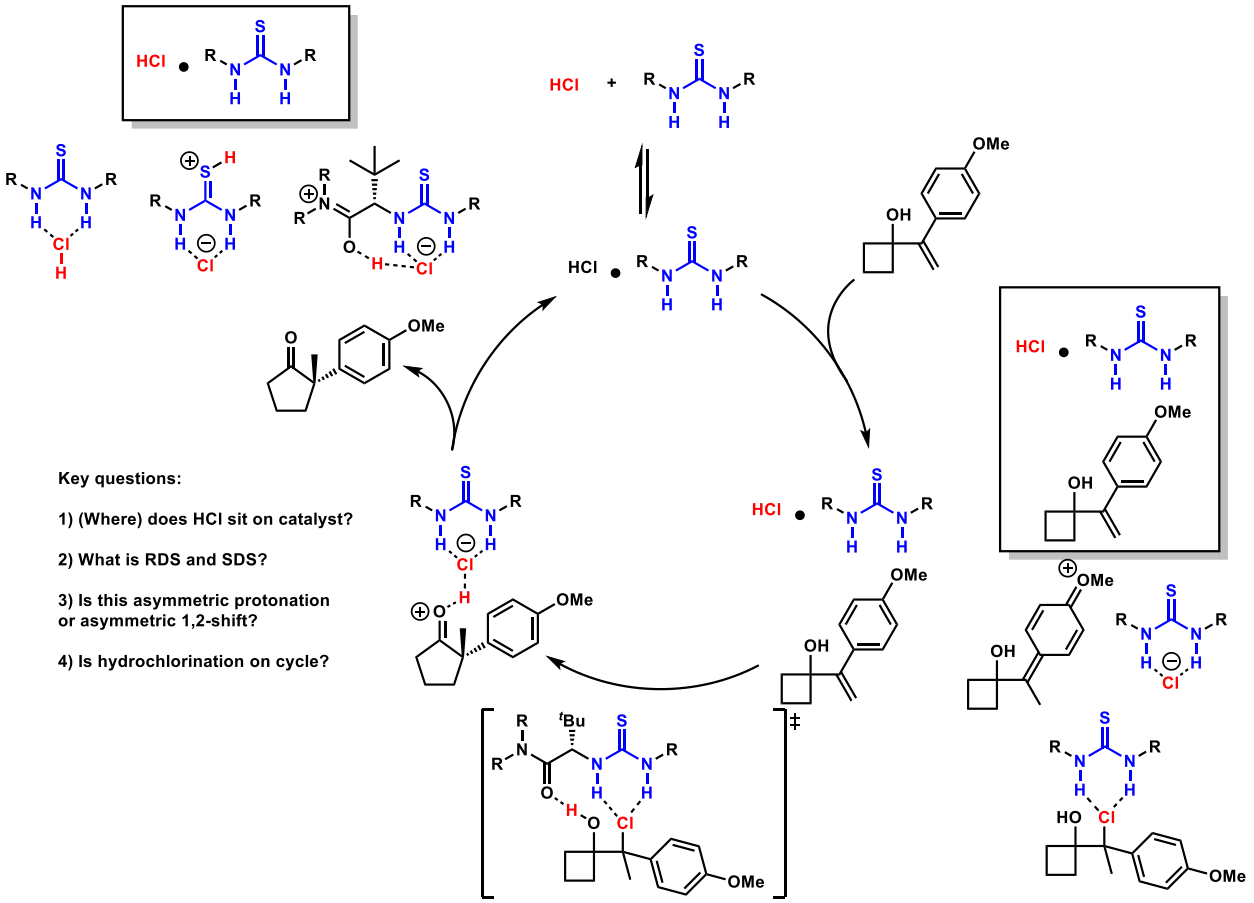

Figure 5.14 Hypothesized catalytic cycle for the HCl and thiourea co-catalyzed semipinacol rearrangement, with plausible intermediates and transition states depicted

A number of mechanistic questions exist about this catalytic cycle, and will be summarized below. First, the fundamental association between catalyst and thiourea is not understood, including the binding geometry and stoichiometry. In figure 5.14, three possibilities for 1:1 HCl·thiourea adducts are depicted. Preliminary computational data suggest that the energetic minimum for the HCl·thiourea adduct is dual hydrogen-bonding to the chloride, which engages in a bridge hydrogen bond with the protonated catalyst amide. Interestingly, in the case of the pyrrole based catalysts, preliminary computations suggests a similar adduct in which the dual hydrogen-

bonding to the chloride is preserved, but the chloride engages in a bridged hydrogen bond with the protonated catalyst amide as the ground state (Figure 5.15). Amide protonation and thiourea protonation were found to be disfavored by 1.8 and 6.3 kcal/mol respectively at M06-2X/6-31g(d).

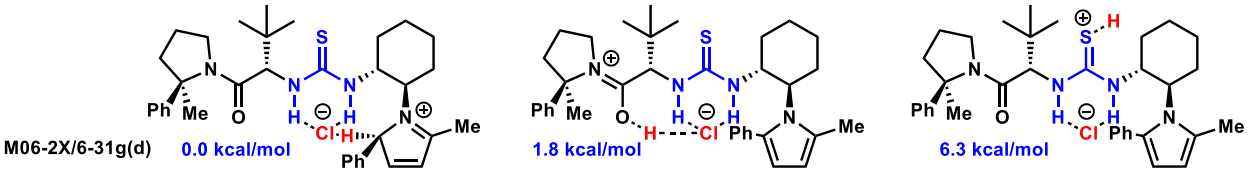

Figure 5.15 Binding geometries and energetics for the HCl·thiourea adduct with pyrrole catalyst

A number of pieces of mechanistic evidence point to the ability of thioureas to increase the rate of the reaction, which may or may not be achieved through acidification of HCl. First, the reaction proceeds to just 7% conversion with HCl alone and to 100% conversion with an appropriate thiourea. Second, a 20 fold excess of HCl to thiourea only decreases the enantioselectivity moderately. Binding studies should be conducted to experimentally determine the binding stoichiometries.

The next mechanistic question is what are the rate and selectivity determining steps of this transformation. While there is no evidence, two steps seem likely, either rate determining protonation to form a chiral adduct which rapidly rearranges, or rate determining rearrangement. In the former case, either step could be selectivity determining, whereas in the latter only rearrangement could be selectivity determining. This implies that enantioinduction could be occurring from an asymmetric protonation or rearrangement. To attempt to answer this question, a dihydronaphthyl vinyl cyclobutanol substrate was made to see if the addition of DCl would set the β-stereocenter in diasteromeric purity with respect to the α-substituent. Unfortunately, a number of substrates were synthesized, but it seems trisubstituted olefins bearing substitution at the β-carbon do not undergo productive chemistry.

Last, is the question of whether or not hydrochlorination is on-cycle, off-cycle or an irrelevant process. One could imagine the reversible addition of chloride to the benzylic carbocation to get to a covalent 3° chloride intermediate, depicted in Figure 5.14. One enantiomer of this intermediate could more effectively undergo a catalyzed stereospecific chloride abstraction with concerted 1,2-rearrangement. Attempts to synthesize the tertiary chloride failed. To test this hypothesis in a related system, one could start from the 1,2-diol, especially enantioenriched 1,2-diol and look for enenatioselectivity or enantiospecificity in the rearrangement step.

5.4 Conclusion and outlook

In conclusion, an enantioselective thiourea and HCl cocatalyzed ring-expansion semipinacol rearrangement to set α-quaternary cyclobutanones and cyclohexanones was achieved in moderate ee. Catalyst, substrate, and conditions optimizations led to an enantioselectivity of 78% in the cyclopropanol rearrangement and 65% in the cyclobutanol rearrangement. Preliminary mechanistic evidence and experimental observations suggest that the thiourea may be enhancing the Brønsted acidity of HCl, allowing for enantioselective catalysis over racemic background HCl catalysis.

The ability to activate strong Brønsted acids with hydrogen-bond donor catalysts would be a complimentary strategy the recent developments in the chiral BINOL acid field. In some ways the HBD approach is more appealing, as it leverages the ability to activate off the shelf strong acids, such as HCl and TfOH, which have decades of precedent in catalyzing well-established reactions with pro-chiral substrates.

Recently, triflate anion and squaramide hydrogen bond-donors have emerged as a highly productive and enantioselective combination in the context of TMSOTf catalyzed reactions. It follows that squaramide may be particularly capable of activating TfOH or R_3SOH toward

enantioselective catalysis, and this was not explored here. Future studies should look to this system for inspiration. Last, recent unpublished work has shown that HCl and HBr can be used with thioureas and squaramides respectively, in a non-substrate buffered reaction to afford high levels of enantioselectivity.

5.5 Experimental

5.5.1 General procedure for the HBD catalyzed semipinacol rearrangement of 10 and 12

Substrates **10** and **12** were synthesized via addition of lithiated α-bromostyrenes to cyclobutanone and cyclopentanone via reported procedures.[224][225] 1-dram vials were equipped with flea stir bars and placed in an oven overnight. The oven-dried vials were allowed to cool to room temperature after which 0.01 mmol of thiourea (0.1 equiv.) A stock solution of 0.1 M substrate and 0.1 M triphenylmethane as internal NMR integration standard was made in the solvent of interest and 1 mL was added to the vial. The vials were then capped and put under nitrogen atmosphere. The reactions were cooled to 0 °C in an ice water bath for 10 minutes after which 1 M HCl in ether was added (0.01 equiv, 0.01 mmol) via syringe. After 10 minutes, nitrogen lines were removed, reactions were sealed with electrical tape and moved to a 4 °C freezer in which stirring was possible. Reactions were generally run overnight, for 12-24 hours.

To work reactions up, solid K_2CO_3 was added at 4 °C and allowed to stir for an hour to guarantee consumption of HCl. The reactions were then warmed to room temperature, filtered through cotton and rotary evaporated. Unreacted substrate, especially cyclopropanol **12** can rearrange on silica in a racemic fashion, artificially lowering the enantioselectivity. Thus, no

[224] Alazet, S.; Preindl, J.; Simonet-Davin, R.; Nicolai, S.; Nanchen, A.; Meyer, T.; Waser, J. Cyclic Hypervalent Iodine Reagents for Azidation: Safer Reagents and Photoredox-Catalyzed Ring Expansion. *J. Org. Chem.* **2018**, *83* (19), 12334–12356.

[225] Shu, X.; Zhang, M.; He, Y.; Frei, H.; Toste, F. D. Dual Visible Light Photoredox and Gold-Catalyzed Arylative Ring Expansion. *J. Am. Chem. Soc.* **2014**, *136* (16), 5844–5847.

further purification was performed. Crude reaction NMRs were integrated against triphenylmethane internal standard to quantify conversion and yield, and products were separated on chiral HPLC. The spectral data for cyclobutanone **13** match the literature values.[226]

NMR spectral data for 11:

2-(4-methoxyphenyl)-2-methylcyclopentan-1-one (11):

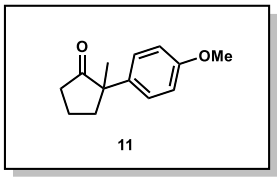

11

^{1}H NMR (400 MHz, cdcl$_3$) δ 7.26 – 7.22 (m, 2H), 6.92 – 6.84 (m, 2H), 3.79 (s, 3H), 2.59 – 2.46 (m, 1H), 2.40 – 2.30 (m, 2H), 2.05 – 1.80 (m, 3H), 1.37 (s, 3H).

5.5.2 Additional screening in the semipinacol rearrangement

A comprehensive solvent screen was conducted with cyclobutanol substrate **10** and thiourea catalyst **7h**. This revealed that alkane solvents were optimal for enantioselectivity; thus an extrensive alkane solvent screen was run and the data are in Figure 5.16. At room temperature, cyclohexane was found to give the best ee at 62%. The effect of temperature on enantioselectivity and yield was then conducted with toluene and heptane (due to cyclohexane freezing at 4 °C). Optimal results were obtained for both solvents at 0 °C, with both catalyst providing complete conversion at that temperature. To see the effect of these new conditions on suboptimal catalysts, the optimal arylpyrrolidine thiourea **7a** and squaramide **4e** were reexamined and found to only have marginally improved enantioselectivities under these new conditions.

[226] Nemoto, H.; Miyata, J.; Hakamata, H.; Nagamochi, M.; Fukumoto, K. A Novel and Efficient Route to Chiral A-Ring Aromatic Trichothecanes—The First Enantiocontrolled Total Synthesis of (-)-Debromofiliformin and (-)-Filiformin. *Tetrahedron* **1995**, *51* (19), 5511–5522.

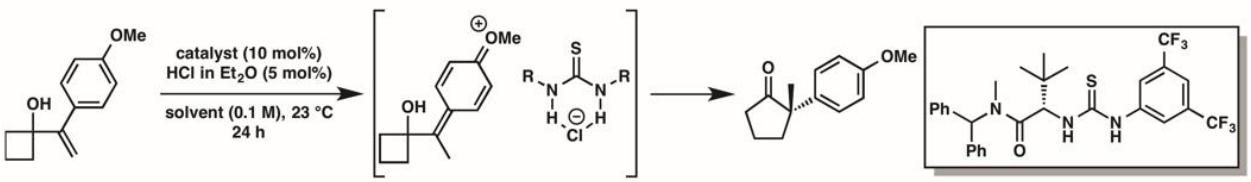

alkane solvent screen

solvent	yield	ee
toluene	100%	46%
pentane	100%	56%
hexanes	100%	57%
cyclohexane	100%	62%
heptane	100%	59%

effect of temperature on yield and selectivity

temperature	solvent	yield	ee
23 °C	toluene	100%	46%
0 °C	toluene	100%	52%
–20 °C	toluene	79%	38%
–40 °C	toluene	37%	50%
23 °C	heptane	100%	59%
0 °C	heptane	90%	65%
–30 °C	heptane	16%	34%

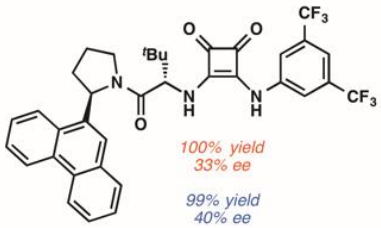

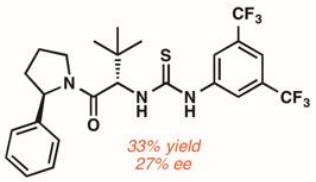

All yields determined via NMR against triphenylmethane standard

Figure 5.16 Solvent and temperature optimization in the semi-pinacol rearrangement of **10**

When the substrate was switched to the cyclopropanol **12** and the optimal pyrrole containing catalyst had been identified, conditions were reoptimized around this combination of substrate and catalyst (Figure 5.17). An extensive solvent screen identified toluene and cyclohexane as optimal for enantioselectivity and conversion. Given the more prevalent HCl catalyzed background reaction for this substrate, the catalyst to acid ratio was tested again to ensure HBD catalysis is outcompeting background. Based on the data, it appears the dual catalytic system is outcompeting HCl catalysis alone, given the relatively constant enantioselectivities and what appears to be a kinetic dependence on the concentration of thiourea catalyst. Last, early reaction time points were taken to determine whether or not enantioselectivity is flat over the course of the reaction; this is found to be the case.

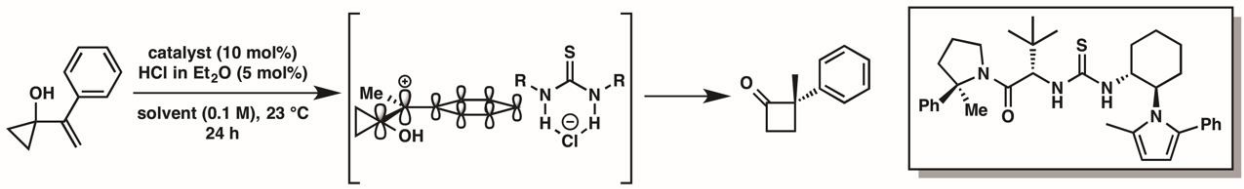

Solvent screen

solvent	conversion	ee
heptane	84%	71%
cyclohexane	86%	77%
toluene	91%	78%
DCM	32%	ND
MTBE	decomp	ND
Et_2O	13%	ND
THF	decomp	ND

Catalyst to acid ratio studies (in heptane)

catalyst/acid (mol%)	conversion	ee
1/5	31%	68%
2/5	55%	59%
5/5	79%	69%
10/5	84%	71%
20/5	55%	ND
10/10	100%	76%

Time point studies (in cyclohexane)

time (h)	yield	ee
3	65%	76%
6	59%	77%
12	72%	77%
24	55%	79%
48	50%	74%

10 mol% HCl

Figure 5.17 Conditions reoptimization around cyclopropanol substrate **12**

Some pyrrole catalyst screening is presented in Figure 5.13; however, the catalyst screens conducted were much more extensive. When holding the thiourea cyclohexyldiamino pyrrole constant, a number of *t*-leucine amide catalysts were tested (Figure 5.18). Among these, fully substituted aryl pyrroldines are uniquely good an all provide the same level of enantioselectivity. Interestingly the structurally similar non-fully substituted pyrrole, prolinol ether, and indoline catalysts tested all provide 0% yield with ~40% starting material decomposition. The pyrrolidine with pseudo C_2 symmetric TBSO groups gives decent conversion with 69% ee. It is known that the role of the methyl substituent on arylpyrrolidine locks the conformation into the amide *Z*-conformer. It is possible that the presence of any population of *E*-conformer is disastrous to reactivity. Given the computations suggesting that proton rests on catalyst amide, pyrrolidine conformation may explain the difference in ability of these catalysts to promote the rearrangement.

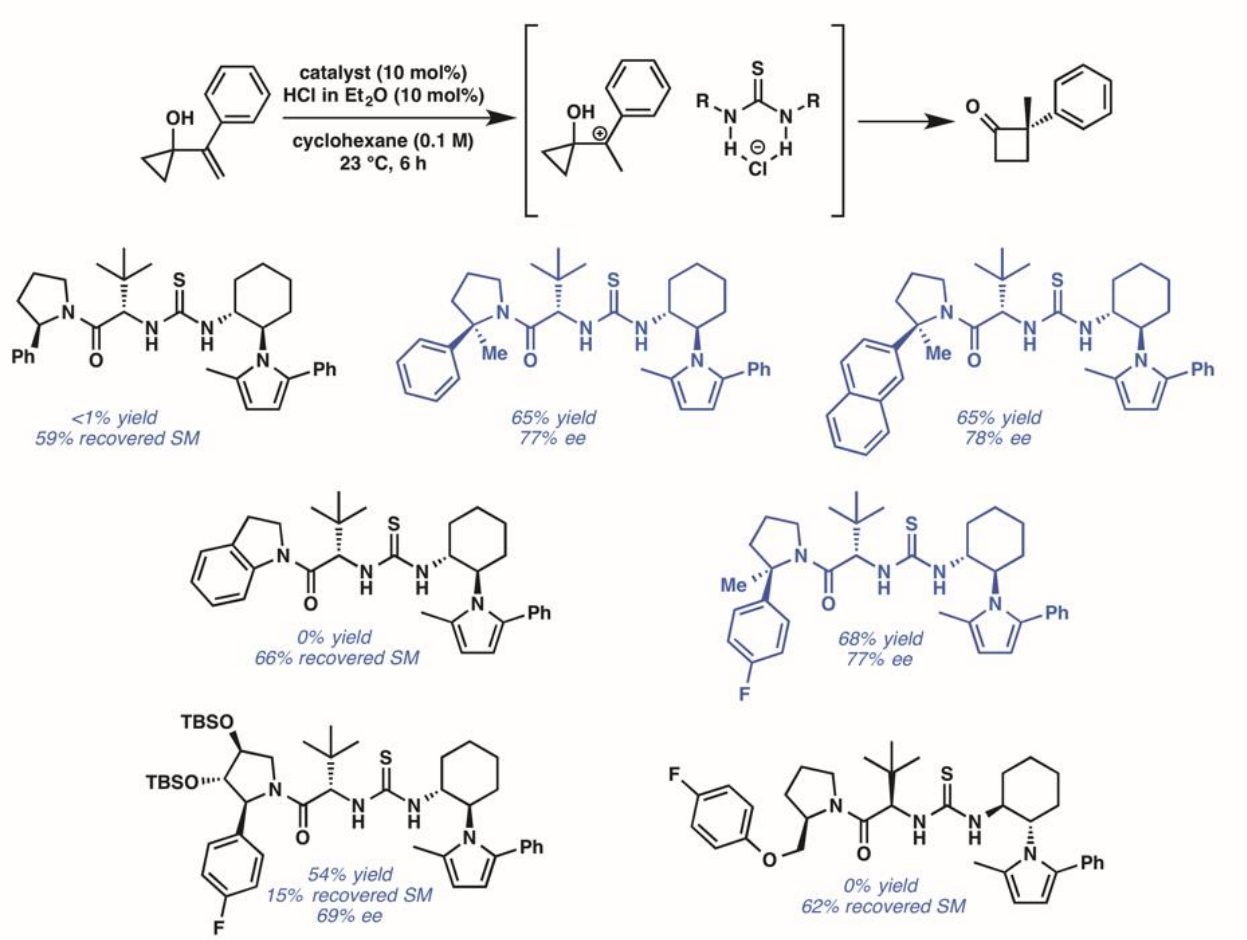

Figure 5.18 Effect of catalyst pyrrolidine variations on the yields and enantioselectivities of the thiourea cyclohexyldiamino pyrrole HCl co-catalyzed semi-pinacol rearrangement of **12**

Next, the effect of changing the pyrrole portion, while holding the rest of the catalyst constant was tested (Figure 5.19). It was found that as long as the pyrrole is 2,5-alkyl,aryl substituted electronic and arene expanse modifications have very little impact on the enantioselectivity. Both 2,5-dialkyl and 2,5-diaryl pyrroles also give relatively similar levels of enantioselectivity, as does replacing the pyrrole with a carbazole; although interestingly, the carbazole flips the sense of enantioselectivity of the transformation. Since this is relatively high-enantioselectivity and vastly different than all other pyrroles tested, this may be a handle for further reaction optimization.

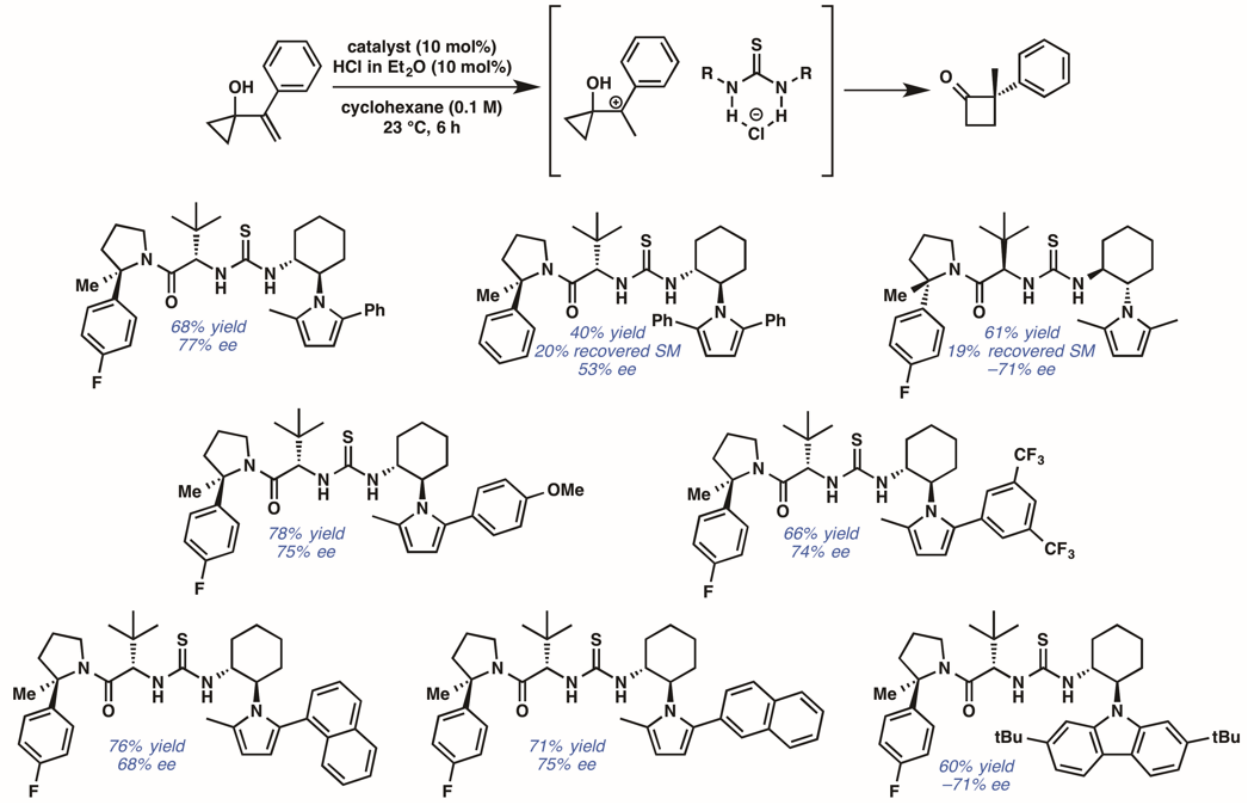

Figure 5.19 Effect of catalyst pyrrole variations on the yields and enantioselectivities of the thiourea cyclohexyldiamino pyrrole HCl co-catalyzed semi-pinacol rearrangement of **12**

Last, this catalyst has 4 stereocenters, thus there are 8 diastereomeric possibilities for the same constitutional isomer. Based on previous reports, it seemed likely this was the optimal diastereomer.[227] Figure 5.20 investigates the effect of diastereomeric catalysts, as well as more fundamental changes to the catalyst structure. As anticipated, the initially tested diastereomer was optimal. The catalyst that is epimeric just at the *t*-leucine stereocenter provides low yield and near racemic product. The catalyst that only preserves the arylpyrrolidine center gives moderately high conversion and enantioseletivity, at –56% ee. Changing the diamine scaffold from C_2 symmetric to pseudo-meso was not tested. This indicates that all catalyst stereocenters are important, but the relative stereochemistry between *t*-leucine and the diamine is essential. Next, we evaluated the

[227] Kennedy, C. R.; Guidera, J. A.; Jacobsen, E. N. Synergistic Ion-Binding Catalysis Demonstrated via an Enantioselective, Catalytic [2,3]-Wittig Rearrangement. *ACS Cent. Sci.* **2016**, *2* (6), 416–423.

urea analog of the optimal catalyst, which provided near identical results to the thiourea. To verify that the pyrrole is essential, fully substituted and non-fully substituted pyrrolidine thioureas **7a** and **7a'** were tested. Like the non-fully substituted version of the optimal catalyst, the **7a** gave minimal yield and near racemic product, whereas the fully substituted thiourea **7a'** provided the same yield as optimal catalyst, 71%, but near racemic product. This indicates that the presence of the pyrrole is indeed essential in optimal catalyst.

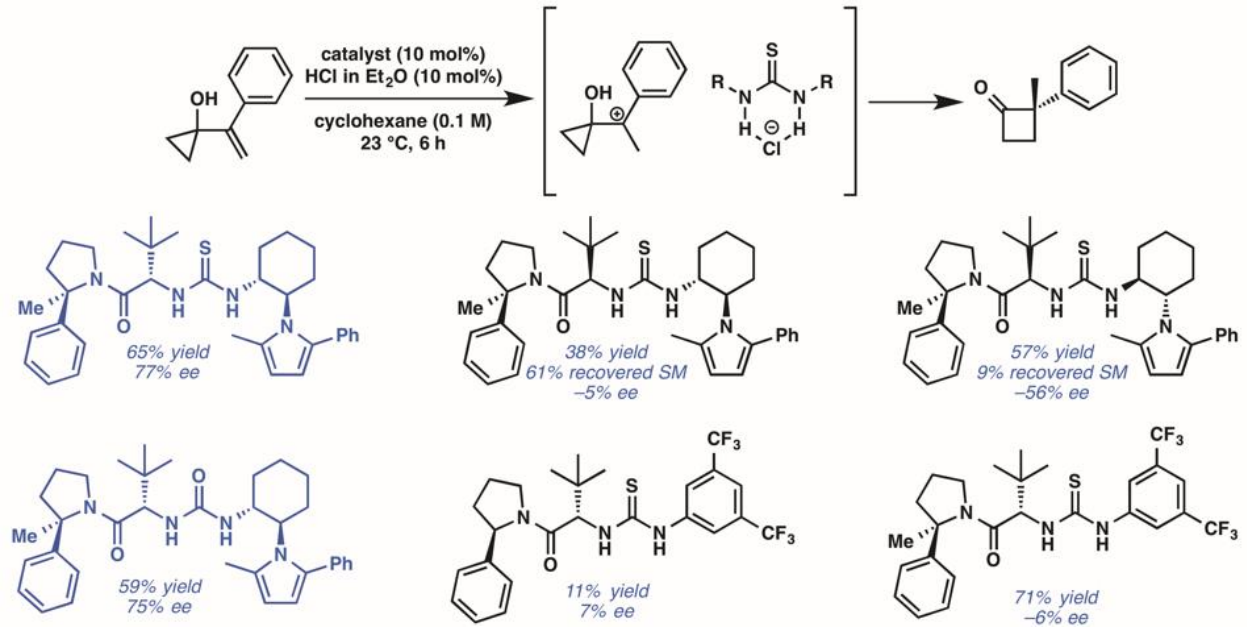

Figure 5.20 Effect of catalyst diasteromers and other structural variations on the thiourea HCl co-catalyzed semi-pinacol rearrangement of **12**